Exploration of New Combinatorial Therapy Candidates for Tongue Squamous Cell Carcinomas

Dissertation

zur Erlangung des
Doktorgrades der Naturwissenschaften (Dr. rer. nat.)

der

Naturwissenschaftlichen Fakultät I – Biowissenschaften

der Martin-Luther-Universität Halle-Wittenberg,

vorgelegt

von Herrn **Ali Hmedat**
geb. am 30.01.1985 in Irbid, Jordan

Gutachter:
1. Prof. Dr. Stephan Feller
2. Prof. Dr. Markus Pietzsch
3. Prof. Dr. Fred Schaper
Tag der Verteidigung: 11. Januar 2022

Acknowledgements

Table of Contents

List of Abbreviations

3-MA	3-methyl-adenine
ALL	Acute lymphoblastic leukaemia
AO	Acridine orange
APS	Ammonium persulfate
AT	AT13387 (a HSP90 inhibitor)
ATP	Adenosine triphosphate
AVO	Acidic vesicular organelle
BC	Bicarbonate
BSA	Bovine serum albumin
CAS	CRK-associated substrate
CDK	Cyclin-dependent kinase
CLL	Chronin lymphoblastic leukaemia
CML	Chronic myeloid leukemia
CRC	Colorectal cancer
CT	Cetuximab
DAPI	4',6-Diamidino-2-phenylindole dihydrochloride
DAS	Dasatinib
DMEM	Dulbecco's Modified Eagle Medium
DMF	Dimethylformamide
DMSO	Dimethyl sulfoxide
DOC	Deoxycholic acid
DX	Dexamethasone
ECL	Enhanced chemiluminescence
ECM	Extracellular matrix
EDTA	Ethylenediaminetetraacetic acid
EGF	Epidermal Growth Factor
EGFR	Epidermal Growth Factor Receptor
EGTA	Ethylene glycol bis (aminoethyl ether) tetraacetic acid
EIA	Expected if Additive
ERK	Extracellular signal-regulated kinase
FAK	Focal adhesion kinase
FDA	Food and Drug Administration
FITC	Fluorescein isothiocyanate
FL	Fluticasone
GC	Glucocorticoid
GCR	Glucocorticoid receptor
GDP	Guanosine diphosphate
GSH	Glutathione
GST	Glutathione S-transferase
GTP	Guanosine triphosphate
HC	Hydrocortisone
HEPES	2- (4- (2-hydroxyethyl) -1-piperazinyl) ethanesulfonic acid
HER2	Human epidermal growth factor receptor 2
HGF	Hepatocyte Growth Factor
HNC	Head and neck cancer

HNSCC	Head and neck squamous cell cancer
HPV	Human papillomavirus
HRP	Horseradish peroxidase
HSP90	Heat shock protein 90 kDa
HSP90i	Heat shock protein 90 inhibitor
IC50	Concentration at 50% inhibition
IMT	Imatinib
IP	Immunoprecipitaion
LB	Luria/Miller
LP	Lapatinib
M	Marker (for protein size)
mAb	Monoclonal antibody
MAPK	Mitogen-activated protein kinase
MMP	Matrix metalloproteinases
MP	Methylprednisolone
NBT	Nitroblue tetrazolium chloride
NCI	National Cancer Institute
NEAA	Non-essential amino acid
NSCLC	Non small cell lung carcinoma
OSCC	Oral squamous cell carcinoma
PARP	Poly-ADP-ribose polymerase
PBS	Phosphate-buffered saline
PI	Propidium Iodide
PI3K	Phosphatidylinositol-4,5-bisphosphate 3-kinase
PIT	Protease inhibitor tablet
PMSF	Phenylmethylsulfonylfluoride
PTK	Protein tyrosine kinases
PVDF	polyvinylidene difluoride
Rb	Retinoblastoma protein
RBD	RAS binding domain
Rcf	Relative centrifugal force
RIPA	Radio immunoprecipitation assay
RNAse A	Ribonuclease A
ROS	Reactive oxygen species
rpm	Revolutions per minute
RRA	Relative receptor affinity
RT	Room temperature
RTK	Receptor tyrosine kinase
SA-β-gal	Senescence-associated-β-galactosidase
SD	Standard deviation
SDBB	Semi dry blot buffer
SDS	Sodium dodecyl sulfate
SDS-PAGE	Sodium dodecyl sulfate-polyacrylamide gel electrophoresis
SEER	Surveillance, Epidemiology, and End Results
Ser	Serine
SFK	SRC family kinase
SH2	SRC-homology 2

ST	Staurosporine
STAT	Signal transducer and activator of transcription
TAS	TAS-116 (a HSP90 inhibitor)
TB	Terrific Broth
TBS	Tris buffered saline
TBST	TBS with 0.1% Tween
TEMED	Tetramethylethylenediamine
TGF	Transforming Growth Factor
Thr	Threonine
TKI	Tyrosine kinase inhibitor
Tris	Tris (hydroxymethyl) aminomethan
TSCC	Tongue squamous cell carcinoma
Tyr, Y	Tyrosine
UC	Ultraclean
V	Vehicle
WHO	World health organization
WT	Wilde type

Chapter 1 Introduction

1.1 Cancer

'Cancer', in a broader sense, refers to more than 277 different types of cancer diseases [1]. According to the World Health Organization (WHO), it is a leading cause of death globally second only to cardiovascular disease. Globally, cancer was responsible for an estimated 9.6 million deaths in 2018. About 1 in 6 of overall deaths are due to cancer [2]. While great steps have been made in the treatment of cancer over the past 50 years, it remains to be a major health concern and, therefore, great efforts are made to search for new therapeutic approaches.

Cancer develops often as a series of successive mutations in genes so that change cellular functions. The cancer cell can be characterized by classic hallmarks of cancer including proliferation, resistance to cell death, induction of angiogenesis, avoidance of growth suppressors, dissemination, invasion and metastasis [3]. In general, cancer disrupts cellular regulatory networks and results in the dysfunction of vital genes. These disturbances affect the cell cycle and lead to abnormal proliferation [4]. Furthermore, it has become evident that not only the cancer cell alone but also the surrounding tumor microenvironment is contributing to the hallmark properties [5] [6]. An inflammatory state is another characteristic of cancer which is driven by cells of the immune system, enabling tumor progression in various ways [7].

Chemical compounds have an obvious role in inducing gene mutations and cancer cell development. For instance, smoking includes many carcinogenic chemical compounds that cause lung cancer [8]. There are also numerous environmental chemical substances with carcinogenic properties that can lead to genetic disorders and gene mutations [9] [10] [11] [12].

Viruses [13] [14] [15] and bacteria [16] are other carcinogenesis factors. In 2018, an estimated 2.2 million infection-attributable cancer cases were diagnosed worldwide, corresponding to 25 cases per 100 000 person years [17]. The radiation of certain wavelengths also has enough energy to damage DNA and cause cancer [18].

1.2 Tongue Cancer

1.2.1 Epidemiology

Head and neck cancer (HNC) is a diverse group of oncological entities, originating from various tissue types and organ localizations all situated in the topographical region of the head and the neck (Figure 1) [19] [20] [21] [22]. HNC represent the sixth most common cancer type worldwide with approximately 650,000 new patients diagnosed annually, resulting in more than 330,000 deaths every year [23]. More than 90% of head and neck cancers are squamous cell carcinomas (HNSCC) that arise from the mucosal surfaces of the tongue, oral cavity, oropharynx and larynx [24].
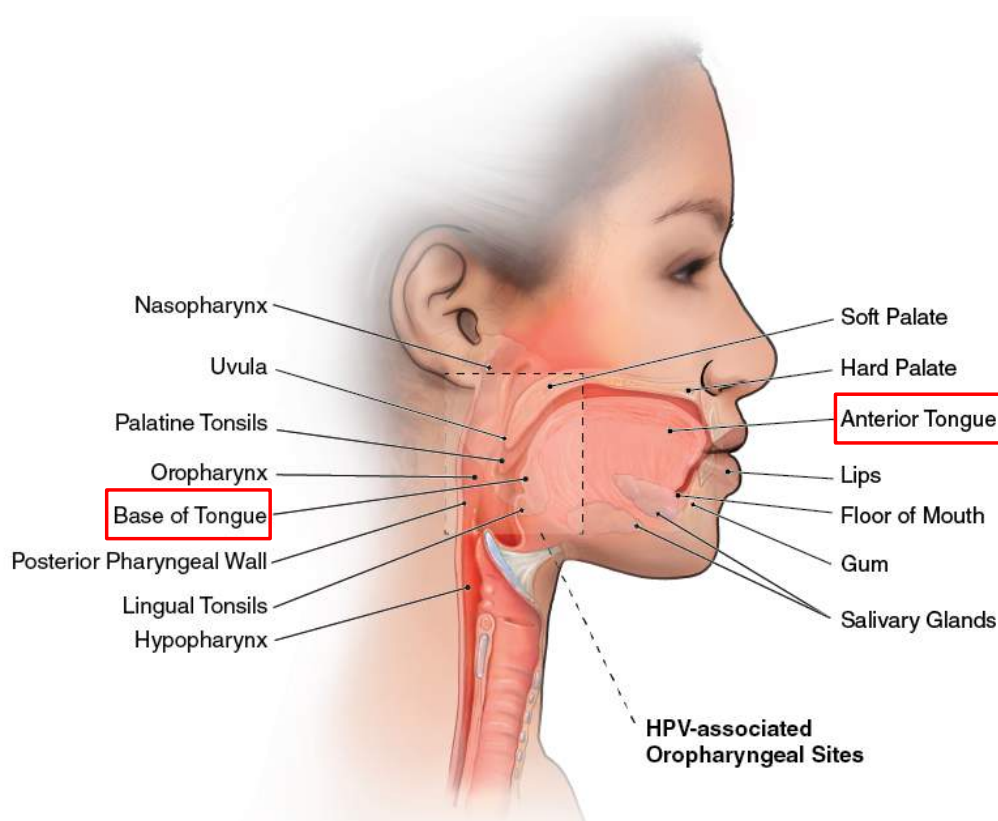
Figure 1. Head and Neck Cancer Regions

This figure illustrates the location affected by HNSCC. Tongue cancer is the main focus of this thesis (red boxes). Figure from the Centers for Disease Control and Prevention (CDC). Boxes were added [25]. HPV: Human papillomavirus.

Up to one-half of all HNSCCs occur in the oral cavity [26] and oral cancer is the 11th most common malignancy in the world. In 2018, it was estimated that 354,900 cases of oral cancer occurred worldwide, with 177,400 deaths [27]. About 90% of tumors are subtyped to Oral Squamous Cell Carcinoma (OSCC). The incidence and mortality of this tumor show variability according to the geographic locations in which it is diagnosed, however in the last decade an increase was seen in the percentage of young patients, especially patients with tongue cancer [28]. Several countries in Europe showed a significant increase of oral cancer prevalence, such as Germany, especially in men [29].

According to the International Classification of Diseases (10th revision, ICD-10), oral cavity cancer includes cancer of the lip (ICD-10: C00), cancer of the tongue (ICD-10: C01-02), and cancer within other regions of the oral cavity (Figure 1). The buccal (cheek) mucosa is the most common site for oral cancer in South and Southeast Asia; in all other regions, the tongue is the most common site [30]. Regional variations in the site of occurrence relate to the major causes, which are alcohol and smoking in Western countries, and betel quid and tobacco chewing in South and Southeast Asia [31].

Squamous cell carcinoma of the tongue (TSCC) is the most common intraoral malignancy worldwide (40-50% of OSCC) and in a number of countries it is a serious public health problem with significant morbidity and mortality [26,32,33,34,35,36]. Tongue cancer's global epidemiology shows significant geographic variation. It is a severe health problem in many countries including India (male incidence rates up to 6.5 per 100,000 persons per year) and parts of Europe (male incidence rates in France up to 8.0 per 100,000 persons per year) [32].

39.5% of diagnosed oral cavity cancer cases in Germany between 1997 and 2006 localized on the tongue. The median age at diagnosis ranged between 59 and 62 years [37] . On the other hand, according to the National Cancer Institute, the estimated number of new tongue cancer cases in 2020 is 17,660 which represent 1% of all new cancer cases in the USA. The estimated number of deaths in 2020 is 2,830 which represent 0.5% of all cancer deaths. The rate of new cases of tongue cancer was 3.5 persons per 100,000 per year and the death rate was 0.7 per 100,000 persons per year. These rates are based on 2013–2017 cases and deaths [38]. The incidence of TSCC has been steadily increasing from 1980 (10% increase overall) whereas the incidence of other OSCC sites has been decreasing suggesting a changing epidemiological trend [34 39 40 41].

Global data on the mortality of tongue cancer are difficult to obtain, because studies on mortality rates of oral cancer mostly do not refer to specific sites. Another problem is that few studies focus specifically on tongue cancer. In most cases, tongue cancer and other intraoral cancers are grouped together with lip cancer and in many cases also salivary gland tumors, both of which are known to have distinct patterns of incidence and mortality [32]. This classification of 'oral' or 'mouth' cancer, while simplifying epidemiological descriptions and increasing the overall number of cases available for analysis, has the disadvantage of masking trends in the individual subsites including the tongue.

Carcinoma of the tongue has always been regarded as a disease that affects men more than women, with the highest incidence occurring in the sixth to the eight decades of life. It rarely occurs below the age of 20 years [42]. Furthermore, recent studies report an increased incidence of carcinoma of the tongue in young patients, particularly those less than 40 years old who are more likely to never have been smokers or drinkers. This is extremely troubling as in this group the disease tends to have aggressive tumor biology with a correspondingly poor prognosis, with a high risk of loco-regional relapse, survival rates inferior to those of HNC group and need for a more aggressive therapy [39 43 44]. However, considering the most recent studies, prognostic results in this patient group are heterogeneous and no specific etiopathogenic agent has been identified to date that may provide a clear explanation for such a trend [45].

1.2.2 Risk Factors and Etiology

Using tobacco, including cigarettes, cigars, pipes, chewing tobacco, and snuff are the largest risk factors for HNC. Smoking has been shown to be closely linked with carcinoma of the tongue. Carcinogens in tobacco smoke and their metabolites covalently bind to deoxyribonucleic acid (DNA) and form DNA adducts. These adducts are responsible for critical mutations during DNA replication. The risk for TSCC increases both with the number of cigarettes smoked and duration of smoking, but returns almost to normal after smoking has been stopped for over 10 years [46 47 48 49] . Smokers of high tar cigarettes increase their cancer risk ten-fold [47]. The association between smoking history and OSCC demonstrate a strong association between a history of smoking and carcinoma involving the posterolateral tongue and the floor of the mouth [50].

In Europe, the US and Australia, smoking has significantly decreased over the past three decades with the introduction of limits on tobacco companies. However, e.g. in the Middle East, Jordan has surpassed Indonesia to have the highest smoking rates in the world partially due to widespread interference in policymaking by multinational tobacco companies [51]. According to a government study carried out in 2019 in collaboration with the WHO, more

than eight out of ten Jordanian men smoke or regularly use nicotine products including e-cigarettes. The study found that Jordanian men who smoke daily consume an average of 23 cigarettes a day. These rates are severely high and predict a future public health catastrophe including a large number of new tongue cancer cases [51]. One study about oral cancer in Jordan revealed that 76% of patients were smokers, whereby the floor of the mouth was the most common site for oral cancer, followed by the tongue [52]. Additionally, narghile (waterpipe) smoking was found to be an independent risk factor associated with the development of oral cancer at a younger age [53]. Public health programs have been successful in reducing the use of tobacco, and therefore the incidence of OSCC overall has been decreasing over the past 20 years [54] [55]. However, there has been a dramatic increase in the incidence rates of tongue cancers [56] [57] [58] [59].

A combination of tobacco consumption by chewing or smoking together with high alcohol consumption synergistically increases the carcinogenic effects [49] [60]. It is possible that the increased incidence of carcinoma of the tongue in women is partially related to changed smoking and drinking habits [61]. Frequent and heavy consumption of alcohol increases the risk of intraoral carcinoma and is often seen together with a history of smoking [42] [62]. The systemic effects of alcohol are mainly due to the hepatic damage. Alcohol addiction leading to cirrhosis and other diseases inhibits the detoxification of carcinogenic compounds [63]. Some forms of alcohol may be more harmful than others, and moderate intake of wine is less dangerous than beer and spirits [47] [49]. Associations between other dietary components and TSCC have revealed that a high intake of green vegetables, carrots, fresh fruits and tea seemed to be associated with reduced risk of TSCC [47] [64] [65]. Coffee or hot beverage consumption in general or cooking practices, such as smoking, pickling, or charcoal grilling, did not increase the risk of TSCC [65]. Separate studies have found that a high intake of vegetables, whole-grain bread and pasta, and vitamin E supplements are protective [47] [66].

There is solid evidence that incidence and prevalence of HPV-associated HNSCC is increasing [67] [68]. Recent publications show an increased incidence of HPV infections in HNSCC of approximately 50% with HPV16 being the most prevalent type in at least 90% of this cancer [69] [70] [71]. The majority of HPV-driven cancers of the head and neck are oropharyngeal squamous cell carcinoma comprising the tonsils and base of the tongue. In 2007, HPV16 was recognized as a risk factor for oropharyngeal cancer. Research indicates that approximately 79% and 73% of cases of tonsil and of base of tongue cancer respectively are caused by HPV, while in other oropharyngeal parts the presence of HPV is lower (17%) [72] [73] [74]. In contrast to this clear picture in oropharyngeal cancer, where the prognostic relevance of biologically active HPV infection is established, no such clear association can be found for OSCC. However, several publications analyzing larger groups of OSCC patients emphasize that HPV DNA, especially of HPV16, is present in 10–25% of tumors of the oral cavity, which is higher than in the healthy control population but smaller than in oropharyngeal cancer [75] [76] [77] [78]. One study concluded that HPV is significantly more common in base of tongue cancer than in mobile tongue cancer, and that it has a positive impact on disease-specific survival in patients with base of tongue cancer [79].

The epidemiology of oral HPV infections is not well understood. However, HPV viruses have long been known to be present in the genital area and to be a significant cause of cervical, cancer. It is thought that an increased number of people are engaging in sexual activity with multiple partners and engage in oral sex practices and as a result are contracting HPV in the head and neck region, resulting in a higher rate of oropharynx cancers. Nevertheless, it is not certain what leads to the development of this type of cancer and whether there are other

risk factors involved. The major role of HPV in cancer development is that its genes and gene products are capable of disturbing the cell cycle machinery. HPVs encode two major oncoproteins namely, E6 and E7. The E6 and E7 proteins have been shown to bind and inactivate the p53 and Rb tumor suppressor genes, respectively, thereby disrupting the cell cycle control with loss of control of DNA replication, DNA repair, and apoptosis [80][81][82].

Fungal infections caused by *Candida* species, in particular, *Candida albicans* have been involved in the pathogenesis of oral premalignant lesions. However, whether *Candida* invasion is a secondary event or causal in oral premalignant lesions is still uncertain and debatable [83]. Poor oral hygiene, poor dental status and chronic ulceration have been suggested to promote neoplasm in the presence of other risk factors. Due to the presence of coexisting risk factors like smoking and alcohol consumption, there is difficulty in obtaining evidence of whether dental factors influence oral cancer development. Nevertheless, mechanical irritation by scraping with a pulp cleaner was recorded to significantly increase the incidence of a chemical carcinogen‑induced TSCC [80].

Patients with Fanconi anaemia also have a higher proportion of HNSCC in the oral cavity, the vast majority of which involve the tongue, compared with the general population. On the cellular level, one of the typical features of this disorder is a high degree of genomic instability [84]. Fanconi anaemia genes are established as tumor susceptibility genes for familiar cancers and the mutations in these genes are a cause of hereditary susceptibility for many tumors. Despite aggressive treatment, the outcome of HNSCC in patients with Fanconi anaemia is significantly poorer and even after the cure of the primary HNSCC, patients with Fanconi anaemia are more likely to develop second primary cancers than the general population [85][86].

1.2.3 Tumor Biology and Genetics

Carcinogenic genetic alterations are considered to be good candidates for molecularly targeted therapeutic interventions against cancers [87]. The understanding of the genetic origins of oral cancers has grown significantly and it is frequently recognized that accumulation of genetic variations in proto-oncogenes and tumor suppressor genes lead to OSCC through a multistep process [88][89]. Recognizing the genetic factors implicated in oral carcinogenesis further will provide a basis for understanding and potentially preventing the spread of oral cancers worldwide. Genetic instability in the tumor caused by segregation of chromosomes [90][91][92], genomic copy number [93][94], loss of heterozygosity [95], telomere instabilities [96], misregulations of cell cycle checkpoints [97], DNA damage repairs [98] and defects in NOTCH signaling pathways [99] are involved in causing oral cancer.

Major molecular determinants in HNSCC development are the abrogation of p53 and retinoblastoma (Rb) pathways that lead to uncontrolled cell replication [100][101][102]. However, high concentrations of abnormal p53 protein can be found in over half of OSCC, particularly in those patients who smoke and drink heavily. Therefore, it is highly likely that this is one of the sites of genetic damage induced by these carcinogens [103][104][105]. Consistently, several studies have shown that Benzopyrene is a potent cigarette smoke carcinogen that forms guanine adducts at p53 mutation hotspot sites and could contribute to the mutational profile of p53 [106][107]. Mutations in EGFR-MEK [108][109], MET [110][111], NOTCH [100], PI3K- AKT [102] and PTEN [112] pathways are also frequently observed in HNSCC. These mutations cooperate to create aberrant mitogenic and survival signaling. The resulting changes in metabolism and tumor hypoxia contribute to resistance to current therapies and tumor recurrence [62].

The majority of the current publications have focused on HNSCC as a single entity [113]. However, epidemiological evidence suggests that biological differences and clinical characteristics do exist between the different head and neck sites, subsites and populations affected by this disease [114]. Even within the oral cavity alone, there are distinct clinical behaviors of tumors arising from the oral tongue, buccal, alveolar, and hard palate [61]. These data raise the important need to consider HNSCC not as one condition but as a spectrum of different diseases requiring separate genomic analysis.

One analysis which investigated the mutational features of TSCC revealed recurrent mutations in genes of therapeutic and prognostic significance in patients with tongue cancer [99]. In this study, apart from the mutations in p53, the most prominently mutated pathways were EGFR, ERRB, mitogen-activated protein kinase (MAPK), and NOTCH signaling pathways as well as adherens junction and focal adhesion pathways. Overall, 55 % of the TSCC samples had mutations in at least one gene affecting the MAPK pathway, while EGFR, Notch, and ERBB signaling families were modified in 52 %, 32 % and 23 % of cases, respectively [99]. Of note, mutations in genes in the Notch pathway and the chromatin remodeling family were associated with poor prognosis in individuals with oral tongue tumors.

Tumor microenvironment regulation has been implicated in the progression and invasion of many human cancers [115]. Matrix metalloproteinases (MMPs) are implicated in degrading the extracellular matrix that encapsulates tumors, allowing for invasion and promoting angiogenesis within tumors. An analysis of microarray data from OSCC samples originating from the tongue showed increased expression of MMP9 compared to normal tissue. In this study, loss of E-cadherin expression and MMP9 protein overexpression was found to be a significant predictor of poor prognosis, disease recurrence and poor disease-free survival in TSCC patients [116].

Moreover, increased concentrations of circulating prolactin in male patients with carcinoma of the tongue were found to be associated with a poor prognosis in the absence of tumor prolactin receptors [117] [118]. It was suggested that tongue cancer cells produce prolactin, and this ectopically produced prolactin might be acting as a major local growth promoter employing autocrine and paracrine mechanisms [119]. One study shows that advanced tongue cancer patients with poor prognosis had significantly elevated levels of molecular markers like tissue polypeptide specific antigen and epidermal growth factor, low level of insulin-like growth factor [120].

1.2.4 Premalignancy

Leukoplakia and erythroplakia are well recognized premalignant lesions of the tongue [121]. It is estimated that up to half of OSCC may arise from premalignant lesions. Malignant transformation rates of oral leukoplakia range from 0.13 to 17.5%, while the rates of five-year cumulative malignant transformation range from 1.2 to 14.5%. Some reports found a high incidence of malignant transformation in older patient [121]. There is an increased risk of malignant transformation in areas of leukoplakia on the tongue and on the floor of mouth compared to other oral sites. Most oral leukoplakias occur in patients who smoke, and almost half of these lesions will undergo some improvement if the patient stops smoking [121]. Most cases of leukoplakia do not turn into cancer, but some leukoplakias are either cancer when first found or have pre-cancerous changes that can progress to cancer if not properly treated. Despite an ongoing debate about the rate of malignant transformation in these lesions, it is known that erythroplakia has a higher risk of malignancy than leukoplakia [42].

1.2.5 Diagnosis

OSCC is usually painless and asymptomatic in the early stages and prompts the patient's self-referral only when symptoms develop [122]. Despite the immediate accessibility of the oral cavity to direct examination, these malignancies are therefore still often not detected until a late stage and, as a result, the survival rate for oral cancer has remained essentially unchanged over the past three decades [123]. The five-year survival rate for small tumors approaches 80% but falls to 30% for stage 4 disease [124]. Late diagnosis results in more expensive, aggressive and disfiguring treatments, lower survival rates and lower quality of life among survivors [125] [126].

The diagnostic skills and activities of the professional (primary care physician or dentist) first contacted by the tongue cancer patient in primary care have a profound effect on the patient's survival [127]. For early detection of oral cancers, dentists have an essential role as they are the persons who see and observe oral cavity during routine dental checkups and can help identify suspicious lesions before having any symptoms [128]. Patients who are suspected of having cancer at the initial visit and are hence referred naturally have the best prognosis. In contrast, the undiagnosed patients who are left without any follow-up have a significantly longer delay resulting in a poorer survival even after the other known prognostic factors are adjusted [127]. Physical examination and biopsy may be used initially to diagnose oral or oropharyngeal cancer. HPV testing may be done on a sample of the tumor removed during the biopsy since it has been linked to a higher risk of oropharyngeal cancer. Once mouth cancer is diagnosed, the extent (stage) of the disease can be determined by endoscopy, imaging tests which may include X-ray, computed tomography (CT), magnetic resonance imaging (MRI) and positron emission tomography (PET) scans, among others [129].

1.2.6 Symptoms

Many oral cancers do not present visually detectable signs or symptoms while in the premalignant or localized stage when they are most treatable [130]. Tongue cancers can occur on the front of the tongue (oral tongue cancer) where it may be more likely to be seen and felt. Or it may occur at the base of the tongue, where it attaches to the bottom of the mouth with few signs and symptoms (oropharyngeal tongue cancer). Cancer at the base of the tongue is usually diagnosed at an advanced stage when the tumor is larger and cancer has spread into the lymph nodes of the neck.

The most common early symptom of tongue cancer is a sore on the tongue that doesn't heal and that bleeds easily. It might also cause mouth or tongue pain. Other symptoms of tongue cancer may include a red or white patch on the tongue that persists, a tongue ulcer that persists, pain when swallowing, mouth numbness, a sore throat that persists, bleeding from the tongue with no apparent cause and a lump on the tongue that persists [127]. Patients rarely present with dysphagia or difficulty with speech. There is often a leukoplakic or erythroplakic component to the lesion, and small size does not preclude invasion [131].

1.2.7 Stages and Grades

Tongue cancer is classified using stages and grades. The stage indicates how far cancer has spread. Each stage has three potential classifications:

T refers to the size of the tumor (a small tumor is T1 and a large tumor is T4).

N refers to whether or not cancer has spread to neck lymph nodes. N0 means cancer has not spread, while N3 means that it has spread to many lymph nodes.

M refers to whether or not there are metastases in other body parts.

The grade of cancer refers to how aggressive it is and how likely it is to spread and correlates with the TNM stage. The tongue cancer grade can be low (slow-growing and unlikely to spread), moderate or high (very aggressive and likely to spread) [132]. TSCC stages are indicated using Roman numbers I through IV. A lower stage, such as stage I, indicates a smaller cancer confined to one area. A higher stage, such as stage IV, indicates a larger cancer or that cancer has spread to other areas of the head or neck or to other areas of the body.

1.2.8 Prognosis

The tongue is disadvantaged because of its special histologic structure, rich lymphatic network and highly muscularized formation, which makes it poorly implemented to protect itself from invasion and metastasis [133]. TSCC is consequently more frequently associated with metastasis to draining lymph nodes than any other cancer of the oral cavity [134] and the presence of nodal metastasis in the neck is the most important prognostic factor. Metastasis is responsible for most cases of mortality and is a result of the acquisition of properties such as growth signal, insensitivity to anti-growth signals, sustained angiogenesis, cell migration and invasion [3]. Patients with TSCC have a significantly worse prognosis than those with similar lesions of the oropharynx, larynx, hypopharynx, and other oral cavity sites [135]. The prognosis depends or varies with nodal involvement, tumor thickness, and the status of the surgical margins [136].

As stated before, cancer staging is considered an important tool in predicting the treatment and survival outcomes of TSCC patients. The TNM classification is currently the mainstay of clinical staging of TSCC patients [137]. Despite its widespread use, this system has been criticized for not considering the biological behaviour and heterogeneity of individual cancers [138] [139]. Therefore, it is important to supplement the TNM staging system with new histological features and biomarkers. TSCC currently lacks reliable prognosticators that can predict outcome and response to therapy [140]. Prognostic factors in HNC could be searched for by using various methods, such as morphological studies, genetic studies, cell and tissue cultures, animal models, and serum or saliva samples [141] [142].

Angiogenesis and lymphangiogenesis promote cancer cell growth and metastasis [143]. TSCC is characterized by an extensive and well-developed vascular and lymphatic system [144]. Therefore, identification of biomarkers that associate with TSCC progression and metastasis, such as blood microvessel density (MVD) and lymphatic vessel density (LVD), could enhance prognostic and therapeutic approaches. In one study, several MVD and LVD markers were reviewed in 13 clinical studies but the results of almost all markers were controversial. It was found that higher expression of MVD/LVD markers were commonly, but not always, associated with shorter survival in TSCC patients. However, D2-40, a specific marker for the lymphatic endothelium, predicted low overall survival in this study [145].

Several studies have looked into sociodemographic factors like age, gender, race and lifestyle as prognostic signs in TSCC, but were found to have only weak prognostic value [146]. For example, there is no agreement in the literature about the prognostic value of age in patients with mobile tongue cancer. Studies show that patients younger than 40 years have

an increased frequency of tumor recurrence, distant metastases and cancer-related deaths compared to older patients [147] [148]. Other studies, however, report that younger age is associated with better survival [149] [150] or have found no relation between age and prognosis [151] [152]. In people under 65 years, survival rates fell from 47% to 39% between 1968 and 1987 in Scotland, with the highest increase recorded among subjects from the more socially deprived areas [153].

Some studies have shown that relative survival rates in men are lower than in women with tongue cancers [154] [155] while others have found no such association [156]. One study reported significant mortality in the African American adult male population compared with white Americans, mainly because they had a higher proportion of tongue cancer, and presented more often with the late-stage disease than white Americans. It was suggested that this is due to white Americans having better access and utilization of healthcare [157].

1.2.9 Survival

The five-year relative survival rate for tongue cancer, which compares the survival of people with cancer to the expected survival rate for people without cancer, depends on the cancer stage. According to the American Cancer Society, which relies on information from the SEER (Surveillance, Epidemiology, and End Results) database (www.seer.cancer.gov), maintained by the National Cancer Institute, if the cancer has spread far, the five-year relative survival rate is only 39%. If cancer has only spread locally, for example, to lymph nodes in the neck, the relative survival rate is 68%. If it has not spread beyond the tongue, the five-year relative survival rate is 81% [158]. Early diagnosis of tongue cancer allows for more treatment options, with fewer side effects, and a good five-year survival rate.

However, an individual study analyzed 176 patients with TSCC of the anterior two-thirds of the tongue with its base. It has been noted that no significant difference in survival between the two locations when survival rates were compared stage by stage. The decreased overall survival frequently reported for patients with squamous cell carcinoma of the tongue base compared with the survival for patients with tumors of the mobile tongue may be due to the disproportionately high number of patients with cancer of the tongue base who present with advanced disease [159].

Statistical analysis using data from the SEER database demonstrated an increase in TSCC among young adults. However, the five-year relative survival for oral tongue cancer was overall higher among younger adults aged 20–44 years (64%) compared with adults aged 45+ years (51%) [41]. In the United States, the average 5-year survival rate for African Americans people is lower than for white Americans with OSCC whereby the disease is at a significantly more advanced stage in African-Americans than in white Americans at the time of diagnosis [141] [160].

The overall estimate for the five-year survival of patients with TSCC in Germany was 48.1% between 1997 and 2006. Survival decreased from 61.1% in patients aged 15–44 years to 43.9% in patients aged 65–74 years. The age-standardized five-year relative survival estimates were much higher for women (56.0%) than for men (44.9%). Tumor stage and grade were strongly related to survival: it varied between 67.4% (local stage) and 6.2% (distant stage) as well as between 65.2% (grade 1) and 41.1% (grade 3 and 4) [37]. A detailed study of oral cancer in Scotland observed that survival is lower among people from lower

socioeconomic groups and the recent increases in occurrence have primarily occurred in these groups [153].

1.2.10 Treatment

TSCC is an aggressive cancer frequently associated with a poor prognosis due to the presence of metastasis in cervical lymph nodes [161]. Five-year survival rates have remained essentially unchanged over the past 20 years despite advances in diagnosis and management. Treatment failure in TSCC patients is most frequently due to local and regional recurrences [139]. Surgery is often the primary treatment of T1 and T2 tumors of the anterior two-thirds of the tongue, and in combination with radiotherapy for the larger, more posteriorly placed lesion. For those with unfavorable histology small lesions of the anterior tongue probably function better after surgery alone [162].

Curative surgery aims to excise the carcinoma with a margin of normal tissue, but in the tongue this can be difficult. The tumor may be deeply infiltrating making it difficult to decide where the resection margin should be placed. Also, the tongue has no midline septum to restrict tumor spread [42]. The midline septum could act as a boundary that restricts tumor spread within the compartment and along the muscle fibres it contains. Occult nodal metastasis can be expected in over 30% of patients with T1 and T2 and if the nodes are affected then the chance of cure falls by half [163] [164]. Given the difficulties of surgical excision and the high incidence of neck failure, most specialists would agree to give postoperative radiotherapy to patients with close or involved surgical margins and those with evidence of extranodal spread [165] [166].

Total glossectomy is done for advanced carcinoma involving the base of tongue and the primary treatment modality in advanced carcinoma of the tongue (including T2 > 3 cm) [167]. It has high associated mortality and morbidity [168] and considerable subsequent functional impairment. There is a high incidence of failure to obtain clear surgical margins [169]. Most patients can achieve adequate speech but the main problem remains swallowing without aspiration. Generally, the long-term prognosis after total glossectomy is poor; one series reported that 85% of patients died within 18 months [170], and other series have documented a three-year survival of less than 50% [169].

Radiotherapy may be given as single treatment or as an adjunct to surgery. It is as effective as surgery for small tongue lesions and may be chosen as a primary treatment when surgery would result in severe disability and when clearance would be difficult to achieve. Radiotherapy is often used in addition to surgery and currently tends to be given postoperatively. Many oncologists suggest adjunctive radiotherapy for large tumors if surgical margins are close to or involved with tumor, or after neck dissection where there are many positive nodes [171] [172].

Radiotherapy may be delivered by an external beam, by a radioactive implant (brachytherapy) or by a combination of the two. External beam radiotherapy used to treat carcinoma of the tongue clearly results in the irradiation of a large amount of surrounding normal tissue, often resulting in the short-term complication of painful mucositis and candida infection, plus the long-term complications of loss of taste and occasionally mandibular osteoradionecrosis [173]. Brachytherapy has the advantage of high radiation dose delivery to the tumor while minimizing dose delivery to the surrounding normal tissues. When used alone for T1 and T2 tumors, five-year survival rates of 61% and 74%,

respectively, can be achieved [174] but the results for larger tumors are poor [175]. Better oncological and functional disease control is obtained by using brachytherapy in conjunction with lower dose external beam irradiation, but this is associated with soft-tissue necrosis [176] [177].

Conventional chemotherapy has a limited role in the primary management of carcinoma of the tongue but is sometimes considered as an adjunct in advanced disease. It is usually used adjunctively or palliatively in cases of very large, unresectable lesions or distant metastasis. Many studies report that chemotherapy does not increase overall survival in HNC patients. However, one study suggested the potential benefits of neoadjuvant chemotherapy in the oral cavity [178]. Platinum compounds and Fluorouracil are of the most commonly used chemotherapy agents.

Cetuximab, an EGFR inhibitory monoclonal antibody, was approved for the treatment of locally advanced and metastatic HNSCC in December 2012 in Japan [179]. 21 patients with locally advanced and recurrent metastatic OSCC were treated with Cetuximab. The overall response rate was 57.1%, with a complete response rate of 33.3% [180]. Phase III trials demonstrated that Cetuximab used in combination with radiotherapy in HNSCC and in combination with Platinum-based chemotherapy as first-line treatment for metastatic HNSCC [181]. Combination treatments were found to improve the overall survival and prolonge progression-free survival.

Another study included 50 patients with TSCC. Adjuvant radiotherapy or chemoradiotherapy was administered to 42 patients after surgery. The concurrent chemotherapy regimen was most commonly a weekly treatment with Carboplatin and Paclitaxel, which was given in 24 patients (70%). Weekly Cetuximab was a component of concurrent systemic therapy for 6 patients (20%). One patient received adjuvant chemotherapy with Cisplatin, Paclitaxel, and Fluorouracil after radiotherapy completion. Despite these aggressive therapies, patients had a low rate of local tumor control and survival, particularly among those with stage I-II disease [136].

The use of Paclitaxel, Ifosfamide, and Cisplatin for induction chemotherapy followed by concomitant Paclitaxel and Carboplatin with radiotherapy was found to be an effective treatment for stage III and IV squamous cell carcinoma of the base of tongue in patients who initially respond to the treatment [182]. This study was a single-institution prospective phase II trial and toxicity was not assessed in a quantitative manner.

Results from a new clinical trial suggest that neoadjuvant immunotherapy for oral cavity cancers may elicit tumor regression, which could provide long-term benefits for patients. In this randomized trial, two neoadjuvant doses of Nivolumab given with or without Ipilimumab led to complete or partial tumor shrinkage in most patients and did not result in the delay of any standard treatment [183]. The identification of new target molecules in TSCC and the use of combination therapies may therefore improve the response and the survival rate.

1.3 Targeted Therapy

It has long been thought that targeting genetic differences between tumor and normal cells may deliver comparatively large therapeutic windows and significant patient benefits. Targeted therapy uses drugs or other substances to attack cancer cells more than normal cells. It can affect specific genes and proteins that are involved in the growth and survival of

cancer cells. It can also alter the tissue environment that helps cancer grow and survive or it can target cells related to cancer growth, like blood vessel cells [184]. Targeted therapy can be used by itself or in combination with other treatments, such as standard chemotherapy, surgery, or radiation therapy [185]. Targeted therapies include tyrosine kinase inhibitors (TKIs) [186], angiogenesis inhibitors [187], proteasome inhibitors [188], immunotherapies [189], hormones [190], apoptosis inducers [191] and other signal transduction inhibitors [192].

In the past two decades, the discovery of oncogenes and tumor suppressor genes and the completion of human genome sequencing supported some major advances in the knowledge of the molecular mechanisms leading to cancer. Subsequently, such newly gained biological and genetic information rapidly prompted the introduction of a large number of new targeted cancer therapies [193]. The functional consequences of genetic and epigenetic changes are, however, sometimes not immediately apparent from DNA-based or transcriptional studies but may be revealed only by in-depth analyses of signaling pathway activities and biological assays. The heterogeneity of cancer cell signaling is a significant obstacle for the effective development and clinical use of molecularly targeted therapies. Signaling pathways regulated by protein kinases are the frequent targets of somatic mutations, leading to many human cancers. Of the more than 100 dominant oncogenes known to date, many encode protein tyrosine kinases (PTKs) [194].

PTKs play key roles in cellular signal transduction, cell cycle regulation, cell division, and cell differentiation. Ninety PTKs are encoded in the human genome and among them 58 are receptor type and 32 are nonreceptor tyrosine kinases [195]. Dysregulation of PTK-activated pathways, often by overexpression, gene amplification, or genetic mutation, is a causal factor underlying numerous cancers, disease progression and drug resistance [196]. Several receptor protein and cytoplasmic tyrosine kinases are known to be mutated and/or overexpressed in human cancer. These include the EGFR, HER2, insulin and insulin- like growth factor (IGF) receptors, SRC, ABL and PI3K, among others [197]. Inactivation of several of these kinases with exogenous inhibitors has resulted in an antitumor effect in preclinical models of cancer. At this time, several tyrosine kinase inhibitors(TKIs) of variable target specificity have been approved by the Food and Drug Administration (FDA) for treatment of patients with a variety of cancers [198].

Because of the increase of TSCC incidence especially in young people, its high risk of recurrence and its poor prognosis, the search for timely and effective clinical treatments for TSCC has become an important topic. Although there are several promising, novel targeted therapies for patients with HNSCC including EGFR monoclonal antibodies (Cetuximab, Panitumumab), EGFR tyrosine kinase inhibitors (Gefitinib, Erlotinib, Lapatinib), vascular endothelial growth factor (VEGF) inhibitor (Bevacizumab), vascular endothelial growth factor receptor (VEGFR) inhibitors (Sorafenib, Sunitinib and Vandetanib) and inhibitors of PI3K [199], there is no particular targeted therapy for TSCC until now. Therefore, more efforts are necessary to identify new molecular targets to further improve treatment.

1.4 Preliminary Work

1.4.1 Tyrosine Phosphorylation Profile for a TSCC Line Panel

As a contribution to a better understanding of the signaling activities and to identify therapeutic targets or prognostic markers for tongue cancers, 34 TSCC lines were subjected to Western blot analysis of the protein tyrosine phosphorylation status using an anti-

phosphotyrosine antibody (Jessica Doondeea, Oxford University; Figure 2 and S1). The analysis revealed that TSCC cells exhibit a distinct tyrosine phosphorylation pattern with a notable and uniform phosphorylated band at around 130 kDa possibly indicative of a prominent role of a single kinase or kinase family in TSCC. Further information on the cell lines (including relatively sparse clinical information) can be found in [200]. For comparison, a panel of colorectal cancer (CRC) cells shows a striking diversity in the phosphorylation profile (Figure 3) [201].
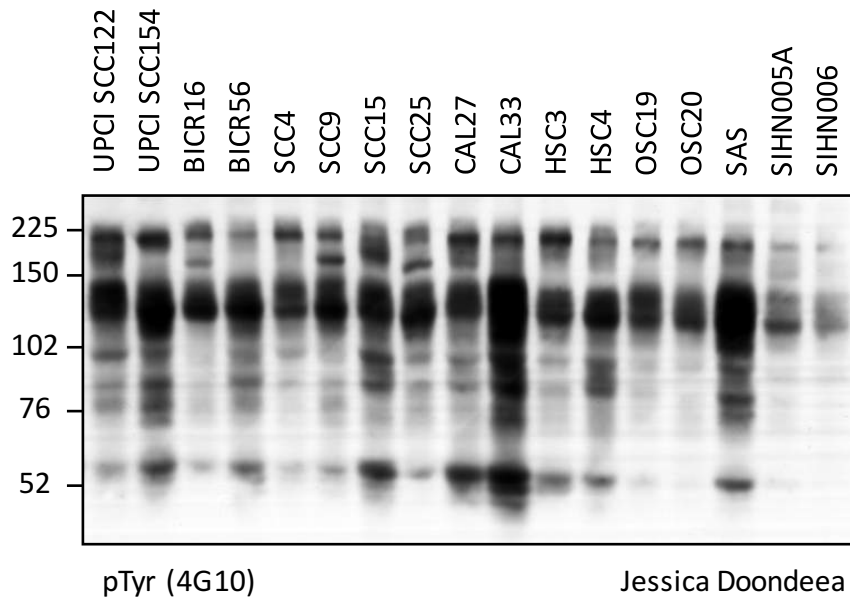
Figure 2. Tyrosine phosphorylation profile for a tongue squamous carcinoma cell (TSCC) line panel shows a prominent phosphorylated band at around 130 kDa

Equal amounts of total lysates from 17 TSCC lines were separated by SDS-PAGE and analyzed by Western blotting with an anti-phosphotyrosine antibody (4G10). Protein size markers are indicated on the left side. This work was done by Jessica Doondeea (Oxford University).
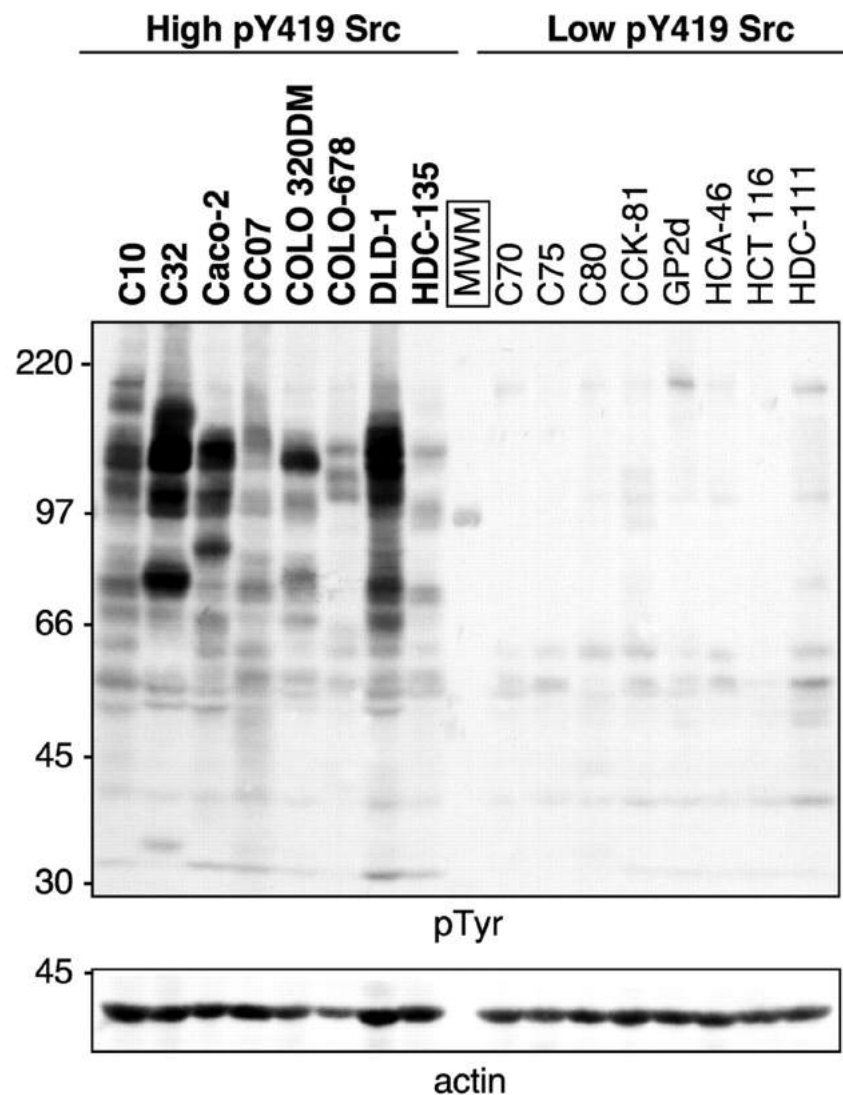
Figure 3. Variable tyrosine phosphorylation patterns in a colorectal cancer cell panel

Total cell lysates from 16 CRC lines were grouped by high or low SRC kinase activity. Cell lysates were separated by SDS-PAGE and analyzed by Western blotting with an anti-phosphotyrosine antibody (4G10). MWM, molecular weight marker. Protein size markers are indicated on the left side. The membrane was stripped and re-probed for actin (lower panel). Figure from [201].

1.4.2 Identification of p130CAS as Overexpressed and Activated in TSCCs

Identifying the proteins overexpressed and activated in TSCC will enable us to think rationally about which pathways to manipulate to suppress the disease. To recognize the outstanding 130 kDa band, total cell lysates from the 34 TSCC lines were analyzed by Western blotting for total level and phosphorylation status of the conserved key adaptor protein p130CAS since it is a well known substrate protein of several oncogenic tyrosine kinases. p130CAS has a molecular weight of 90 kDa but migrates at 130 kDa in SDS-PAGE gel. The results are shown in Figure 4 and S1 and reveal a strong and quite similar expression of p130CAS in terms of absolute protein levels. The protein was phosphorylated in all TSCC lines on pY410 to a varying degree. However, this antibody against a specific phosphorylation site does not necessarily reflect the overall phosphorylation detected by the 4G10 antibody. Therefore, it is believed that p130CAS is at least one major component of the 130 kDa phospho-tyrosine signal detected in all TSCC lines of the panel. This data

14

suggests that p130CAS or the kinase responsible for its phosphorylation could be exploited as a potential molecular therapeutic target for TSCC. The multiple bands of 130CAS observed in TSCC lines may result from different splice variants or phosphorylation states.

Jessica Doondeea
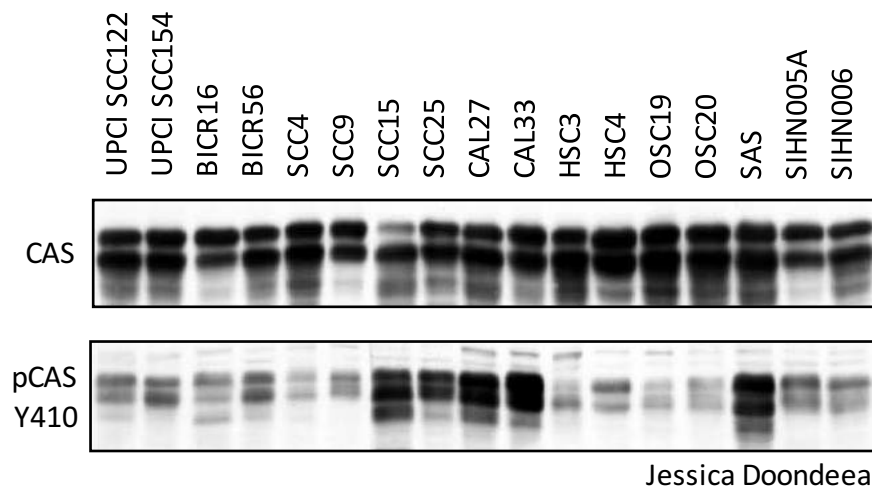
Figure 4. p130CAS is prominently expressed in a panel of tongue squamous carcinoma cells (TSCC) and highly phosphorylated

Total cell lysates were separated by SDS-PAGE and analyzed by Western blotting. Immunoblots were probed as indicated with antibodies against phospho-p130CAS (pCAS Y410) and total p130CAS (CAS) (Jessica Doondeea, Oxford University).

1.5 p130CAS

p130CAS (p130 CRK-associated substrate, also known as BCAR1) belongs to the CAS family of adaptor proteins and can act as a docking protein for several signaling partners. p130CAS is an widely expressed adaptor molecule and was originally identified by its ability to associate with CRK and as a protein that, upon transformation by v-SRC and v-CRK oncogenes, is highly phosphorylated on tyrosine residues [202]. Due to its ability to associate with multiple signaling partners, p130CAS contributes to the regulation to a variety of signaling pathways leading to cell adhesion, migration, invasion, apoptosis, hypoxia and mechanical forces (Figure 5). Recently, results from RNA interference (RNAi) suggest that p130CAS has a role in cell transformation and cancer progression [203]. Alterations of p130CAS expression and the resulting activation of selective signaling are determinants for the occurrence of different types of human tumors [204].

The major post-translational modification of p130CAS is phosphorylation on Tyrosine, Serine and Threonine residues. Most p130CAS tyrosine phosphorylation occurs in the substrate domain, which contains 15 repeats of a YxxP sequence. During extracellular matrix (ECM) binding or growth factor and hormone stimulation, integrins, receptor PTK, estrogen receptors and G-protein coupled receptors regulate p130CAS through the activation of SRC family kinases and the formation of a p130CAS-SRC complex [203]. These stimuli trigger p130CAS tyrosine phosphorylation and its translocation from cytosol to the cell membrane. p130CAS lacks any enzymatic or known transcriptional activity but acts as a platform for multiple proteins due to the presence of multiple tyrosine residues in the substrate domain, which allows extensive changes in phosphorylation that drive the formation of multi-protein signaling complexes [205].
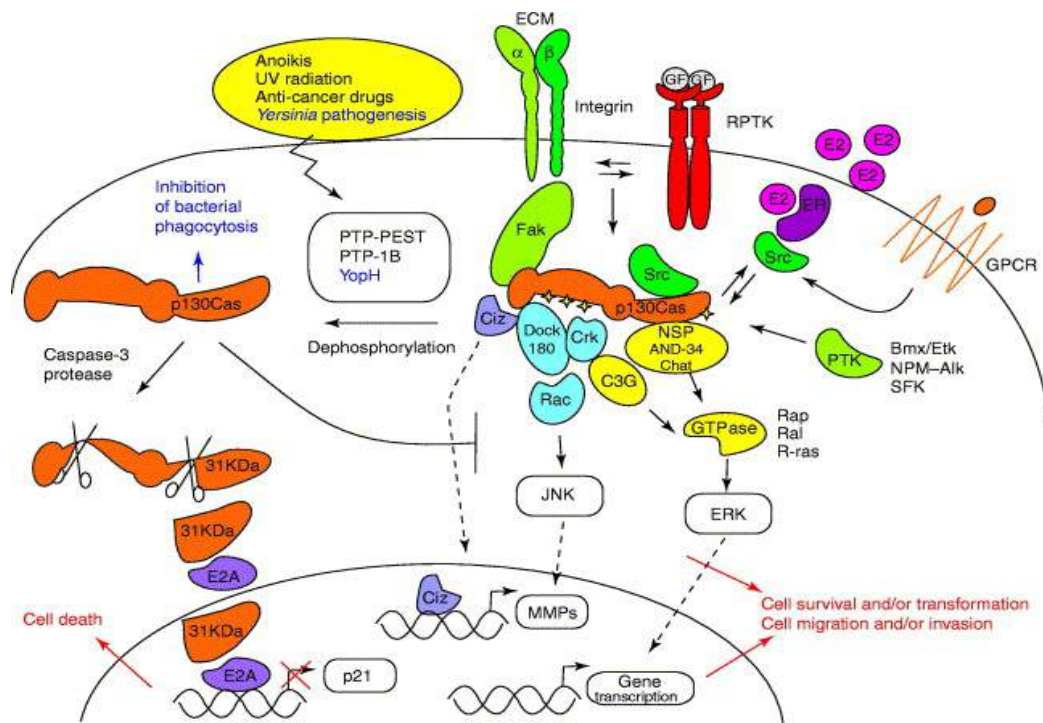
Figure 5. p130CAS is a multifaceted scaffold for signaling networks

p130CAS is regulated by activation through SRC kinases and the formation of a p130CAS-SRC complex. After tyrosine phosphorylation, p130CAS recruits adaptors and effectors that activate downstream pathways, resulting in cell survival, increased cell motility, invasion or transformation. P130CAS dephosphorylation by phosphatases supports cleavage by proteases into a smaller fragment, which enters the nucleus and contributes to cell death. Figure from [203].

p130CAS is an important transducer of survival signals (Figure 5). Various pro-survival signals arising from the ECM, soluble growth factors and hormones proceed through their respective receptors, then through FAK and SRC, to p130CAS, activating the small GTPases RAS and RAC, as well as JNK and ERK1/2 [206]. p130CAS might also have a direct role in death signaling by generating a C-terminal 31-kDa fragment during multiple pro-apoptotic stimuli, such as detachment from the ECM, treatment with anticancer drugs or UV irradiation. Induction of p130CAS cleavage by Caspase-3 or other proteases generates a fragment that can heterodimerize with the transcription factor E2A and then translocates to the cell nucleus, where it contributes to cell death by physically preventing E-box binding by E2A. p130CAS cleavage correlates temporally with the onset of apoptosis, loss of FAK from focal adhesion sites and the attenuation of p130CAS-Paxillin interactions [207] [208].

In the past years, several observations suggest that aberrant activation of the p130CAS signaling network signature in different types of tumors leads to up-regulation of key regulatory signaling pathways promoting cell transformation [204]. p130CAS is necessary for transformation mediated by several oncogenes, such as SRC and HER2 as well as the oncogenic fusion protein nucleophosmin (NPM1)–anaplastic lymphoma receptor tyrosine kinase (ALK) [209] [210] [211]. Furthermore, p130CAS has been shown to be required for KRAS, BRAF, PTEN and PIK3CA oncogene-dependent proliferation [212]. In the case of SRC transformation, for example, SRC requires p130CAS for the organization of actin into podosomes, the activation of MMP2 and the formation of lung metastases *in vivo* [213].

p130CAS overexpression has been discovered in human breast, prostate, ovarian, lung, colorectal, pancreatic and hepatocellular carcinoma, as well as in glioma, melanoma,

anaplastic large cell lymphoma and chronic myelogenous leukaemia, although the exact mechanisms that drive p130CAS overexpression in cancer have not yet been identified [202] [203] [214]. It has frequently been reported that in human breast cancers, overexpression of both HER2 and p130CAS is associated with increased proliferation, metastasis and poor prognosis [215] [216]. p130CAS silencing in HER2-transformed breast cancer cells is sufficient to inhibit tumor growth *in vivo* and correlates with the downregulation of proliferative and survival pathways, such as SRC and AKT activation, FAK phosphorylation and Cyclin D1 expression [211]. In Estrogen receptor (ER)-positive human breast tumors, overexpression of p130CAS associates with intrinsic resistance to tamoxifen treatment and high risk of relapse in a large subset of human breast cancer samples [217] [218] [219]. p130CAS silencing in HER2-dependent breast carcinoma impairs migration and invasion *in vitro*, as well as the formation of lung metastases *in vivo* [211].

The high levels of p130CAS in human breast cancer have been correlated with resistance to the cytotoxic agent Adriamycin. In particular, p130CAS-dependent SRC, AKT and ERK1/2 activation and inhibition of apoptosis are considered to be essential for conferring resistance to Adriamycin. Because p130CAS is frequently expressed at high levels in breast cancers, these findings raise the possibility of resensitizing p130CAS-overexpressing tumors to chemotherapy through the interruption of p130CAS signaling pathways [220]. Moreover, in breast and lung cancer, p130CAS expression has been correlated to the acquirement of mesenchymal characteristics, therefore supporting its role in driving malignancy and metastasis propagation [221].

Silencing of p130CAS may provide a novel approach for therapeutic targeting p130CAS. Interestingly, injection of BCAR1-specific siRNAs into the mammary gland of transgenic mice harbouring HER2-dependent spontaneous adenocarcinoma was sufficient to inhibit HER2 signaling and to reduce tumor initiation. This means that p130CAS might be a potential therapeutic target for HER2-dependent tumors [211].

The non-catalytic nature of p130CAS makes it difficult to develop specific inhibitors. However, structure-based design of inhibitors could be developed to target specific domains of this adaptor protein, especially the SH3 domain or possibly regions that are involved in binding with specific signaling effectors, such as PI3K, SRC, FAK and AKT. To this end, new insights on protein-protein interactions could be obtained by the analysis of the crystal structure of p130CAS domains, enabling the search for competitors and specific inhibitors. So far, only the crystal structure of the p130CAS SH3 domain has been resolved. This structure enables modeling of the docking interactions to its ligands, for example from FAK, and supports structure-based drug design of inhibitors of the CAS-FAK interaction [222]. Recently, the p130CAS/HER2 interaction in breast cancer served as a potential target for the discovery and development of new anticancer agents. Computer strategies, *in vitro* proteomic approaches and cellular models showed that the SH3 domain of p130CAS binds a specific sequence of the HER2 intracellular domain and were used to identify two molecules with potential inhibitory activity *vs.* p130CAS/HER2 interaction. They significantly affect cell proliferation and sensitivity to Trastuzumab [223].

Due to the absence of specific inhibitors for p130CAS, alternative strategies are needed. It is well known that oncogenic SRC family kinases (SFKs) such as v-SRC in fibroblasts cause hyperphosphorylation of tyrosyl residues on multiple cellular proteins [224]. v-SRC transformed mouse fibroblasts show a strongly tyrosine-phosphorylated protein at 130 kDa [225]. As mentioned before, during SRC transformation, SRC was found to need p130CAS for the organization of actin into podosomes, the activation of MMP2 and the formation of lung

metastases *in vivo* [213]. Also, the C-terminal region of p130CAS contains a SRC binding domain and the association between p130CAS and activated SRC kinase is essential for the tyrosine phosphorylation and activation of p130CAS [203]. Therefore, SRC kinase inhibitors have been proposed as alternative options to counteract p130CAS hyperactivation. Bosutinib, a novel SFK inhibitor, has been reported to prevent breast cancer cell migration and invasion by inhibiting the SRC-FAK-p130CAS signaling pathway [226].

1.6 SRC Kinase

SRC is a member of a family of structurally related kinases called SRC family of protein tyrosine kinases that includes eight members: SRC, YES, FYN, FGR, LCK, HCK, BLK and LYN. SRC, a non-receptor tyrosine kinase, is a critical component of multiple signaling pathways that regulates fundamental cellular processes, including cell growth, differentiation, cell shape, migration and survival, specialized cell signals, metastasis and angiogenesis [227] [228]. To carry out these activities, SCR interacts with numerous cellular factors, including integrins, growth factor receptors, G-protein coupled receptors and cytokine receptors to initiate their downstream signaling cascades. SRC activity is regulated by intramolecular interactions controlled by tyrosine phosphorylation, and SH2 and SH3 domains of SRC mediate protein-protein interactions with sequences containing phosphotyrosine and proline-rich motifs [229]. SRC can cooperate with receptor kinases to signal through downstream effectors, such as PI3K/PTEN/AKT, RAS/RAF/MEK/ERK1/2 and STATs (Figure 6) [230] [231]. SRC also interacts with FAK, which plays an important role in integrin signaling. Phosphorylated FAK interacts with multiple cellular proteins to modulate cell adhesion, migration and invasion [231].
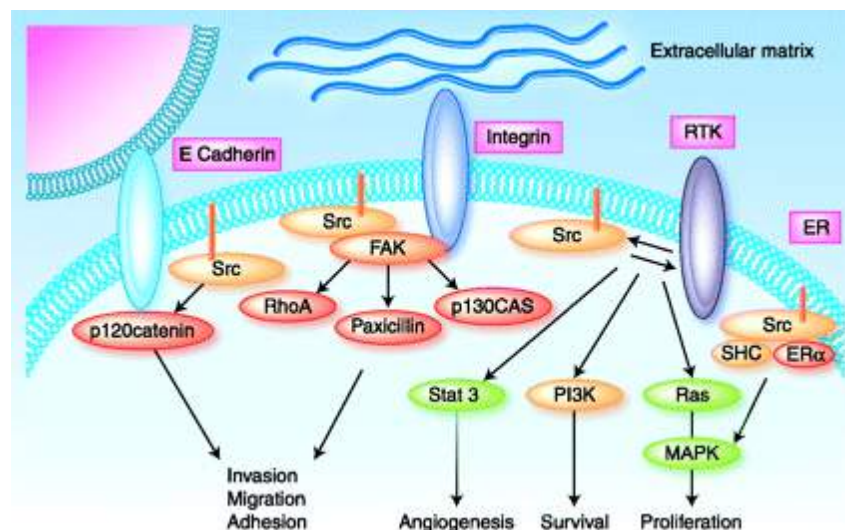
Figure 6. The intracellular functions of the SRC kinase

SRC integrates and regulates signaling from multiple transmembrane receptor-associated tyrosine kinases leading to activation of intracellular target proteins including PI3K, FAK, RAS, and STAT3. These actions can modulate cell survival, proliferation, differentiation, and angiogenesis. SRC, through interactions with integrins and E-Cadherin, also plays a prominent role in the regulation of cell motility, adhesion and invasion. Figure from Mayer and Krop [232].

Unlike BRAF or EGFR mutants for example, SRC is not a primary driver of tumorigenesis, but rather it is a participant in many pathways promoting cell division and survival [233]. Although SRC is rarely mutated in cancer [234] [235], SRC kinase is frequently overexpressed and/or

aberrantly activated in epithelial and non-epithelial cancers [236]. Activated SRC is commonly found in colorectal and breast cancers, and high SRC protein and kinase activity has also been reported in many other human cancers including lung, colon, breast, ovarian, endometrial, pancreatic and head and neck cancers [236] [237]. Although several mechanisms may account for these increases, including increased transcription, activation is likely primarily a consequence of genetic and epigenetic alterations in tumor cells. As these epigenetic changes accumulate, SRC activity increases during cancer progression, with the highest expression and/or activity of SRC observed in metastases [238] [239]. SRC activity can be predictive of poor prognosis [240].

SFK activity levels were found to be strongly correlated with global levels of tyrosine-phosphorylated proteins in CRC lines (Figure 3) [201]. In betel quid (BQ)-induced chewing oral cancer, it has shown that BQ extract can significantly induce *in vitro* oral cancer cell motility, including migration and invasion, through the activation of SFKs. It was also shown that SFKs activities are located at the invasion front of OSCC, suggesting a possible function of SFKs in basement membrane penetration and stromal invasion inside the tumor mass. This study concludes that SFKs may represent a potential biomarker of invasion and therapeutic target in BQ-induced OSCC and TSCC [241]. Thus, it is anticipated that blocking signaling through the inhibition of the kinase activity of SRC will be an effective means of modulating aberrant pathways that drive oncogenesis and metastasis.

Dasatinib (formerly: BMS-354825) is a potent oral TKI of ABL, SRC, LCK, FYN, YES, platelet-derived growth factor receptor, c-KIT and other kinases. It is an example of a promiscuous inhibitor and has a potent broad-spectrum tyrosine kinase inhibition profile (Figure 7). Dasatinib possesses an inhibitory spectrum far beyond its "target" kinases. One reason for this lack of selectivity is that the ATP-binding site is highly conserved between kinases and therefore can represent a promiscuous target [242]. Dasatinib is FDA-approved for the treatment of chronic myelogenous leukaemia refractory or intolerant to Imatinib [243] or as first-line treatment for chronic-phase chronic myelogenous leukaemia [244] and in patients with Philadelphia chromosome-positive acute lymphoblastic leukaemia [245]. There are active research studies evaluating the molecular mechanisms of Dasatinib on human solid tumor cells such as prostate cancer, HNSCC, non-small cell lung cancer, breast cancer [246] [247] [248] [249] [250]. Also, The drug is undergoing numerous clinical trials for the treatment of various solid tumors [251] [252] and for acute lymphoblastic leukaemia [253].
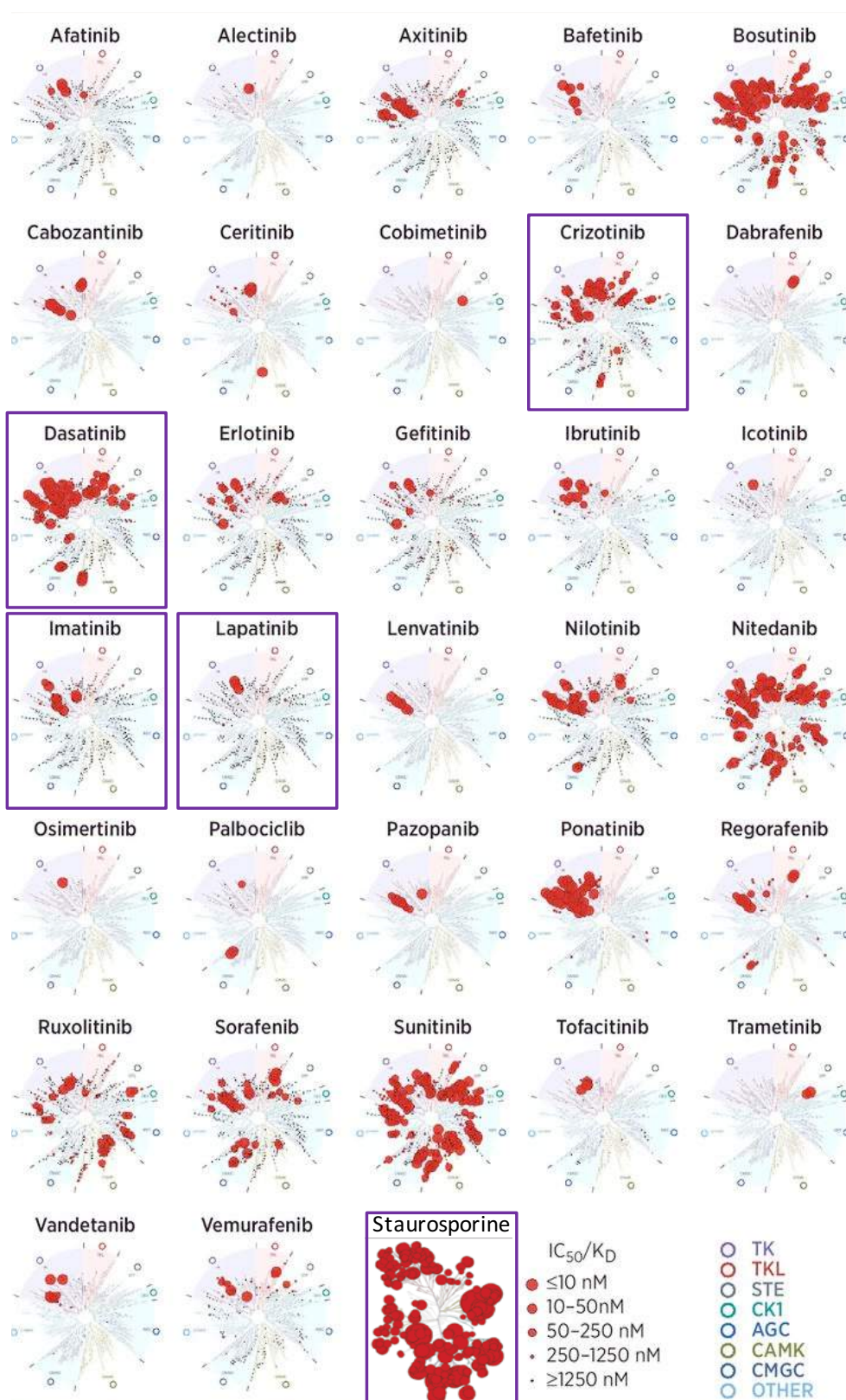
Figure 7. Kinome responses to FDA-approved chemical inhibitors of kinases

The selectivity and potency of approved kinase inhibitors are highly variable. Kinases found to bind are marked with red circles; white larger circles indicate the higher affinity binding. The kinome binding maps of Dasatinib, Imatinib, Crizotinib and Lapatinib (TKIs used in the current research) compared to the pan-inhibitor Staurosporine, which affects more than 250 kinases, are marked with purple boxes. Figure adapted from [242].

K_d is the equilibrium dissociation constant.

As SRC is not a primary driver of tumorigenesis, it is unlikely that anti-SRC monotherapy will be highly efficacious in the treatment of cancers. Along the same line, Dasatinib as a single agent has only modest or no significant clinical activity on many types of solid tumors, including non-small cell lung cancer [254], prostate cancer [255], breast cancer [256 257], melanoma [258] and HNSCC [259].

Significant limitations of Dasatinib and other TKIs in cancer treatment have many potential reasons. The rate of developing acquired resistance to TKIs is extremely high and acquired resistance even appears to be inevitable in certain diseases [260 261]. Studies have shown that cancer cells adapt to chronic therapy through common mechanisms which include secondary mutations of the target or activation of an alternative signaling pathway [262]. Furthermore, complexity and redundancy in signaling pathways and differences between tumor subclones confer robustness on cancer cells, allowing tumors to survive TKIs treatments [263]. Moreover, the high intratumoral heterogeneity predicts poorer prognosis and poorer response to TKIs [264]. Low effectiveness of TKIs in some clinical studies may be also due to poor patient selection. The drug effects of TKIs can be drastically different in two patients. It can work wonders in one, but have no effect at all in another individual. The genetic makeup of a patient's tumor is of enormous predictive value for the efficacy of a TKI. For example, in unselected NSCLC patients, only 15 of 58 in Japan and 1 of 61 in the USA responded to the Gefitinib (EGFR inhibitor) treatment [265]. EGFR mutations were found in lung cancer samples from patients who responded to Gefitinib therapy and in a lung adenocarcinoma cell line that was hypersensitive to growth inhibition by Gefitinib, but not in Gefitinib-insensitive tumors or cell lines which suggest that EGFR mutations may predict sensitivity to Gefitinib.

Many studies have evaluated all kinds of strategies to overcome the limitations of the TKIs. A major direction is to develop new inhibitors, either very specific toward a certain type of acquired mutation or multitargeted to inhibit a broader spectrum of pathways. However, the development of new drugs takes long, is risky and very costly method [266].

Combination therapy is common in the field of chemotherapy. It produces tremendous improvements in patient outcome and leaves less chance for the tumor to acquire resistance to TKIs [267]. Combinations of targeted agents represent a potentially effective approach to simultaneously inhibiting multiple pathways, suppressing feedback reactivation of compensatory signaling networks, and therefore to prevent a recurrence. The efficiency of such therapies depends strongly on the nature of the single components: how they can be delivered, how they are metabolized, and how and to which extent they can enter the cell and reach their targets of action. Currently, nearly all chemotherapeutic regimens involve cocktails of drugs [268].

Recently, Phase I/II studies combined Dasatinib with a selection of drugs to treat various solid tumors. Several randomized phase II trials are investigating Dasatinib in combination with endocrine therapy, such as Letrozole, Exemestane or Fulvestrant, for patients with Estrogen-positive metastatic breast cancer and these results are awaited [269]. Somlo and colleagues reported on a Phase I trial using Dasatinib plus Capecitabine for progressive advanced breast cancer [270]. The combination appears to be well tolerated without significant toxicity. Araujo and co-workers reported on a Phase I/II study of Dasatinib in combination with Docetaxel for patients with castration-resistant progressive prostate cancer [271]. However, the results from a randomized phase III trial of Dasatinib+Docetaxel versus Docetaxel showed that the addition of Dasatinib to standard chemotherapy did not improve overall survival [272].

Haura and colleagues conducted a Phase I/II study utilizing the combination of Erlotinib, an EGFR inhibitor and Dasatinib in patients with advanced NSCLC. They determined that this combination may be promising in cancers known to harbour EGFR and SFK cooperation [273]. On the other hand, another study that used the same combination therapy demonstrated no use for this combination in molecularly unselected NSCLC [274]. Patients with operable stage II–IVa HNSCC were randomized to 7–21 days of a neoadjuvant combination of Erlotinib and Dasatinib [275]. The study showed that Erlotinib significantly decreased tumor size in HNSCC, with no additive effect from Dasatinib. Another Phase II trial clinical trial utilized Dasatinib and Cetuximab in biomarker-unselected patients with Cetuximab-resistant, recurrent/metastatic HNSCC. The clinical benefit and the overall survival from the Dasatinib+Cetuximab combination in this study were improved among patients with low serum interleukin-6. This trial was then modified and redesigned as a biomarker-enriched Phase II study enrolling patients with undetectable interleukin-6 [276] [277].

1.7 High-Throughput Drug Combination Screen

Low effectiveness of Dasatinib in clinical studies may be due to poor patient selection. Thus, it is vital to perform procedures to select the population of patients responsive toward Dasatinib and other TKIs. All the published clinical trials of Dasatinib for HNSCC, as a single treatment or in combination therapy, involved unselected HNSCC patients and no particular focus on tongue cancer.

Previously, in our group, it was found that p130CAS prominently expressed in a panel of TSCCs and highly phosphorylated (Figure 4 and S1). p130CAS has no specific inhibitors but the association between p130CAS and activated SRC kinase is essential for the tyrosine phosphorylation and activation of p130CAS. Therefore, Dasatinib has been proposed as alternative options to counteract p130CAS hyperactivation. However, single-agent Dasatinib in unselected population of patients with HNSCC was not promising [259] therefore further studies of combination therapies that include Dasatinib are desired to avoid developing of acquired resistance or poor response.

Preliminary work in our group aimed to find synergistic combinations to treat tongue cancer employing the former result. Therefore, high-throughput screens were performed to discover possible synergistic candidates using FDA-approved drugs. Repurposing of FDA-approved drugs with possible synergistic effects on TSCC might shorten the critical path to new drug development, which is long, risky and very expensive. To identify compounds that can be combined with Dasatinib for targeted therapy of TSCC, three different cell lines were chosen to recognize drugs with a broad spectrum of activity. To facilitate future animal experiments, cell lines were also chosen for suitability in xenografting. The selected SAS, CAL27 and BICR56 cell lines have different levels of phosphorylated p130CAS and also different sensitivities to Dasatinib. In a pilot screen, 97 FDA-approved cancer drugs and 16 additional self-selected drugs (at concentrations of 0.4, 2 and 10 µM) were combined with Dasatinib (at concentrations of 0, 0.03 and 0.06 µM) and screened across these TSCC cell lines in 2 technical replicates for their impact on cell viability. The final DMSO concentrations did not exceed 0.1%. The resazurin assay was used to evaluate metabolic activity as a surrogate marker for cell viability. All dilutions and liquid handling were performed with robotic equipment.

For very few wells, the technical replication did not work (30 of 10368), for others the robot had problems to transfer the correct volumes (108 of around 10368). Those wells were

removed from the analysis (1.3% of the total). All of the remaining sample wells on each plate were normalized with the average value for all DMSO wells in the same plate. Then the averages for the normalized values on each plate pair were calculated. The ratio of surviving cells in combination treatment relative to surviving cells in one-drug-only treatment was calculated. The values were sorted according to effect size to identify the most promising candidates. Figure 8 shows compounds that may exhibit synergistic activity in at least two cell lines. This work had been done by Dr. Marc Lewitzky (MRC Weatherall Institute of Molecular Medicine) in collaboration with Dr. Daniel Ebner and Elena Seraia (Target Discovery Institute) at Oxford University.

SAS	CAL27	BICR56	Target
	Geldanamycin	Geldanamycin	HSP90
MK-1775		MK-1775	WEE1
	Erlotinib Gefitinib Lapatinib	Erlotinib Gefitinib Lapatinib	EGFR
Imatinib	Imatinib		ABL
Crizotinib	Crizotinib		MET

Figure 8. Candidates from a pilot drug screen for combination therapy of TSCC lines with Dasatinib (DAS) and FDA-approved drugs

In this screen, SAS, CAL27 and BICR56 cells were treated with a panel of 97 FDA-approved cancer drugs and 16 additional individually selected drugs at concentrations of 0.4, 2 or 10 µM with or without DAS for 48 h. Cell viability was quantified by resazurin calorimetric assay. The amount of reduced resazurin (resorufin) produced is directly proportional to the metabolic activity of cells. The table shows promising candidates for synergistic activity in at least two cell lines (Marc Lewitzky, Oxford University).

Several hits from this screen had been identified previously by other groups as promising candidates for combination with Dasatinib. As described earlier, Cetuximab and Erlotinib (EGFR inhibitors) had been used in combination with Dasatinib for HNSCC treatment in clinical trials [275] [277]. In 2018, two clinical trials showed that combination of Crizotinib and Dasatinib has limited tolerability with a high rate of adverse events. Also, responses and durable stable disease were limited [278] [279]. One study suggests that the combination therapy of Imatinib and Dasatinib achieves long-term molecular response in Imatinib-resistant and Dasatinib intolerant patients with advanced CML. However, this study contains two patients only [280]. Heat shock protein 90 inhibitor (HSP90i) and WEE1 kinase seemed to be promising candidates for further investigations.

These results indicated that the screen setup used can produce useful first hints for further analysis. Therefore, another larger high throughput screen was carried out which combined 1600 compounds (at concentrations of 0.4, 2 and 10 µM) with 2 concentrations of Dasatinib (0 and 0.03 µM) in 2 technical replicates to evaluate their synergistic activity against the same three TSCC cell lines. Cell viability was again evaluated by resazurin assay. From a total of 720 plates, 26 plates were removed due to unacceptable differences in between the

technical replicates. Further 45 of 34560 individual well pairs were removed due to differences in between the technical replicates as well. The viability data for treated cells were normalized to the average value for all DMSO control cells in the same plate. Then the averages for the normalized values on each plate pair were calculated. The ratio of surviving cells in combination treatment relative to surviving cells in drug only treatment was calculated. For $\log_2$-transformed values, statistical outliers were identified as promising candidates for synergy with Dasatinib. This work was done by Dr. Marc Lewitzky (MRC Weatherall Institute of Molecular Medicine) in collaboration with Dr. Daniel Ebner and Elena Seraia (Target Discovery Institute) at Oxford University.

β-adrenergic agonists and Corticosteroids appeared frequently in the SAS cell line as possible synergistic candidates (Figure 9). It has been showen that SRC kinase binds to the β-adrenergic receptor via phospho-Tyr350 and is required for the receptor desensitization (decrease its response to an agonist). Therefore, Dasatinib as SRC inhibitor abolishes the ability of SRC to be recruited/activated in response to the agonist and thereby impairs β-adrenergic receptor desensitization, leading to overstimulation [281]. Long-term overstimulation of the β-adrenergic receptor in response to an agonist can cause cardiovascular diseases, including cardiac hypertrophy, stroke, coronary artery disease, and heart failure [282]. Therefore, using Dasatinib with β-adrenergic agonists is usually not recommended.

However, Corticosteroids can help with cancer treatment in a variety of ways and play a vitally important role in the treatment of patients with advanced cancer, as will be discuss further in chapter 5. Fluticasone, which is a synthetic glucocorticoid, showed encouraging activity with Dasatinib in two cell lines with different concentrations and seems to be a promising candidate for combination treatment (Figure 9 and S3). We, therefore, decided to analyse HSP90 inhibitors and Corticosteroids in more details.

DAS 400 nM
GENTIAN VIOLET
FENOTEROL HYDROBROMIDE
ISOPROTERENOL HYDROCHLORIDE
BETAMETHASONE –DIPROPIONATE
ADRENOLONE HYDROCHLORIDE
RACTOPAMINE HYDROCHLORIDE
ETHYLNOREPINEPHRINE
FLUOCINOLONE ACETONIDE
TRIAMCINOLONE ACETONIDE
FLUDROCORTISONE ACETATE
TRIAMCINOLONE
ACRISORCIN
FLUMETHAZONE PIVALATE
TRIAMCINOLONE DIACETATE
TULOBUTEROL HYDROCHLORIDE
GRAMICIDIN
BUDESONIDE
BETAMETHASONE SODIUM PHOSPHATE
FLUOROMETHOLONE
TRETINOIN
MEDROXYPROGESTERONE ACETATE
FLUTICASONE PROPIONATE
POTASSIUM p-AMINOBENZOATE
NOREPINEPHRINE
HYDROCORTISONE VALERATE
NYLIDRIN HYDROCHLORIDE
HYDROCORTISONE PHOSPHATE
HYDROCORTISONE HEMISUCCINATE
FLUMETHASONE
EPINEPHRINE BITARTRATE
DESONIDE
FLUOCINONIDE
ALBUTEROL
ISOXSUPRINE HYDROCHLORIDE
GALLAMINE TRIETHIODIDE
METHYLTHIOURACIL
DEXAMETHASONE SODIUM PHOSPHATE

DAS 2 µM
ISOFLUPREDONE ACETATE
ALBUTEROL
BETAMETHASONE VALERATE
EPHEDRINE HYDROCHLORIDE
NOREPINEPHRINE
FENOTEROL HYDROBROMIDE
ADRENOLONE HYDROCHLORIDE
EPINEPHRINE BITARTRATE
AZACITIDINE
HYDROCORTISONE PHOSPHATE
ISOXSUPRINE HYDROCHLORIDE
DOBUTAMINE HYDROCHLORIDE
ISOPROTERENOL HYDROCHLORIDE
RITODRINE HYDROCHLORIDE

DAS 10 µM
OXYQUINOLINE SULFATE
THONZONIUM BROMIDE
RACTOPAMINE HYDROCHLORIDE
METHYLBENZETHONIUM CHLORIDE
CYCLOSPORINE
NOREPINEPHRINE
ADRENOLONE HYDROCHLORIDE
ISOPROTERENOL HYDROCHLORIDE
BETAMETHASONE SODIUM PHOSPHATE
PROTIONAMIDE
NYLIDRIN HYDROCHLORIDE
TEGASEROD MALEATE
THIOSTREPTON
ALBUTEROL
HYDROCORTISONE ACETATE
THIOGUANINE
RACEPHEDRINE HYDROCHLORIDE
PIMOZIDE
GENISTEIN
FLUOCINONIDE
TRYPTOPHAN
CALCIUM CHLORIDE
FLUTICASONE PROPIONATE
SULFADOXINE
HYDROXYPROGESTERONE
HYDROCORTISONE VALERATE
EPHEDRINE HYDROCHLORIDE
EPINEPHRINE BITARTRATE
TRICLABENDAZOLE
AZATADINE MALEATE
ISOXSUPRINE HYDROCHLORIDE
HYDROCORTISONE PHOSPHATE
RITODRINE HYDROCHLORIDE
SALINOMYCIN, SODIUM
HYDROCORTISONE HEMISUCCINATE

ADRENERGIC RECEPTOR AGONIST
GLUCOCORTICOIDS
CHOLINE
SEROTONINE/DOPAMINE

Figure 9. High-throughput screening results for compounds acting synergistically with DAS in SAS cells

In this screen, 1600 compounds at 3 different concentrations with or without DAS were tested against 3 TSCC lines. Cells were treated for 72 h and the viability was quantified by resazurin calorimetric assay. Different colors represent target groups of potentially synergistic compounds. β-adrenergic agonists and Glucocorticoids also appear for BICR56 cells (Marc Lewitzky, Oxford University). The compounds were ordered according to their effect size in combination with DAS. Compounds active in all cases were underlined. See CAL27 and BICR56 screening results in Supplementary Information (Figure S2 and S3).

1.8 Aim of the Thesis Research

The tongue remains the most common intraoral site for oral cancer worldwide with hotspots in several countries; it is a serious public health problem with significant morbidity and mortality. While the incidence of the tongue cancer appears to be stable or falling in some regions of the world, in other areas it is rising, particularly among younger people. If cancer has spread to a distant part of the body, the overall five-year survival rate drops to 39%. At present, there is no definitive evidence of an improvement in survival by existing therapies although, for theoretical reasons, many approaches are being increasingly utilised. So, alternative treatment options are urgently required and it is sensible to evaluate combinations of currently accepted therapeutics. Therefore, the principal goal of this thesis is to find a new targeted therapy for TSCC.

More specifically, the aims are:

To utilize the obtained results from the TSCC lines phosphorylation profile and the high throughput screens to establish and appraise preclinical treatments potentially useful in TSCC.

To combine Dasatinib with possible candidates and evaluate the activity in 2D and 3D cultures focusing on synergistic combinations.

To obtain knowledge about the mechanism of action of the combination treatments, which may further contribute to the development of even more potent strategies and to understand possible resistance mechanisms.

To begin to test the most promising combination treatment in the animal experiments.

Chapter 2 Materials and Methods

2.1 Materials

2.1.1 Equipments

-150 °C freezer	MDF-C2156VAN-PE	Panasonic
-80 °C freezer	MDF-974-PE	Panasonic
Autoclave	VX-150	Systec
Bacterial shaker	Innova 4200	New Brunswick Scientific
Bacterial shaker, coolable	Innova 43	New Brunswick Scientific
Biological safety cabinets class 2	MARS II	Labocence
BioPhotometer	Model #6131	Eppendorf
Block heater	QBD2	Grant
Cell counter	Countss II FL	Invitrogen
Centrifuge, cell culture	Rotanta 460R	Hettich
Centrifuge, large volume low speed	J-6MI	Beckman Coulter
Centrifuge, medium speed	Avanti J-25	Beckman Coulter
Centrifuge, microcentrifuge tubes	5427R	Eppendorf
Digital camera	Alpha 5100 SEL30M35	Sony
Digital camera	Coolpix E5400	Nikon
FACS	MACS Quant Analyzer	Miltenyi BioTec
Fastblot	015-200	Biometra
Gel imaging system	Syngene G:BOX	VWR, Avantor
Incubator for bacterial plates (no CO_2)	B6030	Heraeus
Incubator, cell culture (CO_2)	CB150	Binder
Inverted Microscope	Eclipse TS100	Nikon
Luminometer	GM3000	Promega
pH meter	Lab 875	SI analytics
Plate reader	Infinite M Plex	Tecan
Semi-Dry transfer cell	221BR	Bio-Rad
Sonicator	Sonopuls HD 2200	Bandelin
Waterbath	WNB 7	Memmert

2.1.2 Consumables

Bacteriological Petri Dish, 100x15 mm, sterile	Falcon, #351029
Blotting paper	Whatman, #GB46
Cell culture dish, 100x20 mm, sterile,	Corning, #430167
Cell culture flasks with filter lid, 25 cm^2, sterile	Corning, #430639
Cell culture flasks with filter lid, 75 cm^2, sterile	Corning, #430641
Cell culture plates, 48-well, sterile	TPP, #92148
Cell culture plates, 6-well, sterile	Corning, #3516
Cell culture plates, 96-well, sterile	Corning, #3596
Counting slide chamber	Invitrogen, #C10283
Cryogenic vial	Corning, #430487
Cuvette, 1.5 ml	Ratiolab, #2712120

Pipet tips   Corning, #4112 and #4129
Pipettes (Polystyrene), 2 ml, sterile   Corning, #4486
Pipettes (Polystyrene), 5 ml, sterile   Corning, #4487
Pipettes (Polystyrene), 10 ml, sterile   Corning, #4488
Pipettes (Polystyrene), 25 ml, sterile   Corning, #4489
Pipettes (Polystyrene), 50 ml, sterile   Corning, #4490
PVDF Transfer membrane   Merk Millipore, #IPVH00010
Reagent reservoir, 50 ml, sterile   VWR, #613-1174
Scraper, large, sterile   Sarstedt, #83.1831
Scraper, small, sterile   Corning, #3010
Tubes with lid, 15 ml, sterile   Corning, #430791
Tubes with lid, 50 ml, sterile   Corning, #430829

2.1.3 Reagents and Chemicals

Cell culture
Difco Nobel Agar   BD Biosciences, #214220
DMEM (1x)   Gibco, #41966-029
DMEM (1x), no phenol red   Gibco, #21063-030
DMEM (5x)   ThermoFisher, #31600-083
DMSO   Roth, #A994.1
Fetal Bovine Serum   Biowest, #S1860-500
Glucose   Gibco, #A24940-01
MEM NEAA (100x)   Gibco, #11140-035
Nitroblue tetrazolium chloride   Roth, #4421.3
PBS pH 7.4 (1x)   Gibco, #10010-015
Penicillin/Streptomycin 1%   Gibco, # 15140-122
Resazurin sodium salt   Sigma Aldrich, #199303
Sodium Bicarbonate   Sigma Aldrich, #S5761
Trypsin (10x)   Gibco, #15400-054
Trypan blue   Invitrogen, #T10282

Phosphatase inhibitors
Phosphatase Inhibitor Cocktail 2 100x   Sigma Aldrich, #P5726
Phosphatase Inhibitor Cocktail 3 100x   Sigma Aldrich, #P0044
Sodium molybdate   Sigma Aldrich, #S6646
Sodium orthovanadate   Sigma Aldrich, #S6508

Protease inhibitors
Antipain dihydrochloride   Roth, #2933.2
Aprotinin   Roth, #A162.3
EDTA   Roth, #8043.2
Leupeptin   Serva, #51867.03
Pepstatin   Roche, #11524488001
cOmplete Protease Inhibitor Cocktail with EDTA   Roche, #11836145001

PMSF   Sigma Aldrich, #AP7626

Molecular weight standards

BlueEye Prestained Protein Marker   Jena Bioscience, #PS-104

Precision Plus Protein Standards   BIO-RAD, #1610375

Antibodies

For antibodies used in this thesis refer to table at the end of the Materials and Methods chapter (2.3).

Detergents

Deoxycholic acid (DOC)   Sigma Aldrich, #D6750

Nonidet P-40 (NP-40)   Sigma Aldrich, #13021

Triton X-100   Roth, #3051.3

Tween 20   Roth, #9127.1

Enhanced Chemoluminescence (ECL) Detection kits

Pierce ECL Western Blotting Substrate   ThemoFisher, #32109

Western Bright Sirius   Advansta, #K-12043-D10

Blocking reagents

Albumin from Chicken egg   Sigma Aldrich, #A5378

Bovine serum albumin (IgG-free)   Roth, #3737.4

Skimmed milk powder   Sucofin #32106297811

Investigated compounds and drugs

AT13387   Hycultec, #HY-14463

Crizotinib   Selleckchem, #S1068

Dasatinib   Hycultec, #HY-10181

Dexamethsone   Sigma Aldrich, #D4902

Fluticasone   MedChem Express, #HY-B0154

Ganetispib   Selleckchem, #S1159

HSP990   Selleckchem, #S7097

Hydrocortisone   Sigma Aldrich, H4001

Imatinib   Hycultec, #HY-50946

Luminespib   Selleckchem, #S1069

Methypredisolone   Selleckchem, #S1733

Staurosporine   Selleckchem, #1421

TAS-116   Chemgood, #C-1315

XL888   Hycultec, #HY-13313

Kits

Caspase-Glo 3/7 Assay   Promega, #G8091

CellTiter-Glo Luminescent Cell Viability Assay   Promega, #G7571

Senescence β-Galactosidase Staining Kit   Cell Signaling Technology, #9860

Dyes and stains

Acridine Orange (AO)	Sigma Aldrich, #235474
Annexin V-FITC	Miltenyi BioTec, #130-092-052
Coomassie (Brilliant blue G 250)	Roth, #9598.1
Coomassie (Brilliant blue R 250)	Serva, #17525
DAPI	Sigma Aldrich, #D9542
Propidium iodide (PI)	Miltenyi BioTec, #130-093-233
Trypan blue	Invitrogen, #T10282

Miscellaneous

Acrylamide/Bis-acrylamide sol. 30% (37.5:1)	Roth, #P3029.1
Ampicillin	Roth, #K029.2
APS	Roth, #P9592.2
ATP	Roth, #HN35.3
Bacto™ dehydrated agar	ThemoFisher, #214010
Bromophenol blue	Bio-Rad, #161-0404, Bio-Rad
BSA for Bradford assay standards	Serva, #11930
DMF	Cell signaling, #12767
EGTA	Roth, #3054.1
Ethanol	Roth, #P9065.1
GammaBind G Sepharose	GE Healthcare, #17-0885-01
GDP 100mM	Sigma Aldrich, #PG7127
Glutathione (GSH) agarose beads	ThemoFisher, #16101
Glycerin	Roth, #3783.1
GTPγS	Jena Bioscience, #73765
HCl	Roth, #P074.1
HEPES	Roth, #9105.3
InstantBlue	Expedeon, #ISB1L
Isopropyl-β-D-thiogalactopyranoside (IPTG)	Roth, #2316.4
LB medium, granulated	Roth, #6673.2
Mercaptoethanol	Roth, #P4227.3
Methanol	Sigam Aldrich, #32212
MgCl2	Roth, #2189.1
MnCl2	VWR, #10152
NaCl	Roth, #9265.2
NaOH	Roth, #6771.1
Propanol	ThemoFisher, #33539
RNAse	Sigma Aldrich, #R6513
SDS	Roth, #P0183.3
TB medium, granulated	ThemoFisher, #BP9728
TEMED	Roth, #P2367.2
Tris	Roth, #5429.5

2.1.4 Solutions and Buffers

Note: in the current work, ultraclean (UC) H_2O was used in all protocols for solutions and buffers preparation.

2.1.4.1 Stock Solutions

Tris HCl, 1 M
1 M   Tris base
Dissolved in H_2O and adjusted with HCl to pH 6.8, 7.5 or 8.8.

2.1.4.2 Protease and Phosphatas Inhibitors

Antipain hydrochloride (1000x stock: 5 mg/ml in H_2O, stored at -20 °C)
Aprotinin (100x stock: 1 mg/ml in H_2O, stored at 4 °C)
Ethylenediaminetetraacetic acid (EDTA) (stock: 0.5 M in H_2O, adjusted to pH 7.5, stored at RT)
Leupeptin (1000x stock: 0.5 mg/ml in H_2O, stored at -20 °C)
Pepstatin A (1000x stock: 0.7 mg/ml in methanol, stored at -20 °C)
Protease inhibitor cocktail tablet (25x stock: one tablet/2 ml H_2O, stored in aliquots at -20 °C)
Phenylmethylsulfonylfluoride (PMSF) (500x stock: 100 mg/ml in DMSO, stored at -20 °C)
Sodium molybdate (100x stock: 100 mM in H_2O, stored at RT)
Sodium orthovanadate (100x stock: 100 mM in H_2O, stored at RT).

2.1.4.3 Cell Lysis Buffers

RIPA 100 lysis buffer
20 mM   Tris-HCl pH 7.5   Add H_2O to 70% of the end volume
1 mM   EDTA pH 7.0
100 mM   NaCl
1% (v/v)   Triton X-100   Stir 5 min before adding DOC
0.5% (w/v)   DOC   Stir 5 min before adding SDS
0.1% (w/v)   SDS   Stir 5 min
Add H_2O to end volume.
Inhibitors
1:100   Phosphatase inhibitor cocktail 2 (100x)
1:100   Phosphatase inhibitor cocktail 3 (100x)
1:40   Protease inhibitor cocktail (25x)
Buffer was stored at 4 °C and inhibitors were added freshly before use.

MLB cell lysis buffer
25 mM   HEPES pH 7.5
150 mM   NaCl
10 mM $MgCl_2$
1 mM   EDTA
10% (v/v)   Glycerol
1% (v/v)   NP-40
0.25% (w/v) DOC
Inhibitors
1:100   Aprotinin (1mg/ml)
1:1000   Antipain (5 mg/ml)

1:1000   Leupeptin (0.5 mg/ml)
1:1000   Pepstatin (0.5 mg/ml)
1:100   Phosphatase inhibitor cocktail 2 (100x)
1:100   Phosphatase inhibitor cocktail 3 (100x)
1:40   Protease inhibitor cocktail (25x)
1:100   Sodium molybdate (100 mM)
1:100   Sodium orthovanadate (100 mM)
1:500   PMSF (100 mg/ml)
Buffer was stored at 4 °C and inhibitors were added freshly before use.

Lysis buffer for kinase assays
50 mM   Tris-HCl, pH 7.5
150 mM   NaCl
1% (v/v)   Triton X-100
1 mM   EGTA
1 mM   EDTA
1% (v/v)   Glycerol
Inhibitors
1:1000   Leupeptin (0.5 mg/ml)
1:100   Aprotinin (1mg/ml)
1:500   PMSF (100 mg/ml)
1:100   Sodium orthovanadate (100 mM)
1:100   Phosphatase inhibitor cocktail 2 (100x)
1:100   Phosphatase inhibitor cocktail 3 (100x)
1:40   Protease inhibitor cocktail (25x)
Buffer was stored at 4 °C and inhibitors were added freshly before use.

2.1.4.4 Bradford Protein Quantification Assays

Preparation of 4x Bradford stock solution
250 mg of (Coomassie) Brilliant blue G was dissolved in 120 ml of ethanol and mixed thoroughly. When the dye is completely dissolved, 250 ml of concentrated phosphoric acid was added carefully to the dye-ethanol mixture. After mixing thoroughly, H_2O was added to the final volume of 500 ml. The stock was stored at RT in complete darkness.

Preparation of 1x Bradford solution
To 12.5 ml of 4x Bradford stock solution, H_2O was added to a final volume of 50 ml. The solution was mixed, stood for 15–30 minutes, then filter through a paper filter and stored in complete darkness at RT. This solution can be used for 2-3 months.

BSA solution for Bradford assay
BSA was dissolved in H_2O to a concentration of 10 mg/ml (100x stock), aliquoted into 0.5 ml aliquots and stored at -20 °C. To make a 1x stock, one aliquot was thawed and mixed with 49.5 ml of H_2O. 1 ml aliquots of 0.1 mg/ml BSA were made and stored at -20 °C.

2.1.4.5 SDS-PAGE and Western Blot

4% Stacking gel (15 ml)
2 ml   Acrylamide/Bis-acrylamide solution
1.6 ml   1 M Tris HCl pH 6.8

0.15 ml   SDS 10%
1.35 ml   Glycerol 50%
Fill up with water to the final volume and mix thoroughly.
0.15 ml   APS 10%
15 µl   TEMED

12% Separation gel (15 ml)
6 ml   Acrylamide/Bis-acrylamide solution
5.65 ml   1 M Tris HCl pH 8.8
0.15 ml   SDS 10%
Fill up with water to the final volume and mix thoroughly.
0.125 ml   APS 10%
10 µl   TEMED

All SDS gel components, except of APS and TEMED, were mixed and filled up with H_2O to the final volume. Finally, APS and TEMED were added, the solution was mixed thoroughly and the gel was cast. To obtain other gel percentages, the amount of Acrylamide/Bis-acrylamide solution in the separating gel is varied as follows:

4 ml   Acrylamide/bis-acrylamide solution (8% gel)
5 ml   Acrylamide/bis-acrylamide solution (10% gel)
6 ml   Acrylamide/bis-acrylamide solution (12% gel)
7 ml   Acrylamide/bis-acrylamide solution (14% gel)
8 ml   Acrylamide/bis-acrylamide solution (16% gel)

10x SDS-PAGE buffer
250 mM   Tris
1.9 M   Glycine
1% (w/v)   SDS
Dissolve in H_2O. Store at RT.

4x SDS protein gel sample buffer
70 mM   Tris HCl, pH 6.8
5% (v/v)   Mercaptoethanol
40% (v/v)   Glycerol
3% (w/v)   SDS
0.05% (w/v) Bromophenol blue
Aliquots were stored at -20 °C. Before use, aliquots were warmed up to room temperature and mixed well to dissolve the SDS completely.

Tris buffered saline (TBS)
20 mM   Tris HCl, pH 7.5
100 mM   NaCl

TBST
TBS with 0.1% (v/v) Tween 20

Blocking buffer for Western blots
TBST with 5% (w/v) low-fat dry milk (not for phospho-specific antibodies) or TBST with 5% (w/v) IgG-free BSA (for phospho-specific antibodies)

Blocking buffer for Far Western blots
TBS with:
0.1% (v/v)	Tween 20
10% (w/v)	Low-fat dry milk
1 mM	Sodium orthovanadate
5 mM	EDTA

Semidry blot-buffer
48 mM	Tris
38.6mM	Glycine
0.037% (w/v)	SDS

Autoclaved and stored at RT.

Blot stripping buffer
60 mM	Tris HCl pH 6.8
2% (w/v)	SDS

Dissolved in H_2O and stored at RT.
Mercaptoethanol was added to final concentration of 0.1% immediately before use.

2.1.4.6 RAS•GTP Pull-Down Assay

100x GTPyS (10 mM)
2 mg of GTPyS was dissolved in 0.371 ml H_2O. 50 µl aliquots were prepared, frozen in liquid nitrogen and stored at -80 °C

100x GDP (100 mM)
10 mg of GDP was dissolved in 0.226 ml H_2O. 50 µl aliquots were prepared, frozen in liquid nitrogen and stored at -80 °C.

2.1.4.7 MET Kinase Assay

Washing buffer
20 mM	Tris HCl, pH 7.5
100 mM	NaCl
1% (v/v)	Triton X-100
1 mM	EGTA
1 mM	EDTA
2.5% (v/v)	Glycerol

10x Kinase buffer
200 mM	HEPES, pH 7.4
30 mM	$MgCl_2$
30 mM	$MnCl_2$
1 mM	Sodium orthovanadate, added immediately before use.

ATP (20 mM)
ATP stock (100 mM) was prepared in H_2O, adjusted with NaOH to pH 7 and stored at -80 °C. ATP stock was diluted 1:5 immediately before use with UC water.

Substrate
A recombinantly expressed His-hGAB1 (613-694) fusion protein was diluted to 2 µg/ml with H_2O. This protein was designed and provided by a member of our group (Dr Marc Lewitzky).

2.1.4.8 Senescence β-Galactosidase Staining (Cell Signaling Technology, #9860)

Fixative solution: The 10x Fixative Solution was diluted 1:10 with distilled water (1x solution).

Staining solution: The 10x Staining Solution was redissolved by heating to 37 °C with agitation then diluted 1:10 with distilled water (1x solution).

X-gal: 20 mg of X-gal was dissolved in 1 ml DMF to prepare a 20 mg/ml stock solution. X-gal solution was stored at -20 °C in a light-resistant container for up to one month. Polypropylene plastic or glass should be used to make and store X-gal. Polystyrene is not suitable.

β-Galactosidase staining solution:
930 µl	1x Staining Solution
10 µl	100x Solution A
10 µl	100x Solution B
50 µl	20mg/ml X-gal stock solution

Note: The β-Galactosidase staining solution should have a final pH of 6.0 (pH of 5.9-6.1 is acceptable). pH differences can affect the staining, a low pH can result in false positives and a high pH can result in false negatives. HCl or NaOH was used to adjust the pH.

2.1.4.9 Caspase-Glo 3/7 Assay

Caspase-Glo 3/7 Reagent (Promega Kit, #G8091):
Caspase-Glo® 3/7 buffer and lyophilized Caspase-Glo® 3/7 substrate were equilibrated to RT before use. The contents of the Caspase-Glo® 3/7 buffer bottle were transferred into the amber bottle containing the Caspase-Glo® 3/7 substrate. Contents were mixed by swirling or inverting until the substrate is thoroughly dissolved to form the Caspase-Glo® 3/7 reagent. The reconstituted Caspase-Glo® 3/7 reagent was stored at -80 °C for few months.

CellTiter-Glo Reagent (Promega Kit, # G7571):
The CellTiter-Glo® buffer was thawed and equilibrated to RT prior to use. The lyophilized CellTiter-Glo® substrate was equilibrated to RT and 10 ml of CellTiter-Glo® buffer was transferred into the amber bottle containing CellTiter-Glo® substrate to reconstitute the lyophilized enzyme/substrate mixture. Contents were mixed by gentle vortexing, swirling or inverting the contents to obtain a homogeneous solution. Reconstituted CellTiter-Glo® reagent could be stored at -80 °C up to 21 weeks.

2.1.4.10 Bacterial Culture and Expression of Recombinant Proteins

LB (Luria/Miller) medium (1 liter)
25 g LB granulate (Roth, #6673.2) was dissolved in 950 ml H_2O. LB medium was filled up to 1 liter with H_2O and autoclaved for 21 minutes at 121 °C.

Terrific Broth (TB) medium (1 liter)
47.6 g granulated powder was (ThemoFisher, #BP9728) dissolved in 950 ml H_2O. 4 ml glycerol was added. Then, the TB medium was filled up to 1 liter with H_2O and autoclaved for 21 minutes at 121 °C.

LB agar plates
25 g of LB granules and 15 g of Bacto dehydrated agar powder were added to 1 liter H_2O. The medium was heated and stirred until the powder was completely dissolved. Afterwards, the medium was autoclaved for 21 minutes at 121 °C. The medium was cooled down to 45 °C and appropriate antibiotics were added. After thoroughly mixing, about 25-30 ml medium was poured per Petri dish (10 cm diameter) and left to solidify at RT. Plates were stored upside-down in sealed plastic bags for max. 4 weeks at 4 °C.

TPE lysis buffer
1% (v/v)	Triton X-100
100 mM	EDTA pH 7.5
1x	PBS

Dissolved in H_2O and mixed well after each addition. Before use cool to 4 °C and add protease inhibitors if required.

GSH-bead wash buffer (GSH-WB)
50 mM	Tris pH 7.5
100 mM	EDTA pH 7.5
0.1 % (v/v)	Tween 20

Chill before use.

2.2 Methods

2.2.1 Cell Lines and Culture Conditions

TSCC cell lines SAS, CAL27 and BICR56 were used in this study (Table 1). The SAS cell line was purchased from the Japanese Collection of Research Bioresources Cell Bank (#JCRB0260), the CAL27 cell line from the American Type Culture Collection (ATCC, #4098560) and the BICR56 cell line from the European Collection of Cell Cultures (ECACC, #06031002).

Cultures were maintained as monolayers in DMEM (with high glucose and sodium pyruvate) supplemented with 10% fetal bovine serum, 1% penicillin/streptomycin and 1% NEAA at 37 °C in a humidified atmosphere with 10% CO_2. Medium with supplements is referred to as 'medium' in this work. Cells were split when reaching 85-90% confluence. In short, cells were washed with PBS and detached by incubation with trypsin at 37 °C for a few minutes. The process was stopped as soon as cells detached by the addition of medium and cultivation was continued in a new sterile flask (Corning, #430639 and #430641).

Table 1. Origin and tumor characteristics of the investigated TSCC cell lines

	SAS	CAL27	BICR56
Source/reference	Yoshida *et al.*, 1993 [283]	Gioanni *et al.*, 1988 [284]	Edington *et al.*, 1995 [285]
Biopsy taken from	Primary tumor (tongue)	Primary tumor (middle of the tongue)	Primary tumor (tongue)
Tumor stage (T)	T3	T4	T4
Lymph node stage (N)	N2	N2	N1
Metasatsis	No	No	No
Doublig time (h)	21	35	48
HPV$^+$	No	No	No
p53 mutation (AA)	p.E336*	p.H193L	p.Y126C
other mutaion	HSP90AA1 (p.K564E)	NRAS (p.R68T, p.D92N)	

2.2.2 Preparation of Compounds

The investigated compounds were insoluble in water. They were initially dissolved in Dimethyl sulfoxide (DMSO) and further diluted with culture medium for analysis. A broad range of stock solutions of test compounds were prepared (from 200 mM to 1 nM), aliquoted to small volumes to avoid repeat thaw-freeze cycles and stored at -80 °C for further use. The final concentration of DMSO never exceeded 0.1 %, which was found to be non-toxic to the cells.

2.2.3 Resazurin Colorimetric Assay

In the present work, the cytotoxicity of all compounds in 2D culture was evaluated by resazurin colorimetric assay. The resazurin assay is based on the reduction of oxidized non-fluorescent blue resazurin to a red fluorescent dye (resorufin) by the mitochondrial respiratory chain in live cells. The amount of resorufin produced is directly proportional to the number of living cells. The resazurin dye can be measured in fluorescence or absorbance mode. However, fluorescence mode measurement offers greater assay linearity, reproducibility, robustness and sensitivity.

Exponentially growing TSCCs were washed with PBS, shortly trypsinated and counted. Then cells seeded into 96-well plates (Corning, #3596) at the appropriate cell densities to prevent confluence of the cells during the period of the experiment. For SAS, CAL27, BICR56 cell lines 8000, 5000, and 3500 cells/well were seeded respectively. After 24 h, the cells were treated with 200 µl of serial dilutions of the investigated compounds and DMSO as vehicle control (Mock) for 72 h. After treatment, the supernatant medium from the 96-well plates was discarded and each well was washed with 100 µL of PBS. The wells were then stained with 100 µL of 0.1% of resazurin in DMEM (no phenol red) for about 2 h at 37 °C. Resazurin stock solution was prepared in 35 mg/ml PBS concentration and stored at 4 °C. After staining, the fluorescence was measured at 590 nm using the plate reader (TECAN Infinite M Plex). The percentages of surviving cells related to Mock-treated cells were determined.

2.2.4 Cell Viability Assay with the Trypan Blue Exclusion Method

Trypan blue dye exclusion assay is used to determine the number of viable and/or dead cells in a cell suspension. It is based on the principle that living cells possess intact cell

membranes that block this dye which is large and negatively charged, whereas dead cells do not [286].

Cells were plated in 6-well plates (Corning, #3516) at the suitable cell quantities per well. For SAS, CAL27, BICR56 cell lines, 240,000, 150,000, and 100,000 cells/well were seeded, respectively. The following day, cells were exposed to different concentrations of agents and DMSO as vehicle control (Mock). After 72 h exposure cell proliferation was assessed with an automated cell counter (Countess II FL, Invitrogen). Briefly, 10 μL of cell suspension was mixed with 10 μL of Trypan blue and pipetted into a disposable Countess chamber slide. The slide was inserted into the instrument and cells counted. The live (viable) cells do not take up the blue dye, whereas dead (non-viable) cells do. Cell viability was calculated using the ratio of total live cells in treated samples normalized to total live cells in the Mock-treated sample.

2.2.5 Morphological Evaluation by Phase-Contrast Inverted Microscope

Microscopic investigation was performed to identify the morphological features of treated cancer cells in comparsion to Mock-treated controls. For this purpose, SAS cells were seeded in 6-well plates (Corning, #3516) at 240,000 cells/well. After 24 h, cells were treated with different concentrations of the investigated compounds and DMSO as vehicle control (Mock). After 72 h exposure, cell growth was evaluated with an inverted microscope (Eclipse TS100, Nikon) and photos were taken by digital camera (Coolpix E5400, Nikon). Images of SAS cells were captured of 10x and 20x magnifications.

2.2.6 3D Soft Agar Assay

2.2.6.1 Preparation of Materials and Reagents

A. Preparation of 5x DMEM Powdered Medium (ThermoFisher, #31600-083)

1. To a mixing container that is as close to the final volume as possible, 1800 mL of RT distilled water was added to the powdered medium with gentle stirring.
2. The inside of the package was rinsed to remove all traces of powder.
3. 7.4 g of sodium bicarbonate was added to the medium (3.7 g/L, pH 7.0-7.4).
4. The pH was adjusted to 0.2 and 0.3 units below the desired final working pH of 7.0-7.4 by slowly adding, with stirring, 1 N NaOH or 1 N HCl. The pH may rise by 0.1 to 0.3 units upon filtration.
5. The final volume (2 L) was adjusted with distilled water.
6. The medium was processed immediately into sterile containers by membrane filtration with a 0.2 μm filter using a positive-pressure system.
7. The prepared medium was aliquoted in 4 x 500 ml bottle and stored at 4 °C up to 3 months.

B. Bicarbonate (BC) water: 3.7 g of sodium bicarbonate was mixed with 1000 ml of sterile ultraclean water. The mixture was autoclaved prior usage.

C. 1.8% nobel agar: 1.8 g of noble agar was added to 100 ml of sterile ultraclean water in 100 ml glass bottle with closable lids for long-term storage. Noble agar will not dissolve completely with agitation alone. The noble agar mixture was autoclaved against a 100 ml reference. This mixture can be made in advance and stored at 4 °C but needs to heated again at the time of the experiment until the agar has completely dissolved.

D. 2x DMEM (2M): 150 ml 2M sufficient for 4 plates was prepared by mixing of 48 ml of 5x DMEM, 5.16 ml of glucose 200g/L and 66.84 ml of BC water. 3 ml was removed from the mixture, then 30 ml of fetal serum bovine and 3 ml of penicillin/streptomycin were added.

E. 1x DMEM (1M): 45 ml of BC water was mixed with 45 ml of 2M.

F. Nitroblue tetrazolium chloride (NBT): NBT was prepared by making a 0.5 mg/ml stock solution in 1x PBS. This was used at the end of the experiment to stain the colonies.

G. 2M3V (2M with 3x highest concentration of DMSO): 175 µl of DMSO was added to 35 ml of 2M.

H. 2M3C (2M with 3x final concentration of compound): Three times the required concentration was prepared in 2M. In G and H, the final DMSO concentrations should be 3 µl/ml.

2.2.6.2 Preparation before Plating Agar Layers

A. 7.5 ml of 1M (50 ml tube) for 1st agar layer and 4 ml of sterile UC water (50 ml tube) for 2nd agar layer were prewarmed to 42 °C in a waterbath.
B. The 1.8% agar solution was liquefied in a microwave completely and cooled down to 42 °C in a waterbath. While heating in a microwave, the solution should be monitor closely to avoid boiling over.
C. 7.5 ml 1.8% agar was mixed with 7.5 ml 1M and kept at 42 °C. This is sufficient for two plates.
D. 4 ml 1.8% agar was mixed with 4 ml sterile UC water and kept at 42 °C. This is sufficient for two plates.
E. Compound stock solution(s) and compound dilutions were prepared in 2M (15 ml tubes).
F. 2 x 0.5 ml aliquots and 1 x 1.5 ml aliquot of 2M3V and 2M3Cs were aliquoted into Eppendorf tubes (0.5 ml) and 15 ml tubes (1.5 ml).
G. The Eppendorf tubes for the 1st and 2nd layers were incubated in two thermoblocks (42 °C).
H. 48-well plates (TPP, #92148) were labeled appropriately for each cell line or condition being investigated.

2.2.6.3 Plating of the 1st Layer (agar, bottom layer)

A. 1 ml agar-1M mixture was added to 0.5 ml aliquots of 2M3V or 2M3Cs. Tubes were vortexed and kept at 42 °C in the thermoblock.
B. 2x 48-well plates were placed on a prewarmed glass plate (42 °C) under the sterile hood. Only the inner 24 wells of the 48-well plates were used, to avoid edge effect.
C. Tubes were vortexed again and 0.2 ml per well were plated.
D. plates were left for at least 30 min to harden at room temperature, in the cell culture hood.

2.2.6.4 Plating of the 2nd Layer (cells in agar, middle layer)

A. 0.5 ml agar-UC water mixture was added to 0.5 ml aliquots of 2M3V and 2M3Cs. Tubes were vortexed and kept in a 42 °C thermoblock.

B. Cells were trypsinized, diluted with 1M and counted. Approximately, 90,000 cells/ml were required for SAS cell line and 100,000 cells/ml were used for CAL27 and BICR56 cell lines. The cell tube was incubated in at 37°C until use.

C. 0.5 ml cells in 1M were added to 1 ml aliquots of 2M3V and 2M3Cs (compound-agar mixture). Tubes were vortexed and kept in a 42°C thermoblock.

D. Tubes were vortexed again and 0.2 ml per well were plated (6,000 cells/well).

E. Plates were left for at least 30 min to solidify agar at RT, in the cell culture hood.

2.2.6.5 Plating of the 3rd Layer (medium, top layer)

A. 20 ml 1M was mixed with 20 ml BC water. This was sufficient for 2 plates.

B. 3 ml of the mixture was added to 1.5 ml aliquots of 2M3V and 2M3Cs.

C. Tubes were mixed well and 0.2 ml per well was plated.

D. The 24 outer wells of the 48-well plates were filled with 0.5 ml normal medium (to prevent the agar layers from drying out).

E. The plates were incubated in the cell culture incubator for at least 2 weeks. Plates were not stacked.

F. 3 x 1 ml aliquots of this mixture (1M+BC water) were aliquoted into Eppendorf tubes and stored with the rest in the 15 ml tube at -20 °C.

G. The wells were fed every 3 to 4 days with 70 µl of the stored 3rd layer mixtures.

2.2.6.6 Staining the Plates and Counting Colonies

Cells were stained by adding 70 µl of NBT solution per well and plates were incubated overnight at 37 °C. Once colonies were stained, photographs of wells were taken using a Sony Alpha 5100 camera with a SEL30M35 macro lens and the colonies were counted using image analysis software (ImageJ 1.50i). A diameter of 50 µM was used as a cut-off for counting viable colonies for the quantitative analyses.

2.2.7 Cell Lysis

Cells were plated in a 100 mm diameter culture dishes (Corning, #430167) at 1,300,000, 850,000 and 650,000 cells/dish for SAS, Cal27 and BICR56 cell lines, respectively. After 24 h, cells were treated with the indicated compounds and concentrations. At the end of the treatment, cells were washed with PBS and extracted with RIPA lysis buffer in the presence of the appropriate concentrations of protease and phosphatase inhibitors. Lysates were agitated for 30 minutes in the cold room and then cleared by centrifugation (20,800 rcf, 25 min, 4 °C). The supernatant was transferred into fresh tubes and the protein concentration was determined by the Bradford assay.

2.2.8 Protein Quantification Assays (Bradford Assay)

Protein concentrations were determined according to the method of Bradford. The Bradford protein assay is a spectroscopic analytical procedure used to measure the concentration of protein in a solution. Before the measurement of samples, a standard curve was prepared with BSA stock solution (0.1 mg/ml):

50 µl H_2O (blank control)
20 µl   BSA solution + 30 µl H_2O
40 µl   BSA solution + 10 µl H_2O

60 µl	BSA solution
80 µl	BSA solution
100 µl	BSA solution
120 µl	BSA solution

950 µl of 1x Bradford solution is added into each tube and rapidly mixed. After 10 min the absorption at 595 nm is measured. The standard curve allows the calculation of protein concentration in unknown samples.

2.2.9 SDS Polyacrylamide Gel Electrophoresis (SDS-PAGE)

Proteins were separated by size on a polyacrylamide gel according to the method of Laemmli [287]. Initially, the protein was mixed with 4x SDS PAGE sample buffer and denatured at 95 °C for 5 min. The SDS-PAGE sample buffer contains β-mercaptoethanol to reduce disulfide bonds in the protein and sodium dodecyl sulfate (SDS) which associates with hydrophobic residues of the proteins and covers the proteins with negative charges. The denatured protein samples were then loaded onto a discontinuous polyacrylamide gel which is composed of a stacking gel (pH 6.8) and a separating gel (pH 8.8). The separating gel was cast with a concentration appropriate to the molecular size of the proteins to be separated. The stacking gel ensures the simultaneous entry of the sample into the separating gel. A constant voltage of 150 V for 120 minutes was used for the separation of proteins. The separating gel then separates the negatively charged proteins according to their size enabling molecular weight estimation.

2.2.10 Immunoblotting (Western Blot)

The polyacrylamide gel was removed from the electrophoresis chamber and proteins were transferred from the gel onto a polyvinylidene difluoride (PVDF) membrane by semi-dry blotting. Six layers of chromatography paper were immersed in semi-dry blot buffer (SDBB) and placed onto the blotter surface. PVDF membrane pre-wetted in methanol for a few second and equilibrated in SDBB for a few minutes was positioned on top of the filter papers. Then the gel was placed carefully onto the membrane and six further layers of pre-wetted filter papers were applied on top. Air bubbles were removed after each step by lightly rolling with a glass pipette. A constant voltage of 20 V for 1 hour or 25 V for 30 min (depending on the transfer device) was used for the transfer of the proteins. The PVDF membrane was then incubated in blocking buffer (5% of BSA or milk in TBST) appropriate for the individual antibody and shaken in the solution for at least 1 h at room temperature to saturate non-specific binding sites on the membrane.

Because of the high concentrations of phosphoproteins in milk, blocking with milk is commonly not compatible with the detection of phosphorylated proteins. 5% BSA blocking solution was used for these antibodies by default. The membrane was incubated with the primary antibody in plastic wrapping overnight at 4 °C on a nutator. After washing three times for 10 min in TBST, a horseradish peroxidase (HRP)-coupled secondary antibody in TBST was added and incubated for at least 1 h. After washing three more times with TBST for 10 min, a freshly mixed enhanced chemiluminescence (ECL) detection solutions was applied. The light produced by catalytic oxidation of luminol in the detection solution through the HRP was detected with a chemiluminescence imaging system (Syngene G: BOX).

2.2.11 Blot Stripping

Blots were incubated 3x 15 min at 50 °C in pre-warmed blot stripping buffer, with gentle shaking. Afterwards, the membrane was rinsed 4 x 10 min in TBST, then blocked again for 1 h before reprobing.

2.2.12 Active RAS Pull-Down Assay [288]

Small GTP-binding proteins (or GTPases) serve as molecular switches in signal transduction pathways. Like other small GTPases, RAS is active when bound to GTP and inactive when bound to GDP.

2.2.12.1 Cell Lysis

SAS cells were seeded overnight in 100 mm diameter cell culture dishes (1,300,000 cells /dish) and treated for 72 h. The culture medium was removed carefully and the cells were gently rinsed once with ice-cold PBS. 0.5-1.0 mL of MLB lysis buffer with appropriate protease and phosphatase inhibitor concentrations was used to extract the cells. The cell lysates were transferred into microcentrifuge tubes and incubated on ice for 5 min. The tubes were centrifuged at 20,800 rcf for 15 min (4 °C) and the supernatants (total lysates) transferred to new pre-chilled tubes. The protein concentrations were determined by Bradford assay as described before.

2.2.12.2 GTPγS or GDP Treatment Controls

The following treatments, GTPγS (positive control) and GDP (negative control), were performed, to ensure the pull-down procedures are working properly. 500 µg of cell lysate was used for each treatment. For best results, GTPγS and GDP stock solutions were aliquoted to minimize freeze/thaw cycles and stored at -80 °C.

Into three tubes with 500 µg lysate each, 10 µL 0.5 M EDTA pH 8.0 (for a final concentration of 10 mM) was added. MLB was added to a final volume of 500 µl in each tube. Into 2 tubes, 5 µL of 10 mM GTPγS (for a final concentration of 0.1 mM) was added. 5 µL of 100 mM GDP (for a final concentration of 1 mM) was added into the third tube. The samples were vortexed and incubated at 30 °C for 15 min with constant agitation. The reaction was terminated by placing the sample in ice and adding 32 µL of 1M MgCl$_2$ (for a final concentration of 60 mM). The samples were vortexed again and used for GST-RAF1-RBD pull-downs.

2.2.12.3 Affinity Precipitation of Activated RAS (RAS•GTP)

A bottle of GSH bead suspension was swirled to thoroughly resuspend the beads then 40 µl of GSH-suspension (1:1) for each sample were was transferred into each 1.5 ml tubes. The tubes were centrifuged at 20,800 rcf for 2 min (4 °C) and the supernatants were discarded. Bacterial lysate containining GST-RAF1-RBD (obtained as a gift from Shalloway lab) [288] was thawed on ice and 150 µl each (around 44 µg as determined in a test pull-down) was added to all but one tube. 26 µg of purified GST-tag was added into the last tube which contains GTPγS, as another negative control. MLB was added to an end volume of 300 µl and the tubes were agitated for 1 h in the cold room. The tubes were centrifuged at 20800 rcf for 2

minutes (4 °C) and the supernatants were removed. After that, the beads with the immobilized GST-fusion proteins were washed two times with 300 µl of MLB buffer and 500 µg of lysate was added. The total volume was filled up with MLB to 500 µl. Then, the tubes were agitated for 1 h in the cold room, centrifuged for 2 min (20,800 rcf, 4 °C) and the supernatants were aspirated. Subsequently, the beads were washed twice with 300 µl of MLB buffer and 100 µl of SDS-PAGE sample buffer was added and mixed with each sample. Samples were heated for 5 min at 95 °C and shortly spun down in a cool centrifuge. Finally, 50 µl of the supernatants (without disturbing the beads at the bottom of the tube) were separated in 12% SDS-PAGE and analyzed by Western blotting with a RAS antibody.

2.2.13 MET kinase assay

2.2.13.1 Cell Lysis

SAS cells were seeded in 100 mm diameter cell culture dishes (1,300,000 cells/dish) and lysed by kinase lysis buffer containing the appropriate inhibitors. The cell lysate was agitated in the cold room for 1 h and centrifuged at 20800 rcf for 25 min (4 °C). The supernatant was transferred to a new tube and the protein concentration was determined by Bradford assay.

2.2.13.2 Preclearing

20 µl amounts of G sepharose beads in a 1:1 suspension with 20% ethanol were transferred into 1.5 ml tubes (10 µl packed beads each). The tubes were centrifuged at 100 rcf for 1 min (4 °C). Supernatants were removed and beads were washed with 500 µl of lysis buffer (without inhibitors) two times. Then, the beads in each tube were mixed with 500 µg of protein cell lysate (which was equivalent to a volume of around 150 µl) in the cold room for 1 h. Samples were centrifuged (100 rcf, 2 min, 4 °C), and the pre-cleared supernatants were transferred into new tubes. The beads were discarded.

2.2.13.3 Immunoprecipitation

Subsequently, three types of immunoprecipitations were prepared. 5 µg of mouse isotype control (Cell Signaling Technology, #5415) was added to one tube containing lysate, 5 µg of MET antibody (Cell Signaling Technology, #8198) was added to one tube containing no lysate and 5 µg of MET antibody was added to tubes containing lysates for immunoprecipitation.

Table 2. Types of samples used for immunoprecipitation

Sample	Isotype control	No lysate control	Immunoprecipitation (IP)
Lysis buffer	X	Same volume as lysate	X
Lysate	500 µg	X	500 µg
Antibody	5 µg isotype control	5 µg MET antibody	5 µg MET antibody

Samples were agitated for 2 h in the cold room. Further 20 µl of 1:1 suspension of G sepharose beads were transferred into each 1.5 ml tubes (10 µl packed beads). Tubes were centrifuged at 100 rcf for 1 min at 4 °C and supernatants were discarded. Immunopreciptation samples were added to the tubes with the new beads and mixed in the cold room for 1 h. Then, the samples were centrifuged and the supernatants discarded. The

immunocomplexes were washed with 500 µl of washing buffer three times and subsequently the supernatants were aspirated. The beads were kept on ice.

2.2.13.4. Kinase Assay Sample Preparation

Table 3. Samples preparation for the MET kinase assay

Sample	Isotype control	No lysate control	No substrate control	No ATP control	Mock	Drug
UC water (µL)	80	80	85	80	80 - drug volume	80 - drug volume
10x kinase buffer (µL)	10	10	10	10	10	10
Substrate (µL)	5	5	X	5	5	5
DMSO (µL)	X	X	X	X	drug volume	X
Drug (µL)	X	X	X	X	x	drug volume
IP type (from table above)	Isotype control	No lysate control	IP	IP	IP	IP

Note: DMSO concentration was kept as low as possible. Dilutions of DX, Crizotinib and DMSO were prepared in washing buffer. A recombinantly expressed His-hGAB1 (613-694) fusion protein was used as substarte.

Prepared samples were added onto the immunocomplexes and incubated in a thermomixer (22 °C) for 5 min. 5 µl of 20 mM ATP was added to all of the samples (expect for the 'No ATP control') in 15-second intervals to start the kinase reaction. Then, samples were incubated in the thermomixer (22 °C) for 30 min. Afterwards, the kinase reaction was stopped by adding 50 µl of SDS-PAGE sample buffer in 15-second intervals. Samples were immediately heated for 15 minutes at 95 °C and centrifuged at 20,800 rcf for 1 min (4 °C). 7.5 µg of the total cell lysate and 30 µl of the supernatants were separated by SDS-PAGE (8% and 16% layers) and analyzed by Western blotting with pGAB1 (Tyr627), total MET and pMET (Tyr1234/1235) antibodies.

2.2.14 Far Western Blotting

SAS cells were seeded in 100 mm diameter cell culture dishes (1,300,000 cells/dish) and then treated for 6 h with the indicated concentration of each compound or DMSO as vehicle control (Mock). The culture medium was removed carefully and the cells were gently rinsed once with PBS. RIPA lysis buffer with 1x PIT and 3x phosphatase inhibitor cocktails 2 and 3 was used to extract the cells. The cell lysates were agitated in the cold room for 1 h and centrifuged at 20,800 rcf for 25 min (4 °C). The supernatants were transferred to new tubes and the protein concentrations were determined by Bradford assay.

Equal amounts of cell lysates were separated by SDS-PAGE and transferred onto PVDF membranes. Membranes were blocked in 10% nonfat dry milk in TBST plus sodium orthovanadate (1 mM) and EDTA (5 mM) at 4 °C overnight. On the next day, 5 µl of GST-fused SH2 domains (1 µg/µL) were diluted in 45 µl of TBST to final concentration of 0.1 µg/µl and incubated for 60 min in ice with 3 µg of anti-GST-conjugated horseradish peroxidase (anti-GSH-HRP, Abcam, #ab58626). For the binding reaction, the labeled probes were incubated with the blocked membranes in nonfat dry milk at a final concentration of 1 µg/ml for 60 min at RT. Subsequently, the membranes were washed three times for 10 min in TBST, and the bound probe was detected by chemiluminescence using the ECL kit.

2.2.15 Flow Cytometry Analysis

2.2.15.1 Cell Cycle Analysis

The DNA of cells can be stained by a variety of DNA binding dyes. The usefulness for quantification of these dyes is that they are stoichiometric, i.e. they bind in proportion to the amount of DNA present in the cell. Cells that are in S phase and G2/M phase will have more DNA than cells in G1; therefore, they will take up proportionally more dye and will fluoresce more brightly. Cells which have doubled their DNA content in G2/M phase will be approximately twice as bright as cells in G1 [289]. DAPI is commonly used in cell cycle analyses since it preferentially binds double stranded DNA, when cells are permeabilized, allowing it to intercalate with and saturate the nucleic acids. DAPI will also bind to double stranded RNA, but then emits at a longer wavelength near 500 nm. However, to entirely avoid the last problem, RNAse A was used to degrade and remove any RNA present.

TSCCs were seeded in 6-well plates for 24 h and treated with the indicated concentration of each compound or DMSO as vehicle control (Mock) for 72 h. Then the supernatant (which contains the floating dead cells) from each well and the attached cells belonging to the same well were collected into 5 ml test tubes. Cells were centrifuged (500 rcf, 5 min, 4 °C), washed with 1 ml PBS and fixed in 3 ml of cold ethanol at -20 °C overnight. Cells must be fixed or permeabilized to allow entry of the dye which is otherwise actively pumped out by living cells. While cells can be fixed with aldehydes for cell cycle analysis, ethanol fixation is favoured. The crosslinking nature of aldehydes can weaken the DNA staining when using intercalating dyes (e.g. DAPI), resulting in less precise measurement [290].

Afterwards, cells were centrifuged (500 rcf, 5 min, 4 °C), washed in PBS and the cell pellet was taken and resuspended in 1 mL of DAPI solution (1:10,000 of DAPI 20 mg/ml and 1:5,000 of RNAse A 10 mg/ml) for staining. Prepared samples were stored in the dark for 30 min at 37 °C then washed with PBS. Cell fluorescence was measured by FACS. The maximum excitation of DAPI bound to DNA, is at 359 nm, and emission is at 461 nm. Histograms of cell numbers vs. linear integrated blue fluorescence were recorded and the distribution of cells in different cell cycle phases was determined with MACSQuant Analyzer 10 (Miltenyi Biotec) flow cytometer. A total of 10,000 events were analyzed using the FlowJo (version 10) software.

2.2.15.2 Apoptosis Evaluation by Annexin V-FITC/Propidium Iodide (PI) Staining

TSCCs were seeded in 6-well plates for 24 h and treated with the compounds or DMSO as vehicle control (Mock) as indicated in each experiment. Then cells were collected by short trypsinization, centrifuged (500 rcf, 5 min, 4 °C), washed with PBS and resuspended in 100 µl of 0.5% BSA in PBS containing 10 µL of Annexin V solution. Cells were stained for 30–60 min in ice then washed with 1 ml of 0.5% BSA/PBS. After Annexin V staining, cells were stained automatically by FACS with PI (1µl per 100 µl of cell suspension) to exclude the dead cells (Figure 10). The quantitative analysis for apoptosis was performed by MACSQuant Analyzer 10 (Miltenyi Biotec) flow cytometer. A total of 10,000 events were analyzed using the FlowJo (version 10) software.
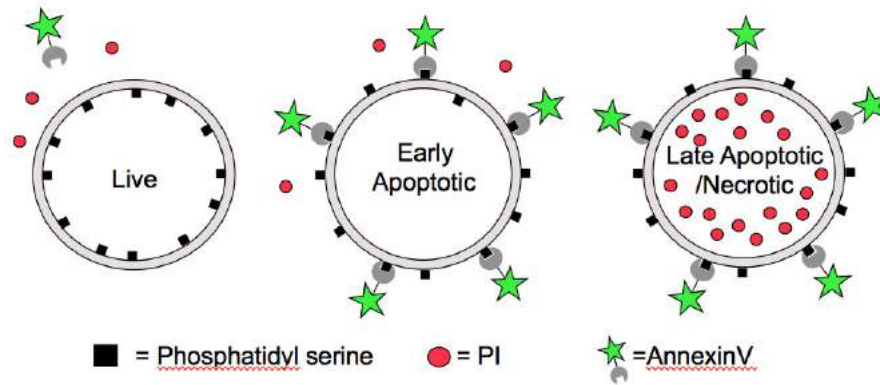
Figure 10. Apoptosis detection by Annexin V/Propidium Iodide assay

An early event in apoptosis is the flipping of phosphatidylserine of the plasma membrane from the inside surface to the outside surface. Annexin V binds specifically to phosphatidylserine and FITC labelled Annexin V can be used to detect early apoptotic cells (Excitation / Emission: 494 / 518 nm). PI is a nuclear stain used in conjunction with labeled Annexin V to measure membrane integrity (Excitation / Emission: 535 / 617 nm.). The cell membrane integrity excludes PI in viable and early apoptotic cells, whereas late apoptotic and necrotic cells are permeable to PI. Therefore, dual parameter FACS analysis allows for the discrimination between viable, apoptotic and necrotic cells. Figure from [291].

2.2.15.3 Analysis of Autophagy by Acridine Orange (AO) Staining

AO is a fluorophore that accumulates in a protonated form inside acidic vesicular organelles such as autolysosomes. AO is used to study late-stage autophagy and can be assessed by using fluorescence microscopy or flow cytometry (Figure 11).
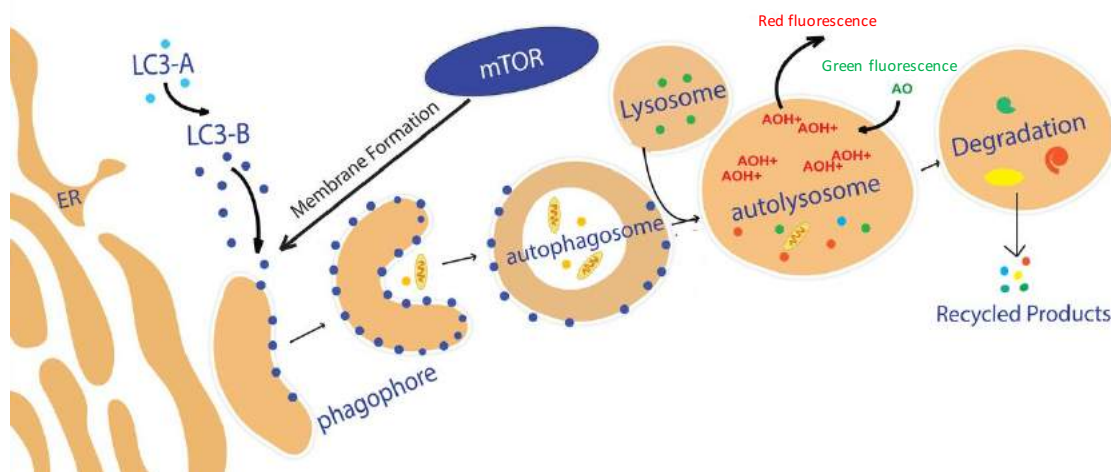
Figure 11. Acridine Orange staining for autophagy analysis by flow cytometry

The first step in autophagy induction involves the formation of a double-membraned autophagosome that engulfs cellular materials and subsequently fuses with the lysosome to form an autolysosome, where cellular materials are degraded. At neutral pH, AO is a hydrophobic green fluorescent molecule (530 nm) and when protonated (AOH$^+$) emit bright red fluorescence (680 nm). Figure adapted from [292].

TSCCs were seeded in 6-well plates for 24 h and treated with the indicated concentration of each compound or DMSO as vehicle control (Mock) for 72 h. Cells were washed and trypsinated,

consequently collected and centrifuged (500 rcf, 5 min, 4 °C). Then, cells were washed with PBS before staining with 500 µl of 10 µM AO solution for 15 min at 37 °C in the dark. Afterwards, cells were washed with PBS and the cell pellet was resuspended in 500 µL PBS for flow cytometry analysis with a MACSQuant Analyzer 10 (Miltenyi Biotec) flow cytometer. A total of 10,000 events were analyzed using the FlowJo (version 10) software.

2.2.16 Caspase-Glo 3/7 Assay

The Caspase-Glo® 3/7 Assay provides a luminogenic Caspase 3/7 substrate, which contains the tetrapeptide sequence, in a reagent optimized for Caspase activity, luciferase activity and cell lysis. Caspase 3/7 activity (Figure 12) in the treated TSCCs was determined using a Caspase-Glo® 3/7 assay kit (Promega, #G8091) according to the manufacturer's instructions. Additionally, the number of viable cells in the culture based on quantitation of the present ATP, which signals the presence of metabolically active cells, was determined by CellTiter-Glo® kit (Promega, #G7571) according to the manufacturer's instructions.
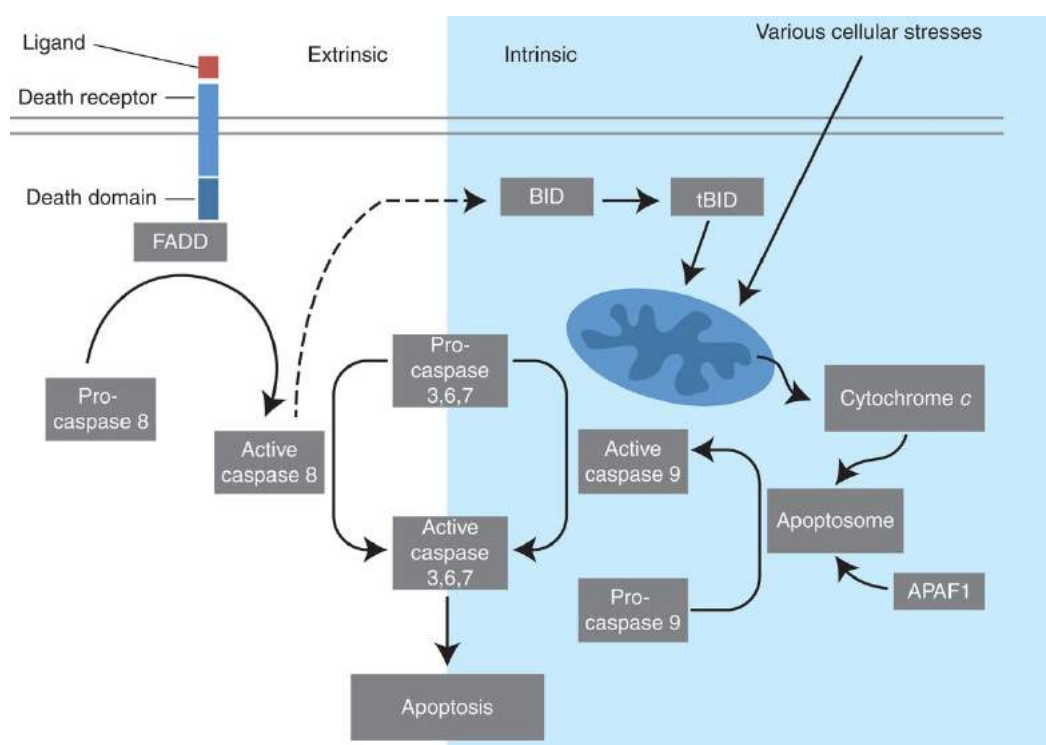
Figure 12. Extrinsic and intrinsic pathways of apoptosis

An early, biochemical event in the apoptotic process is the activation of the caspase cascade. Caspase activation involves the cleavage of the in-active Caspase by enzymes (often other Caspases) into an active form. The extrinsic apoptosis pathway is activated through the binding of a ligand to a death receptor, which in turn leads to activation of Caspase 8. Active Caspase 8 then either initiates apoptosis directly by cleaving and thereby activating executioner Caspase (3, 6, 7) or activates the intrinsic apoptotic pathway through cleavage of BID to induce efficient cell death. The intrinsic or mitochondrial apoptosis pathway can be activated through various cellular stresses that lead to cytochrome *c* release from the mitochondria and the formation of the apoptosome resulting in the activation of Caspase 9 which then initiates apoptosis by cleaving and thereby activating executioner Caspases. Figure from [293].

TSCCs were seeded in 6-well plates for 24 h and treated with the indicated concentration of each compound or DMSO as vehicle control (Mock). Growth medium was removed and

trypsinized cells were washed with PBS. 50 µl of PBS-suspended cells were transferred into white opaque 96-well plates to facilitate luminescence measurement. 50 µl of Caspase-Glo® 3/7 reagent was added and mixed in each well. The plate was covered with a plate sealer or lid and incubated at RT for 30-60 minutes. Adding Caspase-Glo® 3/7 Reagent to cell lysate lead to caspase cleavage of the substrate and generation of a luminescent signal, produced by luciferase. The luminescence of each sample was measured in a plate-reading luminometer as directed by the luminometer manufacturer (Promega, Glomax discover, GM3000).

At the same time, the total cell content was determined by mixing 50 µl of CellTiter-Glo® reagent with 50 µl of cell suspension in a white opaque 96-well plate. The plate was incubated at RT for 10 min to stabilize the luminescent signal and luminescence was recorded by the luminometer (Promega, Glomax discover, GM3000). Finally, the measured Caspase activity was normalized to the corresponding total cell content as determined by ATP concentration.

2.2.17 Senescence Detection by β-Galactosidase Staining

To detect the senescent stage of the cells, treated TSCCs were stained using a Senescence-associated β-galactosidase (SA-β-gal) Staining Kit (Cell Signaling Technology, #9860) according to the manufacturer's instructions. All solutions were prepared freshly before use and volumes stated here are for one well of a 6-well plate.

TSCCs were seeded in 6-well plates for 24 h and treated with the indicated concentration of each compound or DMSO as vehicle control (Mock) for 72 h. The growth medium was removed and the cells were washed with PBS (2 ml/well). Then, the cells were fixed in 2% paraformaldehyde for 15 minutes at RT (1 ml/well), washed twice with PBS and then incubated with staining solution overnight at 37 °C (1 ml per well) in a dry incubator without CO_2. The presence of CO_2 can cause changes to the pH which may affect staining results. On next day, while the β-galactosidase was still on the plate, the cells were checked under the Eclipse microscope for the development of blue color (10x and 20x magnification) and photographed with a Nikon camera (Coolpix E5400). For long-term storage of the plates, the β-Galactosidase staining solution was removed; the cells were covered with 70% glycerol and stored at 4 °C.

2.2.18 Bacterial Culture and Expression of Recombinant Proteins

2.2.18.1 Transformation of Bacteria

A 30 µl aliquot of competent *E.coli* (BL21 (DE3), Agilent Technologies, #200131) was thawed on ice. 1 µl plasmid in H_2O or TE buffer was added and the solution was mixed by stirring with the pipette tip. The mixture was left on ice for 15 min and then heat-shocked for 90 sec at 42 °C. Bacteria were returned onto the ice for 5 min. After cooling, 100 µl LB medium at RT was added and the bacteria were incubated for 1 h at 37 °C with agitation. 50 to 100 µl of bacterial suspensions were plated onto LB agar plates with the appropriate antibiotics.

2.2.18.2 GST-Fusion Protein Expression

5 ml of LB medium with ampicillin (100 mg/ml) was inoculated by transfer of a single colony of transformed bacteria from a selection plate. This starter culture was grown at 220 rpm and 37 °C until the medium became cloudy. 1 ml of the starter culture was then added to 300 ml of LB buffer with ampicillin for an overnight culture at 220 rpm and 37 °C. On the next day 30 ml each of the culture was added into 2 liter Erlenmeyer flasks containing 600 ml TB medium and ampicillin. The suspension was incubated for 2-3 h at 37 °C until reaching an OD600 of 0.8 - 1. Expression of GST-fusion proteins was induced with 0.1 mM IPTG and continued for 3 h at 25 °C and 130 rpm. Bacteria were harvested after the transfer of the cell suspension into centrifuge beakers by spinning at 4,000 rpm and 4 °C (J6-B, Beckman). The bacterial pellet was kept on ice for immediate lysis or stored frozen at -80 °C.

For the purification of the GST fusion protein, the bacterial pellet was resuspended thoroughly in TPE lysis buffer with protease inhibitors (aprotinin, antipain, leupeptin, pepstatin A and PMSF; for concentrations see 2.1.4.3 protease inhibitors). The lysate was sonicated on ice for 3 x 1 min intervals to break up genomic DNA and centrifuged at 20,000 rcf and 4 °C for 40 min to remove cell debris (Avanti J-25, Beckman; JA-20 rotor).

2.2.18.3 GST-Fusion Protein Purification

Appropriate amounts of GSH beads were added into the bacterial lysates and incubated overnight on a nutator at 4 °C. The sepharose beads were washed twice with TPE buffer and three times with GSH wash buffer to remove unbound bacterial proteins. GST-fusion protein was eluted with a buffer of 100 mM GSH in water adjusted with 1 M Tris pH 8.8 to pH 7. Elution was achieved by overnight incubation of beads and elution buffer at a 2:1 volume ratio on a nutator at 4 °C. The eluate was dialyzed three times against 5 liters of 5 mM Tris HCl pH 7.5 and precipitate, if any, was removed by centrifugation for 30 min at 20,000 rcf. The protein concentration was determined by Bradford assay. The integrity of the fusion protein was analyzed by SDS-PAGE and Coomassie InstantBlue staining. The SH2 domain constructs and the expression of the recombinant proteins had been described previously [294] [295].

2.3 List of Antibodies Used

Table 4. List of antibodies used in the current work

Antibody	Epitope/Comment	Source	Details	Blocking	Dilution
4G10	4G10 hybridoma	Mouse	Druker et al., 1989 [296]	BSA	1:1000
Actin		Mouse	Sigma Aldrich, #A5441	BSA	1:2000
AKT		Rabbit	Cell Signaling Technology, #4685	BSA	1:1000
Anti-GST (HRP)		Goat	Abcam, #ab58626	Milk	1:5000
Caspase 3 (3G2)		Mouse	Cell Signaling Technology, #9668	Milk	1:1000
CDC25C		Mouse	BD Biosciences, #556576	BSA	1:1000
CDK1 (CDC2)		Mouse	Cell Signaling Technology, #9116	Milk	1:1000
CDK2		Rabbit	Cell Signaling Technology, #2546	BSA	1:1000
CDK4		Rabbit	Cell Signaling Technology, #12790	BSA	1:1000
CDK6		Rabbit	Cell Signaling Technology, #13331	BSA	1:1000
CRKL		Mouse	Cell Signaling Technology, #3182	Milk	1:1000
Cyclin B1		Rabbit	Cell Signaling Technology, #12231	BSA	1:1000
Cyclin D1		Mouse	Cell Signaling Technology, #2926	Milk	1:1000
Cyclin D3		Mouse	BD Biosciences, #610279	BSA	1:500
Cyclin E1		Rabbit	Cell Signaling Technology, #20808	BSA	1:1000
EGFR		Mouse	BD Biosciences, #610016	BSA	1:2000
ERK 1/2		Rabbit	Upstate Biotechnology, #06-182	BSA	1:2000
GAB1		Rabbit	Bethyl Laboratories, #A303-288A	BSA	1:1500
Glucocorticiod receptor		Rabbit	Cell Signaling Technology, #12041	BSA	1:2000
Histone H3		Rabbit	Cell Signaling Technology, #9715	Milk	1:1000
HRP anti-Goat IgG	secondary antibody	Donkey	Jackson ImmunoResearch, #705-036-147		1:5000
HRP anti-Mouse IgG	secondary antibody	Donkey	Jackson ImmunoResearch, #715-036-151		1:5000
HRP anti-Rabbit IgG	secondary antibody	Donkey	Jackson ImmunoResearch, #711-036-152		1:5000
HSP90 (AC88)		Mouse	Enzo, #ADI-SPA-830	BSA	1:1000

Antibody	Epitope/Comment	Source	Details	Blocking	Dilution
MET (L41G3)		Mouse	Cell Signaling Technology, #3148	Milk	1:1000
Mouse (G3A1) mAb IgG1	Isotype control	Mouse	Cell Signaling Technology, #5415		
MYC		Mouse	Sigma Aldrich, #M4439	BSA	1:500
NF-KB p65 (C20)		Rabbit	Santa Crus Biotechnology, #sc-372	Milk	1:1000
p130CAS		Mouse	BD Biosciences, #610271	BSA	1:1000
p21 waf1		Rabbit	Cell Signaling Technology, #2947	BSA	1:1000
p27 Kip1		Mouse	BD Biosciences, #610241	BSA	1:500
PARP (46D11)		Rabbit	Cell Signaling Technology, #9532	Milk	1:1000
Paxillin		Mouse	BD Biosciences, #610620	BSA	1:1000
phospho-AKT	Ser473	Rabbit	Cell Signaling Technology, #4060	BSA	1:1000
phospho-CDK1	Tyr15	Rabbit	Cell Signaling Technology, #9111	BSA	1:1000
phospho-CRKL	Tyr207	Rabbit	Cell Signaling Technology, #3181	BSA	1:1000
phospho-EGFR (D7A5)	Tyr 1068	Rabbit	Cell Signaling Technology, #3777	BSA	1:1000
phospho-ERK 1/2	Thr202/Tyr204	Rabbit	Cell Signaling Technology, #9101	BSA	1:2000
phospho-GAB1	Tyr307	Rabbit	Cell Signaling Technology, #3234	BSA	1:1000
phospho-GAB1	Tyr627	Rabbit	Cell Signaling Technology, #3233	BSA	1:1000
phospho-Histone H3	Ser10	Mouse	Cell Signaling Technology, #9706	Milk	1:1000
phospho-MET (D26)	Tyr 1234/1235	Rabbit	Cell Signaling Technology, #3077	BSA	1:1000
phospho-p130CAS	Tyr410	Rabbit	Cell Signaling Technology, #4011	BSA	1:1000
phospho-p130CAS	Tyr249	Rabbit	Cell Signaling Technology, #4014	BSA	1:1000
phospho-Paxillin	Tyr118	Rabbit	Cell Signaling Technology, #2541	BSA	1:1000
phospho-PKC (pan)	Ser660	Rabbit	Cell Signaling Technology, #9371	BSA	1:1000
phospho-SRC	Tyr416	Rabbit	Cell Signaling Technology, #2101	BSA	1:1000
phospho-STAT1	Tyr701	Rabbit	Cell Signaling Technology, #9167	BSA	1:1000
phospho-STAT3	Tyr705	Mouse	Cell Signaling Technology, #9138	Milk	1:1000
phospho-STAT3	Ser727	Rabbit	Cell Signaling Technology, #9134	BSA	1:1000
phospho-STAT5	Tyr694	Rabbit	Cell Signaling Technology, #9351	BSA	1:1000

Antibody	Epitope/comment	Source	Details	Blocking	Dilution
phospho-STAT6	Tyr641	Rabbit	Cell Signaling Technology, #9361	BSA	1:1000
phospho-WEE1	Ser642	Rabbit	Cell Signaling Technology, #4910	BSA	1:1000
PKC alpha		Mouse	BD Biosciences, #610108	BSA	1:1000
PTEN		Rabbit	Cell Signaling Technology, #9188	BSA	1:1000
p-Tyr-1000		Rabbit	Cell Signaling Technology, #8954	BSA	1:2000
RAS		Mouse	BD Biosciences, #610002	BSA	1:1000
SKP2 p45		Mouse	Santa Crus Biotechnology, #sc-74477	Milk	1:1000
SRC	327 monoclonal	Mouse	Lipsich et al., 1983 [297]	BSA	1:1000
STAT5 (D2O6Y)		Rabbit	Cell Signaling Technology, #25656	BSA	1:1000
STAT6		Rabbit	Cell Signaling Technology, #9362	BSA	1:1000
WEE1		Rabbit	Cell Signaling Technology, #4936	BSA	1:1000

Chapter 3 Treatment of TSCCs with Dasatinib alone

3.1 Overview

TSCC lines exhibit considerable levels of expression and tyrosine phosphorylation of the adaptor protein p130CAS and the latter is probably caused by high levels of SRC kinase activity (Figure 4 and S1). The non-catalytic nature of p130CAS makes it difficult to develop specific inhibitors. However, SRC kinase is essential for the tyrosine phosphorylation and activation of p130CAS. Therefore, SRC kinase inhibitors like Dasatinib were applied in our laboratory to inhibit SRC and its downstream potential targets like p130CAS. Dasatinib is the clinically most used SRC inhibitor and the safety and tolerability of Dasatinib treatment have already been extensively tested in patients with hematologic malignancies. To evaluate the potential of Dasatinib alone in the treatment of TSCC, a variety of assays to measure its effects on cell proliferation, colony formation, cell cycle distribution, apoptosis, autophagy and numerous signaling pathways were used in the current work.

To further investigate the growth inhibition potential of Dasatinib in TSCCs in this thesis research, a resazurin assay was used to evaluate cell viability in three TSCC lines (SAS, CAL27, and BICR56). The resazurin assay is commonly used in cytotoxicity assays for primary screening of new anticancer agents and it has the ability to measure early indicators of toxicity which is an essential factor in drug discovery and evaluation. The resazurin calorimetric assay is based on the reduction of oxidized non-fluorescent blue resazurin to a red fluorescent dye (resorufin) by the mitochondrial respiratory chain in live cells. The fluorescent product can be detected by microplate photometer. The amount of resorufin produced and its fluorescent signal is directly proportional to cell viability [298].

Resazurin assay has some advantages over other metabolic assays like MTT and other tetrazolium reduction assays. The MTT assay produces a non-soluble formazan salt and the cells have to be lysed to solubilize this salt before the absorbance can be measured. Resazurin do not require cell lysis, keeping cell intact and allowing kinetic monitoring of the same samples at different timepoints. Also, MTT is colorimetric based assays, while resazurin can be measured using colorimetric or more sensitive fluorescence detection. Moreover, the resazurin reduction assay is slightly more sensitive than the tetrazolium reduction assays. All these advantages make resazurin a more comfortable and quicker metabolic assay and therefore it has been used by numerous groups for high throughput screen applications [299].

3.2 Dasatinib (DAS) Reduces TSCC Lines Viability in a Dose-Dependent Manner and Inhibits SRC Activation

Three investigated TSCC lines (SAS, CAL27 and BICR56) were treated with serial dilutions of DAS for 72 h. Their cell viability was then determined by the resazurin colorimetric assay. After treatment at the indicated concentrations, the viability was inhibited in a dose-dependent manner in all cell lines (Figure 13.A). These results indicate that DAS has strong an *in vitro* cytotoxic activity against TSCCs, which exhibit a high expression level of p130CAS. However, the SAS cell line shows less response to DAS than the other 2 cell lines with BICR56 seemingly the most sensitive one. In the SAS and Cal27 cell lines, Dasatinib at very high concentrations was not able to completely kill all cells which suggests that the effects of Dasatinib on cell growth are at least in part cytostatic and not cytotoxic.

A

B
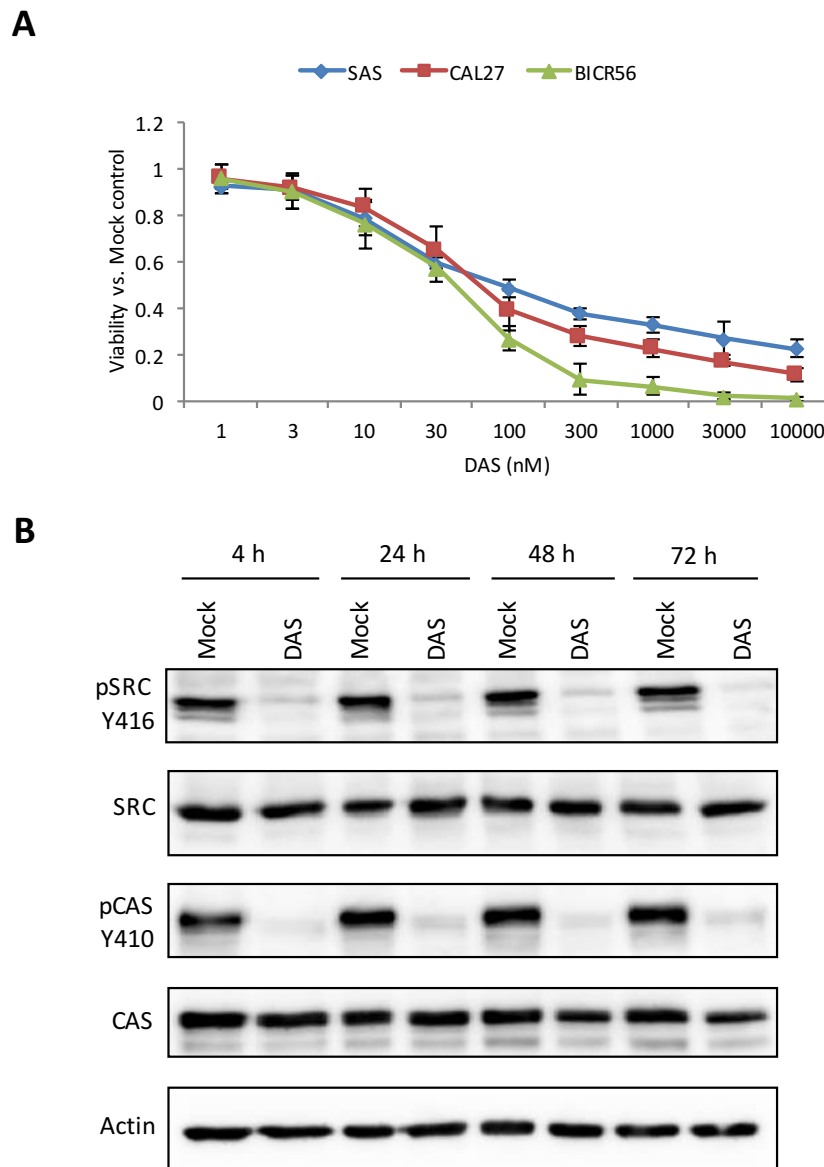
Figure 13. Dasatinib (DAS) reduces TSCC line viability in a dose-dependent manner and inhibits SRC activation and phosphorylation of SRC and p130CAS in the SAS cell line

(A) Dose-response curves of DAS in TSCC cell lines as determined by resazurin assay
SAS cells were treated with serial dilutions of DAS for 72 h. The amount of reduced resazurin (resorufin) produced is directly proportional to the metabolic activity of cells. Data represent fluorescence measurements normalized to Mock-treated cells. The dose response curves show mean values ± SD of three independent experiments with six parallel measurements in each case.

(B) DAS causes rapid and prolonged inhibition of SRC and p130CAS phosphorylation in SAS cells
Cells were treated with DMSO as vehicle control (Mock) or 100 nM of DAS for the shown time points before extraction. Total cell lysates were separated by 9 % SDS-PAGE and immunoblots were probed with the indicated antibodies. Antibodies that detect the phosphorylated state of SRC at Tyr416 and p130CAS at Tyr410 were used to monitor the change in tyrosine phosphorylation over time. The other blots analyze total protein abundance. The immunoblots shown here are representative of three separate experiments. Actin was used as a loading control.

Preclinical studies in a wide variety of solid tumor cell lines have shown that Dasatinib consistently inhibits cell proliferation, adhesion, migration and invasion but infrequently induces apoptosis. These effects support predominantly a cytostatic rather than cytotoxic function of Dasatinib [300] [301]. Because cytostatic agents are likely stop the growth of tumors

and could prevent the development of metastases without affecting tumor shrinkage, this information is important for the clinical setting and the endpoints of potential clinical trials should be selected accordingly.

Many of the targeted drugs are cytostatics, disrupting cell signaling and replication, but do not lead to an immediate decrease of tumor burden [302]. However, the distinction between cytotoxic and cytostatic drugs is not always clear cut in practical medicine. Cytotoxic compounds can also induce a cytostatic effect at low doses on apoptosis-resistant cells. Cytostatic effects often also result in cell death, for example by mitotic arrest, which is a condition that is poorly tolerated by any cell and must either be escaped or resolved by cellular death Hence this is a cytotoxic activity of primarily cytostatic agents [303].

To examine whether SRC and p130CAS inhibition is induced by Dasatinib in SAS cell line, their phosphorylation was detected after treatment with Dasatinib for several time periods. 100 nM of DAS was used to determine the inhibitory activity as this concentration is sufficient to reduce the cell viability to approximately 50% of after 72 h treatment (Figure 13.A) and is clinically achievable in humans [304]. Not unexpectedly, DAS caused almost complete inhibition of SRC and p130CAS activity, as measured by phosphorylation of Y416 and Y410, respectively, by Western blotting. These results are in agreement with data published in the literature [305] [306] [307]. This inhibition was seen at all time points examined (Figure 13.B). Because the pSRC Y416 antibody is likely to cross-react with the autophosphorylation sites of other SRC family members (LYN, FYN, LCK, YES and HCK) [201] [295], when phosphorylated at equivalent sites, the multiple bands observed in TSCC lines could be due to different SRC family kinases (SFKs) being activated and detected, but also may result from different splice variants or phosphorylation states. Also, it is likely that SFKs other than SRC are inhibited by Dasatinib. Dasatinib can inhibit other kinases like ABL, platelet-derived growth factor receptor and c-KIT. To confirm whether SFKs are responsible for the tyrosine phosphorylation of p130CAS, TSCCs were treated with the SFK-selective inhibitor compound PP2, a negative control compound PP3, or compound solvent (DMSO). The results clearly showed that pY-p130CAS was greatly reduced upon SFK inhibition (data not shown).

3.3 Dasatinib Treatment Elicits no Significant Decrease of ERK 1/2, AKT and EGFR Phosphorylation in SAS Cells

To evaluate the effect of SRC and p130CAS inhibitions by DAS on ERK 1/2, AKT and EGFR phosphorylations, SAS cells were treated with DMSO as vehicle control (Mock) or 100 nM of DAS for several time points. Substantial suppression of ERK 1/2 and AKT activity was noted after 24 h in Mock and DAS-treated SAS cells (Figure 14). It is well known that inhibition of cell proliferation occurs at high cell density by contact inhibition [308] [309]. In fibroblasts, epithelial and endothelial cells, cell-to-cell contact at high cell density causes downregulation of ERK and AKT phosphorylations [310] [311] [312] [313]. It has been suggested that the altered redox environment upon contact inhibition may contribute to the regulation of ERK inactivation by increasing protein levels of MAP kinase phosphatases (MKP-1, MKP-2, and MKP-3) [310]. Also, another study demonstrated that the decline in ERK and AKT phosphorylation was related to the Serine/Threonine phosphatase (protein phosphatase 1, PP1) activity, which was increased at the high cell density [314]. Cell-cell contacts also may modulate PI3K levels (p110 α subunit) in order to establish contact inhibition and confluence arrest, which reduces AKT activity [315].
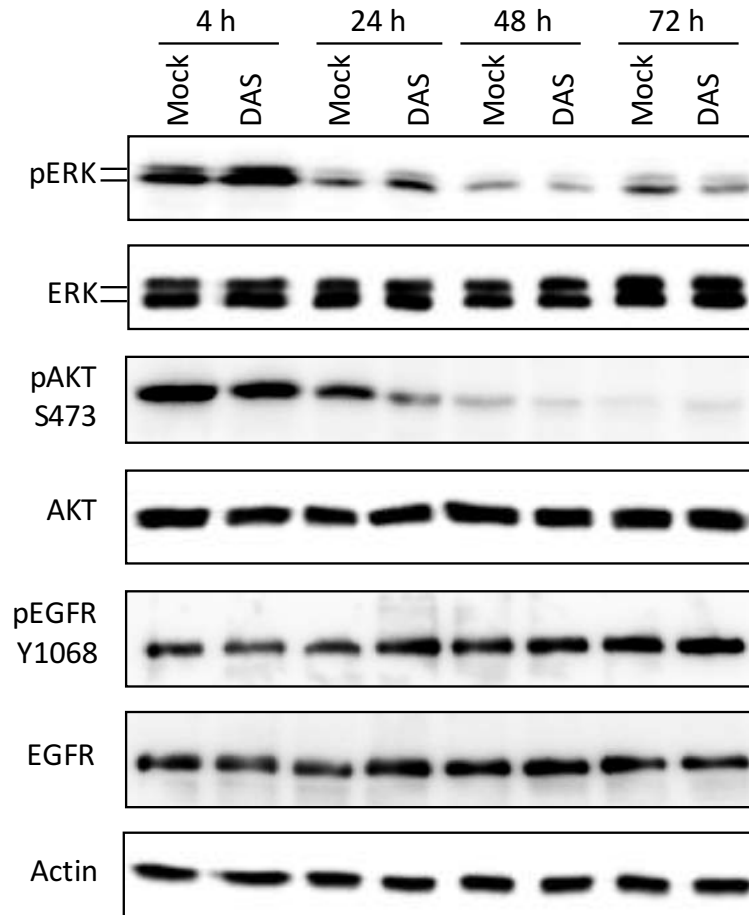
Figure 14. Dasatinib as a single treatment shows no substantial reduction of ERK 1/2, AKT and EGFR phosphorylation over time in SAS cells

SAS cells were treated with DMSO as vehicle control (Mock) or 100 nM of DAS for the shown time points before extraction. Total cell lysates were separated by SDS-PAGE and immunoblots were probed with the indicated antibodies. Antibodies that detect the phosphorylated state of ERK1/2 at Thr202/Tyr204 AKT at Ser473 and EGFR at Tyr1068 were used to monitor the changes in tyrosine phosphorylation over time. The other blots analyzed total protein abundance. The immunoblots shown here are representative of two separate experiments. Please note that the phosphorylation levels of ERK1/2 fluctuated over the investigated time points.

DAS neither downregulated EGFR nor substantially inactivated EGFR and its downstream signaling effectors AKT and ERK 1/2 (Figure 14). Instead, phospho-ERK 1/2 was slightly upregulated after 4 and 24 h treatment. In agreement with the current work, another study which investigated the role of Dasatinib in apoptosis induction in HNSCC found that SAS cell line showed similar behavior with less response to Dasatinib as single treatment after 48 h [316]. SAS cells treatment with 1 µM of Dasatinib for 24 h did not inactivate ERK, AKT or EGFR. SAS cells were initially considered to be Dasatinib-resistant cells. However, after EGFR was knocked down, Dasatinib could induce inactivation of AKT and ERK 1/2 and apoptosis which means that EGFR may play a role in Dasatinib-induced apoptosis. In the same study, two other TSCC lines (SCC-25 and HSC3) exhibited a higher response to Dasatinib than the SAS cell line after 48 h treatment. It was found that inactivation of AKT and ERK 1/2 and down-regulation of EGFR but not SRC correlated with Dasatinib sensitivity, which explains the poor response and high aggressiveness of SAS cells. Nevertheless, Dasatinib showed a cytostatic effect on all three investigated TSCC lines [316].

The MAPK pathway regulates various cellular activities and is deregulated in one-third of all cancers. The effects of ERK activation differ by cell type and influence various cellular processes such as proliferation, differentiation, survival, migration, and angiogenesis [317] [318] [319]. SRC has been described to activate the RAS/RAF/MEK/ERK pathway via recruitment of SHC and SHP2 proteins [320]. It has been observed here that ERK was slightly activated after treatment with Dasatinib. This result is in agreement with other findings which suggested that ERK activation could be enhanced as a secondary effect of Dasatinib treatment [305] [306] [321] [322]. The enhancement in phosphorylation of ERK, is known for their roles in the prevention of apoptosis and the increase of proliferation and survival [323]. ERK activation was found to mediate resistance to Dasatinib and could explain the cytostatic effect of Dasatinib in many cancers where it does not significantly kill cells or inhibit growth and survival [321] [322]. However, ERK activity was found not detectably associated with the speed of cell growth in some cancer cell lines [324].

Packer *et al*. reported that the weak binding of Dasatinib to BRAF and CRAF (weak RAF inhibitors) induces BRAF: CRAF heterodimer as well as BRAF and CRAF homodimer formation, thus leading to paradoxical activation of both BRAF and CRAF, followed by the activation of MEK and ERK [325]. Considering the complex mechanisms involved in the activation of the RAS-RAF-MEK-ERK pathway, further studies will be needed to better understand the effect of Dasatinib-induced activation of ERK.

To counteract ERK activation, MEK inhibitors could be evaluated in TSCCs as a single treatment or in combination with Dasatinib. Two MEK inhibitors, Trametinib and Cobimetinib, were approved by the FDA and the European Medicines Agency (EMA), especially for metastatic melanoma [326]. Consequently, several preclinical researches suggest the MEK and SRC combination inhibition as a promising approach to attenuate tumor growth and improve the efficacy of targeting the ERK/MAPK pathway in NSCLC [327], melanoma [328] and ovarian cancer [329]. This synergistic combination was supported for further evaluation in clinical trials. Here, in my studies, preliminary results showed an additive to slight synergistic activity of the combination of Dasatinib and Trametinib in SAS cell line in 2D culture (data not shown). This combination could be pursued and considered as a future plan to be evaluated in several TSCC lines in 2D and 3D culture. However, understanding the exact mechanistic signaling pathways mediated by this treatment would be of interest.

Chapter 4 Dasatinib and Imatinib Combination Treatment

4.1 Overview

Clinical trials have revealed that Dasatinib as monotherapy is not efficacious in the treatment of many cancers. As discussed before (section 3.2), Dasatinib as a single agent has very low or no significant clinical activity on many types of tumors, including non-small cell lung cancer [254], prostate cancer [255], breast cancer [256], melanoma [258] and HNSCC [259]. Considering this, using Dasatinib in combination with other therapeutic agents was hypothesized as a reasonable strategy and may be necessary to realize the benefits of Dasatinib's cytostatic effects on TSCCs. This could involve combining this potentially cytostatic therapy with another targeted therapy or with nonspecific cytotoxic agents. High throughput screens performed by members of our research group at Oxford University, as described in section 1.7, produced a list of possible candidates for synergistic activity with Dasatinib (Figure 8 and 9). Imatinib initially showed a strong effect with Dasatinib in SAS and CAL27 cell lines, and therefore was thought to be a possible synergistic candidate.

Imatinib was one of the earliest drugs targeted against a specific molecular target and is still one of the most effective therapeutics in this class. Imatinib is a selective TKI specifically directed against ABL, BCR-ABL, KIT, PDGFRA (Figure 7) [330]. The fusion protein BCR-ABL, a constitutively active variant of the ABL kinase, is the main cause of chronic myeloid leukemia (CML). Being an inhibitor of BCR-ABL, Imatinib rapidly and dramatically improved the treatment of CML and led to important changes in management. It received FDA approval for CML treatment in May 2001 and became the first-line therapy [331]. Imatinib increased, for many patients, the median survival of 3 to 5 years beforehand to a survival rate similar to that of the general population [332] Furthermore, it has also shown promising results in the treatment of gastrointestinal stromal tumors [333], chronic eosinophilic leukemia [334], Philadelphia chromosome-positive acute lymphatic leukaemia [335], steroid-refractory chronic graft-versus-host disease because of its anti-PDGFR action [336] and malignant melanoma [337].

Despite this major clinical advance in the treatment of CML, Imatinib resistance has become a challenging problem. The existence of patients resistant to Imatinib was noticed soon after the introduction of the drug into clinical practice [338]. Fortunately, most imatinib-resistant BCR-ABL mutants are sensitive to Nilotinib and Dasatinib, next-generation drugs that provide vital second-line treatments. Nilotinib and Dasatinib have also shown superior efficacy to Imatinib in newly diagnosed CML, inducing faster and higher rates of complete cytogenic response and major molecular responses. Consequently, both drugs are approved by the FDA to be utilized in patients with newly diagnosed CML in chronic phase [339] [340]. Dasatinib is structurally distinct from Imatinib, as it was originally developed as a SRC kinase inhibitor, but also binds both active and inactive conformations of ABL [341]. Compared with Imatinib, Dasatinib exhibits increased potency but reduced selectivity [342]. *In vitro* studies have shown that Dasatinib is at least 300-fold more potent than Imatinib against unmutated ABL [343].

For an ABL inhibitor combination strategy to work, it is crucial that Imatinib does not interfere with the ability of the SRC/ABL inhibitor Dasatinib to reach its binding site within the ABL kinase domain, even when co-administered with Imatinib at concentrations above typical clinical levels. One study reported that Dasatinib retained its full inhibitory capacity even when co-administered with Imatinib at high concentration (2500 nM) and in some cases, additive antiproliferative effects were observed in CML cells. This study also demonstrated the potential use of a combined ABL inhibitor approach for eradicating weakly Imatinib-resistant mutants [344]. In 2016, this preclinical work was translated into a very small

clinical trial which suggested that combination of Dasatinib and Imatinib may achieve long-term molecular response and provide an additive/synergistic antileukemic effect [280]. However, this study contained only 2 patients.

4.2 Combination of Imatinib with Dasatinib Shows no Significant Improvement in Viability Reduction of TSCCs

Since Dasatinib and Imatinib cotreatment showed a strong combination effect on cell viability in the HTP screen, which would be difficult to explain if both compounds target the same signaling pathway, it was assumed that Imatinib may affect other alternative targets. A combination of Dasatinib and Imatinib could target a wider range of signaling pathways and thereby target resistant clones and later on minimize acquired drug resistance. To test the potency of this combination, TSCCs were initially treated with a serial dilution of IMT (Figure 15) then individual concentrations of IMT were combined with serial concentrations of DAS to assess the synergistic activity (Figure 16, S4 and S5). IMT failed to reduce TSCCs viability within the achievable pharmacological concentrations (2 to 5 µM) [345] [346]. The reduction of cell viability by 50 µM of IMT could be the type of response associated with non-specific cytotoxicity observed at supra-physiologic concentrations for many kinase inhibitors. Many observations support the position that the targeted effects of IMT occur in the nanomolar or very low micromolar ranges, while effects in high micromolar range represent non-specific effects on a range of biological processes that lead to cell death [347] [348] [349].
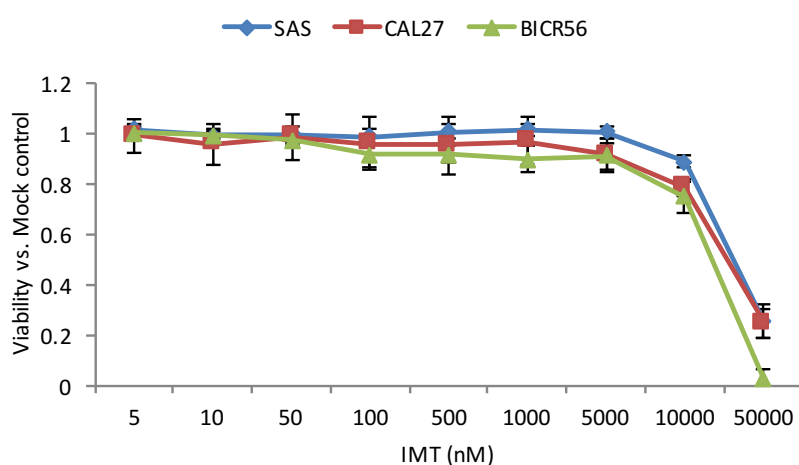
Figure 15. Imatinib (IMT) does not reduce TSCC lines viabilities at clinically relevant concentrations in 2D culture

Cells were treated with a serial dilution of IMT for 72 h and analyzed via resazurin calorimetric assay. Data represent fluorescence measurements normalized to Mock-treated cells. The dose-response curves show mean values ± SD of three independent experiments.

TSCCs were also treated with serial dilutions of DAS with or without a physiologically achievable concentration of 2.5 µM of IMT. To evaluate if the combination of both drugs is synergistic, the Bliss independence (Bliss, 1939) model, based on the idea of probabilistic independence, was utilized. The model proposes that, if two agents act in such a manner that neither one interferes with the other, but each contributes to a common result [350] [351], the expected cell viability (Expected If Additive (EIA)) can be calculated by the product of the

surviving fractions for each individual treatment. For example, if the treatment with one agent results in a surviving population of 80% and treatment with another agent results in a surviving population of 70%, we would expect for a combination of both agents a surviving fraction of 56% (0.8 x 0.7 = 0.56). If the surviving fraction for the actual combined treatment was smaller than the expected additive effect (actual < EIA), it was considered to be synergistic, if it was the same its additive (actual = EIA), or if it was larger it was considered to be antagonistic (actual > EIA) activity.

Treatment of SAS cells with increasing concentrations of Dasatinib at a fixed concentration of 2.5 µM IMT which, on its own did not have any effect on cell viability (Figure 15), did not show any improvement in Dasatinib activity in comparison to Dasatinib single treatment (Figure 16, S4 and S5). Combining Dasatinib with a higher concentration of 10 µM IMT, which is supra-physiological concentration [346], with a serial dilution of DAS shows at best a negligible improvement in DAS activity (Figure 16, S4 and S5). IMT concentrations of 400 nM and 5 µM were tested and they also did not exhibit any significant additive or synergistic activity with DAS in SAS, CAL27 and BICR56 cells (data not shown). This data suggest that Imatinib does not exhibit any synergistic or even additive activity with Dasatinib in the normal physiological concentration or even higher in 2D culture.

Different results have been reported by Rossi *et al.* in gastrointestinal stromal tumor (GIST) [352]. Treatment of GIST mice with Imatinib plus Dasatinib produces an increased clinical response in an additive manner and down-regulated four oncogenic cascades in GIST: the PI3K, SRC, MAPK and STAT pathways. Imatinib is front-line therapy for GIST but eventually, patients develop acquire resistance. It has been found that tumor maintenance and Imatinib resistance occur due to enhancement of integrin signaling by Imatinib and consequently FAK, SRC and LYN activation. This could explain the additive activity of SRC inhibitor Dasatinib in GIST.

In TSCC, there is no contribution from Imatinib in cell survival inhibition with or without Dasatinib within the normal physiological concentration or even with greatly higher concentration. This could be explained by complete ABL inhibition with Dasatinib, which is much more potent against ABL than Imatinib (300-fold) [343], without any additional benefits or role for Imatinib in extra targets. Another possibility could be that ABL and other Imatinib targets are not overexpressed nor highly activated in TSCC. A similar outcome for a Dasatinib+Imatinib combination was seen for cases of highly Imatinib-resistant mutants of CML cells [344]. In this study, treatment of CML cells expressing the Y253F mutation of BCR-ABL with Dasatinib alone was already very efficient in inhibiting CML cells (IC_{50} of 2.3 nM), whereas addition of 0.75 µM or 1.5 µM Imatinib only insignificantly decreased the IC_{50} to 1.8 nM or 1.5 nM, respectively [344].

Based on the obtained results in this work, Dasatinib+Imatinib combination in TSCC is not considered to be sufficiently promising for a follow-up and further alternative therapeutic options should be assessed.

A

B
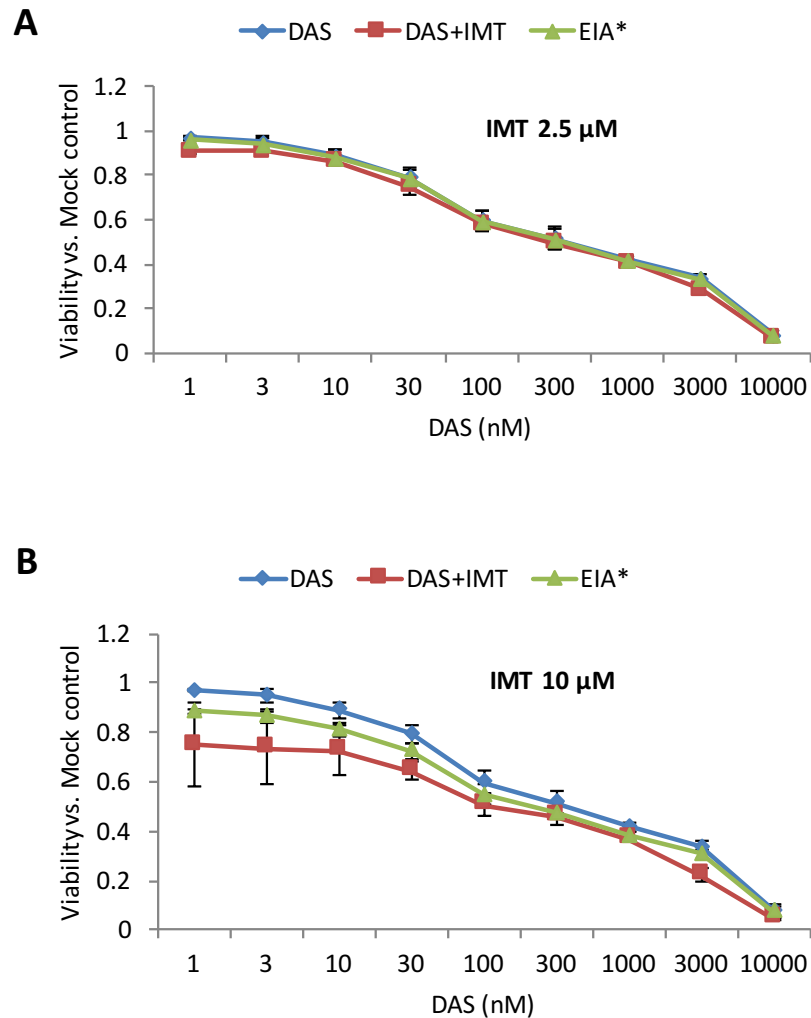
*Expected If Additive (EIA)

Figure 16. Imatinib (IMT) shows no additional activity when added to DAS in 2D cultured SAS cells

SAS cells were treated with a serial dilution of DAS and the indicated concentration of IMT for 72 h. Cell inhibition activity of DAS, as measured by resazurin calorimetric assay, was not detectably improved by addition of 2.5 µM of IMT or even with 10 µM of IMT (super pharmacological concentration). Cell viability upon treatment with 2.5 µM and 10 µM is 98% and 82% respectively. Data represent fluorescence measurements normalized to Mock-treated cells. The dose response curves show mean values ± SD of three independent experiments with six parallel measurements in each case.

Chapter 5 Dasatinib and HSP90 Inhibitor Combination Treatments

5.1 Overview

Heat shock proteins (HSP) are a family of proteins that are produced by cells in response to exposure to stressful conditions. They were first described as proteins expressed by *Drosophila* larvae upon short term exposure to an increased temperature [353], but are now known to be also expressed in many biological systems during other stresses including exposure to cold [354], UV light [355] and wound healing or tissue remodeling [356]. At least five main families of HSPs have been described. These families are categorized according to their molecular weight: HSP100, HSP90, HSPP70, HSP60, and HSP27. HSPs account for 1–2% of total protein in unstressed cells. However, when cells are heated, the fraction of heat shock proteins increases to 4–6% of cellular proteins [357]. HSP90 proteins are the most common representatives of the heat shock-related proteins.

HSP90 family proteins are a ubiquitously expressed molecular chaperones that maintains cell protein homoeostasis under normal and, especially, stress conditions. There are several members in the HSP90 family: cytoplasmic HSP90α (constitutive expression) and HSP90β (inducible expression), mitochondrial TRAP, and endoplasmic GRP94. The cytoplasmic forms are particularly important for cell survival [358]. HSP90 and its paralogues/homologues have three structural domains: an N-terminal domain, which contains the ATP binding site, is connected to a middle domain through a variable charged linker, and a C-terminal domain which is responsible for HSP90 dimerisation. HSP90 catalyzes the decomposition of ATP into ADP and a free phosphate ion, hence they are called ATPases [359]. The charged linker domain was found to be essential in the chaperone function, interaction, and flexibility [360]. HSP90 forms homodimers with the contact sites localized within the C-terminus in an open conformation of the dimer. HSP90 is a highly dynamic and flexible chaperone that can adjust its conformation to the broad variety of substrates (client proteins) with which it works. Large conformational rearrangements are also required for the activation of these client proteins. One driving force for these rearrangements is the intrinsic ATPase activity of HSP90 which is essential for the chaperone cycle and binding the HSP90 client proteins [361].

In normal cells, HSP90 is involved in folding, modifications, and functionality of key proteins necessary for cell survival and proliferation. It is also involved in regulating the activity, maturation, localization, protection and turnover of a large set of client proteins in the cytoplasm [362] [363]. These clients are involved in activities such as transcription, translation, mitochondrial function, cell cycle and signaling kinase. A list of HSP90 interactors can be found here [364].

The function of HSP90 is controlled by a group of co-chaperones that controls its ATPase cycle, which allows client acquisition and selection [365]. In contrast to other chaperone systems, HSP90 recognizes a metastable structural element in its clients rather than a primary amino acid sequence. This explains its ability to promote conformational maturation step and enables clients to bind to ligands, but also to interact with cofactors and complete their biological function [366]. To date, many HSP90s clients have been reported to play an essential role in many cellular processes including cell cycle control, cell survival, hormone and many of these are also involved in tumorigenesis [365] [367] [368] [369].

HSP90 stabilizes various growth factor receptors [370], some signaling molecules including PI3K and AKT proteins and mutant proteins such as SRC, the fusion oncogene BCR-ABL, and mutant forms of p53 that appear during cell transformation. It appears that HSP90 can act as

a "protector" of less stable proteins produced by DNA mutations [371]. Hence, tumor cells are particularly dependent on HSP90, much more than normal cells. The dependence of multiple oncogenes on HSP90 can make cancer cells hypersensitive to HSP90 inhibition; and therefore HSP90 inhibitors could play a major role in cancer treatment [372]. Also, cancer cells actively utilize HSP90 in the repair of damaged proteins and, in this way, HSP90 contributes to sustaining survival and proliferation [373]. The overexpression of HSP90 is often detected in cancer and is correlated with aggressive behavior and poor outcome like gastric cancer, myelodysplastic syndrome and breast cancer [374] [375] [376]. Although immunohistochemistry had revealed HSP90 expression in TSCC, there was no correlation found between HSP90 staining and survival period, stage, lymph node metastasis, histological grade or p53 immunostaining [377].

Targeting HSP90 leads to the accumulation of unfolded proteins which involves alterations in the transcriptional and translational aspects of stressed cells and leads to cell death if the cells cannot overcome the stress [378]. Therefore, HSP90 inhibition was proposed to be an efficient anticancer strategy, either by itself or in combination with other drugs. To date, numerous specific pharmacological inhibitors targeting both, the N- and the C-terminal domain, of HSP90 have been identified. HSP90 inhibition became a novel approach of anticancer activity, in which the drug acts not by binding to the oncoprotein or by inhibiting the enzymatic activity, but by binding to a molecular chaperone complex causing dissociation of the oncoprotein from the protective activity of the chaperone and subsequent degradation [379].

At least 18 HSP90 inhibitors (HSP90i) have entered the clinic, all of which, though structurally distinct, target the ATP-binding site of the chaperone N-terminus. Currently, there are only five HSP90 inhibitors in clinical trials and there is no FDA-approved drug in this class, yet [380]. The major problem, apart from high toxicity [381], is that there exist very few predictive or pharmacodynamic biomarkers for predicting the anticancer activity in a particular setting [382]. Another problem is that, in cancer, HSP70 can partially substitute for HSP90 function, rendering cells resistant to the treatment [383]. However, at least some HSP90 inhibitors accumulate in malignant cells to a greater extent than the surrounding tissue which make them more toxic to malignant cells than to normal tissues [384]. In support of this observation, Kamal and coworkers confirmed that the apparent accumulation of HSP90 inhibitors in tumor cells following systemic administration could result from the increased affinity of HSP90 present in cancer cells as compared to normal cells [385]. HSP90 derived from tumor cells had a 100-fold higher binding affinity for HSP90i than did HSP90 from normal cells. Tumor cells were found to contain HSP90 complexes in an activated, high-affinity conformation to facilitate malignant progression, and that may explain the high affinity and represent a suitable target for cancer treatments by HSP90i.

A recent review summarizes 15 phase II clinical trials using HSP90 inhibitors alone or in combination therapy and found that HSP90 inhibitors may be beneficial against a variety of oncogene‑addicted cancer types, including those developing resistance to specific receptors [386]. However, only tumor types driven by client proteins that are hypersensitive to HSP90 inhibition will be susceptible to the effects of HSP90 inhibitors. The lack of efficacy of HSP90 inhibitors in the initial phase II studies was potentially due to treatment-associated toxicity leading to insufficient doses of drugs being given and infrequent schedules of administration, which leads to a lack of adequate inhibition of target proteins [386]. To maximize the benefit of the HSP90 inhibition, treatment-response biomarkers and rational combinational protocols

should be developed. The last issue could be solved by finding proper synergistic treatments which could reduce HSP90i intake to acceptable non-toxic dose.

The first-generation HSP90 inhibitor Geldanamycin showed promising synergistic activity with Dasatinib during the high throughput screen in two TSCC cell lines (Figure 8). Geldanamycin is a natural product derived from *Streptomyces* and binds to the N-terminal nucleotide pocket of HSP90, leading to inhibition of the ATPase activity [387]. Despite promising *in vitro* and *in vivo* efficacy, Geldanamycin failed to reach any clinical trial owing to its poor solubility, chemical and metabolic instability, and hepatotoxicity [388] [389] [390]. However, Geldanamycin served as a starting point for various drug discovery programs which ultimately led to the development of distinct chemical entities [391].

5.2 TSCCs are Highly Sensitive to HSP90 Inhibitors in 2D Culture

Due to the preclinical limitations of Geldanamycin, six other HSP90 inhibitors that belong to the second generation of inhibitors were investigated in this work. Initially, the inhibitors were tested for their cytotoxic activity in TSCC and then for their synergistic activity with Dasatinib. These compounds share the ability to bind the N-terminal ATPase site of HSP90 with higher affinity and lesser toxicity than Geldanamycin and prevent the chaperone from cycling between its ADP- and ATP-bound conformations. AT13387, TAS-116, Ganetispib, Luminespib, HSP990 and XL888 had been enrolled in clinical trials, however, only three are still undergoing clinical evaluation (AT13387, TAS-116 and XL888) [380].

TSCCs were treated with serial dilutions of the investigated inhibitors for 72 h. The chemosensitivity of the TSCCs was determined by employing a resazurin colorimetric assay as presented in Figure 17 and S6. The three cell lines were found to be very sensitive to the HSP90 inhibitors and all exhibited a response within the achievable peak plasma concentrations of the drugs. All inhibitors showed a steep dose-response curve which means that very little response before the IC_{50} was seen. Also, a drug concentration slightly above the IC_{50} can lead to high levels of inhibition and any small increases of drug concentration can produce a large increase in cytotoxic activity. The plateau in this curve suggests that after a certain threshold dose, further increases do not lead to enhance response. However, this is in contrast to most other classes of therapeutic agents, which exhibit a sigmoidal dose-response relationship with a linear relationship between dose and response over a relatively broad range of drug doses [392]. Most anticancer agents which have a steep dose-response relationship have a narrow therapeutic index [393]. Although the prediction of the IC_{50} from the steep dose-response curve is difficult, it is still useful for predicting the *in vitro* response to chemotherapy.

HSP90 inhibitors as single-agents exert predominantly cytostatic effects rather than cytotoxic effects in both preclinical models and in patients [394]. Modulating a driver oncoprotein with two inhibitors, using a combination of a drug that directly inhibits its kinase function together with overall protein level, could be particularly damaging for the cancer cell. It has been noted that ATP-competitive kinase inhibitors not only suppress enzymatic activity but also block access of kinase clients to the HSP90 chaperone machinery, resulting in client degradation [395]. HSP90i combination with other, more molecularly targeted, agents may also help to enhance tumor-selective killing *in vivo* [396]. This could give new mechanistic insight into the action of protein kinase inhibitors and increases the exciting possibility that simultaneous treatment with both a kinase inhibitor (e.g. SRC

inhibitor) and an HSP90i may not only enhance the suppression of kinase activity but also potentiate the depletion of driver oncoproteins [397].

A

B
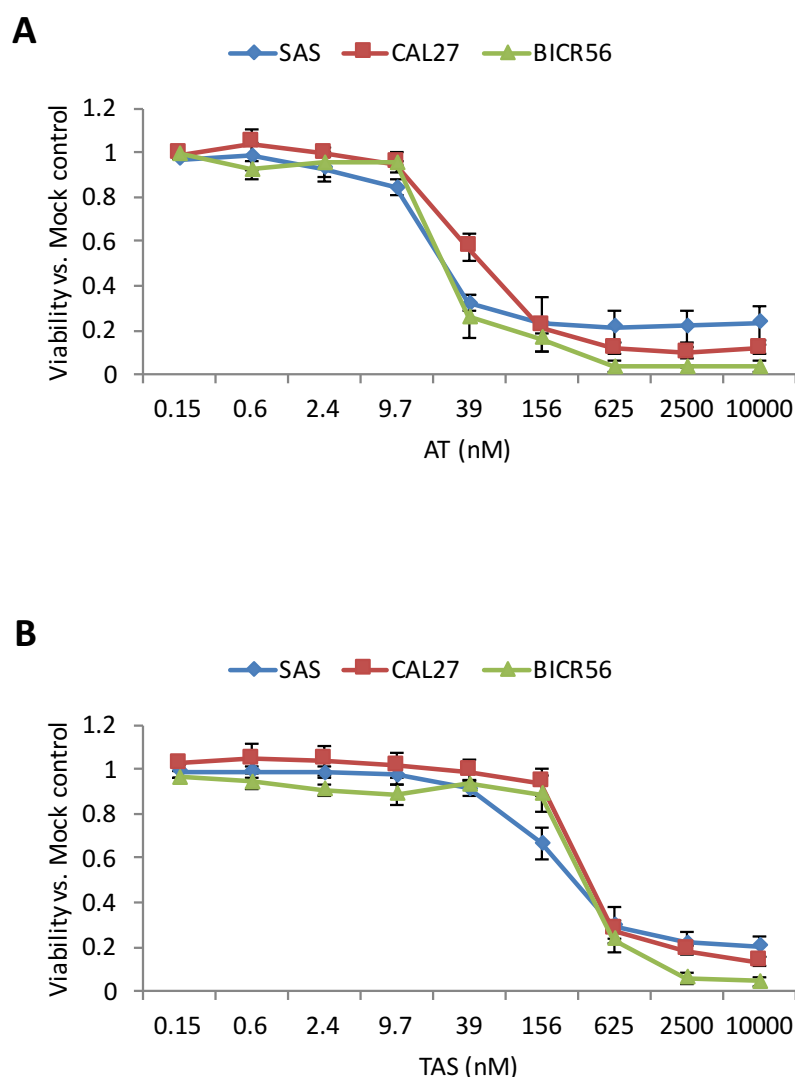
Figure 17. HSP90 inhibitors reduce TSCC line viabilities in a dose-dependent manner

TSCC lines were treated with serial dilutions of (A) TAS-116 (TAS) or (B) AT13387 (AT) for 72 h and analyzed by resazurin colorimetric assay. Data represent fluorescence measurements normalized to Mock-treated cells. The dose-response curves show mean values ± SD of three independent experiments with six parallel measurements from separate wells in each case.

HSP90 inhibitors have been found to potentiate the activity of various chemotherapeutic agents including TKI. HSP90 inhibitors affect multiple targets including signaling kinases, which prevents oncogene switching and results in a more prolonged and robust inhibition of downstream signaling pathways in cancer cells than it is possible to achieve with individual TKIs like Dasatinib [398] [399]. To date, there are no clinical trials that have tested SRC and HSP90 inhibition combination therapy. However, many other TKIs were combined with HSP90i in different cancers. For example, it has been shown that targeting HSP90 by 17-AAG can prevent the escape of breast cancer cells from EGFR-inhibition by Gefitinib. Gefitinib was found to induce SRC activation which mediates downstream signaling rebound in SKBR3 cells and the combination of HSP90i and Gefinitinb was more effective and long-lasting than Gefinitinb alone [398].

AT13387 in combination with the BRAF inhibitor Vemurafenib in melanoma was found to delay the emergence of resistance and cell lines with acquired Vemurafenib resistance or with acquired resistance to both BRAF and MEK inhibitors were found to be still sensitive to HSP90i treatment [400] . Moreover, the capacity of HSP90i Ganetespib to potentiate the *in vivo* activity of particular EGFR TKIs (Erlotinib and Afatinib) had been proven in NSCLC and could provide a possible rationale for combining these agents as part of novel treatment strategies to overcome mechanisms of resistance across a spectrum of NSCLC patients [399]. However, the clinical efficacy of TKI and HSP90i combinations is still under investigation [401].

5.3 Dasatinib Synergizes with HSP90 Inhibitors to Reduce TSCCs Viability in 2D Culture

The cytotoxic activities of Dasatinib in combination with the six HSP90 inhibitors were evaluated in 2D culture for a possible synergistic activity in TSCCs. In preliminary screens, several concentrations of HSP90 inhibitors were tested in combination with serial dilutions of Dasatinib and analyzed using the resazurin colorimetric assay to assess the cell viability. Additionally, defined concentrations of Dasatinib were combined with serial dilutions of the HSP90 inhibitors to look for possible synergistic activity. Based on these preliminary data (data not shown), AT13387 (AT, Onalespib) and TAS-116 (TAS) exhibit promising additive to slight synergistic activity with Dasatinib in TSCC in 2D culture and were chosen for further analysis. Importantly, they are also till currently undergoing clinical evaluation alone or in combination therapy in advanced solid tumors, NSCLC, GIS, HNSCC, breast cancer and recurrent melanoma [401 402 403 404 405 406 407]. The last feature is a very important point for future clinical application.

AT13387 and TAS-116 are structurally distinct ATP-competitive HSP90 inhibitors. AT13387 is a member of resorcinol-derived HSP90 inhibitors and has similarity to radicicol which is a macrocyclic antibiotic originally isolated from the fungus *Monosporium bonorden* [408]. AT13387 was discovered following optimization of a resorcinol-containing lead generated through a fragment-based drug discovery approach. The resorcinol core is maintained as a critical element for binding in a number of molecules that entered clinical trials including NVP-AUY922, KW-2478, and STA-9090. TAS-116 ,on the other hand, is a novel and selective inhibitor of HSP90α and HSP90β and has a different structure from Geldanamycin-derived HSP90 inhibitors that showed excess hepatotoxicity or brain-penetrable HSP90 inhibitor that have neurological toxicities [409]. One of the most notable HSP90-related adverse events universally observed to differing degrees in the clinical setting is visual disturbance. TAS-116 has shown less ocular toxicity than conventional HSP90 inhibitors [410]. Testing two structurally different HSP90 inhibitors should help to confirm that the obtained effect is related to the mechanism of action, which is HSP90 inhibition, but not associated, with an off-target effect of a single drug or drug class.

TSCCs were treated with serial dilutions of Dasatinib with and without a constant concentration of AT or TAS. Cell viability was determined by resazurin colorimetric assay after 72 h. Both AT and TAS concentrations investigated can significantly reduce cell viability (Figure 17) and are clinically achievable in the plasma. Dasatinib dose-response curves and combination dose-response curves are shown in Figure 18, S7 and S8. Expected additive effects were calculated by using the Bliss Independence model as described above (section 4.2) to evaluate potential synergy. Over the investigated concentration range of Dasatinib, the addition of 30 nM of AT or 300 nM of TAS causes a cytostatic effect on SAS cells which

significantly differs from treatment with Dasatinib alone (Figure 18). The combination treatments showed an additive to slight synergistic effect in TSCCs.

A

B

*Expected If Additive (EIA)
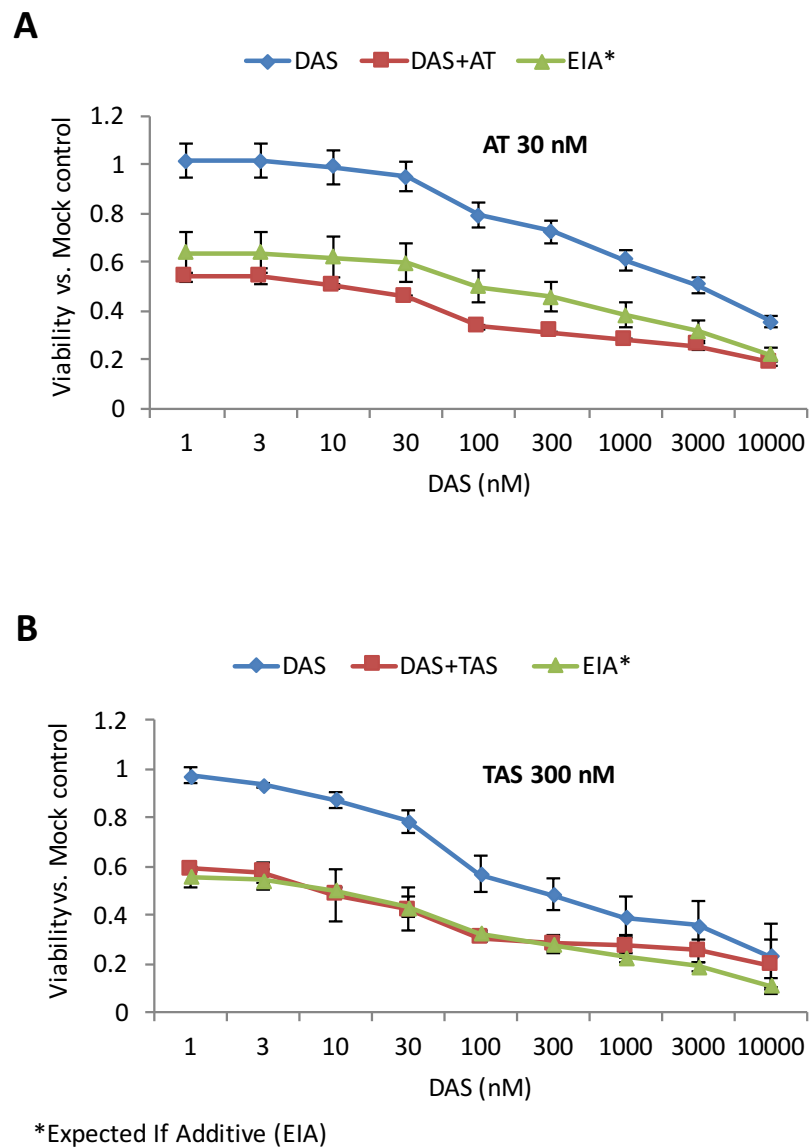
Figure 18. Combined treatment of SAS cells with DAS and HSP90 inhibitors demonstrates an additive or a weak synergistic effect on cell line viability

SAS cells were treated with serial dilutions of DAS plus (A) 30 nM of AT or (B) 300 nM of TAS for 72 h. Cell viability after treatment was measured by resazurin colorimetric assay. The cell inhibition activities of DAS alone and HSP90 inhibitors alone were measured in the same experiment and used to calculate the expected values. Data represent fluorescence measurements normalized to Mock-treated cells. The dose response curves show mean values ± SD of three independent experiments with six parallel measurements in each case.

5.4 Reduction of Soft Agar Colony Formation Activity by Dasatinib is Potentiated by HSP90 Inhibitors in TSCCs

5.4.1 Overview

Most of the cell-based data assume that cells in 2D monolayer reflect the essential physiology of real tissues. However, it is generally known that the plastic or glass substrates that are commonly used for cell culture are not representative of the cellular conditions observed in organisms. In fact, tissue-specific construction, mechanical and biochemical signals and cell-cell communication are lost under such simplified conditions. Studies have shown that growing cells within 3D scaffolds reduces the similarity gap between cell cultures and physiological tissues [411]. 3D cell cultures that allow physiological cell-cell and cell–ECM interactions can mimic the specificity of real tissues better than conventional 2D cultures. It can be assumed that a 3D approach has the potential to improve the physiological relevance of cell-based assays and advance the modeling of biological systems from cells towards organisms.

The soft agar colony formation assay measures the ability of cells to proliferate in semi-solid matrices and is an important pre-clinical technique that can be used to assess the tumorigenicity of a wide range of cancer cells (breast, prostate, ovarian, and others) with regards to their sensitivity to drugs, hormones and a multitude of other treatment conditions [412]. In this environment, non-transformed cells are unable to rapidly propagate in the absence of anchorage to the extracellular matrix and undergo apoptosis, a process known as anoikis. In contrast, cells that have undergone malignant transformation lose their anchorage dependence and able to grow and form colonies within the semi-solid soft agar matrix [413].

5.4.2 DAS, AT and TAS Reduce 3D Soft Agar Colony Formation in a Dose-Dependent Manner in the SAS Cell Line

To further validate the efficacy of tumor growth inhibition by DAS, TAS and AT in TSCC lines in 3D culture, soft agar assays were employed. SAS cells were seeded into soft agar layers and treated with serial dilutions of the investigated compounds. Cells were maintained in culture for an additional 14 days to allow the formation of colonies with continuous feeding as described in the experimental section (2.2.6). The rate of colony formation in soft agar varies depending on the cell type. Therefore, the number of cells to start was optimized and adjusted accordingly before seeding. In addition, the colony size varies depending on the growth rate of each cell line. Hence, a predefined cut-off for colony size of 50 µM diameter was used to count viable colonies for the quantitative analyses. Only colonies above the size cut-off were quantified to avoid inclusion of non-proliferating cells derived from the initial plating.

The individual drugs tested reduce colony formation in a dose-dependent manner as shown in Figure 19.A and C. Colony formation reduction in the treated SAS cells compared to the Mock-treated cells indicates anchorage-independent growth inhibition which is a hallmark of anoikis (apoptosis) resistance and the path to further steps in metastasis [413]. As in 2D culture (Figure 17), AT13387 and TAS-116 demonstrated nanomolar potencies against SAS cells in soft agar, whereas Dasatinib was less potent in 3D soft agar than 2D culture, as presented in dose-response curves in Figure 19.B and C. Only at 10 µm DAS was there a notable decrease in colony formation compared to control values. CAL27 and BICR56 cell lines are more

sensitive to Dasatinib in 3D soft agar culture and their 2D and 3D dose-response curves correlated more closely than SAS cell line (Figure S9). However, in general, Dasatinib exhibited less activity in 3D soft agar in all TSCC lines.
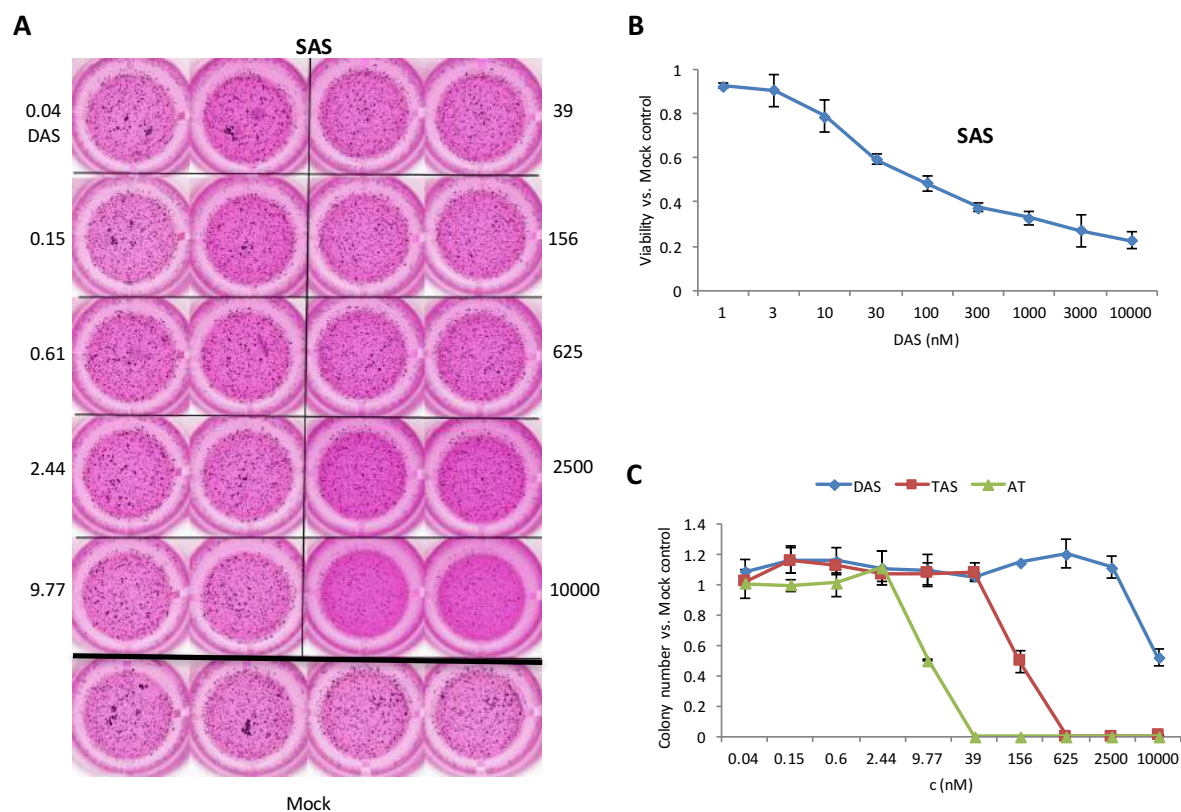
Figure 19. 2D and 3D assays show a reduction in cell viability and colony formation in a dose-dependent manner in SAS cells after treatment with DAS, AT and TAS

(A) Image of colonies from SAS cells treated with the indicated nM concentrations of DAS in a 3D soft agar colony formation assay
SAS cells were treated with DMSO as vehicle control (Mock) or a serial dilution of DAS. Cells were continuously fed for 14 days and colonies were counted after staining with NBT overnight. The image is representative of two separate experiments.

(B) Dose response curve of SAS cells cultured in 2D and treated with DAS as determined by resazurin colorimetric assay
SAS cells were treated for 72 h with DMSO as vehicle control (Mock) or a serial dilution of DAS. Data represent fluorescence measurements normalized to Mock-treated cells. The dose-response curve shows mean values ± SD of three independent experiments with six parallel measurements in each case.

(C) Dose response curves of SAS cells treated with DAS, AT and TAS as determined by colony formation in 3D soft agar assay
SAS cells were treated with DMSO as vehicle control (Mock) and serial dilutions of DAS, TAS or AT. Four wells were counted for each treatment condition. Colony numbers were normalized to Mock-treated cells. The dose-response curves show mean colony number values ± SD of two independent experiments.

This is not entirely unexpected. several studies document that cells cultured in 3D models are usually less sensitive to anticancer drugs than those in 2D cultures [414] [415]. Hsieh and colleagues showed that unstable culture conditions, which sometimes occur *in vitro*, and the type of culture method can significantly influence cellular metabolic activity, cell

70

proliferation and, ultimately, changes in cell sensitivity to tested drugs [416].The considerations for variations in drug response between 2D and 3D cultures may include a decrease in drug penetration and gradients or reduced access to compounds in the 3D medium [417] [418]. This effect may be caused by physiological differences due to hypoxia, changes in the cell cycle, altered gene expression, augmented survival signaling and DNA repair [419] [420] [421]. Also, the activation of genes involved in cell survival and drug sensitivity due to limited diffusion through the soft agar can reduce sensitivity [422].

It was shown that cancer cell lines grown in 2D and 3D models can have very different gene expression levels of various genes responsible for the proliferation, chemosensitivity, angiogenesis and invasion [423]. One possible explanation for the observed difference between 2D and 3D responses to Dasatinib was reported by Schmidt *et al.* [424]. In this study, substantial shifts in gene expression between 2D and 3D growth of 12 HNSCC lines including 3 TSCC lines (CAL27, SCC4 and PE/CA.PJ41) were detected. While cell adhesion and cell junction gene expression increased, DNA replication/cell cycle genes, as well as base excision DNA repair genes expression, decreased in HNSCC. Also, it found the upregulation in genes involved in the cytochrome P450-mediated metabolism of xenobiotics, including drugs.

Dasatinib could mainly repress adhesion in TSCC by inhibition of focal adhesion complex including CRKL, Paxillin and p130CAS (Figure 13.B) [305] [306]. Upregulation of adhesion genes may therefore interfere with this activity and reduce Dasatinib effectiveness. Also, it was hypothesized that a deficiency in DNA mismatch repair may explain some forms of multicellular resistance [420]. Cytochrome P450 is responsible for the metabolism of many drugs including Dasatinib which is metabolized and eliminated primarily through cytochrome P450 according to clinical and preclinical data [425]. Also, it has been shown that elevated levels of this enzyme may contribute to drug resistance [426]. Dasatinib is a substrate for cytochrome P450 and, as this drug exhibits decreased efficacy in 3D cells, it is likely that the increased P450 activity in 3D cells could be at least partially responsible for the decreased drug efficacy observed in 3D cells. However, AT13387 and TAS-116 are not metabolized by cytochrome P450.

As an increase in tyrosine kinase receptors has previously been associated with resistance to TKIs, it could be the case that the overexpression of these receptors in 3D cells mediates part of the resistance of the cells cultured in 3D to the effects of Dasatinib, in comparison to 2D [427]. Moreover, increased levels of drug transporters like PGP and BCRP were found to reduce the levels of substrate drugs within cells in 3D, therefore this may contribute to the decrease in drug efficacy observed in 3D cultures [428]. The considerations for changes in drug response between 2D and 3D cultures may also be related to the reduction in Dasatinib stability during the long treatment time (14 days or more) or pH change. It was shown that Dasatinib undergoes degradation under light, acidic, basic and oxidative conditions which may reduce the drug uptake [429].

Another method like the 3D spheroid assay could be used to confirm the previous results and to determine cell viability, proliferation and migration in 3D culture. Recently, spheroid formation in low-attachment round-bottom plates has become popular as the method offers a simpler workflow and is suitable for high-content imaging. By staining with vital cell-specific dyes like fluorescent dyes, real-time monitoring of drug effects can be monitored with this assay using bright-field and fluorescence microscopy or IncuCyte™ [430]. Also, the soft agar colony formation assay has been modified, in more recent years, to address specific needs. One variation involves the incorporation of fluorometric dye to allow for high-throughput colony counting [431].

5.4.3 HSP90 Inhibitors Potentiate the Soft Agar Colony Formation Reduction Effect of DAS in TSCCs

Having found growth-inhibiting potentials of DAS and HSP90 inhibitor combinations in 2D culture, the effects of combining both types of inhibitors on colony formation of TSCC were assessed in soft agar culture. Constant doses of AT and TAS were chosen from the dose-response curves (Figure 19) for the subsequent experiments. Both concentrations are clinically relevant and slightly reduced the colony formation in the 3D soft agar culture. SAS cells were treated with DMSO as vehicle control (Mock) and serial dilutions of DAS with or without 10 nM of AT and the colony formations after 14 days of incubation are presented in Figure 20.A and B. The colony formation assays show that DAS inhibits the clonogenic ability of SAS cells in a dose-dependent manner (Figure 20.A) and combining Dasatinib with 10 nM of AT significantly potentiates colony formation inhibition (Figure 20.B).

The number of colonies was quantified as described in the experimental section (2.2.6.6). Colony numbers after treatment with DAS alone and with DAS+AT are presented in Figure 20.C. The colony number after treatment with AT alone was counted within the same experiment (Figure 20.B) and it was used to calculate the expected values (EIA) by multiplication of the surviving fractions as described previously (section 4.2). The calculated values determined whether drugs combinations had synergistic (actual < EIA), additive (actual = EIA) or antagonistic (actual > EIA) activity.

The result shows that AT at a noncytocidal concentration (10 nM) synergistically potentiated the cytotoxic effects of DAS on SAS cells in 3D culture and confirm obtained results from 2D culture experiments (Figure 18.A). To exclude that the synergistic effect is particular to one HSP90i or specific to one cell line, other TSCC lines (CAL27 and BICR56) and additional HSP90i (TAS-116) were tested as well. Treatment of CAL27 and BICR56 cells with DAS+AT also exhibit synergistic outcomes (Figure S9). Also, a synergistic result was achieved by combining 100 nM of TAS with a serial dilution of DAS in SAS cell line (Figure 21). These results show that this synergistic interaction with Dasatinib is not related to one TSCC line or limited to an individual HSP90i but can be obtained in several TSCC lines and with several HSP90 inhibitors. It was not possible to evaluate this synergistic effect with higher concentrations of AT or TAS, because at these concentrations the colony formation reduction was already very high (data not shown). In summary, it is important to consider 3D in addition to 2D culture methods in pre-clinical studies of the new targeted and anti-cancer drugs. However, since results from 2D and 3D experiments always do not translate well into clinical results [432], in the next step animal experiment with SAS cell xenografts in mice will be used to test for synergistic activity between Dasatinib and HSP90 inhibitors.
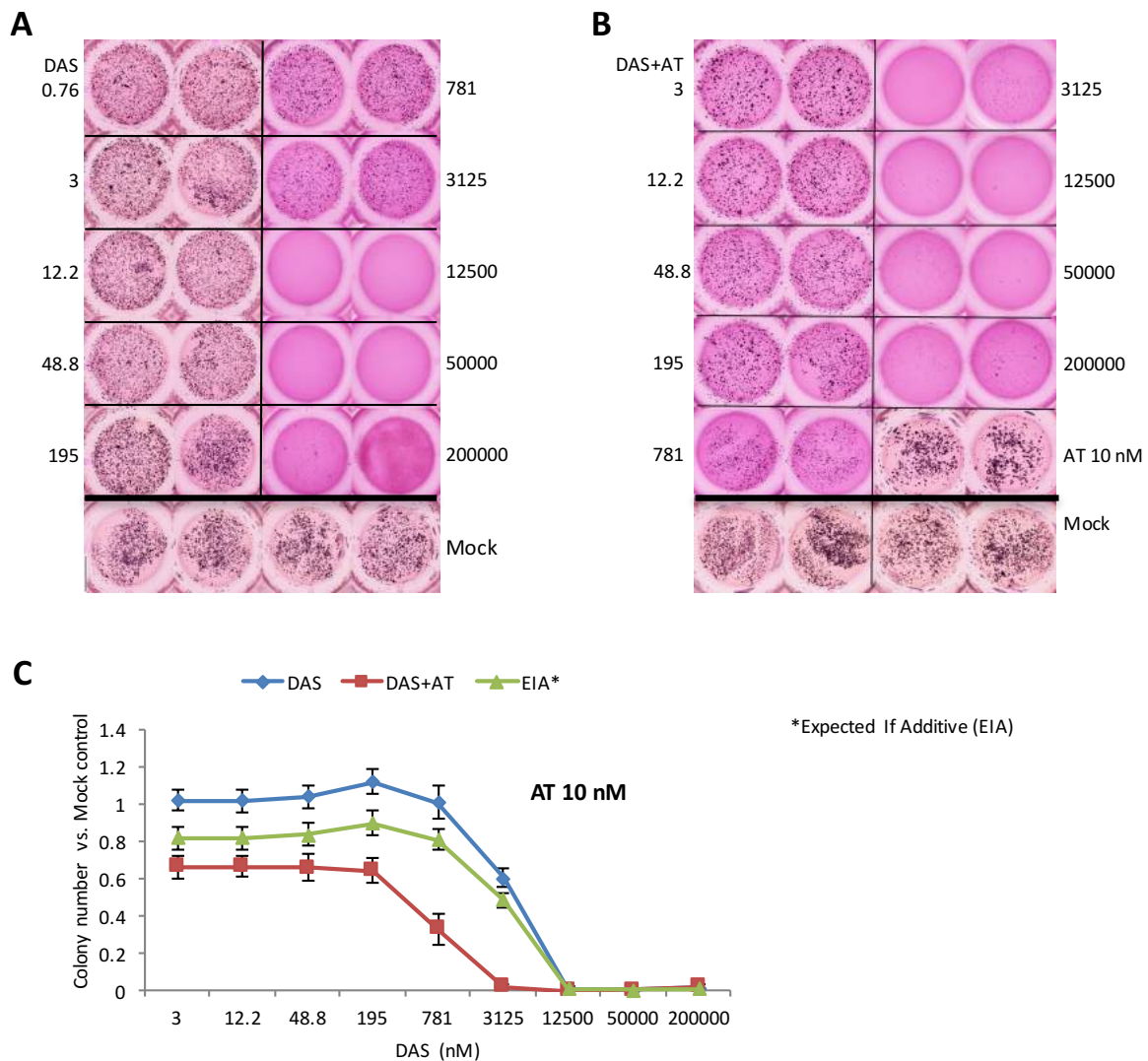
Figure 20. 3D soft agar colony formation assay shows that AT potentiates the colony formation reduction activity of DAS in SAS cells

(A) and (B) Respective images of colony formation of SAS cells treated by the indicated concentrations of DAS without (A) or with (B) a fixed dose of AT (10 nM) for 14 days
Figures are representative of three independent experiments.

(C) Quantification of colony formation in 3D soft agar culture shows a synergistic effect of DAS and AT in SAS cells
Quantification of colony numbers from soft agar plates as shown in (A) and (B). Colony numbers for DAS alone and AT alone were counted within the same experiment and used to calculate the expected values by multiplication of the cell colony fractions. Data represent means of colony numbers normalized to Mock-treated cells. The dose response curves show mean values ± SD of three independent experiments. 2 to 4 wells were counted in each case.

The investigated drugs in this work have different cellular mechanisms of action. Therefore, the activity of a drug combination could depend largely on how well drugs complement each other. TSCC is usually associated with metastasis to draining lymph nodes and the presence of nodal metastasis in the neck is the most important prognostic factor [433]. Inhibition of anchorage-independent growth in the soft agar 3D culture by DAS+AT combination treatment appears to be an attractive anti-metastatic approach to reduce tumor progression [413]. This combination therapy may allow increased efficacy at low doses of Dasatinib and HSP90 inhibitors, therefore reducing side effects and toxicity which are the main limitations

for using HSP90i [386]. Also, it could minimize the occurance of resistance, which is a pressing problem in treating cancers, by using two drugs with different mechanisms of action.
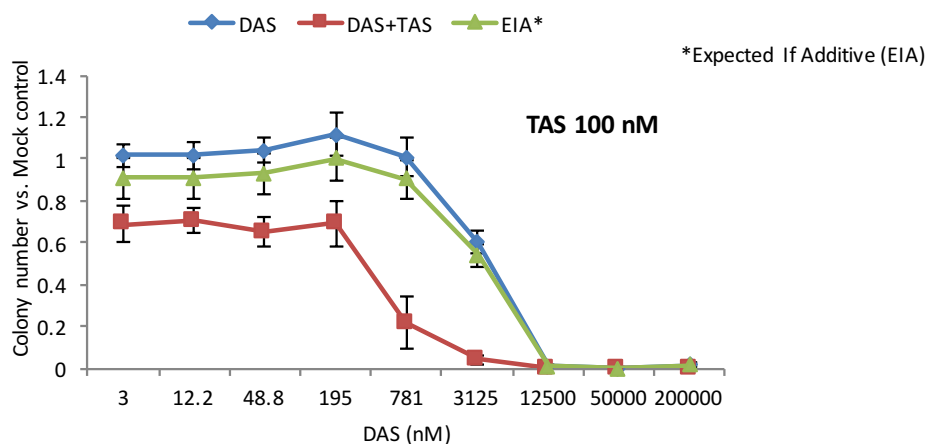
Figure 21. Colony formation quantification by 3D soft agar assay reveals that TAS, another HSP90 inhibitor, enhances the inhibition activity of DAS in SAS cells

SAS cells were treated with DMSO as vehicle control (Mock) and serial dilutions of DAS with or without 100 nM of TAS for 14 days. The colony numbers after treatment with DAS alone and with TAS alone were counted within the same experiment and used to calculate the expected values by multiplication the cell colony fractions. Data represent means of colony numbers normalized to Mock-treated cells. The dose-response curves show mean values ± SD of three independent experiments. 2 to 4 wells were counted in each case.

5.5 Characterizing DAS+AT Activity in TSCCs

Signaling pathways which could be potentially modulated by combination treatment of TSCCs with DAS and AT were investigated further in an attempt to determine a mechanism of action for their synergistic behavior. For this purpose, 50 nM of DAS and 30 nM of AT were used to treat TSCCs for 72 h in 2D culture. Both concentrations were sufficient to produce a significant reduction in cell viability individually and in combination treatment (Figures 13 and 18) and are easily achievable under physiological conditions. Total cell lysate was collected for each treatment condition, separated by SDS-PAGE based on the molecular weight of the investigated protein, blotted onto a PVDF membrane and probed with antibodies as described in the experimental sections (2.2.9 and 2.2.10). Antibodies were used to visualize the phosphorylated forms and the total level of the investigated proteins. β-Actin (Actin) was used as a loading control to assure that protein loading was the same in all lanes. It is a highly conserved protein that is involved in cell motility, structure, and integrity. The expression level of this protein is very strong and does not vary drastically under many different conditions.

5.5.1 Phosphorylation Profile Changes upon DAS and AT Treatments

It is well known that SRC causes hyperphosphorylation of tyrosyl residues on multiple cellular proteins. The development of monoclonal antibodies like 4G10 or PY1000 that identify nearly all of the phosphorylated tyrosine residues, irrespective of the surrounding

sequences, enables researchers to detect the phosphorylation state of many proteins at the same time through the use of anti-phosphotyrosine Western blotting [434]. To investigate how SRC or HSP90 inhibition impact on the global state of phosphotyrosine levels in the TSCC lines, the three cell lines treated with DAS and AT, were analyzed by Western blotting of total cell proteins with the anti-phosphotyrosine 4G10 antibody. As expected, inhibition of SRC kinase activity by Dasatinib in the TSCC lines reduces the total tyrosine phosphorylation as shown by the phosphorylation profile (Figure S10). By contrast, HSP90 inhibition mainly leads to depletion of client proteins levels and has a less dramatic effect on the phosphorylation status (Figure S10) [435]. However, HSP90 inhibition effects are sometimes not restricted only to the reduction of client proteins: since many clients are actively involved in a variety of signal transduction pathways, the loss of their activity ultimately leads to changes in gene expression programs controlled by the signaling output of those pathways [435].

5.5.2 Dasatinib, but not AT13387, Inhibits SRC Downstream Targets Phosphorylation in TSCCs

Since Dasatinib is a multi-targeted kinase inhibitor and targets many SRC family kinase members, its effect on the phosphorylation of possible SRC downstream targets in the TSCCs was investigated. It was also examined whether HSP90 inhibition could modulate Dasatinib activity by reducing the expression or the activity of SRC itself or its targets. For this purpose, several SRC downstream targets, which contribute in cell adhesion, migration, and invasion including Paxillin, p130CAS and CRK-like (CRKL) were examined. Also, the phosphorylation of the GRB2-associated-binding protein 1 (GAB1) which provides binding sites for multiple effector proteins was assessed. Additionally, the activity of Signal Transducer and Activator of Transcription (STAT) family proteins upon DAS and/or AT treatments were investigated. STATs are transcriptional factors capable of integrating inputs from different signaling pathways.

TSCCs were treated for 72 h with DMSO as vehicle control (Mock), 50 nM of DAS, 30 nM of AT, or a combination of DAS+AT. Phosphorylations of SRC at Tyrosine 416, p130CAS at Tyrosine 249 and at Tyrosine 410, Paxillin at Tyrosine 118, CRKL at Tyrosine 2017, GAB1 at Tyrosine 307, STAT5 at Tyrosine 694 and STAT6 at Tyrosine 641 were inhibited in three TSCC lines that were treated with only 50 nM of DAS. AT did not reduce protein phosphorylation or total protein levels (Figure 22, S11 and S12). In TSCCs treated with both DAS and AT, the total level of p130CAS was reduced. This reduction was more prominent in the BICR56 cell line and was mainly due to Dasatinib effect (Figure S12). Neither Dasatinib nor AT exhibited any notable reduction on STAT1 and STAT3 phosphorylation or expression.

The effect of SRC inhibition in any given tumor type cannot be predicted precisely, due to the manifold of roles for SRC in controlling fundamental cellular processes. Here, the contribution of SRC in the activation of many possible SRC targets in TSCCs was investigated using the small-molecule inhibitor of SRC, Dasatinib. Initially, treatment of TSCC cells with nanomolar concentrations of Dasatinib almost completely abolished SRC kinase activity as detected by an antibody against the autophosphorylation site of SRC (Tyr416) as shown in Figure 22. Because this antibody cross-reacts with the autophosphorylation sites in other SFKs, it cannot be excluded that SFKs other than SRC are also inhibited by Dasatinib.
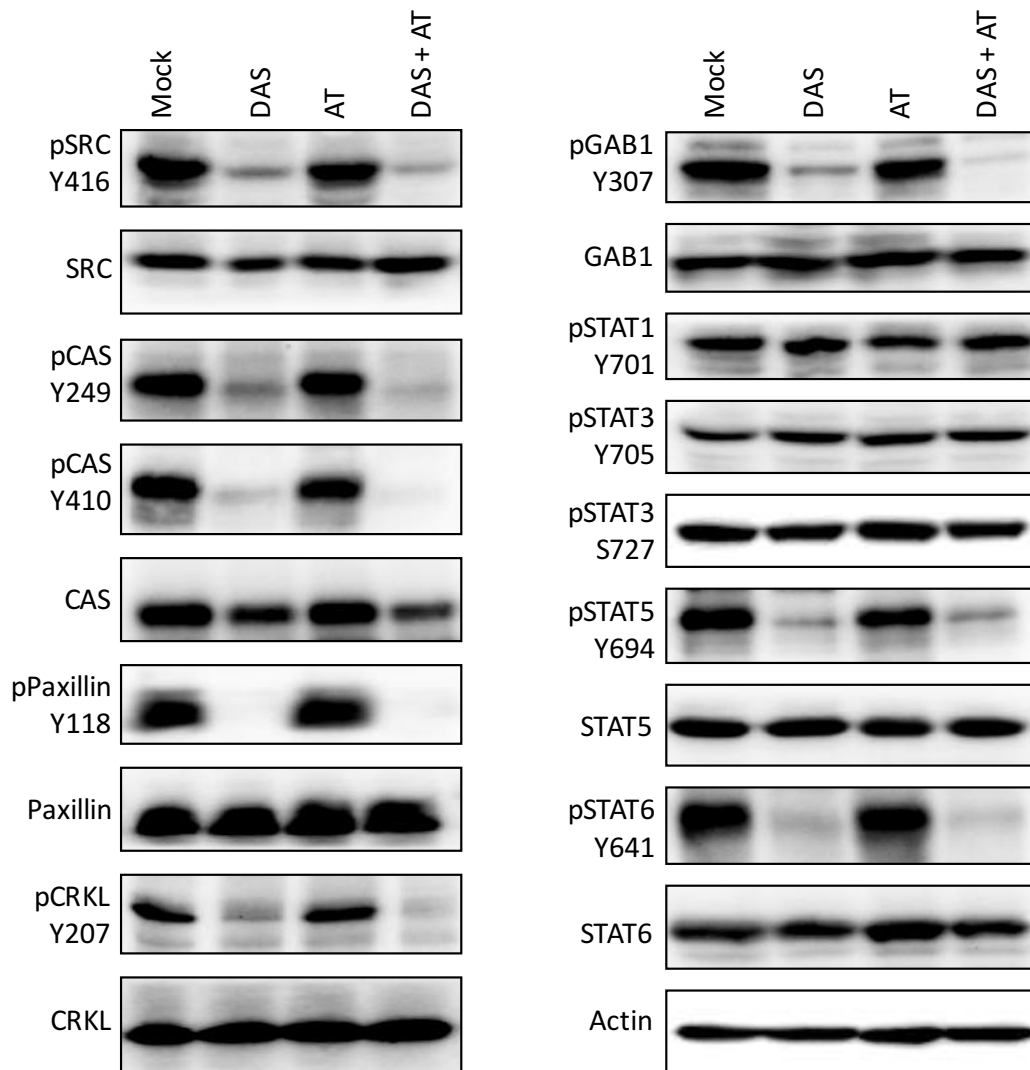
Figure 22. DAS, but not AT, blocks SRC and SRC downstream target phosphorylations in SAS cells

SAS cells were treated for 72 h with DMSO as vehicle control (Mock), 50 nM of DAS, 30 nM of AT, or a combination of DAS+AT. Total cell lysates were generated, separated by SDS-PAGE and analyzed by Western blotting. Antibodies that detect the phosphorylated state of p130CAS at Tyr249 and Tyr410, Paxillin at Tyr118, CRKL at Tyr207, GAB1 at Tyr307, STAT1 at Tyr701, STAT3 at Tyr705 and Ser727, STAT5 at Tyr694 and STAT6 at Tyr641 were used to monitor the changes in phosphorylation. The other blots show total protein abundance. The blots shown in this figure are representative of three independent experiments.

Inhibition of SRC activity correlated with the reduction of phosphorylation of its downstream substrates, Paxillin and p130CAS and CRKL, which are important in cell adhesion, migration, and invasion [436]. p130CAS and Paxillin are components of focal adhesions, which are protein complexes that have important roles in cell morphology and migration by connecting the cell cytoskeleton to the extracellular matrix via integrins. Protein phosphorylation plays important roles in the regulation of focal adhesion formation and turnover [437]. Several components of focal adhesions (FAK, Paxillin, p130CAS, etc.) are phosphorylated at specific tyrosine residues in response to integrin-mediated cell-ECM adhesion by activated FAK/SRC complex, resulting in recruitment of additional signaling intermediates (e.g. GRB2) and activation of downstream signaling pathways (e.g. the RAS-MAPK signaling pathway) [438]. The adapter protein CRKL associates with p130CAS and its translocation to focal adhesions triggers by SRC in a manner dependent on p130CAS. CRKL has critical roles in cell structure

and motility by maintaining cytoskeletal integrity. It plays a role in integrin-induced migration as a downstream effector of SRC by activating small G proteins at focal adhesions [439 440].

Since Tyrosine phosphorylation of focal adhesion proteins is a key signaling initiation event that leads to the recruitment of multiple proteins to focal adhesion sites, phosphorylation inhibition by Dasatinib could disrupt focal adhesion complex and may prevent focal adhesion formation and consequently alteration of cell migration and invasion [441]. TSCC is frequently associated with metastasis to draining lymph nodes and the presence of nodal metastasis in the neck is the most important prognostic factor. Targeting the focal adhesion complex by Dasatinib may therefore help to reduce tumor progression [442 443].

Downregulation in p130CAS expression by Dasatinib therefore might be a promising therapeutic strategy in TSCC. This reduction was more prominent in BICR56 (Figure S12) which may explain its higher sensitivity to Dasatinib in 2D and 3D agar culture. The disassembly and degradation of p130CAS may be controlled by both Caspases and Calpains, depending upon their cellular contexts and this cleavage may not only disrupt focal adhesion complexes but may also impede cell survival signaling [444]. p130CAS can act as a protecting factor against protein degradation, promoting tumorigenesis and progression in some cancers. Interestingly, it has been demonstrated that lowering p130CAS expression in breast cancer cells is sufficient to induce HER2 degradation by autophagy [445]. Therefore, p130CAS reduction, as well as deactivation, may potentiate Dasatinib activity in TSCCs by destabilising other proteins relying on its proper expression.

GAB1 is an adapter protein triggered by activated receptor-type kinases and it also plays a role in intracellular signaling cascades like cellular growth response, transformation and apoptosis. Tyrosine residue 307 is phosphorylated by SRC or MET and serves as a recruitment site for both CRK and PLCγ [446]. In TSCCs, this phosphorylation appears to be based on SRC kinase activity (Figure 22, S11and S12). CRK facilitates tyrosine phosphorylation of GAB1 at Y307 through SRC, contributing to the membrane recruitment of GAB1 to the organization of focal adhesions and enhanced cell migration, thereby possibly promoting human cancer development [447]. This may be counteracted by Dasatinib.

STATs can be activated by cytokine and growth factor receptors, in particular by EGFR as well as by SRC. STAT family members STAT3 and STAT5 promote cancer progression whereas STAT1 plays the opposite role by suppressing tumor growth [448 449]. Persistent STAT3/5 activation raises the susceptibility of healthy cells to carcinogenesis [450 451]. STAT2 and STAT4 seem to have limited roles in tumor biology and are not known to be targets or to be regulated by SRC kinase [452] therefore, they were not investigated in the current work.

STAT1 and STAT3 are well-known targets for SRC kinase, [453 454] but both were not inhibited, neither phosphorylation nor expression, by Dasatinib (Figure 22, S11 and S12). It was found that SRC activated STAT1 upon stimulation by both epidermal growth factor and hypersomatic shock [455]. While STAT3 promotes cell survival/proliferation, motility and immune tolerance and is considered as an oncogene, STAT1 enhances inflammation and innate and adaptive immunity, triggering in most instances anti-proliferative and pro-apoptotic responses in tumor cells that directly hamper tumor growth [456]. It was shown that deficiency of activated STAT1 in HNSCC mediate the escape from cytotoxic T lymphocytes [457]. According to another study concerning OSCC, 18% of analyzed tumor samples exhibited high STAT1 activation which was associated with negative lymph node status and good

prognosis in patients who received chemotherapy [458]. However, in the TSCCs tested here, STAT1 neither downregulated nor activated due to SRC and/or HSP90 inhibitions.

The lack of inhibition of phosphorylation of STAT3 could suggest some of the resistance to Dasatinib in TSCC lines. This could be related to its limited activity in targeting certain pathways associated with cell survival, angiogenesis. Aberrant regulation of the STAT3 oncogene contributes to tumor formation and progression in HNSCC, where hyperactivation of STAT3 is implicated in both treatment resistance and immune escape [459]. Protein tyrosine phosphatase receptors (PTPR) were described to function as tumor suppressors and many members of the PTPR family may be involved in tumor suppression by dephosphorylating STAT3 [460]. Mutations in the PTPR gene family have been described in 31% of HNSCC tumors, independent of HPV status [461]. Reactivation of STAT3 in HNSCC and NSLCC after sustained and specific SRC inhibition is mediated through altered JAK-STAT3 binding and JAK kinase activity and that this compensatory pathway allows for cancer cell survival and proliferation despite durable SRC inhibition [462 463]. STAT3 knockdown found to enhance the cytotoxicity of Dasatinib and provides a rationale for combining SRC and STAT3 inhibition to improve clinical responses [462 463]. Thus, STAT3 can be constitutively activated either as a consequence of enhanced signaling from positive effectors or by decreased activity of negative effectors, as observed in HNSCC.

STAT5, which is inhibited by Dasatinib (Figure 22, S11 and S12), has an alternative pathway of activation that is independent of the JAK kinase activity and dependent on the SRC kinase family. It was reported that STAT5 activation is higher in the HNSCC tumors compared to levels in the corresponding normal mucosa from the same HNSCC patients [464]. Also, it was suggested that constitutive STAT5 signaling enhances tumor growth, invasion and epithelial-mesenchymal transition in HNSCC [465]. Moreover, it was demonstrated that specific targeting of STAT5 isoforms by antisense oligonucleotides resulted in abrogation of STAT5 expression and activation, inhibition of HNSCC growth *in vitro* and *in vivo,* as well as inhibition of STAT5 target genes expression [466]. Therefore, targeting of STAT5 by SRC inhibition appears to have a significant role in Dasatinib anticancer effect in TSCC.

STAT6 is activated by Interleukin-4 and Interleukin-13 through JAK kinases and plays a predominant role in the immune system. However, there is increasing evidence that STAT6 may function in other tissues and organ systems. The mechanistic basis of STAT6 inhibition in TSCC by Dasatinib is still unknown. However, a molecular dynamics study provided evidence for the involvement of LCK (another SRC family kinase which could be inhibited by Dasatinib) in STAT6 activation in T cell [467]. Therefore, STAT6 inhibition could be related to LCK but not SCR inhibition by Dasatinib in TSCC. In HNSCC, inhibitors against STAT5 and STAT6 were able to decrease survival of cancer cells in combination with radiotherapy [468]. Hence, inhibitors against these transcriptional factors may have the potential to improve outcome in HNSCC patients. Taken together, deactivation of STAT5 and STAT6 by SRC inhibition could be a potentially important role of Dasatinib in TSCC and could be pursued in further mechanistic studies.

5.5.3 SRC and HSP90 Inhibition Reduces Receptor Tyrosine Kinases Expression Levels and their Phosphorylation

Receptor tyrosine kinases (RTKs) are a family of transmembrane proteins that mediate many vital physiological processes in both normal and cancerous cells. Molecular therapeutics for treating RTKs expressing cancers are a particularly specific method for treating cancers,

compared to general cell damage with standard cytotoxic therapeutics. MET and EGFR are RTKs that have signaling pathways involved in HNSCC and contribute to disease progression and they are targeted clinically for HNSCC management [469]. Therefore, it has been attempted here to identify the inhibitory effect of DAS+AT combination treatment on EGFR and MET and their downstream effector GAB1.

TSCC lines were treated with DAS and/or AT for 72 h then the total levels and phosphorylations of MET, EGFR and GAB1 were analyzed by Western blotting. Tyrosine phosphorylations of MET at Y1234/1235, EGFR at Y1068 and GAB1 at Y627 were reduced due to the combination treatment (Figure 23). MET phosphorylation in all TSCCs was inhibited most efficiently by a combination of both compounds. The same was found for GAB1 and EGFR. However, in CAL27 and BICR56, AT treatment alone was already sufficient to reduce the EGFR phosphorylation to a very low level that did not decrease much further in the combination treatment. The expression levels of MET and EGFR, but not GAB1, were reduced after the combination treatment in all cell lines with HSP90 inhibition, making the strongest contribution. Interestingly, HSP90 levels showed no significant reduction after inhibitions with single inhibitors or combination treatment.

The tyrosine kinases EGFR and MET strongly interact with HSP90 and are well-established drivers of tumorigenesis and metastasis [470]. Inhibition of SRC and HSP90 reduces proteins stability and activity (Figure 23). Binding of HGF to the extracellular region of MET triggers tyrosine autophosphorylation in the intracellular domain of MET and induces pleiotropic responses, such as proliferation, migration, invasion and angiogenesis in many types of cells [471]. MET is known to be overexpressed OSCC [472][473] and upregulated and functional in 90% of HNSCC cell lines and 84% of patient samples [474][475]. It has been shown that MET activation may represent an early driver in oral premalignancy and a target for chemoprevention of OSCC [473]. The expression of MET is correlated with lymph node metastasis, poor prognosis and decreased overall survival rate of patients with oral cancer [476]. Lim *et al.* investigated the expression of MET associated with cancer invasion and metastasis by studying the clinical and pathological features of TSCC patients and determined that the overexpression of MET promotes invasion of tongue cancer cells. Constitutive activation of MET enhanced migration and invasion of TSCC cells *in vitro* through the expressions of MMP1, 2, and 9, and promoted tongue cancer cell growth *in vitro* and *in vivo* [477]. Therefore, the abrogation of MET receptor kinase activation and the decrease of total protein amounts may to be a promising strategy for the prevention of highly TSCC tumor metastasis.

In future studies, the degradation or inhibition of proteins of interest after different treatments conditions should be evaluated and confirmed upon the 3D culture and later on upon *in vivo* animal experiment. In the 3D culture, a modification in the soft agar assay involves the use of specialized agar solution to allow for retrieval of treated-viable cells after colony formation when protein samples are needed (*e.g.* CytoSelect™ multiwell transformation assays) [431]. Also, following treatment, the 3D spheroids could be harvested for quantitative proteomic profiling to examine the effects of the single and combination therapies on the TSCC lines and understand drug mechanism of action.
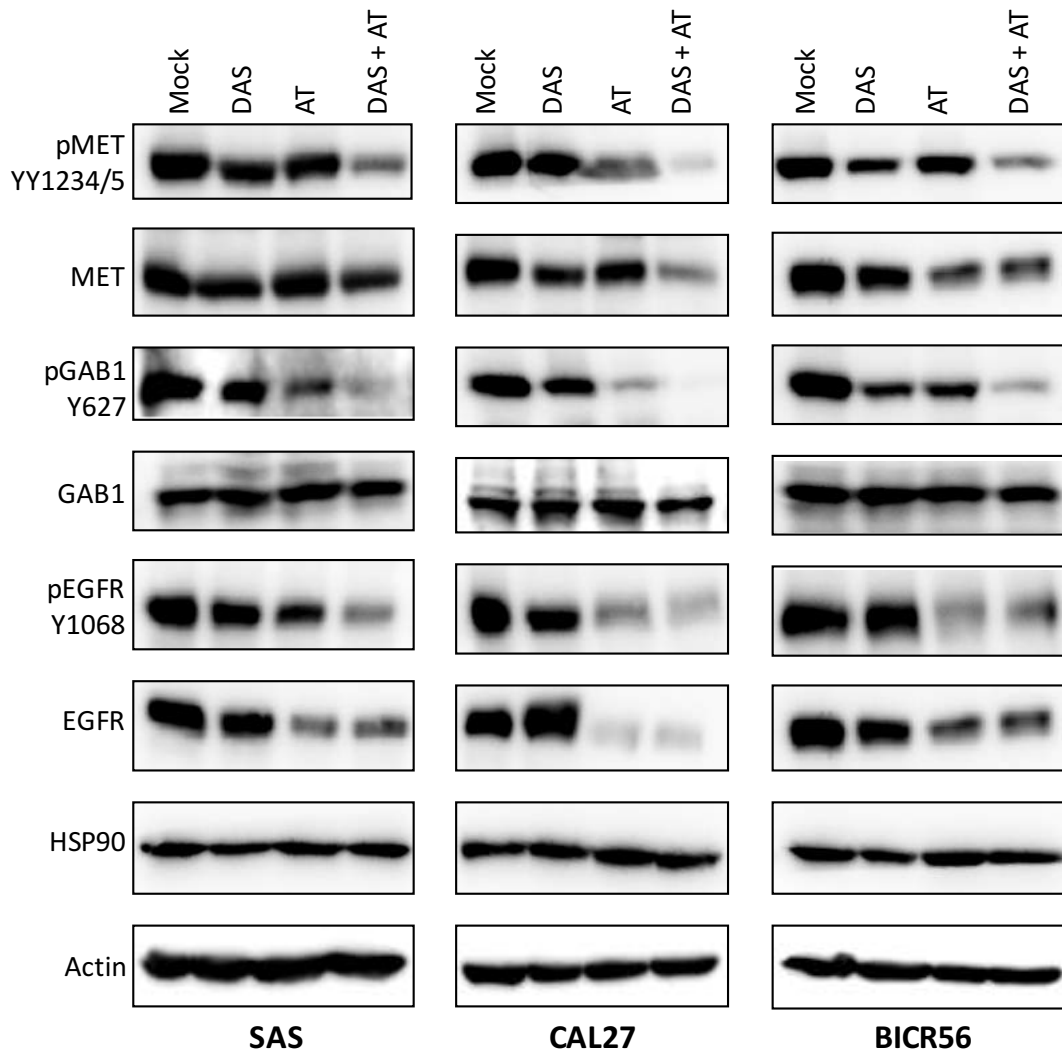
Figure 23. In TSCC lines, EGFR and MET receptor tyrosine kinase downregulation and EGFR, MET and GAB1 dephosphorylation is increased by simultaneous SRC and HSP90 inhibition

TSCC lines were treated for 72 h with DMSO as vehicle control (Mock), 50 nM of DAS, 30 nM of AT, or a combination of DAS+AT. Total cell lysates were generated, separated by SDS-PAGE and analyzed by Western blotting. Antibodies that detect the phosphorylated state of MET at Tyr1234/1235, GAB1 at Tyr627 and EGFR at Tyr1068 were used to monitor the changes in tyrosine phosphorylation. The other blots analyzed total protein abundance. The blots shown here are representative of three independent experiments. Actin was used as a loading control.

The EGFR is involved in many biological processes, such as proliferation, migration, DNA synthesis and adhesion. Many studies have demonstrated EGFR overexpression in more than 80% of the total analyzed OSCC cases [478] [479]. EGFR was also found to be overexpressed in all investigated TSCCs, of which 72% showed very intense expression, making this cancer type a potential target for therapeutic agents against the EGFR receptor [480]. Overexpression of EGFR correlates with a poor prognosis in oral cancer and its activation is associated with a malignant phenotype, inhibition of apoptosis, increased metastatic potential and resistance to anticancer therapy [481] [482]. Several anti-EGFR antibodies (including Cetuximab and Panitumumab) and small-molecule TKIs (including Gefitinib, Lapatinib and Erlotinib) have been developed. However, only the monoclonal antibody Cetuximab is currently approved for the treatment of TSCC [180] [483]. In HNSCC, the Cetuximab response rate is typically not

greater than 25% [179], therefore the role of EGFR expression as a predictor of patient response to EGFR-targeted therapeutic agents remains to be fully elucidated.

EGFR is one of the most potent oncogenic client proteins of HSP90 and mutated EGFR seems to be more sensitive than wild-type EGFR to degradation upon HSP90 inhibition [484] [485]. HSP90i could inhibit EGFR kinase activity by abolishing one of the predominant C-terminal phosphorylation sites of EGFR (Tyrosine 1068) which used to represent ligand-induced activation of EGFR and can bind GAB1 or GRB2, and subsequently activate their downstream signaling pathways [486]. Although EGFR is generally activated through ligand binding and autophosphorylation of its cytoplasmic tail, it is well established that SRC can transactivate EGFR by phosphorylating Tyrosine 845. This event may contribute to full receptor activation [487]. Based on this evidence, SRC and HSP90 inhibition can both contribute by different mechanisms to inhibit EGFR activity.

GAB1 signaling is upregulated by EGFR and MET and growth factors, including EGF and HGF, can induce GAB1 tyrosine phosphorylation and subsequent recruitment of various signaling transducers, such as the SHP2 phosphatase, PLCγ, and PI3K [488]. It was reported that phosphorylated GAB1 can recruit distinct sets of signal transducers to induce different cellular responses [489]. It has been shown that EGF induces transient GAB1 phosphorylation, which stimulates cell growth, whereas HGF induces prolonged GAB1 phosphorylation, which stimulates cell morphological changes and motility [490] [491]. GAB1 has multiple tyrosine residues that are known to be phosphorylated upon activation. Tyrosine 627, if phosphorylated, provides potential binding sites for the SH2 domain-containing SHP2 phosphatase. This binding leads to enhanced SHP2 phosphorylation and activation of the downstream MAP kinase [492]. In some cells, GAB1 phosphorylation and GAB1-SHP2 association are sustained longer in response to HGF than EGF. These effects may explain why HGF promotes more sustained ERK phosphorylation, but the mechanistic details by which MET and EGFR differentially affect the duration of GAB1-SHP2 association have not been fully explored [493].

On the other hand, it was shown *in vitro* kinase assays that SRC may directly phosphorylate GAB1 on Tyrosine 627 [494]. In this study, it was noted that in TSCC, inhibition of GAB1 Tyrosine 627 phosphorylation was correlated MET and EGFR inhibition but not with SRC inhibition during DAS+AT treatment (Figure 23). This action may abolish the induction of GAB1 binding to SHP2 involved in the signal cascade of many growth factors, cytokines and integrin receptors and is also an important part in oncogenic signaling pathways. In TSCC, DAS and AT inhibited SRC, MET and EGFR phosphorylations which are coordinately phosphorylated and activated GAB1 at different sites to transmit the full spectrum of signals to the downstream. GAB1 phosphorylation inhibition could therefore prevent regulation of different aspects of SRC, EGF and HGF elicited cell functions.

5.5.4 DAS+AT Combination Treatment Reduces RAS Activity in SAS Cells

Many reports have shown that the GAB1-SHP2 complex acts directly upstream of RAS [495] [496]. The *ras* gene is one of the most frequently mutated oncogene in OSCC and amplification of wild type RAS in oral cancer results in an overactive mitogenic signal, which in turn, results in an increased proliferative and/or survival response that contributes to the etiology of OSCC [497] [498]. Therefore, targeting RAS would be a potentially effective therapeutic strategy for tongue carcinogenesis. GAB1, through binding and activation of SHP2, is crucial for normal levels of RAS activation [499]. SHP2 is a critical mediator involved in the activation of the

RAS-ERK signaling pathway and SOS1-mediated RAS/GTP-loading [500]. In most signaling pathways, GAB1-SHP2 complex formation is not absolutely essential for RAS-ERK activation; instead, initial RAS-ERK activation occurs then GAB1-SHP2 complexes might serve as 'amplifiers' of initial RAS-ERK pathway activation [501]. The target(s) that SHP2 must dephosphorylate to mediate RAS activation remain only partially known. However, several targets have been proposed like RASGAP, Sprouty, SHPS-1 and CSK [502].

The RAS switch operates by RAS alternating between an active, GTP-bound state and an inactive, GDP-bound state. Many molecules have been described as influencing the RAS GTP-GDP cycle, mainly through two distinct biochemical activities: the guanine nucleotide exchange factors, which regulate the replacement of the nucleotide bound to RAS, favoring the GTP-bound active state, and the GTPase-activating proteins, which increase RAS's low intrinsic GTPase activity and thereby promote the inactivation of RAS proteins [503].

To test the hypothesis that GAB1 inhibition due to kinase suppression impairs the downstream RAS signaling, RAS activation was analyzed by precipitation of RAS•GTP (Figure 24.A). The assay used the RAS-binding domain (RBD) of the RAS effector kinase RAF1. The RAF-RBD domain has been shown to bind specifically to the GTP-bound form of RAS proteins with a high affinity and its binding results in a significantly reduced intrinsic and catalytic rate of hydrolysis of RAS [504]. This makes it an ideal tool for affinity purification of RAS•GTP from cell lysates. A GST-affinity binding tag fused to the RBD allows to "pull-down" the RAF-RBD/GTP-RAS complex with glutathione affinity beads. The amount of activated RAS in SAS cells treated with HSP90i was substantially decreased, without a significant reduction in the total RAS amount (Figure 24.A).

Here it is shown that the amount of the activate RAS, GTP-bound state, can be reduced by HSP90i. This inhibition of RAS activation by HSP90 inhibition has not been reported before. In the current work, the reduction in RAS activity was only checked after 72 h of treatment. However, it was shown that the RAS signaling network-activities proceed in waves [505] and therefore, more time points should be considered in the future. Repression of RAS activation in TSCC with HSP90i could be a promising therapeutic strategy. However, this result should ideally be confirmed in 3D culture and *in vivo* animal experiments first.

In contrast to BRAF and CRAF kinases where their association with HSP90 is essential for both RAF proteins stability and the proper localization in the cell, RAS is not known to be a HSP90 client and can therefore most likely not be targeted directly by HSP90 inhibition [506] [507] [508]. RAS has long been viewed as undruggable due to its lack of deep pockets for binding of small molecule inhibitors. This observation led to the initial belief that RAS may be refractory to direct inhibition [509]. Previous attempts at direct targeting mutant RAS by disrupting its GTP-bound form or by interfering with its cell membrane localization have been unsuccessful [510]. This apparent 'undruggability' has shifted the focus of anti-RAS strategies to the inhibition of more tractable downstream effectors such as the PI3K/AKT and RAF/MEK/ERK signaling pathways [511] [512]. Thus, indirect targeting of mutant RAS by HSP90 inhibitors is a promising therapeutic strategy in many cancers and much evidence supports the RAS mutation status as a marker for predicting responsiveness to these agents [513].
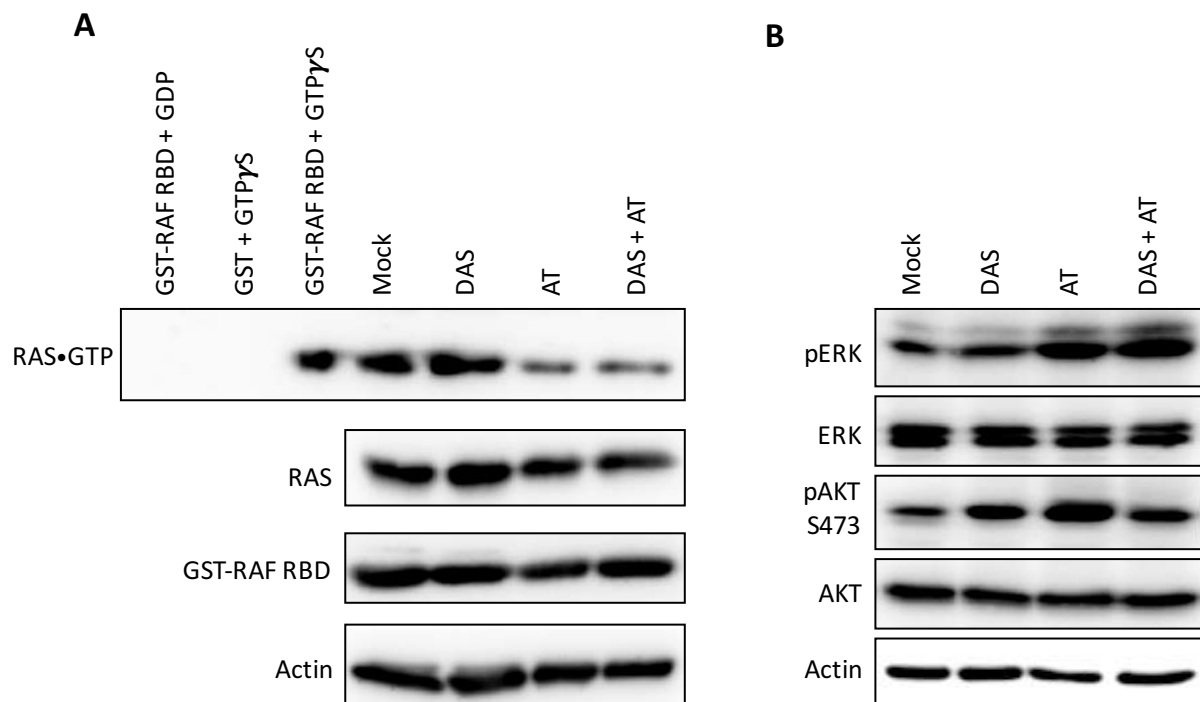
Figure 24. Combination treatment with DAS+AT of SAS cells strongly reduces RAS activity but increases MAPK activity

SAS cells were treated for 72 h with DMSO as vehicle control (Mock), 50 nM of DAS, 30 nM of AT, or a combination of DAS+AT.

(A) RAS pull down activation assays
The GTP-bound form of RAS was precipitated with a glutathione S-transferase fusion protein, corresponding to the RAS binding domain (RBD) of RAF, immobilized on agarose beads. RAS•GTP protein bound to the beads was identified using anti-RAS antibody in an immunoblot. Immunoblot analysis of total cell lysates with RAS antibody confirmed equal levels of total protein. As a negative control, cell lysate was spiked with GDP to inactivate RAS. As a positive control, cell lysate was incubated with GTP𝛾S, a non-hydrolysable analogue of GTP, to activate RAS. A pull down with the GST domain alone from GTP𝛾S-treated cell lysate was used as another negative control. The positive control (GST-RAF RBD + GTP𝛾S) showed a very strong signal which overwhelmed the other signals so finally only a quarter of the total sample was loaded. Actin was used as a loading control.

(B) HSP90 inhibition activates ERK1/2 and AKT phosphorylation despite the reduction in RAS activity
Total cell lysates were generated, separated by SDS-PAGE and analyzed by Western blotting. Antibodies that detect the phosphorylated state of ERK1/2 at Thr202/Tyr204 and AKT at Ser473 were used to detect the change in the phosphorylation levels. The other blots analyzed total protein abundance. The blots shown here are representative of three independent experiments.

There are a number of mechanisms which may explain the reduction of RAS activation by HSP90i. One possible explanation could be the downregulation of client proteins upon HSP90 inhibition which are required for RAS•GTP activation like guanine nucleotide exchange factors [364]. On the other hand, GAB1 binding and activation of SHP2 are, as mentioned above, important for normal levels of RAS activation and inhibition of Tyrosine 627 phosphorylation by HSP90i may prevent SHP2 binding and consequently RAS activation. It has recently been shown that tyrosyl-phosphorylated RAS binds to and is dephosphorylated by SHP2, which in turn promotes RAS binding to RAF and the activation of downstream RAS/RAF/ERK signaling. These results support the assumption that SHP2 reactivates the inactive tyrosyl-phosphorylated RAS via dephosphorylation to begin a new

RAS GTPase cycle [514]. Also, it was demonstrated that SHP2 acts upstream of RAS and functions by increasing the half-life of activated RAS (RAS•GTP) in the cell by interfering with the process of RAS inactivation catalyzed by RAS GTPase-activating protein (RASGAP) [515].

5.5.5 DAS+AT Combination Treatment Increases ERK and AKT Activity in TSCCs

RAS proteins control a great variety of cellular responses and are able to transduce signals from different extracellular stimuli, including growth factors, hormones, and cell-extracellular matrix contacts to many downstream effectors. This includes the Serine/Threonine kinase RAF, which leads to the activation of the ERK pathway that enables the transcription of many regulated genes involved in cell cycle progression [516]. It also includes PI3K, which in turn activates through its second-messenger products AKT, a pathway that supplies a survival signal in many cell systems [517]. Moreover, other proteins have been described as binding directly to RAS in its GTP-bound active form and may be considered effectors contributing to RAS signaling [518] [519].

To examine the possible ERK and AKT deactivation due to RAS•GTP decline, the levels and activities of ERK1/2 and AKT were determined by Western blotting using the same lysate as for the RAS pulldown assay. An increase in phosphorylation at Thr202/Tyr204 demonstrates the activation of ERK1/2 in response to HSP90 inhibition in SAS cells (Figure 24.B). AKT phosphorylation at Serine 473 was moderately raised due to SRC and HSP90 inhibitions. Similar results were obtained in CAL27 and BICR56 cell lines (Figure S13). In CAL27, very strong activation for AKT was observed after HSP90 inhibition. ERK activation in BICR56 was very strong after SRC and HS90 inhibitions. Notably, total expression levels of ERK and AKT were not modified by SRC or/and HSP90 inhibitions in all cell lines.

5.5.5.1 HSP90 Inhibition Increases ERK1/2 Phosphorylation despite the Reduction in RAS Activity

Although RAS activity was decreased due to HSP90 inhibition, ERK activity was unexpectedly increased in SAS cells upon DAS+AT cotreatment. In contrast to the current results, several studies showed that HSP90 inhibitors reduce ERK phosphorylation in other cancer cells without affecting the total ERK protein level [520] [521]. It was found that RAF, the upstream kinase in the RAS-RAF-MEK-ERK pathway, forms a complex with HSP90 and treating cells with HSP90 inhibitors facilitates RAF degradation, thereby downregulating the activity of ERK. However, it became obvious that not all HSP90 clients are equally sensitive to chaperone inhibition. HER2 in breast cancer and ALK in lung cancer, for example, are HSP90 clients that show very high sensitivity to HSP90 inhibition, while the androgen receptor, also an HSP90 client, does not seem to be affected by HSP90 inhibition [522]. STAT3, for example, is also an HSP90 client protein [523] which is not influenced by HSP90 inhibition in TSCC (Figure 22).

Inhibiting tyrosine kinases (SRC by Dasatinib and probably EGFR indirectly by AT in TSCC) or inhibiting their immediate downstream effectors can result in the compensatory upregulation of parallel oncogenic pathways or downstream oncogenic transducers [524]. A well-known case is the inhibition of BRAF that may produce a massive aberrant activation of its last downstream transducer of the cascade RTK/RAS/BRAF/MEK/ERK, resulting clones resistant to the initial targeted therapy [525]. Despite some contrasting evidence, most experimental findings suggest that ERK protects cancer cells from unfavorable conditions

and mediate chemoresistance with different mechanisms, including reduced apoptosis, increased cell proliferation, and up-regulation of drug efflux transporters [526]. However, ERK activity was found not detectably associated with the speed of cell growth in some cancer cell lines [324].

Many mechanisms could contribute to enhance ERK signaling in RAS-independent ways in the presence of pathway inhibitors. These mechanisms are likely complex and cell-specific. This may include increased expression of upstream RTKs or thr formation of CRAF dimers like in Vemurafenib-resistant thyroid cancer cell [527]. Also, it has been shown that MEK increases CRAF phosphorylation and kinase activation. This increase in CRAF kinase activation was found to resemble the activity seen with growth factor stimulation and consequently constitutive activation of ERK in RAS independent way [528]. The ability of MEK to activate CRAF was only partially dependent on MEK kinase activity but required MEK binding to CRAF. Thus, suggests that the binding of MEK results in a conformational change that increases CRAF susceptibility to phosphorylation, or in the stabilization of the phosphorylated-active form.

One of the most common mechanisms of adaptive resistance to targeted inhibitors is an increase of RTKs expression as a result of the loss of feedback inhibition from ERK [529]. A complex network of negative-feedback interactions limits the amplitude and duration of ERK signaling and is mediated directly by ERK-dependent inhibitory phosphorylation of components of the pathway, including EGFR, SOS and RAF [529]. Some data suggest that inhibition of EGFR may redirect downstream signals to depend on other receptor tyrosine kinases, which leads to feedback activation of ERK. MAPK feedback activation induced by EGFR inhibition can depend on the MET receptor, CRAF or NRAS amplification [530]. However, in our experiment, neither MET was activated nor RAS amplified in SAS cells during the current combination treatment.

5.5.5.2 DAS+AT Combination Treatment Increases PKC Phosphorylation in TSCCs

The MEK-ERK pathway can also be activated independently of RAS by protein kinase C (PKC) [531] [532] [533]. PKC isoforms comprise a family of Serine/Threonine kinases that are involved in the transduction of signals for cell proliferation, differentiation and metastasis. Targeting of some tumor-specific pathways leading to PKC activation has been intensively investigated and many studies documented that PKC provides enhanced resistance to apoptosis in response to radiation and chemotherapy [534]. For example, the underlying mechanism of breast cancer antiestrogen resistance includes ERK activation by PKC which also participates in multidrug resistance in breast cancer cells [535]. A positive relationship was found between PKC expression and HNSCC cell size, lymph node metastasis, and clinical stage [536]. It also seems that high nuclear PKC expression has been correlated to a high recurrence of OSCCs and poor survival in patients [537]. In the current work, PKC phosphorylation strongly was increased upon DAS+AT treatment in TSCC lines (Figure S14). Thus, further research is required to decipher the function of the PKC isozymes in tongue cancer generally and in ERK activation. Also, PKC inhibitors could be investigated in TSCC in combination with Dasatinib and other drugs. Some PKC inhibitors showed promising results in pre-clinical studies but are still awaiting the clinical trial phases [538].

Moreover, downregulation of negative regulators of MAPK signaling and subsequent activation of ERK is an alternative possible mechanism that mediates ERK activation independent from RAS in TSCC. The dual-specific phosphatase (DUSP) family, which inhibits

ERK signaling, may become downregulated and lead to ERK activation [539]. It was seen that several DUSPs are modulated in response to heat shock, and some may also interact directly with HSP90. Although this may not have been necessarily shown in TSCC, the heat shock response pathway is a highly conserved one, and it was suspected that some of the mechanistic associations between DUSPs and heat shock response signaling might also exist in different cells [540]. Phosphatase levels could be analyzed by Western blot and activity assays to check this possibility.

5.5.5.3 AKT Activation by DAS and/or AT Treatments in TSCCs

The activation of PI3K/AKT can occur by at least 3 independent pathways including direct binding to RTKs, binding depending on the adaptor protein GRB2 and via RAS [541]. It is not clear which of these pathways predominates in different physiological situations. Some results suggest that PI3K/AKT signaling may be activated by the insulin-like growth factor receptor (IGF1R) to resist tyrosine kinase inhibitions [539]. Another explanation of ERK and AKT activation could be related to the possible degradation of mammalian target of rapamycin (mTOR) which is a client protein for HSP90. mTOR depltion promotes MAPK pathway activation through a PI3K-dependent feedback loop in human cancer [542]. Understanding and inhibiting cell-protective feedback loops may not only improve the response but could also prevent the emergence of drug resistance. ERK and AKT activation could be reduced clinically as both MEK (Selumetinib and Trametinib) and PI3K (Buparlisib and Taselisib) pathway inhibitors are FDA approved.

5.6 Cell Cycle Analysis in TSCC

5.6.1 Overview

Cancer cell proliferation relies on the ability of cancer cells to grow, transition through the cell cycle, and divide. Cell division is usually a highly regulated process that is responsible for the appropriate division of a cell into two daughter cells. The cell cycle combines DNA replication with chromosomal separation in an oscillatory manner. It ensures that the duplicated genetic material is distributed equally to each daughter cell. This process is classically described as four sequential phases as shown in Figure 25: mitosis (M), in which a cell undergoes cell division, pre-DNA synthesis (G1), DNA synthesis (S), and pre-division (G2). Cyclin-dependent kinases (CDKs) are the central players which direct the initiation, progression, and completion of cell cycle events. The timely activation of the CDKs, which allows orderly transition between cell cycle phases, is controlled by their association with Cyclins and CDK inhibitors (Figure 25). Cell cycle progression is primarily controlled by three regulatory processes: phosphorylation of specific proteins by CDKs, CDK dephosphorylation by phosphatases and CDK degradation by the ubiquitin-proteasome system [543].
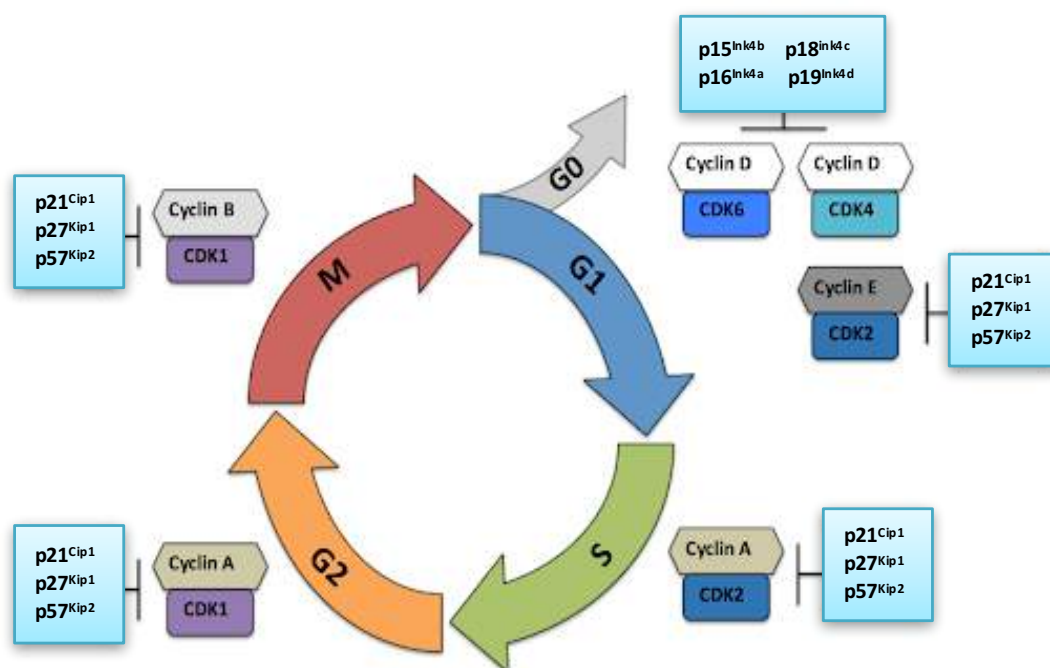
Figure 25. Cell cycle regulation includes a series of events that eventually lead to cell division and duplication

The life cycle of a cell is controlled by various CDK-Cyclin complexes, which affect the progression of cellular proliferation based on their abundance and/or activation state. Various negative regulators like p16, p21, p27 and p57 are present to control the progression through the different stages, based on a series of complex biochemical reactions. Figure adapted from [544].

At cell cycle checkpoints, the order, integrity and fidelity of the major events of the cell cycle are monitored. These include growth to the proper cell size, the full replication and integrity of the chromosomes, and their accurate separation at mitosis [545]. Each checkpoint serves as a potential termination point along the cell cycle, during which the conditions of the cell are assessed, with progression through the various phases of the cell cycle occurring only when favorable conditions are met. This regulation makes sure that cells do not divide under unsuitable conditions, for instance, when their DNA is damaged. There are many checkpoints in the cell cycle but three major ones are the G1 checkpoint, the G2/M checkpoint and the metaphase-to-anaphase transition, also known as the spindle checkpoint.

5.6.2 DAS and AT Treatments Shows Moderate Changes in Cell Cycle Distribution of TSCCs

An essential feature of cancer cells is the deregulation of cell cycle controls [546]. Targeted drug therapy is designed to take advantage of specific genetic alterations that distinguish tumor cells from their normal counterparts. Mutated oncogenes and inactivated tumor suppressors can increase the dependency of cancer cells on G1-phase CDKs, increase replication stress and DNA damage during S phase, and interfere with checkpoints that monitor progression through S/G2/M [547]. These acquired defects generate cancer cell-specific vulnerabilities that provide a window of opportunity for targeted cancer treatments. The successful application of newly developed, targeted therapeutic agents offers reduced dose-limiting toxicities to normal cells [548]. Cytotoxic drugs used to treat cancer usually work in the cell reproduction process. Some are cell-cycle specific drugs that interfere in one phase of the process. However, other chemotherapeutic agents kill cells in all phases [549]. Alkylating agents, for example, can work in any cell cycle phase.

To test whether the DAS+AT combination treatment disturbs the cell cycle process, cell cycle analysis by quantitation of DNA content was carried out by flow cytometry. SRC inhibition induced a slight accumulation of cells in the G1 phase in the CAL27 cell line. HSP90 inhibition promoted cell accumulation in the G2/M phase for all cell lines (Figure 26). In CAL27 the double-treated cells had in the end a similar cell cycle distribution as Mock-treated cells. The G1 or G2/M effect could probably become larger with increasing dosages of DAS or AT, but at these concentrations, the combined treatment effect was too great to quantify, since no cells survived.
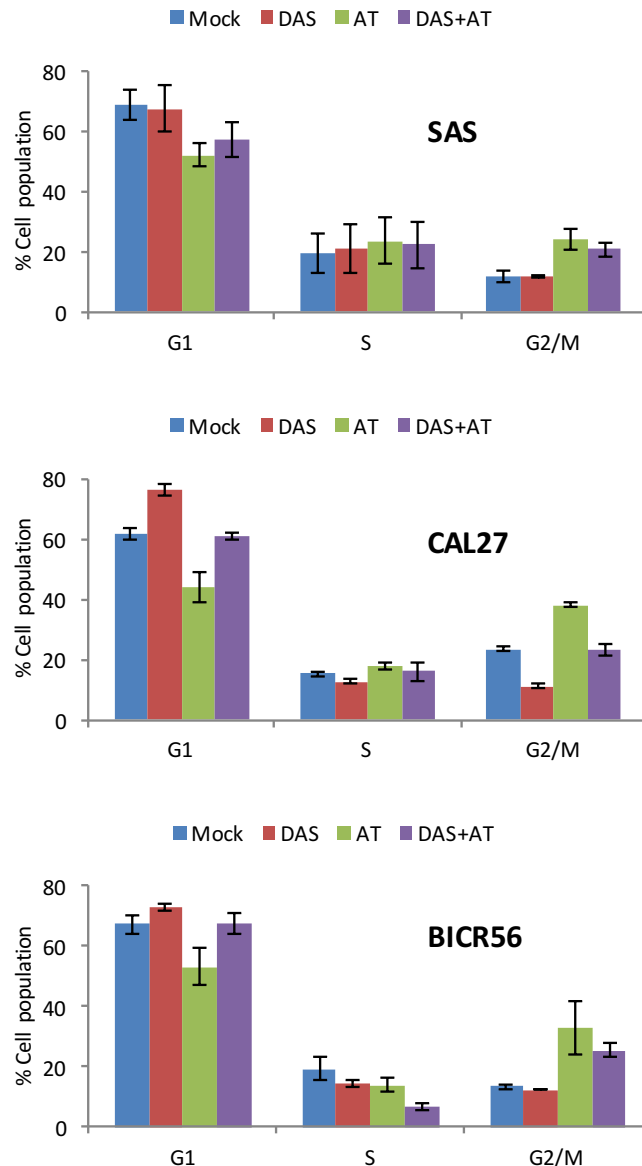
Figure 26. Flow cytometry analysis of TSCC lines treated with DAS and AT shows moderate changes in cell cycle distribution

Cells were treated with DMSO as vehicle control (Mock), 50 nM of DAS, 30 nM of AT, or a combination of DAS+AT for 72 h, fixed overnight and the DNA was stained with DAPI. The DNA content was then determined by flow cytometry. Ten thousand events were measured in each experiment. The cell population was analyzed as cell numbers at each cell cycle phase relative to the total population. No sub-G1 peaks, corresponding to dying or dead cells, were observed following treatment in any of the cells evaluated. Results are expressed as means and standard deviations obtained from three independent experiments.

SRC plays an important role in cell cycle progression in many tumor cells, and suppression of SRC downregulates Cyclin D1 and Cyclin E and upregulates the cell cycle inhibitor p27 Kip1 (p27) [550]. p27 regulates the G1 phase of the cell cycle (Figure 25). SRC has been found to phosphorylate p27 at two discrete sites (Tyrosine 74 and 88), leading to increased p27 proteolysis, reduced p27 inhibitory binding of Cyclin E-CDK2 and impaired p27 inhibition of Cyclin D-CDK4 kinase activity in malignant tissues [551] [552]. The deregulation of p27 by SRC results in increased cell proliferation. SRC inhibitors increase cellular p27 stability and Dasatinib is known to inhibit cell growth by inducing G1 arrest in human breast cancer, esophagus cancer, lymphoma and HNSCC cell lines [553] [554] [555] [556]. It was also demonstrated that Dasatinib induces G1 arrest in the sensitive large B lymphoma cell through inhibition of the SRC-SYK-PLCγ2 pathway. Downregulation of c-MYC, CDK2, CDK, CDK6, Cyclin D2 and Cyclin D3 was detected only in the Dasatinib-sensitive but not in Dasatinib resistant lymphoma cell lines [553].

The G2/M DNA damage checkpoint serves to prevent the cell from entering M-phase with genomic DNA damage, providing an opportunity for repair and stopping the proliferation of damaged cells. The HSP90 chaperone has a number of different cell cycle regulatory proteins as clients, including some involved in G1-S and G2-M transitions. Therefore, inhibition of HSP90 can induce either G1 arrest or G2/M arrest [557]. The final predominant effect on the cell cycle may depend on the net effect of HSP90i on all these proteins. In the current work, the G2-M arrest in TSCCs has been observed upon HSP90 inhibition (Figure 26). Several key regulatory proteins of the G2-M transition (CHK1, CDK1, WEE1, MYT1, CDC25 and POLO-1 kinase) have been identified as HSP90 client proteins [558] [559] and the possible impact of HSP90i on their level could explain the molecular mechanisms of G2/M arrest in TSCCs.

When damage to the mitotic machinery is extreme, the G2-M checkpoint will finally adapt. Failure to arrest the cells at or before mitosis results in the formation of micronucleated cells, aberrant segregation of chromosomes, microtubule misalignment, multicentrosomes, multipolar mitoses, and aneuploidy, leading to eventual cell death [560]. Mitotic catastrophe is a term used to describe these failures in mitosis [561]. Here, it was found that AT can induce G2/M cell cycle arrest in TSCCs. AT was previously reported to induce G2/M cell cycle arrest and interrupts central factors of DNA double-strand break and single-strand break repair in squamous cell carcinoma [562]. Similarly, inhibition of homologous recombination by HSP90i treatment has been reported in prostate and lung cancer [563]. This suggests that G2/M arrest might be a mechanism by which AT inhibits TSCC growth.

5.6.3 DAS and AT Treatments Induce WEE1 Degradation and Strongly Upregulate Phospho-Histone 3

To further examine the changes in cell cycle distribution of TSCCs upon DAS, AT and DAS+AT treatments, the abundance and phosphorylation status of some key cell cycle markers that could be involved were investigated. The expression levels of many G1 and G2/M cell cycle regulators were detected by Western blots and are shown in Figures 27 and S15. The expression level of WEE1, which is a well-known client protein for HSP90, was greatly reduced upon AT treatment in TSCCs. Surprisingly, the reduction of WEE1 phosphorylation at Serine 642 did not correlate well with the general WEE1 depletion and remained relatively high. The phosphorylation of CDK1 at Tyr15 was reduced after DAS+AT cotreatment, possibly due to WEE1 degradation or reduction of the total CDK1 level. Histone 3 phosphorylation at

Serine 10, a sign of meiotic progression, was only slightly increased upon HSP90 inhibition but massively as a result of the combination treatment. Total Histone 3 was also slightly increased in SAS and CAL27 cell lines. The total expression levels of many cell cycle regulator proteins (CDK2, CDK4, Cyclin B1 and Cyclin E1), which are HSP90 clients, did not change upon single or combination treatments (Figure S15). HSP90i treatment alone decreased the protein amounts of CDK6 (Figure S15). However, it became obvious that not all HSP90 clients are equally sensitive to chaperone inhibition as, described earlier.
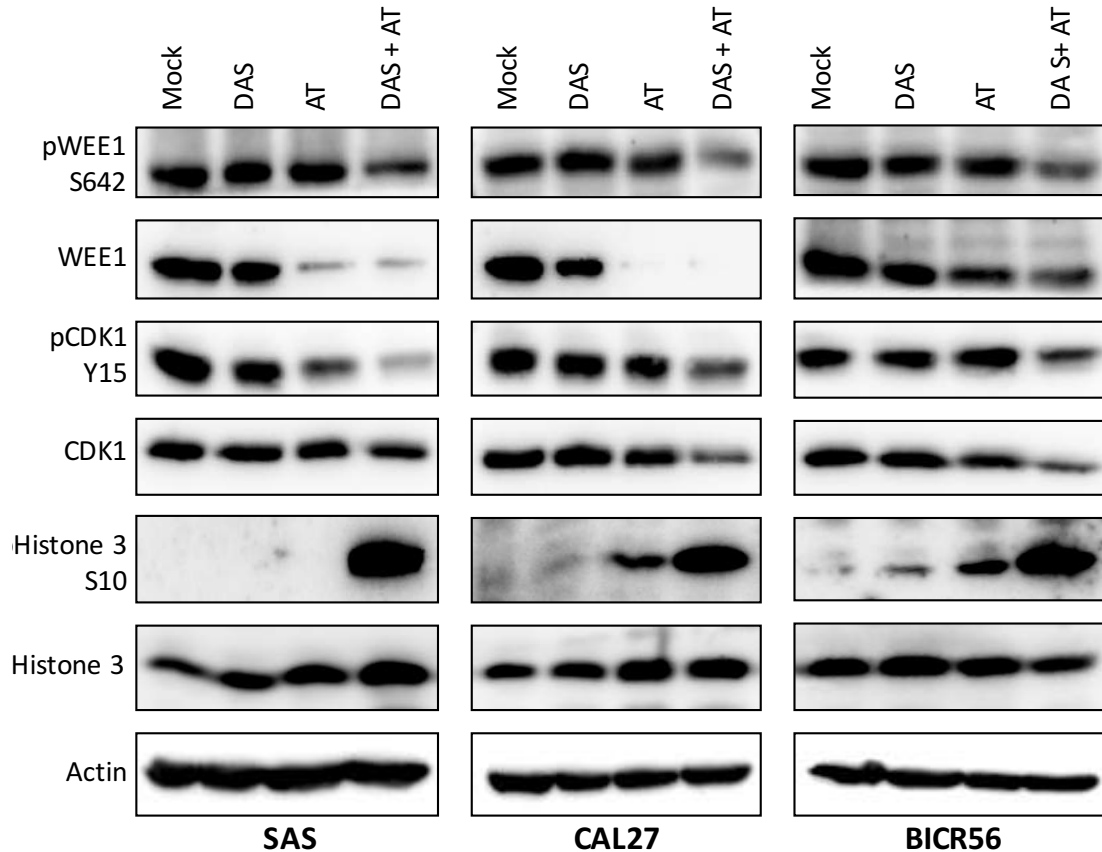
Figure 27. Treatment of TSCC lines with DAS and AT induces WEE1 degradation but an increase in phosphorylation, and also strongly upregulates phospho-Histone 3

Cells were treated with DMSO as vehicle control (Mock), 50 nM of DAS, 30 nM of AT, or a combination of DAS+AT for 72 h. Total cell lysates were generated, separated by SDS-PAGE and cell cycle-related proteins were analyzed by Western blotting. Antibodies that detect the phosphorylated state of WEE1 at Ser642, CDK1 at Tyr15 and Histone 3 at Ser10 were used to monitor the changes in phosphorylation. The other blots analyzed total protein abundance. The blots shown are representative of three independent experiments.

Cell cycle deregulation is a hallmark of tumor cells, and targeting the proteins that mediate critical cell cycle processes is an emerging strategy for the treatment of cancer [564]. The G2/M checkpoint is the most prominent target for many anticancer drugs including HSP90 inhibitors. CDK1/Cyclin B1 and CDK1/Cyclin A complexes play a key role in promoting the G2/M phase transition (Figure 25). Many proteins are known to regulate the activation of CDK1, which controls the G2 to M transition including WEE1, MYT1, CDC25C and others. A critical regulatory step in activating CDK1 during the progression into mitosis appears to be dephosphorylation of inhibitory phosphorylation sites Tyr15 and Thr14 [565]. Phosphorylation at Tyr15 and Thr14 and inhibition of CDK1 is carried out by WEE1 and MYT1 protein kinases, while Tyr15 dephosphorylation and activation of CDK1 is carried out by the CDC25

phosphatase. Reduction of the WEE1 level, which negatively regulates the progression through the G2/M DNA damage checkpoint, could promote mitotic entry by removal of the negative regulation of CDK1 activity and causes cells to enter mitosis without completing DNA repair [566]. However, in CAL27 and BICR56 cells, WEE1 degradation was not sufficient to reduce CDK1 phosphorylation level completely, possibly due to high levels of phospho-WEE1.

The activity of WEE1 is regulated both by protein phosphorylation and degradation. During S and G2 phase, WEE1 is phosphorylated at Serine 642 near its carboxyl terminus, which is required for 14-3-3 scaffolding protein binding. 14-3-3 binding has been shown to function as a positive regulator of WEE1 through protein stabilization or activation of intrinsic kinase activity [567]. However, in contrast, another group has reported that AKT phosphorylates Serine 642 and 14-3-3 binding suppresses the kinase activity of WEE1. Then it is translocated to the cytoplasm [568]. The latter could explain the inconsistency between the reductions of WEE and phospho-WEE level. While the total WEE1 level was strongly reduced by HSP90 inhibition, phospho-WEE1 showed a lesser decrease, possibly due to a paradoxical activation of AKT in TSCC, which increases WEE1 phosphorylation at Ser642.

WEE1 as HSP90 client protein was also found to phosphorylate a conserved tyrosine residue in the HSP90 N-domain and then alters its chaperone activity to favor the stabilization of a number of HSP90-dependent kinases, including WEE1 itself [569]. This suggests that WEE1 degradation by HSP90i may affect more client proteins.

It was shown that the abrogation of WEE1 function enhances the anti-tumor activity of DNA damaging agents such as radiation and some chemotherapy drugs [570]. WEE1 a is highly sensitive HSP90 client in melanoma cells, both *in vivo* and under tissue culture conditions, and it was demonstrated that its degradation maybe the key target of XL888 (another HSP90i) and underlie the anti-tumor activity seen to HSP90i inhibition [571]. Therefore, WEE1 degradation and later on inhibition of CDK1 phosphorylation in TSCCs may strongly explain the activity of AT. At the same line, WEE1 inhibitor MK-1775 shows promising synergistic activity with Dasatinib during the high throuput screen in two TSCC lines (Figure 8). MK-1775 has cytotoxic activity in a number of tumor types, including HNSCC, where it induces senescence through inappropriate mitotic entry [572]. In summary, these data suggest that the WEE1 inhibitor MK-1775 may be a potential therapeutic agent in TSCC, either alone or in combination with other drugs. However, to date, this drug was neither examined in OSCC nor in TSCC.

To determine whether WEE1 degradation due to HSP90 inhibition results in an increased mitotic entry, the phospho-Histone 3 at Serine 10 expression level was analyzed by Western blot (Figure 27). Histone 3 phosphorylation at Ser10 is tightly correlated with chromosome condensation during mitosis, suggesting a functional role for this post-translational modification in chromosome formation [573]. The combination of AT and DAS produced high levels of phosphorylation, indicating entry of a much larger proportion of cells into mitosis, consistent with a strong increase of cells in the G2/M phase observed during the cell cycle analysis (Figure 26). Many kinases are able to phosphorylate Histone 3 at Ser10, for example, cAMP-dependent kinase, activated p21-activated kinase 1 (PAK1), protein kinase C (PKC) δ and the Serine/Threonine kinase PIM1. The kinases that phosphorylate Histone 3 at Ser10 can be divided into kinases that function in signal transduction and mitotic kinases, which indicates that Ser10 phosphorylation might have different functions [574 575 576].

Inhibition of WEE1 kinase activity can override the G2 cell-cycle arrest in HNSCC, causing an accumulation of cells with extensive DNA damage in the M-phase, which can lead to mitotic catastrophe or death [572]. A recent method to distinguish cells in M phase from cells in G2 phase is simultaneous staining of DNA with PI and the mitotic marker phospho-Histone H3 followed by flow cytometric quantitation of DNA content [577]. This method enables rapid and comprehensive analysis of cell cycle profiles (G1, S, G2 and M phase). Also, HSP90 inhibition has been shown to have a significant direct impact on DNA repair mechanisms. HSP90 client proteins include DNA repair proteins such as ATR, FANCA, RAD51 and BRCA2 [578]. Therefore, phosphorylation levels of the DNA damage markers, H2AX and CHK1, at Ser139 and Ser345, respectively, can be examined as an indicator for the increase and persistence of unrepaired DNA damage in TSCCs upon current treatments. H2AX, ATM and CHK2 during DNA damage result in activation and phosphorylation of p53 at Serine 15 which regulates DNA repair [579]. p53 phosphorylation at Serine 15 was greatly increased after AT treatment (data not shown), which may indicate the presence of DNA damage.

Also, the possibly premature mitotic entry, which was indicated by the high level of phospho-Histone 3, suggests the occurrence of mitotic catastrophe, a type of abnormal mitosis characterized by extensive micronucleated and/or giant multinucleated cells, 4N DNA content and death by apoptotic and non-apoptotic mechanisms [580]. Typically, a mitotic catastrophe occurs when cells exit mitosis after failed chromosomal segregation and enter into micronucleated tetraploid interphase. To test this, the cells could be stained with phalloidin and DAPI and scored for the presence of multinucleated cells which is a marker for aberrant mitosis or mitotic catastrophe [581]. It was reported many times that HSP90i-treated cells show aberrant segregation of chromosomes, microtubule misalignment, multicentrosomes, or multipolar mitoses [582 583 584 585]. Mitotic perturbances are correlated with mitotic entry frequencies and mitotic catastrophe.

5.7 Cell Death analysis

5.7.1 DAS and AT Induce neither Apoptosis nor Caspase Activation in TSCCs

It has been shown that unscheduled mitosis results in apoptosis [561 582] or senescence [572] in tumor cells. Therefore, it was decided to test whether sensitization of the SAS cells to Dasatinib by addition of AT13386 could lead to apoptosis or senescence induction.

Apoptosis is a carefully controlled, energy-dependent process of cell death. Induction of apoptosis results in a cascade of characteristic biochemical events leading to changes in cellular morphology and death. Cells undergoing apoptosis display blebbing, cell shrinkage, nuclear fragmentation, and DNA fragmentation [586]. Apoptosis plays a critical role during normal development and homeostasis of adult tissues. Consequently, deregulation of apoptosis is commonly associated with diseases, ranging from cancer to neurodegeneration. In cancer treatments, apoptosis-inducing chemotherapeutic drugs induce DNA damage either directly or indirectly. The cellular response to DNA damage is either repair or cell death. When the repair is incomplete, for example, because the DNA damage is too extensive, cells will undergo apoptosis [587]. However, the evasion of apoptosis is a prominent hallmark of cancer [588].

In cell cycle analysis by flow cytometry with DAPI, the sub-G1 phase represents fragmented low molecular weight DNA content, that is cellular DNA has been degraded within apoptotic cells and released in a very late apoptotic stage. This will yield a population of cells that

binds a quantitative DNA stain, DAPI in this case, to a lesser extent than what is characteristic for G1 cells [589]. During cell cycle analysis in TSCCs, no sub-G1 peaks were observed following treatment of any of the cells evaluated, indicating that the cell growth inhibition resulting from the synergistic interaction of Dasatinib and AT13387 is unlikely to be mediated through apoptosis.

The apparent absence of apoptosis was also confirmed with the Annexin V/PI staining assay, where the percentages of apoptotic cells with positive Annexin V staining were very low (Figure 28.A and S16). Annexin V in conjunction with PI staining is widely used to determine if cells are viable, apoptotic, or necrotic which leads to differences in plasma membrane integrity and permeability (Figure 10). This is based on the principle that normal cells express phosphatidylserine in the inner side of the cell membrane (the side facing the cytoplasm) and when cells undergo apoptosis, the inner membrane flips to become the outer membrane, thus exposing phosphatidylserine. The exposed phosphatidylserine is detected by Annexin V, which is conjugated to FITC and displays a blue fluorescence. The ability of PI to enter a cell is dependent upon the permeability of the membrane; PI does not stain healthy or early apoptotic cells due to the intact plasma membrane. In late apoptotic and necrotic cells, the integrity of the plasma and nuclear membranes decreases, allowing PI to pass through the membranes, intercalate into nucleic acids and display red fluorescence [590] [591].

In the displayed dot plots (Figure 28.A), the x-axis shows Annexin V fluorescence and the y-axis PI fluorescence. Viable cells are found in the lower left quadrant (Annexin V-negative and PI-negative). Early apoptotic cells are found in the lower right quadrant (Annexin V-positive and PI-negative). The upper right quadrant contains necrotic cells or late apoptotic cells (Annexin V-positive and PI-positive). The percentages of apoptotic cells in the lower and upper right quadrants are very low after DAS+AT treatment in all TSCCs which indicates an absence of apoptotic cells. Staurosporine, which leads to the strong induction of apoptosis by inhibiting many intracellular kinases (Figure 7) [592], was used as a positive control (Figure S17.A).

A family of cysteine proteases with aspartate specificity, known as Caspases, plays pivotal roles during apoptosis. They are expressed as inactive proenzymes and become activated by proteolytic processing at internal aspartate residues when cells receive an apoptosis-inducing signal. Caspases are typically activated in the early stages of apoptosis and cleave key cellular components that are required for normal cellular function including structural proteins in the cytoskeleton and nuclear proteins such as DNA repair enzymes [593]. Caspase 3 and Caspase 7 are both activated during apoptosis, irrespective of the specific death-initiating, extrinsic or intrinsic, stimulus (Figure 12). Both proteases are widely considered to coordinate the demolition phase of apoptosis by cleaving a diverse array of protein substrates [594].

The activity of Caspase 3/7 upon DAS and/or AT treatments in SAS cells was evaluated following the manufacturer's instructions through a luminescent method (section 2.2.16). Caspase 3/7 activity was not increased in SAS cells after DAS+AT treatment. SAS cells treated with Staurosporine exhibited very high Casapse 3/7activity (Figure 28.B) compared to Mock-, DAS- or AT-treated SAS cells. These results agree with the cell cycle and Annexin/PI results. These results togather with the previous results (section 5.6.3) for Histone 3 hyperphosphrylation and WEE1 degradation suggest that the underlying synergy between Dasatinib and AT13387 may be based on abnormal mitosis in the absence of apoptosis.
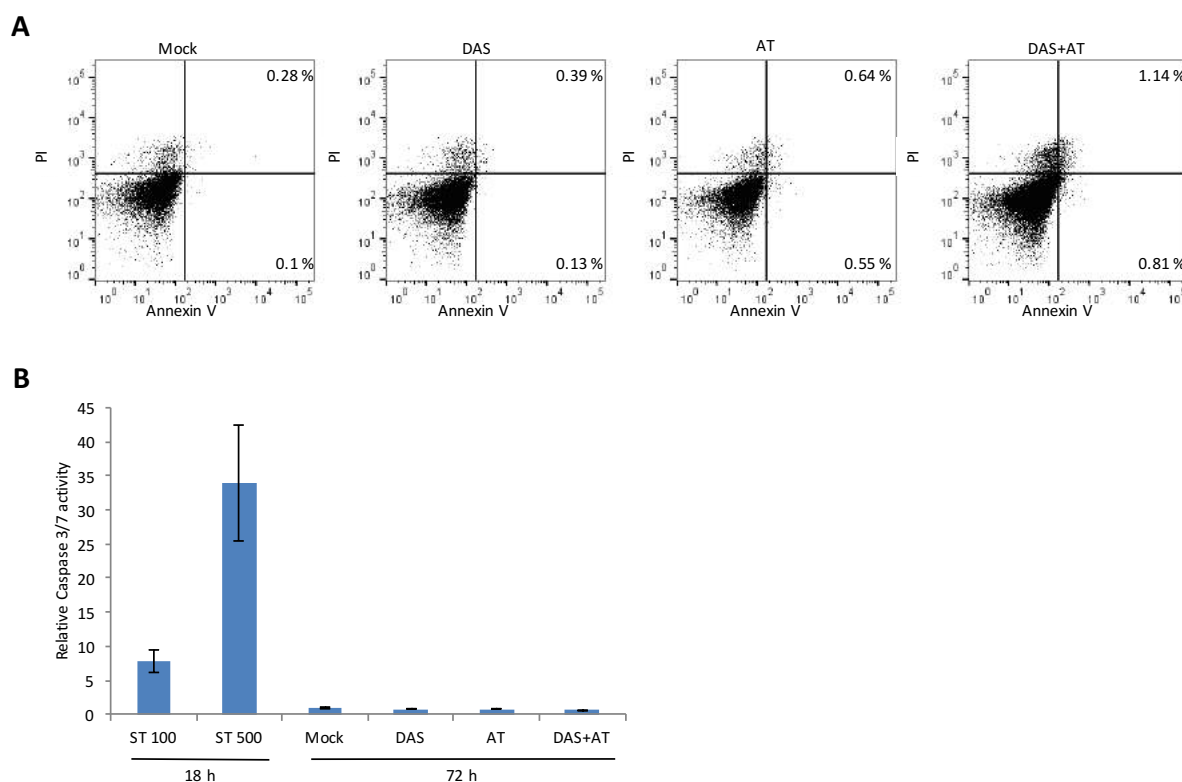
Figure 28. Flow cytometry analysis and a Caspase 3/7 activity assay show no substantial induction of apoptosis due to DAS+AT cotreatment in SAS cells

SAS cells were treated with DMSO as vehicle control (Mock), 50 nM of DAS, 30 nM of AT, or a combination of DAS+AT for 72 h.

(A) Annexin V- Propidium Iodide (PI) staining detects very little increase in Annexin-positive cells
Treated SAS cells were stained with Annexin V and PI for FACS analysis. x-and y-axis indicate Annexin V and PI fluorescence intensity, respectively. Numbers in the right upper and right lower quadrants denote percentages of late and early apoptotic SAS cells, respectively (Annexin V positive). Ten thousand events were analyzed in each experiment. Results are expressed as means taken from two independent experiments.

(B) Caspase 3/7 assay shows no activation of Caspase 3/7 in SAS cells upon treatment with DAS and AT
Caspase 3/7 activity was measured after 72 hours for treated SAS cells. The Caspase 3/7 activity was determined by a Caspase 3/7 Glo® kit (Promega) and normalized to total cell content using a Cell Titer Glo® kit (Promega). The values obtained are presented as level of chemiluminescence signal in the samples. As a positive control, 100 or 500 nM Staurosporine (ST) induced major increase in Caspase activity in SAS cells treated for 18 h. Values are expressed as means with standard deviation obtained from three independent experiments.

There are a variety of molecular mechanisms that tumor cells use to suppress apoptosis and acquire resistance to apoptotic agents, for example, by the expression of anti-apoptotic proteins such as BCL-2 or by the downregulation or mutation of proapoptotic proteins such as BAX [595]. BCL-2 family members protect the integrity of mitochondria, preventing cytochrome C release and the subsequent activation of Caspase 9. BCL-2 expression is associated with a tumor's histologic grade, with the mode of tumor invasion and with a decrease in the apoptosis index in TSCC [596]. It is also possible that p53 mutation in TSCCs (Table 1) could lead to major alterations in the BH3 proapoptotic signaling pathways which provide them with resistance to apoptosis upon treatments [597].

ERK activation, which was noted in TSCCs upon DAS+AT treatment (Figures 24 and S13), has also been shown to inhibit apoptosis in response to a wide range of stimuli including the chemotherapeutic agent. The mechanism by which ERK activation inhibits apoptosis is complicated and varies, depending on the cell and tissue type involved and the cellular regulatory influences that the cell receives [598]. However, ERK can function in a pro-apoptotic manner and induce apoptosis, or it has a dual role in promoting cell survival and cell death [599]. On the other hand, AKT, which is upregulated after DAS+AT treatment (Figures 24 and S13), is an important player in survival signaling by serving as an apoptosis suppressor. Activated AKT phosphorylates and inhibits the pro-apoptotic BCL-2 family members BAD, BAX, GSK3, and FOXO1 without altering their expression levels [600]. Also, AKT promotes nuclear translocation of the ubiquitin ligase MDM2, which counteracts p53-mediated apoptosis [601].

In TSCC, the effect of ERK and AKT activation on apoptosis resistance could be evaluated in the future by using specific ERK or AKT inhibitors. Also, the expression levels of many anti-apoptotic and proapoptotic proteins upon DAS and AT treatment and their impact on apoptosis could be assessed. However, the early apoptotic phase can be very rapid and can often be missed, making cells look either a live or late apoptotic/necrotic [291]. Staurosporine, which was used as a positive control, induced only late apoptotic/necrotic in SAS cells after an 18 h treatment (Figure S17.A). Therefore, it is necessary to perform a time-course experiment to finally prove that cells are in fact crossing through classical early apoptosis before reaching late apoptosis/necrosis.

5.7.2 DAS and AT Treatment Stimulate Senescence in TSCCs

The inhibition of apoptosis has been reported to have little or no effect on the clonogenic survival after treatment with drugs or radiation in many tumor cell lines. Apoptosis reduction in such cell lines could be compensated by an increase in the fractions of cells that undergo permanent growth arrest with phenotypic features of cell senescence or die through the process of mitotic catastrophe [602]. Cellular senescence is a response to nonlethal stress that results in persistent cytostasis with a distinct morphological and biochemical phenotype. Senescence is triggered by multiple types of cellular stress, such as persistent DNA damage, oxidative stress, or oncogene activity [603]. The senescence phenotype, detected in tumors through the expression of specific protein markers, can be generated in cancer cells lacking functional p53 and retinoblastoma protein (Rb) [604]. The most commonly used biomarker of cellular senescence is the senescence-associated β galactosidase (SA-β-gal) which is significantly amplified in senescent cells as a result of increased lysosomal content. The expression of β-galactosidase enzyme, a lysosomal hydrolase, increases with ageing both *in vitro* and *in vivo* and its expression characterizes senescent cells [605].

To detect potential senescence, TSCCs were treated with DAS and/or AT and then stained for SA-β-gal positivity by microscopy as described in the experimental section (2.2.17). Briefly, on exposure to a chromogenic substrate (x-gal), β galactosidase active in senescent cells at pH 6.0 produces a blue precipitate, which is detected by light microscopy. As shown in Figures 29 and S18, DAS alone or together with AT leads to significantly increased levels of SA-β-gal activity. A small increase in SA-β-gal staining was seen in TSCCs following AT treatment. The senescent phenotype distinguishes tumor cells that have survived drug exposure but lost the ability to form colonies from those cells that recover after treatment

[606]. The data obtained here suggest that inhibition of HSP90 in TSCCs exposed to Dasatinib may result in mitotic arrest associated with senescence-like phenotype and not apoptosis.
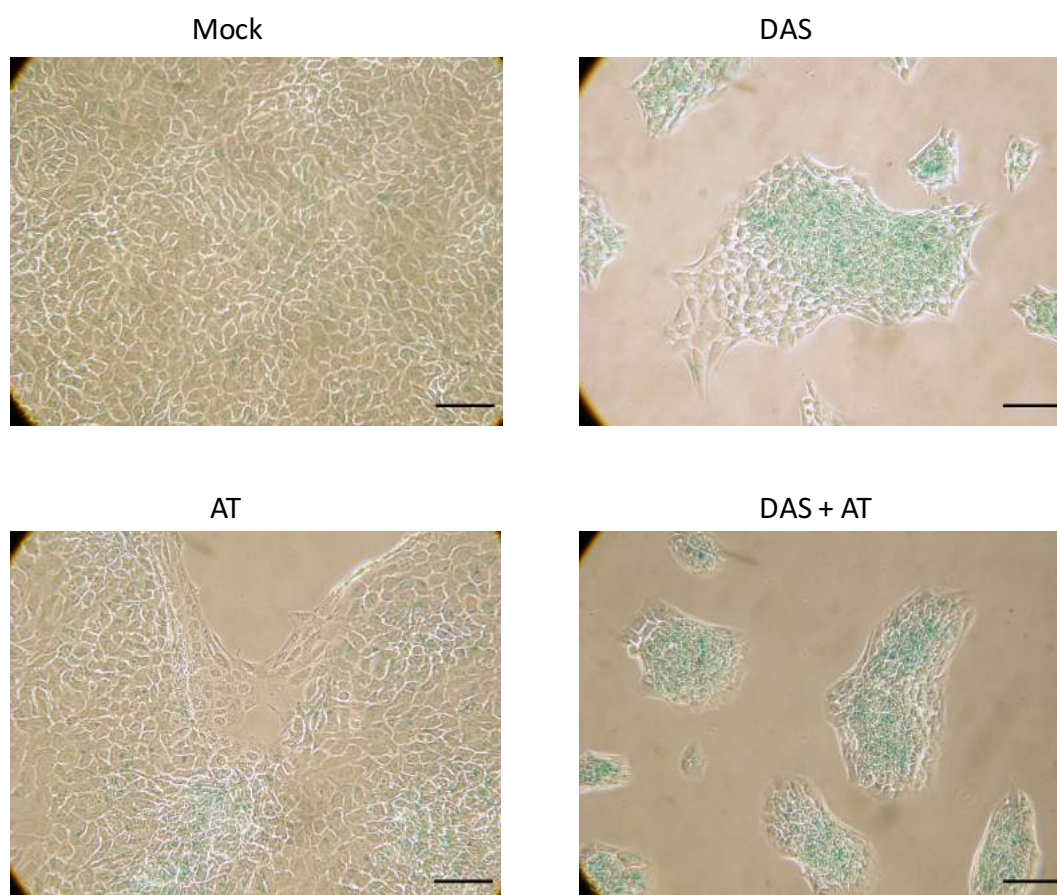
Figure 29. Induction of senescence in SAS cells following DAS and AT treatment

Representative pictures of SAS monolayer cultures stained with senescence-associated-β-galactosidase (SA-β-gal). High activity of pH-dependent β-galactosidase characterizes senescent cells. Accordingly, SA-β-gal positive staining (blue color) indicates aged cells. Cells were treated with DMSO as vehicle control (Mock), 50 nM of DAS, 30 nM of AT, or a combination of DAS+AT for 72 h as indicated in the figure. Then SAS cells were stained with SA-β-gal at 37 °C overnight in a dry incubator (no CO_2). Scale bar = 100 μM.

Senescence has been linked to induction of expression of CDK inhibitors p21 Waf1(p21) and p27 Kip1 (p27), both of which are believed to be necessary for the maintenance of the senescent phenotype in OSCC cells [607]. To determine if DAS+AT treatment induces p21 or p27 expression correlated with the observed senescence phenotype, p21 and p27 protein levels were assayed by Western blot in TSCC lines. The p27 expression but not p21 was slightly increased following the Dasatinib treatment in SAS and BICR56 and more strongly in CAL27. Compared to DAS alone, the addition of AT to DAS did not affect p21 and p27 protein expression in TSCCs (Figure S19).

It was previously shown that prolonged cell cycle arrest leads to posttranscriptional accumulation of the CDK inhibitor p27 that is accompanied by an increase of p27 specifically bound to Cyclin E and a concomitant decrease in Cyclin E-associated kinase activity, thereby preventing phosphorylation of the retinoblastoma protein (Rb) and thus in turn suppressing the expression of proliferation-associated genes which finally induce senescence [608]. However, as discussed before in this chapter, SRC phosphorylates p27 at Tyrosine 74 and 88 leading to increased p27 proteolysis, reduced p27 inhibitory binding of Cyclin E-CDK2 and

diminished p27 inhibition of Cyclin D-CDK4 kinase. SRC inhibition by Dasatinib therefore may increase cellular p27 stability which could partially explain the senescence phenotype in DAS+AT treated TSCCs. However, the slight rise for p27 level especially in SAS and BICR56 may not correlate with senescence outcome and suggest that another mechanism induces senescence.

The tumor suppressor protein p53 mediates the DNA damage-induced checkpoint through the transactivation of p21, which contributes to the induction of cellular senescence owing to its activity as an inhibitor of CDK1, CDK2 and CDK4, leading to growth arrest at specific stages in the cell cycle [609]. The p53 gene is also found to be mutated or deleted in most human tumors [610] including the investigated TSCC lines (Table 1). Abrogation of DNA binding by a mutation in the p53 DNA-binding domain leads to failure of mutant p53 proteins to transactivate p21 and dysregulates the induction of p53-mediated cellular arrest through p21 [611]. The latter may be an explanation for p21-independent senescence in TSCC. However, the role of other CDK inhibitors like p16Ink4a which is found to be active during senescence and induce senescence when overexpressed in cancer cell lines should also assessed in TSCC upon the current treatment [604].

It has been suggested that sustained reactive oxygen species (ROS) production in HNSCC could also play a key role in senescent phenotype [572]. ROS induce genomic damage and act as drivers of signaling networks important for the maintenance of the senescence [612]. Additionally, it was found that ROS produced during senescence inactivate the cytosolic ERK phosphatase DUSP6, resulting in cytoplasmic sequestration of active ERK which was increased upon DAS+AT treatment [613]. In future experiments, ROS levels could be evaluated by flow cytometry analysis, as mentioned earlier. Also, inhibition of ROS using N-acetyl cysteine inhibitors [614], for example, could be employed to elucidate the role of ROS in TSCC senescence and whether ROS-induced senescence has any role in apoptosis resistance.

ERK/MAPK is another known possible mediator of senescence and could lead to a proteasome-dependent protein degradation process targeting proteins required for cell signaling that regulates cell cycle progression, cell migration, mitochondrial functions and RNA metabolism [615]. ERK pathway-induced senescence correlates with increased β-galactosidase activity and induction of classical senescence-associated genes, such as p16/INK4A, p53, and p14-p19/ARF, senescence-associated heterochromatic foci and DNA damage foci [616][617]. So, the role of ERK activation as possible induced for senescence could also be further investigated in TSCC.

Many reports have demonstrated that AKT activation can also induce cellular senescence [618][619][620][621][622]. While induced senescence driven by excessive ERK signaling has been well studied, little is known about the mechanisms supporting the AKT-induced senescence response. However, based on a comparative molecular analysis, it was shown that activated AKT is a weaker inducer of senescence than is activated ERK [623]. Together, these observations point to potentially redundant mechanisms of senescence induction whose relevance depends on the tissue type and the driving inducer.

Senescent cells are known to be resistant to apoptosis induced by genotoxic stress including treatment with cytotoxic drugs [624] and this could also explain the low apoptosis rate in treated TSCCs (Figure 28). Quite often, tumors develop resistance to chemotherapeutic drug-induced apoptosis by senescence induction, which in such cases could serve as a backup strategy to inhibit the growth of tumor cells. It was noticed that senescence induction by chemotherapy results in a stable disease rather than the regression of tumor, a

situation often noticed during treatment by cytotoxic drugs in patients [625]. How cells become apoptosis-resistant during senescence is incompletely understood. Also, it is not fully understood what makes the cell decide between one or the other program. However, recent studies have suggested that senescent cells are resistant to apoptosis a result of the upregulation of BCL-2 family proteins such as BCL-W and BCL-XL. Senescence and apoptosis are alternative cell fates that often can be triggered by the same stressors. Many results indicate that senescence is induced mainly by the low dose of the drugs, and apoptosis predominates at the high dose in cancer cells [604] [626] [627] [628] [629]. The latter fact means that apoptosis could be probably induced in TSCC upon DAS or/and AT treatment with higher dosages of DAS or AT, but at these concentrations, it is difficult to accurately quantify apoptosis since few cells remain. It is also often experimentally difficult to recognise a definitive mode of action for any compound or treatment without conducting assays in thoroughly defined time courses [630]. Therefore, in the future, shorter time points should be implemented to prove that cells are not crossing through early apoptosis since the late time point (72 h), in the current work, may give a wrong conclusion.

5.7.3 DAS and AT Induce Autophagy in TSCCs

The enrichment of lysosomal β-galactosidase activity with the development of the senescent phenotype suggests that some senescent cells may eventually undergo autophagy [604]. Autophagy is a cellular catabolic process by which cytosolic constituents including proteins and subcellular organelles are sequestered in double-membrane vesicles called autophagosomes and degraded by lysosomal hydrolases after fusion of autophagosomes with lysosomes (Figure 11). Autophagy delivers cytoplasmic components to lysosomes for degradation and recycling of the degradation products, such as amino acids, carbohydrates and lipids that are used to synthesize new proteins and organelles or metabolized to supply energy [631]. Therefore, autophagy can help to reduce cellular stress and to maintain cellular homeostasis and cell viability. In contrast, the self-destructive role of autophagy has also implicated autophagy mechanisms in cell death pathways. The autophagic vacuoles in dying cells gave a rise to the term autophagic cell death which is an interesting phenomenon because it leads a cell to its destruction by literally "eating itself" [632]. The characterization of autophagic cell death is revealed by a massive degradation of cellular contents, including portions of the cytoplasm and intracellular organelles.

Furthermore, like apoptosis, autophagic cell death is often found to be suppressed in malignant tumors and involved in tumorigenesis. The occurrence of several cell death modes in a single dying cell and the ability to switch between different cell deaths modes makes it a challenging task to understand the complicated regulation mechanism of programmed cell death and to find the critical path that eventually controls cell death. Inhibition of apoptosis has been shown to activate autophagic cell death in several cases [633] [634]. It has also been shown that autophagy contributes to tumor cell death if induced excessively. In contrast, in some cases, autophagy can support cancer cells survival, proliferation, escape from apoptosis, and therapy resistance [635] [636]. Thus, the relationship between autophagy and apoptosis is complex and many stimuli can induce both processes.

The DAS+AT-treated TSCCs in this study do not display features typical of apoptosis (Figure 28). Growing evidence indicates that nonapoptotic programmed cell death could be associated with autophagy [637] [638]. Therefore, it was decided to assess whether these compounds induce autophagy in TSCC lines. To quantify the accumulation of acidic

components in TSCCs upon DAS and/or AT treatment, FACS analysis of AO–stained cells to evaluate the bright red fluorescence of AOH$^+$ and the green fluorescence of AO was performed (Figures 30 and S20). As shown in Figure 30, DAS and AT treatments increased the red fluorescence which identifies autophagic SAS cells, from 2.1 % to 14.2% and 16.6%, respectively, compared to Mock-treated cells, while the combination treatment further increased the autophagic cells to 31.1% (Figure 30.A).
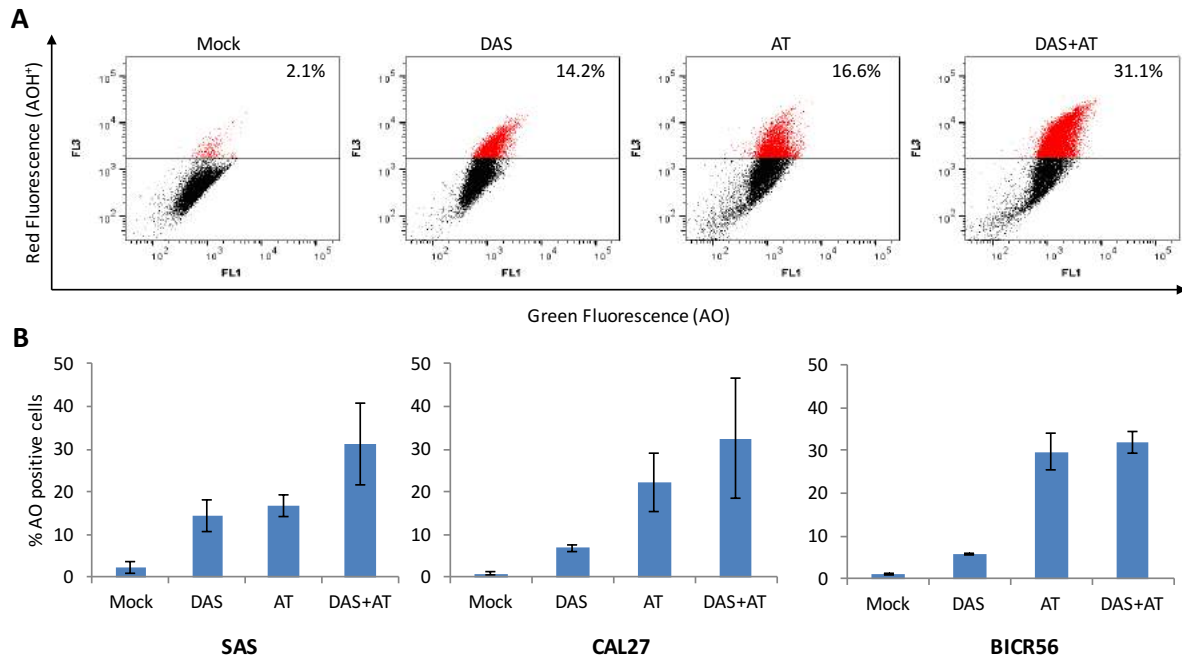
Figure 30. DAS and AT induce autophagy in TSCC lines

(A) Detection of green and red fluorescence in Acridine Orange (AO)-stained cells using FACS analysis

 SAS cells were treated with DMSO as vehicle control (Mock), 50 nM of DAS, 30 nM of AT, or a combination of DAS+AT for 72 h, stained with AO and then analyzed by flow cytometry to quantify the acidic vesicular organelle (AVO) formation. At neutral pH, AO is a hydrophobic green fluorescent molecule. Inside acidic vesicles, AO becomes protonated and trapped within the organelle. Protonated AO (AOH$^+$) forms aggregates that emit bright red fluorescence. FL1 (x-axis) indicates green color intensity, while FL3 (y-axis) shows red color intensity. Representative results from three independent experiments are shown.

(B) Quantification of autophagy
The AO-positive cell population is shown as a percentage of the total cell population in SAS, Cal27 and BICR56 cells. Values are expressed as means and standard deviation obtained from three independent experiments.

Many studies have suggested that autophagy plays a dual role in tumorigenesis. At the early stage, autophagy exerts an antitumor effect and curbs chronic tissue damage, inflammation, and genome instability, while during the late stage, autophagy sustains the energy and nutrient requirements to enable tumor development [639]. However, prolonged activation of autophagy can also lead to cell-death by self-degradation.

To determine whether the autophagy seen in the treated TSCC lines is involved in cell death or apoptosis resistance, siRNA to knock down Beclin-1, which has a central role in autophagy, or autophagy inhibitors like Bafilomycin and Chloroquine could be used. This

approach could determine whether autophagy is required for DAS+AT-mediated cell growth inhibition as a possible alternative death mechanism or apoptosis resistance by measuring cell viability and proliferation or apoptosis markers, respectively. If autophagy induction is found to be a resistance mechanism, autophagy inhibitors could be evaluated as a part of the current combination to facilitate overcoming acquired resistance to antitumor therapy.

In oral cancers, autophagy can mediate tumor suppression or promotion [640]. There are significant associations between autophagy and clinicopathological features or prognosis of OSCC. Evidence indicates that autophagy regulates the radioresistance and chemoresistance of oral cancers [641] [642]. Recently, it was found that the combination of Bortezomib (a proteasome inhibitor) and irradiation treatment induced autophagic cell death in TSCC lines, including SAS cells. This combination treatment was found to reduce tumor necrosis factor receptor-associated factor 6 (TRAF6) protein expression through autophagy-mediated lysosomal degradation, which plays an oncogenic role in tumorigenesis of human oral cancer cells and oral tumor growth [643].

Many reports show a significant increase, *in vitro* and *in vivo*, of autophagic cell death in cancer cells treated with Dasatinib [644] [645] [646]. It was concluded that autophagic cell death induction in cancer cells partially depends on Beclin-1, AKT and BCL-2 [646]. However, other reports suggest that autophagy could mediate resistance to Dasatinib in chronic lymphocytic leukaemia and lung cancer [647] [648]. Targeting autophagy, either by RNA interference or by using novel small-molecule inhibitors could sensitize cancer cell lines to Dasatinib both *in vitro* and *in vivo* by unlocking the apoptotic response.

Currently, autophagy inhibitors, such as Chloroquine, Hydroxychloroquine and 3-methyl-adenine (3-MA), are being developed to overcome resistance in cancer therapy [649] [650]. Multiple clinical trials that include Chloroquine and its derivative Hydroxychloroquine, either alone or in combination with other cancer drugs or radiation, are now being conducted in a wide range of tumors and the results demonstrate some improved clinical outcomes for cancer patients [651] [652]. Both compounds block acidification of the lysosomes, thereby inhibiting the autophagosome-lysosome fusion and hence the autophagic flux. However, high micromolar concentrations of these compounds are required to inhibit autophagy which may limit their clinical use [653].

Many client proteins of HSP90 including Beclin1, BCL-2, RAF-1, AKT, mTOR, and p38 MAPK are involved in the regulation of autophagy [654]. Several reports found that HSP90 inhibitors induce autophagy in cancer cells due to mTOR signaling pathway inhibition, which is the central regulator of autophagy [655] [656]. The treatment with a combination of HSP90i and the autophagy inhibitor 3-MA was found to suppress autophagy and induce much higher apoptosis in osteosarcoma and multiple melanomas than HSP90i alone [656]. It was considered that the autophagy inhibitor 3-MA suppresses a protective mechanism induced by HSP90i in the tumor cells thereby inducing apoptosis. However, another study demonstrated that the HSP90i SNX-2112 potently inhibits the growth of cancer cells via inducing apoptosis and autophagy-related cell death, which is associated with AKT protein degradation in a mechanism dependent on HSP90 inhibition and AKT-mediated inhibition of mTOR activity [657]. This means that it is still under debate whether HSP90 inhibition-induced autophagy in tumor cells is a protective response or is invoked to promote cell death.

One possible explanation for autophagy induction in TSCC lines upon DAS+AT treatment is ERK activation (Figure 24 and S13). Many reports suggested that activation of the ERK pathway promotes autophagy in cancer cells [658] [659] [660]. ERK-dependent autophagic activity is

associated with classical markers of autophagy, such as induction of LC3 and conversion of LC3-I to LC3-II as well as induction of Beclin 1. ERK-mediated autophagic cell death requires prolonged activation of this pathway [661]. Inhibition of the ERK by MEK or ERK inhibitors could be used in the future to evaluate the role of ERK in autophagy induction. Moreover, if autophagy is recognized as a resistance mechanism in TSCCs mediated by ERK activation, MEK inhibitor in combination with DAS or AT will be promising candidates to overcome this resistance.

ROS can also induce autophagy through several distinct mechanisms involving ATG4, catalase, and the mitochondrial electron transport chain [662] [663]. Autophagy serves as a buffer system to control the level of ROS in cells and reduce their toxic effects. The interplay of autophagy and redox response via various signaling pathways may be involved with the modulation of cancer cell homeostasis [664]. The possible important roles of ROS in TSCCs during DAS+AT treatment in autophagy induction, as well as ERK activation, senescence, cell cycle arrest and DNA damage can be further investigated in the future.

5.8 Summary and Future Strategies

The cytotoxic activity of DAS against three TSCC lines was potentiated by the combination with HSP90 inhibitors AT13387 or TAS-116 in 2D and 3D soft agar culture. Considering 3D, in addition to 2D culture methods, in pre-clinical studies is important for the new targeted treatment. However, 2D and 3D *in vitro* results have to be tested and validated in a whole organism, otherwise, they remain doubtful. Therefore, animal experiment (mouse xenografts with SAS cells) with DAS and HSP90 inhibitors will be performed in the near future to confirm the *in vitro* anticancer activity *in vivo*.

DAS, but not HSP90i, was able to inhibit many SRC downstream targets in TSCCs which contribute to cell adhesion, migration, invasion (p130CAS, GAB1, Paxillin and CRKL) and transcription (STAT5 and STA6). Cell migration, invasion, and adhesion are pivotal steps in cancer progression; hence its study and understanding are crucial in order to fight against cancer more effectively. Therefore, in the future, these cellular processes upon single and combination treatments could be evaluated. For example, the scratch assay and the 3D spheroid assay could be used to determine cell migration in 2D and 3D cultures, respectively, upon the current treatments.

Inhibition of HSP90 function leads to the degradation of multiple oncogenic client proteins involved in tumor progression; therefore, multiple signaling pathways can be blocked simultaneously. However, here it was shown that not all HSP90 clients are equally sensitive to chaperone inhibition in TSCC (e.g. STAT3). SRC and HSP90 inhibition reduced receptor tyrosine kinase (MET and EGFR) levels and phosphorylations. This combination treatment also reduced RAS activity but increased ERK and AKT activities. Understanding and inhibiting cell-protective feedback loops may improve the response and prevent the emergence of drug resistance. Therefore, ERK (Selumetinib and Trametinib) and AKT (Buparlisib and Taselisib) pathway inhibitors could be evaluated in the future, alone or in combination treatments to reduce MAPK activation.

DAS and AT treatment led to a G2/M arrest in the cell cycle phase distribution of TSCCs, mainly due to the effect of AT. Cell accumulation in the G2/M phase, WEE1 degradation and phospho-Histone 3 upregulation upon the combination treatment suggest that the underlying synergy between DAS and AT may be based on abnormal mitosis (mitotic

catastrophe). However, other mitotic markers should be evaluated. The absence of a sub-G1 population during cell cycle analysis, a lack of Annexin V-stained cells and absence of Caspase activity in the treated TSCCs indicate that the cell growth inhibition resulting from the synergistic interaction of DAS and AT is unlikely to be caused by apoptosis. On the other hand, DAS and AT treatment stimulated senescence in TSCCs which could be linked to induction of expression of p27. The induction of other classical senescence-associated markers, such as p16/INK4A and p14-p19/ARF should be investigated. DAS and AT also strongly induced autophagy in TSCC lines. Whether the autophagy is involved in cell death or apoptosis resistance should be determined by knockdown of proteins which have a central role in autophagy or by pretreatment of TSCCs with autophagy inhibitors like Bafilomycin and Chloroquine.

Chapter 6 Dasatinib and Glucocorticoid Combination Treatments

6.1 Overview

Glucocorticoids (GCs) are naturally produced by the adrenal cortex and display a large number of physiological effects essential for life. GCs are a type of Corticosteroids, which are a class of steroid hormones, that is lipophilic derivatives of cholesterol. GCs are corticosteroids that bind to the Glucocorticoid receptor (GCR). In technical terms, "corticosteroid" refers to both GCs and mineralocorticoids (as both are mimics of hormones produced by the adrenal cortex), but is often used as a synonym for "Glucocorticoid". In clinical practice, the term "Corticosteroids" usually refers to the Glucocorticoids that encompass a large group of natural or synthetic steroid compounds.

The adrenal glands are endocrine glands which produce both GC and mineralocorticoid hormones. The adrenal cortex comprises three zones, each of which synthesizes steroidal hormones. From superficial to deep, these include the zonas glomerulosa, the source of mineralocorticoids (predominantly aldosterone), reticularis, a source of weak androgens; and fasciculata, the source of GCs (cortisol and cortisone). GCs are distinguished from mineralocorticoids and sex steroids by their specific receptors, target cells, and effects [665]. The primary GC hormone is cortisol, whereas the primary mineralocorticoid hormone is aldosterone. Cortisol has important cardiovascular, metabolic, immunologic, and hemostatic functions. Aldosterone is important in salt and water regulation and therefore critical to the maintenance of intravascular volume and blood pressure.

As with many hormones, the secretion of GCs reflects a balance between positive and negative feedback pathways and is regulated by the hypothalamic-pituitary-adrenal (HPA) axis. The hypothalamus secretes corticotropin-releasing factor (CRF), which stimulates the pituitary to secrete corticotropin (adrenocorticotropic hormone). Corticotropin stimulates the adrenal cortex to synthesize and secrete cortisol. Provided serum concentrations are adequate, cortisol performs vital physiological functions and inhibits the further activity of the HPA axis. As cortisol is consumed during the day, its serum levels diminish and inhibition of the axis wanes. This allows the production of cortisol to start again. This pattern of function is called circadian or diurnal rhythm and occurs at a normal basal rate unless the axis is excited by other factors such as hypoglycemia, trauma, stress or other conditions that demand increased cortisol production [666].

Upon GCs secretion into blood circulation, they play several systemic roles in immune responses, metabolism, cell growth, development, and reproduction. Most of these effects are mediated through the GCR, a member of the nuclear receptor superfamily of transcription factors [667]. GCRα and GCRβ are two isoforms of GCR, generated by alternative splicing of a single gene. GCRα is ubiquitously expressed in nearly all cell types and is responsible for the induction of most GCs-target genes. In contrast, GCRβ does not bind any GCs evaluated yet, and its function remains unknown. GCs act by engagement of the intracellular GCR, which then is translocated to the cell nucleus where the receptor-ligand complex binds to specific GC-response elements on DNA, thus activating genes that mediate GC responses. The activated GCR-GC complex up-regulates the expression of anti-inflammatory proteins in the nucleus (a process known as transactivation) and represses the expression of proinflammatory proteins in the cytosol by preventing the translocation of other transcription factors from the cytosol into the nucleus (transrepression) [668]. It is believed that the adverse effects of GCs are induced by transactivation, whereas the beneficial anti-inflammatory effects are mainly due to transrepression. The number of genes

modulated by GCs are many and the effects are multiple and interactive with other intracellular pathways. Therefore, the effects of GCs on inflammation and the immune system cannot be attributed to a single gene or pathway [669].

The potent anti-inflammatory and immunosuppressive qualities of the GCs have made them important agents in the therapy of many diseases [670]. A variety of synthetic GCs, some greatly more potent than cortisol, have been created for therapeutic use. They differ in pharmacokinetics, pharmacodynamics, potency, duration of effect, and the overlapping mineralocorticoid potency. Cortisol is the standard of comparison for GCs potency [671]. Hydrocortisone is the name used for pharmaceutical preparations of cortisol. GCs are available in multiple forms, including oral tablets and capsules; powders and solutions for parenteral administration; topical creams and lotions for skin disease; eye, ear and nose liquid drop for local application; aerosol solutions for inhalation and liquids or foams for rectal application. The clinical conditions for which GCs are used include, but are not limited to asthma [672], systemic lupus erythematosus [673], rheumatoid arthritis [674], psoriasis [675], inflammatory bowel diseases [676], nephritic syndromes [677], organ transplantation [678], autoimmune hepatitis [679], hypersensitivity reactions [680], cardiogenic and septic shock [681], and, of course, glucocorticoid deficiency diseases such as in Addison's disease [682] and panhypopituitarism [683].

GCs have been used in clinical oncology for over half a century. In particular, GCs are routinely used to help counter some of the side effects of chemotherapy and to help shield healthy tissues in the body from the deleterious effects of chemotherapy. GCs are broadly utilized as an adjuvant during chemotherapy or radiotherapy for minimizing side effects in many cancer types [668,684]. Treatment with GCs improves appetite, reduces weight loss, decreases fatigue, diminishes ureteric obstruction, reduces allergic reactions and prevents nausea and vomiting. GCs are also efficient in relieving pain correlated with bone metastasis by suppressing the synthesis and release of prostaglandins. Furthermore, GCs have important roles in neuropathic and bone pain treatment [685]. GCs are also sometimes used in advanced cancer treatment to reduce side effects for general palliative care [686].

The GCR is not recognized as an oncogene and it is different from other very similar nuclear hormone receptors like estrogen and androgen receptors. For example, in breast cancer, the estrogen receptor drives cell growth, proliferation and metastasis [687] while the androgen receptor plays a comparable role in prostate cancer [688]. Consequently, treatment of these cancers has concentrated on blocking estrogen or testosterone production, or directly blocking steroid binding to their corresponding receptors. In contrast, GCs act through GCR to perform many functions, including arresting growth or stimulating apoptosis in lymphoid tissue [689]. Synthetic GCs, such as Dexamethasone (DX), are routinely included in chemotherapy protocols to induce cell apoptosis in malignant lymphoid cancers, such as acute lymphoblastic leukaemia, chronic lymphocytic leukaemia, multiple myeloma, Hodgkin's lymphoma, and non-Hodgkin's lymphoma. However, despite the effectiveness of GCs in reducing lymphoid disease, as single agents, they did not produce durable remissions [690].

Whether the action of GCs promotes or inhibits tumor progression is controversial in solid cancer. Prior studies have demonstrated that GCs can suppress tumor progression and metastasis [691,692,693,694,695,696,697,698] whereas other investigations found that GCs inhibit chemotherapy-induced cell apoptosis [699,700,701,702,703,704]. This controversial phenomenon may result from different cancer subtypes, differential GCR levels, and the dosage of GCs given. On the other hand, in OSCC, there are possible mechanism-based benefits in the use

of GCs in the treatment of pre-malignant conditions. Oral lichen planus is an example of a pre-malignant condition that has the potential for transformation. Progression to OSCC can occur in up to 5.8% of cases. It was postulated that this chronic inflammation is a factor that may lead to the development of malignancy such as OSCC. The powerful anti-inflammatory effects of GCs may, therefore, be a protective factor in this situation, and they are currently the first-line treatment for this condition [705].

6.2 Fluticasone and Dasatinib Combination Treatment

6.2.1 Overview

During the high throughput screen for drugs that can be combined with Dasatinib, Fluticasone (FL), which is a synthetic GC, improved the viability inhibition activity of Dasatinib in SAS and BICR56 cell lines at different concentrations (Figure 9 and S3). Fluticasone is an antiallergic, anti-inflammatory and immunosuppressive agent that is used, among other things, to treat bronchial asthma and obstructive pulmonary diseases. Other indications may include inflammatory skin diseases, nasal polyps and allergic rhinitis. It is present in preparations as 17α-esters of Fluticasone propionate or Fluticasone furoate. These esters are remarkably stable and remain attached to the FL backbone even during metabolism. Their pharmacological activity is mediated by the entire molecule (backbone + ester) and they share no common metabolites and neither FL propionate nor FL furoate is metabolized to Fluticasone. These ester groups contribute to the physicochemical characteristics of the molecule which impact on solubility, dissolution rate, tissue affinity, and hence pharmacokinetic and pharmacodynamic properties [706].

X-ray crystallography shows the ester derived from 2-furoic acid occupying a discrete pocket of the GCR receptor better than the smaller propionate ester [707]. The resulting enhanced affinity of FL furoate for the target receptor is reflected in the slightly lower daily dose required, compared to FL propionate (110 µg vs. 200 µg). However, during the high throughput screen, FL propionate was investigated in combination with Dasatinib, therefore, it was also used in the current work and hereafter the abbreviation FL indicates FL propionate.

6.2.2 Fluticasone Enhances the Anti-Proliferative Activity of DAS in TSCC Lines in 2D Culture

To appraise the possible synergistic activity between DAS and FL, TSCC lines were treated with serial dilutions of DAS as single agent or in combination with various concentrations of FL. Cell viability was examined by resazurin colorimetric assay after 72 h of treatment. 25 nM of FL was sufficient to enhance cell viability reduction of DAS in the SAS cell line but not in CAL27 or BICR56 cell lines (Figure 31.A, B and C). This concentration is physiologically achievable in the plasma after intravenous dosing [708]. However, FL failed to show any synergistic activity with DAS in CAL27 and BICR56 cells in 2D culture utilizing resazurin colorimetric assay (Data not shown). Only clinically relevant concentrations up to 100 nM of FL were tested in the current work. The cell inhibition activity of FL alone measured in the same experiment and it has on its own no significant effect on cell viability Up to 10 µM concentration, FL showed no notable effect on TSCC viability (Figure S21.A). Therefore, it was not possible to calculate an expected combination treatment effect (EIA).
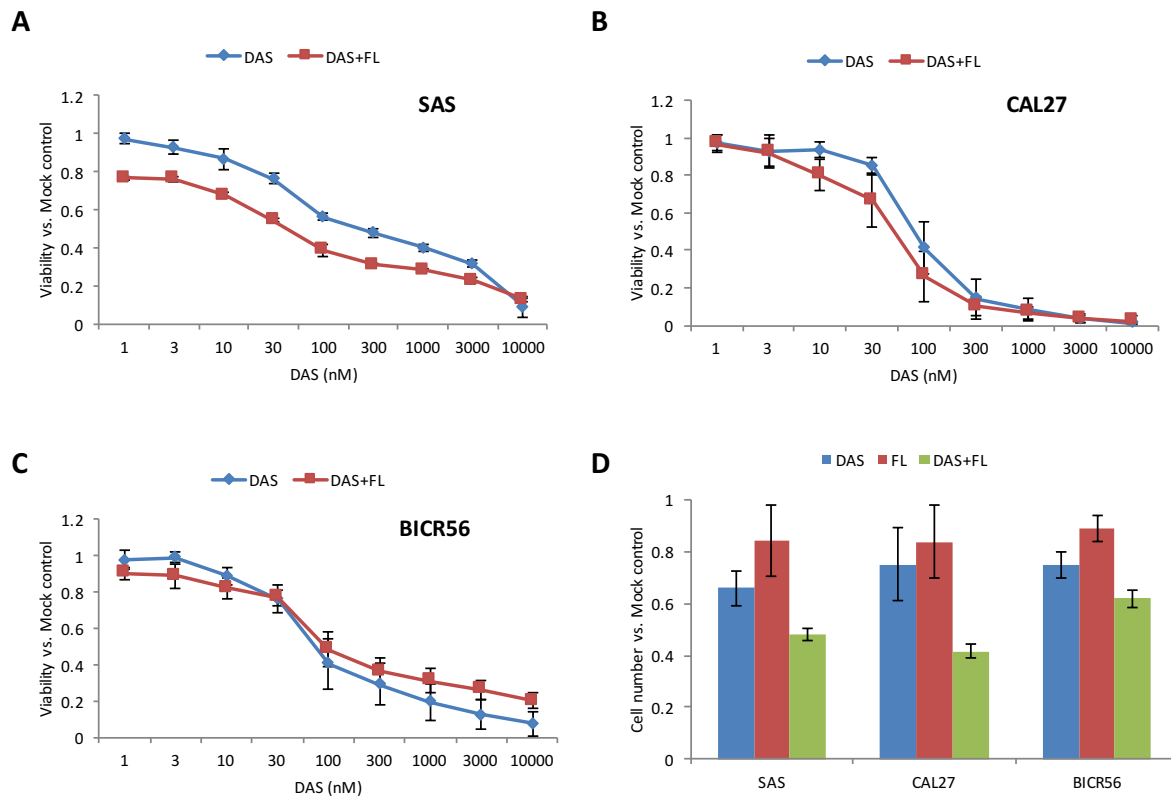
Figure 31. Addition of Fluticasone (FL) to DAS-treated cells reduces cell viability and proliferation in TSCC lines

(A), (B) and (C) FL addition reduces cell viability of DAS-treated cells in (A) SAS cell line but not in (B) CAL27 or (C) BICR56 cell lines
TSCC lines were treated with serial dilutions of DAS with or without 25 nM of FL for 72 h. Cell viability after treatment was measured by resazurin colorimetric assay. The inhibitory activities of DAS alone and FL alone were measured within the same experiment. An expected effect was not calculated here because FL alone has on its own no notable effect on cell viability. Data represent fluorescence measurements normalized to Mock-treated cells. The dose response curves show mean values ± SD of three independent experiments with six parallel measurements in each case.

(D) FL enhances anti-proliferative activity of DAS in TSCC lines
Cells were treated with DMSO as vehicle control (Mock), 50 nM of DAS, 25 nM of FL, or a combination of DAS+FL for 72 h. Cell proliferation was assessed by staining cells with trypan blue (to exclude dead cells) and counting viable cells by automated cell counter. Cell numbers were normalized to Mock-treated cells. Values are expressed as means and standard deviation obtained from three independent experiments.

To analyse a possible cytotoxic effect of the DAS+FL against TSCC lines, trypan blue dye exclusion assay was performed. 50 nM of DAS, which is usually used in the Western blot analysis in the current work, was chosen and combined with 25 nM of FL. After treatment, cells were mixed with dye and then examined to determine whether cells take up or exclude dye. Viable cells have a clear cytoplasm, whereas dead cells will have a blue cytoplasm. The numbers of viable cells were counted by an automated cell counter and normalized to Mock-treated cells (Figure 31.D). The proliferation of all TSCC lines was stronger decreased in the presence of DAS+FL compared with DAS alone. FL individually showed no significant antiproliferative effect.

Trypan blue assay results confirm the possible synergistic activity of DAS+FL combination treatment in SAS cell line which was found in resazurin colorimetric assay. However, there

was also an effect on the CAL27 and BICR56 cell lines which was not seen in the metabolic assay (Figure 31). It is known that the trypan blue assay can significantly overestimate cell viability, thereby undervaluing nonviable cell density and producing an inaccurate estimation of the overall viability of the culture [709]. However, in the current work, using the automated cell counter, we could overcome the main drawback of trypan blue assay which is counting errors due to using the traditional hemacytometer and thus improve the sensitivity and accuracy of this assay. The colorimetric resazurin assay lacks the ambiguous in the identification of stained, nonviable cells and this increases its accuracy in the estimation of culture viability. Therefore, the resazurin assay is considered to be a better choice for the evaluation of cell viability and reported to be more sensitive than trypan blue assay in detecting cytotoxicity [710]. However, since most of cell viability assays including resazurin are applied at time points when the death of some cells in the treated population is still in progress, they cannot sometimes provide precise viability results [711].

Metabolic activity and cell membrane integrity assays are important tools that can be used together to evaluate cell viability. The differences in the results between these cytotoxicity tests in TSCC may arise from different endpoints (targets) measured with these assays. DAS+FL treatment may have a greater effect on plasma membrane integrity than metabolic activity in TSCCs. The discrepancies between viable cell number and metabolic assay signals can also vary greatly depending on the concentrations tested, compound mechanisms of action, phenotypic responses, seeding density and cell types [712]. Many reports demonstrate that metabolic assays underestimate the cell viability and antiproliferative effect of compounds [712] [713]. Careful *in vitro* evaluation of cell viability and proliferation should therefore rely on the colony formation assay as well.

As mentioned above, GCs like Dexamethasone, Hydrocortisone, Methylprednisolone and Prednisolone but not Fluticasone play a vitally important role in the treatment of the side effects of chemotherapy and radiotherapy. Orally administered Fluticasone has very low systemic bioavailability (<1%) compared with inhaled Fluticasone (16.6%) because of poor absorption from the gastrointestinal tract and considerable first-pass metabolism [714]. This may be the reason why Fluticasone is not popular in chemotherapy protocols. However, recent reports have described possible indications for Fluticasone in cancer treatment which may change the current situation. One study tested the efficacy of extended-release Fluticasone propionate intracochlear implant particles to protect against Cisplatin-induced hearing loss and suggested that Fluticasone intracochlear implants are safe and able to provide effective otoprotection against Cisplatin-induced hearing loss in the guinea pig model [715]. Other studies showed that inhalation FL could be an individual treatment option in symptomatic lung patients for radiation-induced pneumonitis grade II after radiotherapy and it may also reduce the risk of systemic steroid-associated adverse effects [716] [717].

The last reports open the door on the possibility of using topical Fluticasone like in combination with Dasatinib in tongue cancer. Systemic administration of drug would of course require the agent to reach the tongue. However, sometimes high doses of medication must be administered to achieve the appropriate drug concentration and to have a therapeutic effect in the tongue. The major advantage of topical GC administration like Fluticasone is in their ability to achieve high local drug levels without the high systemic levels that cause side effects. Therefore, the local administration of Fluticasone can greatly enhance the efficacy of the drug as well as significantly decrease the side effects of systemic GC administration. Also, using a possible extended-release drug delivery technology has a

major advantage by reducing or eliminating the burst release of drug and maintaining a steady drug release over months or years.

6.2.3 DAS+FL Combination Treatment Induces G1 Arrest but not Apoptosis in the SAS Cell Line

The synergistic activity of DAS+FL in the SAS cell line was demonstrated by resazurin colorimetric assay and trypan blue exclusion assay in 2D culture (Figure 31). The current work is the first to describe any role for FL in tongue cancer treatment. So, the molecular mechanisms through which FL enhances the antitumor efficacy of DAS in TSCCs have not been investigated previously. Dasatinib is a well-known SRC kinase inhibitor but the single-agent efficacy of FL or in combination with DAS therapy need to be revealed. For this purpose, flow cytometry analysis was employed initially, to get an idea about a potential impact of FL alone or of FL in combination with DAS on cell cycle distribution and apoptosis induction as a possible death mechanism.

SAS cells were treated with DMSO as vehicle control (Mock), 50 nM of DAS, 25 nM of FL, or a combination of DAS+FL for 72 h. Following treatment, the DNA was stained with DAPI solution and the cell population at each cell cycle phase was determined by flow cytometry analysis based on the DNA content as described in details before (section 2.2.15.1). DAS and FL individually induced G1 arrest (DAS 63.4 ± 0.9, FL 69.2 ± 2.2) which becomes more pronounced upon combination treatment (81.4 ± 1.4) in comparison to Mock control (60.1 ± 1.9) with manifest reductions for the cell populations in S and to a lesser extend G2/M phases (Figure 32.A).

The effect of the DAS+FL combination on the apoptosis induction in SAS cells was investigated by staining the cells after treatment with Annexin V and PI for flow cytometry analysis. As explained in the last chapter (5.7.1), Annexin V in conjunction with PI is used to determine if cells are viable, apoptotic, or necrotic through differences in plasma membrane integrity and permeability. In short, when the cells undergo apoptosis, the inner membrane flips and therefore phosphatidylserine is exposed from the inside surface to the outside surface and detected by Annexin V (Figure 10). PI enters the cell only in late apoptotic and necrotic stages when the integrity of the plasma and nuclear membranes decreases. Based on this, in the displayed dot plots (Figure 32.C), the lower left quadrant represents viable cells: Annexin V-negative and PI-negative; the lower right quadrant represents early apoptotic cells: Annexin V-positive and PI-negative; the upper right quadrant represents necrotic cells or late apoptotic cells: Annexin V-positive and PI-positive. The percentages of apoptotic cells in the lower and upper right quadrants which represent the early and late apoptosis, respectively, are very low in SAS cells. This indicates that no significant apoptosis was induced upon DAS and/or FL treatments. Staurosporine was used as a positive control (Figure S17.A) and strongly induced apoptosis in SAS cells after 18 h treatment as determined by the Annexin V/PI assay.
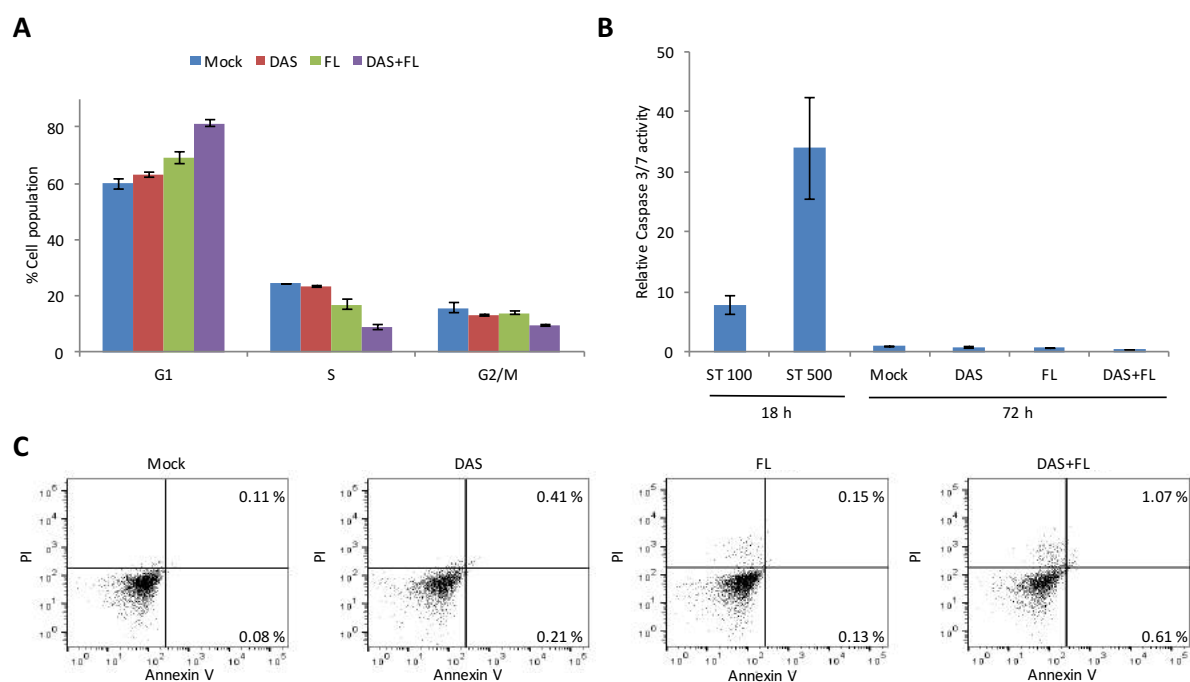
Figure 32. DAS and FL combination treatment induces G1 arrest but not apoptosis in SAS cells

SAS cells were treated with DMSO as vehicle control (Mock), 50 nM of DAS, 25 nM of FL, or a combination of DAS+FL for 72 h. Results are expressed as means and standard deviation obtained from three independent experiments

(A) Cell cycle analysis of SAS cells treated with DAS and FL detects G1 cell cycle arrest
Following treatment, the DNA was stained with DAPI solution and the DNA content was determined by flow cytometry. Ten thousand events were measured in each experiment. The cell population was analyzed as cell numbers at each cell cycle phase relative to the total population. No sub-G1 peaks were observed following treatment of SAS cells.

(B) Caspase 3/7 assay shows no activation for Caspase 3/7
Caspase 3/7 activity was measured after 72 hours of SAS cell treatment with the Caspase 3/7 Glo® kit (Promega) and normalized to total cell content measured by the Cell Titer Glo® kit (Promega). The values obtained are presented as level of chemiluminescence signal in the samples. As positive control, 100 and 500 nM Staurosporine induced major increase in caspase activity in SAS cells treated for 18 h.

(C) Annexin V and PI staining shows no substantial apoptosis induction
Treated SAS cells were stained with Annexin V and PI for FACS analysis. x- and y-axis indicate Annexin V and PI fluorescence intensity, respectively. Numbers in the right upper and right lower quadrants denote percentages of late and early apoptotic SAS cells (Annexin V- positive) respectively. Ten thousand events were analyzed in each experiment.

To confirm that this combination treatment does not induce apoptosis, the activity of Caspase 3/7 upon the single and combination treatments were examined in SAS cells with a Caspase-Glo® 3/7 assay kit according to the manufacturer's instructions as detailed in the experimental section (2.2.16). Normally, Caspase 3 and Caspase 7 are both activated completely during apoptosis, regardless of the specific, extrinsic or intrinsic death-initiating stimulus (Figure 12). As displayed in Figure 32.B, Caspase 3/7 activity was not increased in SAS cells following DAS or/and FL treatment compared to Mock-treated cells. In contrast, SAS cells treated with 100 and 500 nM of Staurosporine for 18 h exhibited very high Caspase 3/7 activity compared to Mock, DAS, FL and DAS+FL treated SAS cells (Figure 32.B). The current outcomes agree with the Annexin/PI results and indicate that the underlying synergy

between Dasatinib and Fluticasone could be related to cell cycle arrest in the absence of apoptosis.

In summary, analysis of Annexin V/PI staining by flow cytometry and Caspase 3/7 activity assay showed no apoptosis induction upon DAS+FL treatment. Additionally, during cell cycle analysis, no significant sub-G1 peaks were present following treatment, suggesting that the cell growth inhibition resulting from the synergistic DAS+FL treatment is unlikely to be mediated through apoptosis. This also implied that G1 arrest is not a consequence of apoptotic cleavage of critical cell cycle regulatory proteins. As discussed in details in the last chapter (5.7.1), TSCC could use a variety of molecular mechanisms to suppress apoptosis by the overexpression of anti-apoptotic proteins, downregulation or mutation of proapoptotic proteins (BH3), high-level expression of ABC transporters, ERK or AKT activation. To further elucidate the mechanism of cell death in SAS cells, the induction of other processes like DNA damage, senescence and autophagy upon DAS+FL treatment should be investigated in the future to gain a better understanding of the DAS+FL synergistic interaction in TSCC.

6.2.4 DAS+FL Combination Treatment Modifies Some Cell Cycle Regulators, p130CAS and MYC in the SAS Cell Line

Western blot analysis was used to evaluate the possible changes in protein expression which may contribute to cell cycle progression (G1 and G2/M), the SRC kinase pathway and other regulatory proteins. To examine the effect of DAS+FL combination treatment on the protein expressions, SAS cell lysates were prepared after 72 h treatment with the same drug concentrations as before and analyzed by Western blotting. Due to the G1 observed cell cycle arrest after treatment (Figure 32.A), changes in some proteins that contribute in G1 progression or arrest were assessed. Treatment of SAS cells with 25 nM of FL resulted in robust degradation of Cyclin D3 protein expression but no effect was seen on Cyclin D1 level by DAS or FL. p27 Kip1 (p27) expression, which is a CDK inhibitor, was strongly upregulated in its expression after treatment with FL and at the same time, the SKP2 level (a negative regulator of p27) was significantly reduced (Figure 33). Interestingly, combination treatment appeared to affect the expression of G2/M-related cell cycle markers. DAS+FL cotreatment strongly reduced WEE1 and CDK1 levels and the amounts of phosphorylated WEE1 and CDK1, indicating inhibited WEE1 activity. However, the CDC25C level (a phosphatase induces M phase by CDK1 activation) was not changed by this combination.

p130CAS total and phosphorylation levels were also examined to detect a possible effect of FL on SRC kinase activity. As expected, p130CAS phosphorylation at Tyr410 was repressed due to SRC kinase inhibition by DAS. However, the combination treatment showed an unforeseen substantial degradation of total p130CAS. On the other hand, the possible influence of DAS+FL treatment on other regulatory proteins like MYC (a major transcription factor), HSP90 (chaperone), NF-KB (another transcription factor) and PTEN (phosphatase) was assessed. Only the MYC level was reduced after the combination treatment (Figure 33).

As discussed in detail in the last chapter (5.6.2), many reports have described that DAS can inhibit cell growth by inducing G1 arrest which is slightly induced by DAS in SAS cells [554] [555]. SRC plays an important role in cell cycle progression in many tumor cells. Suppressing SRC downregulates many cell cycle regulators and upregulates p27 by increasing cellular p27 stability whereas SRC has been found to phosphorylate p27 at 2 discrete sites (Tyrosine 74 and 88), leading to increased p27 proteolysis [551] [552]. However, p27 upregulation in the current combination treatment occured mainly due to the FL treatment. Cyclin D3 and p27

levels are oppositely regulated in SAS cells and are possible candidates for regulating FL-induced G1 arrest (Figure 25).
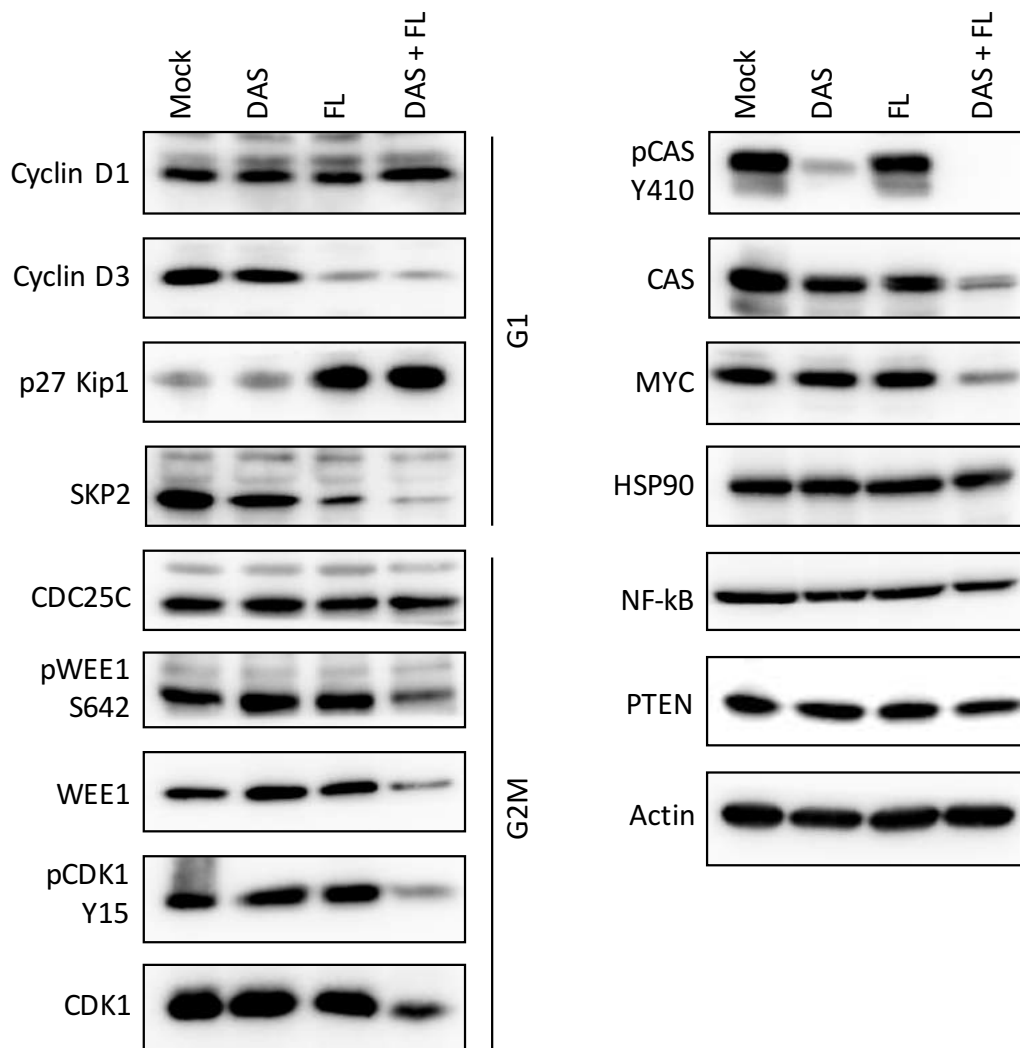
Figure 33. FL and DAS affect some cell cycle regulators, p130CAS and MYC in the SAS cell line Western blot analysis of cell cycle-related proteins, transcription factors and SRC targets in SAS cells treated with DMSO as vehicle control (Mock), 50 nM of DAS, 25 nM of FL, or a combination of DAS+FL for 72 h. Total cell lysates were generated, separated by SDS-PAGE and analyzed by Western blotting. Antibodies that detect the phosphorylated state of WEE1 at Ser642, CDK1 at Tyr15 and p130CAS at Tyr410 were used to detect the change in phosphorylation. The other blots analyzed total protein abundance. The blots shown here are representative of three independent experiments.

As mentioned before, p27 is a Cyclin-CDK inhibitor that arrests the cell cycle at the G1 phase by blocking the activation of Cyclin E-CDK2 complex, preventing the improper entry to the cell cycle [718]. p27 binds to and inactivates Cyclin E-CDK2 in the nucleus, which prevents the subsequent transcription of genes required for G1-S transition [719]. This raises the question of how can FL induce p27 expression? Many groups reported that p27 could be upregulated after Dexamethasone (DX) treatment, another synthetic GC [720] [721] [722]. In lung adenocarcinoma cells, DX was found to induce a progressive accumulation of p27 mRNA that was not associated with a change in mRNA stability. The investigation indicated that a relatively slow rate of transcriptional activation of the p27 gene, that occurs at relatively high GCR levels, accounts for the progressive accumulation of p27 in response to DX

treatment and causes permanent cell cycle blockade [720]. A significant upregulation of p27 mRNA was found in lymphoma cell lines upon DX treatment indicating a transcriptional regulation [721]. However, the relatively moderate induction of p27 mRNA levels by DX did not explain the strong increase of p27 protein in those cell lines. In the same study, DX treatment was found to increases the half-life of p27 protein, which suggests that decreased protein degradation is the primary mechanism of p27 induction by GCs.

Interestingly, DX treatment was observed to decrease the protein and mRNA levels of SKP2, a negative regulator of p27 and an E3 ubiquitin ligase subunit [721]. The F-box protein SKP2 is the substrate-targeting subunit of the ubiquitin-protein ligase SCF ^{SKP2} (SKP1-Cullin1-F-box) complex and is frequently overexpressed in transformed cells. Ubiquitin–protein ligases tag specific target proteins with ubiquitin, which allows the proteasome to recognize and degrade the target. Degradation of p27 is promoted by its phosphorylation on Thr187 by the Cyclin E-CDK2 complex. SKP2 binds to p27 only when Thr187 is phosphorylated; such binding then results in the ubiquitylation and degradation of p27 [723]. Interestingly, in the current work, downregulation of endogenous SKP2 protein by FL was observed in SAS cells. This is could be a distinct regulatory mechanism leading to p27 upregulation.

Both p27 and SKP2 are useful prognostic and therapeutic markers in a variety of cancers. Low levels of p27 often correlate with poor prognosis tongue cancer [724]. Conversely, SKP2 is often overexpressed in cancers and works as an independent marker for the prognosis of malignant diseases [725]. SKP2 exerts its oncogenic function predominantly by the ubiquitin-dependent degradation of p27 [726]. Recent achievements in developing drugs inhibiting SKP2 emphasize the potential importance of the 'SKP2-p27' axis in cancer therapies [723]. Treatment of certain cancer cell lines with a molecule that inhibits the assembly of the E3 ubiquitin ligase complex SCF^{Skp2} re-sensitized these cancer cells to therapeutic agents. The current data suggest that p27 and SKP2 expression might be predictive for a response to Glucocorticoid therapy in tongue cancer. However, this study did not yet address the connection between SKP2 downregulation and p27-induced cell cycle arrest. Therefore, at this stage, it can only be speculated whether SKP2 repression is the cause or the consequence of p27 upregulation and G1 arrest.

A low p27 level is frequently observed in cancers with hyperactive SRC, which results in resistance to cancer therapies [718]. Tyrosine phosphorylation by SRC kinases converts p27 from the inhibitor to the substrate of Cyclin E-CDK2, which further phosphorylates p27 at Thr187, and induces p27 polyubiquitylation and degradation mediated by SCF^{SKP2} E3 ligase. SRC kinase inhibition by Dasatinib and SKP2 downregulation by Fluticasone may synergically increase p27 level and amplify G1 cell cycle arrest.

The initiation of the cell cycle is driven by the transcriptional activation of D-type Cyclins, including Cyclin D1, D2 and D3. D-type cyclins are critical for the activation of CDK4 and CDK6, whose kinase activities are responsible for the early steps in G1 phase progression, mostly by phosphorylating proteins of the Rb family (Figure 25). In TSCC, Cyclin D gene amplification was detected in 88% of the tumors and implies an overall poor survival [727]. Patients with HNSCC strongly positive for Cyclin D had reduced overall and disease-free survival [728]. Recently, it was reported in a meta-analysis that highly expressing Cyclin D3 might be an unfavorable prognostic biomarker for various malignancy patients including HNSCC, which can make great contributions to the clinical diagnosis and treatment [729].

In parallel with p27 upregulation, Cyclin D3 protein level decline after FL treatment (Figure 33). It was suggested that GCs inhibit Cyclin D3 transcription and mRNA stability [730].

Destabilization of Cyclin D3 mRNA was found to be a direct effect of GCs, independent of cell cycle progression and mediated by a GC-induced protein(s) that accelerates the degradation of Cyclin D3 mRNA. Induction of G1 arrest by downregulation of Cyclin D3 was observed in many types of cancer [721] [731]. On the other hand, Cyclin D/CDKs can sequester p27 from the Cyclin E/CDK2 complex and favor progression into S phase [732]. Accordingly, downregulation of Cyclin D3 protein could lead to a release of p27, which is then more available for binding and inhibiting Cyclin E/CDK2, leading to more G1 arrest. To address Cyclin E/CDK2 inhibition by p27 in GC-treated cells more directly, CDK2 complexes could be immunopurified from GC-treated cells and it could be determined if p27 co-immunoprecipitates with CDK2.

c-MYC (hereafter MYC) is a master regulator of many genes and a known transcriptional activator of SKP2 [733] and was downregulated by DAS+FL cotreatment (Figure 33). MYC is also an oncogenic transcription factor that exerts a wide array of biological functions in different cellular models related to cell cycle control, genomic instability, energetic metabolism, protein synthesis, intercellular communication, and control of cell differentiation. The MYC expression is deregulated in a wide array of human solid tumors and often associated with tumor progression in HNSCC [734]. MYC protein was found to be overexpressed in OSCC and is believed to have a key role as an oncoprotein in the tumorgenesis of OSCC, as well as potential as a therapeutic target [735] [736]. In TSCC, high MYC expression correlates with poor prognosis [737] and using DAS+FL combination treatment to reduce MYC level could be a promising strategy in tongue cancer.

Since MYC is an oncoprotein, it is considered a highly desirable therapeutic target. However, despite it significant contribution to cancer, it is commonly thought to be 'undruggable' because of its lack of structured regions amenable to therapeutic inhibition. In spite of this, some small molecule ligands, have been developed to inhibit MYC by by employing its multiple regulatory mechanisms, including *MYC* transcription and mRNA stability, MYC protein stability and degradation, as well as MYC binding to its interactome [738]. Some of these approaches have yielded prototype inhibitors that have entered early clinical trials [739]. However, the clinical responses to MYC inhibitor have been limited, often resulting in relapse, and are therefore inconsistent with their effects on MYC expression [740]. Clinical trials have raised also concerns about the safety of MYC-destabilizing therapeutics, with a number of trials resulting in significant toxicities and disease progression [741].

GCs have been found to repress MYC by an unknown mechanism [742]. It was suggested that DX suppressed the MYC gene at the transcriptional level in human leukemic cells [743]. MYC and p27 show functional antagonism in proliferation: MYC and the loss of p27 cooperate in animal carcinogenesis models and MYC abrogates p27 function in proliferation [744]. The antagonistic effect of MYC on p27 is mediated through several mechanisms. MYC down-regulates p27 at the transcriptional level and it induces Cyclin D and CDK4 expression, which sequester p27 into CDK-Cyclin complexes. In lymphoblastic leukaemia cells, GC-mediated G1 arrest was associated with accumulation of p27 and repression of MYC, Cyclin D3 and their downstream targets [730]. However, in the present work, the MYC level was only reduced after DAS+FL treatment in SAS cells but not with FL alone.

SFKs positively regulate DNA synthesis via the stabilization of MYC mRNA and thus increase the production of MYC. The mechanism of SFK-induced MYC mRNA stabilization is unknown but might involve the activation of a number of effectors including ABL, SHC and STAT3, as these are required for SFK-mediated DNA synthesis in response to mitogens [745]. Mechanistic studies revealed that cancer cells harboring elevated levels of MYC require the LYN kinase for survival and Dasatinib inhibits MYC overexpressing cells by negatively regulating the LYN

protein function [746]. Further studies are necessary to determine the exact molecular mechanisms by which MYC-expressing cells become dependent on LYN. One possible explanation for MYC reduction in SAS cells by combination treatment but not by DAS or FL individually could be related to the transcriptional level and mRNA stability. To address this, MYC mRNA expression could be evaluated upon treatment with DAS or/and FL for stabilization of mRNA and transcriptional activation. It also may be necessary to use higher doses of DAS or FL to fully inhibit MYC activity.

CDK1 modulates the initiation and transition process through mitosis of the cell cycle. Approximately 75 targets of CDK1 have been identified that control critical cell cycle events, such as DNA replication and segregation, transcriptional programs and cell morphogenesis [747]. CDK1 can be regulated by association with its major partner Cyclin B, reversible phosphorylation, and intracellular compartmentalization. CDK1/Cyclin B activity is restricted by the balance between WEE family kinases and CDC25 phosphatases. WEE1 is involved in the terminal phosphorylation and inactivation of CDK1-Cyclin B on Tyr15, resulting in G2 cell cycle arrest in response to DNA damage [748]. A strongly synergistic reduction of WEE1 and CDK1 total proteins levels was noted after the combination treatment (Figure 33). The phosphorylation of WEE1 at Serine 642 was diminished, possibly as a result of the reduction in the amount of total WEE1. The phosphorylation of CDK1 was reduced as well, possibly also due to WEE1 degradation and inactivation or due to the dramatic reduction of CDK1 itself. CDC25C is a phosphatase that activates CDK1 by removing inhibiting phosphate groups and a key enzyme for the transition of the cell into mitosis. The CDC25C total level was not reduced in SAS cells after DAS+FL treatment, suggesting that it has no relation to the reduction of CDK1 phosphorylation level. However, the changes in the expression levels of CDC25C may not correlate with its phosphatase activity. This would need to be tested.

Inhibition of cell cycle checkpoints in the presence of DNA damage, due to radiotherapy for example, results in the accumulation of the damaged DNA, culminating in cell death, as a result of irreparable genetic lesions. The deregulated activity of CDK1, a consequence of WEE1 or CDK1 depletion, has previously been shown to induce replication stress and loss of genomic integrity through subsequent nucleotide shortage and increased firing of replication origins [749]. WEE1 and CDK1 are key regulators of the G2/M transition and WEE1 inhibition consistent is with an induced improper mitotic entry, which could finally lead to mitotic catastrophe, as described during DAS+HSP90 treatment (5.6.3). However, in SAS cells, G1 arrest but not G2/M arrest was induced (Figure 32.A) after DAS+FL cotreatment, associated with WEE1 and CDK1 depletion. One possible explanation for this could be G2/M checkpoint abrogation inducing early cell division and accumulation of more cells in G1 phase, instead of G2/M arrest or mitotic catastrophe. Furthermore, CDK1 activity drops during mitosis because of Cyclin destruction and CDKIs re-expression. This drop in CDK1 activity is essential to exit from mitosis and resets the cell cycle to a basic G1 state of low CDK1 activity [747]. The last fact could be another possible explanation for the G1 arrest, whereas the cell could exit quickly from M phase to G1 phase due to CDK1 depletion by DAS+FL cotreatment.

FL, which reduced Cyclin D3 and increased p27 levels, slightly induced G1 arrest (60.1% to 69.2%) while DAS+FL caused more prominent arrest (60.1% to 81.4 %) which suggests that other factors than p27 and Cyclin D3 could drive this synergistic effect. WEE1 and CDK1 knockdowns (siRNA experiments) in TSCC might thus help to elucidate their effects on cell cycle distribution and cell survival upon DAS+FL treatment. Also, other cell cycle markers like other CDKs, Cyclins and CDK inhibitors could be evaluated in the future to determine if they

have any role in the G1 cell cycle arrest. CDK1 kinase activity was not analyzed in this study, but could also be investigated in the future.

In HNSCC, but also colorectal cancers and sebaceous gland carcinoma [750], CDK1 was found to be upregulated compared to non-cancer head and neck controls. This suggests that the alterations may appear as very early step of carcinogenesis [751]. Overexpression of WEE1 has been observed in several malignancies, including hepatocellular carcinoma, luminal and HER-2 positive breast cancers, glioblastoma and malignant melanoma, where high expression has been shown to correlate with poor disease-free survival [752]. CDK1 and WEE1 depletion by treatment with DAS+FL may be advantageous in these types of cancer. Since CDK1 or WEE1 inhibition make tumor cells sensitive to DNA damaging agents [753], TKI (DAS) and GC (FL), with their limited side effects, could also be investigated in combination with various DNA damaging agents or radiation.

Another question needs to be answered is about the underlying mechanism of how DAS and FL cooperate to deplete WEE1 and CDK1 levels. WEE1 and CDK1 were found to be ubiquitinated by the E3 ubiquitin ligase (SCF$^{\beta TrCP}$) for degradation which suggests that SCF ligases upregulation by DAS+FL cotreatment could be a possible mechanism for WEE1 and CDK1 destruction [754]. The induction of ubiquitin ligase expression in response to exogenous GCs was reported [755], therefore SCF ligase induction by DAS+FL cotreatment could be evaluated in the future. Many kinases and phosphatases, which also affect WEE1 or/and CDK1 stability and induce their degradation, could be possibly modified by DAS+FL treatment. To identify possible candidates, phosphorylation of WEE1 at sites involved in the control of WEE1 stability like Ser53, Ser123 and Ser139 could also be investigated. The recent use of a selective WEE1 degrader instead of a WEE1 inhibitor was 10-fold more potent than a WEE1 inhibitor [756]. Therefore, WEE1 degradation alongside with WEE1 inhibition in TSCC by DAS+FL combination treatment (Figure 33) seems to be an additional advantage over utilizing WEE1 inhibitors, which only inhibit WEE1 kinase activity but not reduced total protein level.

The WEE1 inhibitor (MK-1775) showed promising synergistic activity with Dasatinib in 2 TSCC lines during the high throughput screen (Figure 8). Additionally, WEE1 was observed in this work upon DAS+HSP90i treatment as HSP90 client protein (Figure 27). Additionally, WEE1 inhibition was, surprisingly, the result of the current DAS+FL combination treatment (Figure 33). This suggests that WEE1 is an important target for TSCC therapy. Moreover, the current finding correlates with the results from a kinase-centric chemical proteomics screen which quantified 146 kinases across 34 TSCC lines to identify new targets for individualized diagnosis or therapeutic intervention. The statistical analysis identified WEE1 kinase as having an important role in promoting and maintaining the survival of TSCCs. Apart from WEE1, LYN and EPHA2 (RTKs) were found to be novel targets with therapeutic potential in TSCC [200]. LYN is a member of the SRC kinase family and it is inhibited by Dasatinib. Dasatinib was found also as a very potent inhibitor of EPHA2 in TSCCs in the same study. In agreement with these results SRC and WEE inhibition by DAS+FL cotreatment and DAS+HSP90i cotreatment could possibly be new therapeutic options for TSCC patients.

6.3 Dexamethasone and Dasatinib Combination Treatment

6.3.1 Overview

Fluticasone is a potent synthetic GC that was shown to improve the cytotoxic activity of Dasatinib in TSCC lines in 2D culture especially in SAS cells (Figure 31). However, due to its very low oral bioavailability (1%), the clinical utilization of FL is limited to topical routes of administration for the treatment of asthma, COPD, inflammatory skin diseases, nasal polyps and allergic rhinitis. Systematic administration of the FL is not employed yet in the clinic to manage the side effects of chemotherapy and FL is not known to have any role in tumor progression inhibition. Therefore, it was also decided to investigate more systemically applicable GCs to check whether they also show a synergistic effect with Dasatinib on TSCC line viability.

Dexamethasone (DX) is a synthetic, long-acting GC available in multiple dosage forms that are used as therapy of severe hypersensitivity reactions, shock and control of severe inflammation. DX is the standard GC which is routinely prescribed to patients with advanced cancer in a wide range of doses (0.5 mg up to 16 mg daily) for a variety of reasons: fatigue, stimulation of appetite, night sweats, and to combat the side effects of some chemotherapies both as an antiemetic and to prevent hypersensitivity or allergic reactions [757]. It is also used specifically to decrease oedema associated with primary and secondary tumors of the central nervous system [758] or brain metastases in advanced melanoma [759]. DX is widely used in the treatment of hematologic malignancies and play as a single therapy or in combination with other drugs an essential role in the therapy of acute lymphoblastic leukemia [760], lymphoma [761] and multiple myeloma [762]. DX also has shown some anti-cancer efficacy in several solid tumors, such as prostate cancer [763] and lung cancer [764].

6.3.2 DX Enhances DAS Cytotoxic Activity in 2D-Cultured TSCC Lines

Based on previous reports, DX seems to be the most suitable GC candidate to be assessed in combination with DAS in TSCCs for synergistic activity. The highest plasma concentration of DX ,when humans are administered a single oral or intravenous dose of 4-10 mg of DX, is 100-200 nM [765] [766]. Therefore, 100 nM of DX was chosen to be combined with a DAS to assess the possible synergistic activity. TSCC lines were treated with serial dilutions of DAS as single agents or with DAS+DX combination and then cell viability was measured by resazurin colorimetric assay after 72 h of treatment (Figure 34 A, B and C). DX sensitized all of the investigated TSCC lines to DAS and synergistically enhanced its effect on the cell viability. Cell viability upon DX treatment alone was measured in the same experiment and yielded only a very slight effect on cell viability (Figure S21.B) so that the 'expected if additive' (EIA) effect was not calculated here. Inhibitory activity was increased in presence of DX in all cell lines, with a larger effect in the SAS cell line than in the CAL27 and BICR56 cell lines.

To further explore this synergistic interaction in 2D culture, trypan blue dye exclusion assay was performed to determine the number of viable and/or dead cells after treatments. 50 nM of DAS, which had a significant impact on protein expression in the previous experiments, was combined with 100 nM of DX. After a 72 h treatment, the numbers of viable cells were counted by an automated cell counter and normalized to Mock-treated cells (Figure 34.D). The proliferation of all TSCC lines was reduced more in the presence of DX compared to DAS alone. The reduction in the viable cell by DAS+DX cotreatment was synergistic in all cell lines whereas DX on its own again showed no notable effect.
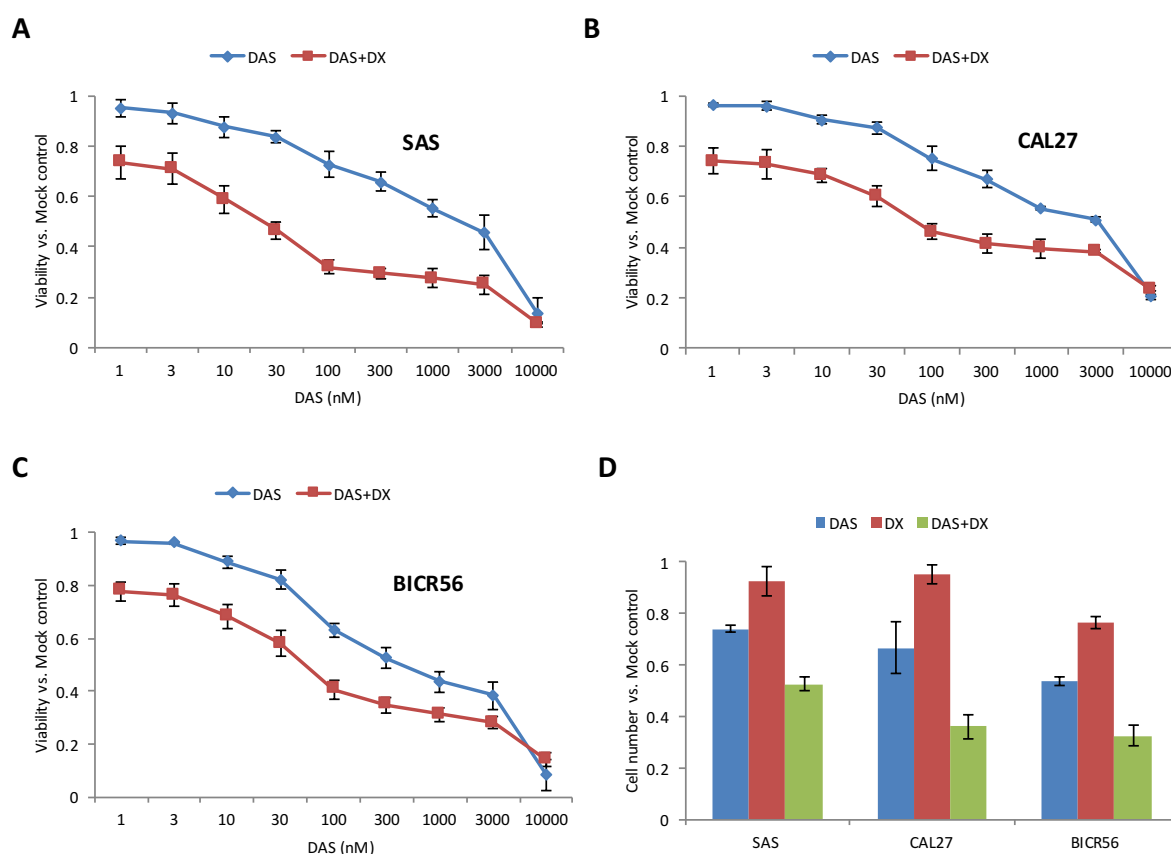
Figure 34. DAS synergizes with 100 nM of Dexamethasone (DX) to repress TSCC lines viability and proliferation in 2D culture

(A), (B) and (C) Addition of DX to DAS-treated cells reduces cell viability of TSCC lines
TSCC lines were treated with serial dilutions of DAS with or without 100 nM of DX for 72 h. Cell viability after treatment was measured by resazurin colorimetric assay. The inhibitory activities of DAS alone and DX alone were measured within the same experiment. An expected effect was not calculated here because DX alone has no notable effect on cell viability. Data represent fluorescence measurements normalized to Mock-treated cells. The dose response curves show mean values ± SD of three independent experiments with six parallel measurements in each case.

(D) Cell proliferation inhibition of DAS in TSCC lines is synergistically improved by addition of 100 nM of DX
TSCC cell lines were treated with DMSO as vehicle control (Mock), 50 nM of DAS, 100 nM of DX, and DAS+DX for 72 h. Cell proliferation was evaluated by staining cells with trypan blue (to exclude dead cells) and counting viable cells by automated cell counter. Cell numbers were normalized to Mock-treated cells. Values are expressed as means and standard deviation obtained from three independent experiments.

6.3.2.1 Clinical Applications of Dasatinib+Dexamethasone Combination Treatment

Dasatinib and Dexamethasone are already utilized clinically in double or even triple therapy for the treatment of acute lymphoblastic leukaemia (ALL) [767]. However, T-cell ALL is frequently characterized by GCs resistance and LCK (SRC kinase family member) was identified to have a critical role in cell proliferation [768]. Combination of DAS with DX resulted in significant drug synergy leading to cell death and the efficacy of this drug combination was underscored in a randomized phase II-like murine trial, recapitulating an early phase human clinical trial. In BCR-ABL[+] (Philadelphia Chromosome[+]) ALL, a triple combination with ABT-199

(inhibitor of the anti-apoptotic protein BCL-2), DX and DAS efficiently attenuates leukaemia progression in primary cell xenotransplantation models [769]. DAS was used mainly for targeting BCR-ABL but not SRC kinase. Triple-agent therapies were superior to the double drug combination DAS+DX both in terms of tumor growth and survival. A Phase II study of DAS and DX as primary therapy for adults with newly diagnosed BCR-ABL$^+$ ALL was published recently. DAS with DX was found to yield complete remission rates comparable to those reported with tyrosine kinase inhibitors combined with conventional chemotherapy [770]. Later on, DAS+DX followed by transplantation were approved to yield similar 3-year survival, comparable to approaches using intensive induction chemotherapy [771].

6.3.2.2. Possible explanations for the role of DX in the synergistic activity with DAS in TSCCs

SAS cells have been reported to produce a large amount of matrix metalloproteinases (MMP9) in comparison to other OSCCs [772]. MMP9 is secreted from tumor cells and involved in cancer invasion and metastasis by degrading extracellular matrices and break down of basement membranes containing type IV collagen, which is an initial step in cancer invasion. DX was found to significantly inhibit the protein production and gene expression of pro-MMP9 in SAS cells and did not affect the viability of the cells [772]. It also suppresses the expression of urokinase-type plasminogen activator (uPA), which is necessary to convert the proenzyme form of MMP9 to its active form. It was suggested that DX can mediate upregulation of IκBα which suppresses NF-κB transcription factor-transactivated expression of MMP9 and uPA [772].

In the future, MMP9 level could be assessed in TSCC lines upon DX single and combination treatments. Then the expression level of MMP9 in the investigated cell lines or even in a larger panel of TSCC lines could be correlated with the synergistic response of TSCCs to DX in combination with DAS. Also, the possible effect of DX on the expression of urokinase-type plasminogen activator and IκBα could be investigated to get possible Knowledge about the underlying mechanisms DX in this synergistic interaction. In the current work, FL treatment showed no on the effect in NF-κB total level obtained by Western blotting from the total cell lysate (Figure 33). Since the expression level is not a good measure for NF-κB activity, NF-κB activation assays could be applied instead, which follows the translocation of the p65 subunit of NF-κB into the nucleus as a hallmark of NF-κB activation. Cytoplasmic and nuclear fractions should be isolated and Western blots of the fractions used to quantify the relative p65 concentration. The ratio of nuclear relative to cytoplasmic p65 concentration provides a numerical estimate of NF-κB activation. Also, the translocation of NF-κB protein from the cytoplasm to the nucleus could be measured using automated fluorescent microscopy computer-assisted image analysis technology [773].

ETS1 is a transcriptional factor that has functions either as transcriptional activator or repressor of numerous genes. It is involved in cell senescence, death, and tumorigenesis and may control the differentiation, survival and proliferation. Phosphorylation of specific Ser/Thr residues in ETS1 enables binding to the COP1 tumor suppressor ubiquitin ligase complex for degradation. Tyrosine phosphorylation of ETS1 by SRC family kinases prevents COP1 binding and induces accumulation of ETS1 promotes which cancer growth [774]. In 2020, ETS1 was found to be a possible target for SRC kinase inhibition by DAS in TSCC where its depletion significantly impaired cell proliferation and survival, as well as cisplatin resistance [775]. Therefore, ETS1 expression and phosphorylation levels should be determined in the

future in TSCC upon DAS single or combination treatments. It was also found that DAS decreased ETS1 expression but increasedof IKKβ/NF-κB signaling in multiple Cisplatin-resistant TSCCs (CAL27 and SCC25) [775]. Simultaneous inhibition of SRC and IKKβ through a DAS and CmpdA (a IKKβ inhibitor) combination synergistically inhibited NF-κB activation and ETS1 expression, suppressed cell proliferation, and induced apoptosis. These findings support the possibility of using Dasatinib in TSCC and may also partially explain the role of DX in the current synergistic activity by inhibition of NF-κB in TSCC as described before [772].

6.3.3 GCs Strongly Potentiate DAS Soft Agar Colony Formation Reduction Power in TSCCs

A 3D soft agar colony formation assay was performed to investigate a potential growth inhibition of DAS+DX treatment in TSCC lines. As discussed in detail in the last chapter (5.4.1), the main advantage for the 3D cell culture is restoring more physiological cell-cell and cell–ECM interactions. Thus, it can mimic the properties of real tissues somewhat better than traditional 2D cultures. Initially, to test whether DX has any effect on TSCC colony formation, SAS cells were treated with a serial dilution of DX and seeded in soft agar for 14 days. As seen on the plate (Figure 35.A) and after counting (Figure 35.B), DX did not cause any substantial colony formation reduction in SAS cells in comparison to Mock-treated cells, even at a high dose of 10 µM which is physiologically unachievable. In contrast, DAS reduced colony formation in a dose-dependent manner as shown in Figure 35.C.

In order to find the optimum DX concentration for the combination treatment with DAS in the 3D culture, various concentrations of DX (3, 10, 30 and 100 nM) were combined with a fixed concentration of DAS (1000 nM for SAS cells, 100 nM for CAL27 and BICR56) and the cells were treated with the indicated concentrations for 14 days (Figure 36.A). The specific DAS concentrations were estimated from the dose-response curves in Figure 35.C. These concentrations individually did not show any substantial colony formation reduction. The SAS cell line is less sensitive to DAS in 3D culture than other TSCC lines, therefore 1000 nM of DAS was used, while in case of CAL27 and BICR56 cells, 100 nm of DAS was enough to produce synergistic activity with DX.

DX enhanced DAS activity in concentration-dependent manner. 30 nM of DX was sufficient to synergistically enhance the colony formation reduction capability of DAS in SAS cells and to a lesser extent in CAL27 cells, while it did not improve DAS activity in BICR56 cells (Figure 36.B). 100 nM of DX was sufficient to show synergistic activity with DAS and significantly reduced the colony formation in all cell lines especially SAS cell line which keeps the behavior to be the most sensitive cell line to this combination treatment even in 3D culture. Even though it would be possible to work with higher concentrations of DX *in vitro*, it was decided here to stay with physiologically obtainable concentrations to avoid generating data with concentrations not feasible for animal experiments and clinical trials. 100 nM of DX is, according to the most published data and pharmacokinetic studies, an achievable and acceptable plasma concentration for normal daily regimen [765] [766] [776]. Based on that fact and the obtained results in this study (Figure 36), 100 nm was used to evaluate synergistic interactions in 3D soft agar culture.
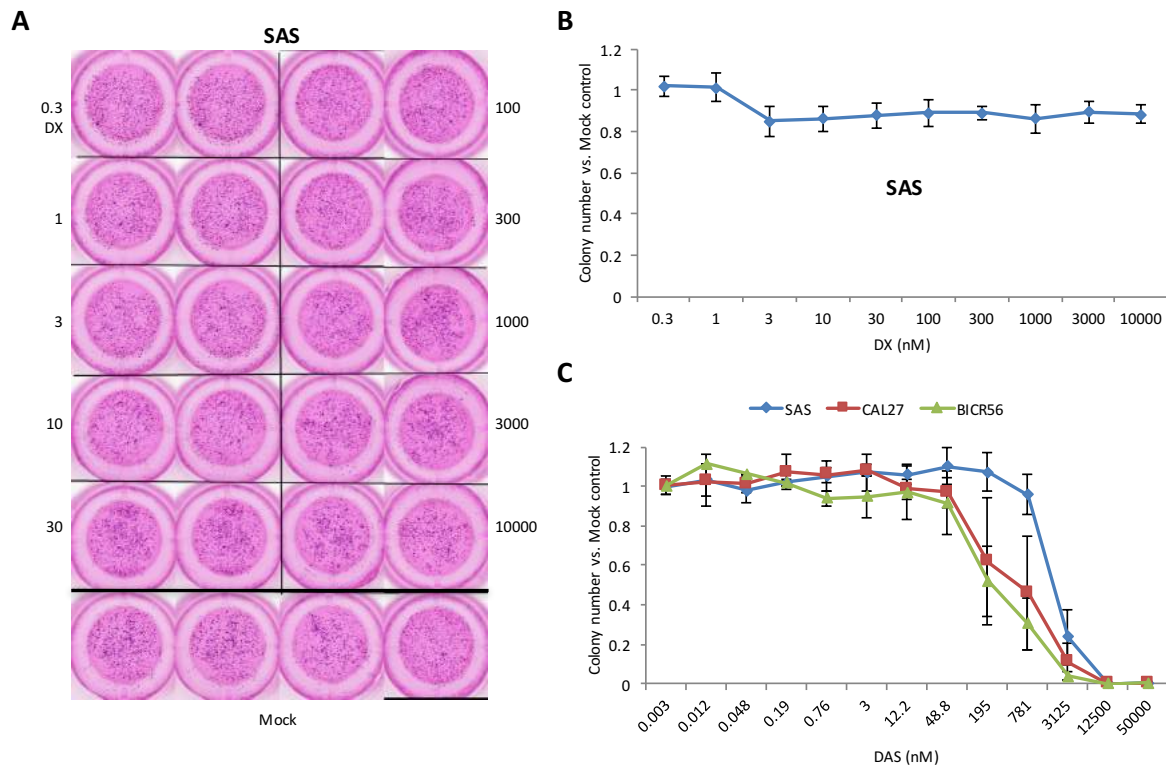
Figure 35. DX alone shows no effect on colony formation in 3D soft agar assay while DAS alone decreases colony formation in TSCC lines in a dose-dependent manner

(A) A representative image of 3D colony formation assay results for SAS cells treated with the indicated concentrations of DX for 14 days
The figure is representative of three separate experiments.

(B) Numerical representation of colony numbers in 3D soft agar culture for SAS cells which were treated with a serial dilution of DX
Colonies were counted and colony numbers were normalized to Mock-treated cells. The dose response curves show mean values ± SD of three independent experiments with 2 wells counted in each case.

(C) Dose-dependent colony formation inhibition of TSCC lines in response to serial dilutions of DAS in 3D soft agar culture
Data represent colony numbers normalized to Mock-treated cells. The dose response curves show mean values ± SD of three independent experiments with 2 to 4 wells counted in each case.

TSCC lines were treated with serial dilutions of DAS or DAS+DX and seeded in soft agar for 14 days. The dose-response curves show that 100 nM of DX synergistically improves colony formation reduction ability of DAS in TSCCs in comparison to DAS single treatment (Figure 37.A, B and C). Since DX alone does not inhibit colony formation (Figure 35.A and B), no expected additive effect was calculated. The half-maximal inhibitory concentration (IC_{50}) which represents the concentration of a drug that is required for 50% inhibition of cell growth was calculated using a four-parameter logistic function in the Sigamaplot 12.5 software. SAS cells which showed the least response to DAS single treatment (IC_{50} = 1963 nM) exhibited very high sensitivity to the combination treatment and the IC_{50} value was reduced by more than 60 times (34 nM) after adding 100 nM of DX (Figure 37.A). CAL27 cells also displayed great responsiveness to the DAS+DX cotreatment in comparison to DAS treatment and the IC_{50} decreased more than 130 times from 428 nM to 3.2 nM, respectively.

DAS+DX cotreatment showed less synergistic activity in BICR56 cells but the IC$_{50}$ was still reduced 13 times from 254 nM to 19 nM in comparison to DAS alone.
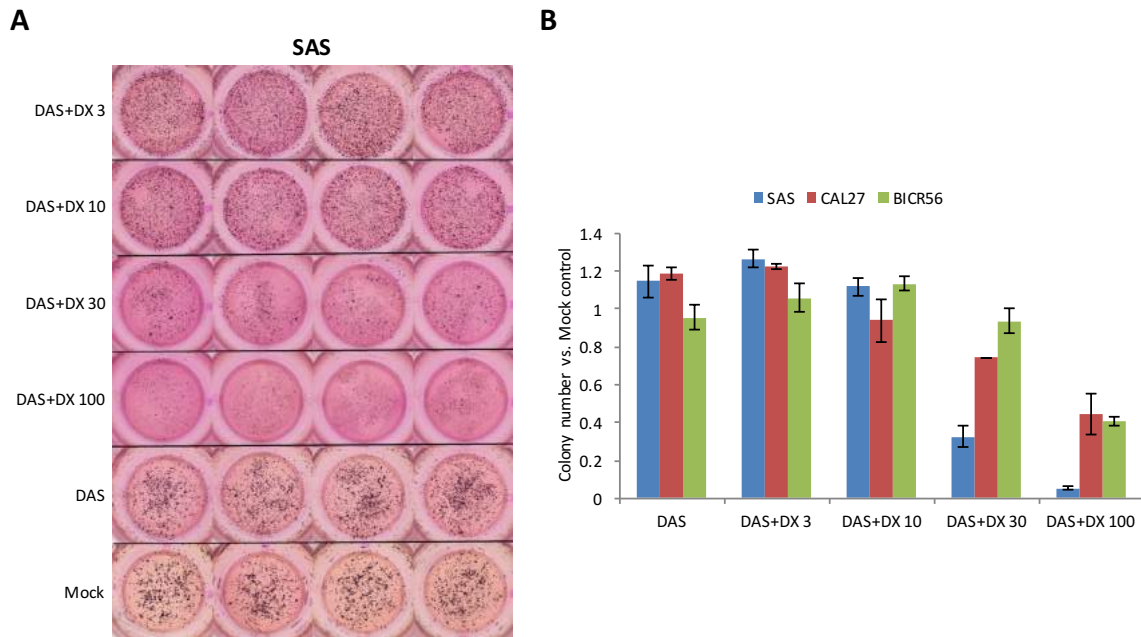
Figure 36. 30 to 100 nM of DX combined with DAS is sufficient to observe a synergistic effect in TSCC lines in 3D soft agar assay

(A) Synergistic reduction of colony formation by the combination of DAS with various concentrations of DX in SAS cells

Cells were treated with DMSO as vehicle control (Mock), 1000 nM of DAS and DAS plus the indicated concentrations of DX for 14 days. The Dasatinib concentration was decided according to the dose response results in Figure 35.C. The figure is representative of three independent experiments.

(B) Bar graph representation of colony formation in TSCC lines

Data represent colony numbers normalized to Mock-treated cells. The Dasatinib concentration was chosen from the dose-response curve in Figure 35.C (1000 nM for SAS cells, 100 nM for CAL27 and BICR56). Values are expressed as means and standard deviation obtained from 3 independent experiments with 4 wells counted in each case.

By comparison, it was previously reported that in a panel of lung adenocarcinoma cell lines, only cells expressing relatively high levels of GCR showed reversible growth arrest [720] [777]. So, GRC status in SAS, CAL27 and BICR56 cell lines was evaluated to find a possible explanation for the difference in the synergistic responses of TSCC lines to GCs (DX or FL) in combination with DAS. As shown in Figure S22, no significant difference was found in GCR expression levels in the three cell lines. However, future analysis for GCR status including a larger panel of TSCC lines may give a more precise perception about the relationship between GCR expression and GC response in TSCCs. If this correlation could be achieved then it could become a prognostic marker for using DAS+GC combination in tongue cancer and maybe other cancers.
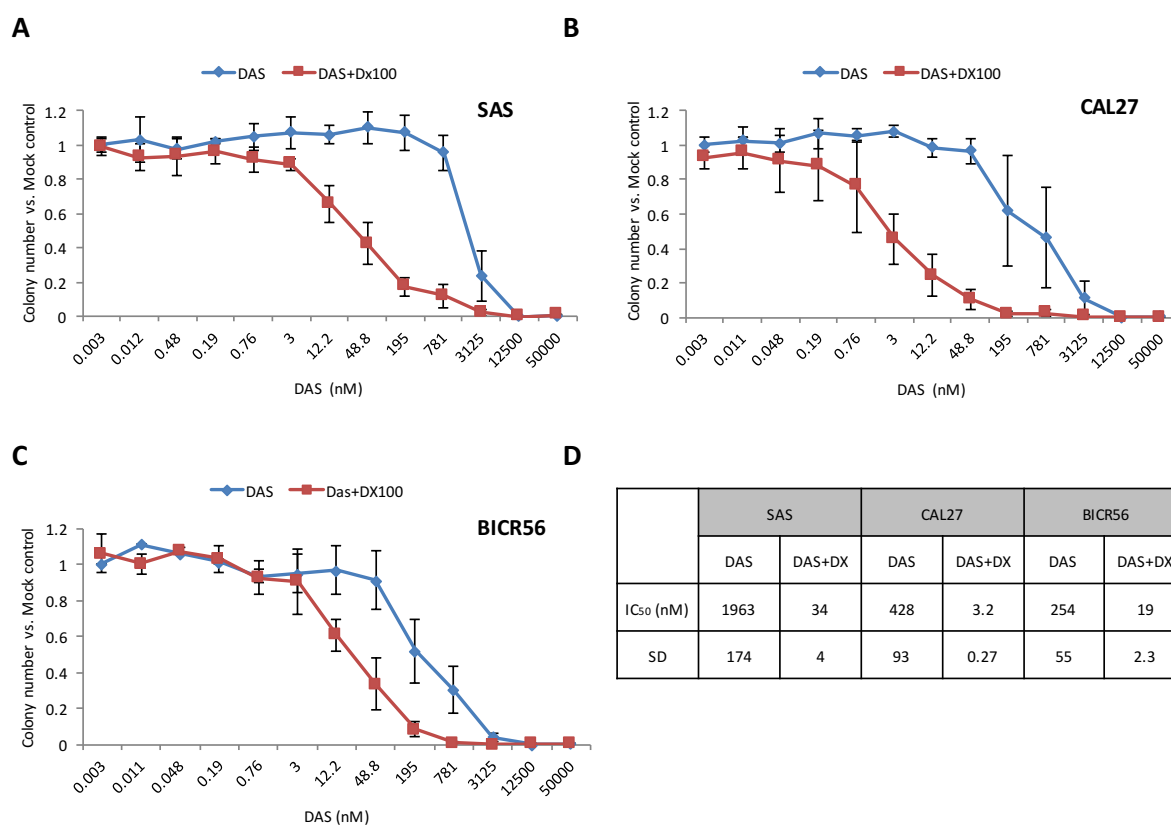
Figure 37. DAS+DX combination treatment shows a strong synergistic effect in TSCC lines and greatly reduces IC$_{50}$ values of DAS in 3D soft agar culture

(A), (B) and (C) Dose response curves of TSCC lines treated, with DAS with or without a constant concentration of DX (100 nM), as determined by colony numbers in 3D soft agar culture
The colony numbers for samples after treatment with DAS and DAS+DX were counted within the same experiment. Data represent colony numbers normalized to Mock-treated cells. An expected effect was not calculated here since DX individually has no notable effect on colony formation as shown before (Figure 35.A and B). The dose response curves show mean values ± SD of three independent experiments with 4 wells counted in each case.

(D) Comparison of the average IC$_{50}$ values for DAS alone and DAS+100 nM DX assessed by colony counting in TSCC cell lines
IC$_{50}$ values, defined as the concentrations of the compound at which 50% of cell growth inhibition occur, were calculated using a four-parameter logistic function in Sigamaplot 12.5 software and are presented as the means ± SD from three independent experiments.

The current results show that TSCC lines cultured in 3D soft agar are remarkably more sensitive to DAS+DX combinations than in 2D cultures. How DX, which itself has no notable activity, increases TSCCs responsiveness to DAS in a 3D culture is unclear. One possible explanation could be a shift in the expression levels of various genes responsible for the proliferation, angiogenesis and invasion by DX. Changes in overall gene expression in 3D culture were reported in TSCC, concerning cell junctions, cell adhesion, cytochrome P450 metabolism, cell cycle, DNA mismatch repair and DNA replication [424]. While cell adhesion and cell junction gene expression was increased in TSCC and could participate in DAS resistance, it is possible that DX transrepresses these genes. Moreover, increased levels of the drug transporters like PGP and BCRP were found to reduce the levels of substrate drugs within cells in 3D culture, therefore this may contribute to the decrease in drug efficacy. So,

it is possible that DX transrepression of DAS transporters increases DAS levels and activities in TSCC.

An overexpression of RTKs in 3D cell cultures has previously been associated with resistance to TKIs [778]. It is possible that receptors which have a great impact on metastasis, like MET, are inhibited in the 3D culture by DX or DAS+DX treatments which potentiate DAS activity and reduces its resistance. However, the role of GCs in TSSC metastasis and invasion reduction, which is indicated by the lack of colony formation, has not been well studied. *In vitro* cell models have shown that GCs can suppress cell migration and invasion through several different mechanisms, such as down-regulation of the GTPase RhoA [694], MMP2/9 or IL-6 [695]. For DX in SAS cells in particular, it was previously found that it significantly inhibits the protein production of MMP9 [772]. Also, it was demonstrated that DX and the highly potent class I histone deacetylase (HDAC) inhibitor Largazole cooperate to induce E-cadherin localization to the plasma membrane in breast cancer and to suppress invasiveness *in vitro* [696].

A novel mechanism for suppressing cancer metastasis by GCs through one of the metastasis suppressor microRNA (miRNA) has been proposed by Lin *et al.* [698]. miR-708 regulates gene expression in a highly specific manner on the post-transcriptional level and suppresses cancer progressions in certain types of cancers. Treatment with DX induces miR-708 transcription, leading to the inhibition of the GTPase Rap1B, which results in the reduction of integrin-mediated focal adhesion formation, inhibition of ovarian cancer cell migration/invasion and impaired abdominal metastasis in an orthotopic xenograft mouse model [698].

Recently, it was reported that SRC kinase activity is high in Burkitt lymphoma (BL) cell lines which have resistance to conventional drugs, including Dexamethasone [779]. Multidrug resistance 1 (MDR1; an efflux pump for xenobiotic compounds) and Survivin (an anti-apoptotic survival factor) expressions were higher in DX-resistant BL cells. Suppressing SRC with Dasatinib restored Dexamethasone sensitivity by reducing Multidrug resistance 1 and Survivin overexpression in DX-resistant BL cells. Also, DAS+DX combination exhibited a synergistic effect on cell proliferation in BL cells. A major difference in the published work is the very high and physiologically not achievable concentration of DX between 20 to 100 μM. Also, in the previous study, the synergistic effect was only examined by trypan blue assay in 2D culture. Nevertheless, this study could possibly provide an explanation for the currently observed synergistic interaction between DAS and DX in TSCC, which could be explored in the future [779].

After the promising results for DAS+DX combinatuin treatment in 3D soft agar, DAS+FL was also tested in 3D soft agar culture for possible synergistic activity with DAS. Initially, TSCC lines were treated with a serial dilution of FL to test whether FL has any impact on the colony formation ability. The dose-response curves in Figure 38.A show that, similar to DX, FL as a single treatment has no visible effect on 3D soft agar colony formation in treated SAS and CAL27 cells compared to Mock-treated cells. To evaluate possible synergistic activity, different concentrations of FL (3 to 100 nM) were combined with a fixed concentration of DAS (1000 nM for SAS cells and 100 nM for CAL27), which were determined from the dose-response curves in Figure 35.C as described before. After 14 days of seeding in soft agar, no colonies were seen in any of the DAS+FL combinations. This indicated that the used concentrations of FL were too high and had a very strong synergistic activity with DAS. Therefore, lower serial concentrations (0.003 to 10 nM) were tested in combination with the same concentrations as before of DAS in SAS and CAL27 cells (Figure 38.C). As shown in

Figure 38.B, 0.3 nM and 1 nM of FL was sufficient to produce strong synergistic colony formation reduction activity with DAS in SAS and CAL27 cell lines, respectively.
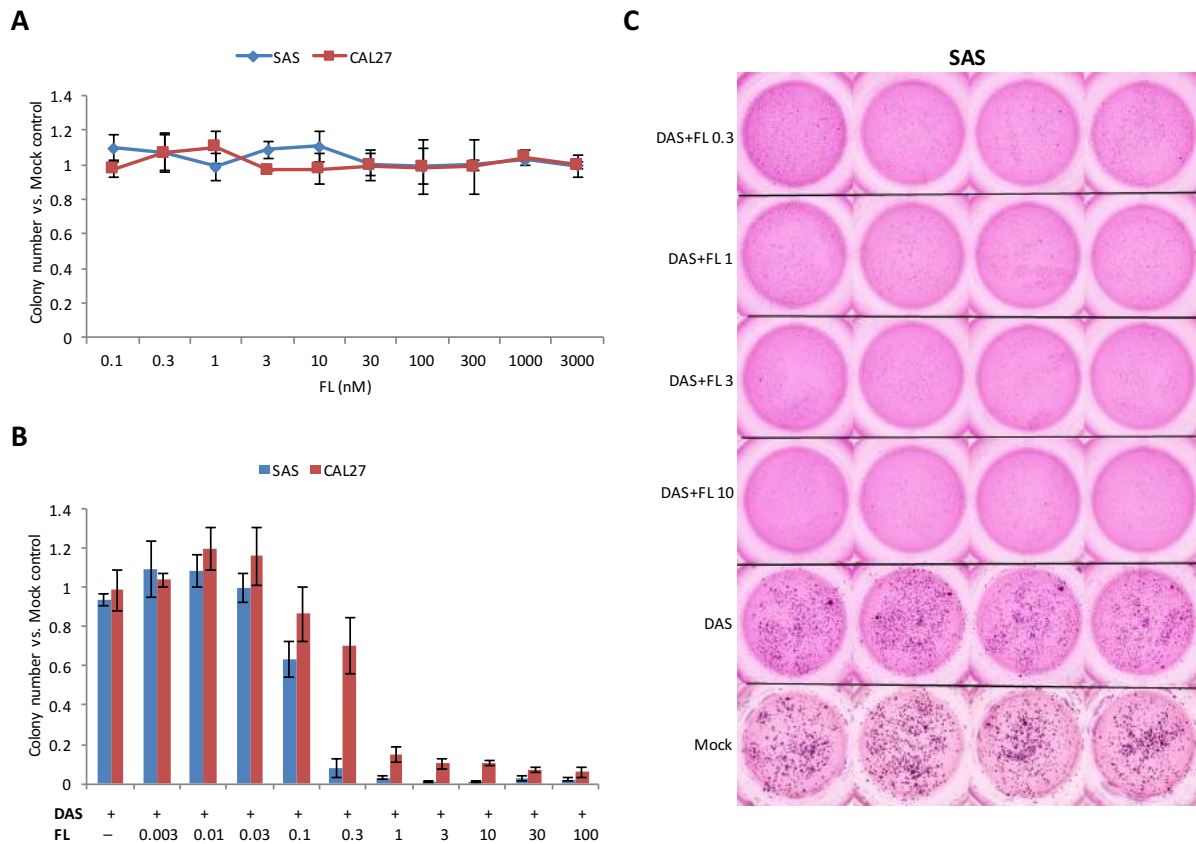
Figure 38. FL single treatment shows no significant effect on colony formation in 3D soft agar assay, while DAS+FL combination treatment displays a very potent synergistic effect in TSCC lines

(A) Numerical representation of colony counts in 3D soft agar culture for SAS and CAL27 cell lines treated with FL alone shows no reduction of colony numbers
TSCC lines were treated with a serial dilution of FL for 14 days. Data represent colony numbers normalized to Mock-treated cells. The dose response curves show mean values ± SD of two independent experiments with 4 wells counted in each case.

(B) Numerical representation of colony count results for TSCC lines treated with DAS and DAS plus a serial dilution of FL (nM) for 14 days in 3D soft agar culture
FL shows more potent synergistic activity with DAS than DX (Figure 34). Dasatinib concentrations were obtained from the dose response curve in Figure 35.C (1000 nM for SAS cells and 100 nM for CAL27). Data represent colony numbers normalized to Mock-treated cells. Bars show mean values ± SD of two independent experiments with 4 wells counted in each case.

(C) 3D colony formation results for SAS cells treated with DMSO as vehicle control (Mock), 1000 nM of DAS and DAS plus the indicated concentrations of FL (nM) for 14 days
The figure is representative of two separate experiments.

This result indicates that FL at 0.3 to 1 nM in combination with DAS significantly inhibits the colony formation of TSCCs while 30 to 100 nM of DX was required to induce a comparable reduction. This means that FL is much more potent than DX in combination with DAS and a lower concentration of FL is enough to exhibit the same synergistic activity in 3D cultured TSCCs. The higher potency of FL could be due to its high relative GCR receptor affinity (RRA). The binding ability of inhaled GCs to GCR is compared with DX which has a binding affinity of

100 while FL has a binding affinity of 1800 [780] [781] [782]. In practical terms, this means that an 18-fold higher concentration of DX at the receptor site is needed to produce the same degree of receptor occupancy as FL. With a higher potency, less FL is needed to exert a synergistic effect with Dasatinib. To prove this assumption, a direct comparison between 100 nM of DX and 10 nM of FL in combination with serial dilutions of DAS was performed in the same experiment. SAS, CAL27 and BICR56 cells were treated with DAS alone, DAS+DX 100 nM or DAS+FL 10 nM and the dose response curves are shown in (Figure S23). 10 nM of FL and 100 nM of DX produced comparable synergistic colony formation reduction in combination with DAS compared to DAS single treatment.

However, the therapeutic efficiency of DAS alone and its synergistic interaction with GCs still needs to be confirmed in the animal experiments (mouse xenografts). SAS and CAL27 xenograft models were established already a few years ago [783] [784]. In a preliminary experiment, the subcutaneous injections of both cell lines produced suitable and measurable tumors for further investigations (data not shown). The next step in the near future will be dosing of the compounds after xenografting to evaluate their *in vivo* activity.

Xenograft mouse models can be divided into ectopic or orthotopic mouse models depending on the tumor location. In ectopic mouse models, tumor cells are subcutaneously injected into the flank or the back, as it was preliminary done in this work, while in orthotopic mice, tumor cells are typically transplanted into an environment that is more similar to the original tumor environment. Orthotopic human SAS and CAL27 oral carcinoma-bearing mouse models have been established [785] [786]. In the current research, utilizing the orthotopic models could provide an opportunity to use the more potent FL topically, which overcomes the pharmacokinetic limitations of this drug. Furthermore, transduction of TSCCs with lentivirus expressing red fluorescent protein followed by injection into tongues of immunodeficient mice generates orthotopic tongue tumors that can be monitored for growth and metastasis by fluorescence measurement with an *in vivo* Imaging System [787].

Also, orthotopic models could be employd to investigate Fluticasone furoate in combination with DAS as a possible synergistic candidate against TSCC. GCR binding kinetics of Fluticasone furoate shows a remarkably fast association and a slow dissociation, resulting in a relative receptor affinity (RRA) of 2989 vs. an RRA of 100 for DX and an RRA of 1800 for Fluticasone propionate which means a 30 times stronger binding than DX [788]. The RRA of Fluticasone furoate exceeds the RRAs of all currently clinically used GCs. This opens the door to application of a very low topical dose of this drug in combination with DAS in the orthotopic model to evaluate the synergistic activity against TSCC and overcome the pharmacological limitations to avoid possible side effects from the systemic treatment.

6.3.4 Characterizing DAS+DX Activity in TSCCs

DAS as SRC kinase inhibitor has a more straightforward signaling mechanism of action in TSCC than DX, namely the inhibition of SRC kinase downstream targets like p130CAS, Paxillin, CRKL, GAB1, STAT5 and STAT6, among others (Figure 22, S11 and S12). Recently it was also shown that DAS decreases the ETS1 (transcription factor) expression in TSCCs, which could partially explain its underlying mechanism of action [775]. How DX contributes to the synergistic effect, especially in the 3D colony formation assay, still needs to be determined. Therefore, possible molecular targets of DX in TSCC were identified to better understand its impact on signaling activities.

6.3.4.1 Phosphorylation Profiles upon DAS and DX Treatments

In many pathways, phosphorylation-mediated cellular signaling relies on a dynamic relationship between proteins, which generates site- and time-specific phosphorylation and dephosphorylation events [789]. The post-translational modification of tyrosine residues by reversible addition of a phosphate group is a powerful signaling switch in a wide range of cellular events which regulate enzymatic activities and protein-protein interactions in cancer cells. Many growth factors act through receptor tyrosine kinases and subsequent phospho-tyrosine-dependent signaling cascades to control cell proliferation, migration, and adhesion. Cells responding to internal or external regulatory inputs modify their phosphorylation status. Cancer cells can therefore often be diagnosed by observing alterations in their qualitative or quantitative phosphorylation profile [790].

As a consequence, examining the phosphorylation profile of a cell is central to the understanding of its signaling pathways. Because diverse cell responses to anticancer treatment are related to alternations in the phosphorylation status of the cell proteome, the determination of the phosphorylation profiles of cancer cells represents an important tool for our understanding of cellular responses. For this purpose, in the current work, the possible alterations in TSCCs phosphorylation profile upon treatment with DAS and/or DX were used, to find possible mechanistic targets, especially for DX. Anti-phosphotyrosine antibodies like 4G10 and PY1000 are widely used as experimental tools to monitor the general phosphorylation status of a cell [434]. Therefore, TSCC lines were treated with DMSO (as a control), 50 nM of DAS, 100 nM of DX or DAS+DX for 72 h. Then they were subjected to Western blot analysis and probed with 4G10 and PY1000 antibodies for characterization of the levels of protein tyrosine phosphorylation. The immunoblot analysis for tyrosine phosphorylation profiles revealed prominent reductions in phosphorylated proteins at apparent molecular weights of around 120 and 135 KDa upon DAS+DX combination treatment (Figure 39 and S24).

As seen in Figure 39, the 4G10 and PY1000 antibody stains show a similar band pattern, although the relative band intensities differ. Even though the recognition specificity of 4G10 and PY1000 antibodies is largely overlapping, utilizing the phosphorylation profiles produced by 4G10 and PY1000 together is an appropriate approach for the identification of a larger number of pY peptides. It was shown that phosphotyrosine antibodies display a sequence preference. For example, the logo analysis of the 4G10-specific peptides reveals a clear enrichment in negatively charged amino acids at positions +1 and, to a lesser extent at −2 and +2 [791].

To confirm this result and to identify the phosphorylated proteins, mass spectrometry (MS) could be used. MS technologies boost the ability to characterize the cell state by allowing the identification of a large number of phosphotyrosine peptides in cell lysates under various physiological and pathological conditions [792] [793] [794] [795]. In principle, it is now possible to perform experiments in which almost the complete phosphotyrosine proteome and its dynamic changes can be monitored. For example, intensity-based label-free MS was previously employed to identify new targets for individualized diagnosis or therapeutic intervention in 34 TSCC lines and identified kinases, including EGFR, NEK9, LYN, JAK1, WEE1, and EPHA2, which are involved in cell survival and proliferation [200].
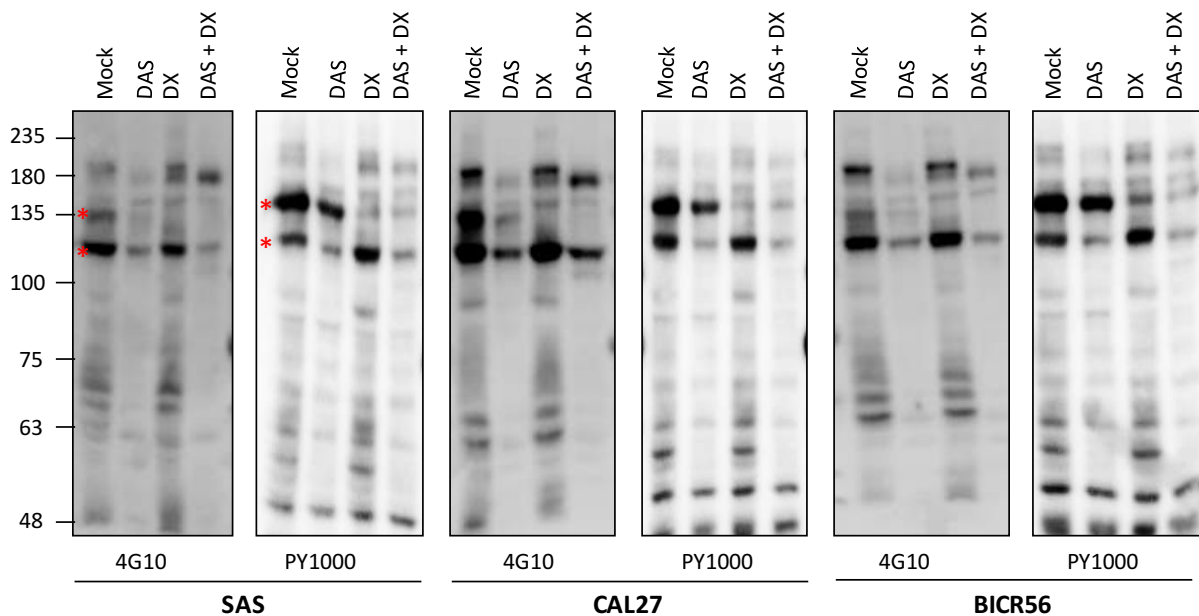
Figure 39. Tyrosine phosphorylation profiles of treated TSCC lines show two major reductions in phosphorylated proteins (around 120 and 135 KDa) upon DAS+DX combination treatment

Cells were treated with DMSO as vehicle control (Mock), 50 nM of DAS, 100 nM of DX or DAS+DX for 72 h before extraction. Total cell lysates were separated by 8 % SDS-PAGE and immunoblots were probed with the anti-phosphotyrosine antibodies 4G10 or PY1000. Protein size markers are indicated on the left. The two most prominently reduced bands are indicated by red asterisks. For a direct comparison of the different cell lines on the same blot see S24.

6.3.4.2 DAS+DX Combination Suppresses MET and SRC Kinase Signaling Pathways in TSCCs

In an intial attempt to identify the two most prominently reduced bands, the membrane which was probed with phosphotyrosine antibody 4G10 was stripped as described in the experimental section (2.2.11) and then reprobed with anti-MET pTyr1234/1235 antibody (145 kDa). The upper band, indicated by the red asterisk (Figure 39), overlayed exactly with the phosphotyrosine MET band and was reduced mainly due to DX treatment. The same membrane was stripped again and reprobed with p130CAS pTyr410 antibody. As expected and shown previously (Figure 4 and 13), the lower band indicated by the red asterisk overlays exactly with the phosphotyrosine p130CAS band, which is highly phosphorylated in TSCC and repressed by SRC kinase inhibitor DAS but not DX (data not shown).

To investigate further these previous results, the phosphorylation of MET at Tyr1234/1235, GAB1 at Tyr627, SRC at Tyr416 and p130CAS at Tyr410 as well as the total protein levels were assessed by Western blotting in TSCC lines treated with the previously used drug

combinations. As shown in Figure 40, MET phosphorylation was greatly diminished upon DX treatment. Also, GAB1 phosphorylation at Tyrosine 627, a downstream target for MET which provides potential binding sites for the SHP2 phosphatase, was inhibited by DX. Both drugs showed no effect on the total protein levels. On the other hand, as shown before, DAS inhibited SRC and p130CAS phosphorylation without any obvious contribution from DX (Figure S25). In agreement with the results from the DAS+FL treatment, DAS+DX synergistically also reduced the total level of p130CAS but not SRC. The total level of GCR was not changed upon the current treatments in the TSCC lines (Figure S25).

Mesenchymal epithelial transition factor (MET) is a RTK activated by HGF. It can activate signaling cascades including the RAS, PI3K, STAT3, FAK and NOTCH pathways, resulting in cell morphogenesis, motility, growth or survival (Figure 41). In normal cells, MET activation is a tightly controlled, ligand-dependent and transient event, whereas in tumor cells, MET is often constitutively activated. Many studies found that the HGF/MET axis is implicated in various human cancers. Genetic and epigenetic gain of functions of this signaling system contribute to cancer development through a variety of mechanisms. Overexpression of HGF/MET has been observed in more than 80% of HNSCC tumors and preclinical and clinical studies linking MET overexpression with cellular proliferation, invasion, migration, and poor prognosis [476]. Overexpression of MET, as reported in OSCC, can facilitate disruption of E-cadherin junctions and enhanced invasion and metastasis [472]. HGF/MET signaling was found to play an important role in the tumorigenic properties of OSCC cells via the AKT, ERK1/2, and NF-κB pathways and plays an essential role in the progression of human OSCC [796].
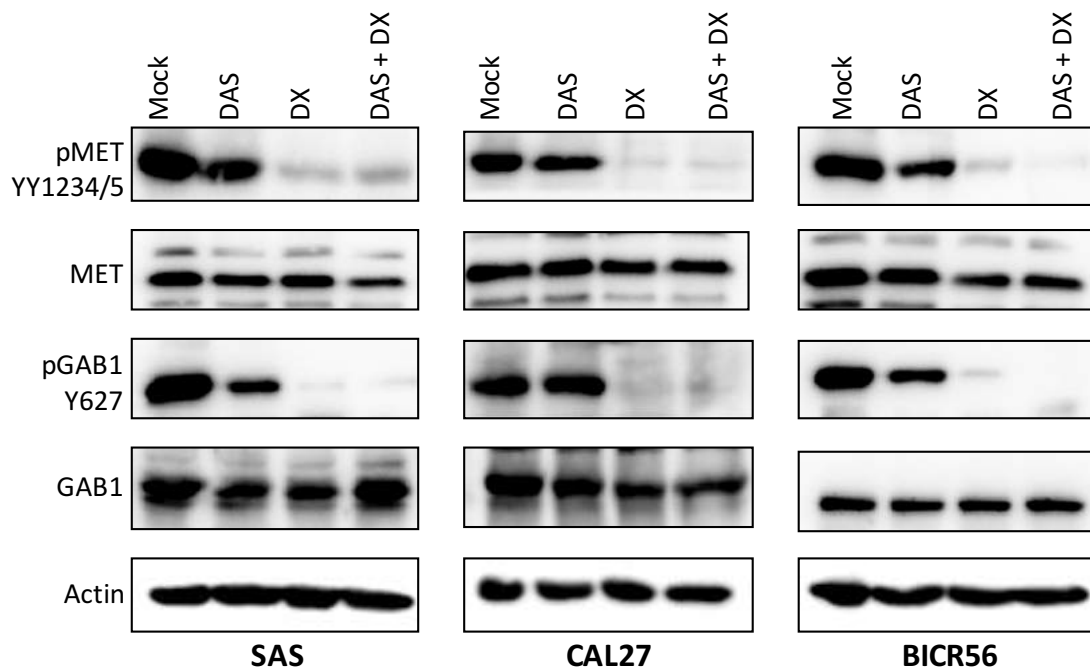
Figure 40. DX or DAS+DX combination treatment suppresses the MET kinase signaling pathway in TSCC lines

Cells were treated with DMSO as vehicle control (Mock), 50 nM of DAS, 100 nM of DX, or a combination of DAS+DX for 72 h. Total cell lysates were generated, separated by SDS-PAGE and analyzed by Western blotting. Antibodies that detect the phosphorylated state of MET at Tyr1234/1235 and GAB1 at Tyr627 were used to monitor the change in tyrosine phosphorylation. The other blots analyzed total protein abundance. The blots shown are representative of three independent experiments.

Activation of the HGF/MET axis can induce different phenotypes, depending on tumor stage: it may provoke proliferation and angiogenesis in primary tumors, stimulate motility to form micrometastases, and regain the proliferation phenotype to form apparent metastases [476]. MET activation can also promote cellular morphogenesis, enabling cells to acquire mesenchymal phenotypes, in part through the epithelial-mesenchymal transition, which contributes to metastasis. In 3D soft agar culture, colony formation is correlated with anchorage-independent growth of cancer cells, which is a key aspect of the tumor phenotype and particularly effects metastatic potential [797]. Therefore, inhibition of MET kinase activity could partially explain the potent DAS+DX synergistic activity in 3D culture.
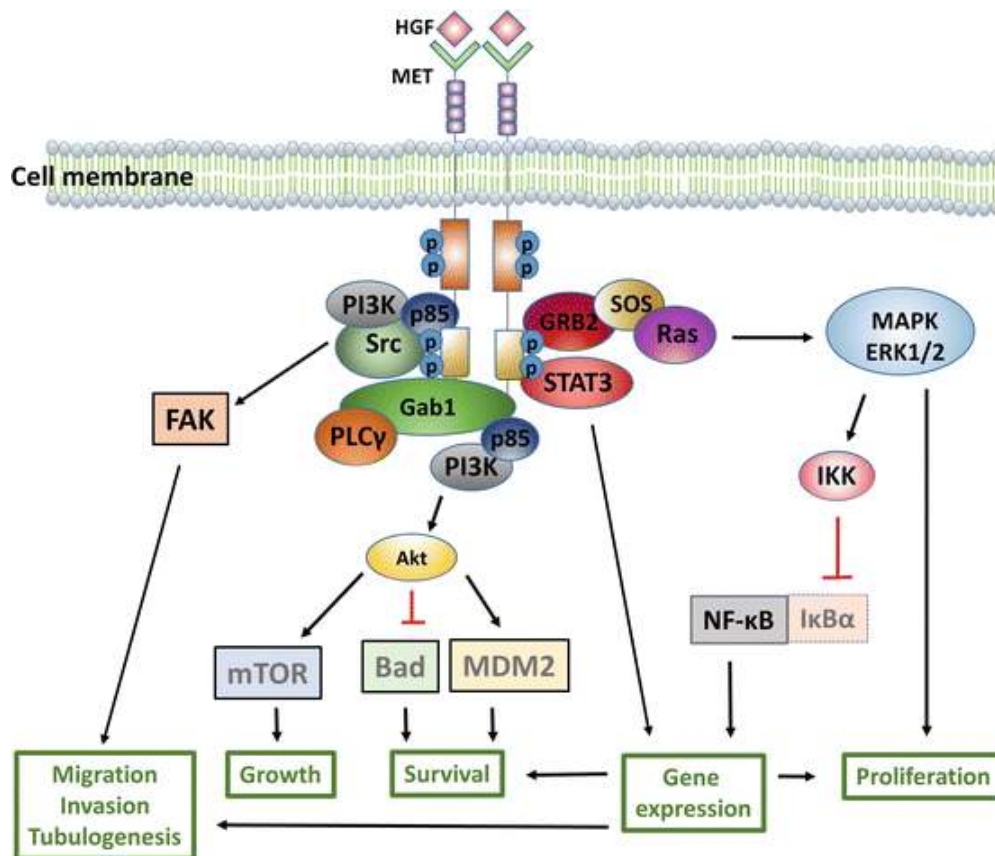
Figure 41. HGF/MET signaling cascades

Upon binding of HGF to its receptor MET, MET signaling is activated by phosphorylation of MET Tyr1234 and Tyr1235 residues and other tyrosines. The activated MET signaling pathway regulates diverse cellular processes including cell proliferation, differentiation, migration, invasion, and survival depending on the cell type investigated. GAB1 is a central player in these regulatory processes. Figure from [798].

In tongue cancer, the main causes of treatment failure are local/regional recurrence, distant metastasis from invasion, and metastasis of tumor cells into adjacent tissue [134]. A previous study off 99 patients with TSCC demonstrated that the expression level of MET was significantly correlated with local and distant metastatic tumor recurrence [799]. Another study found a relationship between MET expression and tumor invasion depth and lymph node metastasis in 71 surgically treated patients with TSCC. In this study, statistically significant correlations between MET expression, lymph node metastasis and >4 mm depth of tumor invasion in patients with TSCC was revealed [477]. Furthermore, high levels of MET expression were associated with decreased patient survival. In the same study, it was also shown that

constitutive activation of MET enhanced migration and invasion of TSCC *in vitro* through the expressions of MMP1, 2, and 9, and promoted tumor cell growth *in vitro* and *in vivo*. As described beforehand, in SAS cells, DX was found to significantly suppress the protein production of MMP9 which is involved in cancer invasion and metastasis by degrading extracellular matrices [772]. Taking all together, DX could therefore potentially sensitize TSCC to DAS and reduce their metastatic activity by inhibiting MET kinase and MMP9 expression.

MET expression is associated with the invasiveness and metastasis of TSCC [477] and therefore it could be a biological and clinical marker for assessing prognosis in patients with TSCC and at the same time an important potential therapeutic target in tongue cancer. Many different strategies have been employed to inhibit aberrant MET signaling in various human cancer cells. These strategies have targeted, directly or indirectly, the MET receptor and/or its ligand HGF. Several agents have been developed to target both the HGF ligand and MET receptor including small-molecule TKIs, mAbs, competitive HGF antagonists and MET receptor decoys. Indirect inhibition of MET signaling can be achieved by blocking MET downstream signaling pathways, such as the MAPK, PI3K or STAT3 pathways, which contribute to the malignant properties of MET.

Several therapies for selectively targeting MET have potent antineoplastic effects in preclinical HNSCC models, with some agents advancing to clinical development [476] [800]. However, despite pre-clinical evidence of anti-cancer activity and initial promising results in early phase trials, most phase II and III trials of MET inhibitors in several tumor types failed to demonstrate clinical efficacy. The main issues behind the failure of these trials have been related to patient selection, like the identification of effective biomarkers to select those patients who are likely to derive the most benefit from targeted MET inhibition, and also related to the primary resistance mechanisms to monotherapy treatment [801].The risk of accumulated toxicity and the potential for overlapping toxicities in combination strategies remain the most common limitations among MET inhibitors in clinical application. Due to challenging toxicity profiles of MET inhibitors, a high number of patients needed dose reductions or discontinued treatment and even lethal toxicity has occurred in some patients [801] [802] [803]. A major reason for that is inhibition of targets beyond MET which are associated with increased toxicity and limit the achievable dose so that MET cannot be inhibited effectively. Moreover, the antitumor activity of fairly nonselective MET inhibitors may be mostly due to their activity against non-MET targets, making it impossible to ascribe drug effects observed in trials specifically to the inhibition of MET [803].

Unlike MET inhibitors, DX is a benign medication that causes little toxicity and is frequently used to control side effects of other anticancer drugs. The low toxicity of DX improves its tolerability and may enable dosing of DX at levels that cause profound inhibition of MET kinase activity. MET inhibition by DX and the synergistic activity of DAS+DX need to be tested *in vivo*. This is can be done by ectopic xenograft or by orthotopic models involving a submucosal injection of TSCC into the tongue of immunocompromised mice, which allows for a more representative microenvironment and assessment of regional and distant metastasis. DX could be also assessed in other cancers for its MET kinase inhibition ability, especially in cancer with known MET overexpression including breast cancer (17%), lung cancer (40%), gastric cancer (>95%), colorectal cancer (78%), ovarian cancer (31%), kidney cancer (70%), pancreatic cancer (>70%) and other HNSCC [804].

MET overexpression/amplification is also an important mechanism for acquired resistance to EGFR-TKIs and EGFR mAbs which occurs in approximately 5–22% of NSCLC patients [805] [806] and 30% of metastatic colorectal cancer patients [807]. Mechanistically, MET amplification

causes EGFR-TKI resistance by activating EGFR-independent phosphorylation of ErbB3 and downstream activation of the PI3K/AKT pathway, providing a bypass pathway in the presence of an EGFR inhibitor. This promotes the proliferation of cancer cells, which ultimately leads to the resistance of patients to EGFR inhibition. Co-targeting of EGFR and MET in TSCC was found to overcome acquired resistance to Erlotinib and to inhibit the invasion and metastasis of Erlotinib-resistant cells [808]. Based on this and taking into consideration the toxicity of MET inhibitors and the MET inhibition activity of DX, combinatorial therapy with DX and EGFR inhibitors could be considered for these cancer cells with resistance to anti-EGFR therapies which carry *MET* amplification and/or protein hyperactivation.

MET kinase inhibition by DX in TSCC is a novel finding and could be a promising therapeutic strategy in TSCC and other tumors, especially cancers dependent on MET. Oral leukoplakia, the most common oral premalignancy, is poorly predictive of cancer risk, and surgical resection has not been shown to reduce oral cancer development [809]. Recent data suggest that MET activation may represent an early driver in oral leukoplakia. MET was also identified as a potential prognostic marker of cancer risk in patients with oral leukoplakia and a predictive marker to prevent malignant transformation in this high-risk population [473]. Therefore, the MET inhibitor Crizotinib was investigated as a chemoprevention strategy of OSCC. Considering the ability of GCs to inhibit MET kinase activity and the relative safety profile, they could be also investigated for their chemoprevention activity.

6.3.4.3 FL and DX Reduce MET Phosphorylation and Activate EGFR in a Concentration-Dependent Manner

In order to investigate this underlying mechanism more closely and to find out whether MET inhibition is associated only with DX or also with other GCs, SAS cells were treated with serial dilutions of FL and DX for 72 h. Surprisingly, 1 nM of either GC was sufficient to inhibit MET phosphorylation with a moderate reduction in the total protein level (Figure 42). In agreement with the previous results, FL was able to downregulate the cell cycle regulator Cyclin D3 and to upregulate p27 which are possible candidates for causing the G1 arrest as discussed before (6.2.4). A higher concentration of DX was necessary to reduce Cyclin D3 and to stimulate p27 in comparison to FL. This observation is in agreement with the relative GCR receptor affinity of the drugs, where FL is 18 times more potent than DX (see 6.3.3). Unexpectedly, DX and FL upregulated and activated EGFR in a dose-dependent manner. A low concentration of 1 nM of FL was sufficient to induce EGFR activation, while a higher concentration of 30 nM of DX was necessary to produce the same effect (Figure 42). The total level of GCR was not changed upon DX or FL treatment.

The previous results have shown that inhibition of MET in TSCC which is associated with the invasiveness and metastasis is related to mechanisms of GC action. To the knowledge of the author of this work, there is currently no published data showing GC-mediated inhibition of MET phosphorylation. MET signaling was found to be important for OSCC and TSCC growth and locoregional dissemination *in vivo* and targeting MET may be an important strategy for therapy by reducing tumor dissemination to regional lymph nodes and inhibition of tumor growth [472][810]. However, it was found that inhibition of MET alone in TSCC exerted an inhibitory effect on the proliferation of Erlotinib-resistant cells in the short term, but it failed to sustain the inhibitory effect in the long term [808]. Also, it was reported that Crizotinib, a potent inhibitor of MET, in combination with radiation did not enhance the effect of

radiation but instead suggested enhanced tumor growth *in vivo* models of oral tongue cancer. Crizotinib was found to inhibit phosphorylation of MET, but did not inhibit phosphorylation of downstream signaling proteins AKT, ERK or SRC. Also, increased activation of SRC was seen TSCC when treated with Crizotinib plus radiation [811].
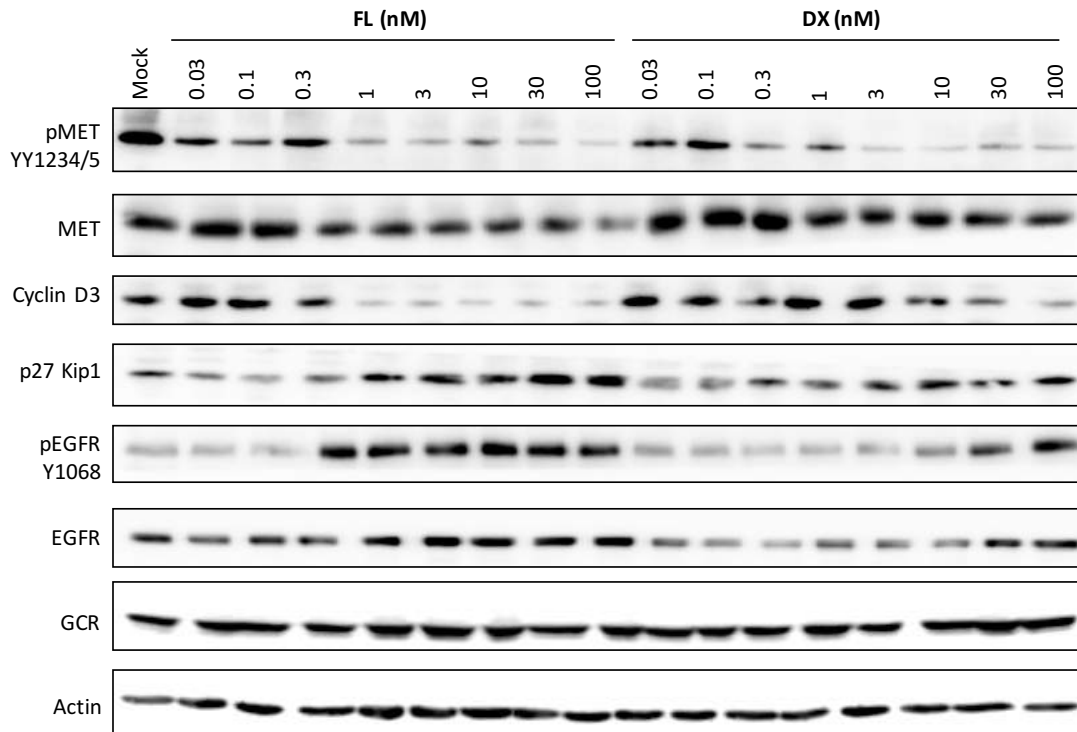
Figure 42. FL and DX reduce MET phosphorylation, deregulate cell cycle proteins and lead to EGFR activation in a concentration-dependent manner

SAS cells were treated with DMSO as vehicle control (Mock) and serial dilutions of FL or DX for 72 h. Total cell lysates were generated, separated by SDS-PAGE and analyzed by Western blotting. Antibodies that detect the phosphorylated state of MET at Tyr1234/1235 and EGFR at Tyr1068 were used to monitor the changes in tyrosine phosphorylation. The other blots analyzed total protein abundance. The blots shown are representative of three independent experiments.

SRC plays an important role in MET and EGFR activation and resistance in HNSCC [811 812 813]. Ligand-independent activation of MET by activated SRC was found to contribute to Erlotinib resistance in HNSCC. MET activation is more dependent on SRC than on EGFR and provides an alternate survival pathway. The level of phospho-SRC in HNSCC was significantly correlated with Erlotinib resistance and MET activation [812]. Sen *et al.* showed that sustained MET activation can mediate resistance to SRC inhibition and that inhibiting SRC and MET together has a synergistic effect on preventing the growth of oral cancer cells [813]. Considering the previous data together, this supports a model in which SRC and MET cooperate to maintain cell survival in HNSCC cells. Dual inhibition of SRC and MET in TSCC by DAS and GC, respectively seems to be a promising therapeutic strategy, by enhancing the efficacy and inhibiting alternative survival pathways.

In the current study, it was observed that the phosphorylation level of MET was significantly decreased upon GC treatments, whereas the phosphorylation and total levels of EGFR were obviously increased in SAS cells (Figure 42). Dual inhibition of MET and EGFR has been shown to result in maximum inhibition of AKT and ERK phosphorylation, and HNSCC tumor growth. Therefore, it was suggested that MET or EGFR can compensate when phosphorylation of the

other receptor is inhibited [814]. Cooperation between MET and EGFR interaction was found by many groups that studied drug resistance after inhibition of either RTK [815].

6.3.4.4 DX is not a Direct Inhibitor for MET Kinase Activity

As MET is inhibited in TSCC and EGFR is upregulated upon GCs treatment and both receptors are potential targets for drug strategies, a more thorough understanding of the crosstalk between MET and EGFR is necessary. To evaluate the kinetics of MET inhibition and EGFR activation and to understand whether DX directly represses MET kinase activity, a time course was performed in SAS cells using 100 nM of DX as presented in Figure 43. MET dephosphorylation occurred rapidly and a prolonged, strong inhibition was achieved within 4 h. This correlated with repression of phosphorylation at Tyr627 of the downstream target GAB1 (Figure 43). Late upregulation of EGFR was becoming prominent after 48 to 72 h, for total and phosphorylation levels, respectively. This result suggests that EGFR is a compensatory but not a concomitant pathway for MET inhibition. In the same direction, this result could explain the effect of MET repression in TSCC which exerts an inhibitory effect on the proliferation of cells in the short term; but, fails to sustain the inhibitory effect in the long term [808]. Rapid MET inhibition could initially reduce cell growth while late EGFR upregulation leads to an alternative survival mechanism.

The somewhat delayed inhibition for MET phosphorylation suggests that DX may not be a direct inhibitor for MET kinase activity (Figure 43). The transport of steroids from the extracellular fluid into animal cells generally occurs by simple diffusion of the free steroid across the cell membrane, but it has also been suggested that a facilitated diffusion systems for steroid hormones exists in some target tissues [816]. The cellular uptake for steroids was found to usually happen within minutes. Given the lipophilic nature of the plasma membrane, it is understandable that DX, which is relatively small hydrophobic molecules, can easily penetrate the bilayer leading to an immediate "uptake" and coupling to specific receptors in an energy-dependent step [817]. Nuclear translocation of the GC-GCR complex occurs within 10-30 min of cell exposure to GC and homodimers of this complex bind to DNA-binding sites termed GC response elements [818]. As shown in Figure 42, 4 h was necessary for DX to exhibit notable MET phosphorylation reduction which means apparently, that DX is not direct MET kinase activity inhibitor. To test this assumption, a MET kinase activity assay was performed as described in detail in the experimental section (2.2.13).
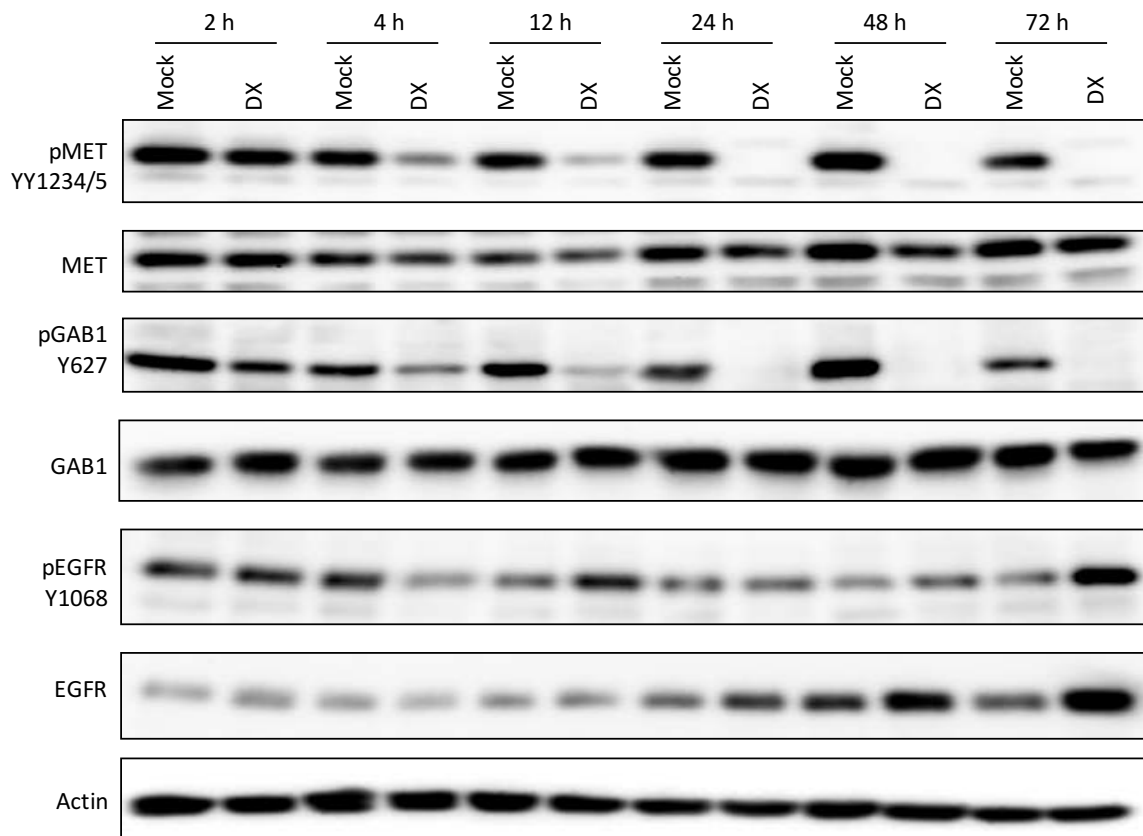
Figure 43. DX causes rapid and prolonged inhibition of MET phosphorylation but late on set EGFR protein abundance increase

SAS cells were treated with DMSO as vehicle control (Mock) or 100 nM of DX for the indicated time points before extraction. Total cell lysates were generated, separated by SDS-PAGE and analyzed by Western blotting. Antibodies that detect the phosphorylated state of MET at Tyr1234/1235, GAB1 at Tyr627 and EGFR at Tyr1068 were used to monitor the changes in tyrosine phosphorylation over time. The other blots analyzed total protein abundance. The blots shown here are representative of three independent experiments.

Shortly, the precleared SAS cell lysate was immunoprecipitated with anti-MET antibody then incubated with ATP plus a recombinant *E.coli*-expressed fragment of GAB1 (aa 613-694), which was used as a kinase substrate. DMSO, 100 nM of DX, 500 nM of DX or 100 nM of Crizotinib (positive control) were added into the kinase reaction. Crizotinib is used in the treatment of NSLCC patients and is also registered for patients with the presence of ALK gene rearrangements after the failure of the first line of treatment based on platinum derivatives. As further controls, an antibody mouse isotype control, a 'no lysate' control, a 'no substrate' control and a 'no ATP' control were included as shown in Figure 44. The result shows that unlike Crizotinib, DX has no direct inhibition of MET kinase activity at the physiologically achievable concentration of 100 nM or even at 5 times higher concentration.

	Total lysate	Isotype control	No lysate control	No substrate control	No ATP control	Mock	DX 100 nM	DX 500 nM	Crizotinib 100 nM	
Anti-MET		−	+	+	+	+	+	+	+	
Lysate		+	−	+	+	+	+	+	+	
Substrate *		+	+	−	+	+	+	+	+	
ATP		+	+	+	−	+	+	+	+	

pMET YY1234/5

MET

pGAB1 Y627 — *C-term. GAB1 aa 613-694
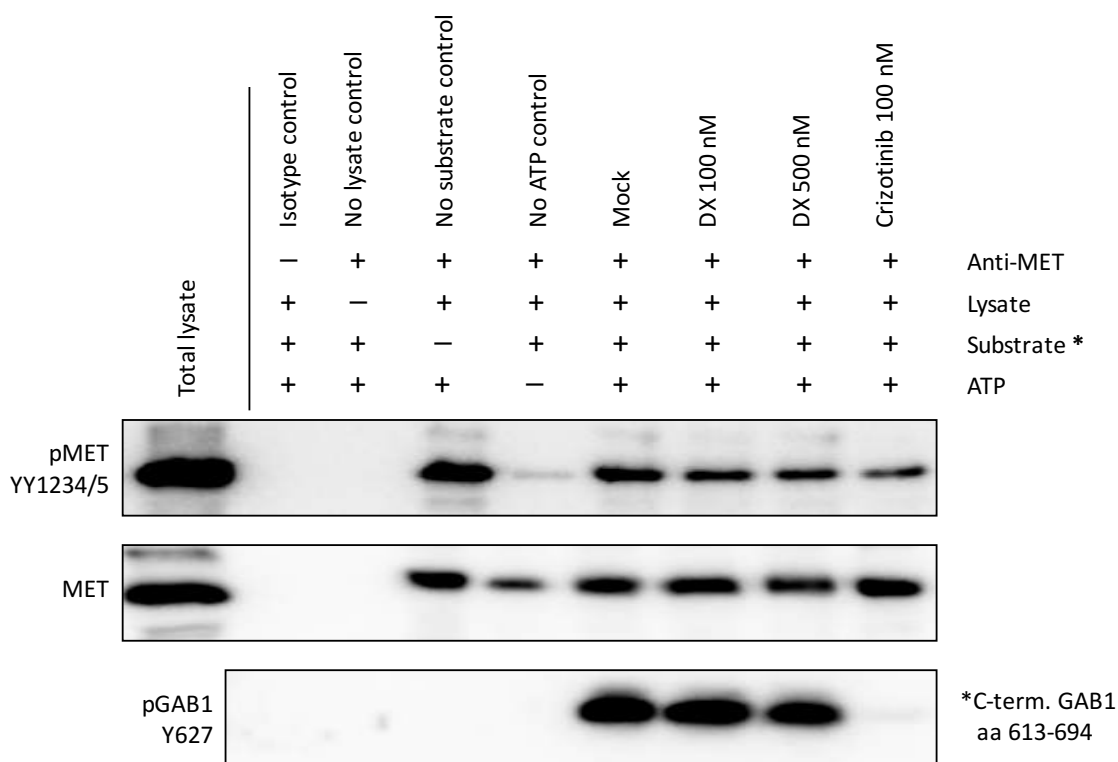
Figure 44. DX shows no direct inhibition of MET kinase activity

SAS cells were lysed with kinase assay lysis buffer and equal amounts of protein cell lysates were precleared with protein G-Sepharose beads for 1 h. The precleared lysate was incubated with anti-MET antibody for 2 h. G-Sepharose beads were added and the mixture was incubated for 1 h. The immunocomplexes were washed with kinase assay washing buffer and mixed with kinase reaction buffer. A recombinant *E.coli*-expressed fragment of GAB1 (aa 613-694) with two MET phosphorylation sites (Tyr627 and Tyr659) was used as a kinase substrate. DMSO, 100 nM of DX, 500 nM of DX or 100 nM of Crizotinib (positive control) were also added to the samples. The kinase reaction was started by ATP addition. As further technical controls an antibody isotype control, a 'no lysate' control, a 'no substrate' control and a 'no ATP' control were included. Lysates were separated by SDS-PAGE and immunoblots were probed with the indicated antibodies. The immunoblots shown here are representative of three independent experiments.

Until now it is not clear how GCs are capable to indirectly inhibit MET kinase activity. Transcriptional regulation of the GC-GCR complex, which inhibits the transcription of genes by direct interaction [668] but also inhibits the transactivation function of other transcription factors such as activator protein 1 and NF-κB [819], could be involved in this MET deactivation. However, it is well possible that MET activation is regulated indirectly by one of the many target proteins of the GC-GCR transactivation activity. Although, it is likely that the GCR is the principal mediator of GC actions, off-target effect could also explain this cellular response to the GC by interaction with other targets. To answer this, GCR could be knocked down to find whether DX shows significant suppressive effects on MET activity through the GCR pathway or through other targets.

GCs have also a multitude of other nongenomic mechanisms that can affect intracellular signaling. These include: effects on membrane lipids, effects on membrane proteins, effects on intracytoplasmic proteins, protein-protein interactions and interactions with GC transporters [818]. A particularly interesting effect on protein-protein interactions in the context of this work is the ability of GCs to dissociate SRC from the GCR-multiprotein

complexes upon binding. This is thought to be responsible for some of the rapid effects of GCs. DX treatment was found to induce HSP90 and SRC release from a cytoplasm HSP90/GCR/SRC complex [820]. This release was inhibited by the inhibitor PP1. Inhibition of SRC release from the same complex by DAS upon cotreatment with DX may potentiate the effects of DX by reducing the level of free and active SRC.

6.3.4.5 DAS+DX Combination Treatment Induces EGFR, ERK 1/2 and AKT Activation in TSCCs

Since EGFR was activated in DX-treated SAS cells, cotreatment with DAS and DX was evaluated to explore whether it could inhibit this upregulation. For that purpose, TSCCs were treated with DMSO as vehicle control (Mock), 50 nM of DAS, 100 nM of DX, or a combination of DAS+DX for 72 h. As presented in Figure 45, DAS+DX treatment was not able to overcome EGFR upregulation by DX. Furthermore, ERK and AKT were activated upon DAS+DX treatment. This could be due to the EGFR upregulation since activation of both ERK and AKT signaling pathways are essential for EGFR-promoted cell growth. However, ERK was activated in SAS and BICR56 cells, even upon DAS treatment, regardless of EGFR upregulation. As discussed in detail in the last chapter (5.5.5), pERK 1/2 and pAKT are upregulated upon DAS+AT treatment in TSCCs despite the repression of RAS and EGFR activity (Figure 23 and 24). Taken together, ERK and AKT activation could be a compensatory or resistance mechanisms not associated with EGFR activation.

Contradictory results were reported about ERK and AKT regulations by DX in different cell lines [821 822 823 824 825 826 827 828]. For example, DX was found to inhibit ERK/MAPK activity by increasing the expression of the MAP kinase phosphatase-1 (MKP-1) gene at the promoter level and attenuating of proteasomal degradation of MKP-1 [822]. Another study reported that ERK activation could enhance the DX-induced phosphorylation of the GCR at Ser211, resulting in the enhancement of GCR transcriptional activity in cancer cells, [829] which means that ERK activation in TSCCs could potentiate DX action instead of being resistance mechanism.

MET inhibition as monotherapy has been reported previously to trigger several survival mechanisms that bypass cell death induced by these agents, including increased expression of the EGFR ligand transforming growth factor (TGF) and of ErbB3, an EGFR family member that has different signal transduction capabilities when it dimerizes with other EGFR family members, especially EGFR [815 830]. Targeting of EGFR signaling by TKIs (e.g. Lapatinib) or mAbs (e.g. Cetuximab) as triple treatment in combination with DAS+DX may improve the outcome and could be a potential therapeutic strategy in TSCC.
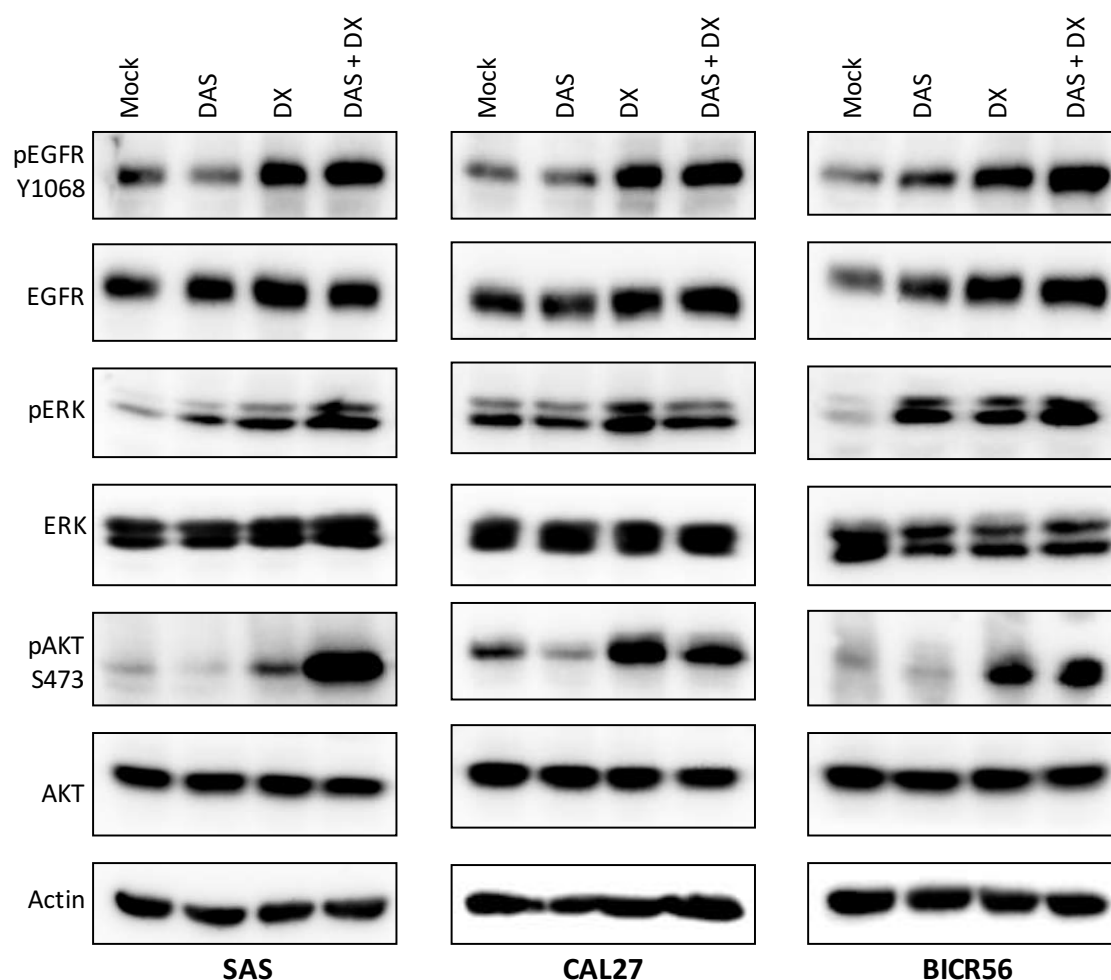
Figure 45. DAS+DX combination treatment induces EGFR, ERK 1/2 and AKT activation in TSCC lines

Cells were treated with DMSO as vehicle control (Mock), 50 nM of DAS, 100 nM of DX, or a combination of DAS+DX for 72 h. Total cell lysates were generated and analyzed by Western blotting. Antibodies that detect the phosphorylated state of EGFR at Tyr1068, ERK 1/2 at Thr202/Tyr204 and AKT at Ser473 were used to monitor the phosphorylation changes. The other blots analyzed total protein abundance. The blots shown are representative of three separate experiments.

6.3.5 EGFR Inhibitors showed Additive to Moderately Synergistic Cytotoxic Activity in Combination with DAS and DX against TSCCs

2D and 3D culture experiments were performed to evaluate the benefit of the EGFR inhibitors, Lapatinib (LP) or Cetuximab (CT), in combinations with DAS and DX in TSSCs. This work was done by another member of our group (Jakob Salzman, MLU) under co-supervision of the author. Lapatinib is a dual reversible inhibitor of EGFR and HER2 tyrosine kinases (Figure 7) and has been shown to significantly inhibit the proliferation of cancer cells overexpressing EGFR and/or HER2. LP binds reversibly to the cytoplasmic ATP-binding site of the kinase, thereby preventing receptor phosphorylation and blocks activation of multiple receptor combinations, including homo-and heterodimers of EGFR and HER2 [831]. It is approved by the FDA in combination with Capecitabine for the treatment of HER2-overexpressing metastatic breast cancer [832][833]. Overexpression of HER2 in HNSCC has been associated with an adverse prognosis in patients with HNSCC [834]. A randomized Phase II study confirmed the safety and tolerability of oral Lapatinib as concomitant and

maintenance therapy during cisplatin-based chemoradiotherapy in locally advanced HNSCC [835]. Furthermore, LP is currently in Phase III trials with chemoradiotherapy in patients with high-risk features after surgical treatment of stage III/IV head and neck cancer [836].

A

B

DAS   DAS+DX+LP   EIA*
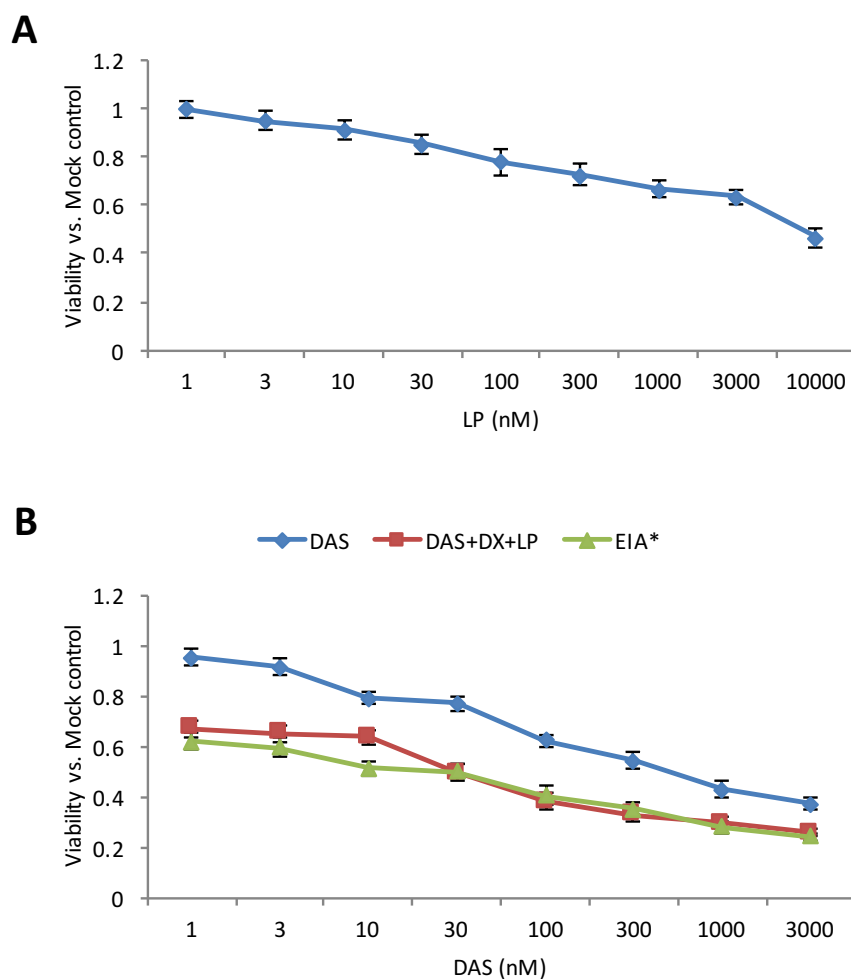
*Expected If Additive (EIA)

Figure 46. Lapatinib (LP) reduces SAS cell viability in a dose-dependent manner and exhibits additive activity with DAS and DX in 2D culture

Cell viability after treatment in (A) and (B) was measured by resazurin colorimetric assay. Data represent fluorescence measurements normalized to Mock-treated cells. The dose-response curves show mean values ± SD of three independent experiments with six parallel measurements in each case. This work was done by Jakob Salzmann (MLU).

(A) SAS cells were treated with a serial dilution of LP for 72 h

(B) SAS cells were treated with serial dilutions of DAS or DAS plus 100 nM of DX and 500 nM of LP for 72 h
The cell inhibition activities of DAS alone, DX alone and LP alone were measured within the same experiment and used to calculate the expected values by multiplication of the surviving fractions. Cell viability upon DX and LP single treatment was 84% and 77% respectively.

In the current work, LP was evaluated for its ability to reduce cell viability and colony formation in 2D and 3D cultures, respectively, alone or in combination with DAS and DX. LP was able to reduce SAS cell viability in 2D culture in a dose-dependent manner but showed only a cytostatic effect at the highest concentrations (Figure 46.A). 500 nM of LP was chosen

to be combined with DAS and DX. As shown in Figure 46.B, LP shows additive activity in combination with DAS and DX in 2D cultured SAS cells. Cell viability after 72 h treatment with each drug alone was measured within the same experiment and used to calculate EIA values by multiplying of the surviving fractions according to the Bliss independence model. LP reduced CAL27 and BICR56 cell viabilities in a dose-dependent manner as well. In combination with DAS and DX, LP showed additive activity in CAL27 cells and synergistic activity in BICR56 cells (data not shown).

In 3D soft agar culture, LP was found to reduce colony formation of SAS cells in a dose-dependent manner (Figure 47.A). 300 nM of LP, which slightly reduced the colony formation by itself, was combined with DAS and DX. SAS cells were treated with serial dilutions of DAS, DAS+DX or DAS+DX+LP. As presented in Figure 47.B, LP showed moderate synergistic activity in combination with DAS and DX compared to DAS+DX cotreatment which already shows strong synergistic activity compared to DAS alone. Colony numbers after LP treatment were counted within the same experiment and were found to be 90% of Mock. These numbers were used to calculate the expected values (EIA) by multiplying colony formation fractions of LP and DAS+DX cotreatment. Taken all together, LP appears to be a promising candidate for combination with DAS and DX to overcome the possible effect of EGFR activation.

The combined inhibition of upstream and downstream tyrosine kinases could be a promising strategy for the treatment of TSCC in combination with DX. However, as more chemotherapeutics are combined, they tend to increase toxicity. Therefore, depending on the outcome of the *in vivo* animal experiment results with DAS+DX cotreatment, it will have to be decided if an addition of LP to the combination of DAS+DX as a triple treatment would be promising to try as well. Also, further investigations are needed to understand the underlying mechanisms of the current synergistic interaction.

A

B

*Expected If Additive (EIA)
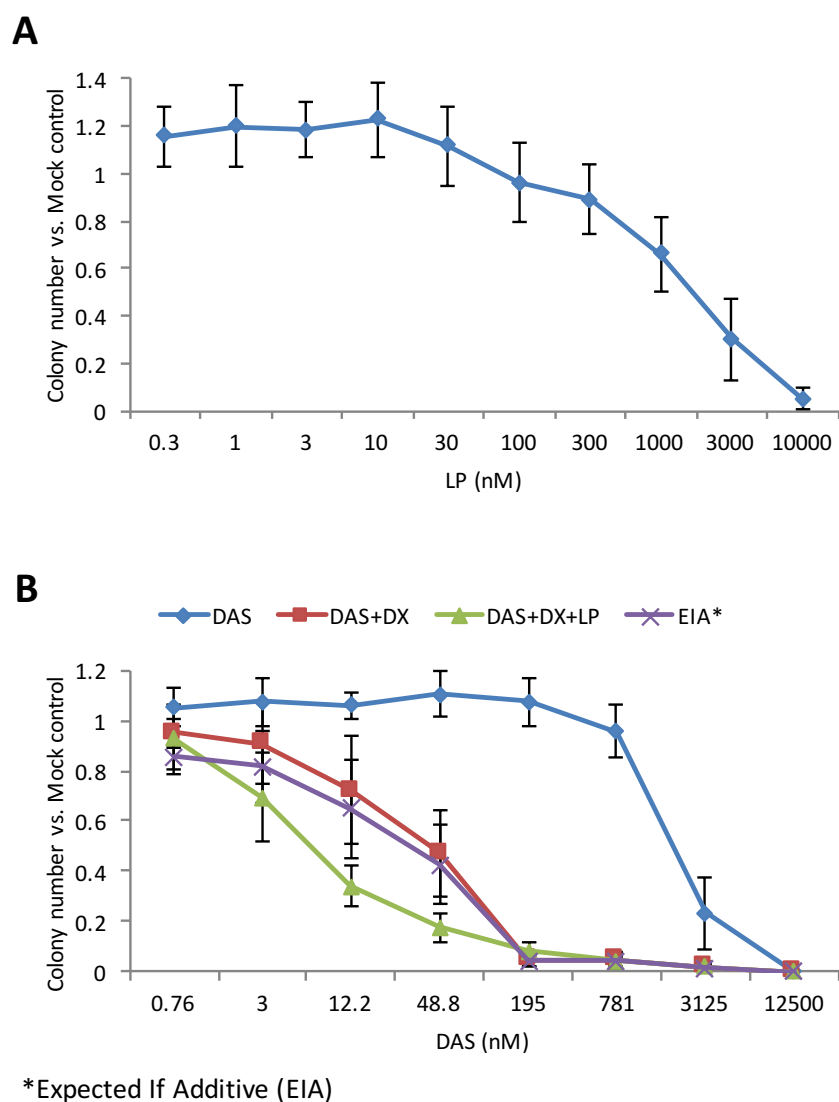
Figure 47. Lapatinib (LP) decreases the colony formation of SAS cells in a dose-dependent manner and exhibits moderate synergistic activity with DAS+DX cotreatment in 3D soft agar culture

Data in (A) and (B) represent means of colony numbers normalized to Mock-treated cells. The dose response curves show mean values ± SD of three independent experiments with 2 wells counted in each case (Jakob Salzman, MLU).

(A) SAS cells were treated with a serial dilution of LP for 14 days before colony counting

(B) SAS cells were treated with serial dilutions of DAS, DAS+DX or DAS+DX+LP for 14 days
100 nM of DX and 300 nM of LP were used in this experiment. The colony numbers were counted following treatment with DAS, DAS+DX, DAS+DX+LP and used to draw dose response curves. Also, colony numbers after LP treatment were counted within the same experiment and used to calculate the expected values (EIA) by multiplication of the colony fraction of LP normalized to Mock with the colony fraction of DAS+DX cotreatment normalized to Mock. LP individually reduced colony numbers to 90% related to Mock (Jakob Salzmann, MLU).

Cetuximab binds specifically to the extracellular domain of EGFR as a competitive antagonist of the endogenous ligands (EGF and TGF) [837]. This process prevents the EGFR from binding to its endogenous ligand, blocking the receptor-dependent transduction pathway and providing many antitumor effects, including cell-cycle arrest, induction of apoptosis, inhibition of angiogenesis, inhibition of metastasis, internalization and downregulation of the EGFR and

enhancement of sensitivity to radiochemotherapy. Cetuximab was approved for the treatment of locally advanced and recurrent/metastatic HNSCC. Phase III trials demonstrated that Cetuximab used in combination with radiotherapy in locally advanced HNSCC [179] and in combination with platinum-based chemotherapy as first-line treatment for recurrent/metastatic HNSCC [181] achieved a higher response rate and a significant increase in overall survival. It has also been reported that Cetuximab used in combination with Paclitaxel is effective when platinum-based chemotherapy fails in recurrent/metastatic HNSCC [838] [839].

*Expected If Additive (EIA)

Figure 48. Cetuximab (CT) moderately decreases SAS cell viability and shows additive activity with DAS and DX in 2D culture

Cell viability in (A) and (B) was measured by resazurin colorimetric assay. Data represent fluorescence measurements normalized to Mock-treated cells. The dose-response curves show mean values ± SD of three independent experiments with six parallel measurements in each case.

(A) SAS cells were treated with a serial dilution of CT for 72 h

(B) SAS cells were treated with serial dilutions of DAS or DAS plus 100 nM of DX and 3000 ng/ml of CT for 72 h.

The cell inhibition activities of DAS, DX and CT individually were measured within the same experiment and used to calculate the expected values by multiplying of the cell viability fractions. Cell viability upon DX and CT treatments were 83% and 75%, respectively (Jakob Salzmann, MLU).

Treatment of SAS cells with a serial dilution of CT showed only moderately decreased cell viability within the clinically relevant concentrations (50000 to 25000 ng/ml) [840] (Figure 48.A). Like LP, CT showed only additive activity in combination with DAS and DX in SAS cells (Figure 48.B). CT also moderately reduced CAL27 and BICR56 cell viabilities in a dose-dependent manner and, in combination with DAS and DX, showed additive activity in CAL27 cells and slight synergistic activity in BICR56 cells (data not shown). On the other hand, in 3D soft agar culture, CT as a single treatment moderately reduced the colony formation of SAS cells in a dose-dependent manner (Figure 49.A). Moreover, CT exhibited mild synergistic activity in combination with DAS and DX compared to DAS+DX cotreatment in SAS cells (Figure 49.B). 50 ng/ml of CT were used in this experiment and colony numbers following CT single treatment were counted within the same experiment. At this concentration, CT individually had no significant effect on colony formation. The colony formation after the treatment with 50 ng/ml of CT was within the range of standard deviations (Figure 49.A) therefore higher concentrations of CT could be used in the future to search for additive or synergistic activity.

Cetuximab was found to display significant therapeutic efficacy in patients with unresectable locally advanced and recurrent/metastatic OSCCs [180]. However, in the current experiments, CT exhibited only a moderate reduction of TSCC viability and colony formation *in vitro* assays, even at the very high concentrations (Figure 48.A and 49.A). The reduced efficacy *in vitro* may be attributed to the lack of an immune component in the current 2D and 3D models. It was demonstrated previously that the *in vivo* antitumor activity of Cetuximab can be associated with a complement-mediated immune response [841]. This process is used by the immune system whereby members of the complement factor family (comprised of at least 20 distinct proteins) recognize antibody-coated cells and facilitate cell lysis resulting in cell death [842]. The immune-dependent mechanisms, which are not achievable *in vitro* cultures or immune-compromised animals, may contribute to an increase in the clinical efficacy of Cetuximab. Therefore, CT could show more promising activity in TSCCs, alone or in combination with DAS and DX in *in vivo* animal experiments if a functional immune system is present.

LP and CT seem to have an additive to moderately synergistic activity in combination with DAS and DX in 2D and 3D cultures. However, Lapatinib offers practical advantages in that, unlike Cetuximab, it is an oral agent and does not cause allergic reactions. Also, TKIs have the advantage over mAbs of oral bioavailability and the potential to inhibit more than one member of the ErbB family, therefore potentially also addressing a mechanism of resistance to EGFR inhibition [835]. The combination of Cisplatin, Fluorouracil, and Cetuximab is a fairly standard treatment for patients with recurrent/metastatic HNSCC but with a high rate of toxicity. A combination of Capecitabine and Lapatinib was found to have survival comparable to the previous combination regimen, and the toxicity of this combination was tolerable [843]. On the other hand, a recent study demonstrated that MET/HGF activation results in OSCC resistance to Cetuximab and tumor recurrence after Cetuximab therapy; thus, inhibition of MET/HGF activity was recommended to restore OSCC sensitivity to Cetuximab [844]. However, MET inhibitors have a severe toxic profile, therefore examining DX in combination with Cetuximab to overcome resistance and MET activation could be a promising strategy in OSCC.

A

B

Figure 49. Cetuximab (CT) reduces colony formation of SAS cells in a dose-dependent manner and exhibits mild synergistic activity with DAS+DX cotreatment in 3D soft agar culture

Data in (A) and (B) represent means of colony numbers normalized to Mock-treated cells. The dose response curves show mean values ± SD of three independent experiments with 2 wells counted in each case.
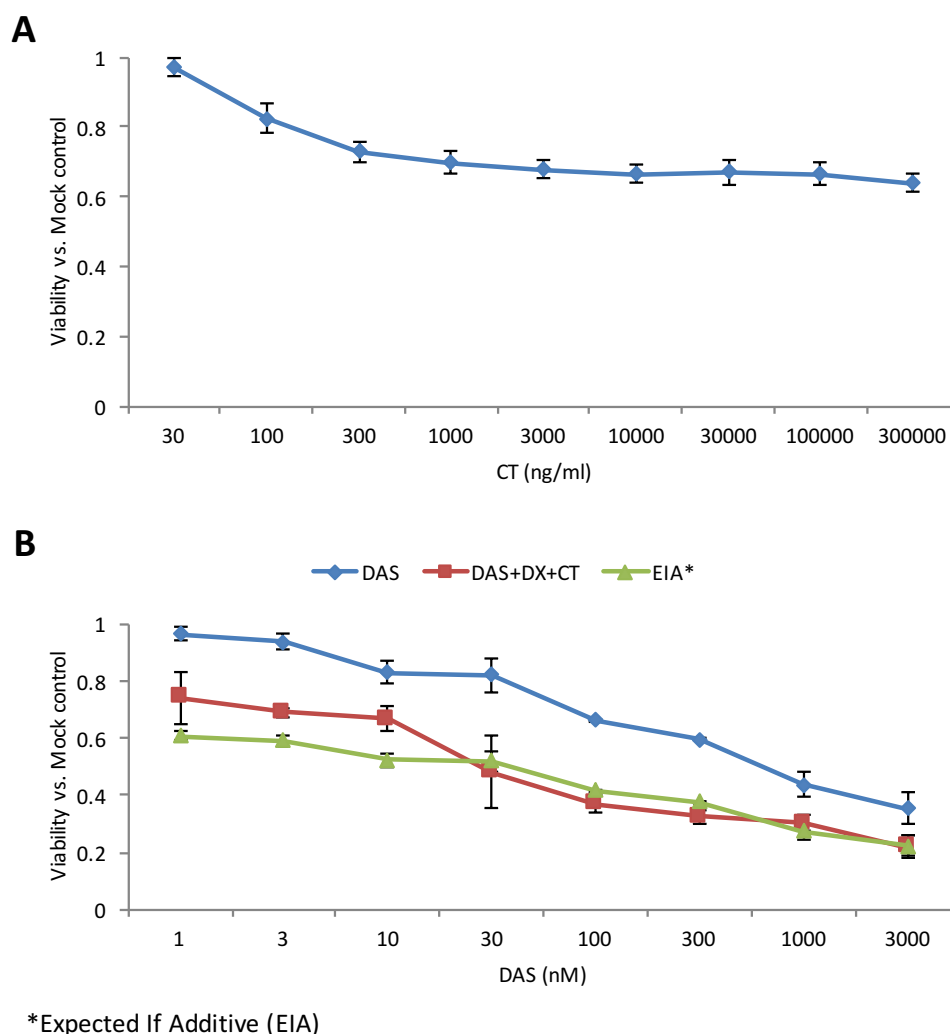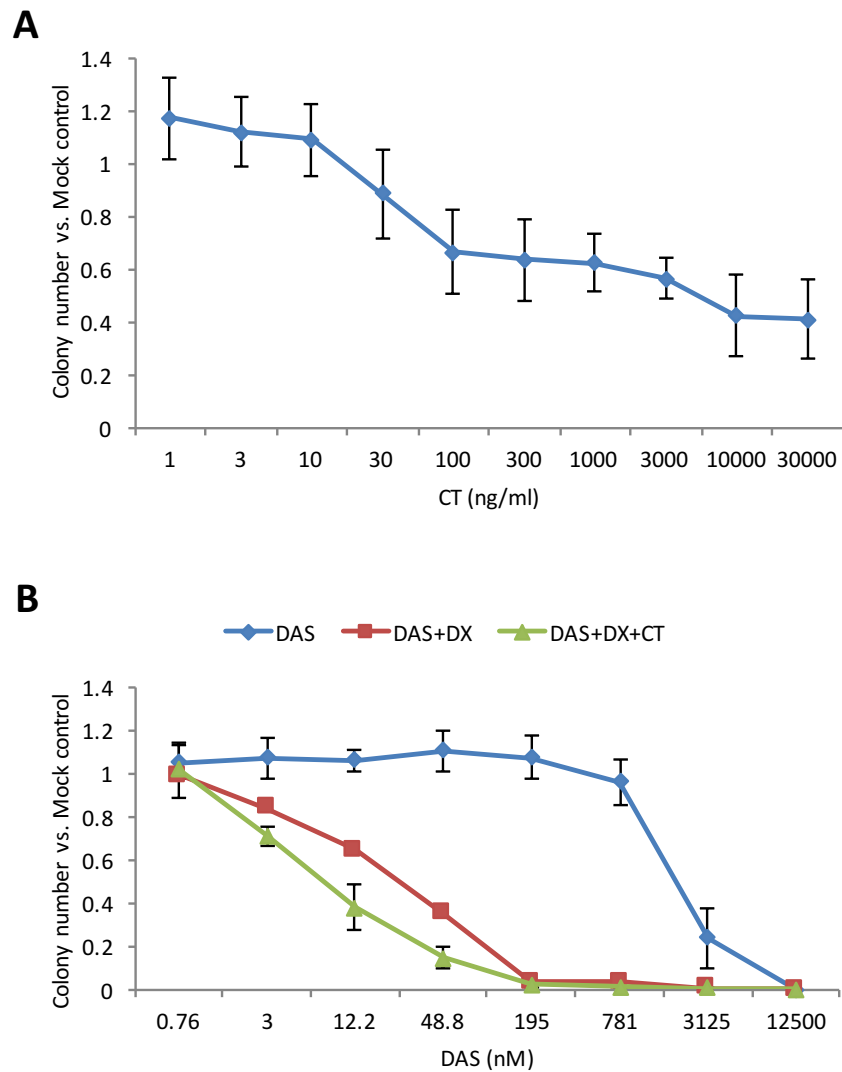
(A) SAS cells were treated with a serial dilution of CT for 14 days then colony numbers were counted

(B) SAS cells were treated with serial dilutions of DAS, DAS+DX or DAS+DX+CT for 14 days
100 nM of DX and 50 ng/ml of CT were used in this experiment. The colony numbers were counted following treatment with DAS, DAS+DX and DAS+DX+CT then used to draw dose response curves. Colony numbers after CT single treatment were counted within the same experiment. An expected effect was not calculated here since CT individually has no notable effect on colony formation (Jakob Salzmann, MLU).

6.3.6 AT13387 Shows Synergistic Cytotoxic Activity in Combination with DAS and DX against the SAS Cell Line

Previously, it was shown that EGFR is downregulated upon HSP90i treatment in TSCCs (Figure 23). This suggests that it may be possible to overcome EGFR activation upon DAS+DX

treatment by combining DAS and DX with the HSP90i AT13387 considering that EGFR is HSP90 client protein. To test this hypothesis, serial dilutions of DAS were combined with 100 nM of DX and 10 or 30 nM of AT. SAS cells were treated for 72 h and then the viability was estimated by resazurin colorimetric assay (Figure S26). AT increased the cell viability reduction by DAS+DX in a dose-dependent manner. Also, DX exhibited synergistic activity in combination with DAS and AT. This synergistic activity was more significant with the low concentration of AT (10 nM). This suggests that combining DX with DAS and AT allows using only a low dose of AT and as a consequence reduce the toxicity which is one of the most limiting factors for its clinical application. Also, DX could play a role in overcoming the possible side effects caused by DAS and/or AT treatments.

Mechanistically, the addition of AT only partially reduced the DX-activated EGFR and it failed to reduce the activated ERK and AKT (Figure S27). MET, p130CAS, Cyclin D3 and WEE1 were downregulated upon the triple treatment while p27 was upregulated. The DAS+DX+AT treatment needs further investigation to understand more about the underlying mechanism. It also needs to be tested in soft agar culture to check for a synergistic interaction in a 3D-system. Like for the EGFRi, it also can be combined with the DAS+DX in animal experiments depending on the result of the initial experiment with DAS+DX.

6.3.7 DAS+DX Combination Treatment Induces G1 Cell Cycle Arrest and Senescence in TSCCs

To determine whether DX has an effect on cell cycle progression alone or in combination with DAS, TSCC lines were treated with DMSO as vehicle control (Mock), 50 nM of DAS, 100 nM of DX, or a combination of DAS+DX for 72 h and then stained with DAPI. The DNA content was determined by flow cytometry (Figure 50). Both compounds individually induced slight G1 cell cycle arrest while combination treatment caused significant G1 arrest. Cell accumulation in S phase was notably reduced and to lesser extent cell accumulation in the G2/M phase. No significant sub-G1 peaks were found following treatment of any of the TSCCs evaluated. This result resembles the effect of DAS+FL treatment on cell cycle distribution. Next, the protein expression of many cell cycle regulators was examined using the same treatment conditions (Figure 51). Western blot analysis showed that the Cyclin D3 level was reduced upon DX treatment. The expression of CDK6, but not of CDK2 or CDK4, was also decreased only upon DAS+DX cotreatment. A similar effect was seen on the levels of phospho-WEE, WEE, Cyclin B1 and to lesser extend on CDK1.

The expression levels of p27 and p21 as major drivers for senescence were evaluated also (Figure 52.A). p27 was upregulated in SAS cells mainly after DX treatment. In CAL27 cells, p27 was upregulated slightly upon DAS or DX treatment and more substantially after the cotreatment. In contrast, p27 was upregulated in BICR cells only in DAS+DX-cotreated cells. Such a heterogeneous response of different cell types is not surprising, given the distinct origins of the tumor cells. However, the p21 level was not changed in TSCCs upon DAS and/or DX treatment. Senescence-associated beta galactosidase assay was performed as described in the experimental section (2.2.17) and SA-β-gal positive staining (blue color) which indicates aged cells was detected by light microscopy (Figure 52.B and S28). DAS and DX individually boosted levels of SA-β-gal positive staining which became more apparent upon the combination treatment.
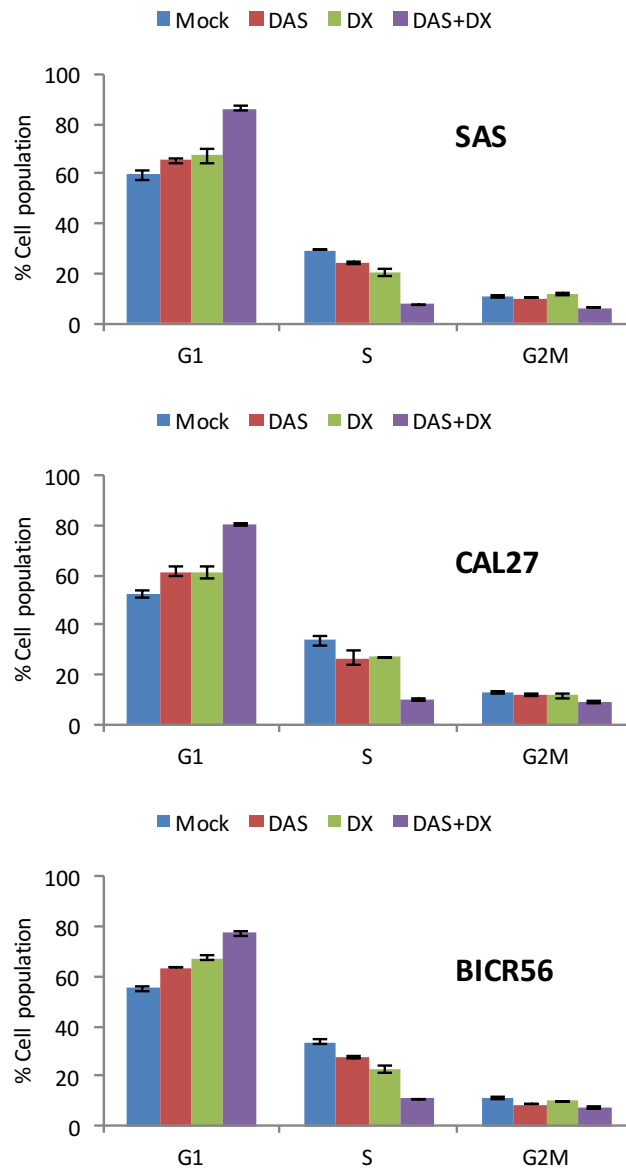
Figure 50. DAS+DX combination treatment induces G1 cell cycle arrest in TSCC lines

TSCC lines were treated with DMSO as vehicle control (Mock), 50 nM of DAS, 100 nM of DX, or a combination of DAS+DX for 72 h. Following treatment, the cells were stained with DAPI and the DNA content was determined by flow cytometry. Ten thousand events were analyzed in each experiment. The cell population displayed as percentage of cells at each cell cycle phase relative to the total population. No sub-G1 peaks were observed following treatment of TSCC lines. Results are expressed as means and standard deviation obtained from 3 independent experiments.
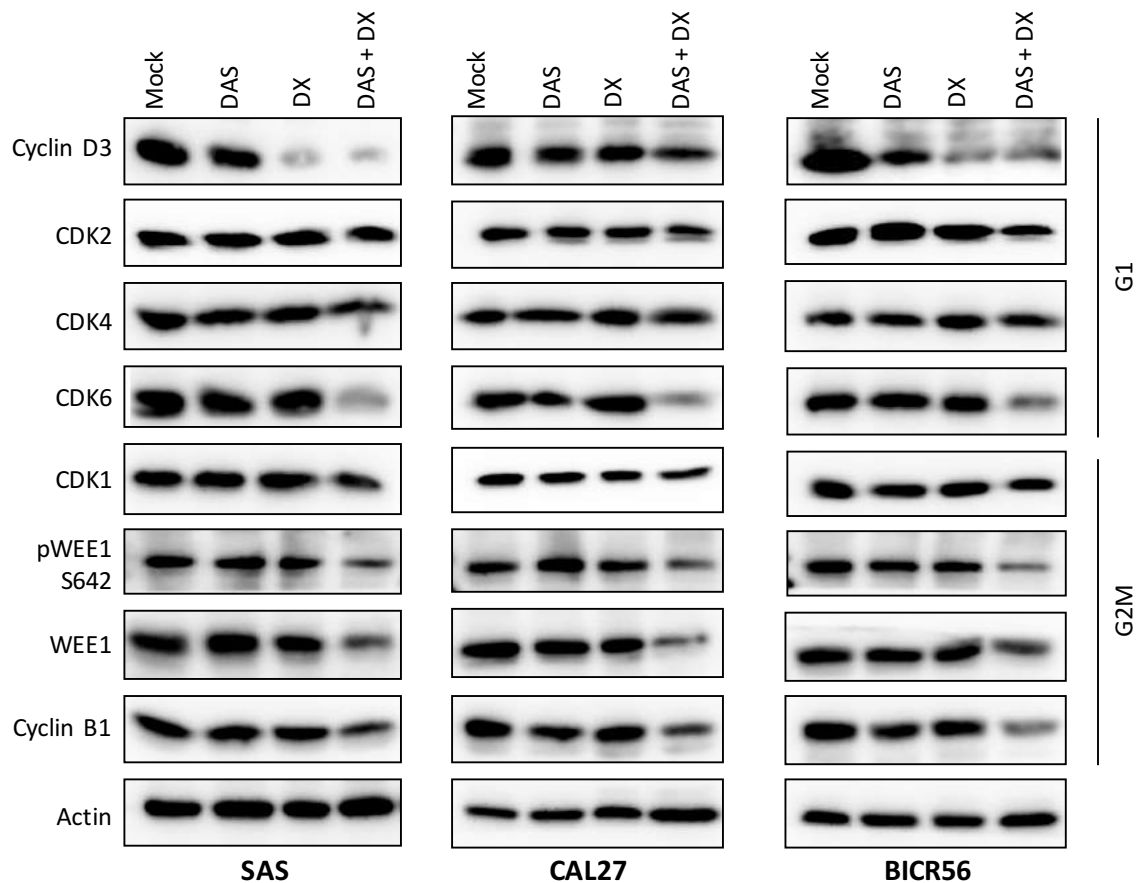
Figure 51. DX+DAS treatment downregulates the expression levels of cell cycle-associated proteins Cyclin D3, CDK6, WEE1 and Cyclin B1

Cells were treated with DMSO as vehicle control (Mock), 50 nM of DAS, 100 nM of DX, or a combination of DAS+DX for 72 h. Total cell lysates were generated, separated by SDS-PAGE and analyzed by Western blotting. An antibody that detects the phosphorylated state of WEE1 at Ser642 was used to monitor the phosphorylation change. The other blots analyzed total protein abundance. The blots shown are representative of three independent experiments.

The previous results indicate that DAS+DX treatment induces substantial cell cycle blockade and a senescence phenotype in TSCC. As discussed in detail in the last chapter (5.6.2), many reports have demonstrated that Dasatinib inhibits cell growth by inducing G1 arrest in many cancers due to increasing cellular p27 stability and downregulation of cell cycle regulators. However, in this work, only a slight G1 arrest was observed upon DAS treatment in TSCCs, maybe due to the low dose of DAS that was used (50 nM). Studies with a variety of cell lines indicate that the antiproliferative effects of GCs may also be mediated by a reversible G1-block in cell cycle progression. Works with glioblastoma cells [845], osteosarcoma cells [846], ovarian cancer cells [847], lung cancer cells [720], bladder cancer cells [695], T-lymphoma cells [721] and lymphoblastic cells [720] have shown that DX leads to cell growth arrest in a time- and dose-dependent manner.

A

SAS   CAL27   BICR56

B
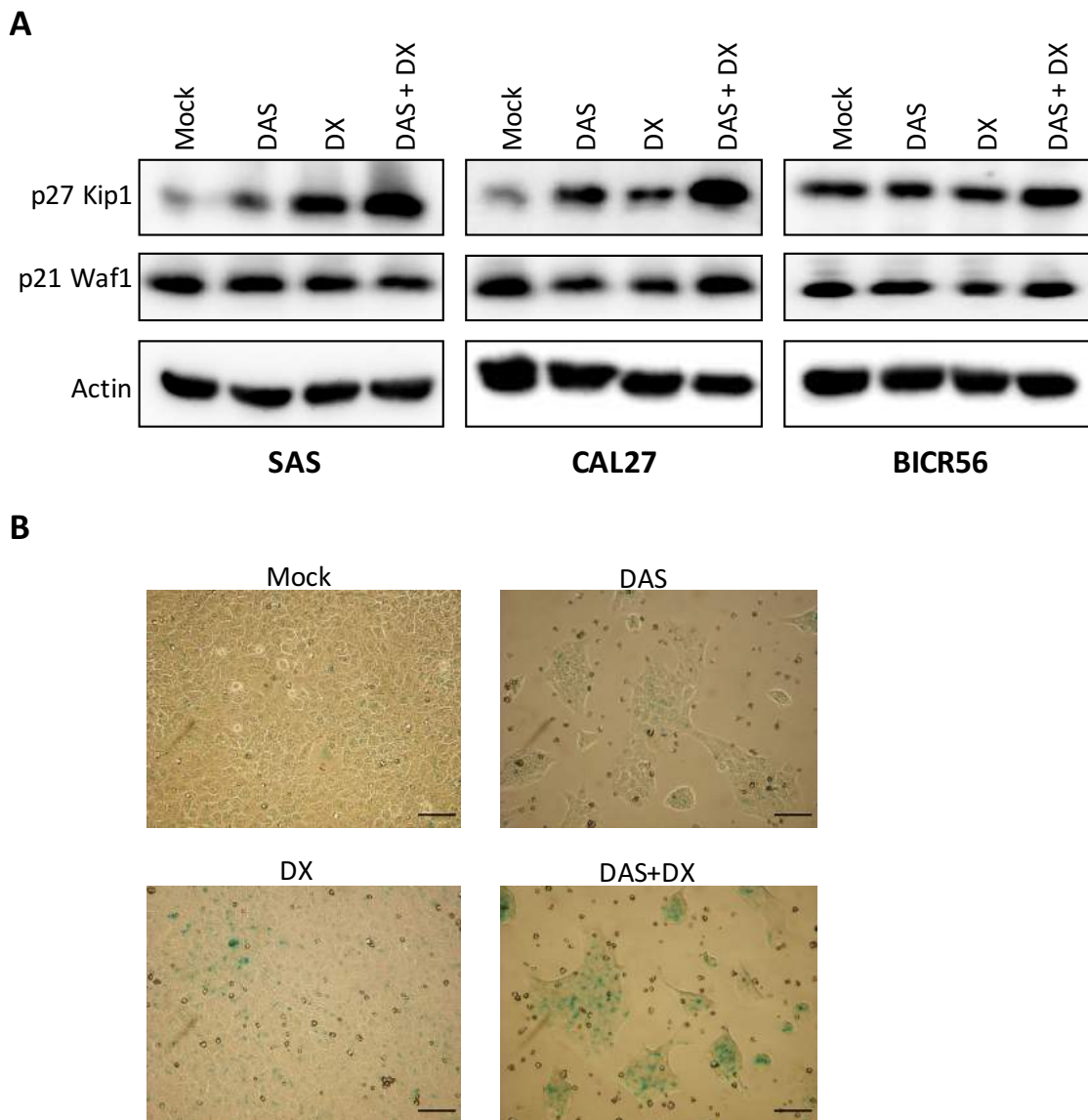
Figure 52. Upregulation of p27, but not p21, may drive cellular senescence in SAS cells upon treatment with DAS and DX

Cells were treated with DMSO as vehicle control (Mock), 50 nM of DAS, 100 nM of DX or a combination of DAS+DX for 72 h.

(A) Total cell lysates were generated and analyzed by Western blotting
The blots shown are representative of three independent experiments. Antibodies that detect the total protein abundance were used.

(B) Representative pictures of SAS monolayer cultures stained with Senescence-associated-β-galactosidase (SA-β-gal)
Expression of pH-dependent β-galactosidase activity characterizes senescent cells. Accordingly, SA-β-gal positive staining (blue color) indicates aged cells. SAS cells were stained with SA-β-gal at 37 °C overnight in a dry incubator (without CO_2). The scale bar = 100 μM.

DX-induced cell growth arrest in TSCC could be related to Cyclin D3 downregulation which is critical for the activation of CDK4 and CDK6 (Figure 25). Cyclin D3 protein levels rapidly decline after DX treatment, most likely through decreased mRNA stability as discussed previously [721]. Also, DX and DAS+DX upregulate p27 which is a Cyclin-CDK inhibitor that can arrest the cell cycle at the G1 phase by blocking the activation of Cyclin E-CDK2 complex and prevent the improper entry into the cell cycle. DX was found to induce a progressive

accumulation of p27 mRNA due to transcriptional activation of the p27 gene [720]. In SAS cells, p27 upregulation was mainly due to DX effect while in CAL27 and BICR56 cells p27 upregulation seems to need SRC inhibition and DX action to increase cellular p27 stability and gene transcription, respectively.

One possible explanation for these findings is that some TSCCs cells can utilize the strong activation of ERK (Figure 45) upon DX treatment to down-regulate p27 expression [324]. This may be mediated by targeting the Thr187 residue on p27, which is linked to its ubiquitinylation and degradation. Therefore, in CAL27 and BICR56 the cooperation between DAS and DX could be necessary to overcome the ERK effect. Another explanation could be related to AKT activation by DX (Figure 45), which was described to phosphorylate and deactivates FOXO transcription factors, causing cytosolic accumulation and thereby preventing FOXO-dependent transcription of p27 mRNA [848]. ERK or AKT activation could be utilized by some TSCCs to override the cell cycle brake p27, while others probably rely on different mechanisms in order to inactivate this important cell cycle brake.

The significant G1 arrest upon the combination treatment could be related to other cell cycle regulators as well. However, CDK2, CDK4 (Figure 51) and Cyclin E (data not shown) levels were not changed upon DAS and/or DX treatments. p27 upregulation which obstructs the Cyclin E-CDK2 complex activity might still explain why DAS+DX-cotreated cells did not enter S phase, despite normal Cyclin E/CDK2 levels.

CDK6 phosphorylates and inactivates the Rb protein to release its binding partner E2F transcriptional activator. This in turn activates genes required for DNA synthetic (S) phase entry and DNA replication. The reduction of this kinase by the DAS+DX cotreatment could inhibit the progression of cells into the S phase of the cell-division cycle. CDK6 inhibition was reported in many cancers and is an inducer for G1 cell cycle arrest and senescence [849] [850] [851]. However, the cell cycle has a complex circuitry of regulation and the role of CDK6 might be more important in certain cell types than in others, where CDK4 or CDK2 can act as protein kinases compensating its role [852]. To findout if CDK6 downregulation is essential for G1 arrest and growth inhibition in TSCCs, CDK6 knockdown or CDK6 inhibitor experiments could be performed.

CDK6 interacts with the NF-κB subunit p65 in the nucleus and is found at promoters of many transcriptionally active NF-κB target genes. It was observed to phosphorylate NF-κB p65 at serine 536 and contributes to the regulation of gene expression [853]. CDK6 recruitment to distinct chromatin regions of genes was essential for proper loading of p65 to its binding sites. CDK6 depletion by the current treatment could alter NF-κB regulation of the expression of inflammatory and tumor-promoting genes. A previous study identified CDK6 as a molecular link between the inflammatory microenvironment and permanent cell cycle progression, two major hallmarks of cancer, and predicted that inhibiting CDK6 will not only affect uncontrolled tumor cell proliferation but also have an impact on innate immune functions arising from stroma or tumor cells [854]. Inhibition of CDK6 activity with a kinase inhibitor was found to inhibit cell proliferation, but does not interfere with the functions of CDK6 as a transcriptional regulator. In contrast, targeted degradation of CDK6 with a bifunctional degrader removed both catalytic and transcriptional CDK6 functions [855]. CDK6 depletion by DAS+DX cotreatment could therefore be a therapeutic strategy in TSCC and could be evaluated in other cancers as well.

Cyclin B1 is a key factor for G2/M phase transition. Cyclin B1/CDK1 complex pushes cell from G2 phase into M phase and hence this is well-known as maturation promoting factor. The

Cyclin B1-CDK1 complex is involved in the early events of mitosis, such as chromosome condensation, nuclear envelope breakdown, and spindle pole assembly. Cyclin B1 overexpression was reported to be involved in early carcinogenesis, cell differentiation and tumor proliferation in OSCC [856]. Also, patients whose TSCC tumors showed overexpression of Cyclin B1 were found to have a poor event-free survival compared with those lacking this feature [857]. The previous data suggest that Cyclin B1 may be a potential tumor marker in TSCC and OSCC and suppression of Cyclin B1, which is associated with a more aggressive biological behavior of tongue cancer, upon DAS+DX treatment seems to be a possible therapeutic strategy. The last results also demonstrate that DAS+DX cotreatment slightly reduce the steady-state level of CDK1 (Figure 51). DAS+DX treatment reduced the expression of a CDK1 partner (Cyclin B1) and induced expression of p27, which is a CDK inhibitor associated with binding to the CDK1-Cyclin B complex and inhibiting its activity (Figure 25).

WEE1 kinase regulates the G2/M checkpoint and WEE1 inhibition leads usually to G2/M arrest and improper mitotic entry. However, abrogation of WEE1 by DAS+DX cotreatment could induce early cell division and accumulation of more cells in the G1 phase. CDK1 and Cyclin B1 are also key regulators of the G2/M but not G1 transition (Figure 25). So, whether or not the reduction of their expression levels upon DAS+DX cotreatment improves this synergistic interaction or has any impact on the strong G1 cell cycle arrest need further investigations. To answer this, CDK1, WEE1 or Cyclin B1 could be knocked down, to find out if they have significant effects on G1 cell cycle arrest or DAS+DX synergistic interaction. The underlying molecular mechanisms for the downregulation of CDK6, WEE1 and Cyclin B1 remain unclear. One or more E2 ubiquitin-conjugating enzymes, E3 ubiquitin-protein ligases or phosphatases may be upregulated after DAS+DX treatment and participate in the degradation of one or all of the previously mentioned proteins. Additional investigations are required to more fully understand the nature of degradation selectivity between CDK4 and CDK6 induced by these compounds. Additionally, whether the depletions of these different cell cycle markers are associated or even linked to p130CAS degradation, which was observed upon DAS+DX cotreatment (Figure S25), still unclear.

G1 cell cycle arrest may lead finally to a senescence arrest phenotype, which is an irreversible loss of cellular proliferative capacity. Senescence β-galactosidase staining analysis showed that in DAS and/or DX-treated cells, the number of positive cells was increased compared to the Mock control group (Figure 52.B). The therapeutic induction of senescence is a potential means to treat cancer through induction of a persistent cytostatic state in tumors. In malignant cells, the irreversible cell cycle blockade that is induced in response to stress stimuli or the activity of tumor suppressors and oncogenes is mediated by the INK4 and Cip/Kip families of CDK inhibitors. p27 and p21 are key proteins representing the classical pathways of senescence by binding and inactivating common G1 Cyclin-CDK targets (Figure 25). Induction of senescence in TSCC by the current treatment seems to be mediated by p27 but not p21. However, induction of other canonical senescence pathways involving proteins such as p16INK4a, and p19ARF should also be evaluated.

DX was reported to induce senescence and inhibit or desensitize tumors by upregulation of various CDK inhibitors [720] [858]. In contrast, other reports demonstrated that DX reduced drug sensitivity by alleviating cellular senescence [859] [860]. Cellular senescence was strongly associated with CDK6 depletion [849] [861] [862] which was seen only upon combination treatment in TSCC (Figure 51). CDK6 reduction could partially explain the strong senescence induction after the DAS+DX cotreatment compared to the DAS or DX treatment (Figure 52.B and S28).

6.3.8 No Induction of Apoptosis was Detected after DAS+DX Treatment in TSCCs

Annexin V/PI staining was used to determine the apoptotic rate of TSCC lines after treatment with DAS and/or DX as described previously. In the dot plots (Figure 53.A and S29), the left upper quadrant indicates necrotic cells due to mechanical injury, the left lower quadrant indicates normal cells, the right upper quadrant and right lower quadrant represent late and early apoptotic cells, respectively. Flow cytometry analysis showed no substantial apoptosis induction in TSCC lines upon single or combination treatments (Figure 53.A and B). However, Staurosporine, which was used as a positive control, effectively induces apoptosis in SAS cells (Figure S17.A). Annexin V/PI results appear to be in agreement with the cell cycle analysis, which shows no sub-G1 peaks following treatment of any of the cells evaluated (data not shown). Sub-G1 normally represents the fragmented low molecular weight cellular DNA which is degraded within apoptotic cells and released at a very late apoptotic stage. Cleaved PARP (89 kDa), which is another hallmark of apoptosis, is also absent upon DAS+DX treatment (Figure 53.C). Staurosporine as an apoptosis inducer produced significant PARP cleavage in SAS cells treated with 500 nM for 18 h. Upon DAS treatment, the PARP band showed a notable shift to a higher molecular weight which could indicate a possible modification like e.g. ubiquitination or phosphorylation. Taken together, the previous results indicate that the cell growth inhibition resulting from the synergistic interaction of DAS and DX is unlikely to be mediated through apoptosis.

GCs can induce apoptosis and have become key elements in the treatment of many hematological malignancies including leukemia and lymphomas. Despite their prevalent clinical use, the mechanisms by which the GCs induce programmed cell death are not clear. Apoptosis may be triggered by direct activation of death-inducing genes or via repression of transcription factor activity, thereby inhibiting the transcription of growth/survival genes [689] [690] [863] [864]. More recent data indicate that GCs can inhibit apoptosis induced by chemotherapy, not only in established cancer cell lines and tumor xenografts, but also in freshly isolated cells from surgical resections from tumors of various origins, including ovary, breast, prostate, pancreas, liver, colon, brain, cervix, bone, skin, and nervous system [695] [865] [866].

In TSCC, no induction of apoptosis was seen with any of the current treatment conditions (Figure 53). Therefore, any impact of DX on apoptosis inhibition here could not be evaluated since DAS by itself did not induce apoptosis. A previous report showed that DX did not exert an anti-apoptotic effect in eight HNSCC lines including CAL27. DX had also no effect on the cytotoxic activity of Cisplatin and Docetaxel in the investigated eight HNSCC lines [867]. Considering this report, which contrasts with other data reported in the literature, it may be concluded that the effect of DX varies both with the type of antineoplastic agent co-administered and the type of cancer. This complex interaction is consistent with the heterogeneous biology of malignant diseases. Thus, patients with HNSCC or TSCC might benefit from the synergistic effects of DX+DAS without any compromise in terms of Dasatinib cytotoxic activity.
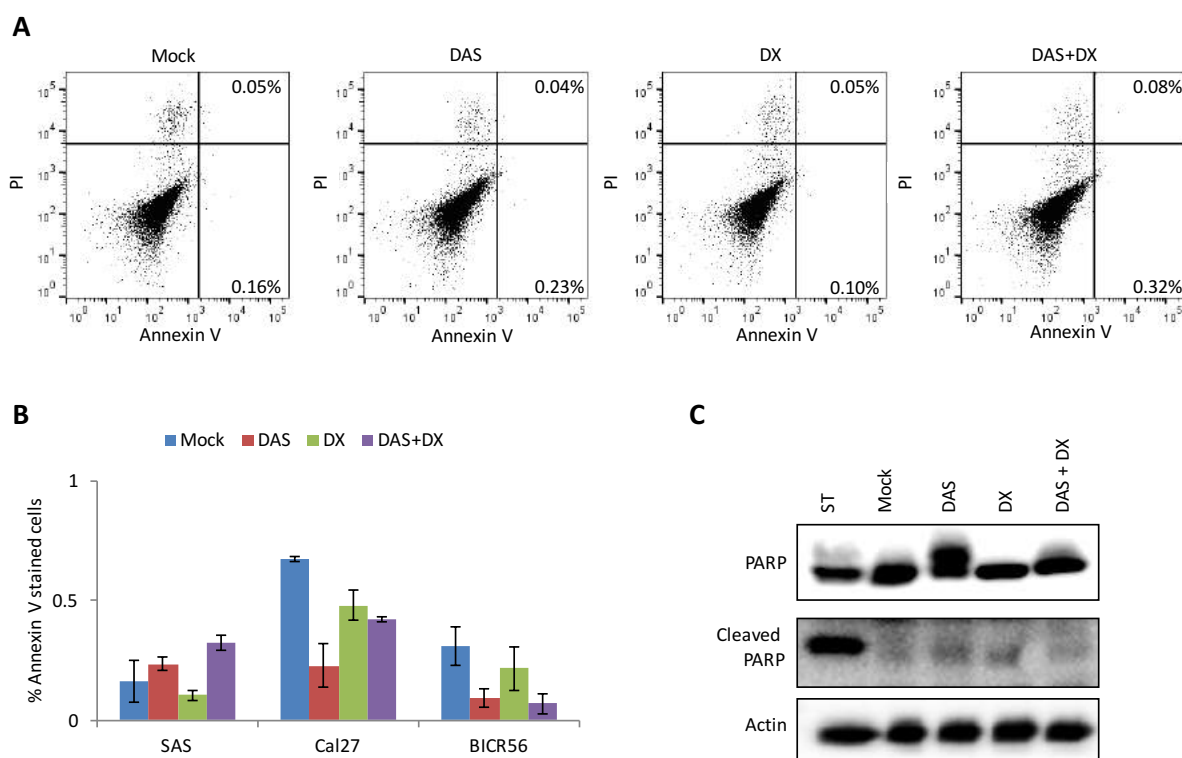
Figure 53. Annexin V and PI staining and the absence of the apoptosis-related marker cleaved-PARP suggests no induction of apoptosis after DAS+DX treatment in TSCC cells

Cells were treated with DMSO as vehicle control (Mock), 50 nM of DAS, 100 nM of DX, or a combination of DAS+DX for 72 h.

(A) Annexin V and PI staining analysis by FACS detects no apoptosis
Treated SAS cells were stained with Annexin V and PI for FACS analysis. X-axis and Y-axis indicate Annexin V and PI fluorescence intensity, respectively. Numbers in the right upper and right lower quadrants denote percentages of late and early apoptotic SAS cells, respectively (Annexin V-positive). Ten thousand events were analyzed in each experiment. Representative dot plots from three independent experiments are shown.

(B) Numerical representation of Annexin V-positive TSCC lines quantified by FACS shows no significant staining for the treated cells
Results are expressed as means and standard deviation taken from 3 independent experiments.

(C) DAS+DX treatment does not induce prominent PARP cleavage
SAS cells were treated as indicated above. As a positive control for PARP cleavage induction, SAS cells were treated with 500 nM of Staurosporine for 18 h. Total cell lysates were generated and analyzed by Western blotting.

PARP is involved in the routine repair of DNA damage in response to a variety of cellular stresses. Caspase-mediated apoptotic cell death is accomplished through the cleavage of several key proteins required for cellular function and survival, including PARP (Figure 12). Cleavage of PARP by Caspases is considered to be a hallmark of apoptosis [868]. The cleavage of PARP from a 116 kDa to an 85 kDa form can be detected at an early stage in apoptosis. Cleavage of PARP in DAS+DX-treated SAS cells was compared to a Staurosporine-treated control. Whereas the 85 kDa form was readily detected in lysates from Staurosporine-treated cells, PARP remained intact in DAS and/or DX-treated cells (Figure 53.C). However, upon DAS treatment, it was noted that the PARP band in general shifted higher compared to protein band in untreated cells. Recent studies indicate that post-translational modifications

such as phosphorylation, acetylation, and methylation are crucial for the regulation of PARP1 activity. Dysregulation of modifications on PARP has been observed in human cancer [869]. Further investigation by liquid chromatography-tandem mass spectrometry, for example, could be utilized to identify the possible PARP modification and understand this phenomenon [870].

6.3.9 DAS+DX Treatment Induces Autophagy in TSCCs

Acridine orange accumulates in a protonated form inside acidic vesicular organelles, causing a metachromatic shift from green to red that can be measured by FACS analysis for studying late stages of autophagy. Autophagy induction was assessed in TSCC lines upon DAS and/or DX treatment as described in the experimental section to quantify the accumulation of the acidic component and assess the volume of acidic vesicular organelles (Figure 11). As shown in Figure 54.A, DAS treatment of SAS cells increased the strength of red fluorescence and the percentage of the autophagic cells from 1.6 % in Mock-treated cells to 6.1% in DAS-treated cells. While DX itself exhibited only little or no autophagy induction, there was a more significant induction upon DAS+DX cotreatment, especially in CAL27 cells (Figure 54.B and S30).

In the context of defective apoptosis, autophagy has been investigated in TSCCs as a possible alternative cell death pathway. Inhibition of apoptosis has also been shown to activate autophagic cell death [633] [634]. When autophagy is induced, parts of the cytoplasm and intracellular organelles are sequestered within characteristic double-membraned or multi-membraned autophagic vacuoles (Figure 11). As shown in Figure 53 and 54, DAS alone or in combination with DX induced a significant amount of autophagy but only a small amount of apoptosis in TSCC lines. However, current results should be confirmed by other methods based on electron or fluorescent microscopy, Western blotting or flow cytometry.

Recent studies have found a dual role for autophagy in several oral diseases. In oral cancer, autophagy can mediate tumor suppression and promotion [640]. The proper amount of autophagy promotes cancer cell survival, whereas a high level of autophagy results in autophagic cell death. Whether autophagy has pro-survival or pro-death effects depends on different factors, including cancer cell type/phase, stress context and the microenvironment. Accordingly, further studies are warranted to better understand whether autophagy is death or resistance mechanism in TSCC upon the DAS+DX treatment. Autophagy could be inhibited by knockdown of proteins that have a central role in autophagy (e.g. ATG5 or Beclin 1) or pretreatment with autophagy inhibitors like Bafilomycin and Chloroquine. After that, cell viability, colony formation and apoptosis should be evaluated.

A

B
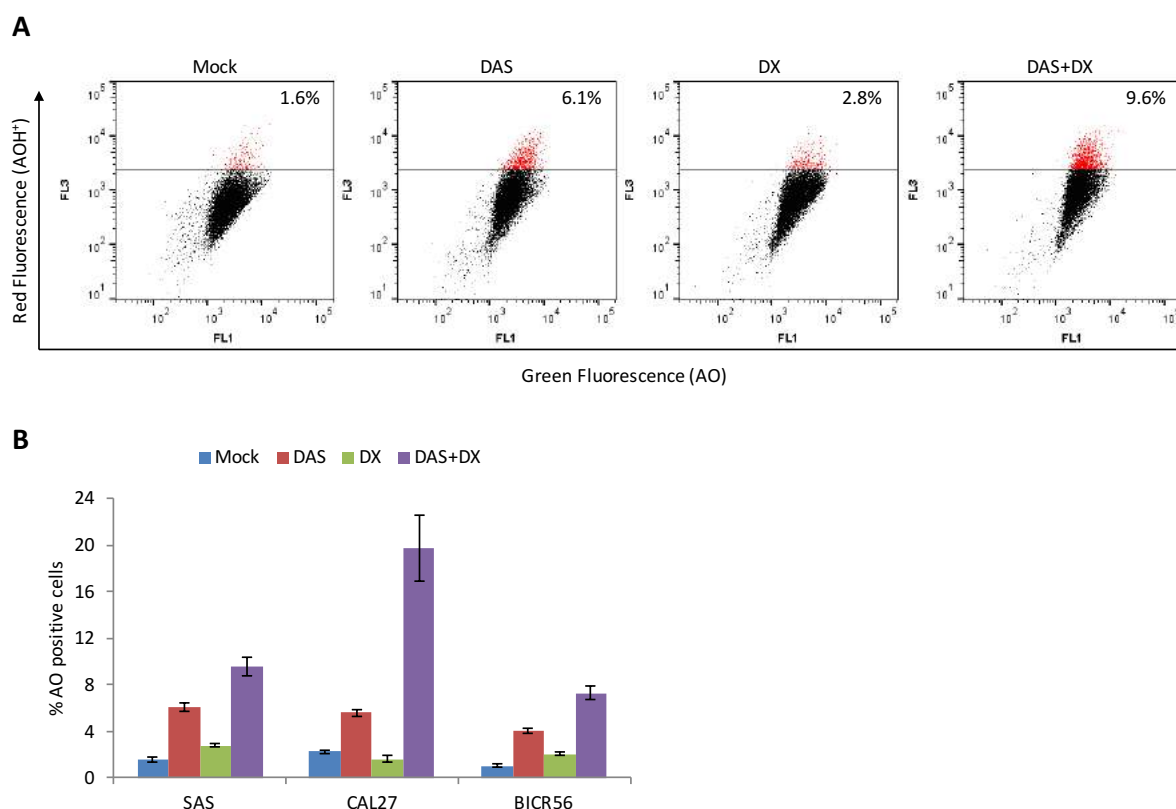
Figure 54. DAS induces autophagy in TSCC lines

(A) Detection of green and red fluorescence in Acridine Orange (AO)-stained cells using FACS analysis

SAS cells were treated with DMSO as vehicle control (Mock), 50 nM of DAS, 100 nM of DX, or a combination of DAS+DX for 72 h, stained with AO and then analyzed by flow cytometry to quantify the acidic vesicular organelle (AVO) formation. At neutral pH, AO is a hydrophobic green fluorescent molecule. Inside acidic vesicles, AO becomes protonated and trapped within the organelle. Protonated AO (AOH$^+$) forms aggregates that emit bright red fluorescence. FL1 (x-axis) indicates green color intensity, while FL3 (y-axis) shows red color intensity. Representative results from three independent experiments are shown.

(B) Quantification of autophagy

The AO-positive cell population is shown as a percentage of the total cell population in SAS, Cal27 and BICR56 cells. Values are expressed as means and standard deviation obtained from three independent experiments.

Interestingly, the synergistic effect of Bortezomib (a proteasome inhibitor) and radiation on the viability of SAS cell line was reported to be autophagic cell death induction [643]. In SAS cells, the tumor necrosis factor receptor-associated factor 6 (TRAF6) protein expression which plays an oncogenic role in tumorigenesis of OSCC and oral tumor growth was reduced through autophagy-mediated lysosomal degradation. There is conflicting evidence about the induction and role of autophagy upon DX treatment in cancer cell lines. DX was found to induce pro-death autophagy [871], to induce autophagy upstream of apoptosis resulting in cell death [872] or to induce autophagy as an apoptosis resistance mechanism [873]. Induction of autophagy has also been shown to overcome Glucocorticoid resistance in acute lymphoblastic leukemia cells [874]. However, in TSCC, DX on its own had only a small effect on autophagy induction while it potentiated autophagy in combination with DAS, especially in the CAL27 cell line. It is supposed that detailed investigations into autophagy, as mentioned before, may lead to a better understanding of its role in TSCC.

6.4 Analysis of other Clinically Used GCs in Combination with DAS in TSCCs

6.4.1 Overview

Generally, DX may be commonly used for cancer management due to its high potency, long duration of action, and minimal mineralocorticoid effect. DX is also the most commonly used GC due to the smaller number of tablets at higher doses, and the option for the intravenous and subcutaneous route if necessary. However, a number of other GCs with varied potencies are used in general medical practice and play very important roles in side-effect management and induction therapy (first line therapy) in many cancers. The most common GCs utilized in cancer therapy beside Dexamethasone include Prednisolone, Methylprednisolone and Hydrocortisone. Different cancer types, differential GR levels, the dosage of GCs given, and even the activity of other hormone nuclear receptors have to be taken into account to choose the appropriate GC [690].

Either Prednisolone or Dexamethasone are being used in the remission-induction therapy in ALL. There are several published studies from large cohorts comparing Prednisolone and Dexamethasone in the treatment of ALL [760] [875] [876]. In the early days of ALL treatment, Prednisolone was the first GC used for induction therapy. Interest in substituting DX for Prednisolone arise from subsequent studies which suggested DX having a more potent anti-leukaemia activity, and better central nervous system penetration [760] [877]. However, DX may be associated with more treatment-related toxicities including infection, bone fracture, osteonecrosis, mood and behavior problems, and myopathy. One clinical trial suggested that adding a physiologic dose of Hydrocortisone to DX treatment can reduce the occurrence of serious neuropsychological adverse effects and sleep-related difficulties in pediatric patients with ALL[878].

The type of GCs is selected based primarily on the route by which it is to be administered and the duration of coverage desired [666]. Selection of the type of GCs-utilized in cancer therapy should also be based on the risk of relapse, the treatment phase, possible side effects and the concomitant chemotherapeutic drugs. Therefore, it was decided to also investigate additional clinically used GCs, namely Methylprednisolone (MP) and Hydrocortisone (HC), for their possible synergistic interaction with DAS in TSCC to give alternatives to using of DX and also to prove the previous synergistic activity. MP is available in an injectable form which allows larger dosages to be given quickly. On the other hand, HC is a synthetic preparation of the steroid hormone cortisol and with MP they are most commonly used GCs for intravenous administration, typically given in emergency or critical situations in which rapid and profound immunosuppression or anti-inflammatory activity is needed. DX and MP are 25 and 5 times, respectively, more potent than HC [879].

6.4.2 HC and MP Exhibit Promising Synergistic Activity with DAS in TSCCs

In order to appraise the possible synergistic interactions between DAS and HC or MP in 2D culture, SAS cells were seeded in 6-well plates then treated with DMSO as vehicle control (Mock), 50 nM of DAS, 300 nM of HC, 150 nM of MP, a combination of DAS+HC or a combination of DAS+MP. After 72, cells were examined under an inverted microscope and photographed to evaluate cell densities upon different treatment conditions. As presented in Figure 55.A, cell density was reduced after DAS but not HC or MP treatment compared to the Mock control. This reduction appears to be potentiated upon DAS+HC and DAS+MP combination treatments. To confirm these results, viable cell numbers were evaluated by

trypan blue staining and counting of unstained cells with an automated cell counter as described before (2.2.4).

A

B
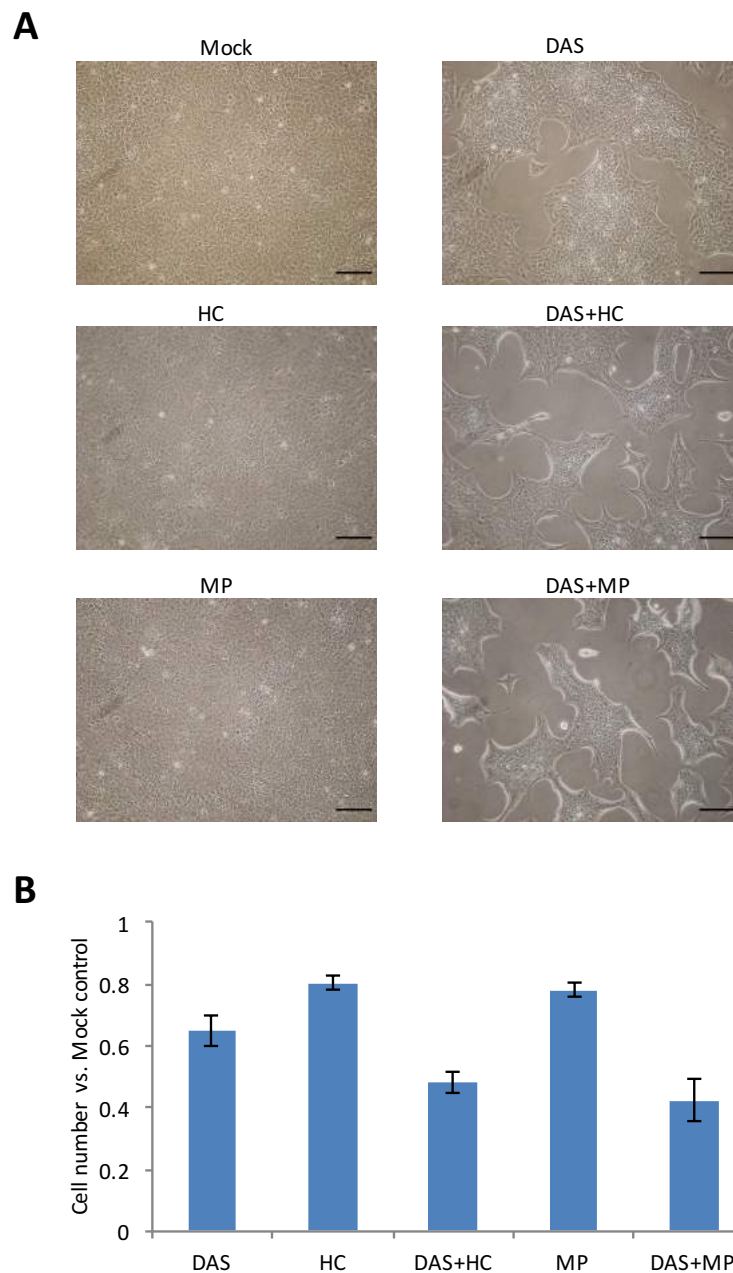
Figure 55. Hydrocortisone (HC) and Methylprednisolone (MP) potentiate DAS-induced anti-proliferation effects in SAS cells

SAS cells were treated with DMSO as vehicle control (Mock), 50 nM of DAS, 300 nM of HC, 150 nM of MP, a combination of DAS+HC or a combination of DAS+MP for 72 h.

(A) Bright field images of SAS cell growth in 2D monolayer culture after 72 h of treatment Images of SAS cells were captured by an inverted microscope using 10x magnifications to give a sense of the cell density (Scale bar = 100 μM).

(B) Graphical representation of the viable SAS cells counts over Mock control Cell proliferation was evaluated by staining cells with trypan blue to exclude dead cells and counting of viable cells by an automated cell counter. Values are expressed as means and standard deviation obtained from three independent experiments.

155

Cell proliferation was reduced to 65% upon DAS treatment compared to the Mock. The antiproliferation activity of DAS was significantly increased upon addition of HC or MP. Viable cell numbers were further reduced from 65% after DAS treatment to 48% and 42% following DAS+HC and DAS+MP combination treatments, respectively (Figure 55.B). The current results indicate that both GCs sensitize SAS cells to DAS in the 2D culture.

Subsequently, the 3D soft agar colony formation assay was used to confirm the earlier results in 2D cultured-TSCC. Initially, SAS and CAL27 cells were treated with serial dilutions of HC or MP. After 14 days, dose-response curves were determined by colony counting. As for FL and DX, no noticeable decrease in colony formation in 3D soft agar assay was found up to 10000 nM for both drugs (Figure 56). To investigate the synergistic activity, serial dilutions of HC or MP were combined with a constant concentration of DAS which had been obtained from the dose response curves in Figure 35.C. DAS concentrations were chosen to not have a striking effect on colony formation (1000 nM for SAS cells and 100 nM for CAL27 cells).
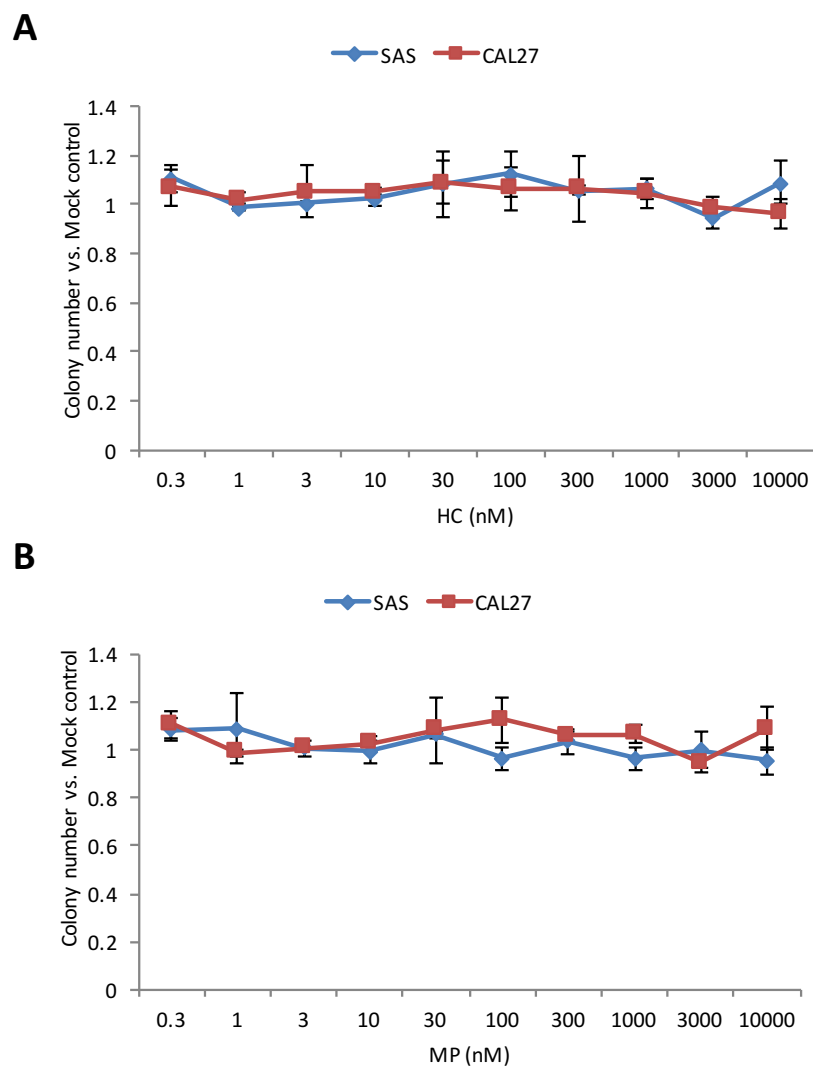
Figure 56. HC and MP as single treatments show no reduction in colony formation in 3D soft agar assay

Dose response curves of SAS and CAL27 cells treated with serial dilutions of (A) HC or (B) MP as determined by colony counting. Colony numbers were normalized to Mock-treated cells. Two wells were counted for each treatment condition. The dose response curves show mean colony number values ± SD of two independent experiments.

Given that all GCs at the used concentrations do not affect colony formation, DAS+HC and DAS+MP combination treatments exhibit strong synergistic colony formation reduction in a dose-dependent manner (Figure 57.A and B). For HC, which is less potent than MP, a higher concentration (at least 300 nM) was needed to show a notable synergistic interaction with DAS. On the other hand, MP shows synergistic interaction with DAS at a concentration comparable to DX (100 nM), yet it is still less potent than DX where a synergistic effect was seen already at 30 nM (Figure 36). All the investigated concentrations of HC and MP are pharmacologically achievable in the plasma level upon normal doses administration [880] [881]. FL is the most potent GC in combination with DAS in TSCCs that was investigated in this research (Figure 38).

Glucocorticoids are often included with other agents in cancer treatment. They are useful in primary combination chemotherapy of both, acute and chronic, lymphocytic leukemia, Hodgkin's and non-Hodgkin's lymphomas, multiple myeloma, breast cancer and prostate cancer [690]. For example, Alemtuzumab, an anti-CD52 monoclonal antibody, plus Methylprednisolone treatment was found to be the most effective of all the reported induction regimens for patients with CLL [882]. High doses of Methylprednisolone were also combined with brain radiotherapy in elderly patients with primary central nervous system lymphoma and showed prolongation of overall survival compared to patients receiving other treatments [883]. Clinical observations indicate that combining GCs with multi-tyrosine-kinase inhibitors could be a successful therapeutic approach. Inhibition of LCK by DAS was found to enhance GC sensitivity and apoptosis in lymphoid cell lines, CML and T-cell ALL[884] [885] [886].

On the other hand, GCs are routinely used to help counter some of the side effects of chemotherapy and help shield healthy tissues in the body from the deleterious effects of chemotherapy. Dasatinib produces several side effects including edemas and pleural effusions, which are supposedly triggered by activated immune cells. Effusion formation in patients treated with Dasatinib can be treated effectively by GCs [887] [888]. It was also reported that Dexamethasone, Hydrocortisone and Prednisolone effectively counteract basophil activation provoked by IgE receptor-mediated histamine release in the presence of Dasatinib and that they can rescue IgE receptor cross-linked basophils from additional costimulatory effects of Dasatinib [889]. The latter data may have additional clinical implications for using GCs in Dasatinib-treated patients to reduce the side effect besides the possible synergistic activity.

In the current study, four GCs (FL, DX, HC or MP) exhibited promising synergistic activity in combination with DAS in TSCC lines. DAS+GC combination treatments synergistically reduced cell viability and proliferation in 2D culture and anchorage-independent growth (colony formation) in 3D soft agar culture. The current robust results obtained by 4 different CGs justify continued investigation of DAS and GC in tongue cancer. The current results give also the chance to choose the suitable GC and dosage form based on the desired effect and the potential side effects in the treated patients. However, since experimental findings cannot be translated easily into clinical practice, *in vivo* trials on a mouse model are planned and will start soon to confirm the present findings.

A

B
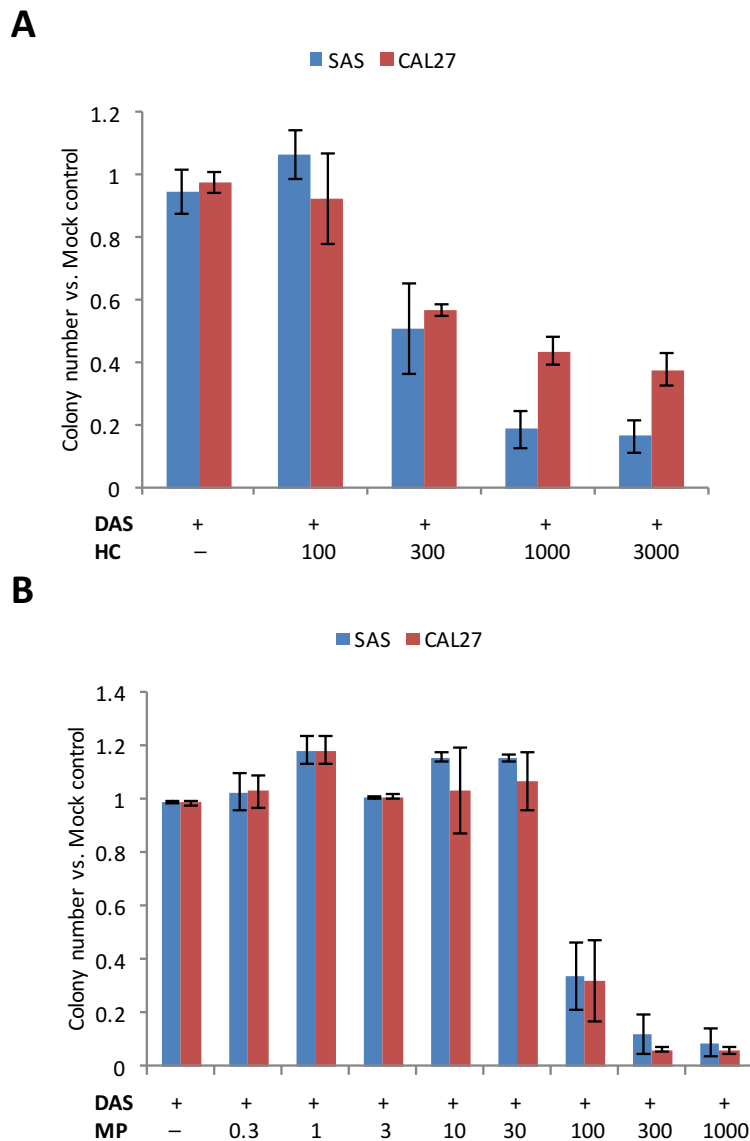
Figure 57. DAS+HC and DAS+MP combination treatments display strong synergistic effects in TSCC lines

Dose-dependent colony formation reduction of TSCC lines in response to a constant concentration of DAS and serial dilutions of (A) HC (nM) and (B) MP (nM) in 3D soft agar culture. DAS concentrations have been obtained from the dose response curves in Figure 35.C (1000 nM for SAS cells and 100 nM for CAL27). Data represent colony numbers normalized to Mock-treated cells. Four wells were counted for each treatment condition. The results show mean values ± SD of two independent experiments with two technical replicates each.

6.4.3 Characterizing DAS+HC and DAS+MP Signaling Effects in SAS Cells

Previously, in this study, it was found that DX and FL inhibit MET phosphorylation in a dose-dependent manner in SAS cells (Figure 42). To determine whether HC and MP do have the same effect, SAS cell line were treated with DMSO as vehicle control (Mock) or a serial dilution of HC (Figure 58) or MP (Figure 59) for 72 h. In comparison to DX and FL, HC and MP were able to reduce MET phosphorylation at very low nanomolar concentrations and in a concentration-dependent manner. In parallel with MET inhibition, phosphorylation of GAB1

at Tyr627, which is direct MET downstream target, was reduced as well by HC or MP in a concentration-dependent manner.
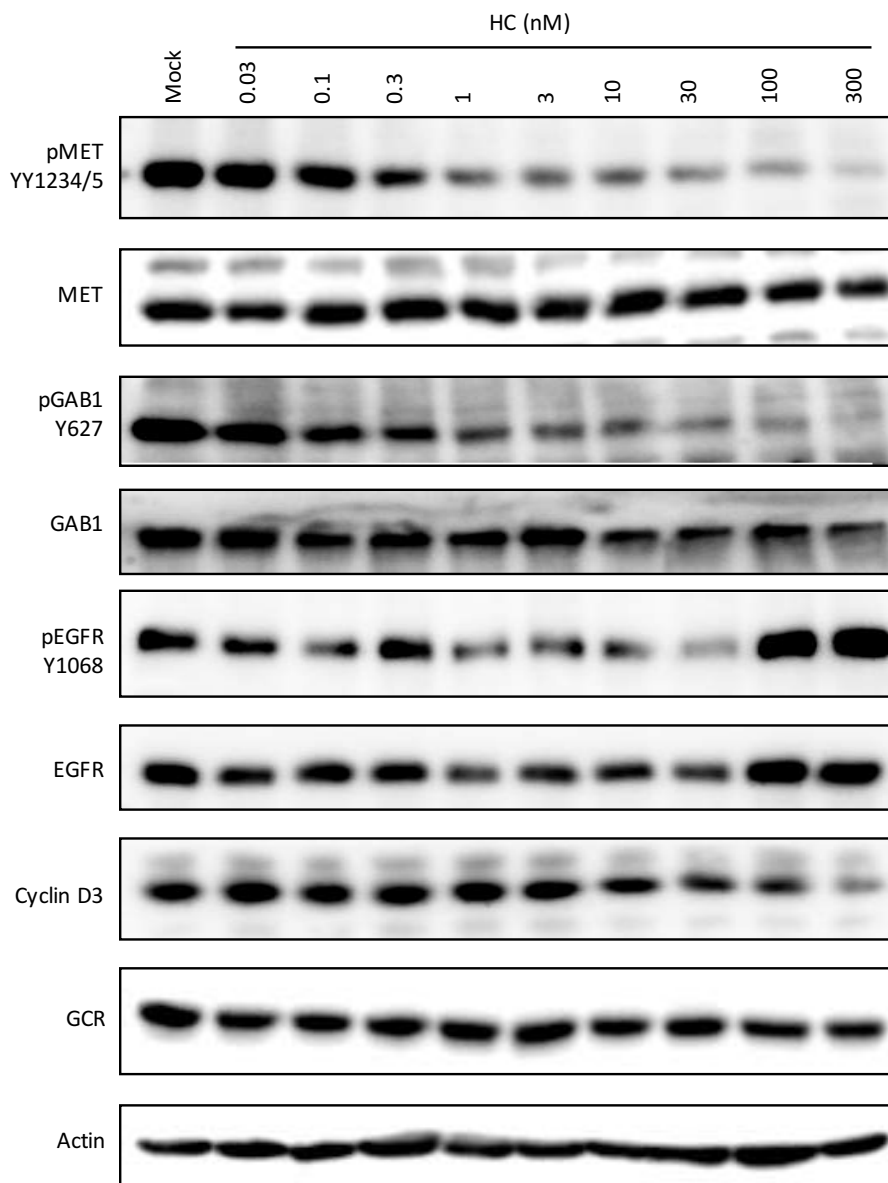
Figure 58. HC inhibits MET and GAB1 phosphorylation, deregulates cell cycle proteins and activates EGFR in a concentration-dependent manner

SAS cells were treated with DMSO as vehicle control (Mock) or a serial dilution of HC for 72 h. Total cell lysates were generated, separated by SDS-PAGE and analyzed by Western blotting. Antibodies that detect the phosphorylated state of MET at Tyr1234/1235, GAB1 at Tyr627 and EGFR at Tyr1068 were used to monitor tyrosine phosphorylation changes. The other blots analyzed total protein abundance. The blots shown are representative of three independent experiments.

EGFR expression and phosphorylation were significantly upregulated only at high concentrations of HC or MP which could be due to a compensatory mechanism upon MET inhibition as discussed before (6.3.4.3). Total protein levels of MET, GAB1 and GCR did not prominently change following HC or MP treatments. The expression level of the cell cycle regulator Cyclin D3 was decreased in a concentration-dependent manner after HC or MP treatments. However, at least 30 nM of HC or MP was necessary to show a notable reduction for Cyclin D3 level which is higher than what was required upon DX or FL

treatments (Figure 42). The last result could be due to GC potency, since both DX and FL are more potent than HC and MP.
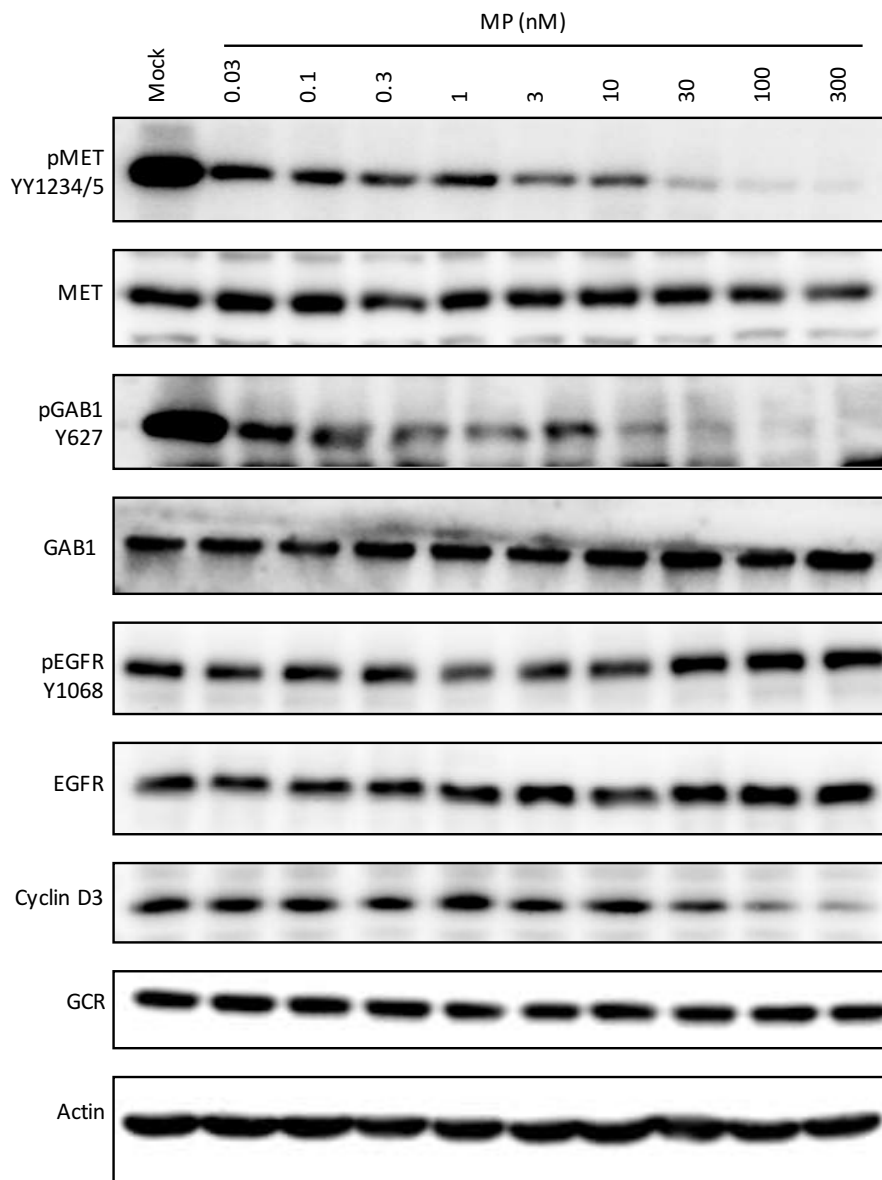
Figure 59. MP inhibits MET and GAB1 phosphorylation, deregulates cell cycle proteins and activates EGFR in a concentration-dependent manner

SAS cells were treated with DMSO as vehicle control (Mock) or a serial dilution of MP for 72 h. Total cell lysates were generated, separated by SDS-PAGE and analyzed by Western blotting. Antibodies that detect the phosphorylated state of MET at Tyr1234/1235, GAB1 at Tyr627 and EGFR at Tyr1068 were used to monitor tyrosine phosphorylation changes. The other blots analyzed total protein abundance. The blots shown are representative of three independent experiments.

All the investigated GCs reduced MET phosphorylation strongly at very low nM concentrations in the 2D culture (Figure 42, 58 and 59). A MET kinase activity assay further demonstrated that DX is not direct MET inhibitor in TSCC (Figure 43 and 44). As mentioned in detail before (6.3.4.4), the mechanism of the MET regulation by GCs is currently unknown. However, the transactivation activity of GR and the off-target activation of related steroid hormone receptors are usually associated with high-dose GCs [890]. MET phosphorylation was inhibited at very low nM concentrations of GCs while higher concentrations were necessary for EGFR upregulation. Based on that, MET inhibition by GCs could be related to their

transrepression activity while EGFR upregulation could be also associated with other GCs mechanisms away from transrepression activity.

DAS+HC and DAS+MP combination treatments were subsequently investigated by Western blot analysis as well, to understand the underlying mechanisms of the current synergistic interactions and to compare this with the previous results. For this purpose, SAS cells were treated with DMSO as vehicle control (Mock), 50 nM of DAS, 300 nM of HC, 150 nM of MP, a combination of DAS+HC or a combination of DAS+MP for 72 h. As uncovered previously, GCs and DAS+GCs treatments inhibit MET phosphorylation and consequently GAB1 phosphorylation at Tyr627 without any notable effect on the total protein levels (Figure 60). In contrast, EGFR expression and phosphorylation were upregulated upon GCs and DAS+GCs treatments. ERK and AKT phosphorylations were also mainly upregulated upon the combination treatments. On the other hand, SRC kinase inhibition by DAS blocked phosphorylation of SRC and its downstream targets p130CAS and Paxillin (Figure 60). No notable effects were seen for the current treatments on the total levels of SRC, Paxillin and GCR. In agreement with the previous results, DAS+GC cotreatments led to p130CAS degradation.
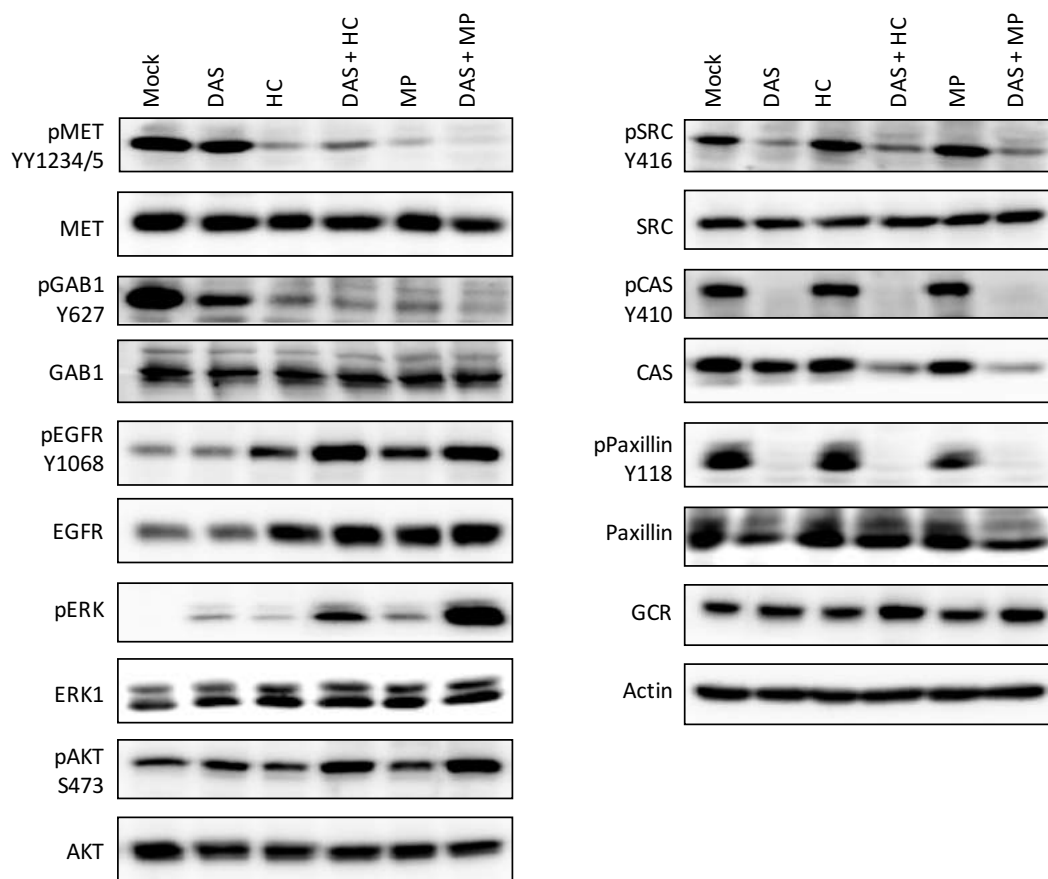
Figure 60. DAS+HC and DAS+MP combination treatments inhibit MET and GAB phosphorylation, activate EGFR, ERK 1/2 and AKT signaling pathways, and block SRC target phosphorylation

SAS cells were treated with DMSO as vehicle control (Mock), 50 nM of DAS, 300 nM of HC, 150 nM of MP, a combination of DAS+HC or a combination of DAS+MP for 72 h. Total cell lysates were generated, separated by SDS-PAGE and analyzed by Western blotting. Antibodies that detect the phosphorylated state of MET at Tyr1234/1235, GAB1 at Tyr627, EGFR at Tyr1068, ERK 1/2 at Thr202/Tyr204, AKT at Ser473, SRC at Tyr416, p130CAS at Tyr410 and Paxillin at Tyr118 were used to monitor the phosphorylation changes. The other blots analyzed total protein abundance. The blots shown are representative of three independent experiments.

As mentioned above, MET promotes tumor invasion and metastasis, which are the main cause of death in cancer patients, therefore, the interfering with MET signaling appears to be a promising therapeutic approach. The unsuccessful clinical outcomes of MET inhibition could be due to underlying resistance mechanisms. One resistance mechanism involves interaction with SRC, thus, targeting the MET and SRC pathways may be effective combination approach to control cancer [813]. One preclinical study showed that among combinations of 12 different tyrosine kinase inhibitors, Crizotinib plus Dasatinib demonstrated the most cytotoxic combination regimen [891]. The combination of Crizotinib and Dasatinib was reported recently to have limited tolerability given the high rate of adverse events in Phase 1 clinical trials [279 892]. GCs are relatively benign drugs which could be administrated safely in high doses (e.g. HC or MP) and could be evaluated with Dasatinib for their MET inhibition activity particularly in TSCC where expression of MET associated with cancer invasion and metastasis with short survival rates [477].

Also, as discussed beforehand, EGFR upregulation upon MET inhibition could be a compensatory mechanism. EGFR inhibitors could be considered with DAS+GCs combination treatments *in vitro* and *in vivo* experiments for their additional anticancer effects as shown previously (6.3.5). However, the current DAS+GCs synergistic interaction should be initially evaluated by *in vivo* trials in a mouse model and then, based on the obtained results, the benefit of EGFR inhibitor addition can be decided. ERK and AKT activation following the combination treatments could be also a compensatory or resistance mechanism associated with EGFR activation (Figure 60). Yet, as discussed in details in the last chapter (5.5.5), these intracellular signaling cascades were activated in TSCC upon DAS+HSP90i treatments despite EGFR inhibition which means other signaling pathways or feedback loops could be involved. The understanding and inhibition of cell-protective feedback loops may not only improve the response rate but also prevent the emergence of drug resistance.

As described earlier (section 1.5), p130CAS regulates signaling for survival, proliferation, invasion, and metastasis by providing a phosphorylation-dependent platform within the adhesion complex. Anoikis is a form of programmed cell death that occurs in anchorage-dependent cells when they detach from the surrounding extracellular matrix. The regulation and function of p130CAS in tumor cell anchorage-independent survival or anoikis resistance has been reported previously [203 893]. Constitutive phosphorylation of p130CAS was found to prevent cells from anoikis, hence contributing to tumor cell anchorage independence and metastasis. p130CAS was found specifically cleaved during anoikis in anoikis-sensitive epithelial cells, but not in anoikis-resistant tumor cells and the expression of the cleaved p130CAS fragment in these cells was sufficient to initiate anoikis and to induce cell death [203 894]. Cleavage of p130CAS was found to be likely the cause, rather than the consequence, of cell death and that the cleavage of p130CAS may participate in the initiation of anoikis.

These observations could provide new insights into understanding DAS+GC synergistic interaction and molecular mechanism of anchorage-independent inhibition of TSCCs in the 3D soft agar assay, which was estimated by colony formation. Taking into consideration p130CAS expression and activation (Figure 4), p130CAS deactivation by DAS treatment, which perhaps is potentiated by p130CAS degradation upon DAS+GC cotreatment, could inhibit cell migration, adhesion and invasion also start anoikis. However, further investigations are necessary to elucidate the exact role of p130CAS dephosphorylation and degradation in the current synergistic interaction.

Paxillin dephosphorylation by DAS could inhibit FAK/Paxillin interaction results in the absence of FAK from focal adhesions, a decrease in the phosphorylation of several adhesion proteins and alteration of cell migration and invasion. A growing number of signaling molecules have been shown to promote or regulate cell migration of cancer cells through the phosphorylation of Paxillin at Tyr118, which alters the organization of focal adhesion, with the consequent promotion of cell motility [895]. The increased phosphorylation of this residue is considered as indicative of metastasis [441]. Previous data showed that maximal tyrosine phosphorylation of Paxillin by SRC and FAK is required for the induction of anchorage-independent signal transduction and proliferation, characteristic of metastatic cells [441]. Paxillin was shown to be involved in the development and progressions of OSCC and to be a potential target for suppress tumor progression [896][897]. It was also considered to be a useful biomarker for OSCC patient management and prognosis. Taken all together, synergistic antiproliferation outcome and anchorage-independent inhibition of TSCCs upon DAS+GC cotreatments could be related to one or more of following effects: p130CAS depletion, Paxillin dephosphorylation or MET inhibition. However, other factors could also be involved.

6.4.4 DAS+HC and DAS+MP Treatments Induce G1 Cell Cycle Arrest but not Apoptosis in SAS Cells

The effects of HC and MP on cell-cycle progression and population distribution were determined by flow cytometry. FACS analysis showed G1 cell cycle arrest in SAS cells upon single treatments (DAS, HC or MP) which became more significant after the combination treatments (DAS+HC or DAS+MP) as presented in Figure 61.A. Similar to the previous results, the current treatments showed no induction for apoptosis indicated by a notable absence of sub-G1 peaks. This observation was confirmed by FACS analysis for Annexin V/PI stained-SAS cells following 72 h treatment with as vehicle control (Mock), 50 nM of DAS, 300 nM of HC, 150 nM of MP, a combination of DAS+HC or a combination of DAS+MP. As displayed in the representative dot plots, there was no increase in cell in the right upper quadrant and right lower quadrant upon single or combination treatments which represent late and early apoptotic cells, respectively (Figure S31).

Subsequently, cells were lysed following the treatment and analyzed by Western blotting (Figure 61.B). CDK inhibitors p27 and p21 were upregulated after GCs and DAS+GCs treatments which could be associated with G1 cell cycle arrest as discussed earlier (Figure 25). Also, Cyclin D3 protein levels declined after GCs and DAS+GCs treatments without any notable change on the Cyclin D1 level. Similar to DAS+DX cotreatment, the CDK6 level but not the CDK4 level was reduced upon DAS+GC combination cotreatments. Cyclin D3 and CDK6 appear in the G1 phase and direct the cell towards the S phase of the cell cycle (Figure 25). Furthermore, the expression levels of G2/M cell cycle markers: WEE1, phospho-WEE1 and Cyclin B1 were decreased after DAS+GC cotreatments. As discussed beforehand, whether downregulation of these regulators have a role in the induction of G1 cell cycle arrest or on the overall DAS+GCs synergistic activity remains unclear and need to be further investigated.
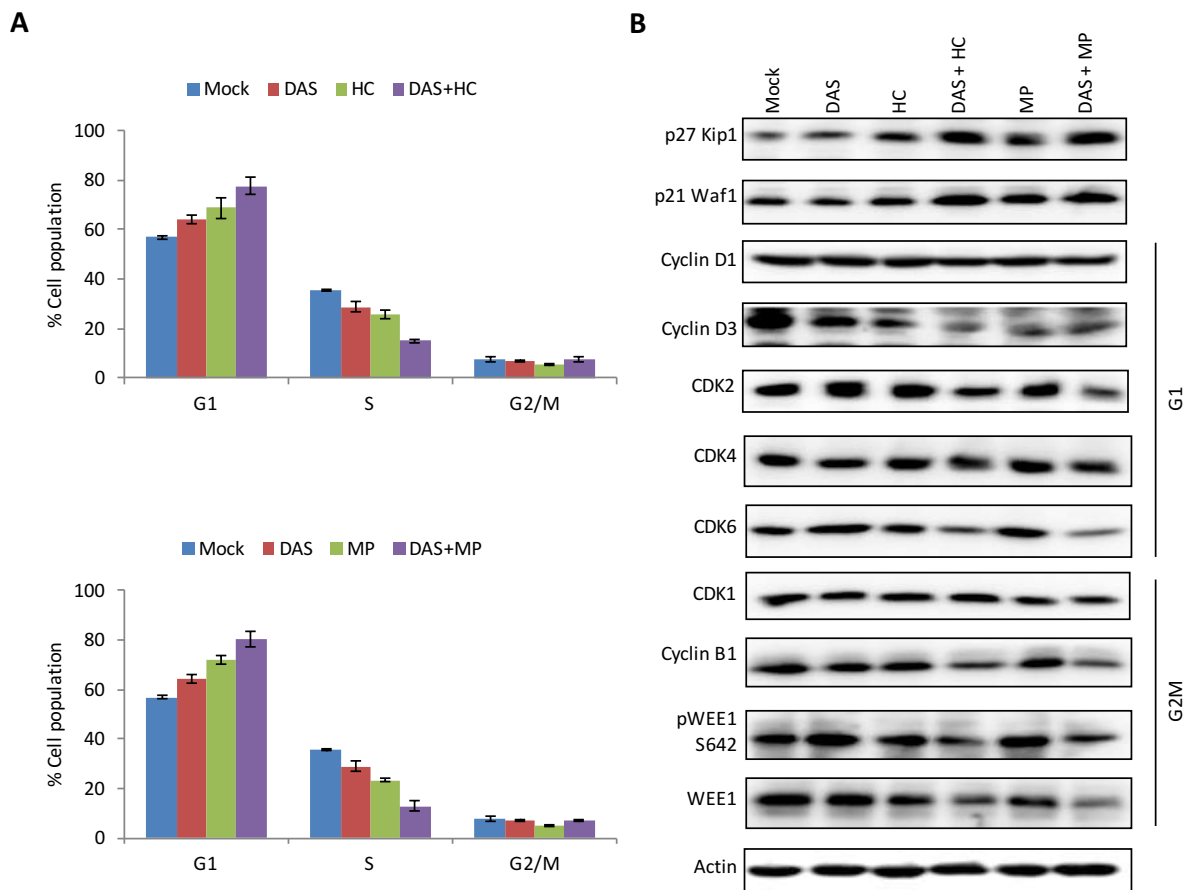
Figure 61. DAS+HC and DAS+MP treatments induce G1 cell cycle arrest in SAS cells and change the expression levels of cell cycle-associated proteins

SAS cells were treated with DMSO as vehicle control (Mock), 50 nM of DAS, 300 nM of HC, 150 nM of MP, a combination of DAS+HC or a combination of DAS+MP for 72 h.

(A) Combination treatments lead to Cyclin D3, CDK6, WEE1 and Cyclin B1 downregulation as well as p21 and p27 upregulation
After treatment, total cell lysates were generated, separated by SDS-PAGE and analyzed by Western blotting. An antibody that detects the phosphorylated state of WEE1 at Ser642 was used to monitor the phosphorylation change. The other blots analyzed total protein abundance. The blots shown are representative of three independent experiments.

(B) FACS analysis shows that combination treatments induce G1 cycle arrest
Treated cells were fixed overnight, the DNA was stained with DAPI and the DNA content was analyzed by flow cytometry. Ten thousand events were measured in each experiment. The cell population was analyzed as cell numbers at each cell cycle phase relative to the total population. No sub-G1 peaks were observed following treatment of any of the cells evaluated. Results are expressed as means and standard deviations obtained from 3 independent experiments.

In conclusion, the previous outcomes showed a very similar mode of action upon different DAS+GC treatments. These are characterized by G1 cell cycle arrest and dergulation of cell cycle regulators (p21, p27, Cyclin D3, CDK2, CDK6, Cyclin B1 and WEE1). However, a few variations were noted: like p21 upregulation upon DAS+HC or DAS+MP cotreatments but not after DAS+DX cotreatment. The last observation could be explained by the low concentration of DX being insufficient to increase the transcription and the expression of p21 in SAS cells. Another variation is CDK2 reduction upon DAS+MP but not DAS+DX or DAS+HC cotreatment. The MP concentration, but not DX or HC concentrations, in

combination with DAS could be sufficient to induce CDK2 degradation. However, as discussed before, the reason for cell cycle markers degradation upon the DAS+GCs cotreatment in TSCCs remains unclear and needs further analysis.

6.5 Exploration of SH2 Domains as Tools to Detect Drug Effects on Protein Tyrosine Phosphorylation with Enhanced Sensitivity

6.5.1 Overview

The SRC Homology 2 (SH2) domain is a protein domain of about 100 amino-acid residues which binds to phosphotyrosine-containing polypeptides via several surface pockets. Specificity is domains provided via interaction with residues that are distinct from the phosphotyrosine. 121 SH2 in 111 human proteins are known. Proteins containing SH2 domains include those kinases, adaptors, phosphatases, ubiquitin ligases, transcription factors, guanine nucleotide exchange factors and phospholipid-based secondary signaling molecules. A central role is played by SH2 domains in connecting activated receptor tyrosine kinases, such as EGFR to cytoplasmic signaling molecules [898]. Additionally, SH2 domains in kinases can be essential in regulating the catalytic activity as exemplified by the SRC kinase family. This establishes the SH2 domain as a key player in the cellular signaling system in a pTyr-dependent manner [899].

The binding affinity of SH2 domains to a pTyr-containing ligand is moderate and considered to be crucial for allowing transient association and dissociation events in cell signaling [899]. Their ability to specifically recognize the phosphorylated state of tyrosine residues has been previously successfully exploited in large-scale proteomics studies. In particular, applications of SH2 domains have been reported for therapeutic and diagnostic purposes [900] [901]. SH2 domain-based probes have been developed and used to profile global pTyr landscapes using peptide dot blotting, Far Western blotting and oligonucleotide tagged multiplex assays [902]. For example, 228 proteins potentially involved in the EGFR pathway were identified, by affinity purification with the glutathione S-transferase (GST)-fused SH2 domain of GRB2 [903]. Machida *et al.* reported the application of domain-based probe technology to profile lung cancer cell lines and demonstrated a significant correlation between EGFR mutations and sensitivity to the EGFR inhibitor Erlotinib with a GRB2 SH2 probe, suggesting a diagnostic value [904].

6.5.2 Expression of GST-SH2 Fusion Proteins in *E.coli*

In this study, a readily available subset of SH2 domains of adaptor proteins (CRKL and NCK), SRC family kinases (FYN, HCK and YES), ABL kinase and the N-terminal SH2 of PI3K were expressed in *E. coli* as GST-fusion proteins as described in the experimental section (2.2.18.2). The advantage of SH2 domain-based detection of tyrosine-phosphorylated proteins is that, in contrast to phosphospecific antibodies, the identification of SH2-binding partners can be linked to signaling pathways inside the cell. SH2 profiling is highly sensitive and throughput is relatively high, thus it is ideal for profiling or detection of phosphotyrosine signaling in cancer cells. That, combined with high affinity binding, as well as the cheap and relatively straightforward expression of many SH2 domains in bacteria, could make them an important tool for phosphotyrosine epitope identification and purification.
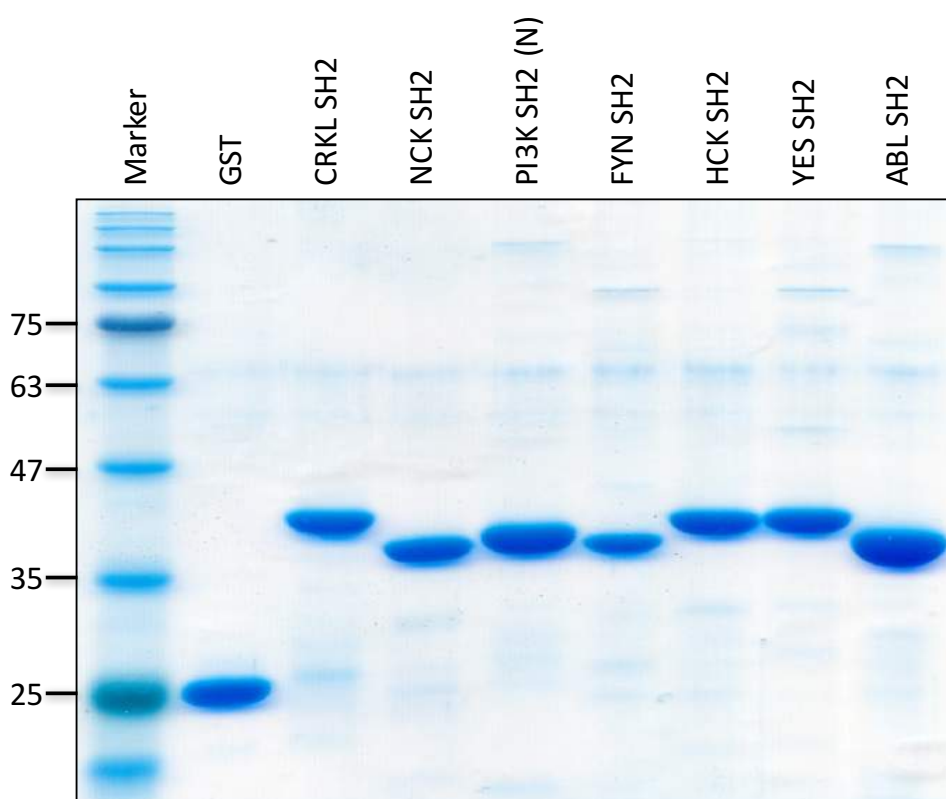
Figure 62. Integrity and purity of _E.coli_-expressed GST-SH2 fusion proteins

Approximately equimolar amounts (ca. 20-40 μg) of recombinantly-expressed SH2 domain fusion protein were separated by 12% SDS-PAGE and stained with InstantBlue.

Since recombinantly expressed proteins can sometimes be subjected to or proteolytic degradation, the integrity of the expressed constructs was first analyzed. For that purpose, equimolar amounts of all GST-fusion constructs expressed in _E.coli_ (BL21 strain) and purified as described in the experimental section, were separated by SDS-PAGE and stained with InstantBlue (Figure 62). All GST and GST-SH2 domains appeared to be intact and were therefore considered to be suitable for use in further experimental procedures.

6.5.3. Detection of Tyrosine-Phosphorylated Proteins by Far Western Blotting

6.5.3.1 Overview

The SH2 domains were used as probes for the detection of tyrosine-phosphorylated binding partners in SAS cells upon DAS and/or DX treatments. The binding of the SH2 domains to different proteins in the SAS cells was investigated by Far Western blotting which allows for the rapid screening and detection of potential protein-protein interactions and provides a method to qualitatively determine relative binding strength. In Far Western blotting, to characterize protein-protein interactions, protein samples of interest are immobilized on a membrane and then probed with a non-antibody protein. In contrast to western blotting, which uses specific antibodies to detect target proteins, Far Western blotting detects proteins based on the presence or the absence of binding sites for the protein probe. With this method it is possible to detect protein-protein interactions and study the effect of post-translational modifications on them without the use of specific antibodies, or even to use specific interaction sequences as probes and investigate their binding partners [905].

In the past, detection of GST-fused proteins often involved biotinylation or the use of GST-specific antibodies. A major drawback of this approach, however, used to be the relatively high background which masked low abundant or weakly phosphorylated proteins. To overcome this, Nollau *et al.* developed a novel technique which relied on the formation of a complex between GST and glutathione conjugated horseradish peroxidase (GSH-HRP), for Far Western blotting [906]. This combination produced a more rapid and sensitive method for phosphotyrosine profiling. However, unfortunately, Sigma Aldrich has discontinued production of this conjugate.

6.5.3.2 Optimization of Far Western Blot Conditions

In the current work, initially, SAS cells were treated with DMSO as vehicle control (Mock), 100 nM of DAS, 100 nM of DX or a combination of DAS+DX for 6 h. Then, equal amounts of lysates (75 µg) were separated by SDS-PAGE and transferred onto PVDF membranes which were then blocked in 10% non-fat dry milk. 1 µg/ml of the GST-fused SH2 domain was used to probe the membrane for 1 h at room temperature. The membrane was washed and incubated with anti-GST–HRP (1:3000) for 4 h at RT then signals were detected by ECL. The protocol had to be optimized as initially a high background signal masked most of the phosphorylated proteins and unspecific signals were detected due to binding of proteins to GST even when GST alone was used as a negative control probe (data not shown). To overcome this, different blocking buffers instead of milk were used (BSA, albumin and BSA+albumin), the initial loading lysate amount was reduced (to 30 µg/well) and the anti-GST-HRP antibody was diluted (up to 1:20000). All these strategies alone or together failed to significantly improve the outcome or reduce the background (data not shown).

It was then decided to include a preclearing step before lysate loading and separation. For this purpose, cell lysates were incubated with an appropriate volume of GST beads and GST protein at 4 °C for 1 h. Next, the mixtures were centrifuged and supernatants were taken and mixed with sample buffer. The protocol was then continued as before. This strategy also exhibited no improvement in the outcomes (data not shown). Incubating the membrane incubated with anti GST-HRP antibody alone without prior probing with any GST-fused SH2 domain showed a strong background by the antibody itself binding to other proteins in cell lysate with the GST. In an attempt to solve this issue, SH2-probed membrane was incubated with an anti-GST mouse antibody without HRP (1:1000) for 3 h at RT. The membrane was washed three times and incubated with anti-mouse secondary antibody (1:5000) for 3 h at RT. After three times washing, signals representing proteins that bound specifically to the probe were detected by ECL. Unfortunately, this approach also did not reduce the strong background (data not shown).

It was reported that pre-incubation of the GST fusion probe with anti-GST–HRP conjugate can be used to reduce the background with some decrease in signal strength [907]. To label the GST fusion probe, 5 µl of GST-fused SH2 domains (1 µg/µL) were diluted in 45 µl of TBST to a final concentration 0.1 µg/µl. This was incubated for 60 minutes in ice with 3 µg of anti-GSH-HRP antibody. This direct labeling method can presumably promote oligomerization of probe and HRP, increasing the avidity of binding to the target and enhancing the signal [907]. In addition, this one-step probing and washing procedure is time-saving and may avoid dissociation of the probe during washes if probe binding is weak. After probe labeling, the preincubated complex was used to probe the membrane for 1 h at room temperature and signals representing proteins that bound specifically to the probe were detected by ECL (Figure 63). To exclude non-specific signals due to the binding of proteins to GST, the same

procedure was also followed with equimolar concentrations of GST alone used as a negative control probe. Due to this modification of the protocol the unspecific binding and the background decreased and low abundant or weakly phosphorylated proteins signal became more obvious.

6.5.3.3. Far Western Blot Analysis of DAS and/or DX Treated SAS Cells with Various GST-fused SH2 Domains

Analysis of treated-SAS cells with several GST-SH2 domains employing Far Western blot assay showed that most of the domains bind to a prominent phosphorylation band around 130 kDa which was reduced upon DAS treatment (Figure 63). Far Western blotting is very different from other commonly used methods to detect and characterize protein-protein interactions, and therefore complements these other approaches. Because the probe protein directly binds to denatured/separated proteins immobilized on a membrane, Far Western blotting detects only direct interactions; by contrast, most other binding assays, such as immunoprecipitation and pull-down assays, may detect both direct and indirect interactions. Thus, the Far Western assay is often used to confirm direct interaction following immunoprecipitation or pull-down assays.

In contrast to western blotting where a target protein is usually known in advance, Far Western blotting can detect proteins based on presence or absence of binding sites without any previous knowledge about their identities. However, with the small SH2 subset utilized in this study, only a very small number of bands were detected. As presented in Figure 63, a key protein band was detected around 130 kDa molecular weight. This protein could be p130CAS which was shown previously to overexpressed and phosphorylated in TSCC lines (Figure 4) and inhibited by SRC kinase inhibitor DAS (Figure 13). To investigate this further, the SH2 domains that showed binding to this band could be used for purification of their binding partners and identification by mass spectrometry. Testing greater panel of SH2 domains could lead to more effective and comprehensive detection of phosphorylated proteins in the future.
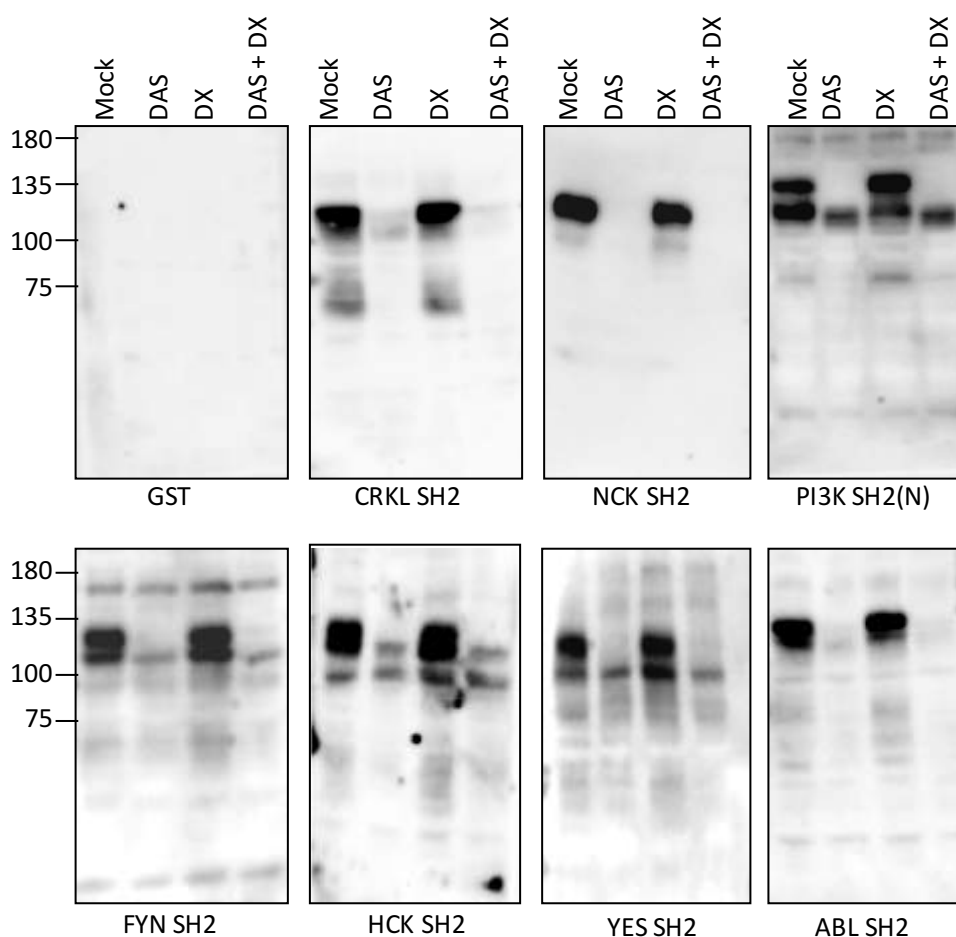
Figure 63. Far Western blot analysis of DAS treated SAS cells with various GST-fused SH2 domains show reductions of prominent phosphorylation bands around 130 kDa

SAS cells were treated with DMSO as vehicle control (Mock), 100 nM of DAS, 100 nM of DX or a combination of DAS+DX for 6 h. Equal amounts of lysates were separated by SDS-PAGE and transferred onto PVDF membranes. Following blocking with milk, each membrane was probed with pre-formed GST-SH2/anti-GST-HRP complexes and the bound probe was detected with ECL. As a control for non-specific background signals, an equimolar amount of GST/ anti-GST-HRP was also used as a probe. The blots shown are representative of two independent experiments.

6.6 Summary and Future Strategies

Four GCs (FL, DX, HC or MP) synergistically enhance DAS cytotoxic activity in 2D and 3D culture of TSCC lines. However, GCs have no notable effect on TSCC viability or colony formation in the 2D and 3D cultures, respectively. This will be further evaluated *in vivo* animal experiment in the near future. So far, the subcutaneous injections of SAS and CAL27 cells produced measurable xenograft suitable for further examinations. The next step will be dosing the compound of interest immediately after xenografting to evaluate their *in vivo* activity. FL shows the most potent synergistic activity in combination with DAS, however, DX is initially preferred to be examined in the animal experiment with DAS due to its favorable clinical and pharmacological features.

p130CAS depletion upon the combination treatments could provide an explanation for DAS+GC synergistic interaction in TSCC lines. p130CAS deactivation by DAS treatment was

potentiated by p130CAS degradation by cotreatment with GC. This may lead to inhibition of TSCCs migration, adhesion and invasion. However, further investigations are necessary to examine the exact role of p130CAS dephosphorylation and degradation and its consequences in the current synergistic interaction.

GCs were found to induce rapid and prolonged inhibition of MET phosphorylation in TSCC in a concentration-dependent manner but this inhibition was not due to a direct effect on MET kinase activity in case of DX. GCs should also be assessed in other cancers for their ability to inhibit MET kinase phosphorylation, especially in cancer with MET overexpression or MET activation as acquired resistance to EGFR inhibitors. Further investigations are required to understand the underlying mechanisms for this action. At the same time, late EGFR upregulation was noted in TSCCs upon GC and DAS+GC treatments. Therefore, EGFR inhibitors (LP or CT) were utilized in this work to overcome EGFR activation. They showed an additive to moderate synergistic cytotoxic activity in combination with DAS and DX in 2D and 3D cultures. However, *in vivo* experiments with DAS+DX+EGFRi treatment are important to establish any potential benefit for a combination of EGFR inhibitors with DAS+DX in a triple treatment. Further investigations are also needed to understand the underlying mechanisms of this interaction.

DAS+GCs combination treatments induce G1 cell cycle arrest and senescence in TSCCs. Upregulation of the p27 level and downregulation the expression levels of cell cycle-associated proteins Cyclin D3, CDK6, WEE1 and Cyclin B1 upon DAS+GC treatments could be associated with these inductions. However, WEE1 and Cyclin B1 are keys regulators of the G2/M and whether or not their depletion upon DAS+GCs cotreatment improves this synergistic interaction or has any impact on the strong G1 cell cycle arrest needs also to be further investigated. No apoptosis, Caspase activity or PARP cleavage was detected after DAS+GCs treatment. On the other hand, autophagy was induced mainly due to the effects of DAS. The role of autophagy in TSCC upon the current treatments as death or resistance mechanism needs also further investigations.

Chapter 7. Conclusions and Future Perspectives

Oral cancer is a common malignancy. In 2018, it was estimated that 354,900 cases of oral cancer occurred worldwide, with 177,400 deaths. Squamous cell carcinoma of the tongue is the most common intraoral malignancy worldwide (40-50% of OSCC) and in several countries, it is particularly a serious public health problem. This aggressive epithelial malignancy is associated with high mortality and severe morbidity among the long-term survivors. The 5-year mortality rate is approximately 50% and the poor survival index has not changed significantly in the past century. Surgery in combination with radiotherapy is still the most commonly used treatment modality. It is curative in certain subsets of patients but these invasive procedures leave many of these patients substantially impaired. In patients who survive, therapy frequently results in significant physical mutilation, compromised speech, taste, mastication and swallowing.

Improvement of patient survival and reduction of the therapeutic-related morbidity requires a better understanding of the biological nature of the disease. Improved understanding is also expected to facilitate the development of novel and more efficient treatment modalities for this lethal disease. The identification of new target molecules in TSCCs and the use of targeted therapies may improve the response and the survival rate. Although there are several promising, novel targeted therapies for patients with HNSCC in clinical use, there is no particular targeted therapy for TSCC until now. Therefore, searching for predictive markers and new targets for treatment in clinically relevant *in vitro* tumor models is essential.

Our work initially utilized 34 TSCC-derived cell lines to identify new molecular targets in tongue cancer. TSCC lines exhibited high levels of expression and tyrosine phosphorylation of the adaptor protein p130CAS. This is probably caused by high levels of SRC kinase activity. Therefore, SFK and their effector proteins could pose promising and potential targets for molecularly based TSCC therapies. Up-regulation of phospho-SFK has been documented in numerous tumors and, in support of our results, an immunohistochemical study conducted independently from our work, reported SFK activation and correlation with prognosis in human TSCC tissues, providing evidence for a role of SFK in TSCC *in vivo* [908]. Based on that, it was hypothesized that Dasatinib as SRC TKI would be useful in treating human tongue cancer cells to inhibit the signaling pathways and to decrease the growth of TSCCs.

SFK inhibition by Dasatinib in the TSCC lines leads to a substantial drop in phosphorylated proteins indicating that SFK is very likely responsible for the elevated pY-protein levels. Dasatinib also reduced TSCCs viability in a dose-dependent manner. However, clinical trials have revealed previously that Dasatinib as monotherapy is not efficacious in the treatment of cancers. Distinguishing features of squamous cell carcinoma are their high degree of cellular heterogeneity, with cell populations at various stages of differentiation, which are able to reverse lineage commitment to proliferative stages as well as enter into quiescent, slow-cycling growth phases [909]. These features might make them particularly difficult to target with monotherapeutic approaches. It was hypothesized that combining Dasatinib with other therapeutic agents could be necessary to realize the benefits of Dasatinib's effects on TSCCs. Drug combinations acting synergistically to kill recurrent resistant cancer cells have become more and more important in cancer chemotherapy. Therefore, high throughput screens with Dasatinib and FDA-approved drugs were performed by members of our laboratory at Oxford University. This produced a list of possible candidates for synergistic activity with Dasatinib (Figure 8 and 9), which were tested in the current work.

Dasatinib was found to exhibit an additive to moderate synergistic activity in combination with HSP90 inhibitors (AT or TAS) in TSCCs. More promising synergistic interactions were seen upon combination of Dasatinib with several clinically applied GCs (FL, DX, HC or MP) in 2D and 3D cultures using resazurin colorimetric assay, trypan blue exclusion assay and 3D soft agar colony formation assay. Animal experiment (mouse xenograft) will be performed in the near future to further establish *in vivo* anticancer activity of Dasatinib and the promising combination treatments in TSCC. SAS and CAL27 xenograftss were performed already and showed good growth in our *in vivo* system. The subcutaneous injections of both cell lines produced suitable and measurable tumors for further investigations. Pending ethics permission, the next step will be dosing of the compound of interest immediately after xenografting to evaluate their *in vivo* activity. Based on the synergistic results, safety profile, clinical and pharmacological features, Dexamethasone was chosen for combination with Dasatinib for initial *in vivo* animal experiments.

The underlying molecular mechanisms of the synergistic interactions were investigated. Both combination treatments (DAS+HSP90i and DAS+GC) showed changes in cell cycle distribution of TSCCs, induced senescence and autophagy but not apoptosis at the investigated concentrations. However, the role of autophagy whether it mediates tumor suppression (autophagic cell death) or promotion (drug resistance), needs to be investigated further in the future. Dasatinib and AT13387 combination treatment seems to induce mitotic catastrophe as indicated by a high expression level of phospho-Histone 3 at Serine 10 as a possible death mechanism. This result should be confirmed by other markers for aberrant mitosis or mitotic catastrophe.

Surprisingly, a very low concentration, in the low nanomolar range, of all investigated GCs was found to induce rapid and prolonged inhibition of MET kinase phosphorylation. To our current knowledge, there are no published data showing GCs inhibition of MET phosphorylation. However, DX showed no direct inhibition of MET kinase activity and therefore, further investigations in the future are warranted to understand the underlying mechanisms for this action. The of MET inhibition activity of GCs in various human tumors could potentially be examined and utilized other types of cancer with MET overexpression, including breast cancer, lung cancer, gastric cancer, colorectal cancer, ovarian cancer, kidney cancer, pancreatic cancer and other HNSCC. This finding could be used, instead of the very toxic MET inhibitors, to manage MET activation which is an important mechanism for acquired resistance to EGFR-TKIs and EGFR mAbs in many cancers.

Again unexpectedly, CGs were found to induce late EGFR activation in a concentration-dependent manner which could act as a compensatory survival mechanism upon MET inhibition. The obtained knowledge about the mechanism of action of the combination treatments would further contribute to the development of more potent strategies and to understand possible resistance mechanisms. Therefore, the benefit of EGFR inhibitors in combinations with DAS and DX to treat TSSCs was examined by another member of our group. Preclinical 2D and 3D experiments revealed that Lapatinib or Cetuximab exhibited an additive to mild synergistic activity in combination with DAS+DX cotreatment in the SAS cell line.

Results using *in vitro* concentrations much higher than those achievable in patients are published frequently. One feature of the current work is the use clinically relevant concentrations *in vitro* testing of agents based on the available human pharmacokinetic data. There are costs to publishing results claiming anticancer activity or mechanisms of action based on clinically unachievable exposures. The most important being the potential

for misallocation of clinical research resources and patients to clinical trials with little or no chance of success.

In summary, this is the first study that utilized a panel of only TSCCs to explore specific targeted therapies for tongue cancer. Also, for the first time, Dasatinib in combination with HSP90i is introduced as a promising strategy for cancer treatment. The current work is also the first to show a very strong synergistic interaction between Dasatinib and clinically used GCs in solid tumors. Based on our knowledge of the published data, it also appears to be the first time that a MET inhibition by GCs has been demonstrated. This should be further evaluated and could potentially be utilized in future for other tumor treatments.

References

1.   Review of cancer from perspective of molecular. *J. Cancer Res. Pract.* **4**, 127–129 (2017).
2.   Cancer. https://www.who.int/news-room/fact-sheets/detail/cancer.
3.   Hanahan, D. & Weinberg, R. A. Hallmarks of Cancer: The Next Generation. *Cell* **144**, 646–674 (2011).
4.   Seto, M., Honma, K. & Nakagawa, M. Diversity of genome profiles in malignant lymphoma. *Cancer Sci.* **101**, 573–578 (2010).
5.   Wang, M. *et al.* Role of tumor microenvironment in tumorigenesis. *J. Cancer* **8**, 761–773 (2017).
6.   Whiteside, T. The tumor microenvironment and its role in promoting tumor growth. *Oncogene* **27**, 5904–5912 (2008).
7.   Gonzalez, H., Hagerling, C. & Werb, Z. Roles of the immune system in cancer: from tumor initiation to metastatic progression. *Genes Dev.* **32**, 1267–1284 (2018).
8.   Aizawa, K. *et al.* Tobacco carcinogen induces both lung cancer and non-alcoholic steatohepatitis and hepatocellular carcinomas in ferrets which can be attenuated by lycopene supplementation. *Int. J. Cancer* **139**, 1171–1181 (2016).
9.   Poon, S. L., McPherson, J. R., Tan, P., Teh, B. T. & Rozen, S. G. Mutation signatures of carcinogen exposure: genome-wide detection and new opportunities for cancer prevention. *Genome Med.* **6**, 24 (2014).
10.   Trafialek, J. & Kolanowski, W. Dietary exposure to meat-related carcinogenic substances: is there a way to estimate the risk? *Int. J. Food Sci. Nutr.* **65**, 774–780 (2014).
11.   Cumberbatch, M. G. K., Cox, A., Teare, D. & Catto, J. W. F. Contemporary Occupational Carcinogen Exposure and Bladder Cancer: A Systematic Review and Meta-analysis. *JAMA Oncol.* **1**, 1282–1290 (2015).
12.   Antwi, S. O. *et al.* Exposure to environmental chemicals and heavy metals, and risk of pancreatic cancer. *Cancer Causes Control* **26**, 1583–1591 (2015).
13.   Burd, E. M. Human Papillomavirus and Cervical Cancer. *Clin. Microbiol. Rev.* **16**, 1–17 (2003).
14.   Yang, P., Markowitz, G. J. & Wang, X.-F. The hepatitis B virus-associated tumor microenvironment in hepatocellular carcinoma. *Natl. Sci. Rev.* **1**, 396–412 (2014).
15.   Yi, Z. & Yuan, Z. Hepatitis C Virus-Associated Cancers. *Adv. Exp. Med. Biol.* **1018**, 129–146 (2017).
16.   Ishaq, S. & Nunn, L. Helicobacter pylori and gastric cancer: a state of the art review. *Gastroenterol. Hepatol. Bed Bench* **8**, S6–S14 (2015).
17.   Martel, C. de, Georges, D., Bray, F., Ferlay, J. & Clifford, G. M. Global burden of cancer attributable to infections in 2018: a worldwide incidence analysis. *Lancet Glob. Health* **8**, e180–e190 (2020).
18.   Gilbert, E. S. Ionizing Radiation and Cancer Risks: What Have We Learned From Epidemiology? *Int. J. Radiat. Biol.* **85**, 467–482 (2009).
19.   Sturgis, E. M., Wei, Q. & Spitz, M. R. Descriptive epidemiology and risk factors for head and neck cancer. *Semin. Oncol.* **31**, 726–733 (2004).
20.   Argiris, A., Karamouzis, M. V., Raben, D. & Ferris, R. L. Head and neck cancer. *The Lancet* **371**, 1695–1709 (2008).
21.   Mehanna, H., Paleri, V., West, C. M. L. & Nutting, C. Head and neck cancer—Part 1: Epidemiology, presentation, and prevention. *BMJ* **341**, (2010).
22.   Mourad, M. *et al.* Epidemiological Trends of Head and Neck Cancer in the United States: A SEER Population Study. *J. Oral Maxillofac. Surg. Off. J. Am. Assoc. Oral Maxillofac. Surg.* **75**, 2562–2572 (2017).
23.   Bray, F. *et al.* Global cancer statistics 2018: GLOBOCAN estimates of incidence and mortality worldwide for 36 cancers in 185 countries. *CA Cancer J. Clin.* **68**, 394–424 (2018).
24.   Vigneswaran, N. & Williams, M. D. Epidemiological Trends in Head and Neck Cancer and Aids in Diagnosis. *Oral Maxillofac. Surg. Clin. N. Am.* **26**, 123–141 (2014).
25.   Head and Neck Cancers | CDC. https://www.cdc.gov/cancer/headneck/index.htm (2020).
26.   Bova, R. J. *et al.* Cyclin D1 and p16INK4A Expression Predict Reduced Survival in Carcinoma of the Anterior Tongue. *Clin. Cancer Res.* **5**, 2810–2819 (1999).
27.   da Cruz Perez, D. E., Passos, K. K. M., Machado, R. A., Martelli-Junior, H. & Bonan, P. R. F. Continuing education in oral cancer during coronavirus disease 2019 (covid-19) outbreak. *Oral Oncol.* **105**, 104713 (2020).
28.   Bray, F., Ren, J.-S., Masuyer, E. & Ferlay, J. Global estimates of cancer prevalence for 27 sites in the adult population in 2008. *Int. J. Cancer* **132**, 1133–1145 (2013).
29.   Ghantous, Y. & Abu Elnaaj, I. [GLOBAL INCIDENCE AND RISK FACTORS OF ORAL CANCER]. *Harefuah* **156**, 645–649 (2017).
30.   Sankaranarayanan, R., Ramadas, K., Amarasinghe, H., Subramanian, S. & Johnson, N. Oral Cancer: Prevention, Early Detection, and Treatment. in *Cancer: Disease Control Priorities, Third Edition (Volume 3)* (eds. Gelband, H., Jha, P., Sankaranarayanan, R. & Horton, S.) (The International Bank for Reconstruction and Development / The World Bank, 2015).
31.   Lambert, R., Sauvaget, C., de Camargo Cancela, M. & Sankaranarayanan, R. Epidemiology of cancer from the oral cavity and oropharynx. *Eur. J. Gastroenterol. Hepatol.* **23**, 633–641 (2011).
32.   Moore, S. R., Johnson, N. W., Pierce, A. M. & Wilson, D. F. The epidemiology of tongue cancer: a review of global incidence. *Oral Dis.* **6**, 75–84 (2000).
33.   Chen, J., Katz, R. V. & Krutchkoff, D. J. Intraoral squamous cell carcinoma: Epidemiologic patterns in connecticut from 1935 to 1985. *Cancer* **66**, 1288–1296 (1990).
34.   Hindle, I. & Nally, F. Oral cancer: a comparative study between 1962-67 and 1980-84 in England and Wales. *Br. Dent. J.* **170**, 15–20 (1991).

35. Mashberg, A. *et al.* Appearance, site of occurrence, and physical and clinical characteristics of oral carcinoma in Torino, Italy. *Cancer* **63**, 2522–2527 (1989).

36. Krolls, S. O. & Hoffman, S. Squamous cell carcinoma of the oral soft tissues: a statistical analysis of 14,253 cases by age, sex, and race of patients. *J. Am. Dent. Assoc.* **92**, 571–574 (1976).

37. Listl, S. *et al.* Survival of Patients with Oral Cavity Cancer in Germany. *PLoS ONE* **8**, (2013).

38. Cancer of the Tongue - Cancer Stat Facts. *SEER* https://seer.cancer.gov/statfacts/html/tongue.html.

39. Patel, S. C. *et al.* Increasing Incidence of Oral Tongue Squamous Cell Carcinoma in Young White Women, Age 18 to 44 Years. *J. Clin. Oncol.* **29**, 1488–1494 (2011).

40. Sp, S. & Gp, Y. Head and neck cancer incidence trends in young Americans, 1973-1997, with a special analysis for tongue cancer. *Arch. Otolaryngol. Head Neck Surg.* **128**, 268–274 (2002).

41. Shiboski, C. H., Schmidt, B. L. & Jordan, R. C. K. Tongue and tonsil carcinoma: increasing trends in the U.S. population ages 20-44 years. *Cancer* **103**, 1843–1849 (2005).

42. Prince, S. & Bailey, B. M. W. Squamous carcinoma of the tongue: review. *Br. J. Oral Maxillofac. Surg.* **37**, 164–174 (1999).

43. Harris, S. L., Kimple, R. J., Hayes, D. N., Couch, M. E. & Rosenman, J. G. Never-smokers, never-drinkers: Unique clinical subgroup of young patients with head and neck squamous cell cancers. *Head Neck* **32**, 499–503 (2010).

44. Layton, S. A., Rintoul, M. & Avery, B. S. Oral carcinoma in pregnancy. *Br. J. Oral Maxillofac. Surg.* **30**, 161–164 (1992).

45. PADERNO, A., MORELLO, R. & PIAZZA, C. Tongue carcinoma in young adults: a review of the literature. *Acta Otorhinolaryngol. Ital.* **38**, 175–180 (2018).

46. Barasch, A., Morse, D. E., Krutchkoff, D. J. & Eisenberg, E. Smoking, gender, and age as risk factors for site-specific intraoral squamous cell carcinoma. A case-series analysis. *Cancer* **73**, 509–513 (1994).

47. Franceschi, S. *et al.* Risk factors for cancer of the tongue and the mouth: A case-control study from Northern Italy. *Cancer* **70**, 2227–2233 (1992).

48. Boffetta, P., Mashberg, A., Winkelmann, R. & Garfinkel, L. Carcinogenic effect of tobacco smoking and alcohol drinking on anatomic sites of the oral cavity and oropharynx. *Int. J. Cancer* **52**, 530–533 (1992).

49. Blot, W. J. *et al.* Smoking and Drinking in Relation to Oral and Pharyngeal Cancer. *Cancer Res.* **48**, 3282–3287 (1988).

50. Schmidt, B. L., Dierks, E. J., Homer, L. & Potter, B. Tobacco smoking history and presentation of oral squamous cell carcinoma. *J. Oral Maxillofac. Surg.* **62**, 1055–1058 (2004).

51. Safi, M. & al-Tahat, J. Jordan smoking rates highest in world amid claims of big tobacco interference. *The Guardian* (2020).

52. Jk, M. Oral cancer in Jordan: a retrospective study of 118 patients. *Croat. Med. J.* **41**, 64–69 (2000).

53. Al-Amad, S. H., Awad, M. A. & Nimri, O. Oral cancer in young Jordanians: potential association with frequency of narghile smoking. *Oral Surg. Oral Med. Oral Pathol. Oral Radiol.* **118**, 560–565 (2014).

54. Franceschi, S., Bidoli, E., Herrero, R. & Muñoz, N. Comparison of cancers of the oral cavity and pharynx worldwide: etiological clues. *Oral Oncol.* **36**, 106–115 (2000).

55. Saman, D. M. A review of the epidemiology of oral and pharyngeal carcinoma: update. *Head Neck Oncol.* **4**, 1 (2012).

56. Marur, S., D'Souza, G., Westra, W. H. & Forastiere, A. A. HPV-associated Head and Neck Cancer: A Virus-related Cancer Epidemic – A Review of Epidemiology, Biology, Virus Detection and Issues in Management. *Lancet Oncol.* **11**, 781–789 (2010).

57. Ramqvist, T. & Dalianis, T. Oropharyngeal Cancer Epidemic and Human Papillomavirus. *Emerg. Infect. Dis.* **16**, 1671–1677 (2010).

58. Chaturvedi, A. K. Epidemiology and Clinical Aspects of HPV in Head and Neck Cancers. *Head Neck Pathol.* **6**, 16–24 (2012).

59. Gillison, M. L. *et al.* Human Papillomavirus and Diseases of the Upper Airway: Head and Neck Cancer and Respiratory Papillomatosis. *Vaccine* **30**, F34–F54 (2012).

60. Jayant, K., Balakrishnan, V., Sanghvi, L. D. & Jussawalla, D. J. Quantification of the role of smoking and chewing tobacco in oral, pharyngeal, and oesophageal cancers. *Br. J. Cancer* **35**, 232–235 (1977).

61. Chen, J., Eisenberg, E., Krutchkoff, D. J. & Katz, R. V. Changing trends in oral cancer in the United States, 1935 to 1985: A Connecticut study. *J. Oral Maxillofac. Surg.* **49**, 1152–1158 (1991).

62. Suh, Y., Amelio, I., Guerrero Urbano, T. & Tavassoli, M. Clinical update on cancer: molecular oncology of head and neck cancer. *Cell Death Dis.* **5**, e1018 (2014).

63. Murti, P. R. *et al.* Malignant transformation rate in oral submucous fibrosis over a 17-year period. *Community Dent. Oral Epidemiol.* **13**, 340–341 (1985).

64. La Vecchia, C., Negri, E., D'avanzo, B., Boyle, P. & Franceschi, S. Dietary Indicators of Oral and Pharyngeal Cancer. *Int. J. Epidemiol.* **20**, 39–44 (1991).

65. McLaughlin, J. K. *et al.* Dietary Factors in Oral and Pharyngeal Cancer. *JNCI J. Natl. Cancer Inst.* **80**, 1237–1243 (1988).

66. Gridley, G. *et al.* Vitamin Supplement Use and Reduced Risk of Oral and Pharyngeal Cancer. *Am. J. Epidemiol.* **135**, 1083–1092 (1992).

67. Kim, L., King, T. & Agulnik, M. Head and neck cancer: Changing epidemiology and public health implications. *ONCOLOGY* **24**, (2010).

68. Jayaprakash, V. *et al.* Human papillomavirus types 16 and 18 in epithelial dysplasia of oral cavity and oropharynx: A meta-analysis, 1985–2010. *Oral Oncol.* **47**, 1048–1054 (2011).

69. Chaturvedi, A. K., Engels, E. A., Anderson, W. F. & Gillison, M. L. Incidence Trends for Human Papillomavirus–Related and –Unrelated Oral Squamous Cell Carcinomas in the United States. *J. Clin. Oncol.* **26**, 612–619 (2008).

70. Hübbers, C. U. & Akgül, B. HPV and cancer of the oral cavity. *Virulence* **6**, 244–248 (2015).

71. Kreimer, A. R., Clifford, G. M., Boyle, P. & Franceschi, S. Human Papillomavirus Types in Head and Neck Squamous Cell Carcinomas Worldwide: A Systematic Review. *Cancer Epidemiol. Prev. Biomark.* **14**, 467–475 (2005).

72. Marklund, L. *et al.* Prevalence of human papillomavirus and survival in oropharyngeal cancer other than tonsil or base of tongue cancer. *Cancer Med.* **1**, 82–88 (2012).

73. Attner, P. *et al.* The role of human papillomavirus in the increased incidence of base of tongue cancer. *Int. J. Cancer* **126**, 2879–2884 (2010).

74. Ramqvist, T., Grün, N. & Dalianis, T. Human Papillomavirus and Tonsillar and Base of Tongue Cancer. *Viruses* **7**, 1332–1343 (2015).

75. Syrjänen, S. *et al.* Human papillomaviruses in oral carcinoma and oral potentially malignant disorders: a systematic review. *Oral Dis.* **17**, 58–72 (2011).

76. Isayeva, T., Li, Y., Maswahu, D. & Brandwein-Gensler, M. Human Papillomavirus in Non-Oropharyngeal Head and Neck Cancers: A Systematic Literature Review. *Head Neck Pathol.* **6**, 104–120 (2012).

77. Reuschenbach, M. *et al.* Lack of evidence of human papillomavirus-induced squamous cell carcinomas of the oral cavity in southern Germany. *Oral Oncol.* **49**, 937–942 (2013).

78. Lingen, M. W. *et al.* Low etiologic fraction for high-risk human papillomavirus in oral cavity squamous cell carcinomas. *Oral Oncol.* **49**, 1–8 (2013).

79. Dahlgren, L. *et al.* Human papillomavirus is more common in base of tongue than in mobile tongue cancer and is a favorable prognostic factor in base of tongue cancer patients. *Int. J. Cancer* **112**, 1015–1019 (2004).

80. Kumar, M., Nanavati, R., Modi, T. & Dobariya, C. Oral cancer: Etiology and risk factors: A review. *J. Cancer Res. Ther.* **12**, 458–458 (2016).

81. Fischer, M., Uxa, S., Stanko, C., Magin, T. M. & Engeland, K. Human papilloma virus E7 oncoprotein abrogates the p53-p21-DREAM pathway. *Sci. Rep.* **7**, 2603 (2017).

82. Herrero, R. *et al.* Human Papillomavirus and Oral Cancer: The International Agency for Research on Cancer Multicenter Study. *JNCI J. Natl. Cancer Inst.* **95**, 1772–1783 (2003).

83. Benner, S. E. *et al.* Regression of oral leukoplakia with alpha-tocopherol: a community clinical oncology program chemoprevention study. *J. Natl. Cancer Inst.* **85**, 44–47 (1993).

84. Schethenbach, K., Wagenmann, M., Freund, M., Schipper, J. & Hanenberg, H. Squamous Cell Carcinomas of the Head and Neck in Fanconi Anemia: Risk, Prevention, Therapy, and the Need for Guidelines. *Klin. Padiatr.* **224**, 132–138 (2012).

85. Kutler, D. I. *et al.* High Incidence of Head and Neck Squamous Cell Carcinoma in Patients With Fanconi Anemia. *Arch. Otolaryngol. Neck Surg.* **129**, 106–112 (2003).

86. Furquim, C. P., Pivovar, A., Amenábar, J. M., Bonfim, C. & Torres-Pereira, C. C. Oral cancer in Fanconi anemia: Review of 121 cases. *Crit. Rev. Oncol. Hematol.* **125**, 35–40 (2018).

87. Herceg, Z. & Hainaut, P. Genetic and epigenetic alterations as biomarkers for cancer detection, diagnosis and prognosis. *Mol. Oncol.* **1**, 26–41 (2007).

88. Califano, J. *et al.* Genetic Progression Model for Head and Neck Cancer: Implications for Field Cancerization. *Cancer Res.* **56**, 2488–2492 (1996).

89. Viet, C. T. & Schmidt, B. L. Understanding oral cancer in the genome era. *Head Neck* **32**, 1246–1268 (2010).

90. Sato, H. *et al.* Prognostic utility of chromosomal instability detected by fluorescence in situ hybridization in fine-needle aspirates from oral squamous cell carcinomas. *BMC Cancer* **10**, 1–8 (2010).

91. Reing, J. E., Gollin, S. M. & Saunders, W. S. The occurrence of chromosome segregational defects is an intrinsic and heritable property of oral squamous cell carcinoma cell lines. *Cancer Genet. Cytogenet.* **150**, 57–61 (2004).

92. Saunders, W. S. *et al.* Chromosomal instability and cytoskeletal defects in oral cancer cells. *Proc. Natl. Acad. Sci. U. S. A.* **97**, 303–308 (2000).

93. Yoshioka, S. *et al.* Genomic Profiling of Oral Squamous Cell Carcinoma by Array-Based Comparative Genomic Hybridization. *PLOS ONE* **8**, e56165 (2013).

94. Zw, Y. *et al.* Genetic alterations of chromosome 8 genes in oral cancer. *Sci. Rep.* **4**, 6073–6073 (2014).

95. Frequent allelic imbalances at 8p and 11q22 in oral and oropharyngeal epithelial dysplastic lesions. *Cancer Genet. Cytogenet.* **161**, 86–89 (2005).

96. Hayakawa, M. *et al.* Electrochemical telomerase assay for screening for oral cancer. *Br. J. Oral Maxillofac. Surg.* **54**, 301–305 (2016).

97. Hsieh, L.-L. *et al.* Characteristics of mutations in the p53 gene in oral squamous cell carcinoma associated with betel quid chewing and cigarette smoking in Taiwanese. *Carcinogenesis* **22**, 1497–1503 (2001).

98. Rawat, G., Urs, A. B., Chakravarti, A. & Kumar, P. DNA damage in buccal cells in oral PMDs and malignant disorders by comet assay: a comparison with blood leukocytes. *Braz. J. Oral Sci.* **18**, e191430–e191430 (2019).

99. Vettore, A. L. *et al.* Mutational landscapes of tongue carcinoma reveal recurrent mutations in genes of therapeutic and prognostic relevance. *Genome Med.* **7**, 98 (2015).

100. Agrawal, N. *et al.* Exome Sequencing of Head and Neck Squamous Cell Carcinoma Reveals Inactivating Mutations in NOTCH1. *Science* **333**, 1154–1157 (2011).

101. Poeta, M. L. *et al.* TP53 Mutations and Survival in Squamous-Cell Carcinoma of the Head and Neck. *N. Engl. J. Med.* **357**, 2552–2561 (2007).

102. Stransky, N. *et al.* The Mutational Landscape of Head and Neck Squamous Cell Carcinoma. *Science* **333**, 1157–1160 (2011).

103. Langdon, J. D. & Partridge, M. Expression of the tumour suppressor gene p53 in oral cancer. *Br. J. Oral Maxillofac. Surg.* **30**, 214–220 (1992).

104. Ogden, G. R., Kiddie, R. A., Lunny, D. P. & Lane, D. P. Assessment of p53 protein expression in normal, benign, and malignant oral mucosa. *J. Pathol.* **166**, 389–394 (1992).

105. Burns, J. E. *et al.* Gene mutations and increased levels of p53 protein in human squamous cell carcinomas and their cell lines. *Br. J. Cancer* **67**, 1274–1284 (1993).

106. Menzies, G. E., Reed, S. H., Brancale, A. & Lewis, P. D. Base damage, local sequence context and TP53 mutation hotspots: a molecular dynamics study of benzo[a]pyrene induced DNA distortion and mutability. *Nucleic Acids Res.* **43**, 9133–9146 (2015).

107. Caponio, V. C. A. *et al.* Computational analysis of TP53 mutational landscape unveils key prognostic signatures and distinct pathobiological pathways in head and neck squamous cell cancer. *Br. J. Cancer* **123**, 1302–1314 (2020).

108. Loeffler-Ragg, J. *et al.* Low incidence of mutations in EGFR kinase domain in Caucasian patients with head and neck squamous cell carcinoma. *Eur. J. Cancer* **42**, 109–111 (2006).

109. Temam, S. *et al.* Epidermal Growth Factor Receptor Copy Number Alterations Correlate With Poor Clinical Outcome in Patients With Head and Neck Squamous Cancer. *J. Clin. Oncol.* **25**, 2164–2170 (2007).

110. Knowles, L. M. *et al.* HGF and c-Met Participate in Paracrine Tumorigenic Pathways in Head and Neck Squamous Cell Cancer. *Clin. Cancer Res. Off. J. Am. Assoc. Cancer Res.* **15**, 3740–3750 (2009).

111. Seiwert, T. Y. *et al.* The MET Receptor Tyrosine Kinase Is a Potential Novel Therapeutic Target for Head and Neck Squamous Cell Carcinoma. *Cancer Res.* **69**, 3021–3031 (2009).

112. Molinolo, A. A. *et al.* mTOR as a Molecular Target in HPV-Associated Oral and Cervical Squamous Carcinomas. *Clin. Cancer Res.* **18**, 2558–2568 (2012).

113. Comprehensive genomic characterization of head and neck squamous cell carcinomas. *Nature* **517**, 576–582 (2015).

114. Rao, S. V. K., Mejia, G., Roberts-Thomson, K. & Logan, R. Epidemiology of Oral Cancer in Asia in the Past Decade- An Update (2000-2012). *Asian Pac. J. Cancer Prev.* **14**, 5567–5577 (2013).

115. Kessenbrock, K., Plaks, V. & Werb, Z. Matrix Metalloproteinases: Regulators of the Tumor Microenvironment. *Cell* **141**, 52–67 (2010).

116. Thangaraj, S. V. *et al.* Molecular Portrait of Oral Tongue Squamous Cell Carcinoma Shown by Integrative Meta-Analysis of Expression Profiles with Validations. *PLoS ONE* **11**, (2016).

117. PATEL, D. D., BHATAVDEKAR, J. M., VORA, H. H. & BALAR, D. B. Circulating prolactin and tumoral prolactin receptors in men with tongue cancer: a preliminary study. *Circ. Prolactin Tumoral Prolactin Recept. Men Tongue Cancer Prelim. Study* **20**, 155–159 (1994).

118. Bhatavdekar, J. M. *et al.* Prolactin: its role in advanced tongue cancer. *J. Surg. Oncol.* **57**, 115–120 (1994).

119. Bhatavdekar, J. M. *et al.* Prolactin as a local growth promoter in patients with locally advanced tongue cancer: GCRI experience. *Head Neck* **22**, 257–264 (2000).

120. Bhatavdekar, J. M., Patel, D. D., Vora, H. H. & Balar, D. B. Circulating Markers and Growth Factors as Prognosticators in Men with Advanced Tongue Cancer. *Tumor Biol.* **14**, 55–58 (1993).

121. Oral Leukoplakia Related to Malignant Transformation. *Oral Sci. Int.* **3**, 45–55 (2006).

122. Neville, B. W. & Day, T. A. Oral Cancer and Precancerous Lesions. *CA. Cancer J. Clin.* **52**, 195–215 (2002).

123. Evans, S. J. W., Langdon, J. D., Rapidis, A. D. & Johnson, N. W. Prognostic significance of STNMp and velocity of tumor growth in oral cancer. *Cancer* **49**, 773–776 (1982).

124. Gurney, T. A., Eisele, D. W., Orloff, L. A. & Wang, S. J. Predictors of quality of life after treatment for oral cavity and oropharyngeal carcinoma. *Otolaryngol. Head Neck Surg.* **139**, 262–267 (2008).

125. Mashberg, A. & Samit, A. M. Early detection, diagnosis, and management of oral and oropharyngeal cancer. *CA. Cancer J. Clin.* **39**, 67–88 (1989).

126. Sciubba, J. J. & Larian, B. Oral squamous cell carcinoma: early detection and improved 5-year survival in 102 patients. *Gen. Dent.* **66**, e11–e16 (2018).

127. Kantola, S., Jokinen, K., Hyrynkangas, K., Mäntyselkä, P. & Alho, O. P. Detection of tongue cancer in primary care. *Br. J. Gen. Pract.* **51**, 106–111 (2001).

128. MESSADI, D. V., WILDER-SMITH, P. & WOLINSKY, L. Improving Oral Cancer Survival: The Role of Dental Providers. *J. Calif. Dent. Assoc.* **37**, 789–798 (2009).

129. Bullock, M. J. Current Challenges in the Staging of Oral Cancer. *Head Neck Pathol.* **13**, 440–448 (2019).

130. LeHew, C. W., Epstein, J. B., Kaste, L. M. & Choi, Y.-K. Assessing oral cancer early detection: clarifying dentists' practices. *J. Public Health Dent.* **70**, 93–100 (2010).

131. Mashberg, A., Morrissey, J. B. & Garfinkel, L. A study of the appearance of early asymptomatic oral squamous cell carcinoma. *Cancer* **32**, 1436–1445 (1973).

132. Scully, C. & Bagan, J. Oral squamous cell carcinoma overview. *Oral Oncol.* **45**, 301–308 (2009).

133. Lim, M. S. RE: Correlational of oral tongue cancer inversion with matrix metalloproteinases (MMPs) and vascular endothelial growth factor (VEGF) expression, by Kim S-H, Cho NH, Kim K, et al. *J. Surg. Oncol.* **93**, 253–254 (2006).

134. Sano, D. & Myers, J. N. Metastasis of squamous cell carcinoma of the oral tongue. *Cancer Metastasis Rev.* **26**, 645–662 (2007).

135. Rusthoven, K., Ballonoff, A., Raben, D. & Chen, C. Poor prognosis in patients with stage I and II oral tongue squamous cell carcinoma. *Cancer* **112**, 345–351 (2008).

136. Rusthoven, K. E. *et al.* Survival and Patterns of Relapse in Patients With Oral Tongue Cancer. *J. Oral Maxillofac. Surg.* **68**, 584–589 (2010).

137. Huang, S. H. & O'Sullivan, B. Overview of the 8th Edition TNM Classification for Head and Neck Cancer. *Curr. Treat. Options Oncol.* **18**, 1–13 (2017).

138. A, P. W. Y. *et al.* Prognostic factors of clinically stage I and II oral tongue carcinoma-A comparative study of stage, thickness, shape, growth pattern, invasive front malignancy grading, Martinez-Gimeno score, and pathologic features. *Head Neck* **24**, 513–520 (2002).

139. Yanamoto, S. *et al.* Predictors of Locoregional Recurrence in T1-2N0 Tongue Cancer Patients. *Pathol. Oncol. Res.* **19**, 795–803 (2013).

140. Almangush, A. *et al.* Prognostic biomarkers for oral tongue squamous cell carcinoma: a systematic review and meta-analysis. *Br. J. Cancer* **117**, 856–866 (2017).

141. Bello, I. O., Soini, Y. & Salo, T. Prognostic evaluation of oral tongue cancer: Means, markers and perspectives (I). *Oral Oncol.* **46**, 630–635 (2010).

142. Goto, M. *et al.* Prognostic significance of late cervical metastasis and distant failure in patients with stage I and II oral tongue cancers. *Oral Oncol.* **41**, 62–69 (2005).

143. Carla, C. *et al.* Angiogenesis in Head and Neck Cancer: A Review of the Literature. *J. Oncol.* **2012**, (2012).

144. Noguti, J. *et al.* Metastasis from Oral Cancer: An Overview. *Cancer Genomics - Proteomics* **9**, 329–335 (2012).

145. Almahmoudi, R. *et al.* Prognostic value of blood and lymphatic vessel markers in tongue cancer: A systematic review. *Cancer Sci.* **110**, 3424–3433 (2019).

146. Woolgar, J. A. Histopathological prognosticators in oral and oropharyngeal squamous cell carcinoma. *Oral Oncol.* **42**, 229–239 (2006).

147. Garavello, W., Spreafico, R. & Gaini, R. M. Oral tongue cancer in young patients: A matched analysis. *Oral Oncol.* **43**, 894–897 (2007).

148. Liao, C.-T. *et al.* Higher distant failure in young age tongue cancer patients. *Oral Oncol.* **42**, 718–725 (2006).

149. Atula, S., Grénman, R., Laippala, P. & Syrjänen, S. Cancer of the Tongue in Patients Younger Than 40 Years: A Distinct Entity? *Arch. Otolaryngol. Neck Surg.* **122**, 1313–1319 (1996).

150. Korpi, J. T. *et al.* Collagenase-2 (matrix metalloproteinase-8) plays a protective role in tongue cancer. *Br. J. Cancer* **98**, 766–775 (2008).

151. Veness, M. J., Morgan, G. J., Sathiyaseelan, Y. & Gebski, V. Anterior Tongue Cancer: Age Is Not a Predictor of Outcome and Should Not Alter Treatment. *ANZ J. Surg.* **73**, 899–904 (2003).

152. Siegelmann-Danieli, N. *et al.* Oral tongue cancer in patients less than 45 years old: institutional experience and comparison with older patients. *J. Clin. Oncol.* **16**, 745–753 (1998).

153. Macfarlane, G. J., Sharp, L., Porter, S. & Franceschi, S. Trends in survival from cancers of the oral cavity and pharynx in Scotland: a clue as to why the disease is becoming more common? *Br. J. Cancer* **73**, 805–808 (1996).

154. Berrino, F. & Gatta, G. Variation in survival of patients with head and neck cancer in Europe by the site of origin of the tumours. *Eur. J. Cancer* **34**, 2154–2161 (1998).

155. Zheng, Y., Kirita, T., Kurumatani, N., Sugimura, M. & Yonemasu, K. Trends in oral cancer mortality in Japan: 1950–1993. *Oral Dis.* **5**, 3–9 (1999).

156. Iype, E. M. *et al.* Squamous Cell Carcinoma of the Tongue Among Young Indian Adults. *Neoplasia N. Y. N* **3**, 273–277 (2001).

157. Shiboski, C. H., Schmidt, B. L. & Jordan, R. C. K. Racial disparity in stage at diagnosis and survival among adults with oral cancer in the US. *Community Dent. Oral Epidemiol.* **35**, 233–240 (2007).

158. Survival Rates for Oral Cavity and Oropharyngeal Cancer. https://www.cancer.org/cancer/oral-cavity-and-oropharyngeal-cancer/detection-diagnosis-staging/survival-rates.html.

159. Ildstad, S. T., Bigelow, M. E. & Remensnyder, J. P. Squamous cell carcinoma of the tongue: a comparison of the anterior two thirds of the tongue with its base. *Am. J. Surg.* **146**, 456–461 (1983).

160. Scully, C. & Bedi, R. Ethnicity and oral cancer. *Lancet Oncol.* **1**, 37–42 (2000).

161. Schuller, D. E., McGuirt, W. F., McCabe, B. F. & Young, D. The prognostic significance of metastatic cervical lymph nodes. *The Laryngoscope* **90**, 557–570 (1980).

162. Finlay, P. M., Dawson, F., Robertson, A. G. & Soutar, D. S. An evaluation of functional outcome after surgery and radiotherapy for intraoral cancer. *Br. J. Oral Maxillofac. Surg.* **30**, 14–17 (1992).

163. Shah, J. P. & Andersen, P. E. Evolving role of modifications in neck dissection for oral squamous carcinoma. *Br. J. Oral Maxillofac. Surg.* **33**, 3–8 (1995).

164. Teichgraeber, J. F. & Clairmont, A. A. The incidence of occult metastases for cancer of the oral tongue and floor of the mouth: Treatment rationale. *Head Neck Surg.* **7**, 15–21 (1984).

165. Matsuura, K., Hirokawa, Y., Fujita, M., Akagi, Y. & Ito, K. Treatment results of stage I and II oral tongue cancer with interstitial brachytherapy: Maximum tumor thickness is prognostic of nodal metastasis. *Int. J. Radiat. Oncol.* **40**, 535–539 (1998).

166. Gourin, C. G. & Johnson, J. T. Surgical treatment of squamous cell carcinoma of the base of tongue. *Head Neck* **23**, 653–660 (2001).

167. Lin, D. T. *et al.* Long-Term functional outcomes of total glossectomy with or without total laryngectomy. *JAMA Otolaryngol. - Head Neck Surg.* **141**, 797–803 (2015).

168. Oncologic and functional considerations of total glossectomy. *Am. J. Surg.* **158**, 297–302 (1989).

169. Harrison, D. The questionable value of total glossectomy. *Head Neck Surg.* **6**, 632–638 (1983).

170. Tiwari, R. M., Greven, A. J., Karim, A. B. M. F. & Snow, G. B. Total glossectomy: reconstruction and rehabilitation. *J. Laryngol. Otol.* **103**, 917–921 (1989).

171. Weber, R. S. *et al.* Treatment selection for carcinoma of the base of the tongue. *Am. J. Surg.* **160**, 415–419 (1990).

172. Zelefsky, M. J., Harrison, L. B. & Armstrong, J. G. Long-term treatment results of postoperative radiation therapy for advanced stage oropharyngeal carcinoma. *Cancer* **70**, 2388–2395 (1992).

173. Robertson, A. G. *et al.* Post-operative radiotherapy in the management of advanced intra-oral cancers. *Clin. Radiol.* **37**, 173–178 (1986).

174. Treatment of oral cancer by interstitial irradiation using iridium—192. *Br. J. Oral Maxillofac. Surg.* **30**, 355–359 (1992).

175. Treatment of oral cancers using iridium-192 interstitial irradiation. *Br. J. Oral Maxillofac. Surg.* **32**, 207–213 (1994).

176. Harrison, L. B. *et al.* Base-of-tongue cancer treated with external beam irradiation plus brachytherapy: oncologic and functional outcome. *Radiology* **184**, 267–270 (1992).

177. Shibuya, H. *et al.* Brachytherapy for stage I & II oral tongue cancer: An analysis of past cases focusing on control and complications. *Int. J. Radiat. Oncol.* **26**, 51–58 (1993).

178. Licitra, L. *et al.* Primary Chemotherapy in Resectable Oral Cavity Squamous Cell Cancer: A Randomized Controlled Trial. *J. Clin. Oncol.* **21**, 327–333 (2003).

179. Bonner, J. A. *et al.* Radiotherapy plus Cetuximab for Squamous-Cell Carcinoma of the Head and Neck. *N. Engl. J. Med.* **354**, 567–578 (2006).

180. Naruse, T. *et al.* Cetuximab for the treatment of locally advanced and recurrent/metastatic oral cancer: An investigation of distant metastasis. *Mol. Clin. Oncol.* **5**, 246–252 (2016).

181. Vermorken, J. B. *et al.* Platinum-Based Chemotherapy plus Cetuximab in Head and Neck Cancer. *N. Engl. J. Med.* **359**, 1116–1127 (2008).

182. Hancock, S. B. *et al.* Treatment of Base of Tongue Cancer With Paclitaxel, Ifosfamide, and Cisplatinum Induction Chemotherapy Followed by Chemoradiotherapy. *The Laryngoscope* **118**, 1357–1361 (2008).

183. Schoenfeld, J. D. *et al.* Neoadjuvant Nivolumab or Nivolumab Plus Ipilimumab in Untreated Oral Cavity Squamous Cell Carcinoma: A Phase 2 Open-Label Randomized Clinical Trial. *JAMA Oncol.* **6**, 1563–1570 (2020).

184. An overall review of targeted therapy in solid cancers. *Curr. Med. Res. Pract.* **7**, 99–105 (2017).

185. Sharkey, R. M. & Goldenberg, D. M. Targeted Therapy of Cancer: New Prospects for Antibodies and Immunoconjugates. *CA. Cancer J. Clin.* **56**, 226–243 (2006).

186. Levitzki, A. Tyrosine Kinase Inhibitors: Views of Selectivity, Sensitivity, and Clinical Performance. *Annu. Rev. Pharmacol. Toxicol.* **53**, 161–185 (2013).

187. Ruegg, C. & Mutter, N. Anti-angiogenic therapies in cancer : achievements and open questions. *Bull. Cancer (Paris)* **94**, 753–762 (2007).

188. Dou, Q. P. & Zonder, J. A. Overview of Proteasome Inhibitor-Based Anti-cancer Therapies: Perspective on Bortezomib and Second Generation Proteasome Inhibitors versus Future Generation Inhibitors of Ubiquitin-Proteasome System. *Curr. Cancer Drug Targets* **14**, 517–536 (2014).

189. Blattman, J. N. & Greenberg, P. D. Cancer Immunotherapy: A Treatment for the Masses. *Science* **305**, 200–205 (2004).

190. El Sayed, R. *et al.* Endocrine and Targeted Therapy for Hormone-Receptor-Positive, HER2-Negative Advanced Breast Cancer: Insights to Sequencing Treatment and Overcoming Resistance Based on Clinical Trials. *Front. Oncol.* **9**, (2019).

191. Noguchi, T. *et al.* miRNA-503 Promotes Tumor Progression and Is Associated with Early Recurrence and Poor Prognosis in Human Colorectal Cancer. *Oncology* **90**, 221–231 (2016).

192. Signal transduction therapy of cancer. *Mol. Aspects Med.* **31**, 287–329 (2010).

193. Yan, L., Rosen, N. & Arteaga, C. Targeted cancer therapies. *Chin. J. Cancer* **30**, 1–4 (2011).

194. Blume-Jensen, P. & Hunter, T. Oncogenic kinase signalling. *Nature* **411**, 355–365 (2001).

195. Lemmon, M. A. & Schlessinger, J. Cell signaling by receptor-tyrosine kinases. *Cell* **141**, 1117–1134 (2010).

196. Kim, H.-J., Lin, D., Lee, H.-J., Li, M. & Liebler, D. C. Quantitative Profiling of Protein Tyrosine Kinases in Human Cancer Cell Lines by Multiplexed Parallel Reaction Monitoring Assays. *Mol. Cell. Proteomics MCP* **15**, 682–691 (2016).

197. Lengyel, E., Sawada, K. & Salgia, R. Tyrosine kinase mutations in human cancer. *Curr. Mol. Med.* **7**, 77–84 (2007).

198. Broekman, F., Giovannetti, E. & Peters, G. J. Tyrosine kinase inhibitors: Multi-targeted or single-targeted? *World J. Clin. Oncol.* **2**, 80–93 (2011).

199. Kozakiewicz, P. & Grzybowska‑Szatkowska, L. Application of molecular targeted therapies in the treatment of head and neck squamous cell carcinoma (Review). *Oncol. Lett.* **15**, 7497–7505 (2018).

200. Wu, Z. *et al.* Quantitative Chemical Proteomics Reveals New Potential Drug Targets in Head and Neck Cancer. *Mol. Cell. Proteomics MCP* **10**, (2011).

201. Emaduddin, M., Bicknell, D. C., Bodmer, W. F. & Feller, S. M. Cell growth, global phosphotyrosine elevation, and c-Met phosphorylation through Src family kinases in colorectal cancer cells. *Proc. Natl. Acad. Sci. U. S. A.* **105**, 2358–2362 (2008).

202. Cabodi, S., Camacho-Leal, M. del P., Stefano, P. D. & Defilippi, P. Integrin signalling adaptors: not only figurants in the cancer story. *Nat. Rev. Cancer* **10**, 858–870 (2010).

203. Defilippi, P., Di Stefano, P. & Cabodi, S. p130Cas: a versatile scaffold in signaling networks. *Trends Cell Biol.* **16**, 257–263 (2006).

204. Maria del Pilar, C. L. *et al.* p130Cas/BCAR1 scaffold protein in tissue homeostasis and pathogenesis. *Gene* **562**, 1–7 (2015).

205. Sakai, R. *et al.* A novel signaling molecule, p130, forms stable complexes in vivo with v-Crk and v-Src in a tyrosine phosphorylation-dependent manner. *EMBO J.* **13**, 3748–3756 (1994).

206. Giancotti, F. G. & Tarone, G. Positional Control of Cell Fate Through Joint Integrin/Receptor Protein Kinase Signaling. *Annu. Rev. Cell Dev. Biol.* **19**, 173–206 (2003).

207. Kook, S. *et al.* Caspase-mediated Cleavage of p130cas in Etoposide-induced Apoptotic Rat-1 Cells. *Mol. Biol. Cell* **11**, 929–939 (2000).

208. Kim, W., Kook, S., Kim, D. J., Teodorof, C. & Song, W. K. The 31-kDa caspase-generated cleavage product of p130cas functions as a transcriptional repressor of E2A in apoptotic cells. *J. Biol. Chem.* **279**, 8333–8342 (2004).

209. Honda, H. *et al.* Cardiovascular anomaly, impaired actin bundling and resistance to Src-induced transformation in mice lacking p130Cas. *Nat. Genet.* **19**, 361–365 (1998).

210. Ambrogio, C. *et al.* p130Cas mediates the transforming properties of the anaplastic lymphoma kinase. *Blood* **106**, 3907–3916 (2005).

211. Cabodi, S. *et al.* p130Cas is an essential transducer element in ErbB2 transformation. *FASEB J. Off. Publ. Fed. Am. Soc. Exp. Biol.* **24**, 3796–3808 (2010).

212. Pylayeva, Y. *et al.* Ras- and PI3K-dependent breast tumorigenesis in mice and humans requires focal adhesion kinase signaling. *J. Clin. Invest.* **119**, 252–266 (2009).

213. Brábek, J. *et al.* Crk-associated substrate tyrosine phosphorylation sites are critical for invasion and metastasis of SRC-transformed cells. *Mol. Cancer Res. MCR* **3**, 307–315 (2005).

214. Tornillo, G., Defilippi, P. & Cabodi, S. Cas proteins: dodgy scaffolding in breast cancer. *Breast Cancer Res. BCR* **16**, 443 (2014).

215. Cabodi, S. *et al.* p130Cas as a new regulator of mammary epithelial cell proliferation, survival, and HER2-neu oncogene-dependent breast tumorigenesis. *Cancer Res.* **66**, 4672–4680 (2006).

216. Tornillo, G. *et al.* p130Cas promotes invasiveness of three-dimensional ErbB2-transformed mammary acinar structures by enhanced activation of mTOR/p70S6K and Rac1. *Eur. J. Cell Biol.* **90**, 237–248 (2011).

217. Dorssers, L. C. J. *et al.* The Prognostic Value of BCAR1 in Patients with Primary Breast Cancer. *Clin. Cancer Res.* **10**, 6194–6202 (2004).

218. van der Flier, S. *et al.* Immunohistochemical Study of the BCAR1/p130Cas Protein in Non-Malignant and Malignant Human Breast Tissue. *Int. J. Biol. Markers* **16**, 172–178 (2001).

219. Flier, S. van der *et al.* BCAR1/p130Cas expression in untreated and acquired tamoxifen-resistant human breast carcinomas. *Int. J. Cancer* **89**, 465–468 (2000).

220. Ta, H. Q., Thomas, K. S., Schrecengost, R. S. & Bouton, A. H. A novel association between p130Cas and resistance to the chemotherapeutic drug adriamycin in human breast cancer cells. *Cancer Res.* **68**, 8796–8804 (2008).

221. Tikhmyanova, N. & Golemis, E. A. NEDD9 and BCAR1 Negatively Regulate E-Cadherin Membrane Localization, and Promote E-Cadherin Degradation. *PLoS ONE* **6**, (2011).

222. Wisniewska, M. *et al.* The 1.1Å Resolution Crystal Structure of the p130cas SH3 Domain and Ramifications for Ligand Selectivity. *J. Mol. Biol.* **347**, 1005–1014 (2005).

223. Costamagna, A. *et al.* Modeling ErbB2-p130Cas interaction to design new potential anticancer agents. *Sci. Rep.* **9**, 1–16 (2019).

224. Martin, G. S. The hunting of the Src. *Nat. Rev. Mol. Cell Biol.* **2**, 467–475 (2001).

225. Renzo, M. F. D., Ferracini, R., Naldini, L., Giordano, S. & Comoglio, P. M. Immunological detection of proteins phosphorylated at tyrosine in cells stimulated by growth factors or transformed by retroviral-oncogene-coded tyrosine kinases. *Eur. J. Biochem.* **158**, 383–391 (1986).

226. Vultur, A. *et al.* SKI-606 (bosutinib), a novel Src kinase inhibitor, suppresses migration and invasion of human breast cancer cells. *Mol. Cancer Ther.* **7**, 1185–1194 (2008).

227. Thomas, S. M. & Brugge, J. S. Cellular functions regulated by src family kinases. *Annu. Rev. Cell Dev. Biol.* **13**, 513–609 (1997).

228. Summy, J. M. & Gallick, G. E. Treatment for advanced tumors: SRC reclaims center stage. *Clin. Cancer Res. Off. J. Am. Assoc. Cancer Res.* **12**, 1398–1401 (2006).

229. Parsons, S. J. & Parsons, J. T. Src family kinases, key regulators of signal transduction. *Oncogene* **23**, 7906–7909 (2004).

230. Diaz, N. *et al.* Activation of stat3 in primary tumors from high-risk breast cancer patients is associated with elevated levels of activated SRC and survivin expression. *Clin. Cancer Res. Off. J. Am. Assoc. Cancer Res.* **12**, 20–28 (2006).

231. c-Src and cooperating partners in human cancer. *Cancer Cell* **6**, 209–214 (2004).

232. Mayer, E. L. & Krop, I. E. Advances in Targeting Src in the Treatment of Breast Cancer and Other Solid Malignancies. *Clin. Cancer Res.* **16**, 3526–3532 (2010).

233. Roskoski, R. Src protein-tyrosine kinase structure, mechanism, and small molecule inhibitors. *Pharmacol. Res.* **94**, 9–25 (2015).

234. Daigo, Y. *et al.* Absence of Genetic Alteration at Codon 531 of the Human c-src Gene in 479 Advanced Colorectal Cancers from Japanese and Caucasian Patients. *Cancer Res.* **59**, 4222–4224 (1999).

235. Irby, R. B. *et al.* Activating SRC mutation in a subset of advanced human colon cancers. *Nat. Genet.* **21**, 187–190 (1999).

236. Irby, R. B. & Yeatman, T. J. Role of Src expression and activation in human cancer. *Oncogene* **19**, 5636–5642 (2000).

237. Summy, J. M. & Gallick, G. E. Src family kinases in tumor progression and metastasis. *Cancer Metastasis Rev.* **22**, 337–358 (2003).

238. Talamonti, M. S., Roh, M. S., Curley, S. A. & Gallick, G. E. Increase in activity and level of pp60c-src in progressive stages of human colorectal cancer. *J. Clin. Invest.* **91**, 53–60 (1993).

239. Site-Specific Differences in pp60c-src Activity in Human Colorectal Metastases. *J. Surg. Res.* **54**, 293–298 (1993).

240. Aligayer, H. *et al.* Activation of Src kinase in primary colorectal carcinoma: an indicator of poor clinical prognosis. *Cancer* **94**, 344–351 (2002).

241. Chen, J. Y.-F. *et al.* Src Family Kinases Mediate Betel Quid-Induced Oral Cancer Cell Motility and Could Be a Biomarker for Early Invasion in Oral Squamous Cell Carcinoma. *Neoplasia N. Y. N* **10**, 1393–1401 (2008).

242. Wilson, L. J. *et al.* New Perspectives, Opportunities, and Challenges in Exploring the Human Protein Kinome. *Cancer Res.* **78**, 15–29 (2018).

243. Talpaz, M. *et al.* Dasatinib in imatinib-resistant Philadelphia chromosome-positive leukemias. *N. Engl. J. Med.* **354**, 2531–2541 (2006).

244. Müller, M. C. *et al.* Dasatinib treatment of chronic-phase chronic myeloid leukemia: analysis of responses according to preexisting BCR-ABL mutations. *Blood* **114**, 4944–4953 (2009).

245. Ottmann, O. *et al.* Dasatinib induces rapid hematologic and cytogenetic responses in adult patients with Philadelphia chromosome positive acute lymphoblastic leukemia with resistance or intolerance to imatinib: interim results of a phase 2 study. *Blood* **110**, 2309–2315 (2007).

246. Nam, S. *et al.* Action of the Src family kinase inhibitor, dasatinib (BMS-354825), on human prostate cancer cells. *Cancer Res.* **65**, 9185–9189 (2005).

247. Johnson, F. M., Saigal, B., Talpaz, M. & Donato, N. J. Dasatinib (BMS-354825) tyrosine kinase inhibitor suppresses invasion and induces cell cycle arrest and apoptosis of head and neck squamous cell carcinoma and non-small cell lung cancer cells. *Clin. Cancer Res. Off. J. Am. Assoc. Cancer Res.* **11**, 6924–6932 (2005).

248. Nautiyal, J., Patel, B. & Majumdar, A. Src inhibitor Dasatinib inhibits growth of breast cancer cells by modulating EGFR signaling. *Cancer Res.* **68**, 4860–4860 (2008).

249. Huang, F. *et al.* Identification of candidate molecular markers predicting sensitivity in solid tumors to dasatinib: rationale for patient selection. *Cancer Res.* **67**, 2226–2238 (2007).

250. Song, L. *et al.* Dasatinib (BMS-354825) Selectively Induces Apoptosis in Lung Cancer Cells Dependent on Epidermal Growth Factor Receptor Signaling for Survival. *Cancer Res.* **66**, 5542–5548 (2006).

251. Evans, T. R. J. *et al.* Phase 2 placebo-controlled, double-blind trial of dasatinib added to gemcitabine for patients with locally-advanced pancreatic cancer. *Ann. Oncol.* **28**, 354–361 (2017).

252. Argiris, A. *et al.* Phase I and pharmacokinetic study of dasatinib and cetuximab in patients with advanced solid malignancies. *Invest. New Drugs* **30**, 1575–1584 (2012).

253. Yilmaz, M., Kantarjian, H., Ravandi-Kashani, F., Short, N. J. & Jabbour, E. Philadelphia chromosome-positive acute lymphoblastic leukemia in adults: current treatments and future perspectives. *Clin. Adv. Hematol. Oncol. HO* **16**, 216–223 (2018).

254. Kelley, M. J. *et al.* Phase II Study of Dasatinib in Previously Treated Patients with Advanced Non-Small Cell Lung Cancer. *Cancer Invest.* **35**, 32–35 (2017).

255. Yu, E. Y. *et al.* Phase II Study of Dasatinib in Patients with Metastatic Castration-Resistant Prostate Cancer. *Clin. Cancer Res.* **15**, 7421–7428 (2009).

256. Herold, C. I. *et al.* Phase II Trial of Dasatinib in Patients with Metastatic Breast Cancer Using Real-Time Pharmacodynamic Tissue Biomarkers of Src Inhibition to Escalate Dosing. *Clin. Cancer Res.* **17**, 6061–6070 (2011).

257. Finn, R. S. *et al.* Phase II trial of dasatinib in triple-negative breast cancer: results of study CA180059. *Cancer Res.* **69**, 3118 (2009).

258. Kluger, H. M. *et al.* A phase II trial of dasatinib in advanced melanoma. *Cancer* **117**, 2202–2208 (2011).

259. Brooks, H. D. *et al.* Phase 2 study of dasatinib in the treatment of head and neck squamous cell carcinoma. *Cancer* **117**, 2112–2119 (2011).

260. Stasi, I. & Cappuzzo, F. Second generation tyrosine kinase inhibitors for the treatment of metastatic non-small-cell lung cancer. *Transl. Respir. Med.* **2**, (2014).

261. Hirsh, V., Melosky, B., Goss, G., Morris, D. & Morzycki, W. A personalized approach to treatment: use of egfr tyrosine kinase inhibitors for the treatment of non-small-cell lung cancer in Canada. *Curr. Oncol.* **19**, 78–90 (2012).

262. Mechanisms of acquired resistance to tyrosine kinase inhibitors. *Acta Pharm. Sin. B* **1**, 197–207 (2011).

263. Lavi, O. Redundancy: A Critical Obstacle to Improving Cancer Therapy. *Cancer Res.* **75**, 808–812 (2015).

264. Morris, L. G. T. *et al.* Pan-cancer analysis of intratumor heterogeneity as a prognostic determinant of survival. *Oncotarget* **7**, 10051–10063 (2016).

265. Paez, J. G. *et al.* EGFR mutations in lung cancer: correlation with clinical response to gefitinib therapy. *Science* **304**, 1497–1500 (2004).

266. Ho, V. W. T., Tan, H. Y., Wang, N. & Feng, Y. Cancer Management by Tyrosine Kinase Inhibitors: Efficacy, Limitation, and Future Strategies. *Tyrosine Kinases Druggable Targets Cancer* (2019) doi:10.5772/intechopen.82513.

267. Batson, S. *et al.* Tyrosine kinase inhibitor combination therapy in first-line treatment of non-small-cell lung cancer: systematic review and network meta-analysis. *OncoTargets Ther.* **10**, 2473–2482 (2017).

268. Mokhtari, R. B. *et al.* Combination therapy in combating cancer. *Oncotarget* **8**, 38022–38043 (2017).

269. Strauss, L. C. *et al.* Three parallel randomized phase II trials of dasatinib plus hormone therapy (HT) in advanced ER+ breast cancer (ER+ ABC). *J. Clin. Oncol.* **28**, TPS133–TPS133 (2010).

270. Somlo, G. *et al.* Dasatinib plus capecitabine for advanced breast cancer: safety and efficacy in phase I study CA180004. *Clin. Cancer Res. Off. J. Am. Assoc. Cancer Res.* **19**, 1884–1893 (2013).

271. Araujo, J. *et al.* Dasatinib and docetaxel combination treatment for patients with castration-resistant progressive prostate cancer: A phase I/II study (CA180086). *J. Clin. Oncol.* **27**, 5061–5061 (2009).

272. Araujo, J. C. *et al.* Overall survival (OS) and safety of dasatinib/docetaxel versus docetaxel in patients with metastatic castration-resistant prostate cancer (mCRPC): Results from the randomized phase III READY trial. *J. Clin. Oncol.* **31**, LBA8–LBA8 (2013).

273. Haura, E. B. *et al.* Phase I/II study of the Src inhibitor dasatinib in combination with erlotinib in advanced non-small-cell lung cancer. *J. Clin. Oncol. Off. J. Am. Soc. Clin. Oncol.* **28**, 1387–1394 (2010).

274. Gold, K. A. *et al.* A phase I/II study combining erlotinib and dasatinib for non-small cell lung cancer. *The Oncologist* **19**, 1040–1041 (2014).

275. Bauman, J. E. *et al.* Randomized, placebo-controlled window trial of EGFR, Src, or combined blockade in head and neck cancer. *JCI Insight* **2**, (2017).

276. Stabile, L. P. *et al.* Abstract CT119: Phase II study of dasatinib in combination with cetuximab in recurrent/metastatic head and neck squamous cell carcinoma. *Cancer Res.* **76**, CT119–CT119 (2016).

277. Stabile, L. P. *et al.* IL6 is associated with response to dasatinib and cetuximab: Phase II clinical trial with mechanistic correlatives in cetuximab-resistant head and neck cancer. *Oral Oncol.* **69**, 38–45 (2017).

278. Broniscer, A. *et al.* Phase 1 trial, pharmacokinetics, and pharmacodynamics of dasatinib combined with crizotinib in children with recurrent or progressive high-grade and diffuse intrinsic pontine glioma. *Pediatr. Blood Cancer* **65**, e27035 (2018).

279. Kato, S. *et al.* Phase I study of the combination of crizotinib (as a MET inhibitor) and dasatinib (as a c-SRC inhibitor) in patients with advanced cancer. *Invest. New Drugs* **36**, 416–423 (2018).

280. Zhu, Y. *et al.* The combination therapy of imatinib and dasatinib achieves long-term molecular response in two imatinib-resistant and dasatinibintolerant patients with advanced chronic myeloid leukemia. *J. Biomed. Res.* **30**, 525–528 (2016).

281. Fan, G., Shumay, E., Malbon, C. C. & Wang, H. c-Src tyrosine kinase binds the beta 2-adrenergic receptor via phospho-Tyr-350, phosphorylates G-protein-linked receptor kinase 2, and mediates agonist-induced receptor desensitization. *J. Biol. Chem.* **276**, 13240–13247 (2001).

282. Shin, E., Ko, K. S., Rhee, B. D., Han, J. & Kim, N. Different effects of prolonged β-adrenergic stimulation on heart and cerebral artery. *Integr. Med. Res.* **3**, 204–210 (2014).

283. Yoshida, H. *et al.* A variant form of laminin is responsible for the neurite outgrowth-promoting activity in conditioned medium from a squamous carcinoma cell line. *Connect. Tissue Res.* **30**, 23–35 (1993).

284. Gioanni, J. *et al.* Two new human tumor cell lines derived from squamous cell carcinomas of the tongue: Establishment, characterization and response to cytotoxic treatment. *Eur. J. Cancer Clin. Oncol.* **24**, 1445–1455 (1988).

285. Edington, K. G., Loughran, O. P., Berry, I. J. & Parkinson, E. K. Cellular immortality: A late event in the progression of human squamous cell carcinoma of the head and neck associated with p53 alteration and a high frequency of allele loss. *Mol. Carcinog.* **13**, 254–265 (1995).

286. Aslantürk, Ö. S. In Vitro Cytotoxicity and Cell Viability Assays: Principles, Advantages, and Disadvantages. *Genotoxicity - Predict. Risk Our Actual World* (2017) doi:10.5772/intechopen.71923.

287. Laemmli, U. K. Cleavage of Structural Proteins during the Assembly of the Head of Bacteriophage T4. *Nature* **227**, 680–685 (1970).

288. Cell cycle-dependent activation of Ras. *Curr. Biol.* **6**, 1621–1627 (1996).

289. Darzynkiewicz, Z., Halicka, H. D. & Zhao, H. Analysis of Cellular DNA Content by Flow and Laser Scanning Cytometry. *Adv. Exp. Med. Biol.* **676**, 137–147 (2010).

290. Darzynkiewicz, Z., Huang, X. & Zhao, H. Analysis of Cellular DNA Content by Flow Cytometry. *Curr. Protoc. Cytom.* **82**, 7.5.1-7.5.20 (2017).

291. admin. Cell Death and Apoptosis. *School of Life Sciences* //www.lifesci.dundee.ac.uk/technologies/flow-cytometry-cell-sorting/techniques/cell-death-and-apoptosis (2015).

292. SenthilKumar, G., Skiba, J. H. & Kimple, R. J. High-throughput quantitative detection of basal autophagy and autophagic flux using image cytometry. *BioTechniques* **67**, 70–73 (2019).

293. McIlwain, D. R., Berger, T. & Mak, T. W. Caspase functions in cell death and disease. *Cold Spring Harb. Perspect. Biol.* **5**, a008656 (2013).

294. Hock, B. *et al.* Tyrosine-614, the major autophosphorylation site of the receptor tyrosine kinase HEK2, functions as multi-docking site for SH2-domain mediated interactions. *Oncogene* **17**, 255–260 (1998).

295. Emaduddin, M., Edelmann, M. J., Kessler, B. M. & Feller, S. M. Odin (ANKS1A) is a Src family kinase target in colorectal cancer cells. *Cell Commun. Signal.* **6**, 7 (2008).

296. Druker, B. J., Mamon, H. J. & Roberts, T. M. Oncogenes, Growth Factors, and Signal Transduction. *N. Engl. J. Med.* **321**, 1383–1391 (1989).

297. Lipsich, L. A., Lewis, A. J. & Brugge, J. S. Isolation of monoclonal antibodies that recognize the transforming proteins of avian sarcoma viruses. *J. Virol.* **48**, 352–360 (1983).

298. Riss, T. L. *et al.* Cell Viability Assays. in *Assay Guidance Manual* (eds. Sittampalam, G. S. et al.) (Eli Lilly & Company and the National Center for Advancing Translational Sciences, 2004).

299. Shum, D. *et al.* A high density assay format for the detection of novel cytotoxic agents in large chemical libraries. *J. Enzyme Inhib. Med. Chem.* **23**, 931–945 (2008).

300. Scott, A. J. *et al.* Evaluation of the efficacy of dasatinib, a Src/Abl inhibitor, in colorectal cancer cell lines and explant mouse model. *PLOS ONE* **12**, e0187173 (2017).

301. Araujo, J. & Logothetis, C. Dasatinib: a potent SRC inhibitor in clinical development for the treatment of solid tumors. *Cancer Treat. Rev.* **36**, 492–500 (2010).

302. Serkova, N. J. & Eckhardt, S. G. Metabolic Imaging to Assess Treatment Response to Cytotoxic and Cytostatic Agents. *Front. Oncol.* **6**, 152 (2016).

303. Rixe, O. & Fojo, T. Is Cell Death a Critical End Point for Anticancer Therapies or Is Cytostasis Sufficient? *Clin. Cancer Res.* **13**, 7280–7287 (2007).

304. Demetri, G. D. *et al.* Phase I Dose-Escalation and Pharmacokinetic Study of Dasatinib in Patients with Advanced Solid Tumors. *Clin. Cancer Res.* **15**, 6232–6240 (2009).

305. Caccia, D. *et al.* Dasatinib reduces FAK phosphorylation increasing the effects of RPI-1 inhibition in a RET/PTC1-expressing cell line. *Mol. Cancer* **9**, 278 (2010).

306. Buettner, R., Mesa, T., Vultur, A., Lee, F. & Jove, R. Inhibition of Src family kinases with dasatinib blocks migration and invasion of human melanoma cells. *Mol. Cancer Res. MCR* **6**, 1766–1774 (2008).

307. Dasgupta, S. K., Le, A., Vijayan, K. V. & Thiagarajan, P. Dasatinib inhibits actin fiber reorganization and promotes endothelial cell permeability through RhoA-ROCK pathway. *Cancer Med.* **6**, 809–818 (2017).

308. Pavel, M. *et al.* Contact inhibition controls cell survival and proliferation via YAP/TAZ-autophagy axis. *Nat. Commun.* **9**, 1–18 (2018).

309. Barriga, E. H. & Mayor, R. Chapter Nine - Embryonic Cell–Cell Adhesion: A Key Player in Collective Neural Crest Migration. in *Current Topics in Developmental Biology* (ed. Yap, A. S.) vol. 112 301–323 (Academic Press, 2015).

310. Wayne, J., Sielski, J., Rizvi, A., Georges, K. & Hutter, D. ERK regulation upon contact inhibition in fibroblasts. *Mol. Cell. Biochem.* **286**, 181–189 (2006).

311. Li, S., Gerrard, E. R. & Balkovetz, D. F. Evidence for ERK1/2 phosphorylation controlling contact inhibition of proliferation in Madin-Darby canine kidney epithelial cells. *Am. J. Physiol. Cell Physiol.* **287**, C432-439 (2004).

312. Viñals, F. & Pouysségur, J. Confluence of Vascular Endothelial Cells Induces Cell Cycle Exit by Inhibiting p42/p44 Mitogen-Activated Protein Kinase Activity. *Mol. Cell. Biol.* **19**, 2763–2772 (1999).

313. Liu, F. *et al.* Cadherins and Pak1 Control Contact Inhibition of Proliferation by Pak1-βPIX-GIT Complex-Dependent Regulation of Cell-Matrix Signaling. *Mol. Cell. Biol.* **30**, 1971–1983 (2010).

314. Kawabata, N. & Matsuda, M. Cell Density-Dependent Increase in Tyrosine-Monophosphorylated ERK2 in MDCK Cells Expressing Active Ras or Raf. *PLoS ONE* **11**, (2016).

315. Yuan, T. L., Wulf, G., Burga, L. & Cantley, L. C. Cell-to-cell variability in PI3K protein level regulates PI3K-AKT pathway activity in cell populations. *Curr. Biol.* **21**, 173–183 (2011).

316. Lin, Y.-C. *et al.* Degradation of epidermal growth factor receptor mediates dasatinib-induced apoptosis in head and neck squamous cell carcinoma cells. *Neoplasia N. Y. N* **14**, 463–475 (2012).

317. McCubrey, J. A. *et al.* Roles of the Raf/MEK/ERK pathway in cell growth, malignant transformation and drug resistance. *Biochim. Biophys. Acta* **1773**, 1263–1284 (2007).

318. Miranda, M. B. & Johnson, D. E. Signal transduction pathways that contribute to myeloid differentiation. *Leukemia* **21**, 1363–1377 (2007).

319. Deng, X., Ruvolo, P., Carr, B. & May, W. S. Survival function of ERK1/2 as IL-3-activated, staurosporine-resistant Bcl2 kinases. *Proc. Natl. Acad. Sci.* **97**, 1578–1583 (2000).

320. Johnson, D. E. Src family kinases and the MEK/ERK pathway in the regulation of myeloid differentiation and myeloid leukemogenesis. *Adv. Enzyme Regul.* **48**, 98–112 (2008).

321. Fang, Y. *et al.* MEK/ERK Dependent Activation of STAT1 Mediates Dasatinib-Induced Differentiation of Acute Myeloid Leukemia. *PLoS ONE* **8**, (2013).

322. Mishall, K. M. *et al.* Sustained activation of the AKT/mTOR and MAP kinase pathways mediate resistance to the Src inhibitor, dasatinib, in thyroid cancer. *Oncotarget* **8**, 103014–103031 (2017).

323. Zou, J. *et al.* Mechanisms shaping the role of ERK1/2 in cellular senescence (Review). *Mol. Med. Rep.* **19**, 759–770 (2019).

324. Kress, T. R., Raabe, T. & Feller, S. M. High Erk activity suppresses expression of the cell cycle inhibitor p27Kip1 in colorectal cancer cells. *Cell Commun. Signal. CCS* **8**, 1 (2010).

325. Packer, L. M. *et al.* Nilotinib and MEK inhibitors induce synthetic lethality through paradoxical activation of RAF in drug-resistant chronic myeloid leukemia. *Cancer Cell* **20**, 715–727 (2011).

326. Cheng, Y. & Tian, H. Current Development Status of MEK Inhibitors. *Mol. Basel Switz.* **22**, (2017).

327. Yuan, M. *et al.* SRC and MEK Co-inhibition Synergistically Enhances the Anti-tumor Effect in Both Non-small-cell Lung Cancer (NSCLC) and Erlotinib-Resistant NSCLC. *Front. Oncol.* **9**, (2019).

328. Ferguson, J., Arozarena, I., Ehrhardt, M. & Wellbrock, C. Combination of MEK and SRC inhibition suppresses melanoma cell growth and invasion. *Oncogene* **32**, 86–96 (2013).

329. Simpkins, F. *et al.* Dual Src and MEK Inhibition Decreases Ovarian Cancer Growth and Targets Tumor Initiating Stem-Like Cells. *Clin. Cancer Res.* **24**, 4874–4886 (2018).

330. Iqbal, N. & Iqbal, N. Imatinib: A Breakthrough of Targeted Therapy in Cancer. *Chemother. Res. Pract.* **2014**, (2014).

331. Capdeville, R., Buchdunger, E., Zimmermann, J. & Matter, A. Glivec (STI571, imatinib), a rationally developed, targeted anticancer drug. *Nat. Rev. Drug Discov.* **1**, 493–502 (2002).

332. Hochhaus, A. *et al.* Long-Term Outcomes of Imatinib Treatment for Chronic Myeloid Leukemia. *N. Engl. J. Med.* **376**, 917–927 (2017).

333. Blanke, C. D. *et al.* Phase III randomized, intergroup trial assessing imatinib mesylate at two dose levels in patients with unresectable or metastatic gastrointestinal stromal tumors expressing the kit receptor tyrosine kinase: S0033. *J. Clin. Oncol. Off. J. Am. Soc. Clin. Oncol.* **26**, 626–632 (2008).

334. Metzgeroth, G. *et al.* A Phase-II-Study To Evaluate Efficacy and Safety of Imatinib in Eosinophilia-Associated Myeloproliferative Disorders and Idiopathic Hypereosinophilic Syndrome. *Blood* **108**, 671–671 (2006).

335. Pfeifer, H. *et al.* Long-Term Outcome of 335 Adult Patients Receiving Different Schedules of Imatinib and Chemotherapy as Front-Line Treatment for Philadelphia-Positive Acute Lymphoblastic Leukemia (Ph+ ALL). *Blood* **116**, 173–173 (2010).

336. Olivieri, A. *et al.* Long-term outcome and prospective validation of NIH response criteria in 39 patients receiving imatinib for steroid-refractory chronic GVHD. *Blood* **122**, 4111–4118 (2013).

337. Hodi, F. S. *et al.* Imatinib for melanomas harboring mutationally activated or amplified KIT arising on mucosal, acral, and chronically sun-damaged skin. *J. Clin. Oncol. Off. J. Am. Soc. Clin. Oncol.* **31**, 3182–3190 (2013).

338. Sawyers, C. L. *et al.* Imatinib induces hematologic and cytogenetic responses in patients with chronic myelogenous leukemia in myeloid blast crisis: results of a phase II study. *Blood* **99**, 3530–3539 (2002).

339. Kantarjian, H. *et al.* Dasatinib versus Imatinib in Newly Diagnosed Chronic-Phase Chronic Myeloid Leukemia. *N. Engl. J. Med.* **362**, 2260–2270 (2010).

340. Saglio, G. *et al.* Nilotinib versus imatinib for newly diagnosed chronic myeloid leukemia. *N. Engl. J. Med.* **362**, 2251–2259 (2010).

341. Lombardo, L. J. *et al.* Discovery of N-(2-chloro-6-methyl- phenyl)-2-(6-(4-(2-hydroxyethyl)- piperazin-1-yl)-2-methylpyrimidin-4- ylamino)thiazole-5-carboxamide (BMS-354825), a dual Src/Abl kinase inhibitor with potent antitumor activity in preclinical assays. *J. Med. Chem.* **47**, 6658–6661 (2004).

342. Shah, N. P. *et al.* Overriding imatinib resistance with a novel ABL kinase inhibitor. *Science* **305**, 399–401 (2004).

343. O'Hare, T. *et al.* In vitro activity of Bcr-Abl inhibitors AMN107 and BMS-354825 against clinically relevant imatinib-resistant Abl kinase domain mutants. *Cancer Res.* **65**, 4500–4505 (2005).

344. O'Hare, T. *et al.* Combined Abl Inhibitor Therapy for Minimizing Drug Resistance in Chronic Myeloid Leukemia: Src/Abl Inhibitors Are Compatible with Imatinib. *Clin. Cancer Res.* **11**, 6987–6993 (2005).

345. Peng, B. *et al.* Pharmacokinetics and Pharmacodynamics of Imatinib in a Phase I Trial With Chronic Myeloid Leukemia Patients. *J. Clin. Oncol.* **22**, 935–942 (2004).

346. Larson, R. A. *et al.* Imatinib pharmacokinetics and its correlation with response and safety in chronic-phase chronic myeloid leukemia: a subanalysis of the IRIS study. *Blood* **111**, 4022–4028 (2008).

347. Chen, Y. *et al.* Idelalisib induces G1 arrest and apoptosis in chronic myeloid leukemia K562 cells. *Oncol. Rep.* **36**, 3643–3650 (2016).

348. Weigel, M. T. *et al.* In vitro effects of imatinib mesylate on radiosensitivity and chemosensitivity of breast cancer cells. *BMC Cancer* **10**, 412 (2010).

349. El-Sisi, A. E., Sokar, S. S., Ibrahim, H. A. & Abu-Risha, S. E. Enhanced anticancer activity of combined treatment of imatinib and dipyridamole in solid Ehrlich carcinoma-bearing mice. *Naunyn. Schmiedebergs Arch. Pharmacol.* **393**, 1113–1129 (2020).

350. Greco, W. R., Bravo, G. & Parsons, J. C. The search for synergy: a critical review from a response surface perspective. *Pharmacol. Rev.* **47**, 331–385 (1995).

351. Roell, K. R., Reif, D. M. & Motsinger-Reif, A. A. An Introduction to Terminology and Methodology of Chemical Synergy-Perspectives from Across Disciplines. *Front. Pharmacol.* **8**, 158 (2017).

352. Rossi, F. *et al.* Imatinib upregulates compensatory integrin signaling in a mouse model of gastrointestinal stromal tumor and is more effective when combined with dasatinib. *Mol. Cancer Res. MCR* **8**, 1271–1283 (2010).

353. Ritossa, F. A new puffing pattern induced by temperature shock and DNP in drosophila. *Experientia* **18**, 571–573 (1962).

354. Matz, J. M., Blake, M. J., Tatelman, H. M., Lavoi, K. P. & Holbrook, N. J. Characterization and regulation of cold-induced heat shock protein expression in mouse brown adipose tissue. *Am. J. Physiol.-Regul. Integr. Comp. Physiol.* **269**, R38–R47 (1995).

355. Cao, Y. *et al.* TGF-β1 mediates 70-kDa heat shock protein induction due to ultraviolet irradiation in human skin fibroblasts. *Pflüg. Arch.* **438**, 239–244 (1999).

356. Guo, J., Chang, C. & Li, W. The role of secreted heat shock protein-90 (Hsp90) in wound healing - how could it shape future therapeutics? *Expert Rev. Proteomics* **14**, 665–675 (2017).

357. Crevel, G., Bates, H., Huikeshoven, H. & Cotterill, S. The Drosophila Dpit47 protein is a nuclear Hsp90 co-chaperone that interacts with DNA polymerase alpha. *J. Cell Sci.* **114**, 2015–2025 (2001).

358. The HSP90 family of genes in the human genome: Insights into their divergence and evolution. *Genomics* **86**, 627–637 (2005).

359. Hoter, A., El-Sabban, M. E. & Naim, H. Y. The HSP90 Family: Structure, Regulation, Function, and Implications in Health and Disease. *Int. J. Mol. Sci.* **19**, (2018).

360. Tsutsumi, S. *et al.* Charged linker sequence modulates eukaryotic heat shock protein 90 (Hsp90) chaperone activity. *Proc. Natl. Acad. Sci. U. S. A.* **109**, 2937–2942 (2012).

361. Krukenberg, K. A., Street, T. O., Lavery, L. A. & Agard, D. A. Conformational dynamics of the molecular chaperone Hsp90. *Q. Rev. Biophys.* **44**, 229–255 (2011).

362. Miyata, Y. & Yahara, I. The 90-kDa heat shock protein, HSP90, binds and protects casein kinase II from self-aggregation and enhances its kinase activity. *J. Biol. Chem.* **267**, 7042–7047 (1992).

363. Wiech, H., Buchner, J., Zimmermann, R. & Jakob, U. Hsp90 chaperones protein folding in vitro. *Nature* **358**, 169–170 (1992).

364. Jackson, S. E. Hsp90: Structure and Function. in *Molecular Chaperones* 155–240 (Springer, Berlin, Heidelberg, 2012). doi:10.1007/128_2012_356.

365. Structure and in vivo function of Hsp90. *Curr. Opin. Struct. Biol.* **10**, 46–51 (2000).

366. Oroz, J., Kim, J. H., Chang, B. J. & Zweckstetter, M. Mechanistic basis for the recognition of a misfolded protein by the molecular chaperone Hsp90. *Nat. Struct. Mol. Biol.* **24**, 407–413 (2017).

367. Burrows, F., Zhang, H. & Kamal, A. Hsp90 Activation and Cell Cycle Regulation. *Cell Cycle* **3**, 1530–1536 (2004).

368. Molecular chaperones, essential partners of steroid hormone receptors for activity and mobility. *Biochim. Biophys. Acta BBA - Mol. Cell Res.* **1803**, 641–649 (2010).

369. The Hsp90 co-chaperone p23 of Toxoplasma gondii: Identification, functional analysis and dynamic interactome determination. *Mol. Biochem. Parasitol.* **172**, 129–140 (2010).

370. Lurje, G. & Lenz, H.-J. EGFR Signaling and Drug Discovery. *Oncology* **77**, 400–410 (2009).

371. Heat shock proteins in cancer: chaperones of tumorigenesis. *Trends Biochem. Sci.* **31**, 164–172 (2006).

372. Yamaki, H., Nakajima, M., Shimotohno, K. W. & Tanaka, N. Molecular basis for the actions of Hsp90 inhibitors and cancer therapy. *J. Antibiot. (Tokyo)* **64**, 635–644 (2011).

373. Trepel, J., Mollapour, M., Giaccone, G. & Neckers, L. Targeting the dynamic HSP90 complex in cancer. *Nat. Rev. Cancer* **10**, 537–549 (2010).

374. Wang, J., Cui, S., Zhang, X., Wu, Y. & Tang, H. High Expression of Heat Shock Protein 90 Is Associated with Tumor Aggressiveness and Poor Prognosis in Patients with Advanced Gastric Cancer. *PLoS ONE* **8**, (2013).

375. Flandrin-Gresta, P. *et al.* Heat Shock Protein 90 is overexpressed in high-risk myelodysplastic syndromes and associated with higher expression and activation of Focal Adhesion Kinase. *Oncotarget* **3**, 1158–1168 (2012).

376. Khan, F., Ricks-Santi, L., Hudson, T., Beyene, D. & Naab, T. HSP90 Expression Associated with HER2 Overexpressing Breast Ductal Carcinomas in African American Women. *Am. J. Clin. Pathol.* **146**, (2016).

377. Ito, T. *et al.* Expression of heat shock proteins in squamous cell carcinoma of the tongue: an immunohistochemical study. *J. Oral Pathol. Med.* **27**, 18–22 (1998).

378. Graner, A. N. *et al.* HSP90 inhibitors in the context of heat shock and the unfolded protein response: effects on a primary canine pulmonary adenocarcinoma cell line. *Int. J. Hyperth. Off. J. Eur. Soc. Hyperthermic Oncol. North Am. Hyperth. Group* **33**, 303–317 (2017).

379. Garg, G., Khandelwal, A. & Blagg, B. S. J. Anticancer Inhibitors of Hsp90 Function: Beyond the Usual Suspects. *Adv. Cancer Res.* **129**, 51–88 (2016).

380. Research, I. I. of A. Molecular Chaperones. Methods and Protocols. *Anticancer Res.* **32**, 715–716 (2012).

381. Seneci, P. Chapter 5 - Selective Disposal of Insoluble Protein Aggregates: Pick, Transport and Remove to Cure. in *Molecular Targets in Protein Misfolding and Neurodegenerative Disease* (ed. Seneci, P.) 183–227 (Academic Press, 2015). doi:10.1016/B978-0-12-800186-8.00005-5.

382. Jhaveri, K. *et al.* Biomarkers that Predict Sensitivity to Heat Shock Protein 90 Inhibitors (HSP90i). *Clin. Breast Cancer* **16**, 276–283 (2016).

383. Munje, C., Shervington, L., Khan, Z. & Shervington, A. Could Upregulated Hsp70 Protein Compensate for the Hsp90-Silence-Induced Cell Death in Glioma Cells? *International Journal of Brain Science* https://www.hindawi.com/journals/ijbs/2014/652643/ (2014) doi:https://doi.org/10.1155/2014/652643.

384. Chiosis, G. & Neckers, L. Tumor selectivity of Hsp90 inhibitors: the explanation remains elusive. *ACS Chem. Biol.* **1**, 279–284 (2006).

385. Kamal, A. *et al.* A high-affinity conformation of Hsp90 confers tumour selectivity on Hsp90 inhibitors. *Nature* **425**, 407–410 (2003).

386. Wang, H., Lu, M., Yao, M. & Zhu, W. Effects of treatment with an Hsp90 inhibitor in tumors based on 15 phase II clinical trials. *Mol. Clin. Oncol.* **5**, 326–334 (2016).

387. Ochiana, S. O., Taldone, T. & Chiosis, G. Designing Drugs Against Hsp90 for Cancer Therapy. in *The Molecular Chaperones Interaction Networks in Protein Folding and Degradation* 151–183 (Springer, New York, NY, 2014). doi:10.1007/978-1-4939-1130-1_7.

388. Samuni, Y. *et al.* Reactive oxygen species mediate hepatotoxicity induced by the Hsp90 inhibitor geldanamycin and its analogs. *Free Radic. Biol. Med.* **48**, 1559–1563 (2010).

389. Khandelwal, A., Crowley, V. M. & Blagg, B. S. J. Natural Product Inspired N-Terminal Hsp90 Inhibitors: From Bench to Bedside? *Med. Res. Rev.* **36**, 92–118 (2016).

390. Cragg, G. M. & Newman, D. J. 1.08 - Natural Product Sources of Drugs: Plants, Microbes, Marine Organisms, and Animals. in *Comprehensive Medicinal Chemistry II* (eds. Taylor, J. B. & Triggle, D. J.) 355–403 (Elsevier, 2007). doi:10.1016/B0-08-045044-X/00011-0.

391. Bagatell, R. & Whitesell, L. Altered Hsp90 function in cancer: a unique therapeutic opportunity. *Mol. Cancer Ther.* **3**, 1021–1030 (2004).

392. Porrata, L. F. & Adjei, A. A. The pharmacologic basis of high dose chemotherapy with haematopoietic stem cell support for solid tumours. *Br. J. Cancer* **85**, 484–489 (2001).

393. Review of therapeutic drug monitoring of anticancer drugs part 1 – Cytotoxics. *Eur. J. Cancer* **50**, 2010–2019 (2014).

394. Banerji, U. *et al.* Phase I Pharmacokinetic and Pharmacodynamic Study of 17-Allylamino, 17-Demethoxygeldanamycin in Patients With Advanced Malignancies. *J. Clin. Oncol.* **23**, 4152–4161 (2005).

395. Polier, S. *et al.* ATP-competitive inhibitors block protein kinase recruitment to the Hsp90-Cdc37 system. *Nat. Chem. Biol.* **9**, 307–312 (2013).

396. Workman, P., Burrows, F., Neckers, L. & Rosen, N. Drugging the cancer chaperone HSP90: combinatorial therapeutic exploitation of oncogene addiction and tumor stress. *Ann. N. Y. Acad. Sci.* **1113**, 202–216 (2007).

397. Samant, R. S., Clarke, P. A. & Workman, P. E3 ubiquitin ligase Cullin-5 modulates multiple molecular and cellular responses to heat shock protein 90 inhibition in human cancer cells. *Proc. Natl. Acad. Sci.* **111**, 6834–6839 (2014).

398. Pashtan, I., Tsutsumi, S., Wang, S., Xu, W. & Neckers, L. Targeting Hsp90 prevents escape of breast cancer cells from tyrosine kinase inhibition. *Cell Cycle* **7**, 2936–2941 (2008).

399. Smith, D. L. *et al.* The HSP90 inhibitor ganetespib potentiates the antitumor activity of EGFR tyrosine kinase inhibition in mutant and wild-type non-small cell lung cancer. *Target. Oncol.* **10**, 235–245 (2015).

400. Smyth, T. *et al.* Inhibition of HSP90 by AT13387 Delays the Emergence of Resistance to BRAF Inhibitors and Overcomes Resistance to Dual BRAF and MEK Inhibition in Melanoma Models. *Mol. Cancer Ther.* **13**, 2793–2804 (2014).

401. Astex Pharmaceuticals, Inc. *A Study of HSP90 Inhibitor AT13387 Alone and in Combination With Crizotinib in the Treatment of Non-small Cell Lung Cancer (NSCLC).* https://clinicaltrials.gov/ct2/show/NCT01712217 (2018).

402. Onalespib and CDKI AT7519 in Treating Patients With Solid Tumors That Are Metastatic or Cannot Be Removed by Surgery - Full Text View - ClinicalTrials.gov. https://clinicaltrials.gov/ct2/show/NCT02503709.

403. Onalespib, Dabrafenib, and Trametinib in Treating Patients With BRAF-Mutant Melanoma or Solid Tumors That Are Metastatic or Cannot Be Removed by Surgery - Full Text View - ClinicalTrials.gov. https://clinicaltrials.gov/ct2/show/NCT02097225.

404. Onalespib in Treating Patients With Locoregionally Advanced Squamous Cell Carcinoma of the Head and Neck Receiving Radiation Therapy and Cisplatin - Full Text View - ClinicalTrials.gov. https://clinicaltrials.gov/ct2/show/NCT02381535.

405. Onalespib and Paclitaxel in Treating Patients With Advanced Triple Negative Breast Cancer - Full Text View - ClinicalTrials.gov. https://clinicaltrials.gov/ct2/show/NCT02474173.

406. A Study of TAS-116 in Patients With Solid Tumors - Full Text View - ClinicalTrials.gov. https://clinicaltrials.gov/ct2/show/NCT02965885.

407. Shimomura, A. *et al.* First-in-Human Phase I Study of an Oral HSP90 Inhibitor, TAS-116, in Patients with Advanced Solid Tumors. *Mol. Cancer Ther.* **18**, 531–540 (2019).

408. Karuso, P. 9.14 - Modern Methods for the Isolation of Natural Product Receptors. in *Comprehensive Natural Products II* (eds. Liu, H.-W. (Ben) & Mander, L.) 513–567 (Elsevier, 2010). doi:10.1016/B978-008045382-8.00210-0.

409. Doi, T. *et al.* Efficacy and safety of TAS-116, an oral inhibitor of heat shock protein 90, in patients with metastatic or unresectable gastrointestinal stromal tumour refractory to imatinib, sunitinib and regorafenib: a phase II, single-arm trial. *Eur. J. Cancer* **121**, 29–39 (2019).

410. Ohkubo, S. *et al.* TAS-116, a Highly Selective Inhibitor of Heat Shock Protein 90α and β, Demonstrates Potent Antitumor Activity and Minimal Ocular Toxicity in Preclinical Models. *Mol. Cancer Ther.* **14**, 14–22 (2015).

411. Chaicharoenaudomrung, N., Kunhorm, P. & Noisa, P. Three-dimensional cell culture systems as an in vitro platform for cancer and stem cell modeling. *World J. Stem Cells* **11**, 1065–1083 (2019).

412. Horibata, S., Vo, T. V., Subramanian, V., Thompson, P. R. & Coonrod, S. A. Utilization of the Soft Agar Colony Formation Assay to Identify Inhibitors of Tumorigenicity in Breast Cancer Cells. *J. Vis. Exp. JoVE* (2015) doi:10.3791/52727.

413. Wang, H., Zhang, Y., Kriska, A. & Chen, H. Chapter 28 - Epigenetic Regulation in Cancer Metastasis. in *Medical Epigenetics* (ed. Tollefsbol, T. O.) 499–514 (Academic Press, 2016). doi:10.1016/B978-0-12-803239-8.00028-4.

414. Loessner, D. *et al.* Bioengineered 3D platform to explore cell–ECM interactions and drug resistance of epithelial ovarian cancer cells. *Biomaterials* **31**, 8494–8506 (2010).

415. Karlsson, H., Fryknäs, M., Larsson, R. & Nygren, P. Loss of cancer drug activity in colon cancer HCT-116 cells during spheroid formation in a new 3-D spheroid cell culture system. *Exp. Cell Res.* **318**, 1577–1585 (2012).

416. Hsieh, C.-H., Chen, Y.-D., Huang, S.-F., Wang, H.-M. & Wu, M.-H. The Effect of Primary Cancer Cell Culture Models on the Results of Drug Chemosensitivity Assays: The Application of Perfusion Microbioreactor System as Cell Culture Vessel. *BioMed Research International* vol. 2015 e470283 https://www.hindawi.com/journals/bmri/2015/470283/ (2015).

417. LaBonia, G. J., Lockwood, S. Y., Heller, A. A., Spence, D. M. & Hummon, A. B. Drug penetration and metabolism in 3D cell cultures treated in a 3D printed fluidic device: assessment of irinotecan via MALDI imaging mass spectrometry. *Proteomics* **16**, 1814–1821 (2016).

418. Kapałczyńska, M. *et al.* 2D and 3D cell cultures – a comparison of different types of cancer cell cultures. *Arch. Med. Sci. AMS* **14**, 910–919 (2018).

419. Griffith, L. G. & Swartz, M. A. Capturing complex 3D tissue physiology in vitro. *Nat. Rev. Mol. Cell Biol.* **7**, 211–224 (2006).

420. Francia, G., Man, S., Teicher, B., Grasso, L. & Kerbel, R. S. Gene expression analysis of tumor spheroids reveals a role for suppressed DNA mismatch repair in multicellular resistance to alkylating agents. *Mol. Cell. Biol.* **24**, 6837–6849 (2004).

421. Riedl, A. *et al.* Comparison of cancer cells in 2D vs 3D culture reveals differences in AKT-mTOR-S6K signaling and drug responses. *J. Cell Sci.* **130**, 203–218 (2017).

422. Trédan, O., Galmarini, C. M., Patel, K. & Tannock, I. F. Drug resistance and the solid tumor microenvironment. *J. Natl. Cancer Inst.* **99**, 1441–1454 (2007).

423. Gurski, L. A., Petrelli, N. J., Jia, X. & Farach-Carson, M. C. 3D Matrices for Anti-Cancer Drug Testing and Development. *Oncol. Issues* **25**, 20–25 (2010).

424. Schmidt, M., Scholz, C.-J., Polednik, C. & Roller, J. Spheroid-based 3-dimensional culture models: Gene expression and functionality in head and neck cancer. *Oncol. Rep.* **35**, 2431–2440 (2016).

425. Levêque, D., Becker, G., Bilger, K. & Natarajan-Amé, S. Clinical Pharmacokinetics and Pharmacodynamics of Dasatinib. *Clin. Pharmacokinet.* **59**, 849–856 (2020).

426. Yao, D., Ding, S., Burchell, B., Wolf, C. R. & Friedberg, T. Detoxication of vinca alkaloids by human P450 CYP3A4-mediated metabolism: implications for the development of drug resistance. *J. Pharmacol. Exp. Ther.* **294**, 387–395 (2000).

427. Corcoran, C. *et al.* miR-630 targets IGF1R to regulate response to HER-targeting drugs and overall cancer cell progression in HER2 over-expressing breast cancer. *Mol. Cancer* **13**, 71 (2014).

428. Breslin, S. & O'Driscoll, L. The relevance of using 3D cell cultures, in addition to 2D monolayer cultures, when evaluating breast cancer drug sensitivity and resistance. *Oncotarget* **7**, 45745–45756 (2016).

429. Madhuri1, M., Kumari1, L. S., Susmitha1, P., Gayatri1, Y. L. & Sahoo2*, S. K. Method development and validation of stability indicating RP-HPLC method for the estimation of Dasatinib in tablet dosage form. *J. Pharm. Res.* 419–423 (2017).

430. Mittler, F. *et al.* High-Content Monitoring of Drug Effects in a 3D Spheroid Model. *Front. Oncol.* **7**, (2017).

431. Borowicz, S. *et al.* The Soft Agar Colony Formation Assay. *J. Vis. Exp. JoVE* (2014) doi:10.3791/51998.

432. Eastman, A. Improving anticancer drug development begins with cell culture: misinformation perpetrated by the misuse of cytotoxicity assays. *Oncotarget* **8**, 8854–8866 (2016).

433. Gonzalez, M. & Riera, A. Tongue Cancer. in *StatPearls* (StatPearls Publishing, 2020).

434. Sawasdikosol, S. Detecting tyrosine-phosphorylated proteins by Western blot analysis. *Curr. Protoc. Immunol.* **Chapter 11**, Unit 11.3.1-11 (2010).

435. Samant, R. S., Clarke, P. A. & Workman, P. The expanding proteome of the molecular chaperone HSP90. *Cell Cycle* **11**, 1301–1308 (2012).

436. Park, T.-J. & Curran, T. Essential roles of Crk and CrkL in fibroblast structure and motility. *Oncogene* **33**, 5121–5132 (2014).

437. Webb, D. J. *et al.* FAK-Src signalling through paxillin, ERK and MLCK regulates adhesion disassembly. *Nat. Cell Biol.* **6**, 154–161 (2004).

438. Wu, C. Focal Adhesion. *Cell Adhes. Migr.* **1**, 13–18 (2007).

439. Li, L., Guris, D. L., Okura, M. & Imamoto, A. Translocation of CrkL to Focal Adhesions Mediates Integrin-Induced Migration Downstream of Src Family Kinases. *Mol. Cell. Biol.* **23**, 2883–2892 (2003).

440. Uemura, N., Salgia, R., Ewaniuk, D. S., Little, M.-T. & Griffin, J. D. Involvement of the adapter protein CRKL in integrin-mediated adhesion. *Oncogene* **18**, 3343–3353 (1999).

441. López-Colomé, A. M., Lee-Rivera, I., Benavides-Hidalgo, R. & López, E. Paxillin: a crossroad in pathological cell migration. *J. Hematol. Oncol.J Hematol Oncol* **10**, (2017).

442. Woo, J. K. *et al.* Daurinol blocks breast and lung cancer metastasis and development by inhibition of focal adhesion kinase (FAK). *Oncotarget* **8**, 57058–57071 (2017).

443. Maziveyi, M. & Alahari, S. K. Cell matrix adhesions in cancer: The proteins that form the glue. *Oncotarget* **8**, 48471–48487 (2017).

444. Shim, S. R., Kook, S., Kim, J. I. & Song, W. K. Degradation of focal adhesion proteins paxillin and p130cas by caspases or calpains in apoptotic rat-1 and L929 cells. *Biochem. Biophys. Res. Commun.* **286**, 601–608 (2001).

445. Bisaro, B. *et al.* p130Cas scaffold protein regulates ErbB2 stability by altering breast cancer cell sensitivity to autophagy. *Oncotarget* **7**, 4442–4453 (2015).

446. Wöhrle, F. U., Daly, R. J. & Brummer, T. Function, regulation and pathological roles of the Gab/DOS docking proteins. *Cell Commun. Signal. CCS* **7**, 22 (2009).

447. Watanabe, T. *et al.* Crk adaptor protein-induced phosphorylation of Gab1 on tyrosine 307 via Src is important for organization of focal adhesions and enhanced cell migration. *Cell Res.* **19**, 638–650 (2009).

448. Bromberg, J. F., Horvath, C. M., Wen, Z., Schreiber, R. D. & Darnell, J. E. Transcriptionally active Stat1 is required for the antiproliferative effects of both interferon alpha and interferon gamma. *Proc. Natl. Acad. Sci.* **93**, 7673–7678 (1996).

449. Shankaran, V. *et al.* IFNγ and lymphocytes prevent primary tumour development and shape tumour immunogenicity. *Nature* **410**, 1107–1111 (2001).

450. Zhang, Y.-W., Wang, L.-M., Jove, R. & Woude, G. F. V. Requirement of Stat3 signaling for HGF/SF-Met mediated tumorigenesis. *Oncogene* **21**, 217–226 (2002).

451. Stat5 Is Essential for the Myelo- and Lymphoproliferative Disease Induced by TEL/JAK2. *Mol. Cell* **6**, 693–704 (2000).

452. Verhoeven, Y. *et al.* The potential and controversy of targeting STAT family members in cancer. *Semin. Cancer Biol.* **60**, 41–56 (2020).

453. Chang, Y.-J., Holtzman, M. J. & Chen, C.-C. Differential role of Janus family kinases (JAKs) in interferon-gamma-induced lung epithelial ICAM-1 expression: involving protein interactions between JAKs, phospholipase Cgamma, c-Src, and STAT1. *Mol. Pharmacol.* **65**, 589–598 (2004).

454. Loh, C.-Y. *et al.* Signal Transducer and Activator of Transcription (STATs) Proteins in Cancer and Inflammation: Functions and Therapeutic Implication. *Front. Oncol.* **9**, (2019).

455. Vasilenko, K. P., Butylin, P. A., Arnautov, A. M. & Nikol'skiǐ, N. N. [The role of SRC kinase in activation of transcription factor STAT1]. *Tsitologiia* **43**, 1031–1037 (2001).

456. Pensa, S., Regis, G., Boselli, D., Novelli, F. & Poli, V. *STAT1 and STAT3 in Tumorigenesis: Two Sides of the Same Coin?* (Landes Bioscience, 2013).

457. Leibowitz, M. S., Andrade Filho, P. A., Ferrone, S. & Ferris, R. L. Deficiency of activated STAT1 in head and neck cancer cells mediates TAP1-dependent escape from cytotoxic T lymphocytes. *Cancer Immunol. Immunother. CII* **60**, 525–535 (2011).

458. Laimer, K. *et al.* STAT1 activation in squamous cell cancer of the oral cavity. *Cancer* **110**, 326–333 (2007).

459. Geiger, J. L., Grandis, J. R. & Bauman, J. E. The STAT3 pathway as a therapeutic target in head and neck cancer: Barriers and innovations. *Oral Oncol.* **56**, 84–92 (2016).

460. Zhang, X. *et al.* Identification of STAT3 as a substrate of receptor protein tyrosine phosphatase T. *Proc. Natl. Acad. Sci.* **104**, 4060–4064 (2007).

461. Lui, V. W. Y. *et al.* Frequent mutation of receptor protein tyrosine phosphatases provides a mechanism for STAT3 hyperactivation in head and neck cancer. *Proc. Natl. Acad. Sci. U. S. A.* **111**, 1114–1119 (2014).

462. Sen, B., Saigal, B., Parikh, N., Gallick, G. & Johnson, F. M. Sustained Src Inhibition Results in STAT3 Activation and Cancer Cell Survival via Altered JAK-STAT3 Binding. *Cancer Res.* **69**, 1958–1965 (2009).

463. Byers, L. A. *et al.* Reciprocal regulation of c-Src and STAT3 in non-small cell lung cancer. *Clin. Cancer Res. Off. J. Am. Assoc. Cancer Res.* **15**, 6852–6861 (2009).

464. Xi, S., Zhang, Q., Gooding, W. E., Smithgall, T. E. & Grandis, J. R. Constitutive activation of Stat5b contributes to carcinogenesis in vivo. *Cancer Res.* **63**, 6763–6771 (2003).

465. Lui, V. W., Xi, S., Raymond, C. L., Koppikar, P. & Grandis, J. R. Activation of STAT5 contributes to tumor growth and epithelial-mesenchymal transition in head and neck cancer. *Cancer Res.* **66**, 1134–1134 (2006).

466. Leong, P. *et al.* Differential function of STAT5 isoforms in head and neck cancer growth control. *Oncogene* **21**, 2846–2853 (2002).

467. Mazumder, E. D. *et al.* A Molecular Model for the Differential Activation of STAT3 and STAT6 by the Herpesviral Oncoprotein Tip. *PLOS ONE* **7**, e34306 (2012).

468. Stegeman, H. *et al.* Combining radiotherapy with MEK1/2, STAT5 or STAT6 inhibition reduces survival of head and neck cancer lines. *Mol. Cancer* **12**, 133 (2013).

469. Elferink, L. A. & Resto, V. A. Receptor-Tyrosine-Kinase-Targeted Therapies for Head and Neck Cancer. *J. Signal Transduct.* **2011**, (2011).

470. Citri, A., Kochupurakkal, B. S. & Yarden, Y. The achilles heel of ErbB-2/HER2: regulation by the Hsp90 chaperone machine and potential for pharmacological intervention. *Cell Cycle Georget. Tex* **3**, 51–60 (2004).

471. HGF: a multifunctional growth factor controlling cell scattering. *Int. J. Biochem. Cell Biol.* **31**, 1357–1362 (1999).

472. Sun, Z. *et al.* Role of c-Met in the progression of human oral squamous cell carcinoma and its potential as a therapeutic target. *Oncol. Rep.* **39**, 209–216 (2018).

473. Saintigny, P. *et al.* Met Receptor Tyrosine Kinase and Chemoprevention of Oral Cancer. *JNCI J. Natl. Cancer Inst.* **110**, 250–257 (2017).

474. Sun, S. & Wang, Z. Head neck squamous cell carcinoma c-Met^{+} cells display cancer stem cell properties and are responsible for cisplatin-resistance and metastasis. *Int. J. Cancer* **129**, 2337–2348 (2011).

475. Arnold, L., Enders, J. & Thomas, S. M. Activated HGF-c-Met Axis in Head and Neck Cancer. *Cancers* **9**, (2017).

476. Rothenberger, N. J. & Stabile, L. P. Hepatocyte Growth Factor/c-Met Signaling in Head and Neck Cancer and Implications for Treatment. *Cancers* **9**, (2017).

477. Yc, L. *et al.* Overexpression of c-Met promotes invasion and metastasis of small oral tongue carcinoma. *Oral Oncol.* **48**, 1114–1119 (2012).

478. O-charoenrat, P., Rhys-Evans, P. H., Modjtahedi, H. & Eccles, S. A. The role of c-erbB receptors and ligands in head and neck squamous cell carcinoma. *Oral Oncol.* **38**, 627–640 (2002).

479. Sarkis, S. A., Abdullah, B. H., Abdul Majeed, B. A. & Talabani, N. G. Immunohistochemical expression of epidermal growth factor receptor (EGFR) in oral squamous cell carcinoma in relation to proliferation, apoptosis, angiogenesis and lymphangiogenesis. *Head Neck Oncol.* **2**, 13 (2010).

480. EGFR protein overexpression and gene copy number increases in oral tongue squamous cell carcinoma. *Eur. J. Cancer* **45**, 1700–1708 (2009).

481. Ang, K. K. *et al.* Impact of epidermal growth factor receptor expression on survival and pattern of relapse in patients with advanced head and neck carcinoma. *Cancer Res.* **62**, 7350–7356 (2002).

482. Ribeiro, F. A. P., Noguti, J., Oshima, C. T. F. & Ribeiro, D. A. Effective targeting of the epidermal growth factor receptor (EGFR) for treating oral cancer: a promising approach. *Anticancer Res.* **34**, 1547–1552 (2014).

483. CETUXIMAB Given for 3 Weeks as Neoadjuvant Treatment in Locally Advanced Tongue Cancer ; A NEW PARADIGM OF TREATMENT - Full Text View - ClinicalTrials.gov. https://clinicaltrials.gov/ct2/show/NCT01760811.

484. Shimamura, T., Lowell, A. M., Engelman, J. A. & Shapiro, G. I. Epidermal growth factor receptors harboring kinase domain mutations associate with the heat shock protein 90 chaperone and are destabilized following exposure to geldanamycins. *Cancer Res.* **65**, 6401–6408 (2005).

485. Sawai, A. *et al.* Inhibition of Hsp90 down-regulates mutant epidermal growth factor receptor (EGFR) expression and sensitizes EGFR mutant tumors to paclitaxel. *Cancer Res.* **68**, 589–596 (2008).

486. Chattopadhyay, A., Vecchi, M., Ji, Q. s, Mernaugh, R. & Carpenter, G. The role of individual SH2 domains in mediating association of phospholipase C-gamma1 with the activated EGF receptor. *J. Biol. Chem.* **274**, 26091–26097 (1999).

487. Tice, D. A., Biscardi, J. S., Nickles, A. L. & Parsons, S. J. Mechanism of biological synergy between cellular Src and epidermal growth factor receptor. *Proc. Natl. Acad. Sci.* **96**, 1415–1420 (1999).

488. The involvement of the docking protein Gab1 in mitogenic signalling induced by EGF and HGF in rat hepatocytes. *Biochim. Biophys. Acta BBA - Mol. Cell Res.* **1833**, 3286–3294 (2013).

489. Chaudhuri, A. *et al.* Distinct Involvement of the Gab1 and Grb2 Adaptor Proteins in Signal Transduction by the Related Receptor Tyrosine Kinases RON and MET. *J. Biol. Chem.* **286**, 32762–32774 (2011).

490. Gual, P. *et al.* Sustained recruitment of phospholipase C-gamma to Gab1 is required for HGF-induced branching tubulogenesis. *Oncogene* **19**, 1509–1518 (2000).

491. Maroun, C. R. *et al.* A conserved inositol phospholipid binding site within the pleckstrin homology domain of the Gab1 docking protein is required for epithelial morphogenesis. *J. Biol. Chem.* **274**, 31719–31726 (1999).

492. Cunnick, J. M., Mei, L., Doupnik, C. A. & Wu, J. Phosphotyrosines 627 and 659 of Gab1 Constitute a Bisphosphoryl Tyrosine-based Activation Motif (BTAM) Conferring Binding and Activation of SHP2. *J. Biol. Chem.* **276**, 24380–24387 (2001).

493. Furcht, C. M., Buonato, J. M. & Lazzara, M. J. EGFR-activated Src family kinases maintain GAB1-SHP2 complexes distal from EGFR. *Sci. Signal.* **8**, ra46 (2015).

494. Chan, P.-C., Sudhakar, J. N., Lai, C.-C. & Chen, H.-C. Differential phosphorylation of the docking protein Gab1 by c-Src and the hepatocyte growth factor receptor regulates different aspects of cell functions. *Oncogene* **29**, 698–710 (2010).

495. Yart, A. *et al.* A critical role for phosphoinositide 3-kinase upstream of Gab1 and SHP2 in the activation of ras and mitogen-activated protein kinases by epidermal growth factor. *J. Biol. Chem.* **276**, 8856–8864 (2001).

496. Cunnick, J. M. *et al.* Regulation of the mitogen-activated protein kinase signaling pathway by SHP2. *J. Biol. Chem.* **277**, 9498–9504 (2002).

497. Ras oncogenes in oral cancer: The past 20 years. *Oral Oncol.* **48**, 383–392 (2012).

498. Al-Rawi, N. H., Merza, M. S. & Ghazi, A. M. PIK3CB and K-ras in oral squamous Cell carcinoma. A possible cross-talk! *J. Orofac. Sci.* **6**, 99 (2014).

499. Cai, T., Nishida, K., Hirano, T. & Khavari, P. A. Gab1 and SHP-2 promote Ras/MAPK regulation of epidermal growth and differentiation. *J. Cell Biol.* **159**, 103–112 (2002).

500. Ahmed, T. A. *et al.* SHP2 Drives Adaptive Resistance to ERK Signaling Inhibition in Molecularly Defined Subsets of ERK-Dependent Tumors. *Cell Rep.* **26**, 65-78.e5 (2019).

501. Gu, H. & Neel, B. G. The 'Gab' in signal transduction. *Trends Cell Biol.* **13**, 122–130 (2003).

502. Dance, M., Montagner, A., Salles, J.-P., Yart, A. & Raynal, P. The molecular functions of Shp2 in the Ras/Mitogen-activated protein kinase (ERK1/2) pathway. *Cell. Signal.* **20**, 453–459 (2008).

503. Simanshu, D. K., Nissley, D. V. & McCormick, F. RAS Proteins and Their Regulators in Human Disease. *Cell* **170**, 17–33 (2017).

504. Studying the Spatial and Temporal Regulation of Ras GTPase-Activating Proteins. *Methods Enzymol.* **407**, 64–82 (2006).

505. An Excitable Ras/PI3K/ERK Signaling Network Controls Migration and Oncogenic Transformation in Epithelial Cells. *Dev. Cell* **54**, 608-623.e5 (2020).

506. Grbovic, O. M. *et al.* V600E B-Raf requires the Hsp90 chaperone for stability and is degraded in response to Hsp90 inhibitors. *Proc. Natl. Acad. Sci. U. S. A.* **103**, 57–62 (2006).

507. Schulte, T. W., Blagosklonny, M. V., Ingui, C. & Neckers, L. Disruption of the Raf-1-Hsp90 molecular complex results in destabilization of Raf-1 and loss of Raf-1-Ras association. *J. Biol. Chem.* **270**, 24585–24588 (1995).

508. Rouhi, A. *et al.* Prospective identification of resistance mechanisms to HSP90 inhibition in KRAS mutant cancer cells. *Oncotarget* **8**, 7678–7690 (2016).

509. O'Bryan, J. P. Pharmacological Targeting of RAS: Recent Success with Direct Inhibitors. *Pharmacol. Res.* **139**, 503–511 (2019).

510. Cox, A. D. & Der, C. J. Ras history. *Small GTPases* **1**, 2–27 (2010).

511. Shimizu, T. *et al.* The clinical effect of the dual-targeting strategy involving PI3K/AKT/mTOR and RAS/MEK/ERK pathways in patients with advanced cancer. *Clin. Cancer Res. Off. J. Am. Assoc. Cancer Res.* **18**, 2316–2325 (2012).

512. Engelman, J. A. *et al.* Effective use of PI3K and MEK inhibitors to treat mutant Kras G12D and PIK3CA H1047R murine lung cancers. *Nat. Med.* **14**, 1351–1356 (2008).

513. Azoitei, N. *et al.* Targeting of KRAS mutant tumors by HSP90 inhibitors involves degradation of STK33. *J. Exp. Med.* **209**, 697–711 (2012).

514. Bunda, S. *et al.* Inhibition of SHP2-mediated dephosphorylation of Ras suppresses oncogenesis. *Nat. Commun.* **6**, 1–12 (2015).

515. Agazie, Y. M. & Hayman, M. J. Molecular Mechanism for a Role of SHP2 in Epidermal Growth Factor Receptor Signaling. *Mol. Cell. Biol.* **23**, 7875–7886 (2003).

516. Lewis, T. S., Shapiro, P. S. & Ahn, N. G. Signal Transduction through MAP Kinase Cascades. in *Advances in Cancer Research* (eds. Vande Woude, G. F. & Klein, G.) vol. 74 49–139 (Academic Press, 1998).

517. Alessi, D. R. & Cohen, P. Mechanism of activation and function of protein kinase B. *Curr. Opin. Genet. Dev.* **8**, 55–62 (1998).

518. Wolthuis, R. M. & Bos, J. L. Ras caught in another affair: the exchange factors for Ral. *Curr. Opin. Genet. Dev.* **9**, 112–117 (1999).

519. Marshall, C. J. Ras effectors. *Curr. Opin. Cell Biol.* **8**, 197–204 (1996).

520. Wu, X. *et al.* Hsp90 is expressed and represents a therapeutic target in human oesophageal cancer using the inhibitor 17-allylamino-17-demethoxygeldanamycin. *Br. J. Cancer* **100**, 334–343 (2009).

521. Dou, F., Yuan, L.-D., Zhu, J.-J. & Wang, K.-Y. Heat Shock Protein 90 Indirectly Regulates ERK Activity by Affecting Raf Protein Metabolism. *Acta Biochim. Biophys. Sin.* **37**, 501–505 (2005).

522. Solárová, Z., Mojžiš, J. & Solár, P. Hsp90 inhibitor as a sensitizer of cancer cells to different therapies (review). *Int. J. Oncol.* **46**, 907–926 (2015).

523. Sato, N. *et al.* Involvement of heat-shock protein 90 in the interleukin-6-mediated signaling pathway through STAT3. *Biochem. Biophys. Res. Commun.* **300**, 847–852 (2003).

524. von Manstein, V. *et al.* Resistance of Cancer Cells to Targeted Therapies Through the Activation of Compensating Signaling Loops. *Curr. Signal Transduct. Ther.* **8**, 193–202 (2013).

525. Obaid, N. M., Bedard, K. & Huang, W.-Y. Strategies for Overcoming Resistance in Tumours Harboring BRAF Mutations. *Int. J. Mol. Sci.* **18**, (2017).

526. Salaroglio, I. C., Mungo, E., Gazzano, E., Kopecka, J. & Riganti, C. ERK is a Pivotal Player of Chemo-Immune-Resistance in Cancer. *Int. J. Mol. Sci.* **20**, (2019).

527. Hanly, E. K. *et al.* Hyperactive ERK and persistent mTOR signaling characterize vemurafenib resistance in papillary thyroid cancer cells. *Oncotarget* **7**, 8676–8687 (2016).

528. MEK-1 activates C-Raf through a Ras-independent mechanism. *Biochim. Biophys. Acta BBA - Mol. Cell Res.* **1833**, 976–986 (2013).

529. Rosell, R. *et al.* Adaptive resistance to targeted therapies in cancer. *Transl. Lung Cancer Res.* **2**, 152–159 (2013).

530. Ma, P. *et al.* Adaptive and Acquired Resistance to EGFR Inhibitors Converge on the MAPK Pathway. *Theranostics* **6**, 1232–1243 (2016).

531. Monick, M. M., Carter, A. B., Flaherty, D. M., Peterson, M. W. & Hunninghake, G. W. Protein kinase C zeta plays a central role in activation of the p42/44 mitogen-activated protein kinase by endotoxin in alveolar macrophages. *J. Immunol. Baltim. Md 1950* **165**, 4632–4639 (2000).

532. Tsao, H.-K., Chiu, P.-H. & Sun, S. H. PKC-dependent ERK phosphorylation is essential for P2X 7 receptor-mediated neuronal differentiation of neural progenitor cells. *Cell Death Dis.* **4**, e751–e751 (2013).

533. Ueda, Y. *et al.* Protein kinase C activates the MEK-ERK pathway in a manner independent of Ras and dependent on Raf. *J. Biol. Chem.* **271**, 23512–23519 (1996).

534. Garg, R. *et al.* Protein kinase C and cancer: what we know and what we do not. *Oncogene* **33**, 5225–5237 (2014).

535. Cooke, M., Magimaidas, A., Casado-Medrano, V. & Kazanietz, M. G. PROTEIN KINASE C IN CANCER: THE TOP FIVE UNANSWERED QUESTIONS. *Mol. Carcinog.* **56**, 1531–1542 (2017).

536. Yang, Y.-L. *et al.* Amplification of PRKCI, located in 3q26, is associated with lymph node metastasis in esophageal squamous cell carcinoma. *Genes. Chromosomes Cancer* **47**, 127–136 (2008).

537. Chu, P.-Y., Hsu, N. C.-H., Lin, S.-H., Hou, M.-F. & Yeh, K.-T. High Nuclear Protein Kinase CβII Expression Is a Marker of Disease Recurrence in Oral Squamous Cell Carcinoma. *Anticancer Res.* **32**, 3987–3991 (2012).

538. Newton, A. C. Protein Kinase C: Perfectly Balanced. *Crit. Rev. Biochem. Mol. Biol.* **53**, 208–230 (2018).

539. Cortot, A. B. *et al.* Resistance to irreversible EGF receptor tyrosine kinase inhibitors through a multistep mechanism involving the IGF1R pathway. *Cancer Res.* **73**, 834–843 (2013).

540. Bhore, N., Wang, B.-J., Chen, Y.-W. & Liao, Y.-F. Critical Roles of Dual-Specificity Phosphatases in Neuronal Proteostasis and Neurological Diseases. *Int. J. Mol. Sci.* **18**, (2017).

541. Castellano, E. & Downward, J. RAS Interaction with PI3K. *Genes Cancer* **2**, 261–274 (2011).

542. Carracedo, A. *et al.* Inhibition of mTORC1 leads to MAPK pathway activation through a PI3K-dependent feedback loop in human cancer. *J. Clin. Invest.* **118**, 3065–3074 (2008).

543. Bai, J., Li, Y. & Zhang, G. Cell cycle regulation and anticancer drug discovery. *Cancer Biol. Med.* **14**, 348–362 (2017).

544. Cancer Genetics - CuboCube. http://www.cubocube.com/dashboard.php?a=1642&b=1691&c=1.

545. Barnum, K. J. & O'Connell, M. J. Cell Cycle Regulation by Checkpoints. *Methods Mol. Biol. Clifton NJ* **1170**, 29–40 (2014).

546. *Cell Cycle Deregulation in Cancer*. (Springer-Verlag, 2010).

547. Sherr, C. J. & Bartek, J. Cell Cycle–Targeted Cancer Therapies. *Annu. Rev. Cancer Biol.* **1**, 41–57 (2017).

548. Diaz-Moralli, S., Tarrado-Castellarnau, M., Miranda, A. & Cascante, M. Targeting cell cycle regulation in cancer therapy. *Pharmacol. Ther.* **138**, 255–271 (2013).

549. Mills, C. C., Kolb, EA. & Sampson, V. B. Development of chemotherapy with cell cycle inhibitors for adult and pediatric cancer therapy. *Cancer Res.* **78**, 320–325 (2018).

550. Liu, X., Du, L. & Feng, R. c-Src regulates cell cycle proteins expression through protein kinase B/glycogen synthase kinase 3 beta and extracellular signal-regulated kinases 1/2 pathways in MCF-7 cells. *Acta Biochim. Biophys. Sin.* **45**, 586–592 (2013).

551. Chu, I. *et al.* p27 phosphorylation by Src regulates inhibition of cyclin E-Cdk2. *Cell* **128**, 281–294 (2007).

552. James, M. K., Ray, A., Leznova, D. & Blain, S. W. Differential Modification of p27Kip1 Controls Its Cyclin D-cdk4 Inhibitory Activity. *Mol. Cell. Biol.* **28**, 498–510 (2008).

553. Yang, C. *et al.* Tyrosine kinase inhibition in diffuse large B-cell lymphoma: molecular basis for antitumor activity and drug resistance of dasatinib. *Leukemia* **22**, 1755–1766 (2008).

554. Dasatinib, a small molecule inhibitor of the Src kinase, reduces the growth and activates apoptosis in pre-neoplastic Barrett's esophagus cell lines: Evidence for a noninvasive treatment of high-grade dysplasia. *J. Thorac. Cardiovasc. Surg.* **145**, 531–538 (2013).

555. Song, Y., Sun, X., Bai, W.-L. & Ji, W.-Y. Antitumor effects of Dasatinib on laryngeal squamous cell carcinoma in vivo and in vitro. *Eur. Arch. Otorhinolaryngol.* **270**, 1397–1404 (2013).

556. Qian, X.-L. *et al.* Dasatinib inhibits c-src phosphorylation and prevents the proliferation of Triple-Negative Breast Cancer (TNBC) cells which overexpress Syndecan-Binding Protein (SDCBP). *PLoS ONE* **12**, (2017).

557. Okamoto, J. *et al.* Inhibition of Hsp90 leads to cell cycle arrest and apoptosis in human malignant pleural mesothelioma. *J. Thorac. Oncol. Off. Publ. Int. Assoc. Study Lung Cancer* **3**, 1089–1095 (2008).

558. Lamoureux, F. *et al.* A novel HSP90 inhibitor delays castrate resistant prostate cancer without altering serum PSA levels and inhibits osteoclastogenesis. *Clin. Cancer Res. Off. J. Am. Assoc. Cancer Res.* **17**, 2301–2313 (2011).

559. Wang, S.-X. *et al.* SNX-2112, a novel Hsp90 inhibitor, induces G2/M cell cycle arrest and apoptosis in MCF-7 cells. *Biosci. Biotechnol. Biochem.* **75**, 1540–1545 (2011).

560. Sato, N. *et al.* A possible role for centrosome overduplication in radiation-induced cell death. *Oncogene* **19**, 5281–5290 (2000).

561. Nomura, M. *et al.* Geldanamycin induces mitotic catastrophe and subsequent apoptosis in human glioma cells. *J. Cell. Physiol.* **201**, 374–384 (2004).

562. Spiegelberg, D. *et al.* The novel HSP90 inhibitor AT13387 potentiates radiation effects in squamous cell carcinoma and adenocarcinoma cells. *Oncotarget* **6**, 35652–35666 (2015).

563. Noguchi, M. *et al.* Inhibition of homologous recombination repair in irradiated tumor cells pretreated with Hsp90 inhibitor 17-allylamino-17-demethoxygeldanamycin. *Biochem. Biophys. Res. Commun.* **351**, 658–663 (2006).

564. Otto, T. & Sicinski, P. Cell cycle proteins as promising targets in cancer therapy. *Nat. Rev. Cancer* **17**, 93–115 (2017).

565. Chow, J. P. H., Poon, R. Y. C. & Ma, H. T. Inhibitory phosphorylation of cyclin-dependent kinase 1 as a compensatory mechanism for mitosis exit. *Mol. Cell. Biol.* **31**, 1478–1491 (2011).

566. Vassilopoulos, A. *et al.* WEE1 murine deficiency induces hyper-activation of APC/C and results in genomic instability and carcinogenesis. *Oncogene* **34**, 3023–3035 (2015).

567. Watanabe, N. WEE1. in *Encyclopedia of Signaling Molecules* 5986–5991 (Springer, Cham, 2018). doi:10.1007/978-3-319-67199-4_101526.

568. Katayama, K., Fujita, N. & Tsuruo, T. Akt/Protein Kinase B-Dependent Phosphorylation and Inactivation of WEE1Hu Promote Cell Cycle Progression at G2/M Transition. *Mol. Cell. Biol.* **25**, 5725–5737 (2005).

569. Mollapour, M., Tsutsumi, S. & Neckers, L. Hsp90 phosphorylation, Wee1, and the cell cycle. *Cell Cycle Georget. Tex* **9**, 2310–2316 (2010).

570. Friedman, J. *et al.* Inhibition of WEE1 kinase and cell cycle checkpoint activation sensitizes head and neck cancers to natural killer cell therapies. *J. Immunother. Cancer* **6**, 59 (2018).

571. He, H. *et al.* Inhibition of Wee1, AKT, and CDK4 underlies the efficacy of the HSP90 inhibitor XL888 in an in vivo model of NRAS-mutant melanoma. *Mol. Cancer Ther.* **12**, 901–912 (2013).

572. Osman, A. A. *et al.* Wee-1 kinase inhibition overcomes cisplatin resistance associated with high-risk TP53 mutations in head and neck cancer through mitotic arrest followed by senescence. *Mol. Cancer Ther.* **14**, 608–619 (2015).

573. Hans, F. & Dimitrov, S. Histone H3 phosphorylation and cell division. *Oncogene* **20**, 3021–3027 (2001).

574. Zhang, N. *et al.* p21-activated kinase 1 activity is required for histone H3 Ser10 phosphorylation and chromatin condensation in mouse oocyte meiosis. *Reprod. Fertil. Dev.* **29**, 1287–1296 (2017).

575. Park, C.-H. & Kim, K.-T. Apoptotic Phosphorylation of Histone H3 on Ser-10 by Protein Kinase Cδ. *PLOS ONE* **7**, e44307 (2012).

576. Zippo, A., De Robertis, A., Serafini, R. & Oliviero, S. PIM1-dependent phosphorylation of histone H3 at serine 10 is required for MYC-dependent transcriptional activation and oncogenic transformation. *Nat. Cell Biol.* **9**, 932–944 (2007).

577. Shen, Y., Vignali, P. & Wang, R. Rapid Profiling Cell Cycle by Flow Cytometry Using Concurrent Staining of DNA and Mitotic Markers. *Bio-Protoc.* **7**, (2017).

578. McLaughlin, M. *et al.* HSP90 inhibition sensitizes head and neck cancer to platin-based chemoradiotherapy by modulation of the DNA damage response resulting in chromosomal fragmentation. *BMC Cancer* **17**, 86 (2017).

579. Meek, D. W. Tumour suppression by p53: a role for the DNA damage response? *Nat. Rev. Cancer* **9**, 714–723 (2009).

580. Mc Gee, M. M. Targeting the Mitotic Catastrophe Signaling Pathway in Cancer. *Mediators Inflamm.* **2015**, (2015).

581. Cinege, G. *et al.* Cellular Immune Response Involving Multinucleated Giant Hemocytes with Two-Step Genome Amplification in the Drosophilid Zaprionus indianus. *J. Innate Immun.* **12**, 257–272 (2020).

582. Zajac, M., Moneo, M. V., Carnero, A., Benitez, J. & Martínez-Delgado, B. Mitotic catastrophe cell death induced by heat shock protein 90 inhibitor in BRCA1-deficient breast cancer cell lines. *Mol. Cancer Ther.* **7**, 2358–2366 (2008).

583. Moran, D. M., Gawlak, G., Jayaprakash, M. S., Mayar, S. & Maki, C. G. Geldanamycin promotes premature mitotic entry and micronucleation in irradiated p53/p21 deficient colon carcinoma cells. *Oncogene* **27**, 5567–5577 (2008).

584. O'Connell, B. C. *et al.* HSP90 Inhibition Enhances Antimitotic Drug-Induced Mitotic Arrest and Cell Death in Preclinical Models of Non-Small Cell Lung Cancer. *PLoS ONE* **9**, (2014).

585. Zaidi, S. *et al.* The HSP90 Inhibitor NVP-AUY922 Radiosensitizes by Abrogation of Homologous Recombination Resulting in Mitotic Entry with Unresolved DNA Damage. *PLOS ONE* **7**, e35436 (2012).

586. Yan, G., Elbadawi, M. & Efferth, T. Multiple cell death modalities and their key features (Review). *World Acad. Sci. J.* **2**, 39–48 (2020).

587. Hassan, M., Watari, H., AbuAlmaaty, A., Ohba, Y. & Sakuragi, N. Apoptosis and Molecular Targeting Therapy in Cancer. *BioMed Res. Int.* **2014**, (2014).

588. Sharma, A., Boise, L. H. & Shanmugam, M. Cancer Metabolism and the Evasion of Apoptotic Cell Death. *Cancers* **11**, (2019).

589. Plesca, D., Mazumder, S. & Almasan, A. DNA Damage Response and Apoptosis. *Methods Enzymol.* **446**, 107–122 (2008).

590. Lakshmanan, I. & Batra, S. K. Protocol for Apoptosis Assay by Flow Cytometry Using Annexin V Staining Method. *Bio-Protoc.* **3**, (2013).

591. Rieger, A. M., Nelson, K. L., Konowalchuk, J. D. & Barreda, D. R. Modified Annexin V/Propidium Iodide Apoptosis Assay For Accurate Assessment of Cell Death. *J. Vis. Exp. JoVE* (2011) doi:10.3791/2597.

592. Belmokhtar, C. A., Hillion, J. & Ségal-Bendirdjian, E. Staurosporine induces apoptosis through both caspase-dependent and caspase-independent mechanisms. *Oncogene* **20**, 3354–3362 (2001).

593. Shalini, S., Dorstyn, L., Dawar, S. & Kumar, S. Old, new and emerging functions of caspases. *Cell Death Differ.* **22**, 526–539 (2015).

594. Walsh, J. G. *et al.* Executioner caspase-3 and caspase-7 are functionally distinct proteases. *Proc. Natl. Acad. Sci. U. S. A.* **105**, 12815–12819 (2008).

595. Amundson, S. A. *et al.* An Informatics Approach Identifying Markers of Chemosensitivity in Human Cancer Cell Lines. *Cancer Res.* **60**, 6101–6110 (2000).

596. Yao, L., Iwai, M. & Furuta, I. Correlations of bcl-2 and p53 expression with the clinicopathological features in tongue squamous cell carcinomas. *Oral Oncol.* **35**, 56–62 (1999).

597. Li, R. *et al.* Targeting Antiapoptotic Bcl-2 Family Members with Cell-Permeable BH3 Peptides Induces Apoptosis Signaling and Death in Head and Neck Squamous Cell Carcinoma Cells. *Neoplasia N. Y. N* **9**, 801–811 (2007).

598. Lu, Z. & Xu, S. ERK1/2 MAP kinases in cell survival and apoptosis. *IUBMB Life* **58**, 621–631 (2006).

599. Smirnova, I. S., Chang, S. & Forsthuber, T. G. Prosurvival and proapoptotic functions of ERK1/2 activation in murine thymocytes in vitro. *Cell. Immunol.* **261**, 29 (2010).

600. Zhou, H., Li, X.-M., Meinkoth, J. & Pittman, R. N. Akt Regulates Cell Survival and Apoptosis at a Postmitochondrial Level. *J. Cell Biol.* **151**, 483–494 (2000).

601. Los, M., Maddika, S., Erb, B. & Schulze-Osthoff, K. Switching Akt: from survival signaling to deadly response. *BioEssays News Rev. Mol. Cell. Dev. Biol.* **31**, 492–495 (2009).

602. If not apoptosis, then what? Treatment-induced senescence and mitotic catastrophe in tumor cells. *Drug Resist. Updat.* **4**, 303–313 (2001).

603. Collado, M. & Serrano, M. Senescence in tumours: evidence from mice and humans. *Nat. Rev. Cancer* **10**, 51–57 (2010).

604. Ewald, J. A., Desotelle, J. A., Wilding, G. & Jarrard, D. F. Therapy-Induced Senescence in Cancer. *JNCI J. Natl. Cancer Inst.* **102**, 1536–1546 (2010).

605. Morgunova, G. V., Kolesnikov, A. V., Klebanov, A. A. & Khokhlov, A. N. Senescence-associated β-galactosidase—A biomarker of aging, DNA damage, or cell proliferation restriction? *Mosc. Univ. Biol. Sci. Bull.* **70**, 165–167 (2015).

606. Singh, R., George, J. & Shukla, Y. Role of senescence and mitotic catastrophe in cancer therapy. *Cell Div.* **5**, 4 (2010).

607. Todd, R. *et al.* Cell Cycle Dysregulation in Oral Cancer. *Crit. Rev. Oral Biol. Med.* **13**, 51–61 (2002).

608. Liu, S. *et al.* Senescence of human skin-derived precursors regulated by Akt-FOXO3-p27 KIP1 /p15 INK4b signaling. *Cell. Mol. Life Sci.* **72**, 2949–2960 (2015).

609. Abbas, T. & Dutta, A. p21 in cancer: intricate networks and multiple activities. *Nat. Rev. Cancer* **9**, 400–414 (2009).

610. Perri, F., Pisconti, S. & Della Vittoria Scarpati, G. P53 mutations and cancer: a tight linkage. *Ann. Transl. Med.* **4**, (2016).

611. Pfister, N. T. & Prives, C. Transcriptional Regulation by Wild-Type and Cancer-Related Mutant Forms of p53. *Cold Spring Harb. Perspect. Med.* **7**, (2017).

612. Correia-Melo, C. *et al.* Mitochondria are required for pro-ageing features of the senescent phenotype. *EMBO J.* **35**, 724–742 (2016).

613. Kim, H. S., Song, M.-C., Kwak, I. H., Park, T. J. & Lim, I. K. Constitutive induction of p-Erk1/2 accompanied by reduced activities of protein phosphatases 1 and 2A and MKP3 due to reactive oxygen species during cellular senescence. *J. Biol. Chem.* **278**, 37497–37510 (2003).

614. Halasi, M. *et al.* ROS inhibitor N-acetyl-l-cysteine antagonizes the activity of proteasome inhibitors. *Biochem. J.* **454**, 201–208 (2013).

615. Deschênes-Simard, X. *et al.* Tumor suppressor activity of the ERK/MAPK pathway by promoting selective protein degradation. *Genes Dev.* **27**, 900–915 (2013).

616. Zou, J. *et al.* Mechanisms shaping the role of ERK1/2 in cellular senescence. *Mol. Med. Rep.* **19**, 759–770 (2019).

617. Cagnol, S. & Chambard, J.-C. ERK and cell death: mechanisms of ERK-induced cell death--apoptosis, autophagy and senescence. *FEBS J.* **277**, 2–21 (2010).

618. Nogueira, V. *et al.* Akt determines replicative senescence and oxidative or oncogenic premature senescence and sensitizes cells to oxidative apoptosis. *Cancer Cell* **14**, 458–470 (2008).

619. Minamino, T., Miyauchi, H., Tateno, K., Kunieda, T. & Komuro, I. Akt-induced cellular senescence: implication for human disease. *Cell Cycle Georget. Tex* **3**, 449–451 (2004).

620. Chan, K. T. *et al.* A functional genetic screen defines the AKT-induced senescence signaling network. *Cell Death Differ.* **27**, 725–741 (2020).

621. Bent, E. H., Gilbert, L. A. & Hemann, M. T. A senescence secretory switch mediated by PI3K/AKT/mTOR activation controls chemoprotective endothelial secretory responses. *Genes Dev.* **30**, 1811–1821 (2016).

622. Astle, M. V. *et al.* AKT induces senescence in human cells via mTORC1 and p53 in the absence of DNA damage: implications for targeting mTOR during malignancy. *Oncogene* **31**, 1949–1962 (2012).

623. Activation of the PIK3CA/AKT Pathway Suppresses Senescence Induced by an Activated RAS Oncogene to Promote Tumorigenesis. *Mol. Cell* **42**, 36–49 (2011).

624. Childs, B. G., Baker, D. J., Kirkland, J. L., Campisi, J. & van Deursen, J. M. Senescence and apoptosis: dueling or complementary cell fates? *EMBO Rep.* **15**, 1139–1153 (2014).

625. What has senescence got to do with cancer? *Cancer Cell* **7**, 505–512 (2005).

626. Nagano, T. *et al.* Identification of cellular senescence-specific genes by comparative transcriptomics. *Sci. Rep.* **6**, (2016).

627. Seluanov, A. *et al.* Change of the death pathway in senescent human fibroblasts in response to DNA damage is caused by an inability to stabilize p53. *Mol. Cell. Biol.* **21**, 1552–1564 (2001).

628. Regulation of Survival Networks in Senescent Cells: From Mechanisms to Interventions. *J. Mol. Biol.* **431**, 2629–2643 (2019).

629. Yosef, R. *et al.* Directed elimination of senescent cells by inhibition of BCL-W and BCL-XL. *Nat. Commun.* **7**, 11190 (2016).

630. Kupcho, K. *et al.* A real-time, bioluminescent annexin V assay for the assessment of apoptosis. *Apoptosis* **24**, 184–197 (2019).

631. Chung, K. M. & Yu, S.-W. Interplay between autophagy and programmed cell death in mammalian neural stem cells. *BMB Rep.* **46**, 383–390 (2013).

632. Kourtis, N. & Tavernarakis, N. Autophagy and cell death in model organisms. *Cell Death Differ.* **16**, 21–30 (2009).

633. Law, B. Y. K. *et al.* Neferine induces autophagy-dependent cell death in apoptosis-resistant cancers via ryanodine receptor and Ca 2+ -dependent mechanism. *Sci. Rep.* **9**, 1–18 (2019).

634. Pal, S., Salunke-Gawalib, S. & Konkimallaa, V. B. Induction of Autophagic Cell Death in Apoptosis-resistant Pancreatic Cancer Cells using Benzo[α]phenoxazines Derivatives, 10-methyl-benzo[α]phenoxazine-5-one and benzo[α]phenoxazine-5-one. *Anticancer Agents Med. Chem.* **17**, 115–125 (2017).

635. Carew, J. S. *et al.* Targeting autophagy augments the anticancer activity of the histone deacetylase inhibitor SAHA to overcome Bcr-Abl-mediated drug resistance. *Blood* **110**, 313–322 (2007).

636. Katayama, M., Kawaguchi, T., Berger, M. S. & Pieper, R. O. DNA damaging agent-induced autophagy produces a cytoprotective adenosine triphosphate surge in malignant glioma cells. *Cell Death Differ.* **14**, 548–558 (2007).

637. Thorburn, A. Apoptosis and Autophagy: regulatory connections between two supposedly different processes. *Apoptosis Int. J. Program. Cell Death* **13**, 1–9 (2008).

638. Jung, S., Jeong, H. & Yu, S.-W. Autophagy as a decisive process for cell death. *Exp. Mol. Med.* **52**, 921–930 (2020).

639. White, E. Deconvoluting the context-dependent role for autophagy in cancer. *Nat. Rev. Cancer* **12**, 401–410 (2012).

640. Tan, Y.-Q., Zhang, J. & Zhou, G. Autophagy and its implication in human oral diseases. *Autophagy* **13**, 225–236 (2017).

641. Jiang, L. *et al.* Inhibition of autophagy augments chemotherapy in human salivary adenoid cystic carcinoma. *J. Oral Pathol. Med. Off. Publ. Int. Assoc. Oral Pathol. Am. Acad. Oral Pathol.* **43**, 265–272 (2014).

642. Nam, H. Y. *et al.* Radioresistant cancer cells can be conditioned to enter senescence by mTOR inhibition. *Cancer Res.* **73**, 4267–4277 (2013).

643. Wu, Y.-H. *et al.* Bortezomib enhances radiosensitivity in oral cancer through inducing autophagy-mediated TRAF6 oncoprotein degradation. *J. Exp. Clin. Cancer Res. CR* **37**, (2018).

644. Milano, V., Piao, Y., LaFortune, T. & Groot, J. de. Dasatinib-induced autophagy is enhanced in combination with temozolomide in glioma. *Mol. Cancer Ther.* **8**, 394–406 (2009).

645. Morita, M. *et al.* Dasatinib induces autophagy in mice with Bcr-Abl-positive leukemia. *Int. J. Hematol.* **105**, 335–340 (2017).

646. Le, X.-F., Mao, W., Lu, Z., Carter, B. Z. & Bast, R. C. Dasatinib Induces Autophagic Cell Death in Human Ovarian Cancer. *Cancer* **116**, 4980–4990 (2010).

647. Li, H. *et al.* Resistance to tyrosine kinase-targeted therapy in lung cancer: Autophagy and metabolic changes. *Meta Gene* **17**, S10 (2018).

648. p53 and autophagy contribute to dasatinib resistance in primary CLL lymphocytes. *Leuk. Res.* **35**, 99–102 (2011).

649. Kwon, Y., Kim, M., Jung, H. S., Kim, Y. & Jeoung, D. Targeting Autophagy for Overcoming Resistance to Anti-EGFR Treatments. *Cancers* **11**, (2019).

650. Kumar, A., Singh, U. K. & Chaudhary, A. Targeting autophagy to overcome drug resistance in cancer therapy. *Future Med. Chem.* **7**, 1535–1542 (2015).

651. Levy, J. M. M., Towers, C. G. & Thorburn, A. Targeting autophagy in cancer. *Nat. Rev. Cancer* **17**, 528–542 (2017).

652. Onorati, A. V., Dyczynski, M., Ojha, R. & Amaravadi, R. K. Targeting autophagy in cancer. *Cancer* **124**, 3307–3318 (2018).

653. Paha, J. *et al.* A novel potent autophagy inhibitor ECDD-S27 targets vacuolar ATPase and inhibits cancer cell survival. *Sci. Rep.* **9**, 1–16 (2019).

654. Xu, C. *et al.* Functional interaction of heat shock protein 90 and Beclin 1 modulates Toll-like receptor-mediated autophagy. *FASEB J. Off. Publ. Fed. Am. Soc. Exp. Biol.* **25**, 2700–2710 (2011).

655. Palacios, C., Martín-Pérez, R., López-Pérez, A. I., Pandiella, A. & López-Rivas, A. Autophagy inhibition sensitizes multiple myeloma cells to 17-dimethylaminoethylamino-17-demethoxygeldanamycin-induced apoptosis. *Leuk. Res.* **34**, 1533–1538 (2010).

656. MORI, M. *et al.* Hsp90 inhibitor induces autophagy and apoptosis in osteosarcoma cells. *Int. J. Oncol.* **46**, 47–54 (2014).

657. SNX-2112, an Hsp90 inhibitor, induces apoptosis and autophagy via degradation of Hsp90 client proteins in human melanoma A-375 cells. *Cancer Lett.* **318**, 180–188 (2012).

658. Xu, C. *et al.* Activation of the SphK1/ERK/p-ERK pathway promotes autophagy in colon cancer cells. *Oncol. Lett.* **15**, 9719–9724 (2018).

659. Shinojima, N., Yokoyama, T., Kondo, Y. & Kondo, S. Roles of the Akt/mTOR/p70S6K and ERK1/2 signaling pathways in curcumin-induced autophagy. *Autophagy* **3**, 635–637 (2007).

660. Gao, H. *et al.* Triptolide induces autophagy and apoptosis through ERK activation in human breast cancer MCF‑7 cells. *Exp. Ther. Med.* **15**, 3413–3419 (2018).

661. Sooro, M. A., Zhang, N. & Zhang, P. Targeting EGFR-mediated autophagy as a potential strategy for cancer therapy. *Int. J. Cancer* **143**, 2116–2125 (2018).

662. Filomeni, G., Zio, D. D. & Cecconi, F. Oxidative stress and autophagy: the clash between damage and metabolic needs. *Cell Death Differ.* **22**, 377–388 (2015).

663. Azad, M. B., Chen, Y. & Gibson, S. B. Regulation of autophagy by reactive oxygen species (ROS): implications for cancer progression and treatment. *Antioxid. Redox Signal.* **11**, 777–790 (2009).

664. Scherz-Shouval, R. & Elazar, Z. ROS, mitochondria and the regulation of autophagy. *Trends Cell Biol.* **17**, 422–427 (2007).

665. Timmermans, S., Souffriau, J. & Libert, C. A General Introduction to Glucocorticoid Biology. *Front. Immunol.* **10**, (2019).

666. Becker, D. E. Basic and Clinical Pharmacology of Glucocorticosteroids. *Anesth. Prog.* **60**, 25–32 (2013).

667. Schoneveld, O. J. L. M., Gaemers, I. C. & Lamers, W. H. Mechanisms of glucocorticoid signalling. *Biochim. Biophys. Acta BBA - Gene Struct. Expr.* **1680**, 114–128 (2004).

668. Lin, K.-T. & Wang, L.-H. New dimension of glucocorticoids in cancer treatment. *Steroids* **111**, 84–88 (2016).

669. Ponticelli, C. & Locatelli, F. Glucocorticoids in the Treatment of Glomerular Diseases. *Clin. J. Am. Soc. Nephrol. CJASN* **13**, 815–822 (2018).

670. Coutinho, A. E. & Chapman, K. E. The anti-inflammatory and immunosuppressive effects of glucocorticoids, recent developments and mechanistic insights. *Mol. Cell. Endocrinol.* **335**, 2–13 (2011).

671. Samuel, S., Nguyen, T. & Choi, H. A. Pharmacologic Characteristics of Corticosteroids. *J. Neurocritical Care* **10**, 53–59 (2017).

672. Alangari, A. A. Corticosteroids in the treatment of acute asthma. *Ann. Thorac. Med.* **9**, 187–192 (2014).

673. Stojan, G. & Petri, M. The risk benefit ratio of glucocorticoids in SLE: have things changed over the past 40 years? *Curr. Treat. Options Rheumatol.* **3**, 164–172 (2017).

674. Cutolo, M. Glucocorticoids and chronotherapy in rheumatoid arthritis. *RMD Open* **2**, (2016).

675. Kleyn, E. C. *et al.* Review of international psoriasis guidelines for the treatment of psoriasis: recommendations for topical corticosteroid treatments. *J. Dermatol. Treat.* **30**, 311–319 (2019).

676. Dubois-Camacho, K. *et al.* Glucocorticosteroid therapy in inflammatory bowel diseases: From clinical practice to molecular biology. *World J. Gastroenterol.* **23**, 6628–6638 (2017).

677. Rheault, M. N. Nephrotic Syndrome: Updates and Approaches to Treatment. *Curr. Treat. Options Pediatr.* **2**, 94–103 (2016).

678. Steiner, R. W. & Awdishu, L. Steroids in kidney transplant patients. *Semin. Immunopathol.* **33**, 157–167 (2011).

679. Cropley, A. & Weltman, M. The use of immunosuppression in autoimmune hepatitis: A current literature review. *Clin. Mol. Hepatol.* **23**, 22–26 (2017).

680. Hox, V. *et al.* Benefits and harm of systemic steroids for short- and long-term use in rhinitis and rhinosinusitis: an EAACI position paper. *Clin. Transl. Allergy* **10**, 1 (2020).

681. Moran, J. L., Graham, P. L., Rockliff, S. & Bersten, A. D. Updating the evidence for the role of corticosteroids in severe sepsis and septic shock: a Bayesian meta-analytic perspective. *Crit. Care* **14**, R134 (2010).

682. Choudhury, S. & Meeran, K. Glucocorticoid replacement in Addison disease. *Nat. Rev. Endocrinol.* **14**, 562–562 (2018).

683. Kim, S. Y. Diagnosis and Treatment of Hypopituitarism. *Endocrinol. Metab.* **30**, 443–455 (2015).

684. Lossignol, D. A little help from steroids in oncology. *J. Transl. Intern. Med.* **4**, 52–54 (2016).

685. Leppert, W. & Buss, T. The role of corticosteroids in the treatment of pain in cancer patients. *Curr. Pain Headache Rep.* **16**, 307–313 (2012).

686. Shih, A. & Jackson, K. C. Role of corticosteroids in palliative care. *J. Pain Palliat. Care Pharmacother.* **21**, 69–76 (2007).

687. Xiao, T. *et al.* Estrogen-regulated feedback loop limits the efficacy of estrogen receptor-targeted breast cancer therapy. *Proc. Natl. Acad. Sci. U. S. A.* **115**, 7869–7878 (2018).

688. Dai, C., Heemers, H. & Sharifi, N. Androgen Signaling in Prostate Cancer. *Cold Spring Harb. Perspect. Med.* **7**, (2017).

689. Smith, L. K. & Cidlowski, J. A. Glucocorticoid-induced apoptosis of healthy and malignant lymphocytes. *Prog. Brain Res.* **182**, 1–30 (2010).

690. Pufall, M. A. Glucocorticoids and Cancer. *Adv. Exp. Med. Biol.* **872**, 315–333 (2015).

691. Keith, B. D. Systematic review of the clinical effect of glucocorticoids on nonhematologic malignancy. *BMC Cancer* **8**, 84 (2008).

692. Karmakar, S., Jin, Y. & Nagaich, A. K. Interaction of glucocorticoid receptor (GR) with estrogen receptor (ER) α and activator protein 1 (AP1) in dexamethasone-mediated interference of ERα activity. *J. Biol. Chem.* **288**, 24020–24034 (2013).

693. Sahu, B. *et al.* FoxA1 specifies unique androgen and glucocorticoid receptor binding events in prostate cancer cells. *Cancer Res.* **73**, 1570–1580 (2013).

694. Rubenstein, N. M., Guan, Y., Woo, P. L. & Firestone, G. L. Glucocorticoid down-regulation of RhoA is required for the steroid-induced organization of the junctional complex and tight junction formation in rat mammary epithelial tumor cells. *J. Biol. Chem.* **278**, 10353–10360 (2003).

695. Zheng, Y., Izumi, K., Li, Y., Ishiguro, H. & Miyamoto, H. Contrary Regulation of Bladder Cancer Cell Proliferation and Invasion by Dexamethasone-Mediated Glucocorticoid Receptor Signals. *Mol. Cancer Ther.* **11**, 2621–2632 (2012).

696. Law, M. E. *et al.* Glucocorticoids and histone deacetylase inhibitors cooperate to block the invasiveness of basal-like breast cancer cells through novel mechanisms. *Oncogene* **32**, 1316–1329 (2013).

697. Yano, A., Fujii, Y., Iwai, A., Kageyama, Y. & Kihara, K. Glucocorticoids suppress tumor angiogenesis and in vivo growth of prostate cancer cells. *Clin. Cancer Res. Off. J. Am. Assoc. Cancer Res.* **12**, 3003–3009 (2006).

698. Lin, K.-T. *et al.* Glucocorticoids mediate induction of microRNA-708 to suppress ovarian cancer metastasis through targeting Rap1B. *Nat. Commun.* **6**, 5917 (2015).

699. Zhang, C. *et al.* Corticosteroid-induced chemotherapy resistance in urological cancers. *Cancer Biol. Ther.* **5**, 59–64 (2006).

700. Gorman, A. M., Hirt, U. A., Orrenius, S. & Ceccatelli, S. Dexamethasone pre-treatment interferes with apoptotic death in glioma cells. *Neuroscience* **96**, 417–425 (2000).

701. Sui, M., Chen, F., Chen, Z. & Fan, W. Glucocorticoids interfere with therapeutic efficacy of paclitaxel against human breast and ovarian xenograft tumors. *Int. J. Cancer* **119**, 712–717 (2006).

702. Rutz, H. P., Mariotta, M., Doeberitz, M. von K. & Mirimanoff, R. O. Dexamethasone-induced radioresistance occurring independent of human papilloma virus gene expression in cervical carcinoma cells. *Strahlenther. Onkol.* **174**, 71–74 (1998).

703. Zhang, C. *et al.* Dexamethasone desensitizes hepatocellular and colorectal tumours toward cytotoxic therapy. *Cancer Lett.* **242**, 104–111 (2006).

704. Gassler, N. *et al.* Dexamethasone-induced cisplatin and gemcitabine resistance in lung carcinoma samples treated ex vivo. *Br. J. Cancer* **92**, 1084–1088 (2005).

705. Azher, S. *et al.* The Non-Conventional Effects of Glucocorticoids in Cancer. *J. Cell. Physiol.* **231**, 2368–2373 (2016).

706. Biggadike, K. Fluticasone furoate/fluticasone propionate – different drugs with different properties. *Clin. Respir. J.* **5**, 183–184 (2011).

707. Biggadike, K. *et al.* X-ray crystal structure of the novel enhanced-affinity glucocorticoid agonist fluticasone furoate in the glucocorticoid receptor-ligand binding domain. *J. Med. Chem.* **51**, 3349–3352 (2008).

708. Mackie, A. E., Ventresca, G. P., Fuller, R. W. & Bye, A. Pharmacokinetics of intravenous fluticasone propionate in healthy subjects. *Br. J. Clin. Pharmacol.* **41**, 539–542 (1996).

709. Altman, S. A., Randers, L. & Rao, G. Comparison of Trypan Blue Dye Exclusion and Fluorometric Assays for Mammalian Cell Viability Determinations. *Biotechnol. Prog.* **9**, 671–674 (1993).

710. Zwolak, I. Comparison of three different cell viability assays for evaluation of vanadyl sulphate cytotoxicity in a Chinese hamster ovary K1 cell line. *Toxicol. Ind. Health* **32**, 1013–1025 (2016).

711. Šatkauskas, S., Jakštys, B., Ruzgys, P. & Jakutavičiūtė, M. Different Cell Viability Assays Following Electroporation In Vitro. in *Handbook of Electroporation* 1411–1424 (Springer, Cham, 2017). doi:10.1007/978-3-319-32886-7_140.

712. Chan, G. K. Y., Kleinheinz, T. L., Peterson, D. & Moffat, J. G. A Simple High-Content Cell Cycle Assay Reveals Frequent Discrepancies between Cell Number and ATP and MTS Proliferation Assays. *PLOS ONE* **8**, e63583 (2013).

713. Wang, P., Henning, S. M. & Heber, D. Limitations of MTT and MTS-based assays for measurement of antiproliferative activity of green tea polyphenols. *PloS One* **5**, e10202 (2010).

714. Singh, S. D. *et al.* Pharmacokinetics and systemic effects of inhaled fluticasone propionate in chronic obstructive pulmonary disease. *Br. J. Clin. Pharmacol.* **55**, 375–381 (2003).

715. Pierstorff, E. *et al.* Prevention of cisplatin-induced hearing loss by extended release fluticasone propionate intracochlear implants. *Int. J. Pediatr. Otorhinolaryngol.* **121**, 157–163 (2019).

716. Zhang, P. *et al.* Post-radiotherapy maintenance treatment with fluticasone propionate and salmeterol for lung cancer patients with grade III radiation pneumonitis. *Medicine (Baltimore)* **97**, (2018).

717. Henkenberens, C. *et al.* Inhalative steroids as an individual treatment in symptomatic lung cancer patients with radiation pneumonitis grade II after radiotherapy - a single-centre experience. *Radiat. Oncol. Lond. Engl.* **11**, 12 (2016).

718. Sun, C. *et al.* Regulation of p27Kip1 phosphorylation and G1 cell cycle progression by protein phosphatase PPM1G. *Am. J. Cancer Res.* **6**, 2207–2220 (2016).

719. Kamura, T. *et al.* Cytoplasmic ubiquitin ligase KPC regulates proteolysis of p27 Kip1 at G1 phase. *Nat. Cell Biol.* **6**, 1229–1235 (2004).

720. Patki, M. *et al.* Chronic p27 Kip1 Induction by Dexamethasone Causes Senescence Phenotype and Permanent Cell Cycle Blockade in Lung Adenocarcinoma Cells Over-expressing Glucocorticoid Receptor. *Sci. Rep.* **8**, 16006 (2018).

721. Kullmann, M. K. *et al.* The p27–Skp2 axis mediates glucocorticoid-induced cell cycle arrest in T-lymphoma cells. *Cell Cycle* **12**, 2625–2635 (2013).

722. Eto, I. Upstream molecular signaling pathways of p27 (Kip1) expression: Effects of 4-hydroxytamoxifen, dexamethasone, and retinoic acids. *Cancer Cell Int.* **10**, 3 (2010).

723. Wu, L. *et al.* Specific Small Molecule Inhibitors of Skp2-Mediated p27 Degradation. *Chem. Biol.* **19**, 1515–1524 (2012).

724. Mineta, H. *et al.* Low p27 expression correlates with poor prognosis for patients with oral tongue squamous cell carcinoma. *Cancer* **85**, 1011–1017 (1999).

725. Chen, Q. *et al.* Targeting the p27 E3 ligase SCF(Skp2) results in p27- and Skp2-mediated cell-cycle arrest and activation of autophagy. *Blood* **111**, 4690–4699 (2008).

726. Nakayama, K. *et al.* Skp2-mediated degradation of p27 regulates progression into mitosis. *Dev. Cell* **6**, 661–672 (2004).

727. Mahdey, H. M. *et al.* Cyclin D1 amplification in tongue and cheek squamous cell carcinoma. *Asian Pac. J. Cancer Prev. APJCP* **12**, 2199–2204 (2011).

728. Rasamny, J. J. *et al.* Cyclin D1 and FADD as biomarkers in head and neck squamous cell carcinoma. *Otolaryngol.--Head Neck Surg. Off. J. Am. Acad. Otolaryngol.-Head Neck Surg.* **146**, 923–931 (2012).

729. Wang, B. *et al.* Prognostic significance of cyclin D3 expression in malignancy patients: a meta-analysis. *Cancer Cell Int.* **19**, (2019).

730. Ausserlechner, M. J., Obexer, P., Böck, G., Geley, S. & Kofler, R. Cyclin D3 and c-MYC control glucocorticoid-induced cell cycle arrest but not apoptosis in lymphoblastic leukemia cells. *Cell Death Differ.* **11**, 165–174 (2004).

731. Goda, A. E., Erikson, R. L., Ahn, J.-S. & Kim, B.-Y. Induction of G1 Arrest by SB265610 Involves Cyclin D3 Down-regulation and Suppression of CDK2 (Thr160) Phosphorylation. *Anticancer Res.* **35**, 3235–3243 (2015).

732. Chiarle, R., Pagano, M. & Inghirami, G. The cyclin dependent kinase inhibitor p27 and its prognostic role in breast cancer. *Breast Cancer Res.* **3**, 91–94 (2001).

733. Bretones, G. *et al.* SKP2 Oncogene Is a Direct MYC Target Gene and MYC Down-regulates p27KIP1 through SKP2 in Human Leukemia Cells. *J. Biol. Chem.* **286**, 9815–9825 (2011).

734. Bhattacharya, N., Roy, A., Roy, B., Roychoudhury, S. & Panda, C. K. MYC gene amplification reveals clinical association with head and neck squamous cell carcinoma in Indian patients. *J. Oral Pathol. Med. Off. Publ. Int. Assoc. Oral Pathol. Am. Acad. Oral Pathol.* **38**, 759–763 (2009).

735. Pai, R. *et al.* Over-expression of c-Myc oncoprotein in oral squamous cell carcinoma in the South Indian population. *ecancermedicalscience* **3**, (2009).

736. Pallavi, N., Nalabolu, G. R. K. & Hiremath, S. K. S. Bcl-2 and c-Myc expression in oral dysplasia and oral squamous cell carcinoma: An immunohistochemical study to assess tumor progression. *J. Oral Maxillofac. Pathol. JOMFP* **22**, 325–331 (2018).

737. Trivedi, T. I. *et al.* Identification of site-specific prognostic biomarkers in patients with oral squamous cell carcinoma. *Neoplasma* **58**, 217–226 (2011).

738. Whitfield, J. R., Beaulieu, M.-E. & Soucek, L. Strategies to Inhibit Myc and Their Clinical Applicability. *Front. Cell Dev. Biol.* **5**, 10 (2017).

739. Allen-Petersen, B. L. & Sears, R. C. Mission Possible: Advances in MYC Therapeutic Targeting in Cancer. *BioDrugs* **33**, 539–553 (2019).

740. Kharenko, O. A. & Hansen, H. C. Novel approaches to targeting BRD4. *Drug Discov. Today Technol.* **24**, 19–24 (2017).

741. Tayyar, Y., Jubair, L., Fallaha, S. & McMillan, N. A. J. Critical risk-benefit assessment of the novel anti-cancer aurora a kinase inhibitor alisertib (MLN8237): A comprehensive review of the clinical data. *Crit. Rev. Oncol. Hematol.* **119**, 59–65 (2017).

742. Schmidt, S. *et al.* Identification of glucocorticoid-response genes in children with acute lymphoblastic leukemia. *Blood* **107**, 2061–2069 (2006).

743. Zhou, F., Medh, R. D. & Thompson, E. B. Glucocorticoid mediated transcriptional repression of c-myc in apoptotic human leukemic CEM cells. *J. Steroid Biochem. Mol. Biol.* **73**, 195–202 (2000).

744. Acosta, J. C. *et al.* Myc Inhibits p27-Induced Erythroid Differentiation of Leukemia Cells by Repressing Erythroid Master Genes without Reversing p27-Mediated Cell Cycle Arrest. *Mol. Cell. Biol.* **28**, 7286–7295 (2008).

745. Abdullah, C., Korkaya, H., Iizuka, S. & Courtneidge, S. A. SRC Increases MYC mRNA Expression in Estrogen Receptor-Positive Breast Cancer via mRNA Stabilization and Inhibition of p53 Function. *Mol. Cell. Biol.* **38**, (2018).

746. Martins, M. M. *et al.* Linking tumor mutations to drug responses via a quantitative chemical-genetic interaction map. *Cancer Discov.* **5**, 154–167 (2015).

747. Enserink, J. M. & Kolodner, R. D. An overview of Cdk1-controlled targets and processes. *Cell Div.* **5**, 11 (2010).

748. Schmidt, M. *et al.* Regulation of G2/M Transition by Inhibition of WEE1 and PKMYT1 Kinases. *Mol. J. Synth. Chem. Nat. Prod. Chem.* **22**, (2017).

749. Magnussen, G. I. *et al.* Combined inhibition of the cell cycle related proteins Wee1 and Chk1/2 induces synergistic anti-cancer effect in melanoma. *BMC Cancer* **15**, 462 (2015).

750. Li, J., Wang, Y., Wang, X. & Yang, Q. CDK1 and CDC20 overexpression in patients with colorectal cancer are associated with poor prognosis: evidence from integrated bioinformatics analysis. *World J. Surg. Oncol.* **18**, 50 (2020).

751. Bednarek, K. *et al.* Recurrent CDK1 overexpression in laryngeal squamous cell carcinoma. *Tumour Biol.* **37**, 11115–11126 (2016).

752. Kim, H.-Y. *et al.* Targeting the WEE1 kinase as a molecular targeted therapy for gastric cancer. *Oncotarget* **7**, 49902–49916 (2016).

753. Lin, Z. P., Zhu, Y.-L. & Ratner, E. S. Targeting Cyclin-Dependent Kinases for Treatment of Gynecologic Cancers. *Front. Oncol.* **8**, (2018).

754. Herrero-Ruiz, J. *et al.* βTrCP controls the lysosome-mediated degradation of CDK1, whose accumulation correlates with tumor malignancy. *Oncotarget* **5**, 7563–7574 (2014).

755. Sato, A. Y. *et al.* Glucocorticoids Induce Bone and Muscle Atrophy by Tissue-Specific Mechanisms Upstream of E3 Ubiquitin Ligases. *Endocrinology* **158**, 664–677 (2017).

756. Li, Z. *et al.* Development and Characterization of a Wee1 Kinase Degrader. *Cell Chem. Biol.* **27**, 57-65.e9 (2020).

757. Cook, A. M., McDonnell, A. M., Lake, R. A. & Nowak, A. K. Dexamethasone co-medication in cancer patients undergoing chemotherapy causes substantial immunomodulatory effects with implications for chemo-immunotherapy strategies. *Oncoimmunology* **5**, (2015).

758. Jessurun, C. A. C. *et al.* Evidence-based dexamethasone dosing in malignant brain tumors: what do we really know? *J. Neurooncol.* **144**, 249–264 (2019).

759. Chukwueke, U., Batchelor, T. & Brastianos, P. Management of Brain Metastases in Patients With Melanoma. *J. Oncol. Pract.* **12**, 536–542 (2016).

760. Li, C. K., Leung, A. W. K. & Lam, G. K. S. Prednisone and dexamethasone in acute lymphoblastic leukemia in children: which is the better option? *J. Xiangya Med.* **1**, (2016).

761. Alekseeva, I. A. *et al.* [Use of dexamethasone in treatment of high- and low-grade non-Hodgkin's lymphoma]. *Vopr. Onkol.* **50**, 726–728 (2004).

762. Stewart, A. K. *et al.* Carfilzomib, Lenalidomide, and Dexamethasone for Relapsed Multiple Myeloma. *N. Engl. J. Med.* **372**, 142–152 (2015).

763. Holder, S. L., Drabick, J., Zhu, J. & Joshi, M. Dexamethasone may be the most efficacious corticosteroid for use as monotherapy in castration-resistant prostate cancer. *Cancer Biol. Ther.* **16**, 207–209 (2015).

764. Wang, L. *et al.* Dexamethasone suppresses the growth of human non-small cell lung cancer via inducing estrogen sulfotransferase and inactivating estrogen. *Acta Pharmacol. Sin.* **37**, 845–856 (2016).

765. Jackson, R. *et al.* Dexamethasone Pharmacokinetics Following Standard and Short Dosing Schedules in Patients on the UKALL2011 Trial. *Blood* **130**, 101–101 (2017).

766. Spoorenberg, S. M. C. *et al.* Pharmacokinetics of oral vs. intravenous dexamethasone in patients hospitalized with community-acquired pneumonia. *Br. J. Clin. Pharmacol.* **78**, 78–83 (2014).

767. Samra, B., Jabbour, E., Ravandi, F., Kantarjian, H. & Short, N. J. Evolving therapy of adult acute lymphoblastic leukemia: state-of-the-art treatment and future directions. *J. Hematol. Oncol.J Hematol Oncol* **13**, (2020).

768. Shi, Y. *et al.* Phase II-like murine trial identifies synergy between dexamethasone and dasatinib in T-cell acute lymphoblastic leukemia. *Haematologica* (2020) doi:10.3324/haematol.2019.241026.

769. Scherr, M. *et al.* Optimized induction of mitochondrial apoptosis for chemotherapy-free treatment of BCR-ABL+acute lymphoblastic leukemia. *Leukemia* **33**, 1313–1323 (2019).

770. Wieduwilt, M. J. *et al.* A Phase II Study of Dasatinib and Dexamethasone As Primary Therapy Followed By Hematopoietic Cell Transplantation for Adults with Philadelphia Chromosome-Positive Acute Lymphoblastic Leukemia: CALGB Study 10701 (Alliance). *Blood* **128**, 2782–2782 (2016).

771. Wieduwilt, M. J. *et al.* A Phase II Study of Dasatinib and Dexamethasone As Primary Therapy Followed By Transplantation for Adults with Newly Diagnosed Ph/BCR-ABL1-Positive Acute Lymphoblastic Leukemia (Ph+ ALL): Final Results of Alliance/CALGB Study 10701. *Blood* **132**, 309–309 (2018).

772. Beppu, M., Ikebe, T. & Shirasuna, K. The inhibitory effects of immunosuppressive factors, dexamethasone and interleukin-4, on NF-kappaB-mediated protease production by oral cancer. *Biochim. Biophys. Acta* **1586**, 11–22 (2002).

773. Trask, O. J. Nuclear Factor Kappa B (NF-κB) Translocation Assay Development and Validation for High Content Screening. in *Assay Guidance Manual* (eds. Markossian, S. et al.) (Eli Lilly & Company and the National Center for Advancing Translational Sciences, 2004).

774. Lu, G. *et al.* Phosphorylation of ETS1 by Src Family Kinases Prevents Its Recognition by the COP1 Tumor Suppressor. *Cancer Cell* **26**, 222–234 (2014).

775. Yang, Z., Liao, J., Cullen, K. J. & Dan, H. Inhibition of IKKβ/NF-κB signaling pathway to improve Dasatinib efficacy in suppression of cisplatin-resistant head and neck squamous cell carcinoma. *Cell Death Discov.* **6**, (2020).

776. Dandona, P. *et al.* Effect of dexamethasone on reactive oxygen species generation by leukocytes and plasma interleukin-10 concentrations: a pharmacodynamic study. *Clin. Pharmacol. Ther.* **66**, 58–65 (1999).

777. Patki, M. *et al.* Glucocorticoid Receptor Status is a Principal Determinant of Variability in the Sensitivity of Non-Small Cell Lung Cancer Cells to Pemetrexed. *J. Thorac. Oncol. Off. Publ. Int. Assoc. Study Lung Cancer* **9**, 519–526 (2014).

778. Rosenzweig, S. A. Acquired Resistance to Drugs Targeting Tyrosine Kinases. *Adv. Cancer Res.* **138**, 71–98 (2018).

779. Tabata, M. *et al.* Dasatinib reverses drug resistance by downregulating MDR1 and Survivin in Burkitt lymphoma cells. *BMC Complement. Med. Ther.* **20**, (2020).

780. Hübner, M., Hochhaus, G. & Derendorf, H. Comparative pharmacology, bioavailability, pharmacokinetics, and pharmacodynamics of inhaled glucocorticosteroids. *Immunol. Allergy Clin. North Am.* **25**, 469–488 (2005).

781. Derendorf, H., Nave, R., Drollmann, A., Cerasoli, F. & Wurst, W. Relevance of pharmacokinetics and pharmacodynamics of inhaled corticosteroids to asthma. *Eur. Respir. J.* **28**, 1042–1050 (2006).

782. Winkler, J., Hochhaus, G. & Derendorf, H. How the lung handles drugs: pharmacokinetics and pharmacodynamics of inhaled corticosteroids. *Proc. Am. Thorac. Soc.* **1**, 356–363 (2004).

783. Jiang, L. *et al.* CAL 27 is an oral adenosquamous carcinoma cell line. *Oral Oncol.* **45**, e204–e207 (2009).

784. Hsiao, Y.-T. *et al.* Curcuminoids combined with gefitinib mediated apoptosis and autophagy of human oral cancer SAS cells in vitro and reduced tumor of SAS cell xenograft mice in vivo. *Environ. Toxicol.* **33**, 821–832 (2018).

785. Chen, Y.-F. *et al.* Establishing of mouse oral carcinoma cell lines derived from transgenic mice and their use as syngeneic tumorigenesis models. *BMC Cancer* **19**, 281 (2019).

786. Hsu, F.-T. *et al.* Synergistic Effect of Sorafenib and Radiation on Human Oral Carcinoma in vivo. *Sci. Rep.* **5**, 1–9 (2015).

787. Demétrio de Souza França, P. *et al.* Fluorescence-guided resection of tumors in mouse models of oral cancer. *Sci. Rep.* **10**, (2020).

788. Valotis, A. & Högger, P. Human receptor kinetics and lung tissue retention of the enhanced-affinity glucocorticoid fluticasone furoate. *Respir. Res.* **8**, 54 (2007).

789. Ardito, F., Giuliani, M., Perrone, D., Troiano, G. & Muzio, L. L. The crucial role of protein phosphorylation in cell signaling and its use as targeted therapy (Review). *Int. J. Mol. Med.* **40**, 271–280 (2017).

790. Ruprecht, B. & Lemeer, S. Proteomic analysis of phosphorylation in cancer. *Expert Rev. Proteomics* **11**, 259–267 (2014).

791. The 4G10, pY20 and p-TYR-100 antibody specificity: profiling by peptide microarrays. *New Biotechnol.* **29**, 571–577 (2012).

792. Ahsan, N. *et al.* Mass Spectrometry-Based Identification of Phospho-Tyr in Plant Proteomics. *J. Proteome Res.* **19**, 561–571 (2020).

793. Breitkopf, S. B. & Asara, J. M. Determining in vivo Phosphorylation Sites using Mass Spectrometry. *Curr. Protoc. Mol. Biol.* **CHAPTER**, Unit18.19 (2012).

794. Vemulapalli, V. *et al.* Time resolved quantitative phosphoproteomics reveals distinct patterns of SHP2 dependence in EGFR signaling. *bioRxiv* 598664 (2019) doi:10.1101/598664.

795. Valdés, A. & Lind, S. B. Mass Spectrometry-Based Analysis of Time-Resolved Proteome Quantification. *PROTEOMICS* **20**, 1800425 (2020).

796. Murai, M. *et al.* Overexpression of c-met in oral SCC promotes hepatocyte growth factor-induced disruption of cadherin junctions and invasion. *Int. J. Oncol.* **25**, 831–840 (2004).

797. Mori, S. *et al.* An Anchorage-Independent Cell Growth Signature Identifies Tumors with Metastatic Potential. *Oncogene* **28**, 2796–2805 (2009).

798. Thewke, D. P., Kou, J., Fulmer, M. L. & Xie, Q. The HGF/MET Signaling and Therapeutics in Cancer. in *Regulation of Signal Transduction in Human Cell Research* 155–181 (Springer, Singapore, 2018). doi:10.1007/978-981-10-7296-3_8.

799. Endo, K., Shirai, A., Furukawa, M. & Yoshizaki, T. Prognostic value of cell motility activation factors in patients with tongue squamous cell carcinoma. *Hum. Pathol.* **37**, 1111–1116 (2006).

800. Seiwert, T. *et al.* Phase II trial of single-agent foretinib (GSK1363089) in patients with recurrent or metastatic squamous cell carcinoma of the head and neck. *Invest. New Drugs* **31**, 417–424 (2013).

801. Puccini, A. *et al.* Safety and Tolerability of c-MET Inhibitors in Cancer. *Drug Saf.* **42**, 211–233 (2019).

802. Choueiri, T. K. *et al.* Cabozantinib Versus Sunitinib As Initial Targeted Therapy for Patients With Metastatic Renal Cell Carcinoma of Poor or Intermediate Risk: The Alliance A031203 CABOSUN Trial. *J. Clin. Oncol.* **35**, 591–597 (2017).

803. Bouattour, M. *et al.* Recent developments of c-Met as a therapeutic target in hepatocellular carcinoma. *Hepatology* **67**, 1132–1149 (2018).

804. Sierra, J. R. & Tsao, M.-S. c-MET as a potential therapeutic target and biomarker in cancer. *Ther. Adv. Med. Oncol.* **3**, S21–S35 (2011).

805. Zhang, Z., Yang, S. & Wang, Q. Impact of MET alterations on targeted therapy with EGFR-tyrosine kinase inhibitors for EGFR-mutant lung cancer. *Biomark. Res.* **7**, 1–7 (2019).

806. Wang, Q., Yang, S., Wang, K. & Sun, S.-Y. MET inhibitors for targeted therapy of EGFR TKI-resistant lung cancer. *J. Hematol. Oncol.J Hematol Oncol* **12**, 63 (2019).

807. Phase II Study of Tivantinib and Cetuximab in Patients With KRAS Wild-type Metastatic Colorectal Cancer With Acquired Resistance to EGFR Inhibitors and Emergence of MET Overexpression: Lesson Learned for Future Trials With EGFR/MET Dual Inhibition. *Clin. Colorectal Cancer* **18**, 125-132.e2 (2019).

808. Huang, K. & Liu, D. Suppression of c-MET overcomes erlotinib resistance in tongue cancer cells. *OncoTargets Ther.* **11**, 5499–5508 (2018).

809. Foy, J.-P., Bertolus, C., William, W. N. & Saintigny, P. Oral Premalignancy: The Roles of Early Detection and Chemoprevention. *Otolaryngol. Clin. North Am.* **46**, 579–597 (2013).

810. Tao, X. *et al.* Silencing Met receptor tyrosine kinase signaling decreased oral tumor growth and increased survival of nude mice. *Oral Oncol.* **50**, 104–112 (2014).

811. Baschnagel, A. M. *et al.* Crizotinib Fails to Enhance the Effect of Radiation in Head and Neck Squamous Cell Carcinoma Xenografts. *Anticancer Res.* **35**, 5973–5982 (2015).

812. Stabile, L. P. *et al.* c-Src Activation Mediates Erlotinib Resistance in Head and Neck Cancer by Stimulating c-Met. *Clin. Cancer Res. Off. J. Am. Assoc. Cancer Res.* **19**, 380–392 (2013).

813. Sen, B., Peng, S., Saigal, B., Williams, M. D. & Johnson, F. M. Distinct Interactions Between c-Src and c-Met in Mediating Resistance to c-Src Inhibition in Head and Neck Cancer. *Clin. Cancer Res.* **17**, 514–524 (2011).

814. Xu, H. *et al.* Dual Blockade of EGFR and c-Met Abrogates Redundant Signaling and Proliferation in Head and Neck Carcinoma Cells. *Clin. Cancer Res.* **17**, 4425–4438 (2011).

815. Steinway, S. N., Dang, H., You, H., Rountree, C. B. & Ding, W. The EGFR/ErbB3 Pathway Acts as a Compensatory Survival Mechanism upon c-Met Inhibition in Human c-Met+ Hepatocellular Carcinoma. *PLOS ONE* **10**, e0128159 (2015).

816. Oren, I., Fleishman, S. J., Kessel, A. & Ben-Tal, N. Free Diffusion of Steroid Hormones Across Biomembranes: A Simplex Search with Implicit Solvent Model Calculations. *Biophys. J.* **87**, 768–779 (2004).

817. McManus, J. M. *et al.* Rapid and structure-specific cellular uptake of selected steroids. *PLOS ONE* **14**, e0224081 (2019).

818. Stahn, C. & Buttgereit, F. Genomic and nongenomic effects of glucocorticoids. *Nat. Clin. Pract. Rheumatol.* **4**, 525–533 (2008).

819. De Bosscher, K. *et al.* Selective modulation of the glucocorticoid receptor can distinguish between transrepression of NF-κB and AP-1. *Cell. Mol. Life Sci. CMLS* **71**, 143–163 (2014).

820. Marchetti, M. C., Di Marco, B., Cifone, G., Migliorati, G. & Riccardi, C. Dexamethasone-induced apoptosis of thymocytes: role of glucocorticoid receptor–associated Src kinase and caspase-8 activation. *Blood* **101**, 585–593 (2003).

821. Shi, W. *et al.* Glucocorticoid receptor–IRS-1 axis controls EMT and the metastasis of breast cancers. *J. Mol. Cell Biol.* **11**, 1042–1055 (2019).

822. Kassel, O. *et al.* Glucocorticoids inhibit MAP kinase via increased expression and decreased degradation of MKP-1. *EMBO J.* **20**, 7108–7116 (2001).

823. Han, S. *et al.* Dexamethasone Inhibits TGF-β1–Induced Cell Migration by Regulating the ERK and AKT Pathways in Human Colon Cancer Cells Via CYR61. *Cancer Res. Treat. Off. J. Korean Cancer Assoc.* **48**, 1141–1153 (2016).

824. Greenberg, A. K. *et al.* Glucocorticoids Inhibit Lung Cancer Cell Growth through Both the Extracellular Signal-Related Kinase Pathway and Cell Cycle Regulators. *Am. J. Respir. Cell Mol. Biol.* **27**, 320–328 (2002).

825. Inhibition of extracellular signal-regulated kinase (ERK) signaling participates in repression of nuclear factor (NF)-κB activity by glucocorticoids. *Biochim. Biophys. Acta BBA - Mol. Cell Res.* **1793**, 439–446 (2009).

826. Andrade, M. V. M., Hiragun, T. & Beaven, M. A. Dexamethasone suppresses antigen-induced activation of phosphatidylinositol 3-kinase and downstream responses in mast cells. *J. Immunol. Baltim. Md 1950* **172**, 7254–7262 (2004).

827. Huang, G.-X., Qi, M.-F., Li, X.-L., Tang, F. & Zhu, L. Involvement of upregulation of fibronectin in the pro‑adhesive and pro‑survival effects of glucocorticoid on melanoma cells. *Mol. Med. Rep.* **17**, 3380–3387 (2018).

828. Yin, L. *et al.* The pro-adhesive and pro-survival effects of glucocorticoid in human ovarian cancer cells. *J. Mol. Endocrinol.* **57**, 61–72 (2016).

829. Pan, X. *et al.* The mechanism and significance of synergistic induction of the expression of plasminogen activator inhibitor-1 by glucocorticoid and transforming growth factor beta in human ovarian cancer cells. *Mol. Cell. Endocrinol.* **407**, 37–45 (2015).

830. Zhang, Y. *et al.* Function of the c-Met receptor tyrosine kinase in carcinogenesis and associated therapeutic opportunities. *Mol. Cancer* **17**, (2018).

831. Kim, H.-P. *et al.* Lapatinib, a Dual EGFR and HER2 Tyrosine Kinase Inhibitor, Downregulates Thymidylate Synthase by Inhibiting the Nuclear Translocation of EGFR and HER2. *PLoS ONE* **4**, (2009).

832. Cameron, D. *et al.* A phase III randomized comparison of lapatinib plus capecitabine versus capecitabine alone in women with advanced breast cancer that has progressed on trastuzumab: updated efficacy and biomarker analyses. *Breast Cancer Res. Treat.* **112**, 533–543 (2008).

833. Geyer, C. E. *et al.* Lapatinib plus capecitabine for HER2-positive advanced breast cancer. *N. Engl. J. Med.* **355**, 2733–2743 (2006).

834. Khademi, B. *et al.* The expression of p53, c-erbB-1 and c-erbB-2 molecules and their correlation with prognostic markers in patients with head and neck tumors. *Cancer Lett.* **184**, 223–230 (2002).

835. Randomised Phase II study of oral lapatinib combined with chemoradiotherapy in patients with advanced squamous cell carcinoma of the head and neck: Rationale for future randomised trials in human papilloma virus-negative disease. *Eur. J. Cancer* **49**, 1609–1618 (2013).

836. Study Of Adjuvant Lapatinib In High-Risk Head And Neck Cancer Subjects After Surgery - Full Text View - ClinicalTrials.gov. https://clinicaltrials.gov/ct2/show/NCT00424255.

837. Lenz, H.-J. Cetuximab in the management of colorectal cancer. *Biol. Targets Ther.* **1**, 77–91 (2007).

838. Péron, J. *et al.* Paclitaxel and cetuximab combination efficiency after the failure of a platinum-based chemotherapy in recurrent/metastatic head and neck squamous cell carcinoma. *Anticancer. Drugs* **23**, 996–1001 (2012).

839. Hitt, R. *et al.* Phase II study of the combination of cetuximab and weekly paclitaxel in the first-line treatment of patients with recurrent and/or metastatic squamous cell carcinoma of head and neck. *Ann. Oncol. Off. J. Eur. Soc. Med. Oncol.* **23**, 1016–1022 (2012).

840. Fracasso, P. M. *et al.* A Phase 1 Escalating Single-Dose and Weekly Fixed-Dose Study of Cetuximab: Pharmacokinetic and Pharmacodynamic Rationale for Dosing. *Clin. Cancer Res.* **13**, 986–993 (2007).

841. Hsu, Y.-F. *et al.* Complement activation mediates cetuximab inhibition of non-small cell lung cancer tumor growth in vivo. *Mol. Cancer* **9**, 139 (2010).

842. Noris, M. & Remuzzi, G. Overview of Complement Activation and Regulation. *Semin. Nephrol.* **33**, 479–492 (2013).

843. Weiss, J. M. *et al.* Capecitabine and lapatinib for the first-line treatment of metastatic/recurrent head and neck squamous cell carcinoma. *Cancer* **122**, 2350–2355 (2016).

844. Yang, H. *et al.* Combination of cetuximab with met inhibitor in control of cetuximab-resistant oral squamous cell carcinoma. *Am. J. Transl. Res.* **11**, 2370–2381 (2019).

845. Kaup, B. *et al.* Time-dependent inhibition of glioblastoma cell proliferation by dexamethasone. *J. Neurooncol.* **51**, 105–110 (2001).

846. Li, H. *et al.* Glucocorticoid Receptor and Sequential P53 Activation by Dexamethasone Mediates Apoptosis and Cell Cycle Arrest of Osteoblastic MC3T3-E1 Cells. *PLOS ONE* **7**, e37030 (2012).

847. Up-regulation of RhoB by glucocorticoids and its effects on the cell proliferation and NF-κB transcriptional activity. *J. Steroid Biochem. Mol. Biol.* **101**, 179–187 (2006).

848. Brandts, C. H., Bilanges, B., Hare, G., McCormick, F. & Stokoe, D. Phosphorylation-independent stabilization of p27kip1 by the phosphoinositide 3-kinase pathway in glioblastoma cells. *J. Biol. Chem.* **280**, 2012–2019 (2005).

849. Goel, S., DeCristo, M. J., McAllister, S. S. & Zhao, J. J. CDK4/6 inhibition in cancer: beyond cell cycle arrest. *Trends Cell Biol.* **28**, 911–925 (2018).

850. Wang, D. *et al.* Antiproliferative effects of the CDK6 inhibitor PD0332991 and its effect on signaling networks in gastric cancer cells. *Int. J. Mol. Med.* **41**, 2473–2484 (2018).

851. Huang, X. *et al.* Prolonged early G1 arrest by selective CDK4/CDK6 inhibition sensitizes myeloma cells to cytotoxic killing through cell cycle–coupled loss of IRF4. *Blood* **120**, 1095–1106 (2012).

852. Kim, S. *et al.* The potent and selective cyclin-dependent kinases 4 and 6 inhibitor ribociclib (LEE011) is a versatile combination partner in preclinical cancer models. *Oncotarget* **9**, 35226–35240 (2018).

853. Buss, H. *et al.* Cyclin-dependent kinase 6 phosphorylates NF-κB P65 at serine 536 and contributes to the regulation of inflammatory gene expression. *PloS One* **7**, e51847 (2012).

854. Handschick, K. *et al.* Cyclin-dependent kinase 6 is a chromatin-bound cofactor for NF-κB-dependent gene expression. *Mol. Cell* **53**, 193–208 (2014).

855. Hantschel, O. CDK6 degradation hits Ph+ ALL hard. *Blood* **135**, 1512–1514 (2020).

856. Patil, G. B. *et al.* Cyclin B1 overexpression in conventional oral squamous cell carcinoma and verrucous carcinoma-A correlation with clinicopathological features. *Med. Oral Patol. Oral Cir. Bucal* **18**, e585–e590 (2013).

857. Hassan, K. A. *et al.* Clinical Significance of Cyclin B1 Protein Expression in Squamous Cell Carcinoma of the Tongue. *Clin. Cancer Res.* **7**, 2458–2462 (2001).

858. Ramnath, N. Induction of Senescence using Dexamethasone to re-sensitize NSCLC to anti-PD1 therapy. *Grantome*.

859. Ge, H. *et al.* Dexamethasone alleviates pemetrexed-induced senescence in Non-Small-Cell Lung Cancer. *Food Chem. Toxicol. Int. J. Publ. Br. Ind. Biol. Res. Assoc.* **119**, 86–97 (2018).

860. Ge, H. *et al.* Dexamethasone Reduces Sensitivity to Cisplatin by Blunting p53-Dependent Cellular Senescence in Non-Small Cell Lung Cancer. *PLoS ONE* **7**, (2012).

861. Tao, Y.-F. *et al.* Molecular mechanism of G1 arrest and cellular senescence induced by LEE011, a novel CDK4/CDK6 inhibitor, in leukemia cells. *Cancer Cell Int.* **17**, 35 (2017).

862. Rader, J. *et al.* Dual CDK4/CDK6 Inhibition Induces Cell Cycle Arrest and Senescence in Neuroblastoma. *Clin. Cancer Res. Off. J. Am. Assoc. Cancer Res.* **19**, (2013).

863. Schmidt, S. *et al.* Glucocorticoid-induced apoptosis and glucocorticoid resistance: molecular mechanisms and clinical relevance. *Cell Death Differ.* **11**, S45–S55 (2004).

864. Greenstein, S., Ghias, K., Krett, N. L. & Rosen, S. T. Mechanisms of glucocorticoid-mediated apoptosis in hematological malignancies. *Clin. Cancer Res. Off. J. Am. Assoc. Cancer Res.* **8**, 1681–1694 (2002).

865. Hou, W. *et al.* The effects of dexamethasone on the proliferation and apoptosis of human ovarian cancer cells induced by paclitaxel. *J. Ovarian Res.* **7**, (2014).

866. Chen, Y.-X. *et al.* Dexamethasone enhances cell resistance to chemotherapy by increasing adhesion to extracellular matrix in human ovarian cancer cells. *Endocr. Relat. Cancer* **17**, 39–50 (2010).

867. Wagenblast, J. *et al.* Does Dexamethasone Inhibit the Antineoplastic Effect of Cisplatin and Docetaxel in Head and Neck Cancer Cells? *Anticancer Res.* **30**, 123–127 (2010).

868. Castri, P. *et al.* Poly(ADP-ribose) polymerase-1 and its cleavage products differentially modulate cellular protection through NF-kB-dependent signaling. *Biochim. Biophys. Acta BBA - Mol. Cell Res.* **1843**, 640–651 (2014).

869. Piao, L., Fujioka, K., Nakakido, M. & Hamamoto, R. Regulation of poly(ADP-Ribose) polymerase 1 functions by post-translational modifications. *Front. Biosci. Landmark Ed.* **23**, 13–26 (2018).

870. Chapman, J. D., Gagné, J.-P., Poirier, G. G. & Goodlett, D. R. Mapping PARP-1 Auto-ADP-ribosylation Sites by Liquid Chromatography–Tandem Mass Spectrometry. *J. Proteome Res.* **12**, 1868–1880 (2013).

871. Xu, J. *et al.* miR-221/222-Mediated Inhibition of Autophagy Promotes Dexamethasone Resistance in Multiple Myeloma. *Mol. Ther.* **27**, 559–570 (2019).

872. Laane, E. *et al.* Cell death induced by dexamethasone in lymphoid leukemia is mediated through initiation of autophagy. *Cell Death Differ.* **16**, 1018–1029 (2009).

873. Jiang, L. *et al.* Inhibition of autophagy overcomes glucocorticoid resistance in lymphoid malignant cells. *Cancer Biol. Ther.* **16**, 466–476 (2015).

874. Bonapace, L. *et al.* Induction of autophagy-dependent necroptosis is required for childhood acute lymphoblastic leukemia cells to overcome glucocorticoid resistance. *J. Clin. Invest.* **120**, 1310–1323 (2010).

875. Teuffel, O. *et al.* Dexamethasone versus prednisone for induction therapy in childhood acute lymphoblastic leukemia: a systematic review and meta-analysis. *Leukemia* **25**, 1232–1238 (2011).

876. Labar, B. *et al.* Dexamethasone compared to prednisolone for adults with acute lymphoblastic leukemia or lymphoblastic lymphoma: final results of the ALL-4 randomized, phase III trial of the EORTC Leukemia Group. *Haematologica* **95**, 1489–1495 (2010).

877. Inaba, H. & Pui, C.-H. Glucocorticoid use in acute lymphoblastic leukaemia. *Lancet Oncol.* **11**, 1096–1106 (2010).

878. Warris, L. T. *et al.* Hydrocortisone as an Intervention for Dexamethasone-Induced Adverse Effects in Pediatric Patients With Acute Lymphoblastic Leukemia: Results of a Double-Blind, Randomized Controlled Trial. *J. Clin. Oncol.* **34**, 2287–2293 (2016).

879. Williams, D. M. Clinical Pharmacology of Corticosteroids. *Respir. Care* **63**, 655–670 (2018).

880. Werumeus Buning, J. *et al.* Pharmacokinetics of oral hydrocortisone - Results and implications from a randomized controlled trial. *Metabolism.* **71**, 7–16 (2017).

881. Siddiraju, S., Lal Prasanth, M. L. & Sirisha, T. A novel LC–MS/MS assay for methylprednisolone in human plasma and its pharmacokinetic application. *Asian J. Pharm. Sci.* **11**, 459–468 (2016).

882. Pettit, A. R. *et al.* Alemtuzumab in combination with methylprednisolone is a highly effective induction regimen for patients with chronic lymphocytic leukemia and deletion of TP53: final results of the national cancer research institute CLL206 trial. *J. Clin. Oncol. Off. J. Am. Soc. Clin. Oncol.* **30**, 1647–1655 (2012).

883. Whole-brain radiotherapy and high-dose methylprednisolone for elderly patients with primary central nervous system lymphoma: Results of North Central Cancer Treatment Group (NCCTG) 96-73-51. *Int. J. Radiat. Oncol.* **65**, 1429–1439 (2006).

884. Harr, M. *et al.* Inhibition of Lck enhances glucocorticoid sensitivity and apoptosis in lymphoid cell lines and in chronic lymphocytic leukemia. *Cell Death Differ.* **17**, 1381–1391 (2010).

885. Serafin, V. *et al.* Glucocorticoid resistance is reverted by LCK inhibition in pediatric T-cell acute lymphoblastic leukemia. *Blood* **130**, 2750–2761 (2017).

886. Combining dasatinib with dexamethasone long-term leads to maintenance of antiviral and antileukemia specific cytotoxic T cell responses in vitro. *Exp. Hematol.* **41**, 604-614.e4 (2013).

887. Quintás-Cardama, A. *et al.* Pleural Effusion in Patients With Chronic Myelogenous Leukemia Treated With Dasatinib After Imatinib Failure. *J. Clin. Oncol.* **25**, 3908–3914 (2007).

888. Fitzgerald, D. B. *et al.* Steroid therapy and outcome of parapneumonic pleural effusions (STOPPE): Study protocol for a multicenter, double-blinded, placebo-controlled randomized clinical trial. *Medicine (Baltimore)* **98**, e17397 (2019).

889. Herrmann, H. *et al.* Glucocorticosteroids Rescue Basophils from Dasatinib-Augmented Immunoglobulin E-Mediated Histamine Release. *Int. Arch. Allergy Immunol.* **159**, 15–22 (2012).

890. He, Y. *et al.* Discovery of a highly potent glucocorticoid for asthma treatment. *Cell Discov.* **1**, 1–13 (2015).

891. Nehoff, H., Parayath, N. N., McConnell, M. J., Taurin, S. & Greish, K. A combination of tyrosine kinase inhibitors, crizotinib and dasatinib for the treatment of glioblastoma multiforme. *Oncotarget* **6**, 37948–37964 (2015).

892. Dasatinib and Crizotinib in Advanced Cancer - Full Text View - ClinicalTrials.gov. https://clinicaltrials.gov/ct2/show/NCT01744652.

893. Wei, L., Yang, Y., Zhang, X. & Yu, Q. Anchorage-independent phosphorylation of p130Cas protects lung adenocarcinoma cells from anoikis. *J. Cell. Biochem.* **87**, 439–449 (2002).

894. Wei, L., Yang, Y., Zhang, X. & Yu, Q. Cleavage of p130Cas in anoikis. *J. Cell. Biochem.* **91**, 325–335 (2004).

895. Pribic, J. & Brazill, D. Paxillin phosphorylation and complexing with Erk and FAK are regulated by PLD activity in MDA-MB-231 cells. *Cell. Signal.* **24**, 1531–1540 (2012).

896. Wu, D.-W. *et al.* Paxillin promotes tumor progression and predicts survival and relapse in oral cavity squamous cell carcinoma by microRNA-218 targeting. *Carcinogenesis* **35**, 1823–1829 (2014).

897. Shekhar, S. & Angadi, P. V. Evaluation of paxillin expression in patients with oral squamous cell carcinoma: An immunohistochemical study. *J. Oral Maxillofac. Pathol. JOMFP* **21**, 318–319 (2017).

898. Wagner, M. J., Stacey, M. M., Liu, B. A. & Pawson, T. Molecular mechanisms of SH2- and PTB-domain-containing proteins in receptor tyrosine kinase signaling. *Cold Spring Harb. Perspect. Biol.* **5**, a008987 (2013).

899. Kaneko, T., Joshi, R., Feller, S. M. & Li, S. S. Phosphotyrosine recognition domains: the typical, the atypical and the versatile. *Cell Commun. Signal.* **10**, 32 (2012).

900. Machida, K. & Mayer, B. J. The SH2 domain: versatile signaling module and pharmaceutical target. *Biochim. Biophys. Acta* **1747**, 1–25 (2005).

901. Lu, X.-L., Cao, X., Liu, X.-Y. & Jiao, B.-H. Recent progress of Src SH2 and SH3 inhibitors as anticancer agents. *Curr. Med. Chem.* **17**, 1117–1124 (2010).

902. Machida, K., Khenkhar, M. & Nollau, P. Deciphering Phosphotyrosine-Dependent Signaling Networks in Cancer by SH2 Profiling. *Genes Cancer* **3**, 353–361 (2012).

903. Blagoev, B. *et al.* A proteomics strategy to elucidate functional protein-protein interactions applied to EGF signaling. *Nat. Biotechnol.* **21**, 315–318 (2003).

904. Machida, K. *et al.* Characterizing Tyrosine Phosphorylation Signaling in Lung Cancer Using SH2 Profiling. *PLoS ONE* **5**, (2010).

905. Wu, Y., Li, Q. & Chen, X.-Z. Detecting protein–protein interactions by far western blotting. *Nat. Protoc.* **2**, 3278–3284 (2007).

906. Machida, K., Mayer, B. J. & Nollau, P. Profiling the Global Tyrosine Phosphorylation State. *Mol. Cell. Proteomics* **2**, 215–233 (2003).

907. Jadwin, J. A., Mayer, B. J. & Machida, K. Detection and quantification of protein-protein interactions by far-western blotting. *Methods Mol. Biol. Clifton NJ* **1312**, 379–398 (2015).

908. Ben-Izhak, O., Cohen-Kaplan, V. & Nagler, R. M. The prognostic role of phospho-Src family kinase analysis in tongue cancer. *J. Cancer Res. Clin. Oncol.* **136**, 27–34 (2010).

909. Dotto, G. P. & Rustgi, A. K. Squamous cell cancers: a unified perspective on biology and genetics. *Cancer Cell* **29**, 622–637 (2016).

Supplemental Data
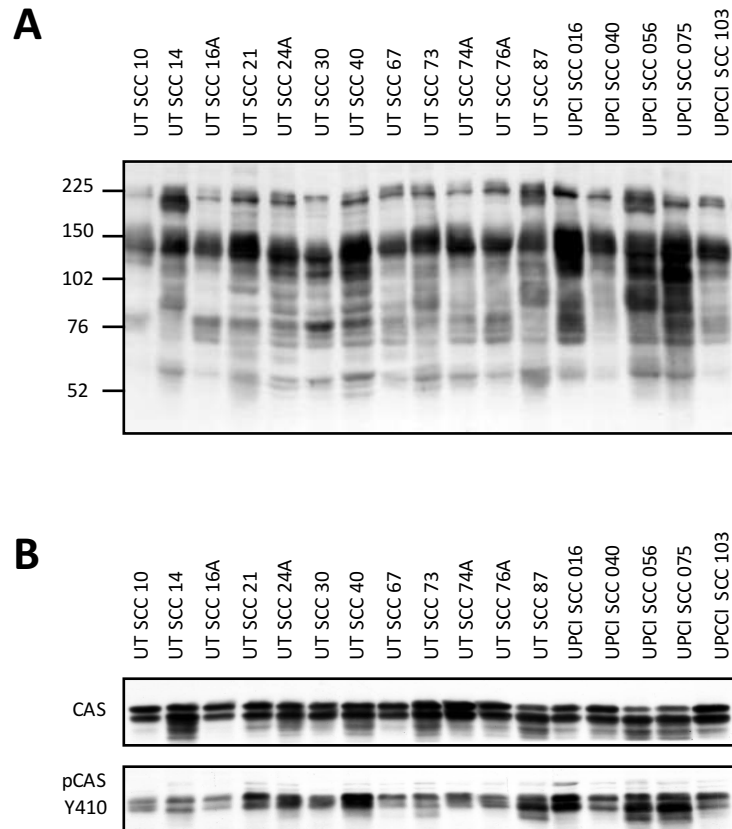
Figure S1. p130CAS is highly expressed in a panel of tongue squamous carcinoma cells

(A) Tyrosine phosphorylation profile for a TSCC line panel displays a prominent phosphorylated band at around 130 kDa
Equal amounts of total lysates from 17 TSCC lines were separated by SDS-PAGE and analyzed by Western blotting with an anti-phosphotyrosine antibody (4G10).

(B) p130CAS is prominently expressed in this panel of TSCC and highly phosphorylated
Total cell lysates were separated by SDS-PAGE and analyzed by Western blotting. Immunoblots were probed as indicated with antibodies against phospho and total p130CAS.

DAS 400 nM	DAS 2 µM	DAS 10 µM
TIMOLOL MALEATE	GENTIAN VIOLET	OXYQUINOLINE SULFATE
	BLEOMYCIN	CHLORHEXIDINE DIHYDROCHLORIDE
	CETYLPYRIDINIUM CHLORIDE	TESTOSTERONE PROPIONATE
	LISINOPRIL	PROPIOLACTONE
	NIKETHAMIDE	SPARTEINE SULFATE
	METHOTREXATE(+/-)	BEPHENIUM HYDROXYNAPTHOATE
	LOFEXIDINE HYDROCHLORIDE	ETHISTERONE
	MEFEXAMIDE HYDROCHLORIDE	TRICLABENDAZOLE
	METHOXAMINE HYDROCHLORIDE	PROGLUMIDE
	ETOPOSIDE	MEGLUMINE
	NORETHINDRONE	PYRIDOSTIGMINE BROMIDE
	MOLINDONE HYDROCHLORIDE	
	PIRACETAM	
	OCTODRINE	
	PHENINDIONE	
	MEFENAMIC ACID	
	LONIDAMINE	
	METRONIDAZOLE	

> ADRENERGIC RECEPTOR AGONIST
> SEROTONINE/DOPAMINE
> ANTHELMINTICS
> STEROIDS
> CNS

Figure S2. High-throughput screening results for compounds acting synergistically with DAS in CAL27 cells

1600 compounds at 3 different concentrations with or without DAS were tested against CAL27 cell line. Cells were treated for 72 h and the viability was quantified by resazurin calorimetric assay. Different colors represent target groups of potentially synergistic compounds (Marc Lewitzky, Oxford University).

DAS 400 nM	DAS 2 µM	DAS 10 µM
VINCRISTINE SULFATE	VINBLASTINE SULFATE	VINBLASTINE SULFATE
PUROMYCIN DIHYDROCHLORIDE	VINCRISTINE SULFATE	VINCRISTINE SULFATE
PIZOTYLINE MALATE	COLFORSIN	AZACITIDINE
	FLUTICASONE PROPIONATE	CYCLOSPORINE
	TRIACETIN	SELAMECTIN
	ISOPROTERENOL HYDROCHLORIDE	THIOGUANINE
		BENZYL ISOTHIOCYANATE
		COLFORSIN
		METHYLPHENIDATE HYDROCHLORIDE
		NITROXOLINE
		COLCHICINE
		DORAMECTIN
		FLUTICASONE PROPIONATE
		THONZONIUM BROMIDE
		CHLOROACETOXYQUINOLINE
		NICORANDIL
		TERCONAZOLE
		METHYLBENZETHONIUM CHLORIDE
		FENOTEROL HYDROBROMIDE
		LEVODOPA
		RACTOPAMINE HYDROCHLORIDE
		TYLOXAPOL
		PODOFILOX
		PHENACETIN

ADRENERGIC RECEPTOR AGONIST
GLUCOCORTICOIDS
SEROTONINE/DOPAMINE
ANTHELMINTICS

Figure S3. High-throughput screening results for compounds acting synergistically with DAS in BICR56 cells

1600 compounds at 3 different concentrations with or without DAS were tested against BICR56 cell line. Cells were treated for 72 h and the viability was quantified by resazurin calorimetric assay. Different colors represent target groups of potentially synergistic compounds. β-adrenergic agonists and Glucocorticoids also appear for SAS cells (Marc Lewitzky, Oxford University).
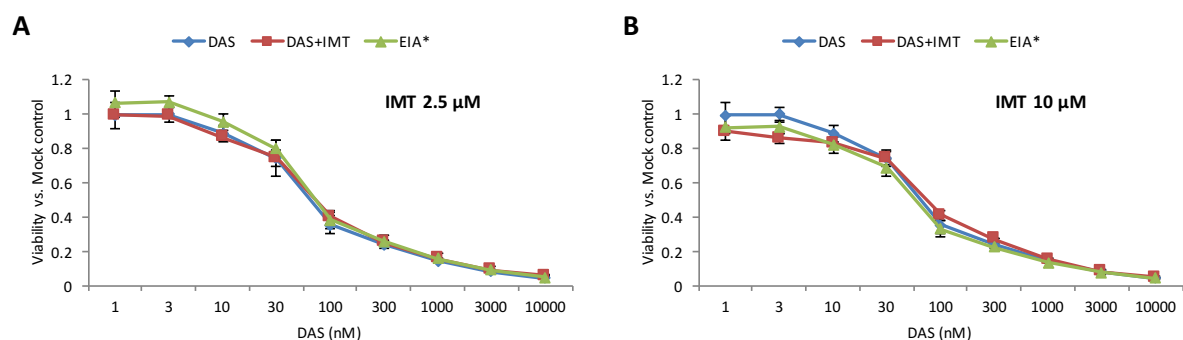
Figure S4. IMT shows no additional activity when added to DAS in 2D cultured CAL27 cells

CAL27 cells were treated with a serial dilution of DAS and the indicated concentration of IMT for 72 h. Cell inhibition activity of DAS, as measured by resazurin calorimetric assay, was not detectably improved by the addition of 2.5 µM or 10 µM of IMT. Data represent fluorescence measurements normalized to Mock-treated cells. The dose response curves show mean values ± SD of three independent experiments.
*Expected If Additive (EIA).
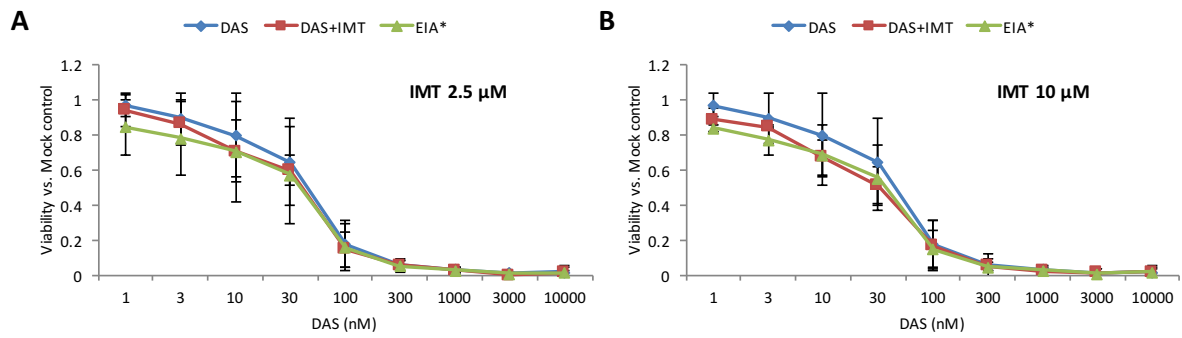
Figure S5. IMT shows no additional activity when added to DAS in 2D cultured BICR56 cells

BICR56 cells were treated with a serial dilution of DAS and the indicated concentration of IMT for 72 h. Cell inhibition activity of DAS, as measured by resazurin calorimetric assay, was not detectably improved by the addition of 2.5 µM or 10 µM of IMT. Data represent fluorescence measurements normalized to Mock-treated cells. The dose response curves show mean values ± SD of three independent experiments.
*Expected If Additive (EIA)
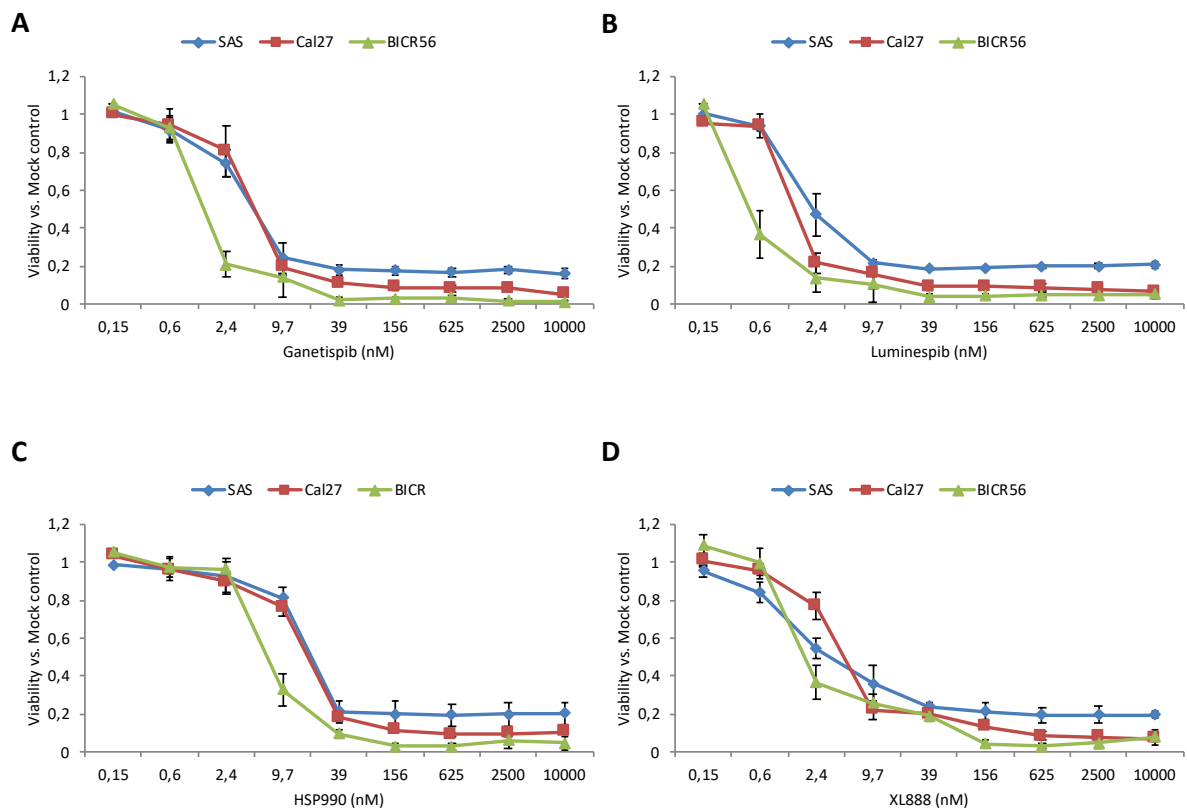
Figure S6. HSP90 inhibitors reduce TSCC line viabilities in a dose-dependent manner

TSCC lines were treated with serial dilutions of (A) Ganetispib, (B) Luminespib, (C) HSP990 or (D) XL888 for 72 h and analyzed via resazurin calorimetric assay. Data represent fluorescence measurements normalized to Mock-treated cells. The dose response curves show mean values ± SD of three independent experiments with six parallel measurements in each case.
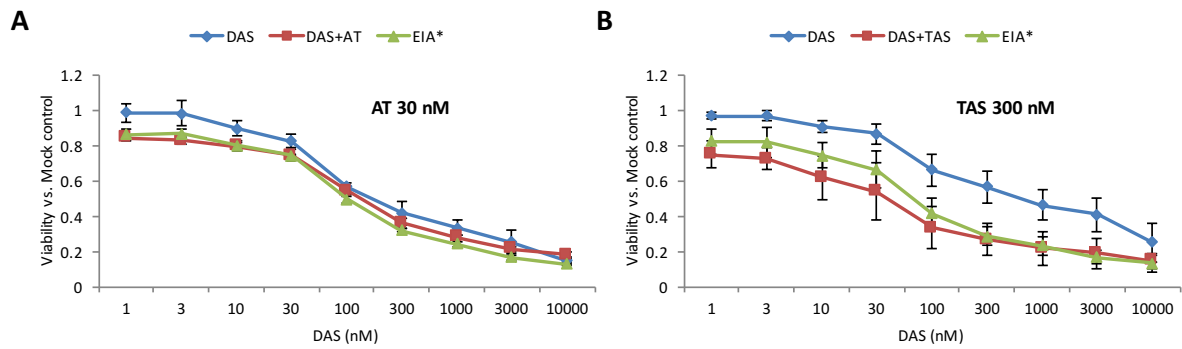
Figure S7. Combined treatment with DAS and HSP90 inhibitors demonstrates an additive or a weak synergistic effect on CAL27 cell line viability

CAL27 cells were treated with serial dilutions of DAS plus (A) 30 nM of AT or (B) 300 nM of TAS for 72 h. Cell viability after treatment was measured by resazurin calorimetric assay. The cell inhibition activities of DAS alone and HSP90 inhibitors alone were measured within the same experiment and used to calculate the expected values. Data represent fluorescence measurements normalized to Mock-treated cells. The dose response curves show mean values ± SD of three independent experiments with six parallel measurements in each case.

*Expected If Additive (EIA)
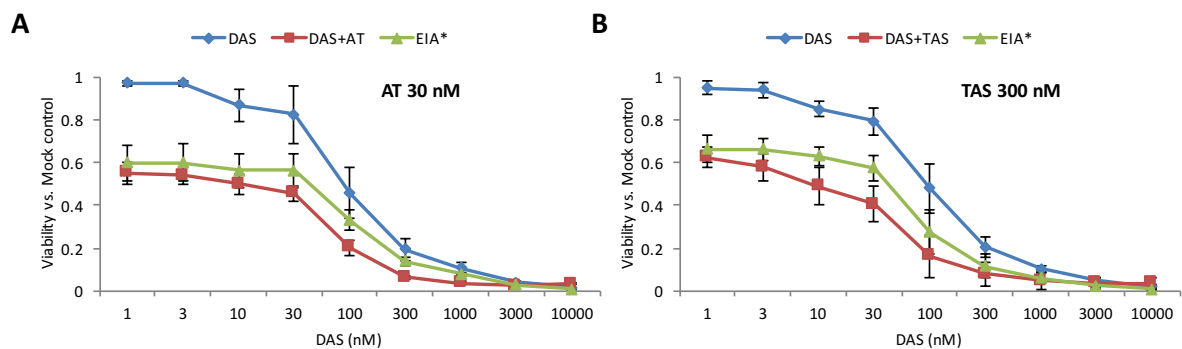
Figure S8. Combined treatment with DAS and HSP90 inhibitors demonstrates an additive or a weak synergistic effect on BICR56 cell line viability

BICR56 cells were treated with serial dilutions of DAS plus (A) 30 nM of AT or (B) 300 nM of TAS for 72 h. Cell viability after treatment was measured by resazurin calorimetric assay. The cell inhibition activities of DAS alone and HSP90 inhibitors alone were measured within the same experiment and used to calculate the expected values. Data represent fluorescence measurements normalized to Mock-treated cells. The dose response curves show mean values ± SD of three independent experiments with six parallel measurements in each case.

*Expected If Additive (EIA)
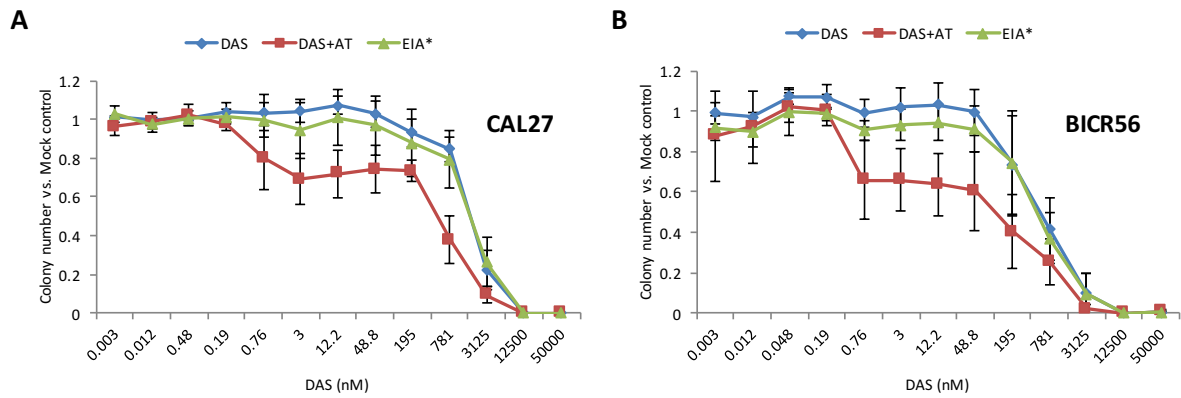
Figure S9. 3D soft agar colony formation assay shows that AT potentiates the colony formation reduction activity of DAS in TSCCs

Colony numbers for DAS alone and AT alone were counted within the same experiment and used to calculate the expected values by multiplying of the cell colony fractions. Data represent means of colony numbers normalized to Mock-treated cells. The dose response curves show mean values ± SD of three independent experiments. 2 to 4 wells were counted in each case.
*Expected If Additive (EIA)
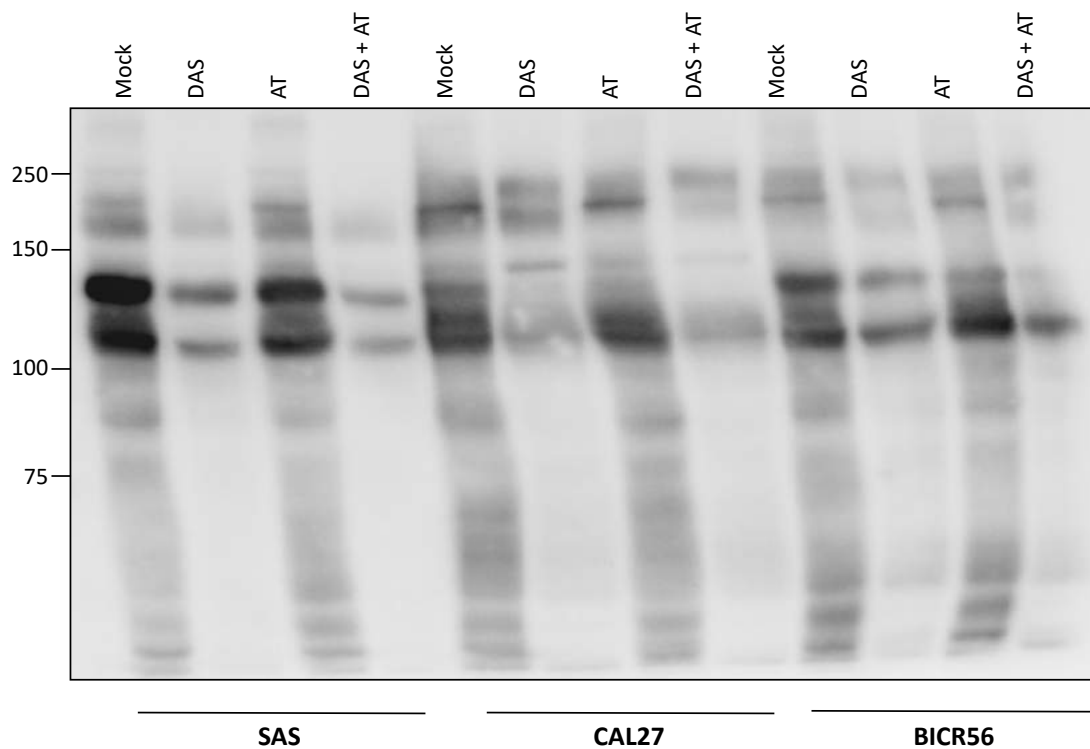
Figure S10. Tyrosine phosphorylation profile for treated TSCC lines shows depletion in phosphorylated proteins upon DAS and DAS+AT treatments

Cells were treated with DMSO as vehicle control (Mock), 50 nM of DAS, 30 nM of AT or DAS+AT for 72 h before extraction. Total cell lysates were separated by 8 % SDS-PAGE and immunoblots were probed with anti-phosphotyrosine antibody 4G10. Protein size markers are indicated on the left.
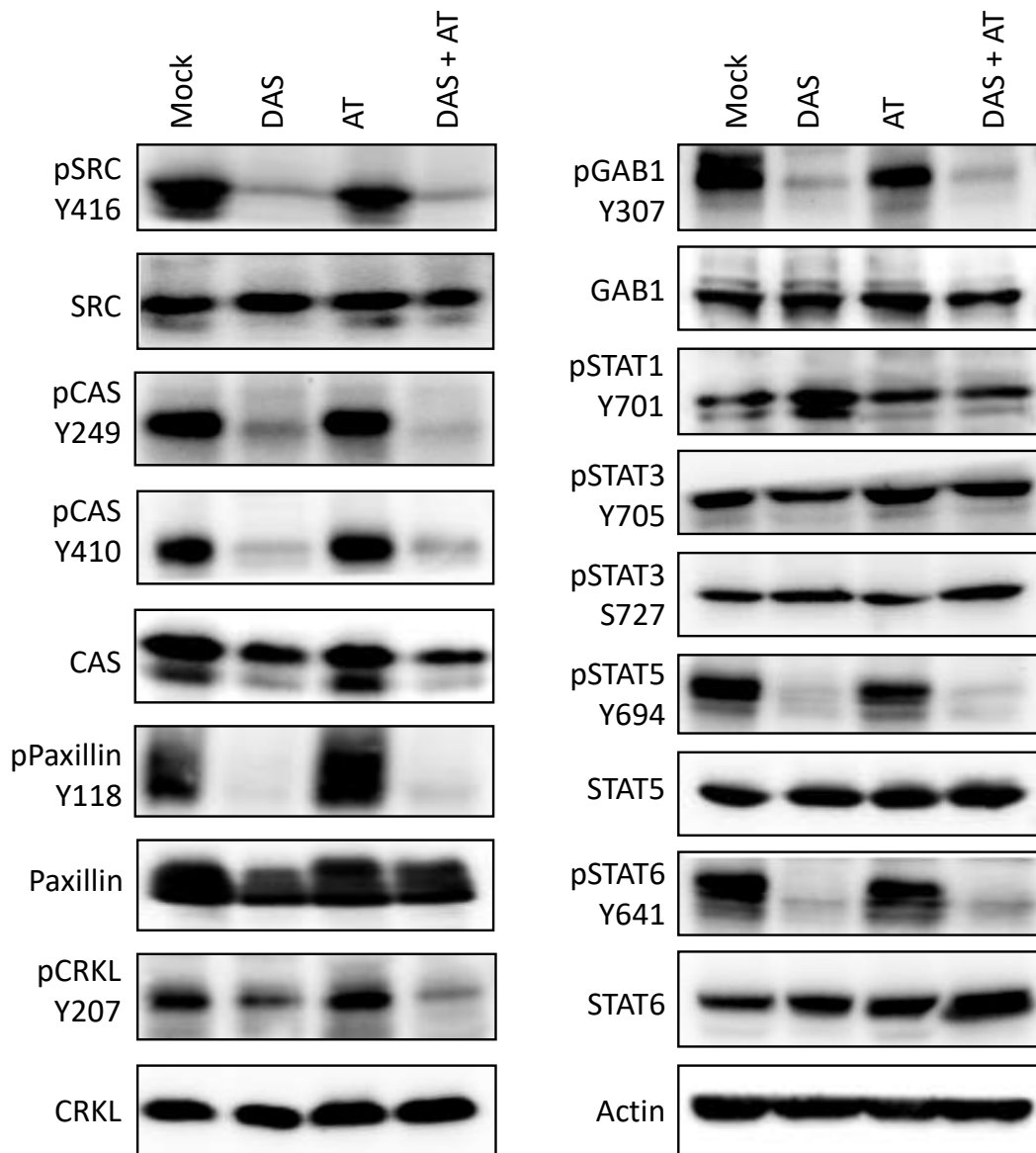
Figure S11. DAS, but not AT, blocks SRC downstream target phosphorylation in CAL27 cells

CAL27 cells were treated for 72 h with DMSO as vehicle control (Mock), 50 nM of DAS, 30 nM of AT, or a combination of DAS+AT. Total cell lysates were generated, separated by SDS-PAGE and analyzed by Western blotting. Antibodies that detect the phosphorylated state of p130CAS at Tyr249 and Tyr410, Paxillin at Tyr118, CRKL at Tyr207, GAB1 at Tyr307, STAT1 at Tyr701, STAT3 at Tyr705 and Ser727, STAT5 at Tyr694 and STAT6 at Tyr641 were used to monitor the changes in phosphorylation. The other blots analyzed total protein abundance. The blots shown in this figure are representative of three independent experiments.
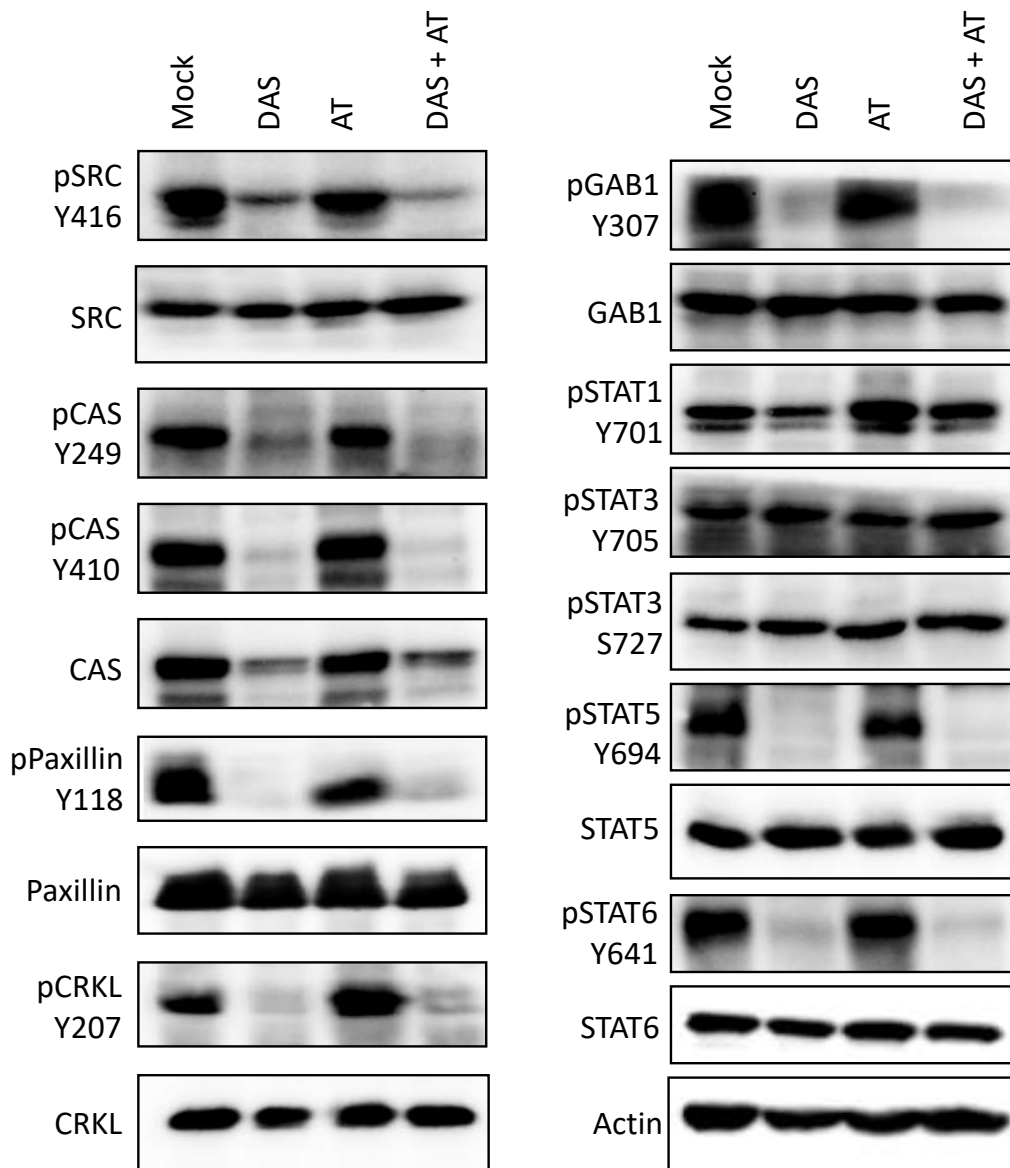
Figure S12. DAS, but not AT, blocks SRC downstream target phosphorylation in BICR56 cells

BICR56 cells were treated for 72 h with DMSO as vehicle control (Mock), 50 nM of DAS, 30 nM of AT, or a combination of DAS+AT. Total cell lysates were generated, separated by SDS-PAGE and analyzed by Western blotting. Antibodies that detect the phosphorylated state of p130CAS at Tyr249 and Tyr410, Paxillin at Tyr118, CRKL at Tyr207, GAB1 at Tyr307, STAT1 at Tyr701, STAT3 at Tyr705 and Ser727, STAT5 at Tyr694 and STAT6 at Tyr641 were used to monitor the changes in phosphorylation. The other blots analyzed total protein abundance. The blots shown in this figure are representative of three independent experiments.
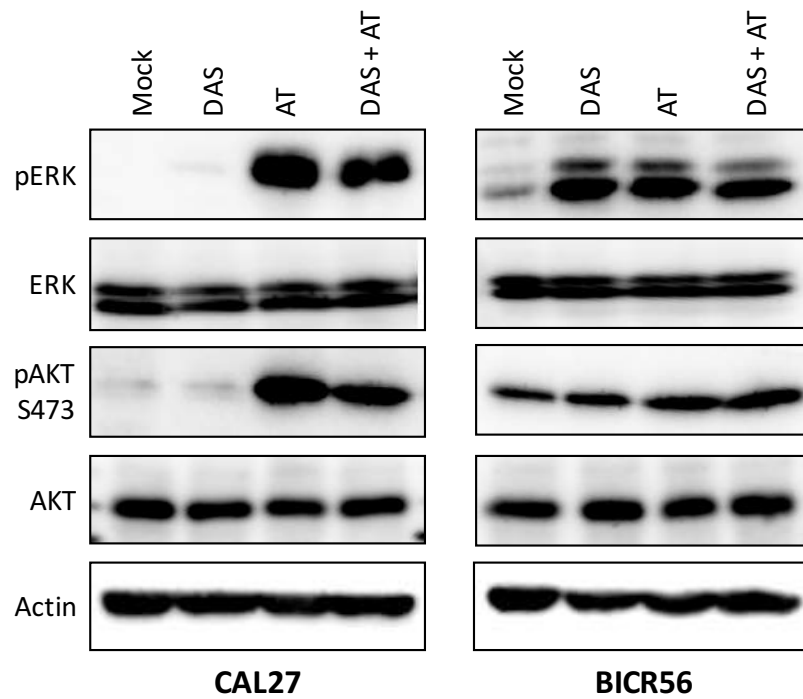
Figure S13. Combination treatment with DAS+AT increases MAPK phosphorylation in TSCCs

Cells were treated for 72 h with DMSO as vehicle control (Mock), 50 nM of DAS, 30 nM of AT, or a combination of DAS+AT. Total cell lysates were generated, separated by SDS-PAGE and analyzed by Western blotting. Antibodies that detect the phosphorylated state of ERK1/2 at Thr202/Tyr204 and AKT at Ser473 were used to detect the change in the phosphorylation. The other blots analyzed total protein abundance. The blots shown here are representative of three independent experiments.
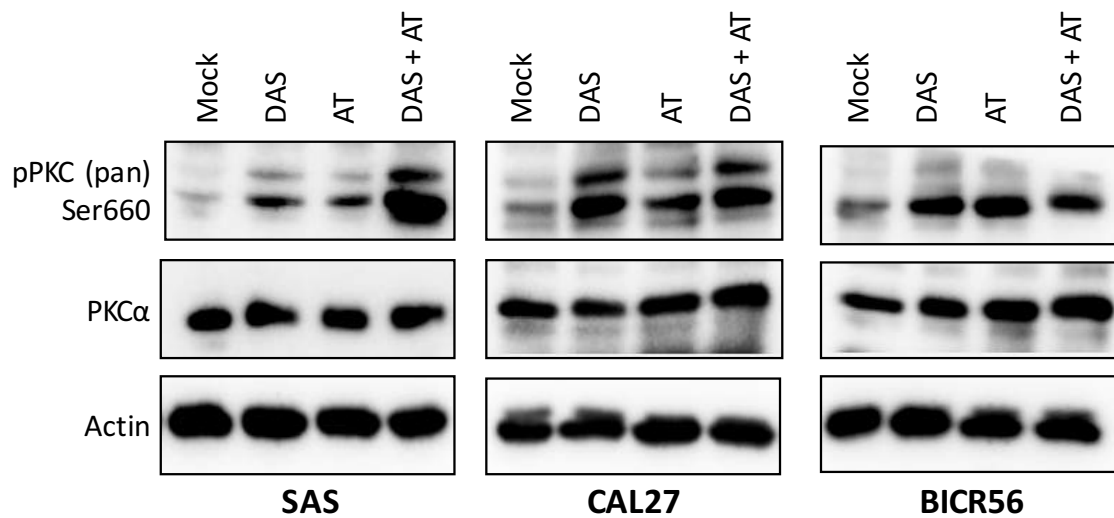
Figure S14. DAS+AT combination treatment increases PKC phosphorylation in TSCCs

Cells were treated for 72 h with DMSO as vehicle control (Mock), 50 nM of DAS, 30 nM of AT, or a combination of DAS+AT. Total cell lysates were generated, separated by SDS-PAGE and analyzed by Western blotting. An antibody that detects the phosphorylated state of PKC α, β I, β II, δ, ε, η and θ isoforms only when phosphorylated at a carboxy-terminal residue homologous to serine 660 of PKC β II was used to recognise the change in the phosphorylation state. The other blots analyzed total protein abundance. The blots shown here are representative of three independent experiments.
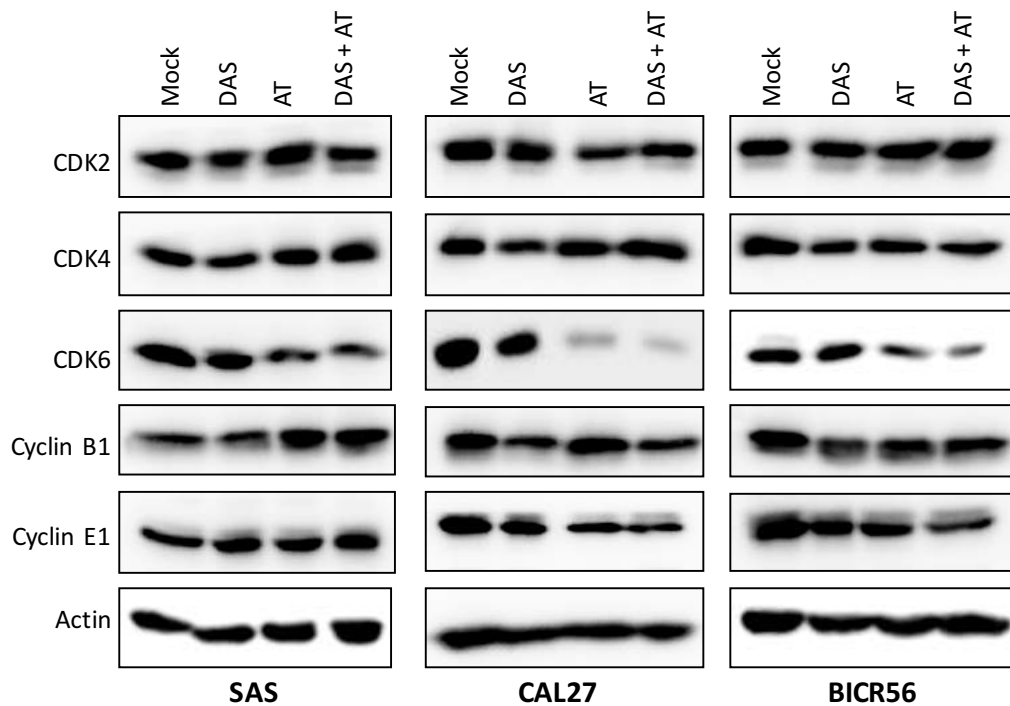
Figure S15. Treatment of TSCC lines with DAS and AT induces CDK6 degradation but have no significant effects on CDK2, CDK4, Cyclin B1, Cyclin E1 expression levels

Cells were treated with DMSO as vehicle control (Mock), 50 nM of DAS, 30 nM of AT, or a combination of DAS+AT for 72 h. Total cell lysates were generated, separated b SDS-PAGE and cell cycle-related proteins were analyzed by Western blotting. The blots shown are representative of three independent experiments.
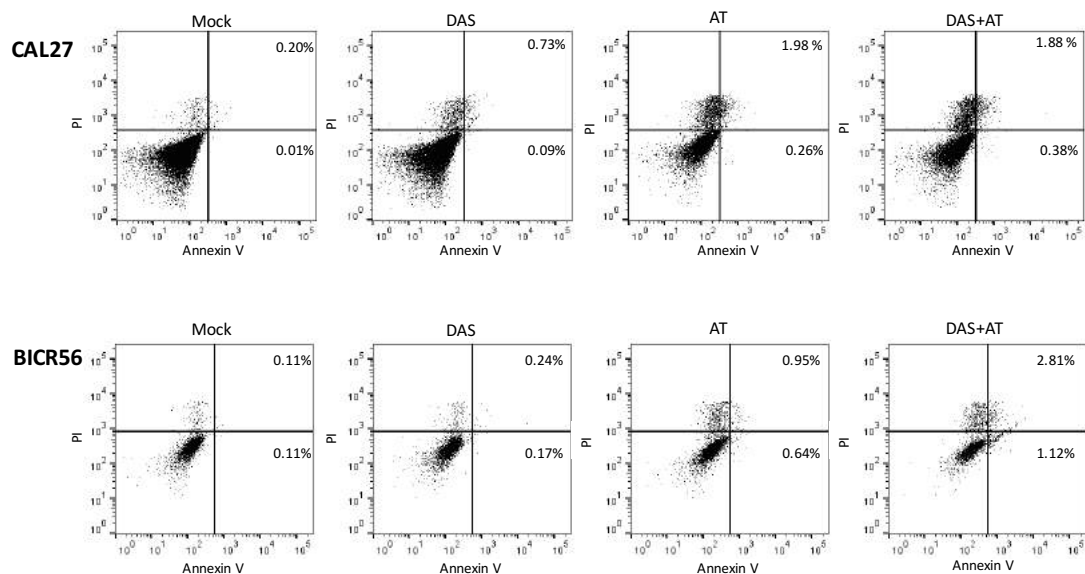
Figure S16. Flow cytometry analysis shows no substantial induction of apoptosis due to DAS+AT cotreatment in TSCCs

 Annexin V- Propidium Iodide (PI) staining detects little increase in Annexin-positive cells. Cells were treated with DMSO as vehicle control (Mock), 50 nM of DAS, 30 nM of AT, or a combination of DAS+AT for 72 h. Treated cells were stained with Annexin V and PI for FACS analysis. x-and y-axis indicate Annexin V and PI fluorescence intensity, respectively. Numbers in the right upper and right lower quadrants denote percentages of late and early apoptotic SAS cells, respectively (Annexin V positive). Ten thousand events were analyzed in each experiment. Results are expressed as means taken from two independent experiments.
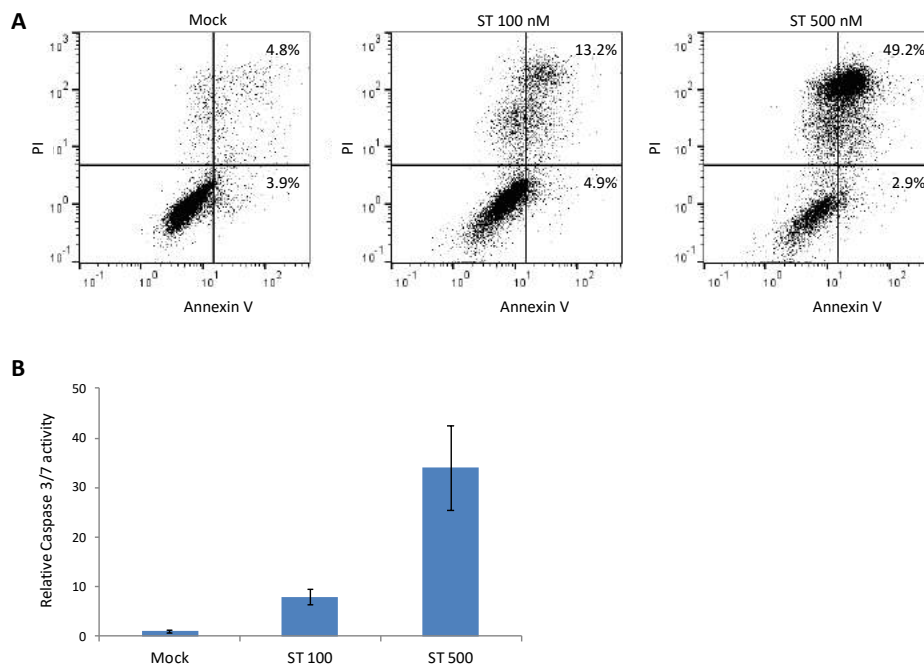
Figure S17. Flow cytometry analysis and a Caspase 3/7 activity assay show a very strong induction of apoptosis due to Staurosporine treatment in SAS cells

SAS cells were treated with DMSO as vehicle control (Mock), 100 nM or 500 nM of Staurosporine for 18 h.

(A) Annexin V/PI staining detects an obvious increase in Annexin-PI-positive cells
Treated SAS cells were stained with Annexin V and PI for FACS analysis. Numbers in the right upper and right lower quadrants denote percentages of late and early apoptotic SAS cells, respectively.

(B) Caspase 3/7 assay shows strong activation of Caspase 3/7 in SAS cells upon treatment with ST
Caspase 3/7 activity was measured after 18 h for treated SAS cells by a Caspase 3/7 Glo® kit (Promega) and normalized to total cell content measured by a Cell Titer Glo® kit (Promega).
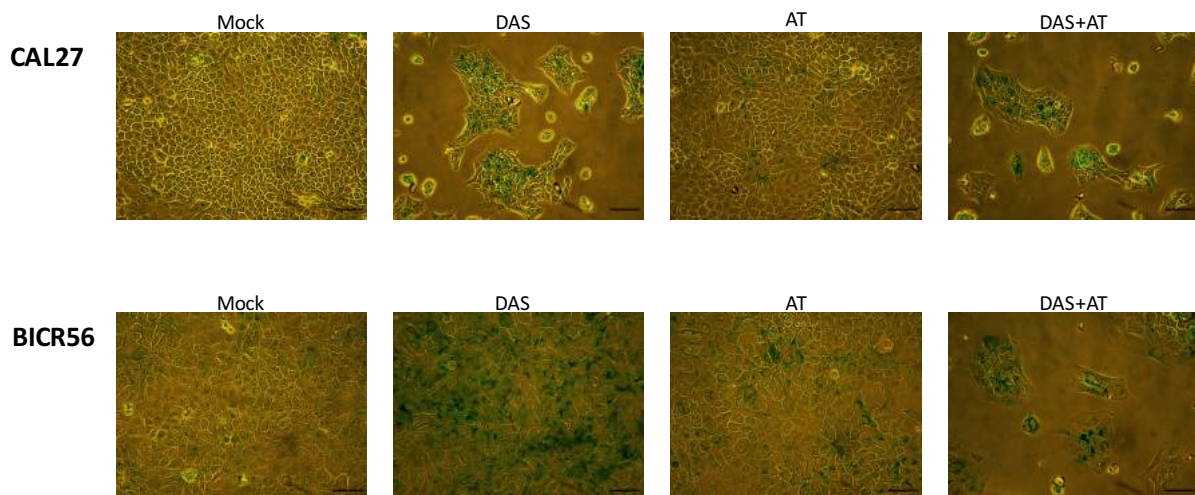
Figure S18. Induction of senescence in TSCCs following DAS and AT treatment

Representative pictures of TSCCs monolayer cultures stained with senescence-associated-β-galactosidase (SA-β-gal). High activity of pH-dependent beta-galactosidase characterizes senescent cells. Accordingly, SA-β-gal positive staining (blue color) indicates aged cells. Cells were treated with DMSO as vehicle control (Mock), 50 nM of DAS, 30 nM of AT, or a combination of DAS+AT for 72 h as indicated in the figure. Scale bar = 100 µM.

SAS **CAL27** **BICR56**
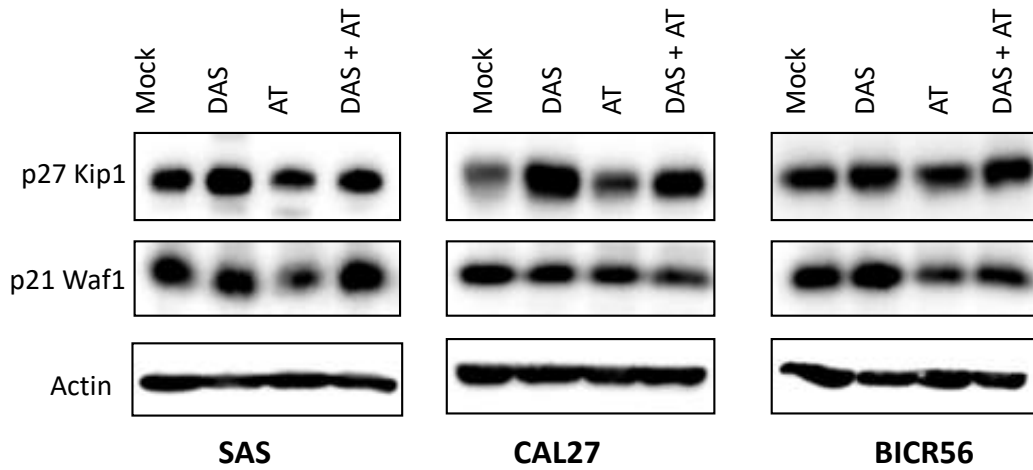
Figure S19. Slight to strong upregulation of p27, but not p21, was observed in TSCCs upon treatment with DAS and DAS+AT which may partially drive cellular senescence

Cells were treated with DMSO as vehicle control (Mock), 50 nM of DAS, 30 nM of AT or a combination of DAS+AT for 72 h. Total cell lysates were generated and analyzed by Western blotting. The blots shown are representative of three independent experiments. Antibodies that detect the total protein abundance were used.
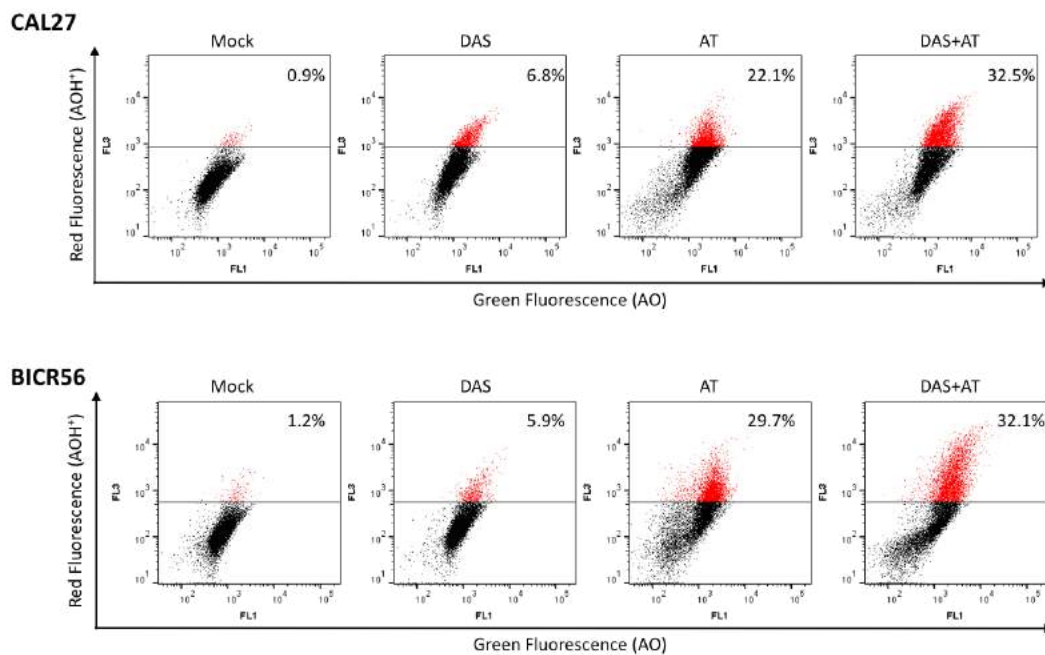
Figure S20. DAS and AT induce autophagy in TSCC lines

Cells were treated with DMSO as vehicle control (Mock), 50 nM of DAS, 30 nM of AT, and a combination of DAS+AT for 72 h, stained with AO and then analyzed by flow cytometry to quantify the acidic vesicular organelle formation. FL1 (x-axis) indicates green color intensity, while FL3 (y-axis) shows red color intensity. Representative results from three independent experiments are shown.
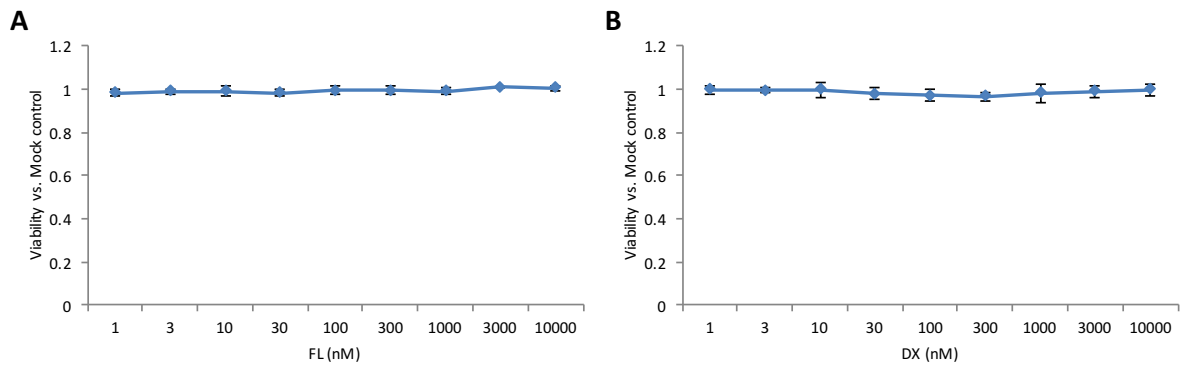
Figure S21. FL and DX were not able to reduce SAS cell line viability in 2D culture

Cells were treated with a serial dilution of FL (A) or DX (B) for 72 h and analyzed via resazurin calorimetric assay. Data represent fluorescence measurements normalized to Mock-treated cells. The dose-response curves show mean values ± SD of three independent experiments.
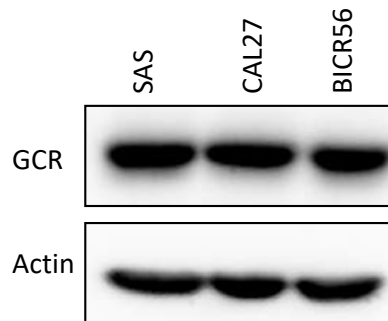

Figure S22. TSCCs show no variable levels of GCR

Equal amounts of total lysates from 3 TSCC lines were separated by SDS-PAGE and analyzed by Western blotting with an anti-GCR antibody.
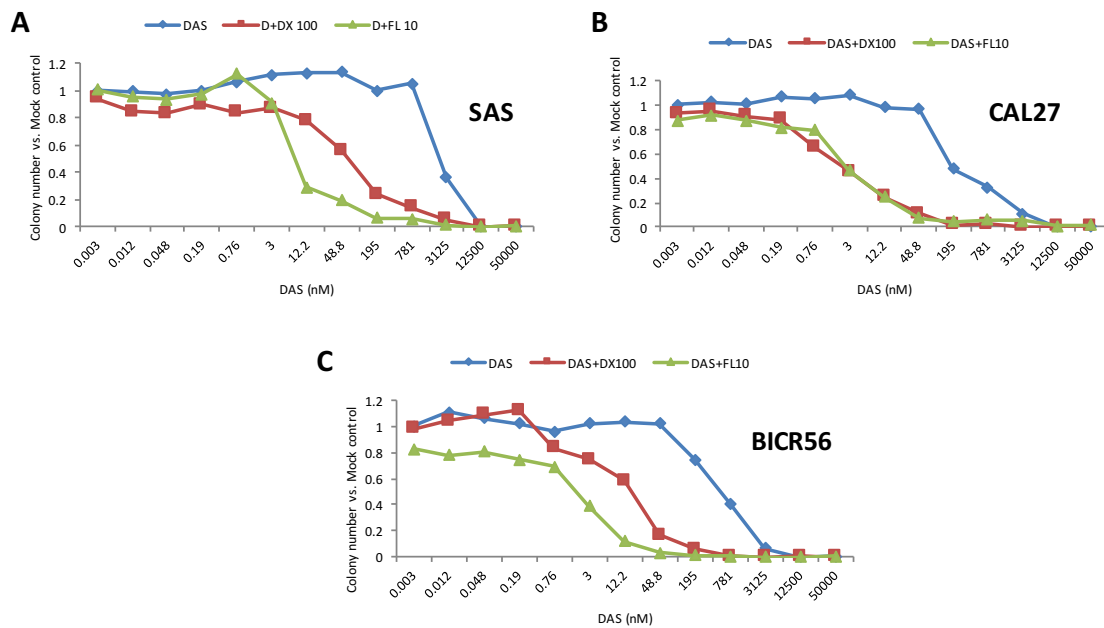
Figure S23. FL is more potent than DX in combination with DAS and both CGs show a strong synergistic effect in TSCC lines in combination with DAS in 3D soft agar culture

Dose response curves of TSCC lines treated with DAS with or without a constant concentration of DX (100 nM) or FL (10 nM) as determined by colony numbers in 3D soft agar culture. The colony numbers for treatment with DAS, DAS+DX and DAS+FL were counted within the same experiment. Data represent colony numbers normalized to Mock-treated cells. An expected effect was not calculated here since DX or FL individually has no notable effect on colony formation as shown before (Figure 30.A and 33.A).
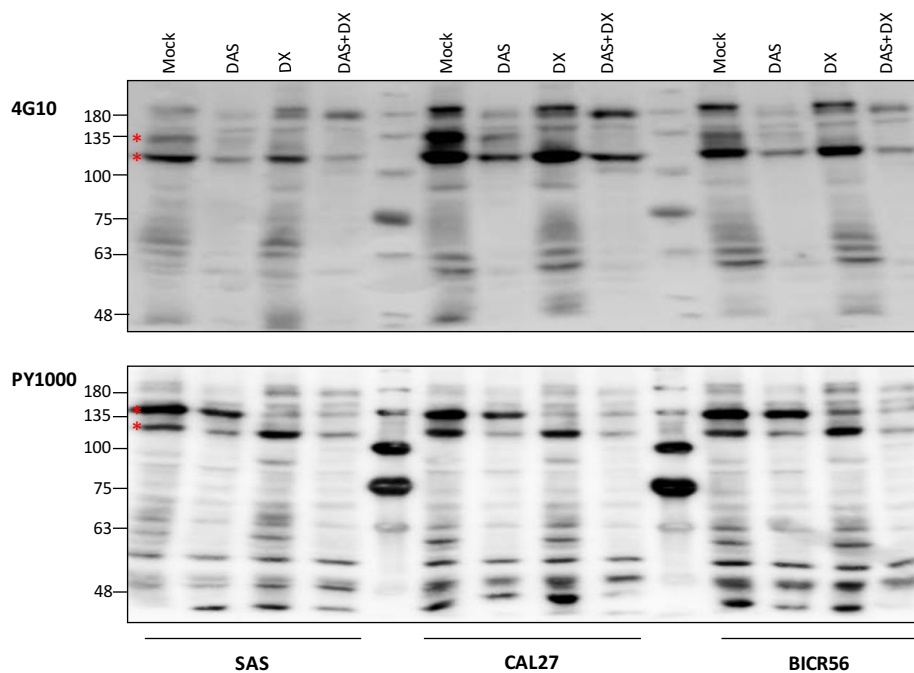

Figure S24. A direct comparison of tyrosine phosphorylation profiles for the treated TSCC lines show two major reductions in phosphorylated proteins (around 120 and 135 KDa) upon DAS+DX combination treatment

Cells were treated with DMSO as vehicle control (Mock), 50 nM of DAS, 100 nM of DX or DAS+DX for 72 h before extraction. Total cell lysates were separated by 8 % SDS-PAGE and immunoblots were probed with anti-phosphotyrosine antibodies 4G10 or PY1000. Protein size markers are indicated on the left. The two most prominently reduced bands are indicated by red asterisks.

216
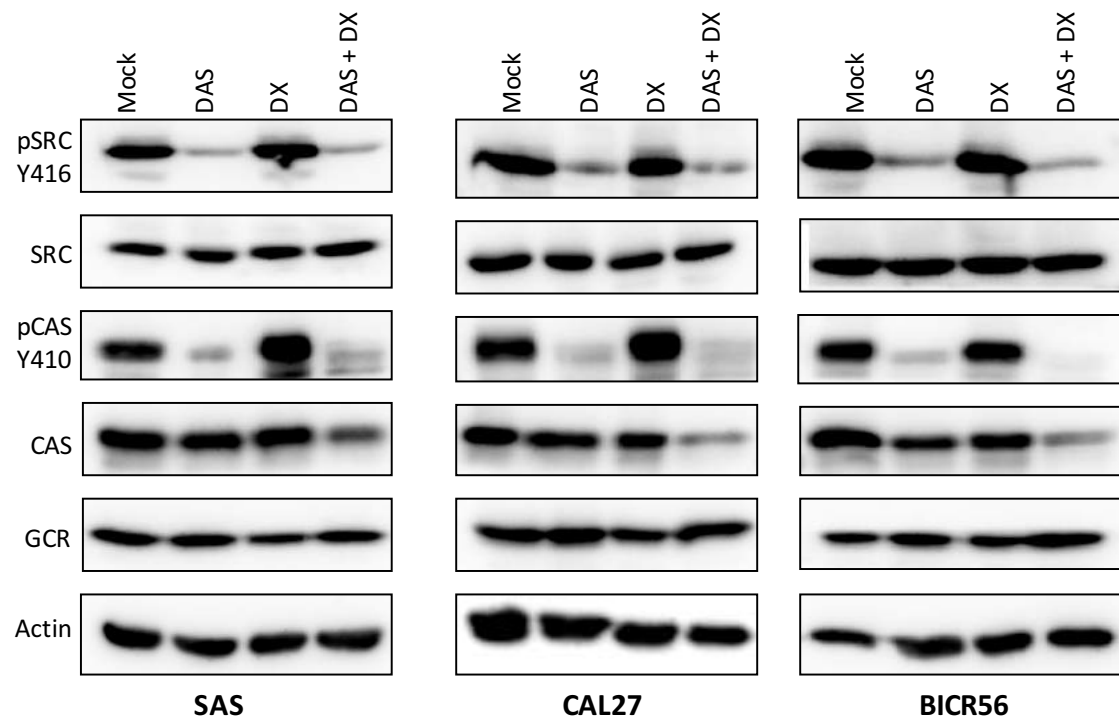
Figure S25. DAS, but not DX, inhibits SRC and its downstream target p130CAS phosphorylations also DAS+DX cotreatment leads to p130CAS degradation in TSCC lines   Cells treated with DMSO as vehicle control (Mock), 50 nM of DAS, 100 nM of DX, or a combination of DAS+DX for 72 h. Total cell lysates were generated, separated by SDS-PAGE and analyzed by Western blotting. Antibodies that detect the phosphorylated state of SCR at Tyr416 and p130CAS at Tyr410 were used to detect the change in phosphorylation. The other blots analyzed total protein abundance. The blots shown here are representative of three independent experiments.
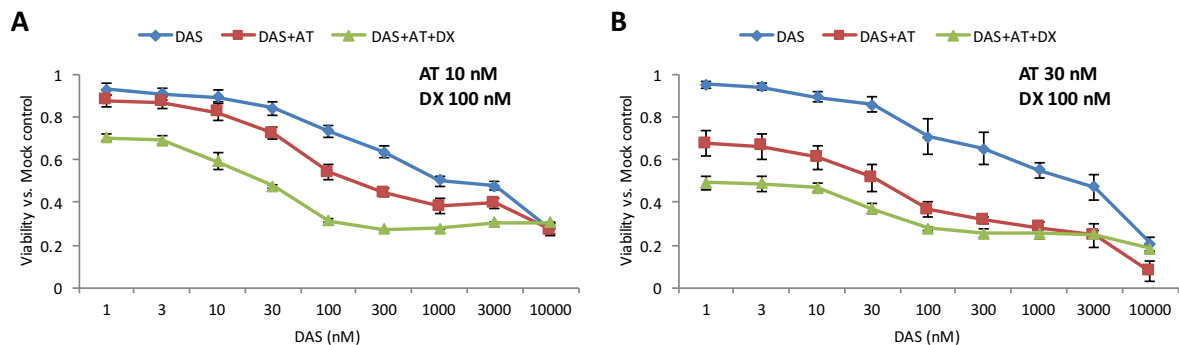

Figure 26. DAS+AT cotreatments synergize with 100 nM of DX to repress SAS cells viability in 2D culture

Cells were treated with serial dilutions of DAS, DAS+AT or DAS+AT+DX for 72 h. Cell viability after treatment were measured by resazurin calorimetric assay. The inhibitory activities of DAS, AT and DX individually were measured within the same experiment. The expected effect was not calculated here because DX alone has on substantial effect on cell viability. Data represent fluorescence measurements normalized to Mock-treated cells. The dose-response curves show mean values ± SD of three independent experiments with six parallel measurements in each case.
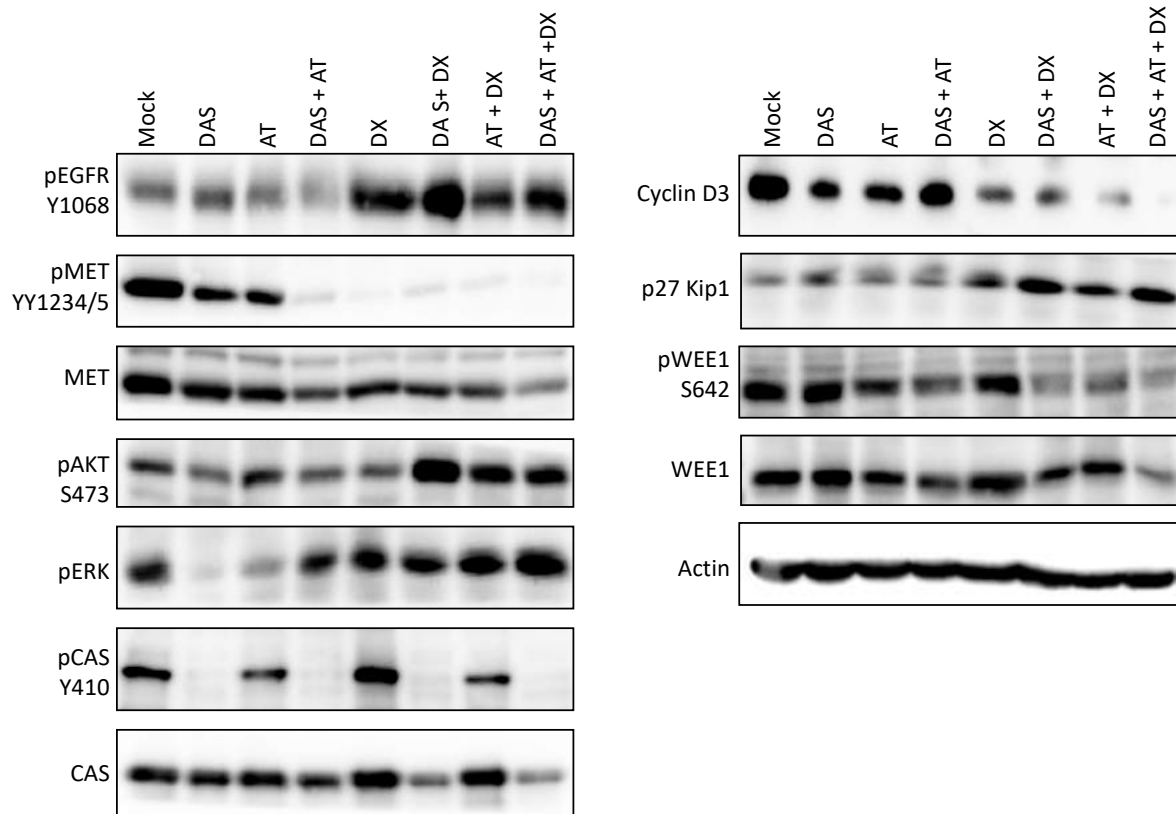
Figure S27. AT slightly reduces EGFR phosphorylation due to DX and DAS+DX treatments but not ERK and AKT activation in SAS cell line
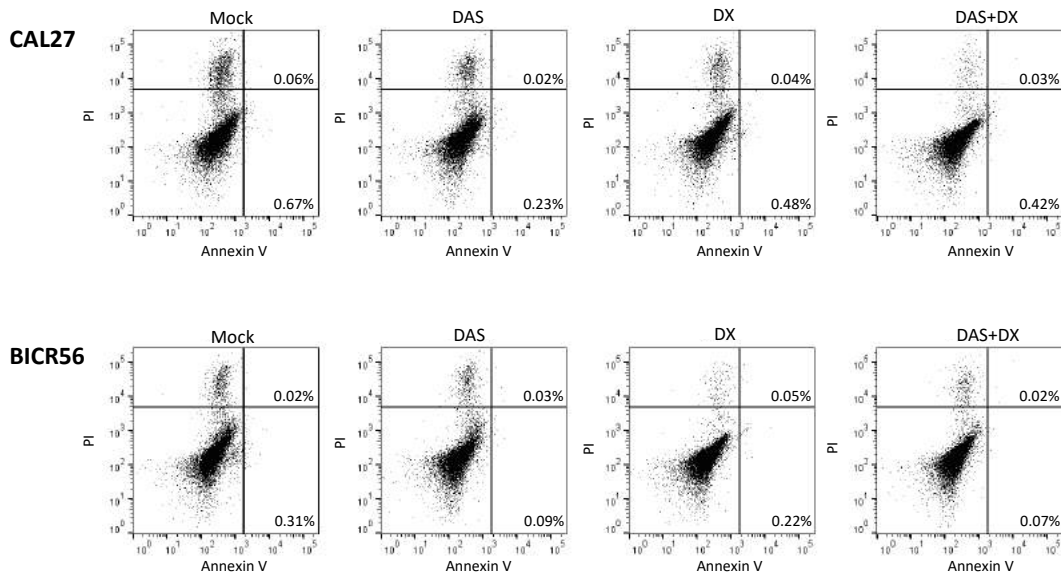
Cells were treated with DMSO as vehicle control (Mock), 50 nM of DAS, 30 nM of AT, DAS+AT, 100 nM of DX, DAS+DX, AT+DX, or a combination of DAS+AT+DX for 72 h. Total cell lysates were generated, separated by SDS-PAGE and analyzed by Western blotting.
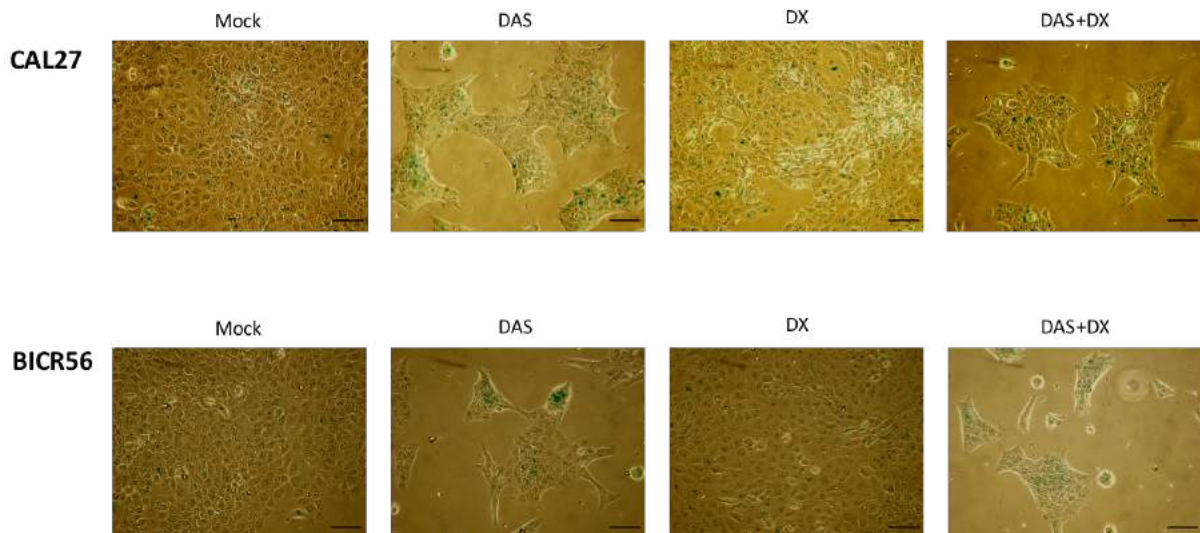
Figure S28. Induction of senescence in TSCCs following DAS and DX treatment

Representative pictures of TSCCs monolayer cultures stained with senescence-associated-β-galactosidase (SA-β-gal). High activity of pH-dependent beta-galactosidase characterizes senescent cells. Therefore, SA-β-gal positive staining (blue color) indicates aged cells. Cells were treated with DMSO as vehicle control (Mock), 50 nM of DAS, 100 nM of DX, or a combination of DAS+DX for 72 h as indicated in the figure. Scale bar = 100 μM.
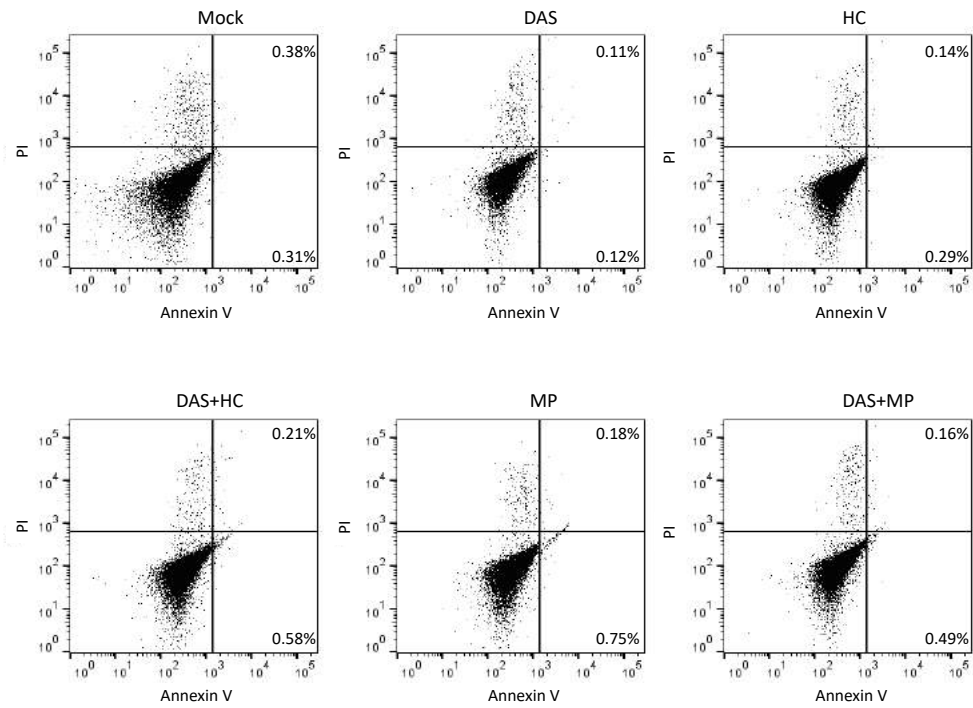
Figure S29. Flow cytometry analysis shows no induction of apoptosis due to DAS and/or DX treatments in TSCCs

Annexin V/PI staining detects no increase in Annexin-positive cells. Cells were treated with DMSO as vehicle control (Mock), 50 nM of DAS, 100 nM of DX, or a combination of DAS+DX for 72 h. Numbers in the right upper and right lower quadrants denote percentages of late and early apoptotic SAS cells, respectively (Annexin V positive). Results are expressed as means taken from two independent experiments.
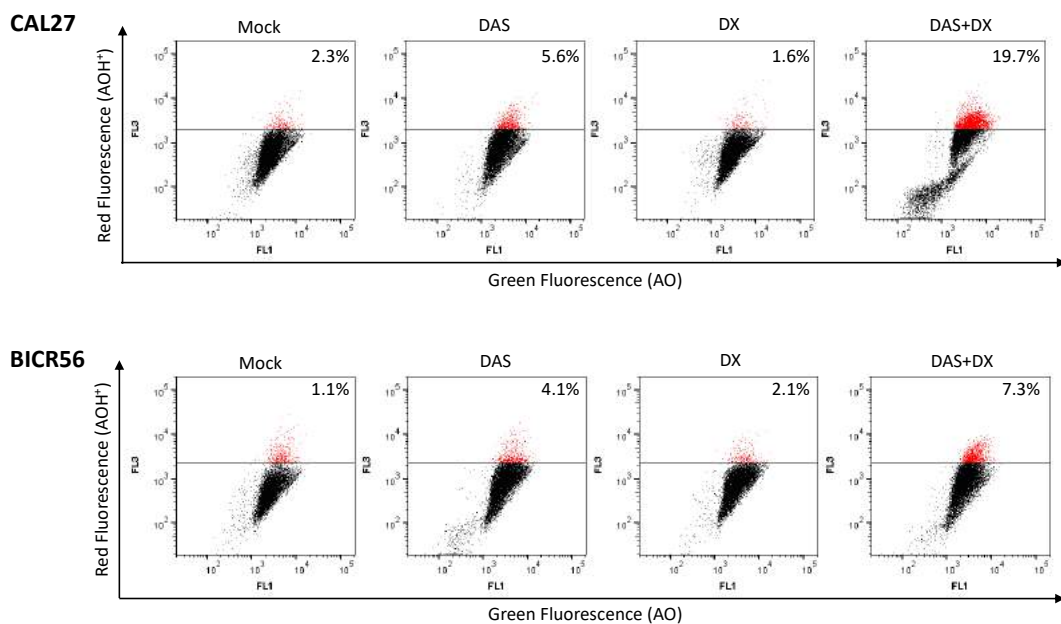
Figure 30. DAS and DAS+DX treatments induce autophagy in TSCC lines

Cells were treated with DMSO as vehicle control (Mock), 50 nM of DAS, 100 nM of DX, and a combination of DAS+DX for 72 h, stained with AO and then analyzed by flow cytometry to quantify the acidic vesicular organelle formation. FL1 (x-axis) indicates green color intensity, while FL3 (y-axis) shows red color intensity. Representative results from three independent experiments are shown.

Figure S31. Flow cytometry analysis shows no substantial induction of apoptosis due to DAS and/or GCs treatments in SAS cells

Annexin V- PI staining detects no significant increase in Annexin-positive cells. SAS cells were treated with DMSO as vehicle control (Mock), 50 nM of DAS, 300 nM of HC, 150 nM of MP, a combination of DAS+HC or a combination of DAS+MP for 72 h. Numbers in the right upper and right lower quadrants denote percentages of late and early apoptotic SAS cells, respectively (Annexin V positive). Results are expressed as means taken from two independent experiments.

Curriculum Vitae

Personal data

Name: Ali Hmedat

Date of birth: 30.01.1985

Place of birth: Irbid/Jordan

Academic qualifications and work experience

Commenced 11/2021	Wissenschaftlicher Mitarbeiter, Molecular Cell Biology Department, Institute of Molecular Medicine, Martin Luther University Halle-Wittenberg
8/2017 – present	PhD candidate, Tumor Biology Department, Institute of Molecular Medicine, Martin Luther University Halle-Wittenberg
9/2016	Master degree in Pharmaceutical Biotechnology, Martin Luther University Halle-Wittenberg
08/2015 – 03/2016	Master thesis, Leibniz Institute for Plant Biochemistry Halle/Germany
09/2014 – 02/2015	Project work, Leibniz Institute for Plant Biochemistry Halle/Germany
09/2010 – 06/2017	Pharmacist, King Abdullah Medical City (KAMC), Saudi Arabia
06/2008 – 08/2010	Pharmacist, Royal Medical Service, Jordan
01/2008 – 05/2008	Medical Representative, Al Hikma Pharmaceuticals Company, Jordan
02/2008	Bachelor of Science in Pharmacy, Jordan University of Science and Technology
01/2005 – 01/2008	Intern, Ma'en Pharmacy, Irbid/Jordan
1998 – 2003	Sammu Secondary High School

List of Publications

Morejón, M.C., Laub, A., Kaluđerović, G.N., Puentes, A.R., **Hmedat, A**.N., Otero-González, A.J., Rivera, D.G., and Wessjohann, L.A. (2017). A multicomponent macrocyclization strategy to natural product-like cyclic lipopeptides: synthesis and anticancer evaluation of surfactin and mycosubtilin analogues. Org. Biomol. Chem. *15*, 3628–3637.

Bassal, M., Abukhalaf, M., Majovsky, P., Thieme, D., Herr, T., Ayash, M., Tabassum, N., Al Shweiki, M.R., Proksch, C., **Hmedat, A.**, et al. (2020). Reshaping of the Arabidopsis thaliana Proteome Landscape and Co-regulation of Proteins in Development and Immunity. Mol. Plant *13*, 1709–1732.

Eidesstattliche Erklärung

Hiermit erkläre ich an Eides statt, dass ich die vorliegende Arbeit selbstständig und ohne fremde Hilfe angefertigt habe. Ich habe keine anderen als die angegebenen Quellen und Hilfsmittel benutzt und die den verwendeten Werken wörtlich oder inhaltlich entnommenen Stellen als solche kenntlich gemacht. Ferner erkläre ich, dass ich mich mit der vorliegenden Dissertation erstmals um die Erlangung eines Doktorgrads bewerbe. Die vorliegende Arbeit ist weder im Inland noch im Ausland in gleicher oder ähnlicher Form einer anderen Prüfungsbehörde zum Zweck einer Promotion oder eines anderen Prüfungsverfahrens vorgelegt worden.

Halle (Saale), 20.3.2021   **Ali Hmedat**